Experimental Fluid Mechanics

R. J. Adrian · M. Gharib · W. Merzkirch
D. Rockwell · J. H. Whitelaw

Springer-Verlag Berlin Heidelberg GmbH

G. S. Settles

Schlieren and Shadowgraph Techniques

Visualizing Phenomena in Transparent Media

With 208 Figures and 48 Color Plates

Springer

Professor G. S. Settles
Penn State University
Gas Dynamics Laboratory
301 D Reber Building
University Park, PA 16802
USA
e-mail: gss2@psu.edu

ISBN 978-3-642-63034-7

Library of Congress Cataloging-in-Publication Data

Settles, G.S. (Gary S.), 1949-
Schlieren und shadowgraph techniques: visualizing phenomena in transparent media / G. S. Settles.
p. cm. – (Experimental fluid mechanics)
Includes bibliographical references and index.
ISBN 978-3-642-63034-7 ISBN 978-3-642-56640-0 (eBook)
DOI 10.1007/978-3-642-56640-0
1. Schlieren methods (Optics) 2. Photography, Shadowgraph. I Title. II Series.
QC 373.S3 S47 2001
535'.2–dc21 2001042034

http://www.springer.de

Originally published by Springer-Verlag Berlin Heidelberg New York in 2001
Softcover reprint of the hardcover 1st edition 2001

Typesetting: Camera ready by author
Cover-Design: design & production, Heidelberg
Printed on acid free paper SPIN: 11013389 61/3111/kk - 5 4 3 2 1

Series Editors

Preface

It makes the most sense in French.[1] Between *microskopie* and *télescopie* come *strioscopie* and *ombroscopie* – schlieren and shadowgraph techniques in English. All of a close family, these optical methods have common parents, grew up together, and are made of the same optical stuff. Though there are hundreds of books on microscopes and telescopes, however, there is no modern book on schlieren and shadowgraph methods, thus the principal justification for this book.

Unlike the microscopes and telescopes, schlieren and shadowgraph instruments are not seeing aids based on size or distance. Instead, they allow us to see the invisible: the optical inhomogeneities in transparent media like air, water, and glass that otherwise cause only ghostly distortions of our normal vision.

These techniques are discussed briefly in many books and papers, but the best and most complete treatments so far are dated and little-known. I might therefore paraphrase Sir James Jeans by claiming that much of my book is merely Schardin [1,2] rewritten and brought up to date.[2]

This book is intended more to be a practical guide and a thinking tool than an exhaustive theoretical treatment of the topic (which would require a separate volume). In the western world few if any schlieren instruments can be bought outright; unlike telescopes and microscopes, schlieren and shadowgraph systems must usually be assembled from components. Though this is actually not very difficult, it can still be frustrating for the inexperienced. Thus Chap. 7 is devoted to practical issues in the selection of components, setup, and adjustment, and Chap. 8 suggests a modest schlieren system anyone can build.

This is a very visual topic. Just in fluid dynamics alone, one clearly sees the nonlinearity and pattern diversity of the governing equations in the wealth of optical images that spill forth. Some of these (e.g. Toepler [3], Mach and Salcher [4], Sabine [5], Cranz and Schardin [6] and Brown and Roshko [7]) have spawned entire fields of study. It is absurd to present such a visual subject in words alone,

[1] Originally from the Latin *striatus* (streaked) and *umbra* (shadow), and the Greek *têle* (far), *micrós* (small), and *skopein* (to look at).

[2] This is especially true in that Springer-Verlag has granted permission to reproduce images from Schardin's classic 1942 monograph on schlieren techniques and their applications [2], and I have followed Schardin's lead on several issues. His scholarship is hard to match, but his German wartime publication is obscure today.

so I made every effort to illustrate the text with the best schlieren images and shadowgrams I could find. The courtesy of colleagues and some good luck allowed me to include a number of classic visualizations, and I thank all those who contributed images. But even Sir Kenneth Clark [8] had to admit that some pictures he greatly admired were inaccessible to him.

For such time-honored techniques there remains a curious lack of familiarity and a misunderstanding of principles that I hope to rectify here. People sometimes confuse these techniques with thermography and paranormal stuff like Kirlian photography and the "human aura." Following recent coverage of some of my schlieren imagery on German public TV, I received a flurry of German inquiries about this "new" technique. One even asked for the English equivalent of the word "Schlieren." These misconceptions are dealt with throughout the text.

I thus hope to fulfill the needs of the novice for basic information, as well as those of the professional for a thorough treatment of the topic. Other goals include making connections among several diverse fields and covering important recent developments. At the end I make an attempt to predict where this topic is headed. Along the way, I try to convey a little of what Ernst Mach called "the charm and the poetry of research" [9].

Consequently this book fails a primary goal if it turns out not very readable. Acronyms, for example, would save some space but the cost is too great: technology must not become the Tower of Babel.

Almost every book requires some difficult choices of scope. Thus the gray area between schlieren and interferometry is explored only briefly here. Further, though several useful instruments embody schlieren optics without actually forming an image, present coverage is limited solely to imaging methods. No attempt is made to cite all of the thousands of literature references in which the subject techniques are mentioned or used. Quantitative methods are discussed in Chap. 10, but the emphasis remains on the qualitative and semi-quantitative visualization of natural phenomena, at which schlieren and shadowgraphy excel.

My audience is the user group of schlieren and shadowgraph methods. I hope they find here a comprehensive resource. On a different level I also try to appeal to all enthusiasts of seeing the invisible. The implications of this field – the optics of inhomogeneous media – are so broad as to span most of science and technology. I try to do justice to this despite my obvious background in fluid dynamics.

The book assumes familiarity with geometric optics, optical components, and calculus, though I do not stress the mathematical background. A few more-advanced topics such as aberrations, diffraction theory, and Fourier optics are also invoked. No attempt is made to review this background in any detail, since it is readily available in many fine textbooks. A few key optical concepts and a derivation are covered in App. A in support of the main text.

Though introduced to schlieren techniques as a teenager in the 1960's, I first had the notion to write this book in 1983. I mentioned this to long-time friend and colleague Wolfgang Merzkirch and it eventually led, with his encouragement, to my writing the actual book.

I am privileged to acknowledge the assistance and friendship of three colleagues, Leonard Weinstein, Horst Herbrich and Peter Krehl, who share my obses-

sion with the optics of inhomogeneous media. Weinstein's inventive genius on this topic is without parallel in the latter 20th Century. Herbrich's approach to applications inspired me in that direction, and Krehl provided the example of a scientist with a determined flair for history.

I am further indebted to Anatol Roshko for pointing out, with characteristic insight, that a book on schlieren techniques should include shadowgraphy too.

Jack North and Felix Weinberg are the only masters of schlieren imaging from the previous generation that I was privileged to know personally. Jack passed away during the writing of this book, but his widow, Nella North, and his colleagues Herbert Pearcey and Eric Rogers have been very helpful.

Heather Ferree, Rossana Quiñones, and Thomas C. Hanson helped illustrate the book with many fine photos shot using the example schlieren system of Chap. 8. I also thank Lori Dodson and J.D. Miller – staff members of the Penn State Gas Dynamics Lab – for their support in this and all our other endeavors.

Mrs. E. Raufelder and Dr. H. Riedesel of Springer-Verlag Heidelberg assisted this project over more years than expected, and I thank them for their patience.

Finally, special thanks are due to the following individuals who assisted the effort in a wide variety of ways: M. Abramowitz, R. C. Benson, P. Bradshaw, Y. D. Chashechkin, A. Davidhazy, J. M. Dewey, I. V. Ershov, H. Kleine, J. Kozák, H. F. Lehr, W. H. McCallum, J. R. Meyer-Arendt, M. Raffel, J. Rienitz, P. Rheinberg, M. T. Settles, J. Srulijes, P. Steehouwer, J. K. Vandiver, A. A. Zheltovodov, and my parents, Charles H. and Stella M. Settles.

Bellefonte, PA, February 2001 Gary S. Settles

Left-to-right: the author, Leonard Weinstein, and Horst Herbrich in Sorrento, Italy, Sept. 1998: the self-proclaimed "world's experts on schlieren photography". (No one else applied for the title.) Photo by Liselotte Herbrich.

About the Author

Gary Settles was born in 1949 and grew up on a farm at the edge of the Great Smoky Mountains in East Tennessee. His interest in fluid dynamics, optics, and experiments began as a teenager with the construction of small subsonic and supersonic wind tunnels, winning awards at the 1967 International Science Fair. He gained industrial and laboratory experience through summer jobs at the US Naval Ordnance Lab, NASA's Ames Research Center, and the Boeing Company, where he worked on both 747 and SST aerodynamics. He studied at the University of Tennessee under an Alcoa Foundation scholarship, receiving the Bachelor of Science Degree in Aerospace Engineering in 1971.

Supported by an NSF Traineeship at Princeton University, he studied shock wave/boundary-layer interactions under Prof. Seymour Bogdonoff, earning his Ph.D. degree in 1976. For three years he was a Research Scientist in the Princeton Combustion Lab Division of Flow Research, Inc., where he led a project to define a national program in energy-efficient pump utilization. He then joined the Research Staff of Princeton University's Mechanical and Aerospace Engineering Dept., where he conducted research and managed the Gas Dynamics Laboratory.

In 1983 Settles was appointed Associate Professor of Mechanical Engineering at Penn State University, where he established the Penn State Gas Dynamics Lab. He was promoted to full professor in 1989. The Penn State Gas Dynamics Lab has become well-known for its work in high-speed viscous-inviscid interactions and optical flow diagnostics. Research by Settles and his students on these topics was honored by the Penn State Engineering Society with its 1986 Award for Outstanding Research and its 1992 Premiere Researcher Award.

The strong visual and artistic nature of the optical flow visualization practiced by Settles has been used in many film and television documentaries, museum exhibits, books, encyclopedias and magazines around the world. Examples include the award-winning film "Search for Solutions," the CBS science series "Universe", the NBC "Today Show," CNN's "Science News," the series "Scientific Imagery" on German Public Television (NDR), the Learning Channel's series "Body Atlas," and the 3-D IMAX film "The Hidden Dimension." Settles has also presented many invited lectures and seminars in the US, Europe, Russia, China, and Japan.

Beginning in 1992, the Penn State Gas Dynamics Lab redirected its research, emphasizing applications of gas dynamics, nozzles, and flow visualization to "non-traditional" problems in areas ranging from surface engineering and materials processing to rheology and aviation security. This has since resulted in several inventions, the world's largest indoor optical flow visualization system, and a new aviation security screening portal based on the human thermal plume.

Fourteen Ph.D.'s and many Masters-degree and undergraduate scholars have been educated by Prof. Settles at Penn State. He currently teaches a 2-semester lecture sequence on compressible flows, and takes recourse in oil painting and classical music as antidotes to the rigors of an academic career.

The Settle/Suttle family immigrated from Yorkshire to Virginia in 1657 [10]

Table of Contents

List of Nomenclature

Man: 'Hello, my boy. And what is your dog's name?'
Boy: 'I don't know. We call him Rover.'

Stafford Beer

Metric units are used throughout this book. Distances units m, cm, mm, and μm are used at various points for convenience. In the special case of photometric units, see Sect. A.1 for more detail. Finally, an attempt is made to maintain consistent notation, as far as possible, with the key precedent works [1,2,98,102,110].

a	grid constant in cutoff plane, also acoustic speed, m/s
a	unobstructed height of source image in cutoff plane
Δa	change in a due to refraction
A	amplitude function; also clear aperture of schlieren objective
B	Luminance, candela/m^2; also grid width constant
b, h	breadth and height of light source slit
c	constant; also denotes the speed of light
C	contrast
d	width of schliere in test area; also diameter of circle of confusion
D	schlieren system aperture (test area diameter); also light source diameter
e	base of natural logarithms; also grid width constant
f	focal length
f/no.	the focal ratio of a lens or mirror, i.e. f/D
f′, f_2	focal length of second lens or mirror
F	Fourier transform; also focal distance coordinate
g,h	lengths; g also denotes gravitational acceleration constant
E, I	illuminance on viewing screen, lux
ΔE	change of illuminance on screen, lux
E*	indirect or unwanted illuminance component, lux
j	imaginary number $\sqrt{-1}$
k	constant; also Gladstone-Dale constant
l, ℓ	length
L	length of light path or of schlieren object in test area, measured along z-axis; also designates a lens
m	image magnification

M	Mach number
n	refractive index
p	static pressure, kPa; also denotes polarizer
r,θ,φ	spherical coordinates (r = radius)
R	range of schlieren system in mm of ray deflection or arcseconds of angle; also specific gas constant and inverse of lens aperture angle
$R_{a,d,ph}$	resolution limits due to aberrations, diffraction, and photographic media
S	Sensitivity; also denotes schlieren object
s	distance coordinate
T	temperature, K; also transmittance function
t	time, seconds; also used as a length coordinate, e.g. thickness
u,v	coordinates normal to optical axis in Fourier plane
V	speed, m/s
w	width coordinate; also wall condition, Wollaston prism
x,y,z	Right-handed Cartesian coordinate system in which the light propagation along the optical axis is in the +z-direction

Symbols

α	aperture angle, radians
β	light-loss factor
β_T	coefficient of thermal expansion, K^{-1}
γ	slope of characteristic curve of photographic film
δ	surface inclination angle, degrees; also diameter of a small feature of a schlieren object, and blur diameter
Δ	represents an increment or change in the quantity which follows
ε	light ray deflection angle produced by schlieren, radians or arcseconds
ϕ, φ	phase function; also number of line pairs contributing to an image point in focusing schlieren, and an angular coordinate
λ	wavelength of light, usually given in μm
μ	fluid viscosity, $N \cdot sec/m^2$
θ	azimuth angle in plane perpendicular to optical axis, degrees; also rotation angle and axis offset angle in a z-type schlieren system
ρ	density, kg/m^3
ξ	constant

Subscripts

0	background or baseline value
1	first schlieren lens or mirror
2	second schlieren lens or mirror
3	focusing lens
b,u	blur, unsharpness
max	maximum
min	minimum
ref	reference value

1 Historical Background

> ...it would open not only a cranney, but a large window...into the Shop of Nature, whereby we might be enabled to see both the tools and operators, and the very manner of the operation itself of Nature...
>
> *Robert Hooke, Observation LVIII,* Micrographia

> When I discover something new it has a musty smell, as if it hadn't been opened since the world began. *Buckminster Fuller*

It has been on my mind for years to tell the history of schlieren and shadowgraph techniques in detail and proper chronological order. This story reveals a connection generally unappreciated amongst the works of several well-known fathers of technology and others not so well-known, at least not in this context. It is the story of a way of seeing the invisible, and of discoveries centuries before their time; discoveries that nonetheless eventually played an important role in far-flung branches of science and technology. Other elements of this history touch on the key role of direct observation and the almost-lost art of ingenious bench-top experiments in physics. Despite beginnings centuries ago, only now can a complete history be written – thanks in large part to the scholarship of several colleagues who have a fine appreciation of history [11-13].

1.1 The 17th Century

The father of the optics of inhomogeneous media is the great enigmatic Robert Hooke (1635-1703) [14]. Destined to remain forever in Newton's shadow, Hooke was nevertheless a surpassing experimental genius in his own right. He observed both the microscopic world and the heavens, discovered and named the cell, fathered the field of elasticity, and made basic contributions to physics, chemistry, meteorology, geology, and biology [15]. Yet Hooke remains faceless to us, since no likeness of him survives [16].

Hooke's contributions of present interest came during his most productive years [14], when he was simultaneously involved with microscopy, telescopy, glass technology, and optical shop testing [17-19], all of which are closely related to the

G. S. Settles, *Schlieren and Shadowgraph Techniques*

present topic. These multifarious endeavors, along with his fascination with atmospheric refraction, led him to establish the optics of inhomogeneous media as a new field of scientific endeavor.

Hooke described this new field in his famous *Micrographia* [17], Observation LVIII, which is a thorough and cogent discussion of light refraction due to density variations in the atmosphere and in liquids. With this background he explained a great many phenomena: the twinkling of stars, convection in fluids, "heat haze," turbulent mixing and eddies, chromatic aberration, stratified flows, hydrostatics, and mirages. Even the modern field of gradient-index optics [20] was presaged. Key among these observations was that of veins (streaks, striae, *schlieren*) in glass.

Hooke's first schlieren method was the direct observation of a thermal air disturbance against a distant light-dark boundary: "...you shall find such a tremulation and wavering of the remote object, as will very much offend your eye" [17]. This unaided visual observation of schlieren effects, in which the pupil of the eye cuts off refracted rays, was not formally recognized as a schlieren technique for three centuries [2]. However, it must have been observed by our curious ancestors even many centuries before Hooke.

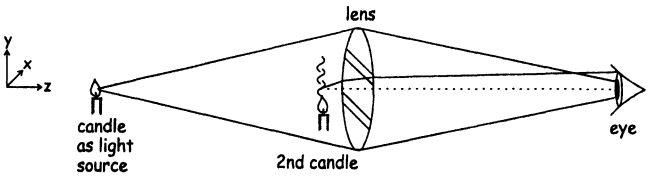

Fig. 1.1. Hooke's original schlieren system, using two candles, a lens, and the human eye.

But, being the premier instrument-maker of his time, Hooke next devised a much better schlieren method [14,21]. He replaced the distant light-dark boundary with the image of a candle flame, projected by a concave mirror or lens upon the pupil of the eye. As shown in Fig. 1.1, this illuminates the entire diameter of the lens to the eye of the observer. A second candle flame, now placed near the lens, refracts some light rays so strongly that they fall outside the pupil and are blocked, thereby revealing the transparent convective plume of the candle through changes in light intensity seen by the eye. Hooke understood this completely, and even diagrammed the refraction of the candle plume in *Micrographia*. Thus began a long, close relationship between the new method of schlieren observation and the ancient candle.

Images from a modern reenactment of this experiment are shown in Figs. 1.2a-b. A lens or mirror with a focal length on the order of 1 m or more is required to see the schlieren effect clearly. Such long-focus optics were, in fact, being ground for telescopes in Hooke's day [17]. A simple candle flame still makes a usable schlieren light source even today – as effective for this experiment as any modern source and better than most lasers.

Hooke went on to point out, almost casually, that the convective plume of a lit candle can also be seen by way of its shadow, as cast by the Sun on white paper [14,22]. He was describing what we now know as the shadowgraph technique, usually attributed to V. Dvorák in 1880 [23]. Two photos from a reenactment of this original shadowgraph experiment are shown in Fig. 1.3. It is such a simple physics experiment that almost everyone has seen it in one form or another, but Hooke was the first to explain it.

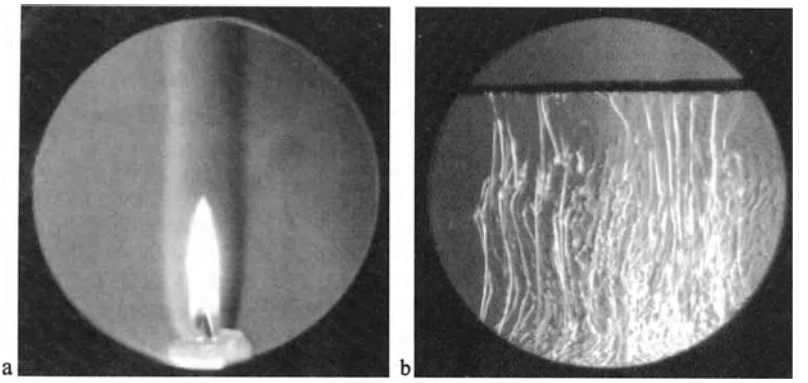

Fig. 1.2. Images from a reenactment of Hooke's schlieren demonstrations before the Royal Society: **a** candle plume, **b** dissolution of "sal-nitre" in water. Photos by author.

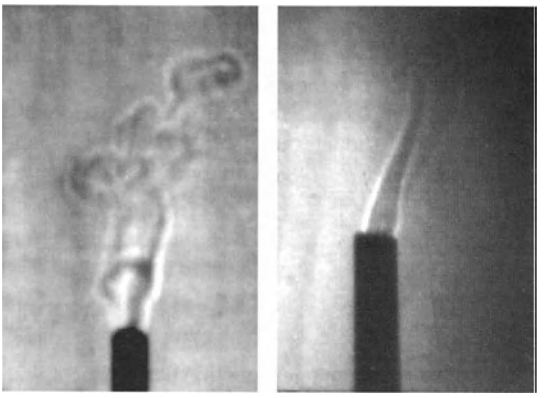

Fig. 1.3. Images from a reenactment of Hooke's original shadowgraph observation, showing the convective plume of a candle in shadows cast by sunlight. Photos by author.

Hooke saw the role of scientific instruments as an extension of human perceptions [24] – in this case to see the invisible. His descriptions of optical refraction [17], the convective plume of a candle [21], and the function of his new visualization techniques are all quite accurate, even by today's standards. But the pressure of his position as curator of experiments for the Royal Society caused him to leave

many fruitful topics only partially explored. He shared this weakness with Aristotle and Leonardo: a technical "butterfly syndrome" that caused him to flit from one fascinating topic to another while seldom completing the study of any [15]. A full account of his optical works was promised for a book called *Dioptricks* that, alas, he never wrote.

Hooke's effect on many technical fields was thus more catalytic than comprehensive [25]. And so it was that the optics of inhomogeneous media, like several of his other discoveries, suffered the fate of being forgotten in his time, rediscovered centuries later, and attributed to others.

From today's perspective it is not surprising that the schlieren technique arose naturally in the early days of microscopy, telescopy and glass technology. It is curious, though, that no one pursued it after it was demonstrated several times by Hooke, circa 1672, to dozens of members of the Royal Society. Here lay the key to unseen worlds, like those of the microscope or the heavens. Had Hooke's lead been followed in the 17th Century, the course of science and technology would have been altered. For one thing, we would not use the term *schlieren* today. (Hooke [22] called his new technique "the way of the concave speculum.")

On the other hand, there was little immediate need for optical flow visualization in the 17th Century. It would not be crucial for ballistics until Victorian times, not for high-speed flight until after World War I. This may help explain the apparent lost opportunity. Robert Hooke discovered much that was novel, that would arise of necessity only centuries later. Once can understand, then, that some of it was overlooked in his day. The schlieren technique was but one of these orphans of genius, a classic example of an idea centuries before its time.

Only about a decade after Hooke's work, Christiaan Huygens (1629-1695) also invented a version of the schlieren technique using a distant light-dark boundary [26]. Huygens is now famous, of course, for his astronomical discoveries, time measurement, kinetic energy formula, and a key optical principle named for him (Sect. A.2.2). He used the schlieren technique to look for striae (*veines du verre*) in glass blanks prior to grinding lenses from them. He also re-invented Hooke's candle-illuminated schlieren technique for similar purposes [14,26]. This approach is part of what we now call *optical shop testing*, a field originated by Huygens, but not generally attributed to him.

1.2 The 18th Century

After Huygens, the thread of the optics of inhomogeneous media is almost lost until the 19th Century, but for one man. The sole known contribution during the 18th Century comes from a most-unlikely source: Marat.

Jean Paul Marat (1743-1793) is remembered as a notorious character of the French Revolution. He is almost forgotten as a physician and scientist, and a key biographer [27] devotes but a few pages to this aspect of his life. Nevertheless in 1780, nine years before the Revolution, Marat published a volume on the physics of fire [28] that contains – apparently – the first optical flow visualization image

ever printed. Shown here in Fig. 1.4a, it is indisputably a shadowgram. A candle flame is flanked by the thermal plumes of heated metal objects. As in Fig. 1.3 the warm air, less dense than the ambient, refracts light outward to form a bright fringe around an inner, darker zone. The laminar candle plume is handsomely drawn in its transition to turbulence. This key observation entered the fluid dynamics mainstream only when officially discovered by Osborne Reynolds a century later.

What can be said here of such a man as Marat? Some biographers discredit his scientific work and label him a charlatan [27]. Asimov [29] blames him for the guillotine death of Lavoisier, in revenge for his rejection of Marat's "foolish homegrown notions on the nature of fire." Conner [30], on the other hand, argues convincingly for the legitimacy of Marat's scientific work.

In any case, Marat's strong account of his Sun-powered shadowgraph projector [28] – he called it a "helioscope" – is certainly convincing. His shadowgrams are a key precedent: since Hooke published no shadowgrams, Marat's are evidently the historical first of their kind.

In the strangest turn of all, the French Academy of Sciences sent a delegation accompanied by Benjamin Franklin to visit Marat's laboratory [30]. With characteristic jocularity, Franklin thrust his bald head into Marat's shadowgraph beam and, sure enough, a rising thermal plume was seen by all (see Sect. 9.4.2). Marat falsely interpreted what he saw, though, as evidence of "igneous fluid."

Eventually Marat's experiments were rejected by the scientific establishment, whereupon he became alienated from it. At the onset of the Revolution his medicine was replaced by radical politics, his fire research by fiery oratory. Marat found the glory he sought as "The Friend of the People," the champion of the poor, the scourge of nobility, and a symbol of boundless revolutionary zeal. On his account the guillotine-blade fell until the streets ran red with blood.

Centuries later we are still ambivalent about Marat [27,30], but his contribution to the present topic remains undeniable. Even despite it, though, shadowgraphy was not to appear again officially for another century.

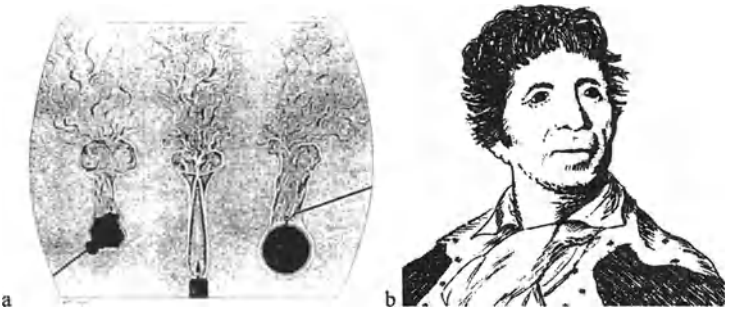

Fig. 1.4. **a** Marat's drawing of thermal plumes, apparently the first published shadowgram [28] **b** Jean Paul Marat (sketch by author based on 1793 portrait by Joseph Boze).

1.3 The 19th Century

According to Rienitz [14], the schlieren principle for optical shop testing can be traced from Huygens in 1685 to the optical practice in Paris at the end of the 18th Century. Coincidence or not, it was in Paris in 1859 that yet another prodigy, J. B. Leon Foucault (1819-1868), made the next important contribution to the optics of inhomogeneous media. Foucault is remembered today for his demonstration of the reduced speed of light in water, his invention of the first gyroscope, and especially his great pendulum experiment. Beside these accomplishments his knife-edge test of astronomical telescope mirrors [31,32] seems rather minor, but it was vital to perfecting telescopes and thus, indirectly, to our present knowledge of the heavens.

It is vital here as well, because it is the first use of an explicit cutoff (mask, stop, diaphragm, filter, *knife-edge*), external to and distinct from the pupil of the eye, for schlieren imaging. With this, the discrimination of regular vs. irregular rays occurs independently of the observer. This cutoff is now recognized as the salient distinguishing feature between schlieren techniques and all related approaches.

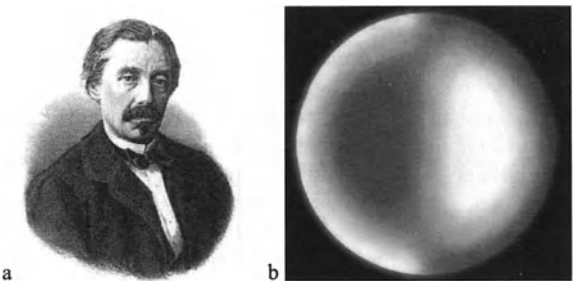

Fig. 1.5. **a** J. B. Leon Foucault [31], **b** "shadow" pattern of a parabolic mirror observed by Foucault's knife-edge test (photo by author).

So, although Huygens was the original pioneer of optical shop testing, Foucault's knife-edge test marks the recognized beginning of the field [31,33]. With this simple but exquisitely-sensitive variant of what we now call the schlieren technique, even amateurs could test the figure of their homemade telescope mirrors with sub-μm accuracy. Porter [34] called it "one of the most delicate and beautiful tests to be found in the realm of physics." The "shadow" pattern of a parabolic mirror under Foucault's knife-edge test is shown here in Fig. 1.5b.

A great hobby of amateur telescope making sprang up in the early 20th Century, feeding the ranks of professional astronomers and supplementing their observations. Even today, modestly-priced parabolic mirrors intended for amateur telescopes provide optics for many of the schlieren instruments in the West.

Like Huygens, Foucault took no apparent notice of any airflows made visible by his knife-edge test, but others did. The Foucault test caught on quickly, and in 1864 Henry Draper [35], an NYU professor and amateur astronomer, published a drawing of the warm air rising from his hand (Fig. 1.6). Draper disliked this, claiming that it "will completely destroy the beauty of an image." Likewise most astronomers, with the exception of Douglass [36], have avoided developing an interest in the atmospheric phenomena that stand between them and the stars.

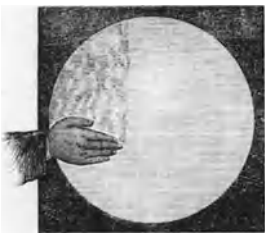

Fig. 1.6. Henry Draper's drawing of the thermal convection from his hand, as observed while testing a telescope mirror.

At about the same time as Foucault – the earlier work of Hooke and Huygens having been forgotten – August Toepler (1836-1912) re-invented the schlieren technique between 1859 and 1864 [3,12]. He had a flair for naming things, and so named his new technique distinctively after optical inhomogeneities in glass, which were known in German as "Schlieren.[3]" When his attention was called to Foucault's work, Toepler admitted the similarity but defended his claim of originality. He noted that Foucault was only concerned with testing mirrors, and did not see the broader value of this technique as a powerful scientific instrument in its own right [37,38]. However, the priority issue was clouded enough that journal editors of the time, including Kirchhoff and Helmholtz, were initially shy to publish Toepler's schlieren method. Some French scientists [38] even claimed that Toepler had appropriated Foucault's method and renamed it. Still today the otherwise-universal term *schlieren* is replaced in the French vocabulary by *strioscopie*. The extent of this confusion at the time is well-illustrated by Mach's [39] reference to the schlieren technique as "the optical method of Foucault and Toeppler (sic)."

Nonetheless Toepler's argument has stood the test of time. Though he did not invent the knife-edge test, he certainly did invent the schlieren imaging technique and was its first and principal developer, proponent, and patriarch.

[3]Hans Jebsen-Marwedel [117] has discussed the meaning of "Schlieren" as a word, an object, and a concept. It is, of course, the plural form of "Schliere," whose English equivalents are "streak," "striation," and "cord." (Though the German noun is always capitalized, in customary English usage the capitalization is dropped.) Its etymology connotes slime, ulceration, turbidity and knottiness, all of which can apply, for example, to flaws in glass. Toepler, however, was the first to apply the term to generic optical inhomogeneities. Given the history of the word schlieren, Jebsen-Marwedel concluded that "Toepler's method could not have had a better name than this."

Little was known of Toepler up to the present, though he ranked among the most prominent scientists of his time. Thanks to Krehl and Engemann [12], we now have a clearer picture of the man and his fascinating scientific career. Briefly, he was born in Brühl, Germany in 1836, and showed an early aptitude for art, music, and science. By age 23 he was already a popular lecturer in chemistry and physics at the Agricultural College of Poppelsdorf (now part of Bonn), and an innovative researcher. During a 5-year period at Poppelsdorf, while earning his Ph.D., Toepler invented, named, and refined his schlieren technique. For the next 15 years he applied the instrument to observe, demonstrate, and publish many diverse phenomena for the first time. The long-neglected optics of inhomogeneous media had finally found a champion.

Fig. 1.7. August Toepler's likeness from his tomb in Dresden (courtesy of Dr. P. Krehl, Ernst-Mach-Institut). The German epitaph reads "He was the first who saw sound." Actually it was shock waves, not sound, that Toepler first saw using his schlieren method.

Toepler's work on the schlieren technique was collected toward the end of his life and published in two volumes of *Ostwald's Classics of Exact Science* [40,41], which can still be found in research libraries. The first volume reproduces his original treatise [3], which was privately published at his own expense (perhaps due to the priority dispute with Foucault), and which is now very rare. It names and introduces the principle of the new instrument, then proceeds to explore previously-invisible aspects of diverse natural phenomena ranging from flames and convection columns to electric sparks.

Toepler was the first to devise a practical apparatus for schlieren observations (Fig. 1.8), including an adjustable knife-edge cutoff, a lantern light source, and a telescope for viewing the image directly. (Nowadays the telescope is replaced either by a ground-glass viewing screen or a camera.) The long-focus lens combination at the center of Toepler's apparatus was named the "schlieren head," a term we still use. He also described an 8-10 minute procedure to set up and align the apparatus "from scratch." This is not difficult, given a little experience, but it often evades the novice (see Chaps. 7 and 8).

Like his predecessors, Toepler began his schlieren investigations with optical shop testing in mind, but he soon broadened his outlook. For example, he noticed that the convection from his hand produced weak schlieren calling for fine optics and a sensitive knife-edge adjustment. By systematic tests he found that air temperature differences less than 1°C were visible, corresponding to a change in re-

fractive index of only one part per million. There followed studies of gas and liquid mixing, the world's first visualization of the human thermal plume, one of the earliest images of Marangoni convection [37], and even the convective heat transfer from plants. While all these observations are understood by geometric optics alone, Toepler also noted the effect of light diffraction in a forming bright halo about opaque objects in his schlieren image. He understood and promoted this new schlieren technique as if it were his own child.

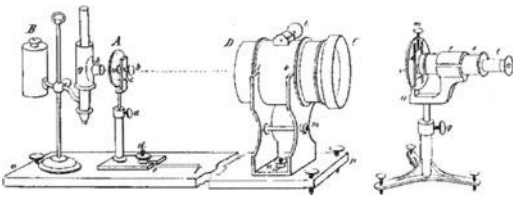

Fig. 1.8. Toepler's original schlieren apparatus [41].

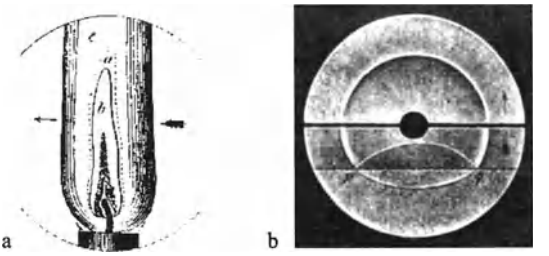

Fig. 1.9. **a** Toepler's drawing of the schlieren image of a candle flame [40]. **b** drawing of the schlieren image of a spherical shock wave from an electric spark in air [37].

Photographic media of sufficient speed for schlieren imaging were not yet available in Toepler's era. So, in time-honored fashion he drew his observations by hand. From his extensive schlieren studies a drawing of a candle flame and another of spherical shock wave motion are reproduced here in Figs. 1.9a and b.

Toepler's early efforts to see sound by the schlieren technique failed, but he soon hit upon the use of an electric spark to generate sharp acoustic disturbances. He called these by various names including "sound waves," but they were actually *shock waves* traveling faster than sound [12]. Toepler saw and illustrated the motion, reflection and refraction of shock waves for the first time, thus starting a field of study that is a key element of physics and engineering to this day. 90 years later one reviewer [42] wrote "The shock wave has been one of the most important and popular subjects for study since the discovery of the schlieren effect." One could say that schlieren and shock waves grew up together.

Using a spark gap as a schlieren light source, Toepler observed this shock wave motion with microsecond flashes. He thus shares credit for the invention of

stroboscopic imaging with W. H. F. Talbot (1800-1877) [43], one of the pioneers of photography. Talbot's interest was mainly in portraiture, however, while Toepler's was the first-ever *scientific* use of high-speed imaging. This work inspired Ernst Mach and, later, the modern pioneer of electronic stroboscopy, Harold E. Edgerton (1903-1990) [44]. Thus we see that modern flashlamps of all sorts were, in some sense, sparked by August Toepler.

All of Toepler's 1864 schlieren treatise [3] was qualitative, i.e. visual rather than numerical or theoretical. He had an excellent physical "feel" for his subject. For example, he proved the outer mantle of a flame to be convection by duplicating it with a hot metal bulb (as did Marat a century before). He felt the shock wave from a spark in a hand-held cork before he ever actually saw it. Then he demonstrated the dependence of the observed shock motion on the speed of sound by varying the air temperature or composition. As Witting [38] remarked, Toepler's original papers give the student a classical example of physical research: they report practical observations and "building-block" experiments designed to reveal a phenomenon or prove a concept. After the schlieren method has done this – which it does superbly – a host of less-general but more-quantitative instruments can be applied to lend numerical values to the details.

Before ending his work on schlieren, Toepler turned to microscopy [45]. Here there was already an observation method for transparent objects, called "oblique illumination," but Toepler found it was but a crude version of schlieren microscopy. Mounting a variable knife-edge cutoff in the back focal plane of his microscope objective, Toepler demonstrated unparalleled sensitivity, ease of adjustment, and uniformity of field illuminance in the microscopy of transparent objects. Despite this, schlieren illumination somehow never assumed a primary role in microscopy and later gave way, along with oblique illumination, to phase contrast and interference methods. That branch of the optics of inhomogeneous media is taken up further in the next section and in Sect. 9.4.7.

Toepler moved on to prestigious university posts in Riga, Graz, and finally Dresden [12]. His other scientific works ranged widely, and included a collaboration with Boltzmann on the physics of hearing [46]. He was famous in later life for these accomplishments, especially his brainchild, the *Toepler schlieren technique*. Eventually an accident and failing health removed him from science at the turn of the century, and he died in 1912 at age 76.

So, two centuries after Hooke introduced it, Toepler succeeded in making a name for the schlieren technique. But this time the atmosphere of experimental physics was more receptive, and applications for the new technique flourished. It was quickly recognized as a valuable tool, and was taken up by many scientists of the time, including Ernst Abbe [47], Robert W. Wood [48], Toepler's son Maximilian [49], and especially Ernst Mach (1838-1916).

Mach's is a household name today because, long after his death, the public imagination is captured by high-speed flight and the breaking of the mystical "sound barrier," linked forever to his name. In fact, his name continues to be appropriated for everything from automobiles to computers to razor blades that advertisers want us to associate with speed. The broader picture of Mach's contribution to the philosophy of science is overlooked, and here, as well, the supersonic

flight and shock waves are more to the point. Several excellent articles on Mach's contribution to gas dynamics form the background for what follows [50-53].

Fig. 1.10. Ernst Mach (photograph courtesy of Ernst-Mach-Institut).

Mach's motto, *"Sehen heißt verstehen"* (seeing is understanding) could be the mantra of modern flow visualization, but it played him false over the atom, whose concept he decried. His philosophy required direct observations of nature in order to maintain honesty and realism in scientific theory. When he heard of Toepler's new schlieren method to see the invisible, it must have appealed to him immediately.

In his 30's and holding the Chair of Experimental Physics at the German University of Prague, Mach had both the tools and the talent to pursue the key physics problems of the late 19th Century. Moreover, he had great intuitive skill with experiments, he paid attention to what others were doing in the field, he kept detailed notebooks, and he was always thinking.

From roots in physiology, Mach took up acoustics. Initial experiments with soot tracing of "sound" waves from sparks were indirect, and were replaced by direct schlieren observations. However, where Toepler's delay circuits were unreliable, Mach's succeeded. Also by this time photographic plates became sensitive enough to permit spark-illuminated schlieren photography (e.g. Fig. 1.11). Combined, these developments allowed precise wave-speed measurements, proving that the waves from sparks were not mere sound waves, they were *supersonic*.

The speed of sound or acoustic speed, "a," was already known for decades to be about 340 m/s. Then Riemann's theory [54] showed, in 1860, that nonlinear waves of finite strength could travel faster than sound. Mach's schlieren observations confirmed this in 1877, and he wrote [55] "...we deal in our experiments with such waves as described by Riemann." Thus the schlieren technique again played a crucial role in establishing the modern field of shock wave physics.

In 1885 Mach and Wentzel [56] recognized that the simple nondimensional parameter V/a (where V is the wave speed) governs the behavior of such shock waves. It took 40 years before Jakob Ackeret [57] suggested that V/a be called the *Mach number* in honor of Mach's contribution. This Mach number is now central to almost all calculations in gas dynamics and high-speed flight, and partly for this reason, every schoolchild now knows Mach's name.

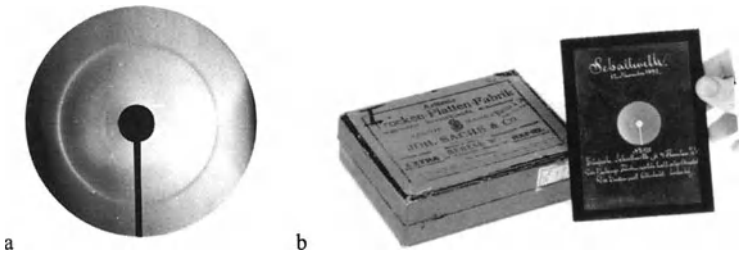

Fig. 1.11. **a** Mach's Schlieren photograph of a spherical shock wave from an electric spark, **b** corresponding original negative plate bearing the confusing title "Schallwelle" (sound wave). Photographs courtesy of P. Krehl, Ernst-Mach-Institut.

The reason also has a lot to do with ballistics. Mach took an interest in 1881 after he heard the Belgian ballistician Melsens [58] present a suspicious description of high-speed projectile motion. Mach doubted Melsens' explanation, and had the tools at hand to test it: μsec spark illumination, delay circuitry, and the schlieren technique. Much of the experimental work was done by his colleague, Prof. Peter Salcher of the Naval Academy in Fiume, Austria, a former student Toepler. Salcher used a rifle known to propel a bullet at supersonic speed. The remarkable schlieren result [4], Fig. 1.12, shows the swept bow shock, tail shock, and turbulent wake of the bullet. Here, in a series of schlieren images, the secrets of supersonic flight were first revealed. This began the field of supersonic aerodynamics, where seeing has been the key to understanding ever since.

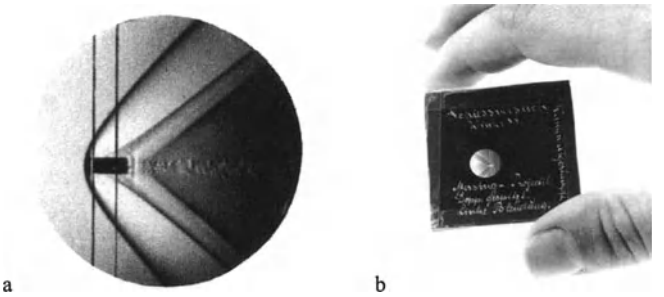

Fig. 1.12. **a** Mach and Salcher's schlieren photograph [4,59] of the oblique shock waves about a supersonic bullet **b** Original negative plate with 5-mm-diameter image. Photographs courtesy of P. Krehl, Ernst-Mach-Institut.

Salcher then suggested to Mach [60] that they check their results by observing a supersonic airstream flowing over a fixed projectile. The experiment was done by exhausting the compressed air supply of a torpedo factory through a converging

nozzle and photographing the result with a schlieren system. One of the resulting images is shown in Fig. 1.13, the first photograph of a supersonic jet ever taken. This experiment also marks the prototype of the *supersonic wind tunnel*, later crucial to advancing high-speed flight.

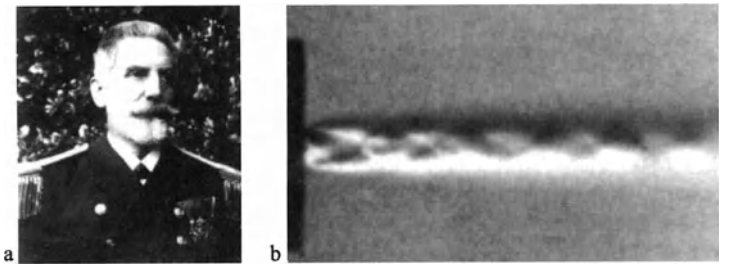

Fig. 1.13. **a** Peter Salcher (1848-1928), courtesy Dr. G. Salcher, Hermagor, Austria. **b** the first schlieren photograph of a supersonic jet [60]. Photos taken a century later can improve upon it only by virtue of better photographic media.

Irregular shock wave crossings in the jet were dubbed "Lyra" by Salcher, but later came to be called "Mach disks." In fact, the experiments were done entirely by Salcher, who coordinated with Mach only by mail. Though Mach provided scientific guidance, recent correspondence discovered by Krehl [61] shows that Salcher's contribution has been underrated. If there is anything left to name in gas dynamics, we should name it for Peter Salcher.

The beginnings of unsteady gas dynamics and supersonic aerodynamics by Mach and Salcher thus depended critically on the schlieren technique. Shock waves, ballistics, supersonic jets, and high-speed wind tunnels were soon to follow. Schlieren first achieved its potential here, in revealing the physical phenomena that led to jet and rocket propulsion, high-speed air transportation, and of course a host of deadly military weapons.

One of Mach's assistants in Prague was Vincenz Dvorák (1848-1922), who later became professor of Physics at the University of Zagreb [12,53]. While he worked with Mach, Dvorák published the first *traditionally-recognized* account [23] of the simple visualization method we now know as the shadowgraph technique (Hooke's and Marat's precedents having been forgotten). Dvorák once again used sunlight focused on a 1-mm aperture to project a diverging light beam across his darkened lab onto a white wall. Refractive phenomena in the middle of the beam appeared as shadows on the wall. The similarity to Marat's forgotten "helioscope" shadowgraph apparatus [28] is remarkable.

Dvorák described many observations, including mixing phenomena in water and the atmosphere, the warm convection from a hand, and electric sparks. In fact, he repeated most of Toepler's original visualizations in order to show that similar results could be had by the simpler means of shadowgraphy.

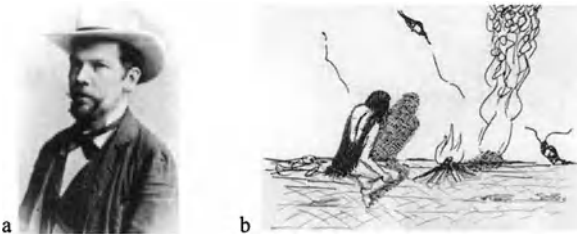

Fig. 1.14. **a** Vincenz Dvorák (1848-1922). **b** prehistoric shadowgraphy (sketch by author).

Yet, with due respect to Dvorák, he lacked Toepler's broad feeling for his subject. He attempted no more than a cursory optical analysis of his technique and showed no shadow photographs, though he had the resources to take them. He also made his discovery an adversary of the schlieren technique, claiming the latter was too complex and expensive and had a too-small field of view. That is not the way it worked out: nowadays schlieren and shadowgraphy are complementary tools. Others [2,62] later clarified that shadowgraphy produces no focused image like schlieren, but merely a shadow, hence it is purely a qualitative tool.

Neither did Dvorák coin the term "shadowgraph," but rather called it only "a new, simple form of schlieren observation." It is not actually a schlieren technique, however, since that requires a knife-edge cutoff and the formation of a real image. Boys [62] published the first shadowgraph *photos* in 1893, a few years after Dvorák and a century after the assassination of Marat. Schardin [1,2,63] named Dvorák's approach the "simple" or "direct" shadow method, which it is still called. The term "shadowgraph" seems to have been first used in this context by Townend [64] in the early 1930's, and was then in common use within a decade [65]. Weinberg [66] rounded out the terminology by naming the record produced by the shadowgraph technique: a "shadowgram."

Despite this official history, shadowgraphy is so simplistic that it must have been observed since ancient times (Fig. 1.14b). Wherever sunlight casts a shadow through disturbed air or water, as Hooke [14] noted, a shadowgram is formed. Rienitz [11] also points out that Augsburg optician Johann Wiesel (1583-1662) used the shadowgraph principle in an instrument for self-examining one's eye, pre-dating even Hooke's shadowgraph observations.

Following Dvorák's publication on shadowgraphy [23], as the 19th Century drew to a close, a London amateur microscopist named Julius Rheinberg (1871-1943) devised a schlieren approach to optically "stain" objects in a microscope [67]. Chemical staining was already used to distinguish transparent objects from their surroundings, but it was messy and it could misrepresent or kill biological subjects under study. Rheinberg saw the value of color contrast to enhance microscopy, and placed color filters in the substage diaphragm of his microscope to color-code the light diffracted by the structure of his subjects. This is the color analog of Toepler's [45] black-and-white microscopical schlieren method, though nothing indicates that Rheinberg knew of Toepler's prior work.

Fig. 1.15. Julius H. Rheinberg (1871-1943). (Photo courtesy of Peter Rheinberg, Graticules Ltd.)

Rheinberg illumination is still used today, a century later, to produce brilliantly-colored microscopic images that are obviously also schlieren images to the trained eye (see Color Plate 1). It reached its zenith in 1933 when Zeiss produced the "Mikropolychromar" microscope illuminator based on Rheinberg's principle [68]. More recently, Rheinberg illumination was eclipsed by differential interference color contrast, but it is still used by a few microscopists with outstanding results.

However, Rheinberg's discovery was broader than this fate implies. It was apparently one of the first uses of color filters in any sort of optical imaging system. It thus set the stage for color schlieren methods (Sect. 5.2) as well as for modern methods of pseudocolor-encoding grayscale images [69], white-light optical processing, and a variety of applications eventually including color television projectors [70]. In principle, Rheinberg's approach encodes information in a white-light image projector by way of the azimuth angle θ, measured in a plane perpendicular to the optical axis. This was named "θ-modulation" decades later [71], and became the basis for the modern field of white-light optical processing [72].

Like his work, Julius Rheinberg was himself equally interesting [73]. At age 24 his microscopy brought him together with Ernst Abbe of the Zeiss optical works in Germany, the father of the modern microscope. At the outbreak of World War I, Rheinberg and his brother Ernest were called upon by the British government to manufacture optical sights and eyepieces formerly obtained only from Germany. Julius coined the term *graticules* for these items, which now appears in the Oxford Dictionary. The firm of Graticules Ltd., now directed by Julius's grandson Peter Rheinberg, thrives to this day in Tonbridge, outside London.

1.4 The 20th Century

Early in the 20th Century, schlieren imaging caught on in the leading experimental physics labs around the world due to the publications by Toepler, Mach, and colleagues. In the US, physicist Robert W. Wood (1868-1955) [74] used it to explore shock wave motion in the air, while in Germany it became a key tool in the lab of the world's leading fluid dynamicist, Ludwig Prandtl (1874-1953).

Prandtl [75] and some of his students at Göttingen University took an interest in supersonic gas flows about the same time that, elsewhere in the world, powered human flight was just beginning. This interest was tweaked by an unlikely application, though: sawmill dust collectors. Theodor Meyer, Prandtl's student, derived the theory of oblique waves in supersonic flows in his 1908 Ph.D. thesis [76] while Ernst Magin [77] made schlieren observations of them. These images are so well-suited to illustrate the phenomena that they are still used today (Fig. 1.16).

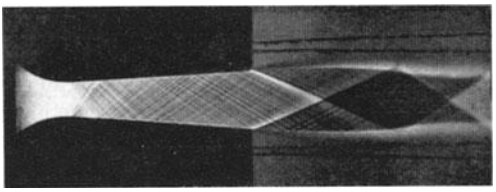

Fig. 1.16. Supersonic nozzle flow pattern photographed in Prandtl's lab [75,77].

Also at the beginning of the 20th Century, the field of ballistics was coming into its own. The world's expert ballistician was also a German: Dr.-Ing. Carl Cranz (1858-1945). As Professor of Ballistics in Berlin, he authored a famous textbook on the topic [78] and trained two generations of students [79]. Given the importance of schlieren to his work, Cranz visited Ernst Mach in Vienna in 1907 to learn more [80]. Subsequently Cranz and his students applied the schlieren technique and high-speed cinematography to bullets in flight, first at 5,000, then 100,000, and finally more than a million frames/second [81].

In this manner the schlieren legacy of Toepler and Mach was handed over by Cranz to his star student, Hubert Schardin (1902-1965). Schardin became Cranz's assistant in 1927 at the Berlin Technical University in Charlottenburg. Cranz was already 69 but still vital. He and Schardin made a crucial contribution to high-speed photography: the multi-spark camera now known as the *Cranz-Schardin camera* [6]. Using shadowgraph or schlieren optics, having no moving parts, and forming up to 24 separate images on a single photograph, this camera enabled the high-speed imaging of physical phenomena at more than a million frames/second – far faster than any other high-speed camera available at the time. With this camera many important studies of explosive events, shock-tube flows, and ballistic impacts were later carried out by Schardin and his colleagues. It became the premier instrument of German ballistics, and is still used 70 years after its invention.

But much more of this history revolves around Hubert Schardin. His 1934 Ph.D. thesis is entitled "The Toepler Schlieren Technique – Principles for its Application and Quantitative Evaluation" [1]. This work provided, for the first time, a solid theoretical background for schlieren imaging. In his early thirties, Schardin was already well on his way to becoming the 20th Century patriarch of high-speed physics and the optics of inhomogeneous media [79].

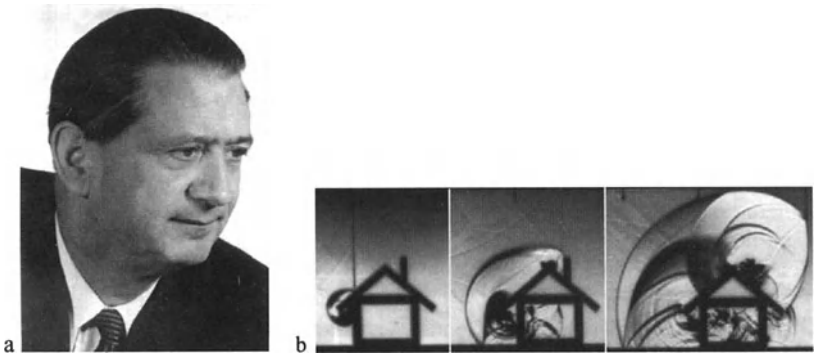

Fig. 1.17. **a** Hubert Schardin (1902-1965), **b** three frames from a Cranz-Schardin-camera schlieren sequence of a blast wave striking a model building (courtesy Ernst-Mach-Institut).

According to Kutterer [80], Schardin learned from Cranz and other professors at Berlin the art of extracting the solution of a difficult technical problem by the simplest-possible means available. This is the clear influence of Toepler's and Mach's school of experimental physics, described earlier. Today, alas, in an age of massive computer power applied to almost everything, this is a lost art.

From Cranz's retirement in 1935 until the end of World War II, Schardin directed the Ballistics and Technical Physics Institutes of the Luftwaffe Technical Academy in Berlin-Gatow. During this period came his second major publication: "Schlieren Methods and Their Applications" [2]. Here we see his mature inventive genius at work in an extensive 136-page monograph, including the almost-casual introduction of several entirely-new schlieren arrangements. (One of these, the lens-and-grid focusing schlieren method to be described in Chap. 4, is only reaching true fruition today.)

Profusely illustrated and including all necessary mathematical rigor, this second key paper of Schardin on schlieren methods [2] is a delight to read. Schardin not only did splendid schlieren and shadowgraphy, but he also had the literary skill to convey his work in comparable style. It includes a section on shadowgraphy, and half of it is devoted to applications spanning a broad range of scientific pursuits. Many of its fine original photographs are reproduced here. Published in German during World War II, it is hard to find today. Nonetheless it has the reputation of the classical reference work [82], and all serious students should read it.

In 1945 Schardin and his research group were caught up in the rift of Germany, and were sought by both the US and France for their ballistics expertise. France made the better offer, and they ended up at Saint-Louis in the French Alsatian region. There, in 1958, Schardin became the first German director of ISL, the German-French Research Institute Saint-Louis, which remains today a world-renowned center for ballistics, shock tubes, and optical flow diagnostics [83]. He also established the Ernst-Mach-Institut in Freiburg, Germany, a sister institute of similar reputation only about 50km from ISL.

Schardin was fascinated by shock tubes, high-speed physics, and color schlieren photography [2] (see Color Plates 2, 9, and 16). He had optical setups in his cellar and attic where his students learned to improvise optical mounts from broomsticks and such [79]. Today a commercial optical mount can cost hundreds of dollars. So, for all of us who ever improvised a knife-edge by a razor-blade taped to a brick, there is comfort in following the footsteps of the master.

Hubert Schardin died of a stroke at age 63, having advanced the knowledge of schlieren methods further than anyone since Toepler. He is remembered for his scientific contributions to ballistics and the physics of all manner of high-speed phenomena, as well as his leadership in defense technology and the establishment of great scientific centers. One of his former students, Reichenbach [79], claims: "Schardin was a researcher and scientist with heart and soul." R. J. North [84] wrote: "Schardin's papers were works of scholarship as well as science. In retrospect they seem as relevant today as when they were written."

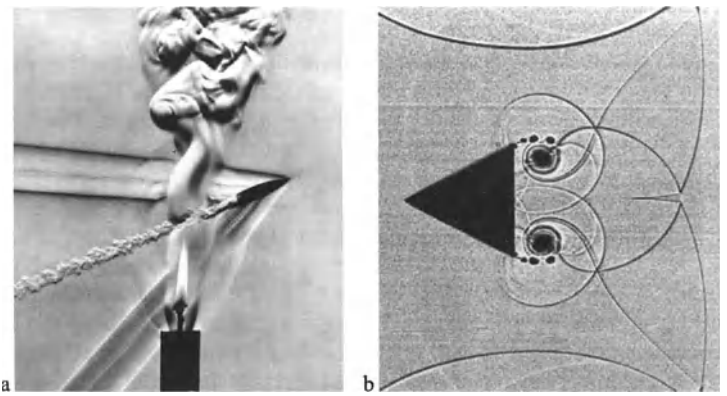

Fig. 1.18. Two famous images by Hubert Schardin. **a** Schlieren photo of a bullet and a candle flame. **b** Shadowgram of shock wave diffraction around a triangular block.

During Schardin's lifetime, historical developments were underway that would soon bring schlieren and shadowgraph techniques into far-wider use. There was only a handful of yearly publications on these techniques from Toepler's time up to about 1930: then things began to change. The publication rate increased until the end of World War II, then ballooned to hundreds of papers per year from the 1960's to the present. All told, the publications involving these techniques now number many thousand.

What caused such growth? As we have seen, the optics of inhomogeneous media began in the UK but then moved to Germany. The first application to benefit from this was ballistics, of value primarily to the military. Air power through the end of World War I was too slow to need much optical flow visualization, but this was set to change. As Germany prepared to rearm, rocket propulsion research

began in earnest at the Army Experimental Laboratory in Peenemünde. By 1939 a large supersonic wind tunnel was designed by a team led by Rudolf Hermann (1905-1991) and put into operation there [85,86]. Its key instrument was a schlieren system built by the Zeiss optical works. Maximilian Toepler (1870-1960), son of August and then a Professor at Dresden Technical University, advised Peenemünde's wind tunnel instrumentation engineer Heinrich Ramm on schlieren flow visualization [12]. One of the resulting photos of a V-2 missile model under test is shown in Fig. 1.19a. Prandtl also came to Peenemünde, watched the schlieren screen, and ran the wind tunnel repeatedly [85]. A major application for schlieren and shadowgraphy thus arose in wind tunnel testing, and the era of high-speed flight and supersonic warfare began.

The story of German wartime rocketry, the Nazi rain of destruction upon England, V-2 rockets built by slave labor in the Mittelwerk, and the simultaneous dawn of the space age is now familiar [85,86]. Wernher von Braun (1912-1977) and the Peenemünde scientists fled to the West after the war, and eventually played a key role in the US space program. Upon Germany's defeat in 1945, the Peenemünde wind tunnels and schlieren equipment (having been moved to Kochel in Bavaria to avoid bombing) were captured by the Allies. Through the controversial Project Paperclip, the supersonic wind tunnel and its German engineering staff were shipped to the States and installed at the Naval Ordnance Lab outside Washington, DC [85]. There, 22 years later, I had the opportunity – as a student intern – to use this historic test facility (Fig. 1.19b).

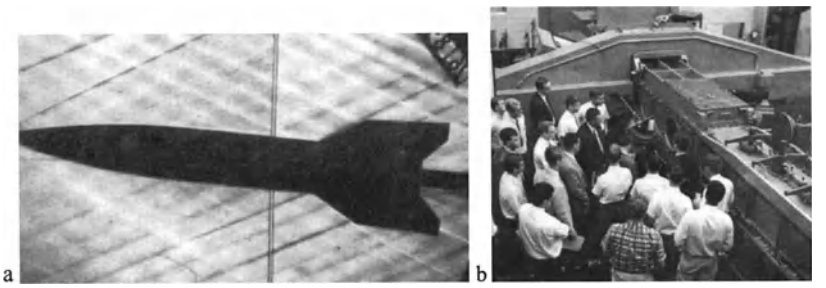

Fig. 1.19. **a** Schlieren photo of a model of the German V-2 missile under test in the supersonic wind tunnel at Peenemünde. **b** The wind tunnel itself, with its schlieren system contained in the bridge-shaped enclosure in the background (US Navy photo).

While rocketry was developing in Germany in the early 1930's, American researchers had no such large supersonic wind tunnels. At the Langley Aeronautical Lab of the National Advisory Committee for Aeronautics, they struggled with the knotty problems of transonic airflow. Complex and dangerous flow disturbances appeared when an aircraft approached the speed of sound [87]. Without flow visualization, wind tunnel tests were blind. Eastman N. Jacobs, wind tunnel chief and amateur astronomer, knew about schlieren optics by way of the Foucault knife-edge test. He had a schlieren system installed in 1933. With it, shock waves

were seen on wing sections even when the initial airflow was subsonic. Schlieren revealed that these shock waves caused boundary layer separation on the wing, akin to stalling the airplane. Efforts began immediately to minimize this problem, if possible, by shrewd wing design [88]. Once again, the schlieren technique provided a crucial glimpse into the Shop of Nature.

Following World War II the emphasis of western high-speed flight research shifted from Germany to the US and the UK. A team of aerodynamicists at Britain's National Physical Laboratory (NPL) continued the struggle over the knotty problems of wing and aircraft design for transonic and supersonic flight. An inspired team of 20 young researchers worked there, with modest resources, under the guidance of Douglas W. Holder (1923-1977). 50 years later, surviving team members still speak fondly of the team spirit and excitement of the time [89-91].

Holder [92] believed in getting at the underlying physics of these airflow problems. Clever use of experimental methods was a key theme of his group's wind tunnel research. Schlieren and shadowgraphy were again crucial in seeing and understanding the complex flows that developed on aircraft wings as the mystical "sound barrier" was approached.

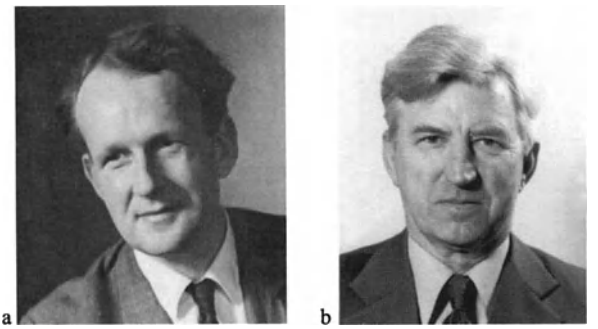

Fig. 1.20. **a** Douglas Holder (photo courtesy Ramsey and Muspratt Collection, Central Library, Cambridge), **b** R. J. North (photo courtesy Mrs. Nella North).

Beyond just using these optics, however, R. J. "Jack" North (1921-1998) of the NPL Aerodynamics Division contributed new substance to the techniques. He introduced the graded filter [93] and a simple multicolored filter [94] as alternatives to the standard knife-edge cutoff. The former (Sect. 5.1.1) allows a broad schlieren measuring range and improved clarity, while the latter (Sect. 5.2) brings color schlieren imagery within the reach of everyone. Holder and North also collaborated with the Shell Film Unit to produce a film entitled "Schlieren," [95] that brought the topic to public attention for the first time.

Using North's graded-filter schlieren method and other measurements, Herbert Pearcey studied the flow over transonic wings in an NPL wind tunnel. His work [96] is now a classic in the annals of aeronautics. He proposed wing-section designs that ameliorated the deadly transonic problem known as "shock-stall" [97].

His "peaky" wing thus allowed subsonic aircraft to fly closer to Mach 1 than ever before. This theme was also taken up by R. T. Whitcomb in the US, leading to what are now called *supercritical* wing sections for efficient transonic flight. Modern commercial jet transports and military fighters depend on this technology. Looking back on this period, Pearcey [90] told me that the success of his research stemmed in large measure from the insight he gained using the schlieren methods of Holder and North.

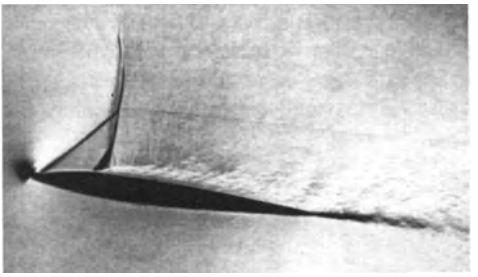

Fig. 1.21. Graded-filter schlieren photo of a 2-D wing section undergoing buffet due to shock-wave induced boundary layer separation, reproduced courtesy of H. H. Pearcey.

In 1963 Holder and North published a small monograph entitled "Schlieren Methods" [98] as part of an NPL series transferring technology to industry. Expanding upon their earlier work [99], it is beautifully illustrated and comprehensive for its size. It surveys the state-of-the-art of schlieren and shadowgraphy in a scholarly manner, and it uniquely covers the practical side of equipment setup, high-speed light sources, and photography of the schlieren image. Along with Schardin's two papers [1,2], Holder and North [98] is a third classic work that every serious student of the schlieren arts should read.

Douglas Holder left NPL in 1961 to become Professor of Engineering Science at Oxford, was elected Fellow of the Royal Society in 1962, and died too young in 1977. Herbert Pearcey and Eric Rogers are retired from illustrious careers in aerodynamics, and have both contributed to this historical account [89,90]. Jack North contributed too, until his death in 1998. Subsequently Mrs. Nella North has graciously provided additional material (e.g. Color Plate 3).

Another schlieren pioneer, Felix J. Weinberg (1928-) was a Czech teenager at the onset of the Holocaust. He survived the concentration camps at Auschwitz and Buchenwald to later become a world leader in combustion research. His 1963 classic book *Optics of Flames* [66] contains authoritative reviews of both schlieren and shadowgraph theory. He is responsible for naming the shadowgram, and is co-author of the definitive paper on lasers as schlieren light sources [100]. Weinberg's insights have enriched every chapter of the present book.

While these postwar developments were going on in the West, schlieren and shadow methods followed a similar path behind the Iron Curtain – with some interesting twists. The famous Russian telescope maker D. D. Maksutov (1896-1964) published a book in 1934 entitled "Schlieren methods in the study of optical systems" [101]. However, unlike Schardin in his Ph.D. thesis [1] of the same

year, Maksutov confined himself to optical shop testing of telescope reflectors and refractors. He also introduced the wire or filament cutoff and the exponentially-curved cutoff in the schlieren focal plane (See Sects. 5.1.2 and 10.2.3). The telescope design for which Maksutov is famous came a decade later.

Still later, a Russian book entitled "Shadow Methods[4]" was published in 1968 by L. A. Vasiliev [102]. This 350-page book is the largest tome ever written on the schlieren technique until now. It can be found in English translation in about a dozen US research libraries. While contemporary with Holder and North [98], it is rather different in emphasis (referencing only 137 sources, many in Russian, compared to twice that number in Holder and North). Vasiliev does not spare mathematical rigor, and emphasizes both quantitative schlieren applications and commercial schlieren instruments of Soviet design. Maksutov's hand is seen in the design of the ubiquitous and famous IAB-451 schlieren instrument, which Vasiliev uses as an example (see Sect. 7.4.1).

Fig. 1.22. L. A. Vasiliev (1931-1982). Photo courtesy of Prof. I. V. Ershov.

Though some of the methods Vasiliev explores in depth (e.g. Maksutov's focal filament and curved cutoff) have never found much use in the West, a great deal of useful material is nonetheless found in Vasiliev's book [102]. His talent for clear explanations shines through an excellent translation by A. Baruch. For one already schooled in the schlieren arts, the differing approaches and views from behind the former Iron Curtain are fascinating. I have therefore referred to Vasiliev often in the chapters that follow.

[4]Here a curious confusion between Russian and English terminology needs explanation. Теневые Методы, or *Tenevye Metody* (literally "shadow methods") is a generic term that includes both schlieren (*Shliren* or *Teplerovski metod*) and true shadowgraphy (*Priamotenevoy metod*). The *schliere* or density nonuniformity itself is *neodnorodnost plotnosti* in Russian. Many Russian authors simply use the term *Tenevye Metody* when referring to schlieren methods, but this is usually translated as "shadow methods," falsely implying shadowgraphy. Dr. A. A. Zheltovodov is thanked for clearing up this confusion.

As for the man himself, Lev Alexandrovich Vasiliev (1931-1982) began his career applying schlieren and interferometer instruments to the gas-dynamic problems of the Soviet space program. He designed several schlieren instruments and his book on this topic [102] became the handbook for a generation of optical scientists in the Soviet Union [103]. He was a Professor in the Moscow Physico-Technical Institute and the author of 4 books, 200 papers, and 30 patents. He died tragically in a mountaineering accident at age 50.

Thus far we've seen several examples of schlieren images and shadowgrams that had a significant impact upon science and technology. A more-recent one demonstrates that this trend is continuing: in 1974, Brown and Roshko [7] published a simple, elegant experiment in which shadowgraphy revealed large coherent structures in the mixing of two planar gas streams. These shadowgrams, one of which is reproduced in Fig. 1.23, spawned a new approach to the understanding of turbulent flows by way of their underlying large-scale structures.

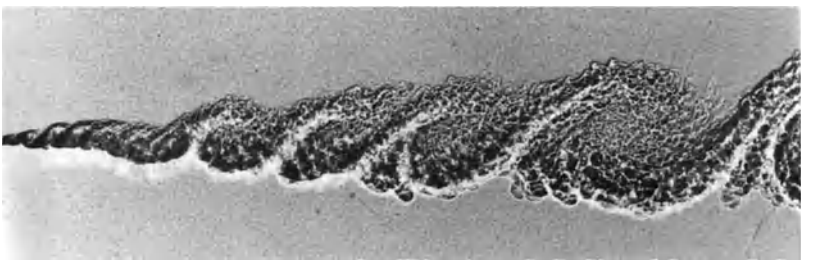

Fig. 1.23. Spark-illuminated "contact" shadowgram of He/N_2 mixing layer (photo courtesy of Prof. Anatol Roshko).

The most-recent history of schlieren imaging concerns novel arrangements for focusing and large fields of view. Ralph Ashby Burton (1925-) wrote his MS thesis on this topic at the University of Texas, Austin, in 1951 [104]. Usually such theses are rather naïve learning experiences, but Burton wrote with authority for a mere 25-year-old. He and several contemporaries independently developed the idea of extended-source schlieren optics that was originally suggested by Schardin [2]. But Schardin overlooked the potential of this approach to yield a large field-of-view, while others [105,106] were chiefly concerned with its sharp-focusing properties. Burton, however, saw large-field-of-view as a fundamental advantage. His work can be found in several publications dealing with schlieren and shadowgraphy in general, and "focusing schlieren" in particular [42,107-109].

Most recently, this theme has been developed further by NASA scientist Leonard M. Weinstein (1940-). Weinstein was an amateur astronomer and photographer as a youth, was trained in physics and engineering, and has been at NASA's Langley Research Center for more than 30 years. There he was involved in high-speed aerodynamics, wind tunnel testing, and instrumentation. Being of an inventive nature, he developed new concepts ranging broadly from instrumentation and

imaging enhancements to solar desalinization of seawater, environmental cleanup techniques, and practical means of space travel.

Around 1990, Weinstein turned his attention to the neglected theme of lens-and-grid schlieren techniques (see Chap. 4). These techniques were never fully developed by Schardin, Burton, or the others who studied them in the mid-20th Century. Weinstein completed the general optical design of these systems and showed them to be more than mere curiosities [110]. For example, on his account several large wind tunnel facilities now use such systems for flow visualization at far less cost than conventional schlieren optics. Applications also abound for the sharp-focusing feature of this approach. More than 70 new schlieren systems have been based on Weinstein's work to date. An August, 1993 discussion between Weinstein and myself led to the world's largest indoor schlieren system, with a field of view of 2.2x2.7 m (see Ref. [111] and Sect. 4.3.5).

Weinstein then had another revolutionary idea: Hooke [17], Huygens [26], and Schardin [2] all observed schlieren against a distant light-dark boundary, but none found much practical use for it. Weinstein realized the potential of this approach with a specially-fitted telescope aimed at the queen of all distant light sources, the Sun [112]. A schlieren cutoff inside the telescope was matched to the edge of the Sun's image and a streak camera recorded a schlieren photograph by scanning the line of schlieren sensitivity across the film. Weinstein demonstrated the practicality of this in 1993, when he photographed a T-38 jet aircraft flying across the face of the Sun at Mach 1.1 and almost 10 km distance from his telescope. The image, shown in Fig. 1.24b, was the largest-scale schlieren image ever captured on film. It was, to say the least, the flow visualization achievement of the decade.

Weinstein's "Schlieren for Aircraft in Flight" is an important new tool for the flight-testing of high-speed airplanes. It was used already for sonic boom research and, more recently, he has adapted a similar approach to rocket-sled testing as well [113] (see Sect. 4.4.1). At the beginning of the 21st Century, Leonard Weinstein's contributions demonstrate that the optics of inhomogeneous media still thrives.

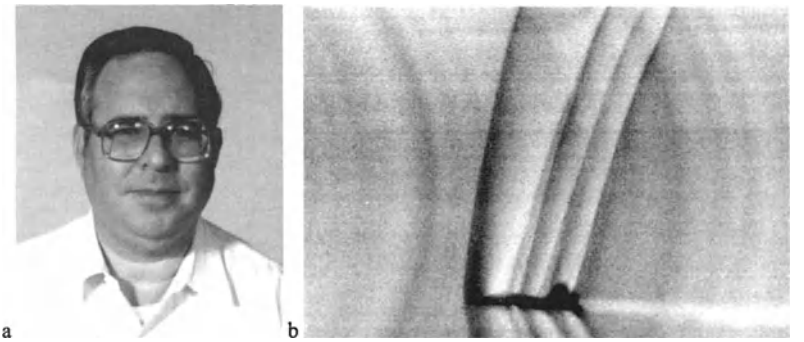

Fig. 1.24. **a** Leonard M. Weinstein. **b** Weinstein's schlieren photograph of a T-38 aircraft in flight at Mach 1.1. The vertical scale of this image is about 28 m.

2 Basic Concepts

> The basic principle of the schlieren technique is the combination of the optical projection of an object with an indication of its light deflection.
>
> *Hubert Schardin* [2]

In this chapter let us examine how the schlieren and shadowgraph techniques work in principle. The details of how they work in practice will come later.

Our eyes – and ordinary cameras – have no way to discern the phase differences in a light beam. We can only see amplitude, color contrast, and (with appropriate sunglasses) polarization. If we could see phase as well, new vistas would open to our view. That is what schlieren and shadowgraph methods do: they translate phase differences into amplitude and sometimes color differences that we can see.

In this book, that feat is accomplished mostly with special optical apparatus only available in recent recorded history. The basic problem, however, is older than life itself. In the ocean, for example, some jellyfish and other organisms are essentially transparent [114]. Neither their predators nor their prey can see them directly. But small differences in refractive index between them and the surrounding seawater cause these creatures to cast visible shadows, whence they can be detected. We now proceed to see how such methods of observation work.

2.1 Light Propagation Through Inhomogeneous Media

Light propagates uniformly through homogeneous media. Starlight, for example, is undisturbed in its long journey through empty space. If Earth's atmosphere were similarly uniform, starlight would reach us as exactly-parallel light rays (per geometric optics), or a perfectly-planar wavefront (per physical optics). The starlight could then be focused to as nearly-perfect a point as diffraction allows: no twinkle.

But the atmosphere is not uniform; it is full of disturbances and inhomogeneities due to turbulence, thermal convection, weather phenomena, and whatnot. These disturbances change the atmospheric density on a relatively-small scale, and with it the refractive index. Rays of starlight become bent. Since the wavefront of

light is always perpendicular to its rays, it becomes wrinkled by phase distortions. Now the image of a star is no longer a point, and it fluctuates on the time scale of the atmospheric disturbances: it twinkles.

This confounds Earth-bound astronomers, driving them even so far as to place a telescope in orbit outside the atmosphere. Yet this annoyance of astronomers is our main interest. While they study the stars, we study the disturbances that alter light propagation through the air, the ocean, or any other transparent medium.

Light slows upon interacting with matter. The refractive index $n = c_o/c$ of a transparent medium indicates this change, where c is the light speed in the medium and c_o is the celebrated universal speed limit, $3x10^8$ m/s, of light in a vacuum.

For air and other gases there is a simple linear relationship between the refractive index and the gas density ρ:

$$n - 1 = k\rho \tag{2.1}$$

The Gladstone-Dale coefficient, k, is about 0.23 cm^3/g for air at standard conditions, given visible illumination. For other gases it may vary roughly from 0.1 to 1.5. In substance, however, the refractive index of common gases varies only in the third or fourth decimal place. Air, for example, at 0°C and 1 bar pressure has n = 1.000292 when trans-illuminated by light from the Sodium-D spectral line. Helium, with n = 1.000035, is distinctly refractive upon mixing with air, despite what appears to be only a minor difference in n. Alcohol vapor, at around n = 1.0008, differs enough from air that its evaporation from an alcoholic drink is clearly visible to schlieren and shadowgraph equipment. Carbon tetrachloride vapor has one of the highest indices of refraction, 1.001768; once a common cleaning fluid, it is now banned due to toxicity.

Also from Eqn. 2.1, n is only weakly dependent upon ρ. A change in air density of two orders of magnitude causes only a 3% change of n. If we are to detect small gas density variations optically, we will need very sensitive optics.

The *refractivity* (n – 1) of a gas, from Eqn. 2.1, depends upon gas composition, temperature and density, and the wavelength of illumination. In many cases the temperature, density, and pressure of gases not too far from atmospheric conditions are further related by the simple perfect-gas state equation,

$$p/\rho = RT \tag{2.2}$$

where R is the specific gas constant. Flowing gases with variable density are called *compressible flows*; they can arise due to temperature differences or high gas speeds. All these possibilities lead to gas disturbances that refract light, and that may be visualized by virtue of this refraction.

n vs. ρ relationships also exist for liquids and solids, but are more complex than Eqn. 2.1 [82]. Moreover, the refractivity is stronger too. For example, although (n – 1) in standard air is only 0.000292, in water it is about 3 orders of magnitude larger; and in transparent plastics and glass, larger still. This means much less optical sensitivity is needed to see refractions in liquids or solids than in air.

The physics of refractivity has some special features that are occasionally useful [82]. For example, k increases slightly with increasing light wavelength λ. Thus refractivity is higher for longer λ, so the weakest disturbances become more detectable in infrared than in visible light. Likewise, refractivity increases notably when a gas is ionized, so a plasma refracts light even when the plasma density is quite low. Finally, some unusual gases (e.g. sodium vapor in air) may absorb significant light, leading to resonant refractivities far higher than the usual.

For all these cases – in the simple view of geometric optics – our interest is in the bending or refraction of light rays. We take the z-axis of a right-handed Cartesian x,y,z coordinate system as the "normal" direction: the optical propagation direction of undisturbed rays approaching a zone of optical inhomogeneity. x,y-pairs now describe planes perpendicular to the normal z-direction. These coordinate directions are shown in Fig. 1.1 for reference.

It can be demonstrated [1,2,115,116] that optical inhomogeneities refract or bend light rays in proportion to their gradients of refractive index in an x,y-plane. (See App. A.6 for the derivation.) The resulting ray curvature is given by:

$$\frac{\partial^2 x}{\partial z^2} = \frac{1}{n}\frac{\partial n}{\partial x}, \qquad \frac{\partial^2 y}{\partial z^2} = \frac{1}{n}\frac{\partial n}{\partial y} \tag{2.3}$$

Integrating once, the components of the angular ray deflection in the x- and y-directions are:

$$\varepsilon_x = \frac{1}{n}\int \frac{\partial n}{\partial x}\partial z, \qquad \varepsilon_y = \frac{1}{n}\int \frac{\partial n}{\partial y}\partial z \tag{2.4}$$

For two-dimensional schlieren of extent L along the optical axis, this becomes:

$$\varepsilon_x = \frac{L}{n_0}\frac{\partial n}{\partial x}, \qquad \varepsilon_y = \frac{L}{n_0}\frac{\partial n}{\partial y} \tag{2.5}$$

where n_0 is the refractive index of the surrounding medium.

These expressions provide the mathematical basis for schlieren and shadowgraph techniques in the following chapters. For now, note that full knowledge of an inhomogeneous region does not necessarily follow from a knowledge of the various ray deflections after having passed through. Clearly, however, the gradients $\partial n/\partial x$ and $\partial n/\partial y$ cause the refraction, not the overall level of n. A region without such gradients is homogeneous and relatively uninteresting. Moreover, Eqns. 2.3 and 2.4 show that light rays are always bent toward the region of higher n. From Eqn. 2.1 for gases, this also means toward the region of higher density ρ.

Finally, this discussion does not essentially depend on whether or not the light beam is coherent. Few of the interesting phenomena are dispersive enough to cause much chromatic separation of white light, and interference phenomena *per se* are excluded from primary consideration here. The advantages and drawbacks of coherent illumination are taken up in detail in Chap. 7 and App. B.

2.2 Definition of a Schliere

> Schlieren, like clouds, are meaningful only in relation to their environment.
>
> *H. Jebsen-Marwedel* [117]

We already have, from Chap. 1, a succinct name for these gradient disturbances of inhomogeneous transparent media: *schlieren* [3,117]. They are relatively-small refractive differences within the overall background [1,2], and by definition they bend light rays in any direction other than the "normal" direction z. [1]

Schlieren may have refractive-index gradients in one, two, or three dimensions: if one or two, then these should be oriented to match the x- and y-axes for best visibility. Three-dimensional schlieren, though certainly observable, cannot be fully characterized by the two-dimensional optical methods primarily covered in this book. Holographic, tomographic and stereoscopic ways around this difficulty are discussed, however, in Sects. 4.6 and 5.3.

Schlieren occur in solids, liquids, and gases. They may result from temperature changes, high-speed flows, or the mixing of dissimilar materials. In glass and plastic, they may be due to inclusions of variable density or to thickness differences in otherwise-homogeneous material. Some schlieren are of complicated structure, others are simple. Some refract light very strongly, others barely at all. Some schlieren are sharply-defined while others are more gradual, but never so gradual as to be indistinguishable from their uniform background.

As a typical example, consider the laminar candle plume shown earlier in Fig. 1.2a as a *schliere* or "schlieren object." It is cylindrical and is oriented vertically, meaning that its gradients that deflect light rays are restricted to the x-direction, and are described by $\partial n/\partial x$. The candle plume has a diameter about the same as that of its candle, in this case 2 cm. Being hotter and less dense than the surrounding air, it acts like a very-weak negative cylindrical lens. [2] Its maximum ray deflection angle ε_x is around 200 arcseconds or 0.06 degree. This may not seem like much, but as schlieren objects go it is far from the weakest. Hooke was able to see it distinctly with his original rudimentary schlieren system, described in the previous chapter. You can see it yourself with the unaided eye, by sighting over the top of a candle flame at a distant, detailed background (see also Sects. 4.3.1 and 9.4.10).

---

[1] For non-parallel-light illumination, *z* is measured along radii from a point light source at a finite distance.

[2] A quantitative schlieren method [118] has been used to estimate the effective focal length of a candle plume: -20 to -25 m.

2.3 Distinction Between Schlieren and Shadowgraph Methods

Schlieren and shadowgraph methods are closely related, but there are several distinctions [1,102]. First, the shadowgram is not a focused optical image; it is a mere shadow. The schlieren image, however, is what it purports to be: an optical image formed by a lens, and thus bearing a conjugate optical relationship to the schlieren object. Second, schlieren methods require a knife-edge or some other cutoff of the refracted light, where no such cutoff is needed or allowed in shadowgraphy. Finally, the illuminance level in a schlieren image responds to the first spatial derivative of the refractive index in the schliere, e.g. $\partial n/\partial x$, as we will see in more detail later. The shadowgram, however, responds to the second spatial derivative or Laplacian, e.g. $\partial^2 n/\partial x^2$. Equivalently, the schlieren image displays the deflection angle ε while shadowgraphy displays the ray displacement resulting from the deflection (more on this in the next section).

Despite these distinctions, both schlieren and shadowgraphy are integrating optical systems that project line-of-sight information onto a viewing screen or camera focal plane. As such, they are most appropriate for 2-D phenomena but still qualitatively useful for any phenomenon. Even when the object under study is non-planar, we nonetheless assume an equivalent "object plane" in which the ray deflections appear to lie [119].

Another distinction between schlieren and shadowgraph techniques lies in the apparatus and the effort required. The great advantage of shadowgraphy is its extreme ease. So little is needed that natural shadowgrams appear all around us without the use of any high technology. Schlieren effects also appear naturally in more-limited circumstances (see Sect. 9.4.10), but they stand out best in the laboratory using lamps, mirrors, and lenses.

In favor of shadowgraphy, note that it readily allows large-scale visualizations and it shows the salient features of a subject without gross changes in illumination. Though it is less sensitive than schlieren in general, particular circumstances can make it more sensitive. For example, $\partial^2 n/\partial x^2$ can be much larger than $\partial n/\partial x$ in gas flows involving shock waves or turbulence, both of which occur around supersonic projectiles [104], for example. Shadowgraphy renders, by way of its double differentiation, fine-scale images of turbulent flows [120,121]. Shock waves, being natural step-functions, produce strong higher derivatives of refractive index that cause them to stand out as stark lines in a shadowgram.

For weaker disturbances overall, however, schlieren holds the advantage of much higher sensitivity. Its unambiguous 1:1 image correspondence with the object of study is often a decisive benefit. It emphasizes, even exaggerates detail in the schlieren object [122] where shadowgraphy usually downplays it. Thus many fields of application are open to the superior sensitivity and adaptability of the schlieren method that are closed to the simpler shadowgraph technique.

2.4 Direct Shadowgraphy

> To understand the shadowgraph, it is necessary to remember that light from a point source is in the form of rays that do not bend or cross unless disturbed.
>
> *R. A. Burton* [42]

Schardin [1,2,63] named the invention of Hooke [17], Marat [28], and Dvorák [123] the "simple" or "direct" shadow method. It is so simple, in fact, that it needs only a light source, the schlieren object S, and a reasonably-flat reflective screen onto which the shadow is cast, as shown below.

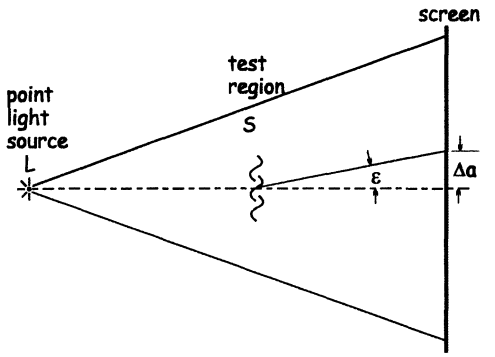

Fig. 2.1. Diagram of the direct shadowgraph method in its simplest form.

A bright "point" light source helps to cast a sharp shadow on the screen, but is not absolutely required. The Sun – with an apparent visual angle of about ½ ° – casts shadowgrams every sunny day (see Fig. 1.3 and Sect. 9.4.10).

Without schlieren object S in the field-of-view, the light source illuminates the viewing screen uniformly. But with S present, some rays are refracted, bent, deflected from their original paths. One such ray is shown in Fig. 2.1. Having suffered a refraction through angle ε, it reaches the screen displaced from its original position by distance Δa. Now it contributes extra illuminance to its new screen point, while its previous position suffers an illuminance deficit.

Generalizing to the entire schlieren object, we see that its optical inhomogeneities redistribute the screen illuminance. It causes previously-regular rays to bend and cross, casting a shadow. Not the same as the shadow of a solid object, [3] this shadowgram is rather the telltale of a wraith.

To consider this shadowgram formation more carefully, we make one concession to complexity by adding a lens in Fig. 2.2a to collimate the light beam from

[3] Long before video and computers, evening entertainment was provided by casting candlelight shadow-plays on a wall. Artful shadowcasters used their hands to portray characters: a duck, a dog, Sherlock Holmes. This was called *shadowgraphy* well before the present connotation arose. An example is seen in the famous Orson Welles movie *Citizen Kane*.

the point source. Moving the source off to the left, toward $z = -\infty$, has the same effect. Now the light rays are parallel before reaching the schlieren object, not diverging as before. The method is still called *direct shadowgraphy*.

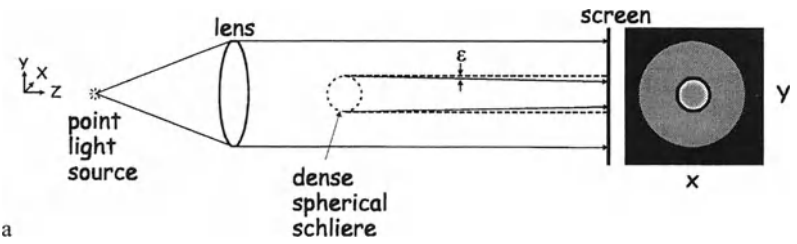

Fig. 2.2. **a** Diagram of parallel-light direct shadowgraph observation of a dense spherical schliere. **b** Shadowgraphy in a kitchen saucepan filled with water and illuminated from above. One large cooking-oil globule and several satellite globules float atop the water. The shadowgram, cast on the bottom of the pan, reveals focusing due to the higher refractive index of the oil.

Here, as before, the principal direction is along the positive z-axis and only the lateral gradients $\partial n/\partial x$ and $\partial n/\partial y$ refract light rays. Without a schlieren object in the beam, an evenly-illuminated spot is projected upon the screen. In place of a screen one may substitute a camera film plane, a sheet of white paper, or a wall.

Now insert in the beam of Fig. 2.2a a spherical schliere of higher refractive index than the surroundings. (In air, this could be a soap bubble containing a heavier gas such as carbon dioxide.) Light refraction is strongest at the boundary between the schliere and its surroundings, where the lateral gradients are strongest. No refraction occurs outside the schliere, or exactly at its center. But the planar wavefront of light approaching the schliere becomes warped upon interacting with it. Light travels more slowly inside it than outside, skewing the wavefront toward its center. Rays of light, propagating normal to the wavefront, are similarly bent toward the center from around the periphery of the schliere. The refraction angle at the periphery is indicated by ε. Thus the dense spherical schliere acts as a positive lens, converging its part of the shadowgraph beam toward an eventual focus much farther out along the optical axis.

Long before that focus occurs, the beam is intercepted by the viewing screen. What appears there is shown to the right in Fig. 2.2a. A dark circular shadow marks the periphery of the schliere. Immediately inside it, the illuminance rises above the background level to form a bright ring that fades back to the background at its center: this is the light displaced from the dark circular shadow. Under ideal

conditions, the outer diameter of the dark band corresponds to the actual diameter of the schliere. A practical example of such focusing is shown in Fig. 2.2b: kitchen-sink shadowgraphy.

Finally, note that this spherical-example schlieren object is only visible to the shadowgraph because it has *varying* lateral refractive index gradients $\partial n/\partial x$ and $\partial n/\partial y$. Indeed these gradients are only equal to zero outside the schliere and at its center, and are maximum at its periphery. Had we chosen instead a large glass wedge with planar non-parallel faces, its uniform gradient would shift the entire beam undisturbed: no shadowgram. Thus differential illuminance shifts only occur in shadowgraphy when there is a change – or gradient – of the refractive-index gradient. It was shown earlier that deflection angle ε is proportional to refractive-index gradients in the observation zone. Consequently it is the gradient of the deflection angle, $\partial\varepsilon/\partial x$ or $\partial\varepsilon/\partial y$, that we observe in a shadowgram in the form of ray displacement. Otherwise written, this is the second spatial derivative or Laplacian of the refractive index, $\partial^2 n/\partial x^2$ or $\partial^2 n/\partial y^2$.

2.5 Simple Lens-Type Schlieren System

To understand the basics of schlieren imaging, it helps to begin as simply as possible with two lenses, geometric optics and a point light source. Building upon that, an extended light source is considered afterwards. Finally, in later chapters and App. B, physical optics and practical apparatus are brought to bear in order to complete the picture.

2.5.1 Point Light Source

As shown in Fig. 2.3, the beam from a "point" source is collimated by a lens as in the previous discussion. Now, however, a second lens refocuses the beam to an image of the point source. From there, the beam proceeds to a viewing screen where a real inverted image of the test area is formed. At this point the optical system is merely a projector, imaging opaque objects in the test area as silhouettes on the screen. Transparent schlieren objects are not imaged at all until a knife-edge is added at the focus of the second lens. In practice, this knife-edge is usually just an ordinary razor blade.

As the knife-edge advances toward the focal point, nothing happens until it rather suddenly blocks the image of the light source, causing the screen to go dark. (This is not entirely realistic, but approximates what happens when a laser light source is used.) Thus one has the choice of a bright or a dark screen: brightfield or darkfield in the language of microscopy. Choosing the former, let the knife-edge be positioned just prior to blocking the image of the source point.

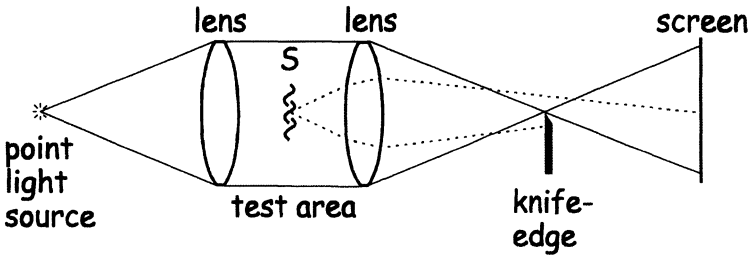

Fig. 2.3. Diagram of a simple schlieren system with a point light source.

If we now add schlieren object S to the test area, it bends light rays away from their original paths. Despite this, however, the second lens focuses the ray from each point in S to a corresponding point in the screen image. Two such rays are shown in Fig. 2.3, one bent upward, the other downward. Both refracted rays miss the focus of the optical system. The upward-deflected ray brightens a point on the screen, but the downward-deflected ray hits the knife-edge. Its corresponding image point is dark against a bright background. For this particular point of the schlieren object, the phase difference causing a vertical gradient $\partial n/\partial y$ in the test area is converted to an amplitude difference, and the invisible is made visible.

Generalizing from this example of individual rays, a finite schlieren object refracts many such rays in many directions. All downward components of these ray deflections are blocked by the knife-edge, painting at least a partial picture of the schlieren object on the screen in shadows on a bright background. The oversimplified example system of Fig. 2.3 will shortly be improved, but nevertheless this is – in basic physical terms – the essence of the schlieren effect.

A word about the orientation of the knife-edge: here shown horizontal, it detects only vertical components $\partial n/\partial y$ in the schlieren object. That is, a simple knife-edge affects only those ray refractions with components perpendicular to it. Refractions parallel to the edge, due to $\partial n/\partial x$, move rays along it but not across it, so there is no change in cutoff or in screen illuminance. A schliere with purely horizontal gradients in Fig. 2.3 remains invisible despite the presence of the knife-edge. Many have said that two schlieren images are needed to completely portray a schlieren object: one with a horizontal and one with a vertical knife-edge.

Those who said it were strictly correct, but they exaggerated the difficulty. An opaque mask with a circular hole can be used in place of the knife-edge to get around this issue if necessary, but that approach has other problems that will become clear later. In practice, a single knife-edge judiciously oriented is often good enough. To illustrate this, three actual schlieren images of the same phenomenon with different cutoffs are shown in Fig. 2.4 [124].

To conclude, the point-source schlieren system discussed in this section is good for illustration, but not very practical. Its operation is "on-or-off," with infinite sensitivity over zero measuring range [125]. In order to take real schlieren pictures like those shown below, an extended light source is generally required.

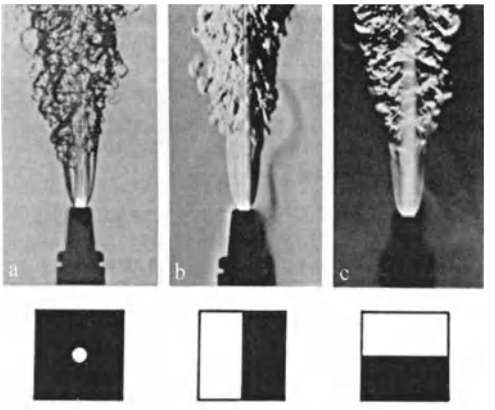

Fig. 2.4. Schlieren photographs of the turbulent flame and mixing phenomena of an oxy-acetylene torch using a circular light source and: **a** circular cutoff, **b** vertical knife-edge, and **c** horizontal knife-edge. Photos by H. Herbrich, reproduced by courtesy of Messer Griesheim GmbH, Industriegase Deutschland, a member of the Hoechst Group.

2.5.2 Extended Light Source

Having covered the elements of the schlieren effect using a point source, we now consider the more realistic case of an extended light source [126-128]. As diagrammed in Fig. 2.5, the dual-lens approach of Fig. 2.3 is retained, but an additional focusing lens is added after the knife-edge.[4] The coordinate frame shows the principal direction along the +z-axis, x and y being the transverse coordinates as before. An incoherent beam of white light originates from the extended source, here shown as a downward-pointing arrow. (It often has the form of a rectangular slit in the x,y-plane, but its specific shape is secondary to the point at hand.) Collimated by the first lens, the light beam traverses the test area and is refocused by the second lens to form an inverted image of the source at the knife-edge.

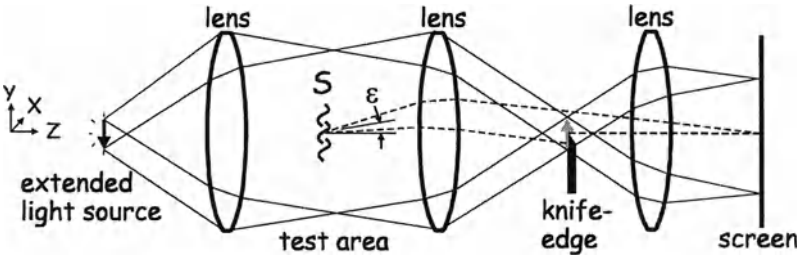

Fig. 2.5. Diagram of a simple schlieren system with an extended light source.

[4] No focusing lens was shown in Fig. 2.3 because, in principle, a point-source optical system has an infinitesimal aperture – like a pinhole camera – and thus infinite depth-of-field. In this case disturbances anywhere along the optical path are automatically in focus.

Because the light source is no longer a point, however, collimation no longer produces exactly-parallel rays. Actually, one can imagine an array of point sources distributed along the vertical height of the extended source, each producing a schlieren beam that focuses to a corresponding point in the light source image at the knife-edge. The extreme rays from the top and bottom of the source are drawn in Fig. 2.5 to illustrate this point.

The knife-edge cutoff blocks a portion of the image of the extended source: say about half. Beyond the knife-edge a third lens (the focusing or camera lens) is used to focus an inverted image of the schlieren test area on a viewing screen.

From the optical properties of lenses [129-132] one recognizes that the light-source and knife-edge planes, as well as the test-area and screen planes, are sets of conjugate optical planes. These sets bear reciprocal Fourier-transform relationships to one another (see App. B). Pairs of conjugate optical planes are crucial in understanding the schlieren effect, for what appears in one also appears undistorted in its mate, but for a possible scale transformation. Thus an accurate image of the light source is focused on the knife-edge in Fig. 2.5, and a true image of the schlieren object S appears on the viewing screen.

Because the light source now has finite size, every point in the test area is illuminated by countless rays within a cone limited by the extremities of the source. Likewise each point in the light source illuminates every test-area point. This lends depth-of-focus to the schlieren system, which it was lacking in the earlier consideration of a point source. It also has a more-important effect: the generation of a *composite light-source image* at the knife-edge plane.

Toepler [37] was first to recognize that this light-source image is the superposition of many separate, weak, "elemental" source images from all points of the test area. For example, if we insert an opaque x,y-mask containing a pinhole into the test area, we still see an image of the entire light source in the knife-edge plane – only much weakened in intensity. Thus each point in the test area contributes an entire elemental source image to the composite image in the knife-edge plane. If no schlieren object is present, then advancing the knife-edge to block more of the composite source image blocks each elemental source image equally. Since every test-area point is therefore equally deprived of light, the screen darkens uniformly. This is a fundamental characteristic of a schlieren image.

Now let one test-area point be subject to refraction by the schlieren object S. Whereas in Fig. 2.3 a single ray was bent, now a ray bundle from all light-source points suffers the refraction angle ε. This bundle – shown by dashed lines in Fig. 2.5 – proceeds to form an elemental source image in the knife-edge plane, now *displaced* from the undisturbed composite source image by virtue of its refraction. This essential concept is illustrated in Fig. 2.6 [98,116,128].

Despite this displacement in the knife-edge plane, the ray bundle originating at a test-area point is returned by the second lens to the same relative position in the conjugate image plane on the screen. This happens, according to the properties of a lens, regardless of the angle ε at which the rays left the test plane. It gives us a way to separate the extraordinary light rays – refracted by schlieren in the test area – from the ordinary rays that provide the general background illuminance. Once separated, the refracted light is marked by a different amount of cutoff at the

knife-edge, then recombined in the schlieren image to yield illuminance variations with respect to the background [66]. The schlieren image is built up of many such points of varying illuminance, corresponding to the shape and strength of the refractive schlieren object.

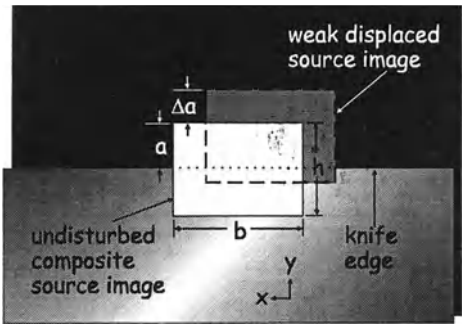

Fig. 2.6. Diagram of the knife-edge plane. A rectangular composite source image is shown about half cut-off, with height *a* remaining unobscured by the knife-edge. Due to refraction at a point in the test area, a weak elemental source image is shifted to the upper right. Its unobscured height, a + Δa, passes extra light to a corresponding point in the schlieren image.

This is a much better arrangement than that of Fig. 2.3: now the extended light source allows a continuous gray-scale schlieren image rather than merely binary black-and-white. This book is full of examples of such schlieren images.

In Fig. 2.6, note that the amount of knife-edge cutoff of the undisturbed composite source image sets the background level of illuminance in the image on the viewing screen. Any displaced elemental source image due to test-area refractions can alter the local illuminance on the screen if it meets two conditions: 1) a component of the displacement must be perpendicular to the knife-edge, and 2) the displacement must not be so large as to move the weak source image entirely onto, or off of, the knife-edge. When the latter occurs, we say the *measuring range* of the schlieren system has been exceeded, since stronger refractions no longer produce corresponding image illuminance changes. Since the weak displaced source image in Fig. 2.6 meets both of the above conditions, it falls within the linear range of the optical system. Had the component of displacement been in the negative rather than positive y-direction, a decrease in image illuminance would have occurred relative to the background level. Of course, horizontal displacements cannot be observed with the horizontal knife-edge of Figs. 2.5 and 2.6: they require a vertical knife-edge orientation.

Within the measuring range of the instrument, the image illuminance E is, by geometric optics, linearly proportional to the amount of knife-edge cutoff. But since

$$\Delta a = f_2 \cdot \varepsilon_y \tag{2.6}$$

where f_2 is the focal length of the second lens, E is also linear in the y-component of refraction angle, ε_y, in the schlieren object. This has been used on many occasions to measure $\partial n/\partial y$ quantitatively by measuring E, then integrating to get n and hence ρ for a gas or liquid. More on this in Chap. 10.

Finally, though a simple lens-type schlieren arrangement has served for this introduction, a few more words are needed regarding practicality. Mirror-type systems are more common but more complicated than the lens-type arrangement for reasons to be covered in the next chapter. The third (focusing) lens in Fig. 2.5 is used to adjust the scale of the schlieren image for various uses. Although frequently used for convenient image sizing, it is not absolutely essential; the second lens, or schlieren objective, can produce a serviceable schlieren image by itself if the distance from the test area to the objective is appropriate. There is, however, one omission from Fig. 2.5 that needs special notice: a bare-bulb light source is seldom adequate for schlieren imaging. Instead, it is common practice to use a condenser lens and slit to define a bright *effective source* with sharp boundaries at the front focus of the first schlieren lens. More on these practical issues is given in Sect. 7.1.

2.6 On the Aspect of a Schlieren Image

> ...a pleasing effect of relief as though the air streams were carved in plaster and illuminated from one side.
>
> *H. G. Taylor and J. M. Waldram* [133]

Several authors [1,34,78,104,116,133,134] have remarked upon the striking appearance of a schlieren image: it has a bas-relief effect, like stone carvings or a landscape seen from above at sunrise or sunset. As illustrated in Fig. 2.4, the direction of illumination appears to be opposite the knife-edge. Goldstein and Kuehn [116] note that illuminated regions (sunlit slopes) occur when n increases in the direction away from the knife-edge. For liquid surface waves [134], the image illuminance is again proportional to the local wave slope. It appears as if someone had carved a contour map of refractive index from solid material, then illuminated it from the side to reveal the gradients.

In fact, someone did, as shown in Fig. 2.7. In the early days of ballistics, decades before computers, interferometry was used to measure the density profile of supersonic projectile flows like that of Fig. 2.7a. A plaster contour model was made as a convenient way to display the tabulated data. When side-illuminated, in Fig. 2.7b, it assumed the aspect of a schlieren image. This analogy fails when it comes to the projectile model itself, but it still provides us a powerful visual parallel between tangible reality and the abstraction of a schlieren image.

Porter [34] was intrigued by the appearance of his telescope mirror undergoing the Foucault test. He even felt there was something uncanny about it. Today, many are still fascinated by the striking appearance of schlieren images. There is an architectural beauty to them, like hieroglyphs. One must consciously try in order to make an ugly one, and the best of them are truly works of art. There is nothing else like them in all of scientific imagery.

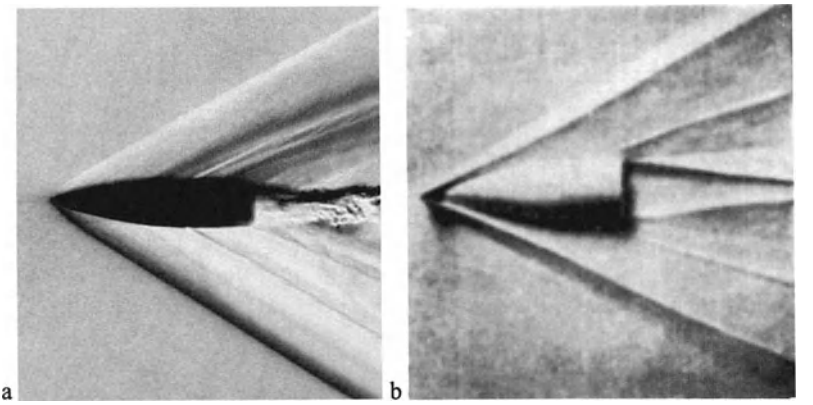

Fig. 2.7. **a** Schlieren photograph of a supersonic bullet by Schardin [2]. **b** Side-illuminated plaster model of the air density distribution about a bullet, from Cranz [78]. Photos reproduced by permission of Springer-Verlag.

3 Toepler's Schlieren Technique

They said 'You have a blue guitar,
You do not play things as they are.'
The man replied, 'Things as they are
Are changed upon a blue guitar."

Wallace Stevens, The Man with the Blue Guitar

'Schlieren apparatus' is a name just as suitable or unsuitable as the name 'telescope,' for as the latter is a scope to see distance, so is the former an apparatus to see Schlieren.

August Toepler [135]

Why do we call it Toepler's technique? Recalling Chap. 1, although Toepler was not the strict originator of schlieren imaging, he made it what it is today. Here, *Toepler's schlieren technique* distinguishes the basic (lens or mirror) schlieren system with slit-source and knife-edge from all the other adaptations that have arisen since his time.

Toepler also stated some lasting design principles for schlieren equipment [12,37]. His apparatus (see Fig. 1.8) was arranged in three sections: the "illuminator," the "schlieren head" or main field lens, and the "analyzer." (Today dual field lenses or mirrors are more often used instead of a single schlieren head.)

A variety of schlieren arrangements is possible, all embodying Toepler's design principles [66]. Our goals in this chapter are to discuss the basic setups, and to consider the salient properties of the resulting schlieren image in detail.

3.1 Lens- and Mirror-Type Systems

Although Toepler originally used the objective lenses of refracting telescopes as schlieren heads, mirror-based systems followed shortly on the strength of Foucault's knife-edge test. There are some distinctions worth noting at the outset.

While lens-type schlieren instruments can be in-line, and therefore relatively simple, mirror-type instruments are inherently folded. This is not a problem for routine work unless one uses too many mirrors. But mirror-based instruments

G. S. Settles, *Schlieren and Shadowgraph Techniques*

tend to be rather more difficult to align, and troublesome off-axis optical aberrations can occur under circumstances to be explained later.

On the other hand, chromatic aberration matters for a lens, but not for a first-surface mirror. In fact, residual chromatic aberration is a problem even for expensive achromatic lenses, due to partial spectrum cutoff by the knife-edge. This causes color anomalies in the schlieren image, which sometimes appears split into halves of spectrally-opposite colors. A narrow-band color filter at the light source eliminates this difficulty (Toepler [3,37]).

Further, modern multi-element lenses require high internal quality and several optical surfaces polished to near-perfection, while mirrors need only one polished surface and little internal quality. These factors weigh in favor of mirrors when cost and field-of-view are considered. Accordingly the largest lens-type schlieren instruments to be found are in the 20 cm-diameter range. Larger systems – except for the special ones described in the next chapter – are always mirror-based.

Some typical commercial prices for schlieren-quality lenses and mirrors are plotted vs. diameter in Fig. 3.1. An exponential rise of cost with diameter is evident, depending upon manufacturer, with the steepest rise in the case of lenses. Lens cost also increases with higher lens power. Mirrors and lenses of larger diameter than those of Fig. 3.1 can be had by special order, but meager data prevent any general comments on cost outside the range shown (see App. D).

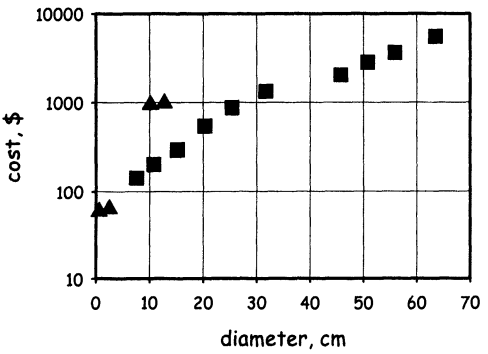

Fig. 3.1. Cost in US$ vs. diameter for achromatic lenses ▲ and parabolic telescope mirrors ■ suitable for use as schlieren field optics. (These data are for example purposes only, and are extracted from commercial catalogs ca. 2000.)

3.1.1 Lens Systems

Sharp high-quality lenses are always favored for schlieren work. The schlieren objects themselves are often quite weak, so lens imperfections can easily mask them. Surface figure within at least $\lambda/2$ over the lens diameter is required for such high-sensitivity work. Correction of both spherical and chromatic aberration is important. Internal striae are annoying, but as Weinberg [66] says: "One or two well charted familiar (streaks) across the field of view...will not seriously interfere with research or teaching." Telescope objectives, projector lenses, and military-surplus aerial camera lenses often make good schlieren field lenses.

Schardin [1,2] discussed Toepler's [41] single-lens schlieren system in detail. Shown in Fig. 3.2, its light source is extended, but must have at least one edge

sharply limited by an opaque mask or knife. The field lens K[1] requires the quality level just discussed, plus a large diameter to provide adequate field-of-view. With only one field lens the schlieren object S is traversed by non-parallel light, which is sometimes a disadvantage. Finally, as Schardin put it, the task of lens K is to reproduce the light-source image in the knife-edge plane, while that of camera-lens O is to focus the schlieren object S upon the image plane S′.

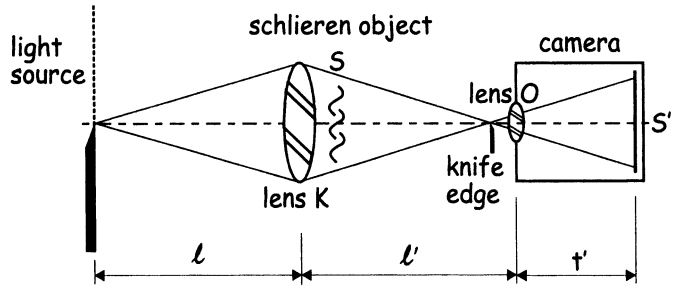

Fig. 3.2. Toepler's single-field-lens schlieren arrangement [2,41]

An improved setup – more in line with current practice – is the dual-field-lens system shown in Fig. 3.3 [2]. Parallel light in the test area between the field lenses is often necessary, especially for 2-D schlieren objects. It provides the least-ambiguous interpretation of $\Delta a = f_2 \cdot \varepsilon$ (Eqn. 2.6) [102]. Thus there is a strong incentive for it in any quantitative and much qualitative schlieren work.

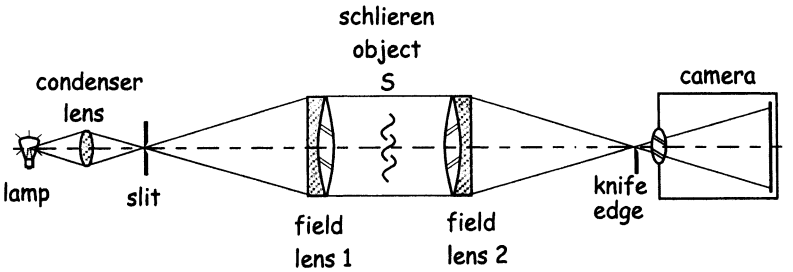

Fig. 3.3. Dual-field-lens schlieren arrangement [2,98,102]

Fig. 3.3 also shows the use of a lamp with a condenser lens and slit to produce a well-defined effective light source, as mentioned at the end of Chap. 2.

[1] K stands for *Kopf* or *Schlierenkopf*, the schlieren head lens. Here we call it the objective (from telescopy) or the field lens, since its diameter defines the schlieren field-of-view.

3.1.2 Mirror Systems

As in the cases of lenses, schlieren field mirrors also require the best quality available. Fortunately, parabolic mirrors that make good telescopes also usually make good schlieren instruments. Several manufacturers supply telescopic parabolas polished to λ/8 or better (See App. D). Keagy et al. [136] used twin 300-cm-diameter λ/10 parabolas for schlieren photography. Holder and North [98] recommend mirrors accurate to at least λ/4 (per 25 mm of diameter), and with no more than 1λ overall figure error. According to Weinberg [66], if the figure is in error by as much as 6λ over the mirror surface, lower schlieren sensitivity results. An older rule also required the mirror thickness to be 12-17% of the diameter for stability [98], but this is now violated in large new-age telescopes [137].

The Z-Type 2-Mirror Schlieren System. Spherical, parabolic, and off-axis concave mirrors are often used in schlieren equipment. But by far the most popular arrangement is the *z-type* Herschellian[2] system using two oppositely-tilted, on-axis telescopic parabolas (Fig. 3.4). The combination of a diverging illuminator beam, an opposite converging analyzer beam, and a parallel beam between the two mirrors suggests the letter *z,* whence the name.

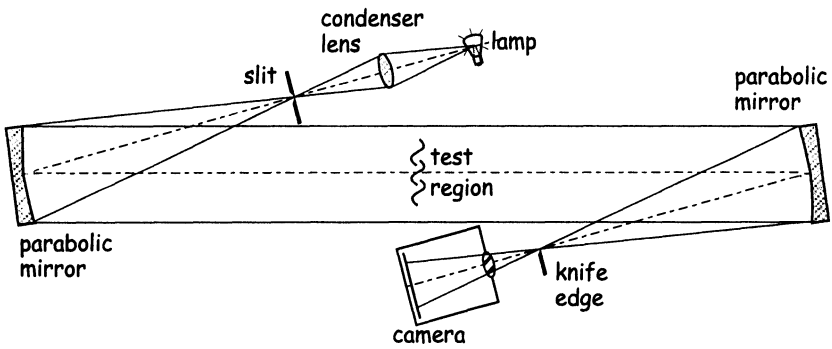

Fig. 3.4. Z-type schlieren arrangement [1,2,98,102].

Though titled, the mirrors are usually symmetrical, on-axis parabolas. Specially-figured off-axis parabolas are quite expensive, and are unnecessary if large-f/number on-axis mirrors are chosen and are carefully aligned [98]. The advantages of parallel light, stated above for lens-type systems, apply equally to the z-

[2] Sir William Herschel (1738-1822), a great astronomer, tilted his parabolic telescope mirror off its axis in order to gain access to the image.

type mirror schlieren system. The advantage of mirrors in place of lenses is primarily found in a larger field-of-view for a given cost.

A minimum distance between the field mirrors of about $2f$, where f is the mirror focal length, is required to provide space for the test area. Longer distances between mirrors do not matter in principle. To shorten the overall length, plane first-surface folding mirrors can be used in the illuminator and analyzer beams. These make the system somewhat more difficult to align and more prone to vibration sensitivity. They also exacerbate optical aberrations by increasing the off-axis angles [66]. Nevertheless they can be essential in cramped quarters.

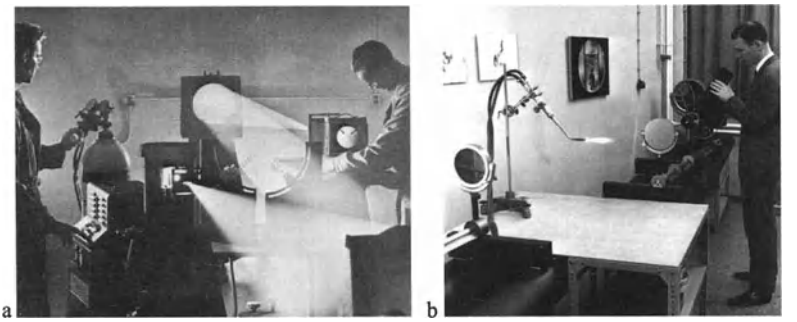

Fig. 3.5. **a** The 300-cm-aperture z-type schlieren system of Keagy, Ellis, and Reid [136,138]. Smoke is used to make the schlieren beam visible by light scattering. Photo courtesy Battelle. **b** The z-type schlieren system that was used to photograph Fig. 2.4. Foreground: oxy-acetylene torch and plane beam-folding mirrors, background: one of two parabolic field mirrors; H. Herbrich adjusting analyzer unit. Photo courtesy of Messer Griesheim GmbH, Industriegase Deutschland, a member of the Hoechst Group.

Despite the strong popularity of the z-type schlieren setup, other parallel-beam mirror systems are used occasionally [139-142]. Chief among these is the Newtonian on-axis system. Newton may have overshadowed Herschel in telescopes, but not when it comes to schlieren equipment: the center of the Newtonian field-of-view is blocked by the on-axis diagonal mirror. In one case a perforated coaxial schlieren mirror setup of the Cassegrain type was used [143] with similar effect. These optics are unpopular for schlieren because an obstruction in the center of the field-of-view is seldom tolerable. Their chief advantage, however, lies in avoiding the off-axis aberrations of the z-type arrangement, discussed next.

Off-Axis Aberrations: Coma and Astigmatism. Most available optical elements are figured for on-axis use, their geometrical and optical axes being coincident. When we deliberately thwart this, as in Figs. 3.4 and 3.5, there is a price to pay. For mirrors, the resulting optical aberrations (see App. A.4) are known as *coma* and *astigmatism* [1,2,65,66,98,126,144]. Both lead to errors in the faithful production of the light-source image in the cutoff plane. If either is allowed to get out of

hand, then there results uneven schlieren-image illuminance even when the test area is schlieren-free.

By definition, coma occurs when the direction of light reflected from a mirror depends on the position of the point of reflection. This is a consequence of tilting the schlieren field mirrors off their optical axes. In result, beginning with a point light source, a comatic optical system spreads the point focus into a line. Different annular zones of the mirror-face focus at different points along this line with different spot sizes [145]. The point focus becomes smeared into a region of flare with a bright core at one end: a "comet," whence the name.

This aberration grows in proportion to the offset angle θ (see Fig. 3.6), and to the inverse square of the mirror f/no. for a given θ. It is thus minimized by keeping θ small and using long-focal-length mirrors. There are other reasons to do this as well, but fortunately, since coma is generated at both schlieren field mirrors, it is possible to cancel its overall effect by tilting the mirrors at equal angles θ_1 and θ_2 in opposite directions from the central optical axis, forming a "z." One must use identical mirrors, of course, and all optical elements must be centered in a common plane: the plane of the page in Figs. 3.4 and 3.6.

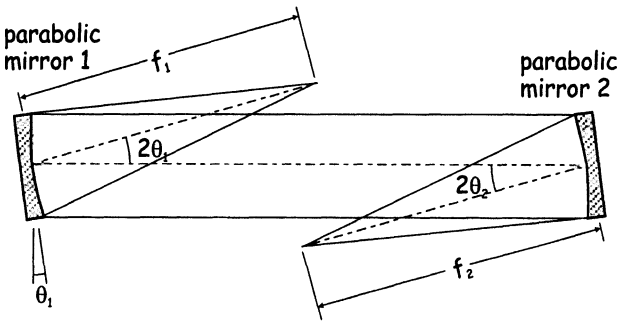

Fig. 3.6. Diagram of z-type schlieren optics for discussion of aberrations.

This is the beauty of the z-type schlieren arrangement: it is free of coma if the mirrors are perfectly and identically figured, and are arranged carefully as just described. The unsymmetrical arrangement in which the illuminator and analyzer beams lie both on the same side should be avoided like the plague, since the coma is doubled rather than cancelled in that case.

Unlike coma, astigmatism cannot be eliminated from the z-type schlieren or any off-axis mirror system. The word literally means *non-point-like*, or failure to focus a point to a point. It arises from differences in path length along the optical centerline and the mirror periphery, as shown in Fig. 3.6. Due to finite off-axis angles θ_1 and θ_2, a point light source is imaged as two short lines at right angles to one another and spaced apart a small distance Δf along the optical axis [66]. Even though θ_1 and θ_2 are minimized and large-f/number mirrors are used, some astigmatism is always present.

Unable to eliminate it, we therefore learn to live with it. Recalling Sect. 2.5.2, a small rectangular-slit light source is used to illuminate the z-type schlieren system. Astigmatism smears or spreads the elemental source images from various points of the test area along two short lines near the focus of the second mirror. The second of these, called the sagittal focus, is illustrated in Fig. 3.7. Here the spreading is horizontal, i.e. in the plane of the schlieren system. If we apply a horizontal knife-edge, then despite the smearing, all elemental source images are equally cut off. Uniform screen illuminance thus results and visible astigmatism errors are avoided. The same holds for the tangential focus, occurring at distance Δf ahead of the sagittal focus, except there a vertical knife-edge is required.

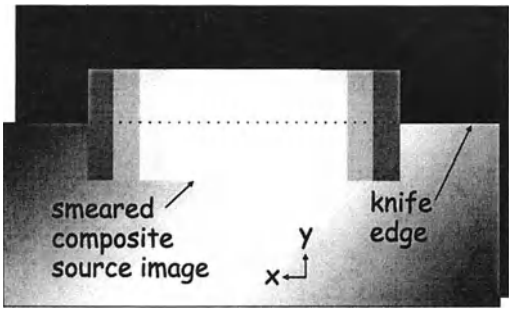

Fig. 3.7. Diagram of tangential focus in a z-type schlieren system, showing horizontal smearing of the light-source image and the proper application of a horizontal knife-edge cutoff.

Thus knife-edge position and orientation are both important in limiting astigmatic effects. In practice one can usually see the shape of the composite light-source image on the knife-edge; this helps the axial adjustment of the cutoff. The desired result is uniform darkening of the schlieren image as the knife-edge is advanced.

Astigmatism in z-type schlieren equipment generally frustrates the use of circular or L-shaped cutoffs, or any cutoff that attempts to mask the light beam in perpendicular directions in a single x,y-plane. Several ways have been devised to get around this restriction, including separate vertical and horizontal cutoffs properly positioned at the tangential and sagittal foci. Δf can be eliminated with some extra trouble by displacing perpendicular light-source slits appropriately along the optical axis [146]. A compensating cylindrical lens can also be used after the light source [147], or a two-spherical-lens compensator before the focus [148]. Best of all, one can stick with an ordinary slit source and knife edge, and avoid these problems of non-uniform cutoff altogether.

Still, other problems can stem from astigmatism [98]. Vertical and horizontal lines in the test area are not sharply focused simultaneously. Distortion errors can also arise in reproducing test-area angles in the schlieren image. These problems are usually negligible for long-focus mirrors, but checking for distortion with an orthogonal test-area grid is advised if true angular reproduction is desired.

The distance between the sagittal and tangential foci can be taken as an index of the astigmatism severity. It is given by the geometric formula [126,149]:

$$\Delta f = f \cdot \sin^2\theta / \cos\theta \tag{3.1}$$

But since larger-f/number mirrors permit smaller angles θ, this can be simplified. In the limit of small θ it becomes $d^2/4f$, where d is the mirror aperture. Obviously, for a given aperture one wants long-focal-length mirrors to minimize the astigmatic separation. The following examples reinforce that point.

In Chap. 8 a small z-type schlieren system is described in detail. It uses twin f/8 parabolas having d = 10.8 cm and f = 86.4 cm. Eqn. 3.1 yields Δf = 2.4 mm for θ = 3° in this system. If f/10 mirrors were substituted, this value would shrink to 2 mm with θ = 2.5°. In neither case is astigmatism much of a problem. By contrast, in Sect. 4.1.2 a large z-type system with short-focus f/5 mirrors is described: d = 0.76 m, f = 3.81 m, and Δf = 38 mm. Astigmatism is very noticeable in this system; it requires careful alignment and adjustment to realize a uniform cutoff.

In summary, recommended practice is to minimize both astigmatism and coma by restricting the offset angles θ to their minimum practical values. Further, mirrors with f/numbers of 6 or greater are strongly recommended. The usual range of mirrors found in z-type schlieren systems is from f/6 to f/12 [98].

The Single-Mirror Coincident System. Following the z-type schlieren arrangement in popularity are several mirror-based systems without the advantages of parallel light. Chief among these is the single-mirror coincident system described by Taylor and Waldram [133]. Schardin described it at about the same time, and attributed it to Hans Boas [78]. Shown in Fig. 3.8, this arrangement is also called "autocollimating" by some, due to its similarity to an autocollimator for aligning a telescope mirror. It also bears a close familial resemblance to Foucault's knife-edge test.

Given a single spherical field mirror, one places the light source on-axis at its radius of curvature (R = 2f). The diverging beam fills the mirror and returns along the coincident path, forming a source image upon the light source itself. This minor difficulty is overcome by using a reflecting knife-edge or a beamsplitter to deflect the returning rays, or else by allowing a small off-axis separation between illuminator and analyzer beams.

The test area lies directly in front of the mirror in diverging light from the source, as well as in converging light reflected from the mirror. Ideally, each point in the test plane is traversed twice by the same ray, which acquires the deflection angle ε once on each pass. Since ε is small and the distance to the mirror is short, this actually does work in practice, yielding the advantage of twice the sensitivity of a single-pass schlieren method.

The lack of parallel light in the test area is a disadvantage that hampers some applications. On the other hand, the perfect coincident on-axis alignment avoids all difficulties with astigmatism and coma. This method is sometimes used for its sensitivity advantage but, more often and most compellingly, when there is only one field mirror available.

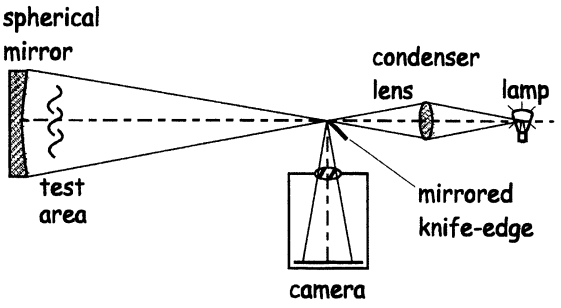

Fig. 3.8. Diagram of the single-mirror coincident schlieren system

The optical alignment shown in Fig. 3.8 is perfect when the field mirror is spherical. But what if the only available mirror is parabolic? In that case optical shop testing practice comes to the rescue, providing a relatively-simple way to add a corrector lens after the light source [150,151]. The spherical aberration of the corrector lens is of opposite sign but similar character to that of the parabolic mirror, hence they can be made to nullify one another. Without this, a uniform schlieren cutoff is impossible for mirrors of shorter focus than about f/10. With it, near-perfect compensation can be had at the expense of adding the corrector-lens flaws (especially chromatic aberration) to the system.

In Sect. 4.1.3 a large (1 m diameter) parabolic-mirror coincident schlieren system with such a corrector lens is described [127]. Then in Sect. 4.3.5 the world's largest indoor schlieren system is shown to be based, at least loosely, on the single-reflector coincidence principle [111].

The Off-Axis Single-Mirror System. Other than the coincidence method just shown, a single mirror can also be used well off-axis, with the test area positioned in the illuminator or the analyzer beam (Fig. 3.9). While Schardin [1,2] found this useful, few have used it since. It is subject to the off-axis aberrations described earlier, but even worse, it demands a mirror perhaps twice the diameter of the desired field-of-view. In conventional mirror-based schlieren optics, field-of-view comes at a high premium and few have the luxury of using mirrors twice as large as necessary. Nevertheless this approach is still used occasionally when only a single mirror is available.

Multi-pass mirror systems. Schardin [1,2] set up a system to visualize very weak disturbances by allowing the light beam to pass through the test area several times. He noted increased sensitivity, as well as susceptibility to vibration and room air currents, and difficulty of adjustment. More recently a similar scheme was suggested for low-density plasma observation [152]. According to Burton et al. [42], "Multiple coincidence systems other than that of the single mirror are seldom used, though many have been devised."

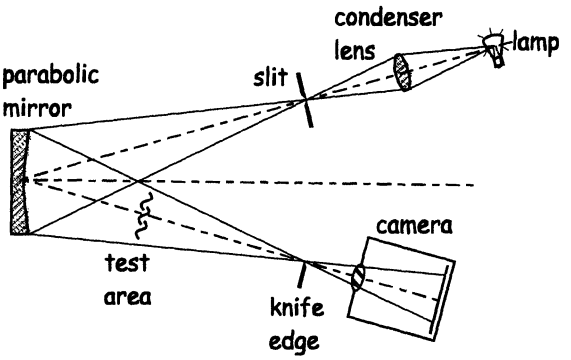

Fig. 3.9. Diagram of the single-mirror off-axis schlieren system

3.2 Sensitivity

> It is true that the greatest sensitivity will show the finest wave structure – and, incidentally, all the flaws in the glass plates
>
> *W. F. Hilton* [122]

> The main advantages of the schlieren techniques are their sensitivity and their simplicity...
>
> *J. Ojeda-Castañeda* [153]

3.2.1 Definition and Geometrical Theory

The sensitivity of a measuring instrument is one of its basic characteristics, relating the instrument's output to the input received. In the case of schlieren optics – at least those considered here – the output is a 2-D image in x and y. More specifically, it is an array of picture elements characterized by amplitude or grayscale contrast variations. With Toepler's schlieren system we do, after all, observe something transparent by producing a grayscale image of it. (Color comes later in Chap. 5.)

It is convenient to use the z-type mirror system here, Figs. 3.4 and 3.6, to illustrate the geometrical optics of schlieren sensitivity [98]. A horizontal source slit orientation and a horizontal knife edge are assumed for convenience. Beginning with the luminance B emitted by the light source (in candela/m^2, see Sect. A.1), one can easily find the illuminance E_0 incident upon the first mirror by way of the inverse square law:

$$E_0 = \frac{B \cdot b \cdot h}{f_1^2} \tag{3.2}$$

where b and h are the breadth and height of the source slit, respectively (recall Fig. 2.6) and f_1 is the focal length of the first mirror. Neglecting any losses, this illuminance level also falls on the test area and the second mirror in parallel light. The schlieren image illuminance is the same as well, in the absence of any knife-edge cutoff, but for a magnification factor m that accounts for image size relative to that of the test area,

$$E_0 = \frac{B \cdot b \cdot h}{m^2 f_1^2} \tag{3.3}$$

Now let the knife-edge block all but a part of the light source image at the second mirror focus, that part having height a, as in Fig. 2.6. Replacing h in Eqn. 3.3 with $(f_1/f_2)a$ to describe the actual unobstructed height of the light source image,

$$E = \frac{B \cdot b \cdot a}{m^2 f_1 f_2} \tag{3.4}$$

Every schlieren image has such a background illuminance or amplitude level; E, often appearing as a middle-gray shade. The illuminance of a point in the image is judged by comparison to this level: above it, below it, or equal to it.

Now consider the case of a schlieren object in the test area that refracts a certain light ray through angle ε having y-component ε_y. We already saw in Fig. 2.6 and Eqn. 2.6 that this causes a weak elemental source image to shift upward in the knife-edge plane by a distance $\Delta a = \varepsilon_y \cdot f_2$. Substituting Δa for a in Eqn. 3.4, one obtains:

$$\Delta E = \frac{B \cdot b \cdot \varepsilon_y}{m^2 f_1} \tag{3.5}$$

which describes the incremental gain of illuminance at the corresponding image point due to the refraction ε_y in the test area.

Contrast in the schlieren image refers to the ratio of differential illuminance ΔE at an image point to the general background level E,

$$C \equiv \frac{\Delta E}{E} = \frac{f_2 \varepsilon_y}{a} \tag{3.6}$$

This image contrast is the output of the schlieren instrument. The input is a pattern of irregular ray deflections ε, resulting from refractive-index gradients in the test area, in an otherwise regular beam. Since the sensitivity of any instrument is basically an influence coefficient, i.e. d(output)/d(input). We can therefore write the schlieren sensitivity – sometimes called *contrast sensitivity* – as the rate of change of image contrast with respect to refraction angle:

$$S = \frac{dC}{d\varepsilon} = \frac{f_2}{a} \tag{3.7}$$

This simple geometric-optical result is accurate and sufficient for most purposes. It provides a measure of schlieren sensitivity independent of any observing or recording means [102]. It also shows that sensitivity is proportional to the focal length of the second parabolic mirror in a z-type system, another reason for longer rather than shorter focal lengths. Further, it reveals that the *unobstructed* height of the source image, a, determines sensitivity, not the overall height h (a common misconception). On the other hand, it is not reasonable that a real instrument can achieve infinite sensitivity when $a \rightarrow 0$. Sect. 3.5 on diffraction reveals how physical optics comes into play in this sensitivity limit.

Eqns. 3.4 and 3.7 demonstrate that Toepler's schlieren technique has a basically-linear response [2]. Not only does image contrast respond linearly to refraction angle ε, but also the background illumination level is linear with respect to the degree of knife-edge cutoff of the source image. To reinforce the latter point, Fig. 3.10 shows Eqn. 3.4 plotted alongside comparable data from the small z-type schlieren system to be described further in Chap. 8. Departures from strict linearity, mostly of concern for quantitative schlieren measurements, occur near 0% and 100% cutoff,[3] as noted by several authors [130,146,154].

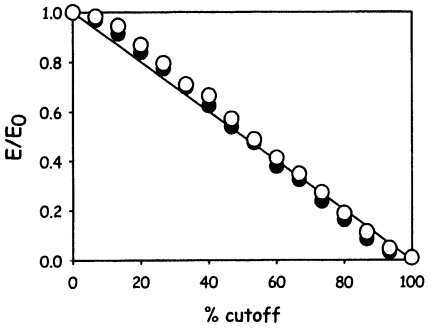

Fig. 3.10. Plot of schlieren image illuminance ratio E/E_0 vs. % knife-edge cutoff. Symbols are experimental data for different E_0 levels; solid line is Eqn. 3.4, f_2 = 86.4 cm, h = 1.5 mm. The nonlinearity of the data near 0% and 100% cutoff is due to uneven source-slit illumination and to diffraction effects.

An important point is raised here by Kean [146]: schlieren system linearity only holds when the *detector* is also linear with respect to image illuminance. This was the case for Fig. 3.10, but is not so for either the human eye or photographic film. Instead, both have an approximately logarithmic response (see App. A). To achieve a linear visual or photographic response, one must then employ a source slit or cutoff with an exponential contour. This issue is taken up in Sect. 5.1.2.

Eqn. 3.5 fails to describe the change in image illuminance once the light source image is shifted entirely off of – or entirely onto – the knife-edge. As noted in Chap. 2, these cases exceed the measuring range of the instrument. Stronger schlieren objects then no longer cause a change of image illuminance. Moreover,

[3] The use of % cutoff in Fig. 3.10 is not a complete index of schlieren sensitivity. From Eqn. 3.7 above, f_2/a is the proper descriptor. Nevertheless, % cutoff is used for convenience so long as f_2 and h are also given.

equal range for darkening as well as brightening of the image only holds when the source image is exactly half cut-off by the knife-edge (i.e. a = h/2). On this account the literature [98] usually recommends that the knife-edge be set at 50% cutoff. But that setting does not simultaneously achieve high sensitivity, as one clearly sees from Eqn. 3.7 and the example shown below in Fig. 3.11. A tradeoff thus occurs between sensitivity and measuring range. This and other issues regarding the schlieren measuring range are considered further in Sect. 3.3.

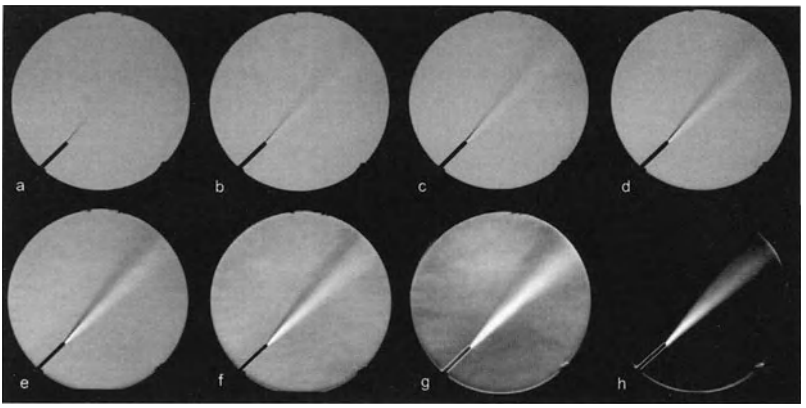

Fig. 3.11. Series of long-exposure schlieren photographs of a turbulent gas jet mixing with air. The degree of knife-edge cutoff of the source image is **a** 0%, **b** 20%, **c** 40%, **d** 60%, **e** 80%, **f** 90%, **g** 95%, and **h** 100%. While 50% cutoff is ideal from the standpoint of measuring range, the need for greater sensitivity often requires a cutoff of 90% or more. Except for **h**, all images were exposed to obtain about the same background gray level. h = 1.5 mm, f_2 = 86.4 cm. Photos by Rossana Quiñones.

The geometric theory of schlieren sensitivity given above is simplest for lens or mirror systems casting parallel light across the test area. The specific test area location, e.g. between the mirrors of a z-type system, is immaterial in this case. Position can matter, though, in non-parallel-light setups like those shown in Figs. 3.2, 3.8, and 3.9. Especially for schlieren objects extending along the optical axis, the light deflection a at the cutoff can become a function of spatial position in the object. Weinberg [66] recommends comparing the product of local ray obliquity and path length through the schlieren object with the desired feature resolution in the image. He concludes: "A parallel beam is, of course, always to be preferred."

Finally, in more casual terms than Eqns. 3.2-3.7, one can associate deflection angles ε directly with a kind of "visual sensitivity index." Those well-trained in the schlieren arts recognize the sensitivity level of an image by the type of disturbances it reveals. This is seldom done in terms of refractive-index-gradients, but may sometimes take a derived form like temperature gradient in degrees/cm. Most handily, however, we rank schlieren in terms of deflection angle ε in

arcseconds, a habit obviously borrowed from astronomy. Schardin tested the sensitivity of a schlieren system by rubbing his thumb and forefinger in the field-of-view. If he could see the warm air this generated, it gave him a sense of the detectable angle ε (5-10 arcseconds, as discussed in the next section).

3.2.2 Sensitivity Examples

Some actual examples help to understand the relationships among Eqns. 3.2-3.7. Consider the small z-type schlieren system of Chap. 8, used as an example throughout the book.

We begin with the photometry of the light source. A typical tungsten-halogen automotive lamp, appropriated for schlieren use, has a 1.5x5 mm filament rated at 55 watts and 12 volts. A typical efficacy of 25 lumens/watt is assumed. The luminous exitance of the filament is thus about 1.8 lumens/m^2 (lux) and the radiant intensity is estimated to be 109 candela. Part of the radiated light is masked at the 1x3 mm source slit in order to have a well-defined effective source. The luminance B of the beam after the source slit is found to be 1.5×10^7 candela/m^2, which is consistent with the literature on tungsten-halogen lamps. Finally, invoking Eqn. 3.2, we find the illuminance incident upon the first mirror to be 60 lux, also confirmed by a direct measurement.

The system considered in this example uses twin f/8 parabolic mirrors of 10.8 cm diameter. A focusing lens forms an image on Polaroid film at 65% full size, or magnification m = 0.65. From Eqn. 3.3 the background illuminance E_0 of the schlieren image with no knife-edge is 140 lux. With 50% knife-edge cutoff this drops to 70 lux.

Now allow a 10-arcsecond refraction in the test area, typical of the refraction angle ε in the plume above a low-power reading lamp. From Eqn. 2.6, Δa = 42 μm in the cutoff plane. Eqn. 3.5 yields ΔE = 5.8 lux above or below the 70-lux background, depending on direction. The contrast of this schliere is, from Eqn. 3.6, about 8%, which is weak but visible (an issue taken up in the next section). Eqn. 3.7 yields a sensitivity of 0.8% contrast change per arcsecond of refraction.

Finally, consider the same 10-arcsecond schliere with 95% knife-edge cutoff. ΔE does not change, of course, but the background level drops to 7 lux and the contrast rises to 83%. A similarly-dramatic rise in contrast is shown in Fig. 3.11 above, using the same apparatus considered in this example.

Schardin [2] gives a similar example of a larger off-axis-type schlieren system with a single 30-cm f/22 spherical mirror. He includes a 50% optical loss factor not considered in the example above. Severe knife-edge cutoff leaves only 60 μm of the source image height unobstructed. In this case the weakest detectable shift of the source image, Δa, is a mere 3 μm due to a refraction of only 0.22 arcsecond.

This emphasizes the point that long-focal-length optics are capable of extraordinary sensitivity levels in principle. Schardin [2] and Kean [146] give examples of one- and two-mirror system with $f_2 > 5$ m. Another example of a large single-mirror coincidence system with high sensitivity is given in the next chapter. D. D. Maksutov, of telescopy fame, used the schlieren technique to measure the gravity-

induced surface curvature of a pool of mercury, from which he was able to estimate the radius of the Earth [101,102].

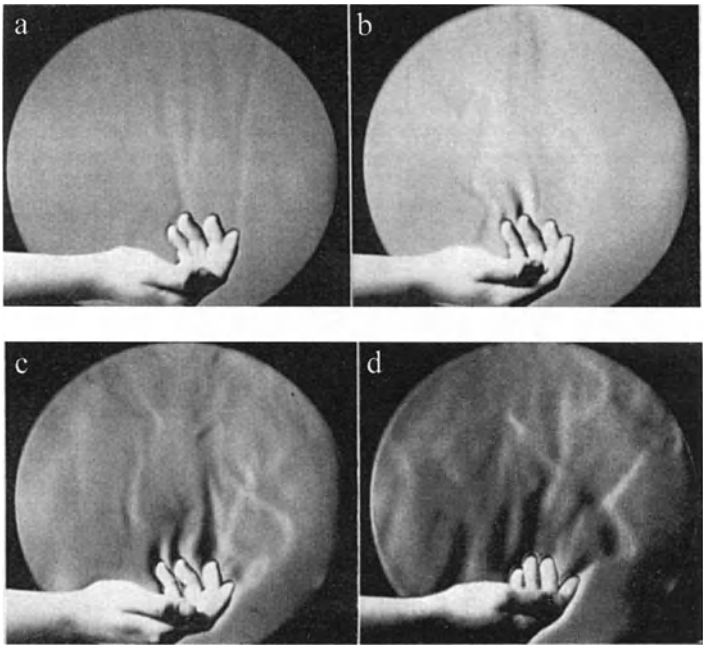

Fig. 3.12. Schardin's [2] images of thermal convection from a human hand with increasing sensitivity settings: **a** system range R= 40″, ε_{min} = 2″, **b** R= 20″, ε_{min} = 1″, **c** R= 5″, ε_{min} = 0.25″, **d** R= 2″, ε_{min} = 0.1″. Photographs reproduced by courtesy of Springer-Verlag.

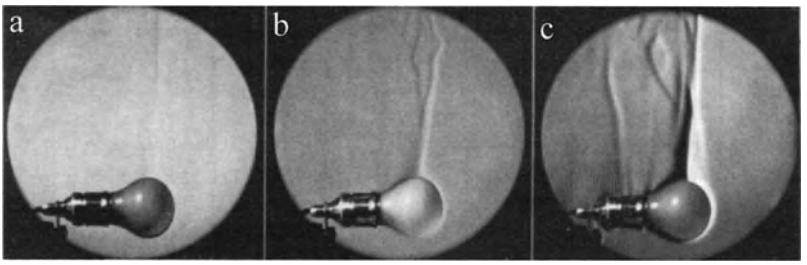

Fig. 3.13. Schardin's [2] images of thermal convection from a light-bulb with increasing sensitivity settings: **a** R= 160″, ε_{min} = 8″, **b** R= 80″, ε_{min} = 4″, **c** R= 5″, ε_{min} = 0.25″. The range has been exceeded just above the bulb in frame c by at least 3″. Photographs reproduced by courtesy of Springer-Verlag.

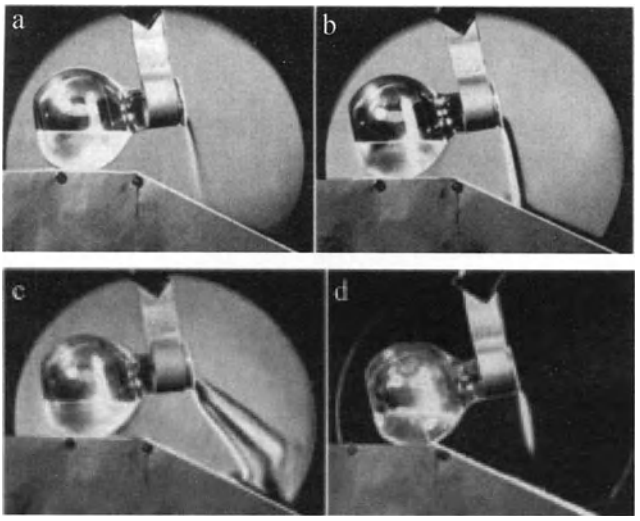

Fig. 3.14. Schardin's [2] images of ether vapor poured from a flask with increasing sensitivity settings: **a** R= 160″, ε_{min} = 8″, **b** R= 20″, ε_{min} = 1″, **c** R= 5″, ε_{min} = 0.25″, **d** ε_{min} = -20″. In frame **d** the knife-edge was deliberately set so that all refractions of strength less than ε_{min} = -20″ were blocked. While producing a poor visualization of the phenomenon, this is sometimes done in order to measure the strongest refractions accurately.

Schardin's [2] fine examples of visual schlieren sensitivity are reproduced here in Figs. 3.12-3.14. The photographs were made with a single-mirror off-axis schlieren system of the type shown in Fig. 3.9, having an effective focal length of 5.15 m. Schardin recorded the unobstructed source-image height for each frame, then calculated both the measuring range R and the minimum-detectable refraction ε_{min} in arcseconds (denoted in the figure captions by double-prime marks). Studying these 60-year-old photos is still an important exercise in learning the schlieren technique by associating the visual appearance of the images with the corresponding refraction angles ε. Violating the measuring range is likewise illustrated.

3.2.3 The Limits of Sensitivity

> In a vacuum there is nothing left to photograph.
> *W. F. Hilton* [122]

Another issue in examining schlieren sensitivity is the minimum discernable contrast ΔE/E in a schlieren image. In Eqn. 3.6, for a given amount of knife-edge cutoff, this threshold determines the least-detectable refraction ε. Schlieren users never seem to get quite enough sensitivity, so the limits of possibility are important to define and understand.

Schardin [2] found $\Delta E/E$ = 5-8% just detectable, but 10% easily so. Speak and Walters [126] could detect 4%, Goldstein and Kuehn [116] 5%. These contrast thresholds were given without indicating the background level, but its importance is shown in Fig. 3.15 [155,156]. For brightly-illuminated images, i.e. above ~ 10 candela/m^2, even a 2% threshold is possible. Weaker illumination raises the threshold dramatically, however. This holds several lessons for schlieren and shadowgraph imaging, but confirms that a contrast threshold of a few percent is reasonable for bright schlieren images.

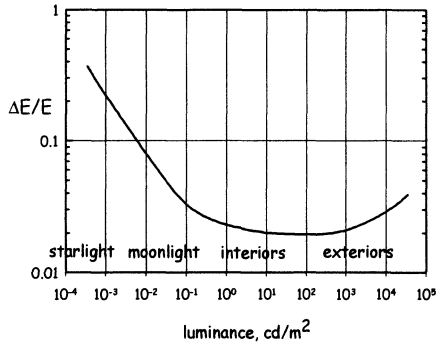

Fig. 3.15. The contrast sensitivity of the human eye as a function of field luminance, adapted from Blackwell [155]. Notation above the luminance axis indicates familiar light levels. The size and geometry of the contrast boundary in an image can also play a role. Results are shown for a target subtending 4 minutes of arc.

Given this contrast threshold and knowing f_2 and the amount of cutoff, one can use Eqn. 3.6 to find the threshold value of refraction ε in arcseconds. Routine values as low as 0.1″ are illustrated in Fig. 3.12, and much smaller claims have been made [146]. The warm convection from the human hand is widely regarded as a visual indicator of high sensitivity [2,65], but at several arcseconds it does not represent a remarkably-small refraction. In any case, threshold values of ε are strongly equipment-dependent.

Other measures are used and sometimes confused in efforts to cite a sensitivity threshold: Toepler claimed to detect 0.6 ° C or 1 part per million in refractive index [37], but did not say over what distance this change occurred. Barnes and Bellinger [65] made the same error, claiming to detect "a 1 ° C temperature change" (1 °C/cm in air, presumably).

By combining Eqns. 2.5 and 3.6 and accepting a 5% contrast threshold, one obtains [98],

$$\left.\frac{\partial n}{\partial x}\right|_{\min} = 0.05 \frac{n_0}{L} \frac{a}{f_2} \tag{3.8}$$

So the minimum detectable gradient – per geometric optics – depends on the medium, the schliere itself, and the schlieren apparatus. For a medium of given n_0, extensive schlieren along the optical z-axis are easiest to see; for if $L \rightarrow 0$, no schlieren will be seen in any case. Further, as amply demonstrated already, one wants a severe knife-edge cutoff and a long focal length f_2 for high sensitivity.

A few other considerations also matter: at high cutoff one can also extend the light-source width b in order to improve the background image illuminance [98]. Also, once a value of $\partial n/\partial x|_{min}$ has been established, schliere of limited extent in x satisfy this criterion with the least absolute change of n. In other words, sharp disturbances like shock waves are still visible long after the gradual ones – like expansion fans – have vanished.

Fluid dynamicists struggle especially with the lower limit of schlieren sensitivity when studying rarefied gas flows [2,98,122,157,158]. Holder and North [98] found that shock waves in air could still be observed by schlieren optics even at a 1% of standard atmospheric density. By analogy with glass testing, their experience indicates that a gradient of 4 λ/cm is needed for excellent schlieren contrast and ¼ λ/cm for detectability. But at 1/40 λ/cm, schlieren in glass are barely noticeable. One can use this knowledge along with Eqn. 3.8 as a rough guide to estimate $\partial n/\partial x|_{min}$, thence minimum gas-dynamic density levels. An example schlieren image of a rarefied hypersonic flow is given in Fig. 3.16.

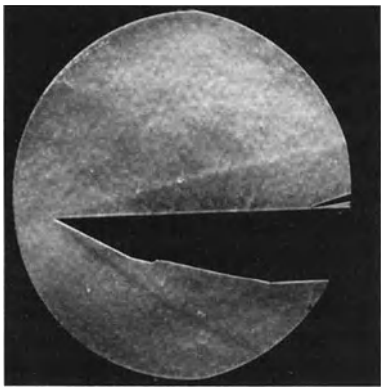

Fig. 3.16. Mach 10 rarefied airflow over a flat-plate test model in a hypersonic wind tunnel. Though there are other features in the flow, only the shock waves from the plate leading edge are visible in this schlieren photo due to low freestream density. Photo courtesy of the Princeton University Gas Dynamics Laboratory.

Nevertheless the geometric theory can only go so far in explaining and predicting the lower limit of schlieren sensitivity, for at high knife-edge cutoff, light diffraction plays a significant role. Schardin [2], Merzkirch [82,158], and Weinstein [159] have looked into this, with results to be discussed in Sect. 3.6.

According to Eqn. 3.6, ΔE/E is not a function of the dimensional background illuminance E, but the visual contrast threshold clearly is (Fig. 3.15). When feasible, increasing the luminous exitance (formerly called brilliance) of the light source raises the background level in a dark schlieren image, lowering the ΔE/E detectability threshold. Dark images are therefore always improved if E can be raised independently. When enough light is available, it may then be possible to increase the cutoff still further until diffraction effects take over. Conversely, from Fig. 3.15, attempts to raise the sensitivity by increasing the cutoff fail when the schlieren luminance drops below about 3 candela/m^2 [160].

Vasiliev [102] gives a list of strategies to achieve the best schlieren sensitivity. Other than the obvious minimization of a/f_2, the quality of each optical component needs careful consideration in order to maintain high sensitivity. Little more can be gained once the optical-quality threshold has been reached. Secondary issues like thermal expansion problems, vibration, and air thermals along the optical path outside test area also take their toll on ultimate sensitivity if allowed.

Finally, in the next section we consider post-processing effects on the schlieren image. Here, additional sensitivity can often be gained after all other strategies are exhausted.

3.2.4 Sensitivity Enhancement by Post-Processing

> The maximum possible contrast consistent with a uniformly gray background
> *W. F. Hilton* [122]

Digital image processing arose only in the last 20 years or so, and was not available for any of the classic works on schlieren methods [1-3,98,102]. Post-processing was then limited to what could be done in the darkroom. Thus the content of this section, while not new to image processing, is at least new to schlieren.

Since contrast is central to schlieren sensitivity, it was understood in the classic works that higher-contrast photographic media improved the sensitivity embodied in the recorded image. Further improvements could also be made later in the darkroom, if necessary, before image use or publication. Today digital image processing is much faster, less frustrating, and less messy than the darkroom, and has a far-broader range of useful tools [161,162].

Some of these tools are edge detection, thresholding and binarization, smoothing and sharpening, pseudocoloring, image correction and restoration, and quantitative image analysis for velocities, intensities, spectra, and feature identification. Since the present concern is contrast sensitivity, though, we limit our attention to methods that enhance image contrast.

Image contrast is about gray levels and how they are used. Typical digital schlieren images today – including many scanned originals reproduced in this book – are 8-bit images capable of resolving 256 gray levels from black to white. The eye, however, can only resolve about 20 of these levels, so superfluous information is present. A glossy 200x250 mm (8x10 inch) black-and-white photograph with 100 lines/mm resolution and an 8-bit grayscale contains four billion bits of information [161]. It is difficult to display it all, and certainly the information in a schlieren negative or original print is much more than is usually displayed digitally or in print. If we reduce the image to only 10 gray levels (3½ bits), a smaller digital file results but obvious contouring boundaries appear. At 20 gray levels or 4½ bits the image looks almost as good as the original. Thus the leeway exists in an 8-bit schlieren image to manipulate gray levels to enhance an image with inferior contrast, or to emphasize certain desired features at the expense of others.

Typical images at the size reproduced here are processed as digital files with 12 lines/mm (300 dpi) resolution, more than 500,000 8-bit pixels, and sizes of 0.5 to 1 Mb. At this writing, Pentium-class desktop computers have the speed and mem-

ory to process such images in near-real-time. Software for this purposes includes Adobe Photoshop, Micrografx Picture Publisher, and the NIH Image freeware for Macintosh platforms, among others. Given such tools, the typical operations found useful in improving schlieren images are linear contrast stretching, histogram equalization, and unsharp masking.

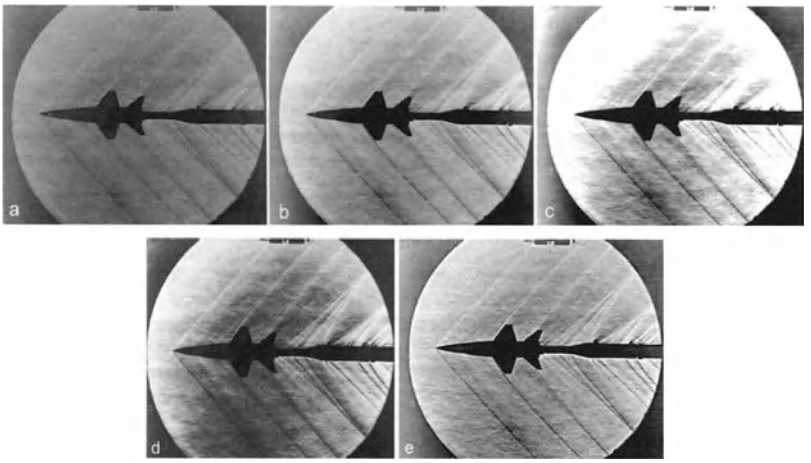

Fig. 3.17. Five versions of NASA-Langley photograph L-62-2577, a Mach 1.4 wind tunnel test of an X-15 hypersonic research aircraft model. **a** as scanned from original photo, **b** linear contrast stretch, **c** overstretch with clipping, **d** histogram equalization, **e** linear contrast stretch plus unsharp masking.

For purposes of illustration an example schlieren image is shown in Fig. 3.17a in its original form (scanned from a glossy photo). This "muddy" image uses only the first 187 of its possible 256 gray levels. A linear contrast stretch transforms the brightest pixel in the image to white, and all other pixels in proportion. The result, Fig. 3.17b, now shows the full range of gray levels from black to white. A useful brightening of the image results, and the flow features show better contrast. Most of the images in this book were contrast-stretched like this for consistency.

It can be overdone, though, if the stretch is carried so far as to clip highlight and shadow information to further enhance mid-tone detail. This is shown in Fig. 3.17c, where severe clipping of highlights violates Hilton's uniform background rule and loses some features of the flowfield.

Related to contrast stretching, but nonlinear, is the process of histogram equalization. Again the full grayscale range is used, but now each gray level is assigned the same number of pixels. The gray levels of the image remain in proper order, but are redistributed across the image histogram. The effect is more useful in some images than others; it is not very useful in this specific example, where Hilton's rule is again violated (Fig. 3.17d).

Finally, there is "unsharp masking." A copy of the digital image is blurred to remove all detail, then subtracted from the original. This removes slowly-varying gradations and enhances detail. In Fig. 3.17e it is applied after a linear contrast stretch. The oblique shock waves are enhanced, but so are the diffraction halos around the test model and the turbulence in wind tunnel window boundary layers. Nonetheless a contrast stretch plus a certain degree of unsharp masking is very effective in improving the schlieren sensitivity in this example.

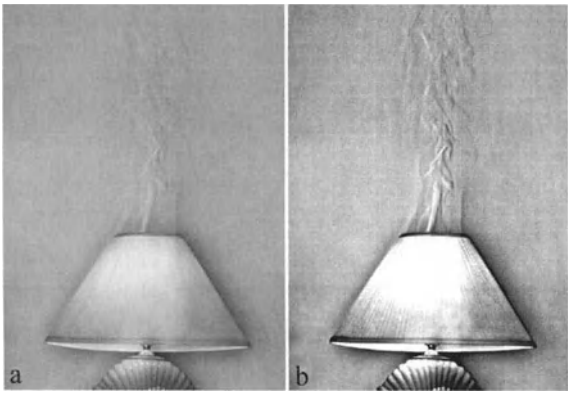

Fig. 3.18. Thermal plume rising from an incandescent lamp in the Penn State Full-Scale Schlieren Facility. **a** original image scanned from low-contrast Polaroid print, **b** enhanced version following a contrast overstretch with clipping and unsharp masking operations. See also Fig. 9.15c.

Weinstein [163] suggests, moreover, that post-processing by combined contrast stretch and unsharp masking can increase the effective sensitivity of many schlieren images after image acquisition. The best results are had with weak originals such as Fig. 3.18a. This was overstretched with clipping to emphasize the narrow tonal range of the convective plume, then further enhanced by unsharp masking to yield Fig. 3.18b. In this case front-lit features of the lamp itself are also overstretched, but that can be avoided by masking selected portions of the image. Fig. 3.18b displays much of the schlieren information that is present in the original but of insufficient contrast to be seen clearly.

Even more can be done if a *tare* or background image is taken without the schlieren object present. Figs. 3.19a and b show the tare and original shadowgrams, respectively, of a Freon jet discharging into air [163]. Unsharp masking, in image c, brings out the detail of the turbulence and the background as well. By subtracting the tare image and stretching the contrast, only the jet features remain in image d. Subtracting a side-offset image and further contrast stretching produces a relief effect, image e. Finally the background is added back in Fig. 3.19f to show important information like the nozzle shape, etc. This example goes beyond what is necessary or desirable in many cases, but it does show the range of possibilities in digital post-processing. It also makes the point that tare images are just as important now as they always were, even in the early days of schlieren imaging when this sort of processing was not yet imagined.

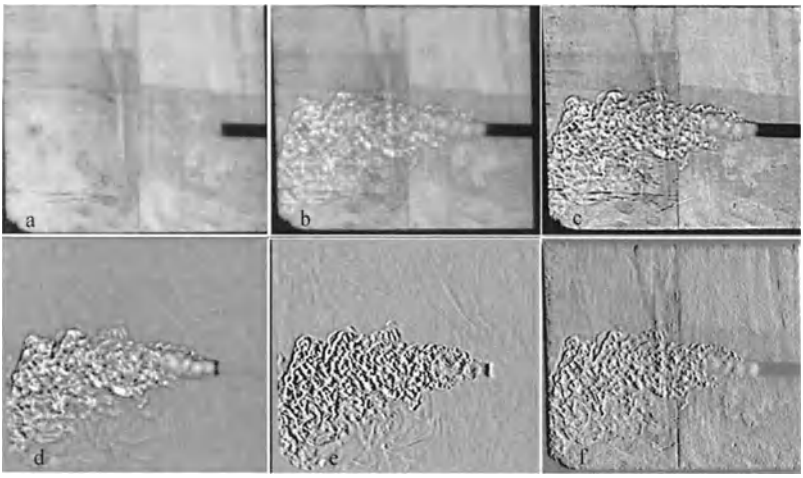

Fig. 3.19. Five versions of a shadowgram of Freon jet mixing in air [163] (see text).

This section has given only a brief summary of what the broad field of digital image processing has to offer schlieren imaging and shadowgraphy. Clearly, though, the ultimate sensitivity is not often reached when a schlieren image is first acquired. If information is there but is not well-revealed, then image enhancement can be quite useful. But if the information is not there in the first place, then bringing it forth in post-processing becomes an exercise in the paranormal: well beyond the present scope.

3.3 Measuring Range

3.3.1 Definition of Measuring Range

As already introduced in the discussion of Fig. 2.6, the measuring range R of Toepler's schlieren technique is the range of schlieren refraction angles ε over which a definite, gradual change in image illuminance occurs [66,98,102,160,164]. This corresponds to the range over which elemental light source images from various points in the test area remain only partially cut off by the knife-edge. Once the source image has shifted entirely off of – or onto – the knife-edge, then the corresponding image point has reached its brightest or darkest value, respectively. Larger deflection angles no longer produce a change in image illuminance. We will call these conditions *over-ranging* above the bright limit and *under-ranging* below the dark limit. The linear range of schlieren illuminance between these limits is

the measuring range or "latitude" of the instrument [66]. It is best reckoned in units of refraction angle ε, i. e. arcseconds. Alternatively it can be measured in terms of displacement Δa in the cutoff plane, which is related to ε through Eqn. 2.6.

3.3.2 Adjustment of Measuring Range

One should usually adjust the range of the Toepler schlieren system so that the maximum refraction angles ε produce approximately "black" and "white" responses in the image [66,122]. This yields maximum contrast, but any larger ε will lose detail in "highlight" or "shadow" regions. One might then say that the instrument has been "tuned" to the phenomenon under observation. Guidance on how to make an *a priori* estimate of ε is given in the next section.

The range of Toepler's schlieren system is varied most directly by adjusting the source slit height, h. For a horizontal 50% knife-edge cutoff, Eqn. 3.6 yields:

$$\varepsilon_{y_{max}} = \frac{\Delta E}{E} \frac{h}{2f_2} \tag{3.9}$$

With a = h/2 at 50% cutoff, this knife-edge setting has equal range in both directions perpendicular to the edge.

While 50% cutoff is universally recommended on this basis, it was already shown in Fig. 3.11 that this setting is not very sensitive when a broad source slit is used. To increase sensitivity at 50% cutoff, the source slit must be narrowed. Thus high sensitivity entails a small measuring range at 50% cutoff, since a is to be minimized per Eqn. 3.7. This leads to a second "universal" statement in the literature: sensitivity and measuring range are inversely proportional. Weinberg [66], however, only partially agrees: "Although sensitivity need not be inversely proportional to range, an increase in one quantity is invariably paid for in some way by a decrease in the other." Kean [146] adds that inverse proportionality only occurs in systems where the sensitivity is constant with respect to a (see Sect. 5.1.2).

In actual practice a broad source slit is commonly used to gain overall illumination, but the cutoff is frequently raised to the vicinity of 90% for improved sensitivity. This causes the instrument to have an uneven measuring range: wide for brightening of the image but quite narrow for darkening. Sensitivity being the paramount concern, this range anomaly is usually ignored. Even when over- or under-ranging occurs, it seldom misleads those familiar with their subjects of observation. But when unfamiliar subjects are first examined, consider taking a variety of images with different knife-edge orientation, sensitivity, and range. Also for the quantitative schlieren measurements covered in Chap. 10, exceeding the measuring range produces spurious and unacceptable results.

Measuring-range anomalies of two distinct types are likely to appear in schlieren images. The first type arises when the source slit is simply too narrow

for the range of light deflections encountered. As exemplified in Fig. 3.20a, large regions of the image can appear binarized in black and white with no apparent schlieren sensitivity except at their boundaries. This example is an extreme case, and should be compared to the images of the same flow having a broader measuring range in Fig. 5.10 and Color Plate 4.

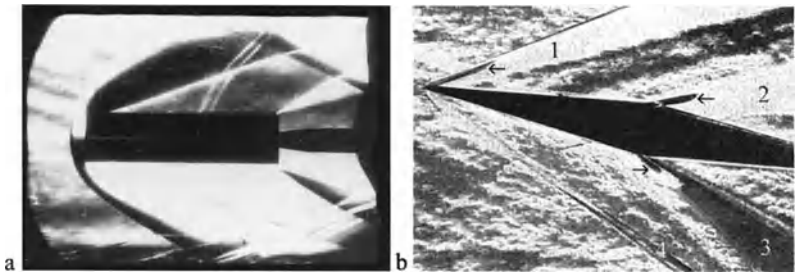

Fig. 3.20. **a** Over-ranged schlieren image of Mach 3 airflow past a blunt cylindrical test model (photo by author). **b** Full-span 2-D double-wedge airfoil model in a Mach 3 airstream (photo courtesy of the Princeton University Gas Dynamics Laboratory).

The second type of anomaly is described by Mair [164], who took an interest in schlieren measuring-range issues in wind tunnel testing. He found that strong gas-dynamic density gradients can cause dark regions to appear in parts of the schlieren image that would normally be bright. An example is Fig. 3.20b, where a horizontal knife-edge enters the schlieren beam focus from below. The three Prandtl-Meyer expansion fans labeled 1-3 have exceeded the measuring range, since no flow details are visible within them. Nonetheless, curious dark bands – indicated by arrows – occur near the origin of each fan. Mair found that these features arise from refractions strong enough not only to over-range the system, but also to actually deflect light onto the knife-edge mount, lens mount, or some other system aperture stop. Such rays are blocked, creating the anomalous dark features. Mair discovered the source of this anomaly by taking pairs of images with cutoffs on opposite sides of the schlieren focus, then examining them for lapses of symmetrical illuminance.

In gas dynamics, shock waves are often the culprits in such range violations. Mair [164] notes that a strong shock reflects glancing light like a mirror. A shock that strong can cause a 2000-arcsecond refraction (more than ½ °). In large wind-tunnel schlieren setups this leads to a displacement Δa of several centimeters in the cutoff plane. The resulting inadvertent-cutoff anomaly is also shown in Fig. 3.20b, where the lower oblique shock (labeled 4) contains dark lines even tho ugh it should be entirely brighter than the background.

Avoiding cases that violate the measuring range of the Toepler schlieren system is not enough, though; the observing/recording instrument must also be taken into account. If it cannot accept or reproduce the full measuring range due to its

threshold or saturation limits, then the overall difficulty still remains. Video "blooming" is one common example, in which the image brightness saturates the video detector.

Finally, Holder and North [93,98] pioneered the used of the *graded filter*, a simple means to extend measuring range at the cost of some sensitivity. More on that topic is given in Sect. 5.1.1.

3.4 Estimating the Sensitivity and Range Required

According to Weinberg [66], "...if it is desired to optimize both range and sensitivity, it is most convenient to estimate the maximum deflection to be expected..., and to arrange the range of the system at that value, thereby automatically utilizing the optimum sensitivity condition for the phenomenon under test." Several authors have given advice on how to make this estimate [2,62,159,164]. Here, we begin with a simple refraction model for schlieren in gases.

Keagy and Ellis [138] and Weinstein [159] have adapted the thin-lens approximation of geometrical optics, Sect. A.3.3, to estimate the refraction due to a gas bubble in air. Recalling Fig. 2.2a, a spherical bubble of denser gas has a focusing effect, like a weak positive lens. The greatest refraction occurs at the periphery of the bubble, where it is given approximately by:

$$\varepsilon_{max} = 2\left(\frac{n}{n_0} - 1\right) \tag{3.10}$$

Here n is the refractive index inside the bubble and n_0 is that of the surrounding atmosphere. The numerical value of ε_{max} is in radians according to the small-angle approximation (Sect. A.2.1), but is routinely converted to arcseconds, by multiplying by 206265, for convenience.

From the Gladstone-Dale Law, Eqn. 2.1, we can write an expression for n/n_0 as a function of gas-bubble density ρ and the surrounding atmospheric density ρ_0,

$$\frac{n}{n_0} = \frac{1}{n_0} + \frac{\rho}{\rho_0}\left(\frac{n_0 - 1}{n_0}\right) \tag{3.11}$$

Using this and Eqn. 3.10 we can see, for example, that a 2% change from atmospheric density is expected to cause about 2.4 arcseconds of refraction. A sensitive schlieren system is needed to reveal it. Likewise for an oxygen bubble in air, with $n_{O_2} = 1.000297$, 2 arcseconds refraction is estimated. A helium bubble in air, on the other hand, is easily observed with n = 1.000036 and a refraction angle ε_{max} over 100 arcseconds.

If air motion is the subject of study, one can similarly estimate refraction angles based on air's compressibility. For example, the 2% density change just discussed corresponds, by way of elementary isentropic gas-dynamic theory [165], to a Mach number of 0.2. Taking the speed of sound at ambient conditions to be 340 m/s, Mach 0.2 in air is equivalent to 68 m/s, 245 km/hr, or 152 miles/hr. This explains why we do not use schlieren optics to examine the airflow around automobiles unless they are very speedy, unless heat transfer from the vehicle is involved, or unless we add thermal or concentration tracers to the airflow as described later in Sect. 5.8.3.

But for a bullet traveling just under the speed of sound, the same gas-dynamic theory predicts a 56% density change, yielding almost 70 arcseconds of refraction per Eqns. 3.10 and 3.11. The field of ballistics, as we saw in Chap. 1 and will see further, can make good use of Toepler's schlieren system.

For supersonic gas motion, shock waves outweigh most other phenomena because of their strong refractions. Schardin [2] applied the Rankine-Hugoniot shock wave theory [165] to calculate and tabulate Δn for shock waves in air. In terms of shock Mach number M_s, his results show that ε in arcseconds is closely approximated by $200(M_s - 1)$ up to about Mach 2.2. Nonlinearity sets in at higher Mach numbers, and for very strong shocks in air, dissociation and eventual ionization of O_2 and N_2 occur in the hot region after the shock.

But even weak shock waves are readily observed by schlieren optics. For example, a schlieren sensitivity of 2 arcseconds is able to reveal shock waves traveling at only Mach 1.01, which is barely supersonic and just beyond the realm of loud sound waves. Such weak shocks are produced, for example, by the burst of a toy balloon (see Fig. 9.18d and Color Plate 5) or by the explosion of the smallest of firecrackers [166].

For high-speed wind-tunnel work, Mair [164] gives an estimate of refraction in a Prandtl-Meyer expansion and Weinstein [159], using Eqn. 3.10, examines the oblique shock wave from a 10° wedge over a Mach number range. This shock is clearly visible with $\varepsilon > 100$ arcseconds under typical testing conditions at Mach 2 in air. At Mach 10, 40 bar and 2000 K stagnation conditions, however, only about one arcsecond of refraction is expected (see Fig. 3.16).

Weinstein [159] recommends $\varepsilon_{min} = 16$ arcseconds and a measuring range of over 300 arcseconds as general guidelines for high-speed wind-t unnel testing. He also notes that sensitivities better than 4 arcseconds should be obtained indirectly using the post-processing techniques described in Sect. 3.2.5.

Finally, for schlieren investigations in liquids and solids, n vs. ρ relationships were briefly discussed in Sect. 2.1 and are treated in more detail by Merzkirch [82]. Comparing the 47-arcsecond refraction from a 1 K temperature change in water with the 3.6-arcsecond refraction from a 10 K change in room air serves as a good example [159]. Water has 1195 times the refractivity of air, but only 129 times the change in refractivity per degree K. Thus schlieren sensitivity is almost always adequate in the schlieren observation of liquids, but the measuring range can easily be exceeded.

3.5 Resolving Power

The resolving power, or resolution, of an optical system is its ability to reproduce fine detail in an image. It is commonly measured in lines/mm (sometimes line-pairs/mm) or arcseconds of angular separation between points just resolvable by the optics. Vasiliev [102] considered the issue for schlieren optics, and distinguished resolution limits due to optical aberrations R_a, photographic materials R_{ph}, and knife-edge diffraction R_d.

It is unlikely that the diffraction limit of resolution [167,168] is often reached in schlieren imaging, since this typically requires resolving better than 100 lines/mm or discriminating points less than one arcsecond apart. The optical quality of the system components, before any photography or knife-edge cutoff is applied, sets a practical resolution limit R_a. For example, tests with the small z-type schlieren apparatus of Chap. 8 show that about 30 lines/mm can be resolved in the test area under optimum circumstances. Similarly, Vasiliev [102] reveals that former Soviet schlieren instruments like the IAB-451 can only resolve 10 lines/mm due to aberrations of the optical components. Ershov [169] lists several such instruments with resolving power in the 1-10 lines/mm range.

In practical terms, high image resolution is not usually so important in schlieren imaging as high sensitivity, adequate range, and uniform cutoff. Given typical field diameters of tens of cm, acceptably-sharp schlieren images result when the resolving power of the optics is a few lines/mm. Besides, as we shall see, diffraction at the knife-edge imposes a more serious resolution limit R_d at high sensitivity settings. For high-sensitivity work at near-full cutoff, however, the unobstructed source-image height a may be only a few μm. If the schlieren field optics are not capable of resolving this small dimension, then they place an effective upper limit on system sensitivity even before diffraction takes over. More on this topic is given in Sect. 4.3.4.

The resolution limit due to the recording medium, R_{ph}, should likewise not normally be a limiting factor except perhaps where small images are necessary, e.g. in cinematography and videography. The effective resolution of modern photographic films is 50-300 lines/mm, with 100 lines/mm being typical in schlieren photography. Only in an extreme case of small image size and grainy film processing is this likely to be more limiting than R_a.

Not so for videography, however (see Sect. 7.3.2): the prevailing RS-170/NTSC North American and Japanese standard for broadcast video is low-resolution, providing only 512×384 pixels [170]. Suppose one images a 108-mm-diameter schlieren field on the video sensor so as to use all 384 vertical pixels; the resulting video schlieren image resolves about 2 line-pairs/mm in the schlieren test area. This usually limits the image resolution beyond all other considerations, but help may eventually be on the way in the form of High-Definition Television. Higher-resolution CCD cameras are already available, of course, with 1000 ×1000 pixel resolution or better, but these are not compatible with the ubiquitous broadcast-video standard.

Finally, Vasiliev [102] recommends capturing large schlieren images to minimize resolution loss due to optical aberrations and film grain. Hosch and Walters [171] also require at least a full-sized image to achieve 10 lines/mm resolution. As a concrete example, the venerable former-Soviet IAB-451 instrument [102] has a 230 mm field diameter. With a 24-mm-diameter image, R_a = 5 lines/mm and R_{ph} = 10 lines/mm. The combined effect yields 3.3 lines/mm test-area resolution at low knife-edge cutoff settings. But, as the cutoff increases toward 100%, the resolution limit due to knife-edge diffraction, R_d, eventually overpowers all other considerations. That issue is considered next.

3.6 Diffraction Effects

> Schlieren effects are geometrical optical phenomena. When the wave nature of light intrudes and produces observable effects, these effects must be treated as errors to be removed if possible.
>
> *Lee Kean* [146]

Actually, Kean's 1962-vintage viewpoint on diffraction is no longer current. Until recently, a proper treatment of the physical-optics aspects of schlieren imaging required laborious hand-calculations, now well-handled by computer (See App. B). Moreover, diffraction is now recognized as an integral, even fundamental part of the schlieren image-formation process, though indeed still a roadblock to high sensitivity and to some quantitative measurements.

Two diffraction effects are of chief concern: the diffraction of light in the test-area, creating halos in the image, and the diffraction of the light-source image at the knife-edge, which limits schlieren sensitivity and resolution.

3.6.1 Diffraction Halos Due to Opaque Edges in the Test Area

A bright band or *halo* about opaque objects in the schlieren image was first observed by Toepler [3], who identified it with light diffraction. Schardin [1,2] explained it well with an approximate theory and physical examples. Later calculations [66,102,126,149] based on Rayleigh's [172] theory of Fraunhofer diffraction, though awkward and one-dimensional, verified Schardin's explanation.

Any opaque edge in the schlieren test area diffracts light broadly in the direction perpendicular to that edge. In the cutoff plane, this diffracted light lies in higher-order diffraction bands outside the geometric light-source image, thus partially evading cutoff by the knife-edge. The schlieren image, being optically conjugate to the test area, "reassembles" this diffracted light at the position of the original opaque test-area edge. As the knife-edge cutoff is advanced, direct illumination of the schlieren image decreases as described earlier, but not so the diffracted light. A narrow, bright diffraction band or halo thus appears around all

opaque edges in the test area that have components parallel to the knife-edge. Its contrast increases with knife-edge cutoff, since the background illuminance is falling, and its appearance reveals that significant cutoff has occurred (see Figs. 3.11g and h, and other examples shown earlier in Figs. 3.16-3.18).

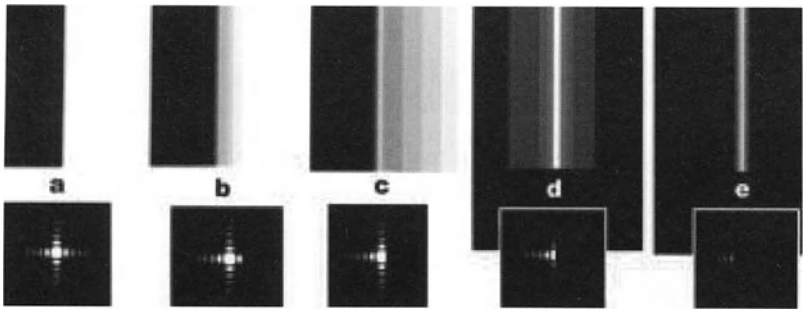

Fig. 3.21. The schlieren-image appearance of a vertical opaque edge in a square test-area aperture, computed for coherent light using GLAD 4.6 (see Apps. B and D). Insets show the "source image" diffraction pattern being progressively cut off from the right by the vertical knife edge in frames a-e. Once the central maximum of the source image is blocked (after frame c), only the diffraction halo of the edge remains in the schlieren image. The stepwise illumination in frames b and c is an artifact of the limited gray levels available in the computed results.

Even at 100% cutoff of the light-source image and beyond, diffracted light still passes the knife-edge to form halos against a black background in the schlieren image (see Figs. 3.21 and 3.22b). Window flaws, dust particles, and a horde of other artifacts all become visible by diffraction once the direct schlieren beam is blocked. Depending upon the level of beam coherence, interference fringes may also appear in the diffraction halos. Since the entire area of the light source contributes to diffraction in the test area, a broad source height h worsens these halo and artifact effects [146].

Despite all this, Schardin [1,2] makes it clear that diffraction halos are not a very serious problem. They outline opaque objects with thin white lines, but do not usually otherwise obscure the schlieren image. One must take care not to confuse them with other bright bands that can appear (e.g. due to test-model misalignment or laminar boundary layers [149], to be illustrated later in Sects. 6.1.3 and 7.2.3). Long-time users of the schlieren technique learn to expect the appearance of diffraction halos as the knife-edge is advanced, and treat them like old acquaintances. Unfortunately this is not the case for the more-disruptive diffraction phenomena that can occur at the knife-edge.

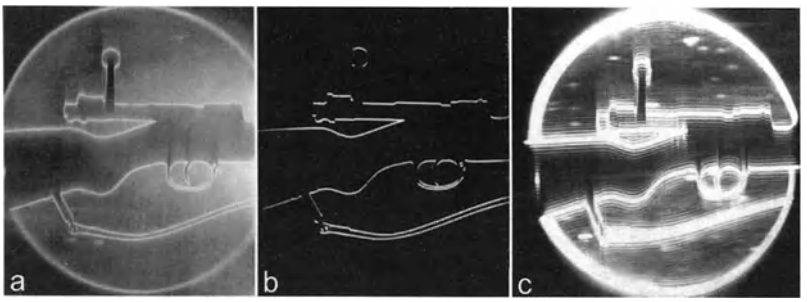

Fig. 3.22. Schardin's [2] images of diffraction halos about a rifle mounted in the schlieren test area. **a** Near 100% cutoff and **b** beyond 100% cutoff by a horizontal knife-edge in white-light illumination. **c** Image-smearing effect of a narrow slit in the knife-edge plane, 100% cutoff, monochromatic light. Photos reproduced courtesy of Springer-Verlag.

3.6.2 Diffraction at the Knife-Edge

The Diffraction Limit of Schlieren Sensitivity. Diffraction provides a natural limit to attempts to increase sensitivity indefinitely by increasing the knife-edge cutoff [2]. Of course, the geometric-optical definition of sensitivity, Eqn. 3.7, does not show this, but rather predicts infinite sensitivity as the unobstructed source image height, a, tends to zero. Recourse to physical optics is necessary to understand what actually happens in this vicinity. The mathematical analysis has been presented by several authors [66,102,126,149], but quickly gets out of hand. We will forego that here in favor of a physical explanation illustrated by experimental, analytical, and computational results.

The unobstructed source image height, a, becomes small as the knife-edge cutoff is advanced. Eventually, a begins to behave like a narrow slit [2]. One side of this "virtual" slit is the knife-edge itself, while the other is the exposed edge of the light-source image parallel to it. The consequences are not as bad as those of an actual narrow slit with two real knife-edges, since diffracted light from the test area is only blocked on one side by a real knife-edge. Nonetheless, the beam approaching the cutoff contains all the information necessary to create a sharp schlieren image, so one must beware not to block too much of it, nor to disrupt it by what amounts to narrow-slit diffraction.

When this happens, light diffracted by edges in test area is diffracted a second time in the cutoff plane. Near full cutoff, this smears the image resolution and creates a diffraction "shadow" emanating perpendicular to the edges of objects in the test area [2]. Examples of this are given in Figs. 3.22a and 3.23. By competing with illuminance variations from refractions ε in the test area, diffraction at the knife-edge thus counteracts any sensitivity gain beyond a certain amount of knife-edge cutoff. This effect is worst near opaque test-area boundaries, and for the smallest schlieren objects no matter where they are located in the field.

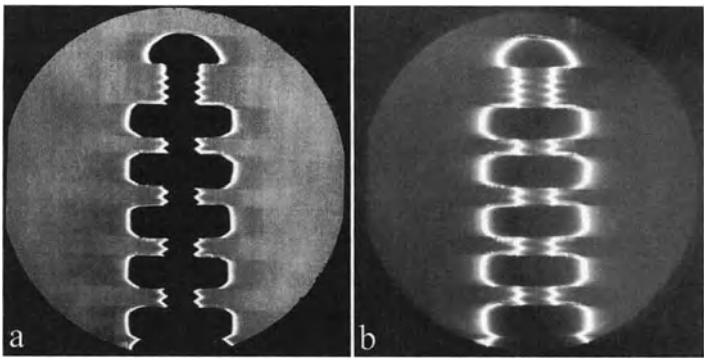

Fig. 3.23. **a** Schlieren image of a bolt with threaded nuts in the test area, vertical knife-edge, h = 1.5 mm, b = 4 mm. **a** 95% cutoff, revealing diffraction "shadows" **b** ~100% cut-off reverses the diffraction shadow illumination. Photos by Heather Ferree.

Finally, at about 100% knife-edge cutoff, the screen darkens sufficiently that there is an illumination reversal in the phenomenon of diffraction shadowing. As shown in Fig. 3.22b, bright shadows now extend into the darkened schlieren field. This is explained once again [2,146] as a second diffraction, at the knife edge, of light already diffracted once at the edges of solid objects in the test area. The diffraction halos – now the brightest parts of the image – are smeared across adjacent darker areas of the schlieren field.

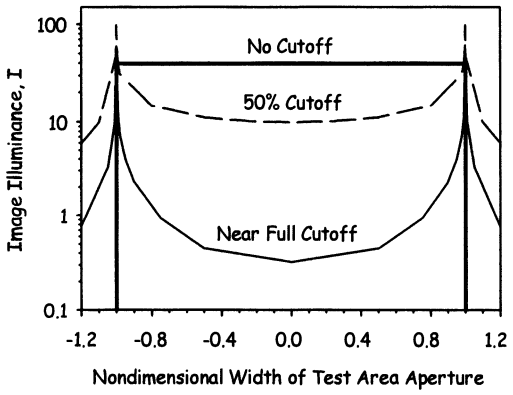

Fig. 3.24. Plot demonstrating diffraction smearing of the edges of a rectangular aperture in the schlieren test area. As knife-edge cutoff is increased, halos appear at the edges and a diffraction "shadow" extends across the open aperture. Adapted from calculations by Speak and Walters [126].

The 1954 hand-calculated example of Speak and Walters [126] also serves to illustrate this phenomenon (Fig. 3.24). The image illuminance I is shown on a logarithmic scale to better represent what the eye or photographic film sees. Without any knife-edge cutoff, a rectangular vertical aperture in the test area appears as a

square-wave when photometrically sampled along a horizontal "cut." At 50% cutoff a halo begins to form at the edges of the aperture, but most of the aperture is still almost evenly-illuminated. Near full cutoff, however, the aperture illuminance becomes nonuniform. A minimum level of I in the center rises steadily to strong peaks – halos – at the aperture edges. Small or weak schlieren objects inside the aperture must compete with this background illuminance gradient, due to diffraction, in order to become visible.

Slit-like effects have been shown for diffraction at the knife-edge near full cutoff, but the effects of an actual slit in the cutoff plane are more serious still (Fig. 3.22c). The slit cutoff is not considered here to be a part of Toepler's method, but rather is covered separately in later chapters.

The Diffraction Limit of Observable Schlieren Size. Several classical authors on schlieren methods have described diffraction effects as a function of the size of a schlieren object [2,66,126]. As Weinstein [159] puts it, "A flow feature may be thought of as a small aperture through which we re-image a portion of the light source onto the cutoff." For small-enough schlieren objects, diffraction spreads the corresponding elemental source image significantly in the knife-edge plane. This has the effect of reducing the amount of cutoff for these objects, hence reducing the effective sensitivity. In this manner sensitivity is diminished upon decreasing the feature size, and schlieren of small lateral extent can be lost entirely due to diffraction smearing [66,126].

Schardin [2] derived a simple expression for this from the diffraction blur that occurs at a "sharp" light/dark boundary in an image. The *unsharpness angle* ε_u subtended by that blur is proportional to the wavelength of illumination, λ, and inversely proportional to the size of the schlieren object, d, thus

$$\varepsilon_u = \xi \frac{\lambda}{d} \tag{3.12}$$

where the proportionality constant ξ has been added to emphasize that the detectable level of ε_u, given a certain combination of λ and d, is somewhat arbitrary.

Schardin then generalized this relationship to predict the minimum observable test-area refraction angle as a function of the diameter of the schlieren object. In this role it is admittedly only a rough guide, but many have accepted it [82,102,119,158] and there is only one known dissenter [146].

Since it is problematical to test this relationship experimentally, the physical optics code GLAD 4.6 (see Apps. B and D) was used to perform a "computed experiment": a circular phase-ripple schlieren object was illuminated with coherent light at $\lambda = 0.6328$ μm, as discussed in Sect. B.2. d, the wavelength of the ripple, was varied over two orders of magnitude, while the ripple phase amplitude was reduced until it could no longer be resolved at 50% knife-edge cutoff. Though the latter step was a subjective judgment, useful results were nonetheless generated for comparison with Eqn. 3.12. These results are plotted in Fig. 3.25.

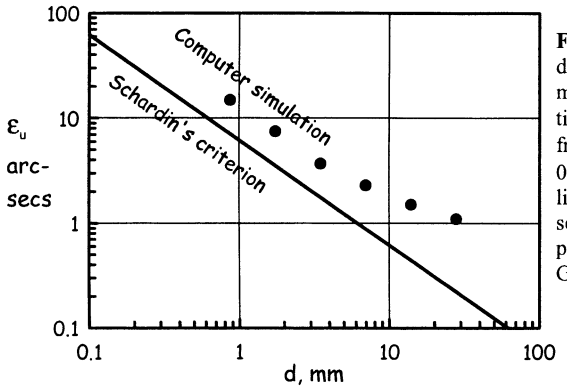

Fig. 3.25. Plot of Schardin's criterion for minimum observable refraction angle ε_u due to diffraction, Eqn. 3.12, λ = 0.6328 μm, ξ = 1 (solid line). Solid points represent results obtained with physical optics code GLAD 4.6 at 50% cutoff.

Nothing can be concluded from the difference in level of ε_u in Fig. 3.25, but Eqn. 3.12 and the six computed points are in substantial agreement regarding the trend. There is only the suggestion in the latter that Schardin's equation may not persist for large schlieren objects with extremely-small refraction angles. In any case, Eqn. 3.12 and Fig. 3.25 are rough guides to the effect of diffraction on the resolution and sensitivity of Toepler's schlieren technique for schlieren objects.

An Example of the Resolution/Sensitivity Compromise. The diffraction constraint on schlieren image resolution, R_d, arises from the knife-edge cutoff of part of the *Fourier spatial frequency spectrum* [171], which is the combination of elemental source images and diffracted light in the schlieren cutoff plane (see App. B). The practical effects, however, are confined to cases of moderate-to-high knife-edge cutoff, where they also obstruct increasing sensitivity as noted earlier.

Traditionally, the resolution of optical systems is tested using a standard target with sets of parallel clear and opaque bars [167,171], e.g. the 1951 USAF resolution target. This test was done using the 10.8-cm-aperture f/8 z-type schlieren system described in Chap. 8. A tungsten-halogen lamp was imaged upon a slit of 1.5 mm width to illuminate the system. The target was imaged at extreme magnification by the second field mirror with no focusing lens. Resolution of test bars parallel to the knife-edge was observed on a ground-glass screen using an eyeloupe magnifier as the knife-edge was advanced. The results are shown in Fig. 3.26

Over 30 lines/mm could be resolved in this test with no cutoff, giving evidence of high quality in the $\lambda/8$ parabolic field mirrors. This resolution degraded slowly up to 50% cutoff (a = 0.75 mm), then more swiftly. In the 70-80% cutoff range the ability to distinguish clear vs. opaque bars was rapidly lost, though diffraction halos remained at their edges. In the 90% cutoff range the resolution fell below 1 line/mm. The resolution of bars perpendicular to the knife-edge remained around 10 lines/mm even at high cutoff, however. Similar results were shown by Hosch and Walters [171] for the case of a slit cutoff of variable width and position.

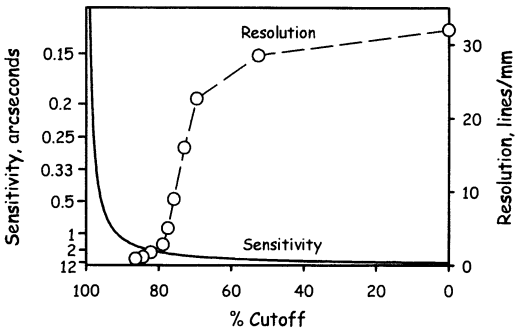

Fig. 3.26. The resolution and sensitivity of a 10.8-cm-aperture f/8 z-type schlieren system, plotted vs. % knife-edge cutoff. Resolution is shown by open circles, while sensitivity is shown by a solid line. In converting sensitivity to refraction angle ε in arcseconds, a 5% visual contrast threshold was assumed. h = 1.5 mm.

Fig. 3.26 further reveals that the system sensitivity increases only slowly from zero cutoff to the "knee" of the curve, at about 90% cutoff in this example. Beyond that, as Schardin [2] says, the sensitivity "increases amazingly with any further cutoff." But since the plotted sensitivity curve is purely from geometric optics (Eqn. 3.6), it becomes unrealistic somewhere in this range. Certainly the extraordinary theoretical sensitivity it indicates is offset by the practical loss of resolution just discussed. Eqn. 3.12 further predicts that fractional-arcsecond sensitivity can only be had with this schlieren system when the diameter of the schlieren object approaches that of the field mirrors.

One may compare the sensitivity curve of Fig. 3.26 with the images shown previously in Fig. 3.11, obtained under the same conditions. The ultimate sensitivity occurs around 95% cutoff ($a \approx 75$ μm), and is about 1 arcsecond. Though 0.1-arcsecond sensitivity should occur at 99% cutoff according to geometric optics, it is not attainable in practice due to the diffraction effects described here.

Conclusion. We have seen that the implications of physical optics are not too restrictive for qualitative schlieren visualizations, where excellent sensitivity can be obtained before diffraction finally takes over. The consequences are more restrictive, however, for the quantitative evaluation of schlieren images by densitometry at high sensitivity [2,171]. This procedure, considered in detail in Chap. 10, is disrupted when nonuniform image illuminance occurs due to diffraction shadows. Severe practical sensitivity limits thus occur in quantitative work.

In summary, Wolter [119] characterizes diffraction effects on schlieren sensitivity by invoking a form of Heisenberg's Uncertainty Principle: "The point of origin of photons and the direction they have taken are always scattered in the measurement of both values, such that the product of their uncertainties is at least equal to the wavelength of illumination."

3.7 Magnification and Depth of Field

Compared to diffraction and sensitivity, magnification and depth-of-field in the schlieren image are simple manifestations of geometric optics. The thin-lens approximation (Sect. A.3.3) is thus used in what follows.

3.7.1 Image Magnification and the Focusing Lens

Without the use of a focusing lens, the schlieren field lens or mirror still forms a real image of the test area so long as the distance ($s + f_2$ in Fig. 3.27) between the two is greater than f_2, the focal length of the second field element. In this case the image magnification m, i.e. the ratio of image to test-area diameters, is given by:

$$m = \frac{f_2}{s} \tag{3.13}$$

This is usually inconvenient, though; since s grows large in order to demagnify the image, the overall length of the optical train becomes unwieldy.

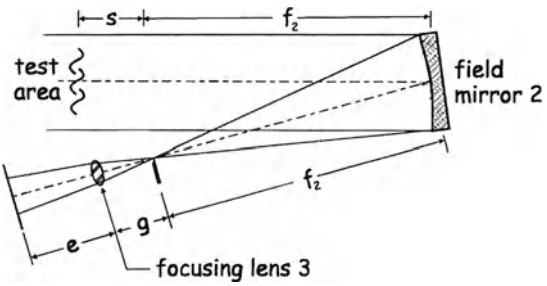

Fig. 3.27. Diagram of the second field mirror and analyzer section of a z-type schlieren system showing notation regarding magnification and the focusing lens.

Including a focusing lens allows one to the control the image size independently. The image diameter for direct viewing on a ground-glass screen should be on the order of 10 cm, whereas for film or video recording it may be only 1 cm. Therefore a selection of focusing lenses or a well-chosen zoom lens becomes a modern necessity in schlieren imaging.

For a desired magnification m, using the notation shown in Fig. 3.27, the thin-lens approximation yields the following expression [98] for the focal length f_3 of the focusing lens:

$$f_3 = \frac{m(f_2^2 - sg)}{f_2 - ms} \tag{3.14}$$

Having thus chosen a focusing lens, the distance e from it to the schlieren image is usually found experimentally. It can be calculated, though, from the expression,

$$e = m\left(f_2 - \frac{sg}{f_2}\right) = \frac{f_3(f_2^2 - sg)}{f_2^2 - sg + f_3 s} \tag{3.15}$$

which is sometimes useful for sizing a camera bellows, extension tube, etc. In both Eqns. 3.14 and 3.15 the distance s is negative if the test area is closer to the second field mirror than its focal length f_2.

High-quality camera lenses are available and are usually affordable, so they are recommended as schlieren focusing lenses to preserve image resolution without distortion [102]. Modern zoom lenses are especially effective for sizing the photographic or video image.

These lenses should be used with wide-open iris apertures to avoid vignetting the image. Likewise the distance g should be minimized in order to keep the schlieren beam diameter small compared to the lens aperture. One wants to avoid any circumstance where the effective focusing-lens aperture limits the measuring range of the schlieren system or blocks higher-order diffracted light that would otherwise contribute to the image resolution.

An example of these calculations is the case of the small 10.8-cm-aperture z-type schlieren system described in Chap. 8. In order to fit the apparatus diagonally on an existing 0.9×1.2-m optical table, the distance from the test area to the second mirror is constrained to 66 cm, making s = -20.4 cm. Then, in order to size the field-of-view appropriately to the width of a 35-mm photographic frame, a demagnification to about 1/3 full-size is required (m = 0.32). Finally, mounting constraints prevent g from being less than 4 cm. Eqn. 3.14 thus yields a required focal length f_3 = 260 mm, and a 100-300 mm telephoto zoom lens is thus suited to the job. The standard f_3 = 50 mm lens found on most 35 mm cameras is inappropriate, and indeed mild-to-moderate telephoto lenses or extenders are needed for most schlieren photography to image the small, distant test area at proper size on the film. This is not also the case for videography, though, due to the much-smaller image sensor involved.

3.7.2 Depth of Field

The depth-of-field of a schlieren instrument is the test-area dimension along the optical axis that may be considered sharply-focused in the schlieren image. The criterion for sharpness-of-focus is arguable, but Weinstein [110] suggests that the circle of confusion due to defocusing should be comparable to the resolution of the optical system.

Recalling Sect. 2.5, a true "point" light source illuminates the schlieren test area with parallel light. At near-infinite f/number there is no preferred position for sharp focus, and the schlieren image is sharp – within the limits of geometric optics – no matter where the test area is located. Of course, all real light sources fail this test due to finite size, some more so than others.

In Toepler's schlieren system a slit-type source of small-but-finite dimensions is intentionally used. (The exaggerated effects of finite source size were illustrated in Fig. 2.5.) Each test-area point is illuminated by a cone of light representing the *aperture angle* of the light source, $\alpha = b/f_1$, where b is the length of the source slit and f_1 is the focal length of the first lens or mirror. On this account a focusing effect now occurs, and a portion of the optical path through the test area can be described as the depth-of-field of the optical system.

Given the (small) aperture angle and a criterion for sharpness-of-focus, a simple estimate of the depth-of-field Δz is found by geometrical optics [173]:

$$\Delta z = \frac{\delta}{\alpha} = \frac{\delta f_1}{b} \tag{3.16}$$

where δ is the acceptable diameter of the circle-of-confusion due to defocusing.

Again we take the case of the 10.8-cm-aperture f/8 schlieren system of Chap. 8 as an example, with b = 3 mm, f_1 = 86.4 cm, and δ = 0.1 mm in order to preserve 10 lines/mm resolution. Eqn. 3.16 yields a 2.9 cm depth-of-field for sharp focus, which is consistent with the ~3.6 cm value observed subjectively in experiments.

Given the small aperture angles of most conventional schlieren systems, depth of field is not usually an issue. While it is necessary to focus the test area sharply on the schlieren image, window defects and other out-of-plane irritants show up all too clearly on most occasions. Still, this topic sets the stage for the next chapter, in which focusing effects and the size of the field-of-view are of primary concern.

4 Large-Field and Focusing Schlieren Methods

> In most cases it is unfortunately impossible to study thermo-hydrodynamic flowfields at full scale, owing to the limited dimensions of the available mirrors.
>
> *Hubert Schardin* [1]

Schardin essentially overlooked the large-scale possibilities of the lens-and-grid schlieren technique which he and H. Maecker pioneered [2]. Sixty years later, this and other opportunities have emerged to free the schlieren technique from its traditional bonds of small scale. Concurrently some of these approaches allow narrow depth-of-field as well, hence the ability to focus upon a "plane" in a 3-D schlieren field. Both possibilities are crucial to the renewed vitality of schlieren imaging.

These specialized schlieren techniques are given chapter status because they are the most important and most recent developments in the field, and because they are expected to play a strong role in the future of schlieren imaging.

4.1 Large Single- and Double-Mirror Systems

4.1.1 Availability of Large Schlieren Mirrors

In Chap. 3 the cost of schlieren-quality parabolic mirrors up to about 65 cm diameter was discussed. We have amateur astronomy to thank for the larger examples of these. At about f/5 – to minimize telescope length – they are short for schlieren use. Nevertheless they make fine z-type systems of large aperture if only simple illumination is used, and if astigmatism is dealt with properly. One manufacturer, Glass Mountain Optics, has supplied very-successful twin ¼ λ 71-cm-diameter parabolic mirrors on lightweight substrates for schlieren use [174,175]. They have the ability to produce mirrors up to 2.5 m diameter (see App. D).

Such large traditional glass schlieren mirrors can be custom-made in the 1-2.5 m diameter range, but they are shockingly expensive. The conventional rule is a

6:1 diameter/thickness ratio, but some are willing to try 14:1 or 15:1 [175]. The optical fabricating industry has undergone an upheaval and several of the traditional stalwarts who once made large monolithic schlieren mirrors are no longer in business. Those who are, as of this writing, are listed in App. D.

At the same time some fresh opportunities may be on the horizon for large schlieren-quality mirrors. For example, new earthbound telescopes now achieve large aperture by way of segmented mirrors: Kodak fabricated 91 thin 1-m hexagonal segments for the Hobby-Eberly Telescope for $16,500 each [137]. Not that any such mirrors are known to be available for schlieren imaging, but the manufacturing technique and the possibility of surplus mirrors is worth noting.

The same can be said for large, light space telescope mirrors [176-178]. The 2.4-m Hubble Space Telescope mirror, for example, is a glass face-sheet with an "eggcrate" backing. Such lightweight mirrors are contemplated for meter-class amateur telescopes, so schlieren imaging cannot be far behind.

Finally, stretchable-membrane mirrors are proposed by Waddell et al. as a cheap, lightweight alternative to conventional glass schlieren mirrors [179-182]. A thin sheet of aluminized Mylar is stretched over a frame, forming an airtight cavity behind the sheet. Removing air from the cavity stretches the membrane into a spherical shape. Mirrors from 0.15 m to 1.2 m in diameter have been demonstrated, and a 2-m mirror is under development. Waddell [183] contemplates still-larger mirrors, but serious questions about their schlieren quality remain.

4.1.2 Examples of Large-Mirror Systems

A number of large conventional mirror-type schlieren systems exists, especially in government wind tunnel laboratories around the world. NASA and the US Air Force, TsAGI in Russia, and defense aerodynamic installations in Europe and Asia account for most of these. They are predominantly z-type parabolic-mirror systems not unlike the original Peenemünde wind-tunnel schlieren system described in Chap. 1. NASA's Unitary Plan tunnels and the Propulsion Wind Tunnel at the USAF Arnold Center are mammoth facilities with schlieren equipment of similar scale. One fine example is the former NASA-Ames 6x6 Supersonic Wind Tunnel, with a 1.3-m z-type schlieren system. Images taken in this facility by the author are shown in Color Plates 6-8. In the 1950's, the windows of this facility bested the 1-m Yerkes Refractor lens, until then the largest transmissive optical element ever cast.

Such large facilities are endangered by high energy costs, the boom-and-bust cycle of the aerospace industry, and the inexorable loss-of-ground of experimental to computational fluid dynamics. Many have already disappeared, including the NASA-Ames 6x6 and the Army BRL tunnel with its 0.9-m schlieren. Astute fans of large mirrors must always keep an eye on the surplus equipment market.

Large industrial wind tunnels typically have optics in the 0.4-0.75-m range, but these too are disappearing. New ones sometimes spring up, though, on an ad hoc basis. Mendonsa [184] describes a modern, expensive schlieren system with 0.6 m off-axis parabolas in a z-type setup, intended for a new hypersonic-flow facility.

Some orphaned schlieren mirrors end up in academia, where there is less fervor to dismantle large facilities. Davies [185] describes a 0.75 m system at the University of Exeter, the parabolic mirror salvaged from an old observatory. Mirrors up to 0.45-m-diameter are used to observe flows at the University of Manchester. The Penn State Gas Dynamics Lab operates a 0.76 m z-type system salvaged from the former MIT Naval Supersonic Wind Tunnel. This system is rather short at f/5, thus giving its users a thorough workout in the elements of astigmatism. Examples of its use include greenhouse modeling ([186] and Fig. 9.9b) and the world's largest stereoscopic schlieren, shot for an IMAX movie and described further in Sect. 5.3. Apparently the largest of all these academic facilities is Penn State's 1-m coincident schlieren system, described next in detail.

4.1.3 Penn State's 1-Meter Coincident Schlieren System

In the 1960's the Unertl Optical Co. made a 1-m f/4 parabolic mirror for use as a collimator in military searchlight testing. The aluminized and overcoated mirror in its massive steel mount eventually served its purpose and was surplused. An amateur astronomy club in New Jersey bought it with a telescope in mind, but had second thoughts on the cost of the observatory. I then bought the mirror from them in 1982 for a small fraction of its original cost. Shown in Fig. 4.1, it has been the workhorse of the Penn State Gas Dynamics Lab ever since [111,127].

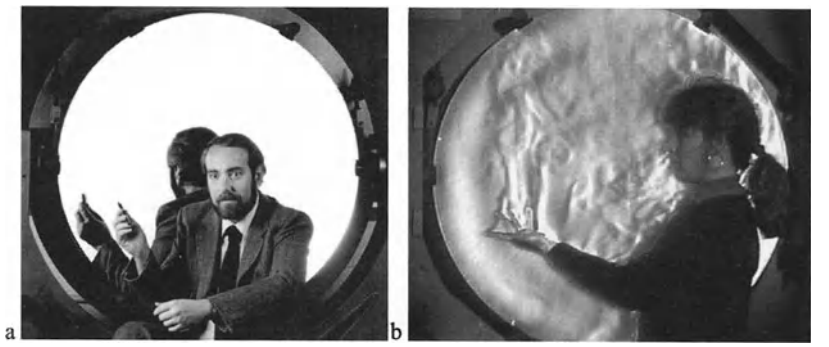

Fig. 4.1. **a** Portrait of the author as a young man, seen against the illuminated mirror of the Penn State Gas Dynamics Lab's double-pass coincident schlieren system, from an original PSU photo by James Collins, 1984. **b** The extraordinary sensitivity of the system is demonstrated by Lori J. Dodson, Lab Manager, 1998 (frame extracted from videotape record).

Since only one such large mirror was available, a single-mirror coincident arrangement was the obvious choice (Sect. 3.1.2). Its optical layout is shown in Fig. 4.2. The difficulty, mentioned earlier, of needing a spherical mirror but having only a parabola was overcome using a *Dall null corrector*. Howard Dall

[150,151] of Dall-Kirkham telescope fame suggested this solution by adding a simple corrector lens after the light source. The spherical aberration of the lens is of opposite sign but similar character to that of the parabolic mirror, effectively correcting the parabola to a sphere. A simple plano-convex lens of d = 6.5 cm and f = 50 cm was bought off-the-shelf and installed exactly 25.9 cm after the source slit of the schlieren system with its convex side toward the source. [1] The illuminator section of the apparatus was then placed on the axis of the parabolic mirror and moved axially until the source image (magnified by the power of the corrector lens) focused exactly at the effective mirror radius-of-curvature R = 2f. Near-perfect compensation was achieved; only a few concentric polishing zones of the ~λ/5 mirror disturb the otherwise-flat schlieren field (Fig. 4.1b).

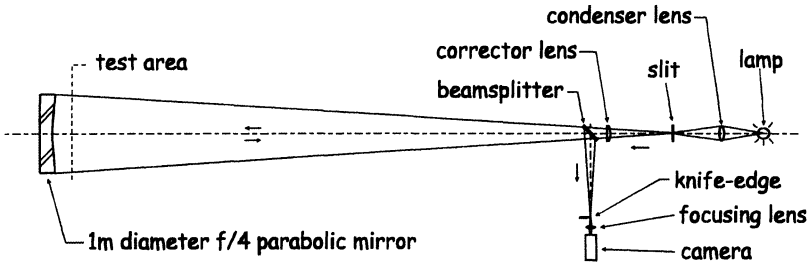

Fig. 4.2. Layout diagram of Penn State's 1-meter coincident schlieren system.

The setup shown in Fig. 4.2 wastes about ¾ of the captured lamp luminance in two passes through the beamsplitter, but in practice a tungsten-halogen lamp still provides plenty of light. The slight spectral dispersion of the corrector lens causes a color gradient across the schlieren image that can be muted by way of a color filter at the source slit.

Precisely-coincident alignment is important in such a large system, whose overall length is about 10 m. Each point in the test area must be traversed twice by the same light ray to avoid double-imaging. If this occurs, then the already-high sensitivity to weak disturbances is doubled. That is exactly what happens in practice, though strong deflections can produce confusing results in the schlieren image, and the system is easily over-ranged.

We can estimate the ultimate sensitivity of this schlieren system as follows: If the light-source slit height h is 1 mm, then at 95% knife-edge cutoff a = 50 μm. Assuming a 5% contrast detection threshold, an elemental source image displacement of Δa = 2.5 μm at the knife-edge is just detectable in the image. The effec-

[1] A similar corrector lens may be specified for any single-mirror coincident schlieren system by following Dall's [150] philosophy of corrector design.

tive optical lever-arm is approximately R = 2f = 8 m long. Eqn. 3.6 yields an amazing 0.06 arcsecond sensitivity that, because of the doubling just discussed, actually becomes 0.03 arcsecond sensitivity in the test area.

Whether diffraction and other system errors in fact allow 0.03 arcsecond sensitivity is doubtful, but the extraordinary sensitivity of such a large mirror-type schlieren system is palpable (Fig. 4.1b). To make proper use of it, lab ventilation must be shut down and people in the lab must stand still for a minute or so to suppress airflow disturbances along the optical path.

This system has been very useful in medical, environmental, and security studies of the human thermal plume [111,127,187-189], of canine olfaction [190], and of thermal flows in materials processing. Schlieren image-correlation velocimetry [191] was developed using it, and Strobe-illuminated color schlieren has been implemented as well. Example images are given throughout the book, and especially in Color Plates 5 and 23-29.

4.2 Traditional Schlieren Systems with Large Light Sources

Schardin [2], Burton [107], Kantrowitz and Trimpi [105], Fish and Parnham [106], and Mortensen [192] all developed the idea of extended-source schlieren optics around 1950. What caused all this spontaneous interest is unclear, but the need for optical imaging of intricate high-speed wind tunnel flows was one contributor. The work of Schardin and Burton resulted in a truly-original schlieren approach, covered in the next section. That of the others, who extended the light-source dimensions of traditional schlieren systems in order to gain sharper focusing, is discussed here.

Recalling Fig. 2.5, a light source of small-but-finite size was illustrated in a simple schlieren system. Here we extend the source dimensions until they are comparable with those of the schlieren field-of-view, as shown in Fig. 4.3. A grid of some type – usually parallel clear and opaque lines – is back-illuminated by a light source and condenser lens to form the effective light source. Light from all points of this source grid is collimated by the first field lens and projected through the schlieren object in the test area. Given the wide aperture of this setup, points in the schlieren object are illuminated not by single rays, but by ray bundles subtending the aperture angle [102]

$$\alpha \approx \tan\alpha = \frac{h}{f_1} \tag{4.1}$$

where h is now the usable height of the source grid. Ray bundles from only the two extreme points on the source grid are shown in Fig. 4.3 for clarity [193].

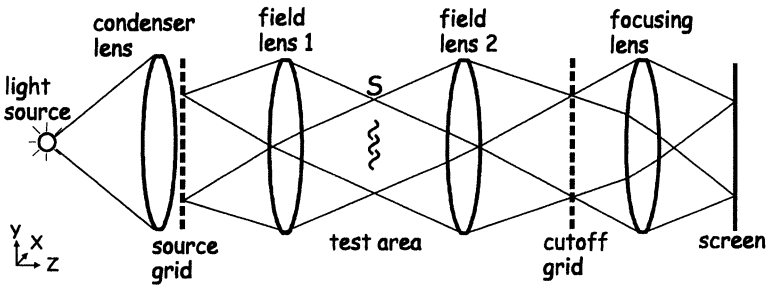

Fig. 4.3. Diagram of a conventional schlieren system modified with large source and cutoff grids for sharp focusing.

Field lens 2 accepts the non-parallel schlieren beam and brings it to a focus on the cutoff grid, which is a matching photographic negative of the source grid. As before, the two grid planes are optical conjugates, as are the test area and the screen image. Disturbances anywhere along the optical path can refract light, but only those in the plane of the test area are sharply-focused in the schlieren image. The schlieren cutoff is adjusted, just as it is in a conventional knife-edge system, by translating the cutoff grid vertically with respect to the image of the source grid.

One may consider each corresponding pair of source-grid slits and cutoff-grid bars in Fig. 4.3 as an individual schlieren system [66,183,193]. One thus has "multiple simultaneous schlieren systems" [105] or "a set of ordinary schlieren instruments at angles to one another" [102]. This a ngular redundancy gives the technique its focusing ability and its appeal.

Few of the original investigators of this technique offered much optical design theory, but Kantrowitz and Trimpi [105] at least discussed characteristics and shortcomings in detail. They were interested in sharp focus, not large-scale imaging and, indeed, Fig. 4.3 shows that the schlieren field-of-view is obviously smaller than the field-lens aperture – typically by about 1/3 – due to vignetting of the extreme rays. It follows that high-quality, well-corrected anastigmatic field lenses are needed, since the illumination is no longer paraxial. Likewise a multi-element focusing lens of high quality and large aperture is called for. Kantrowitz and Trimpi further noted that they could not usefully approach full cutoff, as in a knife-edge system, but got best results with only slight-to-partial cutoff.

They show an interesting example of a 4.8-mm supersonic gas jet in sharp focus and then defocused by various distances. Between 12 and 25 mm of defocus the schlieren image of the jet disappears in their optical system. Invoking Eqn. 3.16 for depth-of-field with $f_1 = 152.4$ mm, $b = 38.1$ mm, and δ = the jet diameter of 4.8 mm, one obtains $\Delta z = 19$ mm in agreement with their experiment.

However, the blurred image of the opaque nozzle exit remains visible in that example. Kantrowitz and Trimpi [105] conclude from this, as do others [102,106], that depth of field also depends upon on the character of the object under study. Extensive opaque objects in the test area are hard to defocus. In the

extreme case of a boundary layer on a flat plate, focusing largely fails in the direction perpendicular to the plate because only the grazing rays actually pass through the boundary layer.

Fish and Parnham [106] give the first theoretical treatment of focusing schlieren optics. They cite as an advantage that out-of-focus optical defects, e.g. defects in wind tunnel windows, will not appear in the schlieren image if they are below a certain size. The diameter of the circle of confusion for such defects is given by

$$d = \ell\alpha = \ell b / f_1 \tag{4.2}$$

where α is the aperture angle subtended by the usable portion of the source grid and ℓ is the distance of the defect from the plane of sharp focus.

Fish and Parnham also show that the vignetting of the effective test area diameter is given by

$$D = D_0 - \ell\alpha = D_0 - \ell b / f_1 \tag{4.3}$$

where D is the usable test area diameter, D_0 is the field lens diameter, and ℓ is here the distance of the test area from either field lens if placed centrally.

Though this discussion refers to a lens-type focusing schlieren system, Fish and Parnham [106] point out that z-type mirror focusing schlieren systems suffer some of these problems even more acutely. Their high-f/number mirrors preclude much sharpness of focus, vignetting is serious, and their off-axis aberration problems are exacerbated by a large light source. Nonetheless, several later examples of such systems are described [194-197]. Evidently, however, one may not casually convert a traditional schlieren setup to an effective focusing system merely by replacing the slit and knife-edge with a matched pair of grids.

More recently, Waddell et al. [183] examined the system of Fig. 4.3 and noted that the periphery, not the center, of the second field lens is most useful for narrow depth-of-field. They added a central stop to this lens in order to lower the depth-of-field further. This was unsatisfactory, though, since it obscured the center of the schlieren field and reduced the schlieren image contrast.

Even more recently there were two separate attempts to model focusing schlieren systems using Fourier optics. Hanenkamp et al. [198] carried out a computational Fourier-optical simulation of the traditional schlieren system with multiple point light sources in order to investigate sharp-focusing effects. The representation of a 3-D phase object is integrated and thus poorly-represented by only a single source, as expected. A marked improvement is shown with 5 distinct sources, verifying the focusing effect. Serafino [199,200] went beyond this by actually modeling a source grid of extended bright bands of white light. She used the analogy between Fourier optics and communications theory to examine the phase distortion of the light beam, the formation of Fourier spatial-frequency spectra in the cutoff plane, the modulation of these spectra by the cutoff grid, and the schlieren image formation. At full cutoff, her results show that the focusing schlieren image is similar to that of darkfield microscopy (covered in Sects. 5.1.3, 9.4.7, and B.4).

In summary, though historically important and a noteworthy step in understanding, conventional schlieren systems with extended sources are seldom used nowadays. Expensive lenses are required, the field-of-view is too small, and there is often not enough focusing effect to be useful. The real potential of focusing and large-scale schlieren lies not here, but rather in the single-lens-and-grid method of Schardin [2] and Burton [107,108], described next.

4.3 Lens-and-Grid Techniques

> Experiment shows that it does not seem to be as sensitive, or quite as easy to use as the parallel light schlieren system.
>
> *R. A. Burton* [104]

Burton [104] succinctly stated the drawbacks of a schlieren system based on a single lens, a large source grid, and non-parallel illumination. Only recently it was shown that the advantages of such a system are nonetheless spectacular: narrow depth-of-field and an unlimited field-of-view. One expects to fret more over the setup and alignment of such a system than that of an ordinary schlieren method.

In this section we progress from the simplest of such arrangements to the most sophisticated, much as Schardin did in 1942 [2].

4.3.1 Simple Background Distortion

> ...the body of the Starrs appear to tremulate or twinkle,...being sometimes magnify'd and sometimes diminished; sometimes elevated, otherwhiles depress'd; now thrown to the right hand, and then to the left.
>
> *Robert Hooke,* Micrographia [17]

Schardin began his treatise [2] by remarking upon schlieren that are visible to the naked eye in windowpanes and above hot railroad tracks (covered further under outdoor applications in Sect. 9.4.10). This introduced the optics of a rudimentary schlieren system in which a distant light-dark boundary (e.g. the horizon) serves as the light source and the balance of the optics is contained in the eye. The optical diagram and an example are shown in Fig. 4.4.

The schlieren object S is observed by the eye or by a camera, which images it inverted upon the retina or film. A light/dark boundary at distance L lies further away than S on the optical axis. The image portrays this inverted light/dark boundary, though it is generally defocused unless the lens iris is severely st opped down, or else both t and L are very large compared to t'. Point P in the schlieren object, at distance t, refracts the light from the light/dark boundary through angle ε. P thus appears bright in the image at P', even though its apparent location P'' lies at a distance e into the dark zone. P and P'' are both described by viewing

angle φ below the optical axis. (In case t = L/2, then φ and ε are of equal magnitude.)

The result of this is that the distant light/dark boundary no longer appears straight in the schlieren image, but rather is distorted due to the refraction of schlieren object S. In Fig. 4.4b an antique mouth-blown windowpane serves this purpose. The light/dark boundary is straight on either side of it, but is distorted through the glass by optical imperfections and thickness variations. The glass is transparent and thus invisible, purely of itself, but is rendered at least partially visible by this distortion of the background.

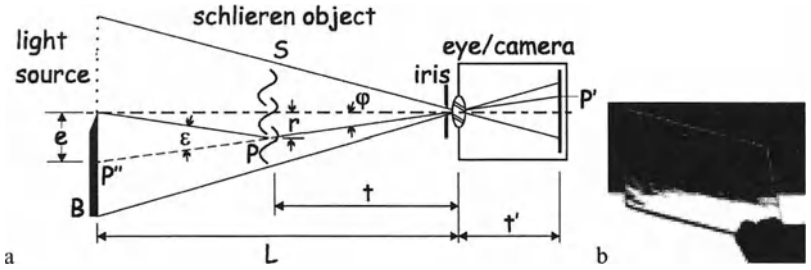

Fig. 4.4. **a** Diagram of Schardin's [2] schlieren method no. 1, simple background distortion. **b** Schardin's photo of a mouth-blown glass windowpane viewed against a distant light-dark boundary (reproduced by permission of Springer-Verlag).

In Fig. 4.4a the light source, schlieren object, and lens are obvious, but where is the schlieren cutoff or knife edge? That role is fulfilled by the iris aperture of the camera or of the eye. Schardin classified this as "schlieren method no. 1," since it constitutes schlieren optics in its simplest generic form. Through its simplicity, it has been much honored by time: Hooke [17] used it to see heat haze and explain the twinkling of the stars. Salcher [60] used it to visualize the original supersonic jet experiments (Fig. 1.13b) against the background of his laboratory window.

However, despite its simple natural occurrence without the aid of apparatus, this schlieren technique suffers the severe limitation that its working range is confined narrowly to the vicinity of the light/dark boundary. Right on this boundary the sensitivity is high, but points of the schlieren object lying off the boundary at significant viewing angles φ must produce large ray deflections in order to become visible. Thus high sensitivity is not available over a significant field of view, and a complete impression of the schlieren image can only be obtained by *scanning* .

Moving the eye or the camera accomplishes this scanning while the other optical elements remain relatively fixed. Sometimes one may take advantage of the natural motion of the schlieren object for this purpose. It is even possible to deliberately design a schlieren apparatus with a moving light source (Sect. 4.4).

4.3.2 Background Grid Distortion

Meanwhile, as Schardin [2] noted, scanning can be avoided by using an array of light/dark edges or stripes in the form of a background grid. This expedient, which he called "schlieren method no. 2," is used in explosions, ballistics, glass testing, and other applications that combine a need for simplicity and a large field-of-view with the lack of any need for high sensitivity [201-208].

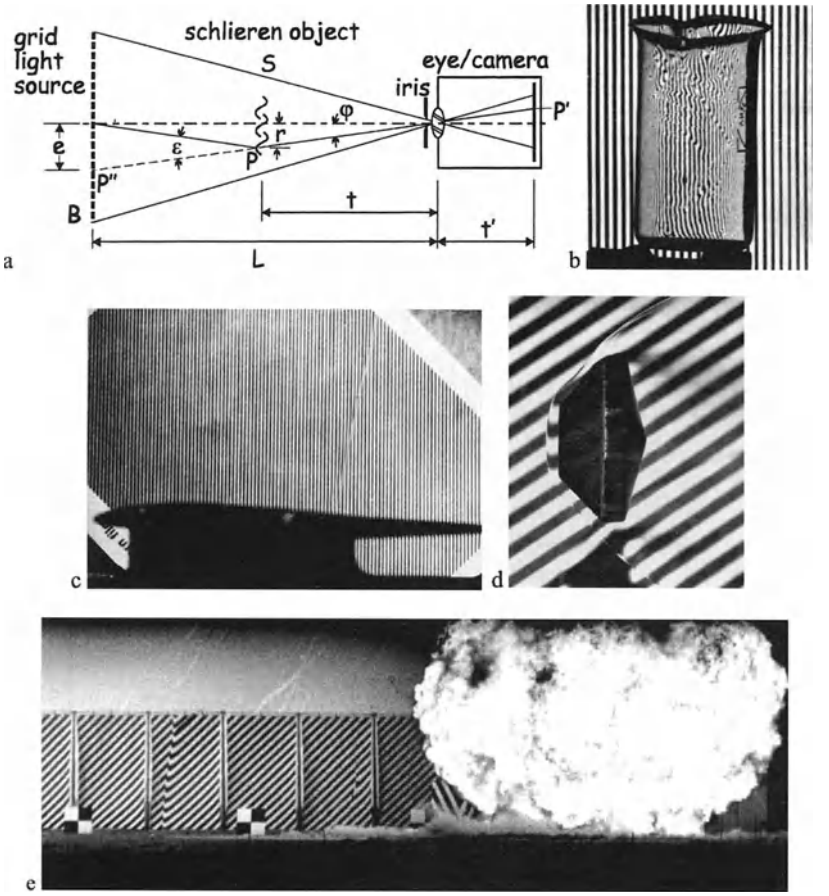

Fig. 4.5. **a** Diagram of Schardin's [2] schlieren method no. 2. **b** Schardin's photo of a glass beaker (courtesy Springer-Verlag). **c** Flow over a transonic airfoil revealing normal shock wave formation [205] (photo by the author and J. P. Crowder). **d** bow shock wave about a ballistic projectile [209] (US Air Force photo). **e** outdoor explosion photograph revealing primary and secondary blast waves against a striped background (in background panels 3 and 5 from the left, respectively). Photo courtesy J. M. Dewey [202,210].

As shown in Fig. 4.5a, the light/dark boundary of each background-grid stripe functions as described in Sect. 4.3.1. Apparent stripe distortion thus reveals the schlieren object in front of the grid over the entire field of view. The eye and brain usually ignore the background and observe a continuous schlieren object where there is actually only discontinuous illumination. Nevertheless this method is inferior to Toepler's method in several respects, and it is only a step along the way to an eventual goal. (Schardin [2] discussed removing the stripes photographically, a measure that can nowadays be done electronically as described later in Sect. 4.5.)

4.3.3 Large Colored Grid Background

Following the idea of background grid distortion, Schardin [2] next proposed making the grid so large that the entire schlieren object subtends an angle less than that of one central white stripe or spot, "*a*." This solves the problem of discontinuous background illumination while still providing schlieren contrast through the distortion of the adjacent stripes or rings, b′, b″, etc. (now colored differently in order to avoid confusion). This "schlieren method no. 3" is diagrammed in Fig. 4.6a.

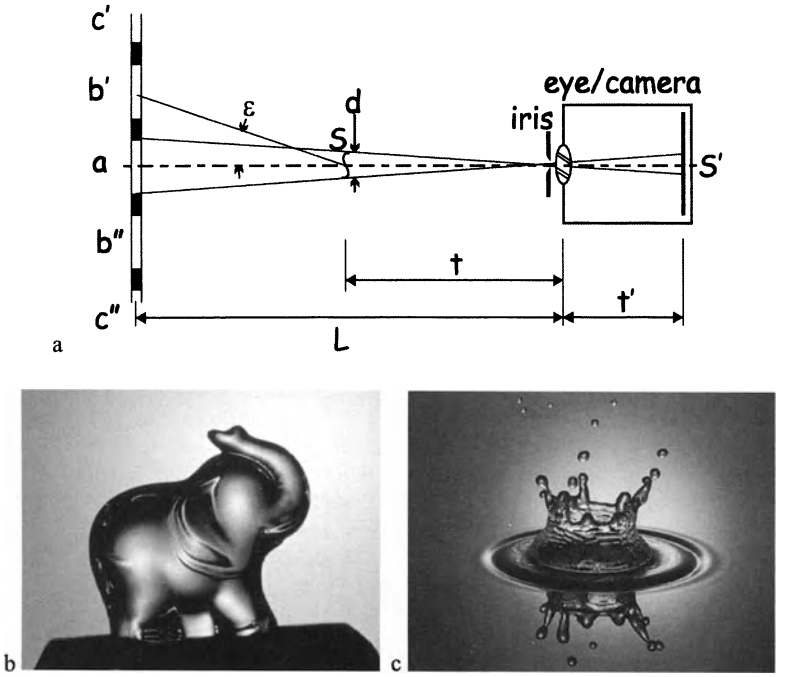

Fig. 4.6. **a** Diagram of Schardin's schlieren method no. 3, the large colored grid background method. **b** Crystal glass elephant figure (photo by Heather Ferree). **c** High-speed flash photo of a water splash (courtesy Prof. A. Davidhazy, Rochester Inst. of Tech.).

This approach is especially useful for strongly-refracting schlieren objects like glass plates and water waves (Figs. 4.6b and c, and Color Plate 9). In fact, this schlieren technique underlies a common method of photographing glassware in dark outline [211]: a spotlight is cast upon a white background to provide a bright central spot. This spot illuminates all parts of the glassware that are not strongly refracting, e.g. the center of the figurine in Fig. 4.6b. The edges of the figurine and its other features refract strongly enough to bring the dark peripheral background onto the optical axis. Streaks and flaws in the glass are also made visible in this way. Photos like Figs. 4.6b and c are not usually called schlieren images, but that is certainly what they are by any consistent definition.

Due to the very-strong refractions of typical glassware (degrees rather than mere arcseconds), a sensitive schlieren system is not necessary or desirable. From Fig. 4.6a, the weakest detectable refractions are characterized by

$$\varepsilon_{\min} \approx \frac{d}{L-t} \tag{4.4}$$

Schardin [2] points out that using this method for large objects at high sensitivity becomes impractical by requiring the distance L-t to be prohibitively long; perhaps hundreds of meters or more.

The same optical principles hold for liquid surface waves, where the refractions are strong and the large colored grid background technique works nicely [212]. Moreover, since every color boundary corresponds to a known refraction angle, quantitative evaluation of the schlieren image becomes possible.

Thinking broadly about this approach, Schardin [2] first suggested using the Sun as the bright spot *a*. In this case the schlieren object should subtend a visual angle of ½° or less. Weinstein [112] adapted a variation of this idea 50 years later to take schlieren photos of high-speed aircraft in flight (Sects. 1.4 and 4.4).

4.3.4 The Modern Focusing/Large-Field Schlieren System

Schardin's Contribution. The first three schlieren methods of Schardin, just discussed, all have limitations that restrict their usefulness, but they nevertheless add up to something very useful. Schardin [2] credits his colleague H. Maecker, of the Ballistics Institute, Luftwaffe Technical Academy, with building an improved lens-and-grid schlieren system to achieve a large field-of-view. Schardin called it "schlieren method no. 4," and clearly saw it as the culmination of a major class of schlieren optics. With it, he introduced the concept of an explicit schlieren cutoff, serving the same purpose as the Toepler knife-edge.

In principle, this improvement can be made upon Schardin's method no. 2 (Fig. 4.5) by recognizing that the grid light source B and the schlieren object S are imaged at different distances L′ and ℓ' in the back focus of lens O. Making use of this, a negative grid – the schlieren cutoff – can be placed at L′ to block the unrefracted light from the source, as shown in Fig. 4.7.

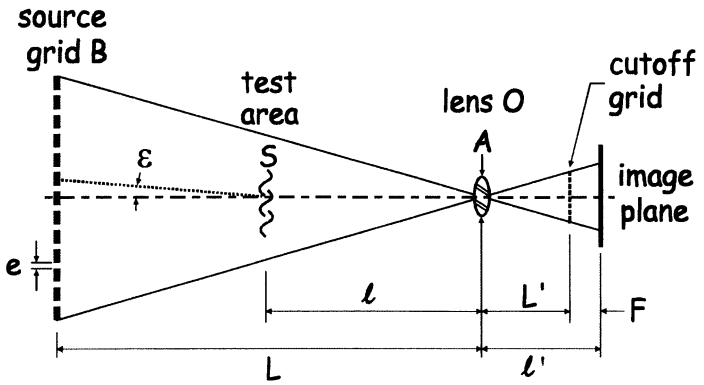

Fig. 4.7. Diagram of Schardin's schlieren method no. 4, the lens-and-grid technique. (The notation is consistent with Fish and Parnham [106] and Weinstein [110] rather than with Schardin [2].)

In practice a photographic film or plate is exposed in place, developed to produce the complementary negative cutoff grid, and then reinstalled precisely in position. When there is no schlieren object present in the test area, all light from the source grid is blocked by this cutoff grid. But a refraction at a point in the schlieren object through angle ε shifts an elemental source-grid image with respect to the cutoff grid, allows light to pass, and brightens a corresponding point in the schlieren image. Such refracting points then appear bright upon a dark background, as in darkfield microscopy. The collection of these bright points defines a schlieren image much as it does in Toepler's method at full knife-edge cutoff.

Actually, though, we already know that schlieren techniques are never at their best with 100% cutoff. Instead, the cutoff grid is deliberately adjusted vertically until each bright stripe of the source grid image is only partially cut off (say 50%). Now the image is illuminated in medium gray, and darkening as well as brightening may occur, depending on the direction of the component of ε normal to the grid bars. Once again, as in Sect. 4.2, each corresponding pair of source-grid stripes and cutoff-grid bars in Fig. 4.7 acts as an individual schlieren system of the single-lens Toepler type. The many resulting individual schlieren images superpose exactly in the image plane only when it is sharply focused upon a conjugate plane in the test area. According to Weinberg [66], "The device may be thought of simply as a number of autonomous schlieren systems whose optic axes are at small angles to each other – angles small enough for the systems to share the (lens). The two outermost systems determine the depth of focus by the angle their axes subtend; the others increase intensity."

The measuring range of this lens-and-grid schlieren system depends upon the spacing of the source gridlines, which can be chosen as a system design parameter. If the range is exceeded, then a maximum brightening of the image gives way to darkening as the refracted light is once again blocked by the adjacent opaque bars of the cutoff grid. For very strong refractions this occurs repeatedly, the elemental

source images being superposed upon the cutoff grid after a shift of several times the grid constant. *Isophotes* – fringes of uniform illuminance – then form in the image (see Figs. 4.8a and b for examples). Schardin saw the utility of these isophotes for quantitative measurements: they are, in fact, curves of constant refraction perpendicular to the stripes of the source grid [2]. When they appear, the schlieren sensitivity curve is no longer a ramp (as in Toepler's system, Fig. 3.10), but rather a "sawtooth" [119]. In that case, assuming both bright and dark source grid bars have the same width e, and letting k = 2, 3, 4, etc., the refraction angle ε can be written [2] as

$$\varepsilon = 2ke / L \tag{4.5}$$

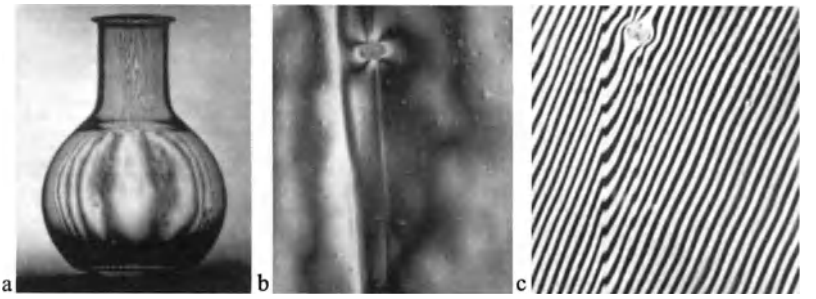

Fig. 4.8. **a** Flask, and **b** mouth-blown glass windowpane, both seen by Schardin's [2] schlieren method no. 4. **c** The same piece of glass as in **b**, but observed with schlieren method no. 2. The "orange-peel" surface defects of the glass are much more visible in **b** than **c** due to continuous illumination and higher sensitivity. The same argument is made in favor of schlieren vs. interferometry where qualitative visualization is concerned. Photos reproduced courtesy of Springer-Verlag.

But here even the far-seeing Schardin missed the point. Referring to Fig. 4.8a, he wrote [2]: "We see from this photograph that the method is very suitable for investigating objects which naturally cause strong light deflections," and he left it at that. In the intervening 60 years this schlieren method was seldom called upon to image such strongly-refracting objects. Sharp focusing, a different characteristic of Schardin's method no. 4, became much more popular, however, and lately Maecker's idea of using it for large-scale schlieren imaging has resurfaced on a grand scale.

Burton's Contribution. Unlike his sharply-focused colleagues (Sect. 4.2), R. A. Burton [42,104,107-109] fundamentally saw method no. 4 as a large-field schlieren system. He cited Schardin's single-lens-and-grid precedent [2], but went well beyond it in the design and practical arrangement of the optics. He was the first to state that "...the field size is not limited to the size of the lens, but to the size of an easily-constructed grid [104]."

Maybe not so easily constructed in every case, but he had the right idea. Taking Fig. 4.7 to extremes, the source grid B becomes so large that the lens aperture A is negligible by comparison. In that case, and for the typical choice of L = 2 ℓ, the field-of-view is half the size of the source grid. The source grid size, however, is limited only by the size of one's space, budget, and imagination (not necessarily in that order). This schlieren system thus promises an enormous field-of-view, completely divorced from the cost of large, high-quality optics. Burton mounted his source grid on the wall; a modern example using the entire wall of a warehouse is given in the next section.

In addition to bringing Schardin's lens-and-grid method to public attention, Burton also identified several of the issues to be managed in making it actually work: resolution loss due to cutoff-grid diffraction, image banding, alignment procedure, and the practical details of the source-grid illumination.

We saw in Sect. 3.6 that diffraction at the schlieren cutoff is troublesome but generally manageable in the case of a single knife-edge. Not so in the case of the cutoff grid in Fig. 4.7 if the slits are too narrow, since each slit spreads the light into diffraction orders that can lead to unacceptable smearing of the image resolution (see Fig. 3.22c for an example). Burton found that he could maintain 4 lines/mm image resolution by observing the following criterion [108]

$$\frac{F}{4b^2} < 8000 \tag{4.6}$$

where F is defined in Fig. 4.7 and b is the open slit width between opaque cutoff gridlines. This criterion, for visible illumination at the sodium D line, has been superceded by versions of Rayleigh's criterion [110,213]. According to Weinstein [110], the resolvable dimension w in the schlieren test area is given by

$$w = \frac{2F\lambda}{mb} \tag{4.7}$$

where m is the image magnification defined in Sect. 3.7, here equal to ℓ'/ℓ. A more-complete physical-optics treatment of the resolution consequences of slit diffraction at the schlieren cutoff can be found in Hosch and Walters [171].

Burton [104,108] also identified the problem of image banding, wherein the shadow of the cutoff grid disturbs the uniformity of the schlieren image background. To hold this illumination difference below 1%, he gave a design criterion that turns out to be very conservative by present standards. Weinstein [110] later proposed a similar criterion that does a better job based on ϕ, the number of pairs of cutoff-gridlines which combine to form the schlieren image:

$$\phi = An(\ell' - L')/2\ell' \tag{4.8}$$

Here A is the schlieren lens aperture in Fig. 4.7, and n is the number of gridlines per mm in the cutoff grid. Weinstein observed in practice that $\phi > 5$ is a minimum

for a reasonably-uniform schlieren background, and that $\phi > 8$ is preferable. Later, an example will demonstrate that even $\phi = 2.8$ proved acceptable in one case.

Finally, Burton recognized that a large source grid relieved the normal schlieren restrictions on lamp size, making possible the use of large flood- or flash-lamps. His thesis [104] contains extensive guidance on such setup and alignment issues, including the expedient of a magnifying glass to align the cutoff grid and the source-grid image. He saw the primary design parameters of a single-lens-and-grid schlieren system as lens focal length, film size, and size of the field-of-view. He also looked forward in 1950 to the general acceptance of lens-and-grid schlieren methods, though it only happened some 45 years later.

Ten years after Burton another Masters candidate, Boedecker [214], further improved lens-and-grid schlieren methods by using a Fresnel lens as a large, cheap condenser to collect the light from the source and direct it toward the schlieren objective. This raised the image illumination perhaps a hundredfold, solving the poor-illumination problem that had plagued the technique of previous investigators. Nevertheless, focusing and large-field schlieren languished in the latter half of the 20th Century, with only a few publications [98,179,215-217] and, probably, many attempts that ended in failure and frustration (present author's included). This situation was changed permanently in the 1990's by the work of Leonard M. Weinstein [110,159,218].

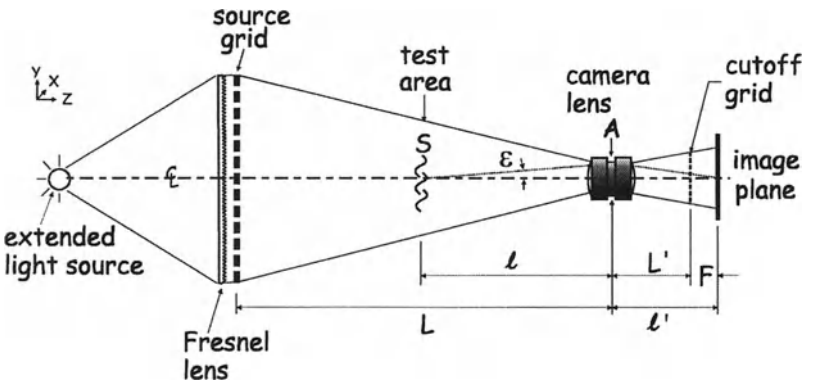

Fig. 4.9. Diagram of Weinstein's modern focusing schlieren system [110].

Weinstein's Contribution. Weinstein solved the remaining design problems that inhibited lens-and-grid schlieren methods, presented the technique ready-to-use in an archival publication [110], and – most importantly – succeeded in popularizing it. He became the August Toepler of focusing schlieren methods.

The modern focusing/large-field schlieren system he championed is illustrated in Fig. 4.9. It differs from Schardin's system, Fig. 4.7, only in the use of the Fresnel lens and a high-quality camera lens, but the working technique and design philosophy have also improved greatly.

With Weinstein's permission, entire segments of his unpublished work "Designing and Using Focusing Schlieren Systems" [159] are paraphrased in the following discussion of modern system design and adjustment.

Designing a Focusing Schlieren System requires tradeoffs among sensitivity, depth-of-focus, image resolution, and the size of the field-of-view. Moreover, only a limited range of imaging lenses is available for this purpose. The required sensitivity should thus be estimated at the outset by considering the possible range of refractions of the schlieren objects to be examined. Experience shows that the desired sensitivity often falls in the 2-16 arcsecond range, assuming the (arbitrary) detectability of a 10% change in image illuminance [159]. The methods of estimating required sensitivity and range, given in Sect. 3.4 for Toepler's schlieren technique, apply here as well.

The depth-of-field of a focusing schlieren system should not automatically be minimized early in the design process, as this might excessively constrain other key system parameters. Instead, an initial compromise leading to a preliminary design ought to be made. Depending upon the availability of the optical components, a redesign may be called for later to accommodate reality.

For a lens with k line-pairs of resolution per mm, the minimum reliable value of a, the unobstructed height of a source-image band at the cutoff grid, is 2 /k mm (i.e., it takes 2 line-pairs to properly define a). The lens one selects must be capable of this resolution. Most suitable lenses – aerial camera, overhead projector, copier, enlarger, and large-format-camera lenses – have 15-60 line-pairs/mm resolution, allowing a minimum a value in the 33 to 133 μm range. This minimum value establishes the limit of system sensitivity.

Sensitivity is based on Eqn. 3.6, with f_2 now replaced by $L'(L - \ell)/L$ according to Fish and Parnham [106]:

$$\varepsilon_{min} = a\frac{\Delta E}{E}\frac{L}{L'(L-\ell)} \tag{4.9}$$

with $\Delta E/E = 0.1$ for a 10% detection threshold, convenient design formulae for ε_{min} and a are:

$$\varepsilon_{min} = 20626a\frac{L}{L'(L-\ell)} \qquad \text{(arcseconds)} \tag{4.10}$$

$$a = 4.85\times10^{-5}\varepsilon_{min}\frac{L'(L-\ell)}{L} \qquad \text{(mm)} \tag{4.11}$$

Eqn. 4.10 gives the minimum schlieren refraction angle detectable by the system for a given degree of cutoff, while Eqn. 4.11 gives the unobstructed height of a source-image band at the cutoff grid, corresponding to a given minimum detectable refraction angle.

Often the test area will be located halfway between the lens and the source grid, in which case (L – ℓ)/L = ½ and L′ ≈ f, the lens focal length. With this simplification we can revert directly to Eqn.3.6, which yields

$$\varepsilon_{\min} \approx 41252\, a / f \qquad \text{(arcseconds)} \tag{4.12}$$

This expression illustrates the typical inverse relationship between ε_{min} and f for several different values of a, as shown graphically in Fig. 4.10.

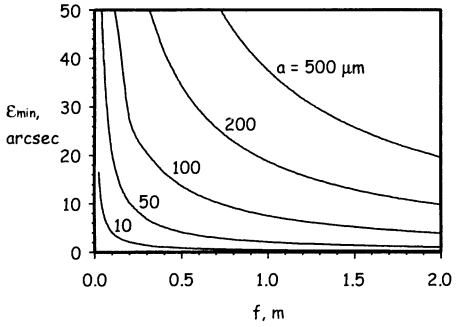

Fig. 4.10. Plot of minimum detectable refraction angle ε_{min} vs. lens focal length f for schlieren systems, according to Eqn. 4.12 (10% detectability threshold assumed). For single-lens-and-grid schlieren methods, long focal length lenses or very-high-resolution lenses with reasonable focal lengths are required for high sensitivity.

Criteria for image resolution w and image banding ϕ were given in Eqns. 4.7 and 4.8, respectively. With them, we can now find suitable values of n, b, and w. If ϕ is chosen too large, the resulting narrow cutoff-grid slits deteriorate the image resolution w through slit diffraction. Similarly, too-small ϕ causes image banding and reduces the image brightness as well. Unless the loss of resolution is overly restrictive, $\phi \approx 10$ is suggested as a starting point. Eqn. 4.8 is then solved for n:

$$n = \frac{2\phi\ell'}{A(\ell' - L')} \qquad \text{(cutoff gridlines/mm)} \tag{4.13}$$

Having determined a and n, we can now find the width of the clear stripes in the cutoff grid, b:

$$b = 1/n - 2a \qquad \text{(mm)} \tag{4.14}$$

As for the image resolution, a convenient simplification can be made of Eqn. 4.7 by choosing λ = 0.5 μm (blue-green light), substituting Eqn. 4.8 in Eqn. 4.7, and using Eqn. 4.14 under the approximation that b >> a:

$$w \approx 0.002 R\phi \qquad \text{(mm)} \tag{4.15}$$

where R = ℓ/A is the test-area distance divided by the lens aperture, or approximately the inverse of the lens aperture angle.

Finally, attention is turned to the depth-of-field of the focusing schlieren system. From Eqn. 3.16, the depth-of-field Δz equals the circle of confusion δ divided by the lens aperture angle, here equal to 1/R. If we claim that defocusing has occurred when the circle of confusion outgrows the image resolution w, then a very narrow depth-of-field results:

$$\Delta z = 2Rw \qquad \text{(mm)} \tag{4.16}$$

Unfortunately this is too narrow to be practical, for refractions just outside this zone will be slightly-blurred but still quite visible in the schlieren image. Instead, a practical (though arbitrary) criterion derives from Weinstein's [110] experience with focusing schlieren systems: $\delta = 2$ mm, or

$$\Delta z = 4R \qquad \text{(mm)} \tag{4.17}$$

Outside the depth-of-field by this definition, fine detail in the schlieren image blurs significantly. Users should feel free, however, to redefine δ otherwise as called for, and some have done so. In [219] for example, coherent structures in a small turbulent jet were blurred but still visible at $\delta = 2$ mm. By $\delta = 8$ mm they had disappeared entirely from view. Quantitatively, the peak in the measured optical power spectrum corresponding to these structures disappeared for δ = 2-3 mm.

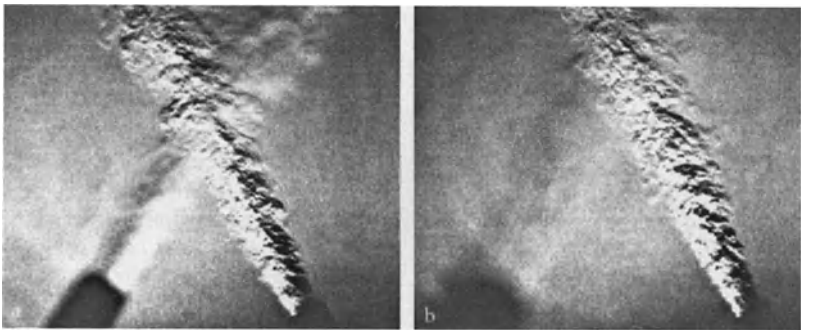

Fig. 4.11. Short-exposure focusing schlieren images of crossed turbulent free jets. The right-hand jet remains in focus while the other is defocused by **a** 19 mm and **b** 38 mm [110]. Photos by L. M Weinstein, reproduced by permission.

Eqns 4.10 through 4.17 define the focusing/large-field schlieren system to the stated level of approximation for design purposes. Once values of a, b, and n have been found, the required cutoff grid is specified. The source grid is then the complimentary image of the cutoff grid, larger by the factor L/L'. Thus the opaque source-grid bars are bL/L' wide and the clear stripes are $2aL/L'$ wide.

Adjusting a Focusing Schlieren System. Once the components thus designed are acquired or fabricated and set up according to Fig. 4.9, one exposes the cutoff grid in place on photographic film mounted at the sharp focus of the source-grid image. High-contrast film is normally used (e.g. Kodalith), and some effort is required to obtain a cutoff grid exposed and developed to produce sharp dark lines separated by clear lines. A measure of success is the *extinction ratio*, the ratio of image illuminance at minimum cutoff to that at full cutoff. An extinction ratio of 10 or higher is needed to reach the best sensitivity that the schlieren system can deliver. If this ratio is only 4, for example, then the actual sensitivity will be only about half as good (or twice ε_{min}) as the value chosen during the design process. The system of Alvi et al. [219] initially had an inadequate 6:1 extinction ratio, later improved to 15:1 by proper attention to cutoff grid exposure [220].

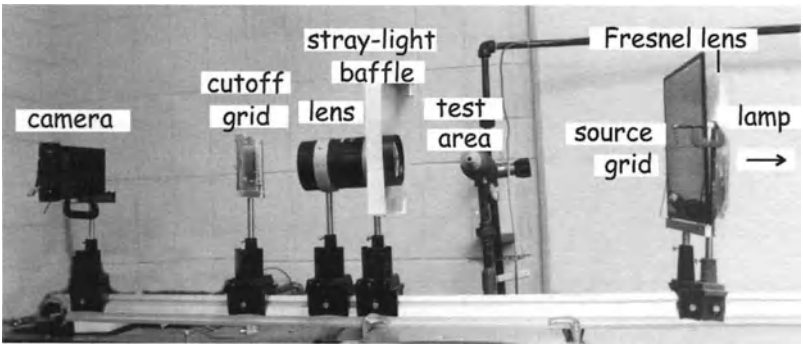

Fig. 4.12. Physical setup of sharp-focusing schlieren system of Alvi, et al. [219,220].

Once a suitable cutoff grid is developed, dried, and reinstalled, the following final adjustment sequence is called for in order to maximize performance [159]: First, all components should be checked for proper height on a common horizontal centerline. With the light source turned on, a sheet of white paper held in front of the lens assists in axially locating and pointing the illuminator assembly (light source, Fresnel lens and source grid) such that the image of the light source is centered on the lens.

For cutoff grid alignment, the analyzer assembly (lens, cutoff grid holder, and image plane) is adjusted until the source grid image and the cutoff grid coincide. This may be done with the sheet of white paper placed against the back of the cutoff grid as a screen, or by direct examination of the cutoff grid from behind using a magnifying lens or eye loupe. Adjust so that reference marks on the source grid line up with their images on the cutoff grid, yielding approximately 100% cutoff. Recheck that the light-source image is still reasonably centered on the lens, and iterate the adjustment if necessary.

The final step is the adjustment of the cutoff grid for even illumination of a sensitive, uniform schlieren image. Competent vernier controls for x, y, and z cutoff-grid position and rotation in the x,y-plane are essential at this stage [104]. Incompetent controls lead to backache, ill temper, and a lot of foul language.

Translate the cutoff grid perpendicular to the direction of its gridlines until the brightest screen image is seen, then slowly drive it back toward full cutoff. As the schlieren image (observed directly on a ground-glass screen or sheet of white paper) begins to darken, non-uniformity or "splotchiness" is usually seen at first. Sometimes moiré fringes appear due to gross source-image/cutoff-grid misalignment. If the non-uniformities are parallel to the gridlines, a grid focus error along the z-axis is indicated. If they are perpendicular to the gridlines, a cutoff-grid rotation error in the x,y-plane has occurred. At first both errors will likely be present, causing non-uniformities or fringes to lie at some angle to the gridlines. The more fringes that appear, the larger is the misalignment error. Focus and rotation errors should be dealt with separately in order to converge upon the best grid alignment and uniform darkening of the schlieren image with the least effort. With experience (and, once again, competent vernier controls), the procedure becomes reasonably routine. Still, even seasoned users of focusing schlieren equipment must remind themselves occasionally that some frustration is expected, and that the merits of the technique are worth the effort required.

Perfect image uniformity at high sensitivity is seldom achieved, and some mild splotchiness across the field-of-view is common. For white-light illumination, color discrepancies often appear in the image, since the present technique places severe demands on the chromatic correction of even the best camera lenses. Since chromatic aberration detracts from schlieren sensitivity, greenish or bluish photographic color-correction filters in front of the camera lens are helpful in black-and-white imaging, or when a shift of the color balance of front-lit objects does not create a problem.

If reasonable image uniformity cannot be had with any cutoff adjustment, or if a dark maximum cutoff is not possible, then troubleshooting is needed. Recheck the grid quality and the spacing and alignment of the key optical elements as previously described. Look for out-of-x,y-plane tilt in all components and correct it if found. Avoid stray light by shielding the cutoff grid (especially during its exposure) and the schlieren image plane with black cloth, bellows, etc. Although the full aperture of the camera lens is used in the design process for minimum depth-of-field and maximum illumination, a 1-stop reduction of aperture in operation sometimes helps to solve image non-uniformity problems. As a last resort, reconsider whether the camera-lens quality is sufficient for the job at hand.

Retroreflective Source Grids [216,221-224]. When large-scale schlieren imaging takes precedence over sharp-focusing, sizeable source grids are required. For simplicity and low cost, the illumination scheme of Fig. 4.9 then gives way to a simple panel coated with commercial retroreflective sheet material, with a pattern of lines or spots painted-on or superposed using a mask. The illumination then comes from lamps near the camera lens, illuminates the source grid uniformly, and is reflected back toward the lens with high gain. This simulates a self-illuminated

source grid at reduced cost and weight. A US Patent was issued to J. T. Heineck for this approach in 1996 [222].

Commercial retroreflective plastic sheet material is available in several varieties (see App. D). These are mass-produced for highway signs, and some of them have an imbedded pattern which is not itself retroreflective. This pattern is disadvantageous for present purposes, since it shows up in the cutoff grid and detracts from the intended line pattern. High retroreflective gain is important, thus the frontlighting of a retroreflective source grid should be as near the optical axis as possible. The cost of the retroreflective material is in the \$30-\$70/m ^{2} range.

Applications. The idea of focusing and large-field schlieren techniques flourished following Weinstein's [110,218] seminal work, whereas previously it had been a mere curiosity [225-232]. Vasiliev [102] foresaw the potential value of large-field schlieren to industry, and indeed the industrial applications now range from combustion research [233,234] and thermal-spray technology [111,235] to ventilation [186,232,236] and leak detection [237]. The leading application is still aerodynamics and wind-tunnel testing [197,219,220,222-226,230,238-240]. Several large focusing schlieren systems have been built for NASA wind tunnels: cheaper than mirror systems, they also avoid wind-tunnel window problems [238]. The largest of all these burgeoning single-lens-and-grid schlieren instruments is discussed next as a specific example.

4.3.5 Penn State's Full-Scale Schlieren System

More than 20 years ago, I was approached by the (now-defunct) International Harvester Corp. with a request for a schlieren photograph of the heat transfer from a full-scale tractor. I thought it impossible with any existing equipment, but joked that I would try it if they had the influence to borrow the Hale Telescope Mirror from Mt. Palomar (see Fig. 9.36). They did not, of course, but it prompted me to consider schlieren imaging on a scale grand enough to examine full-sized vehicles, equipment, and people. No such opportunity arose until August 1993 when, during a discussion with Leonard Weinstein, it became clear that it was feasible – given a building of sufficient size – to construct by far the largest indoor schlieren system in the world.

Making this actually happen posed several significant challenges. Funding, for example, was sought from various government and industry sources to no avail. Eventually it was built as an internal project of the Penn State Gas Dynamics Lab on a very-limited initial budget. Later improvements were "bootstrapped" by funded full-scale schlieren projects.

The second challenge, finding suitable housing, was similarly discouraging at the outset. Essentially no engineering college has such large space unused and available. This challenge was eventually met by finding and obtaining the use of a 12.2 x 13.7 m Penn State warehouse building (Fig. 4.13a) formerly used for cold fruit storage.

The limited size of this building required some optical design compromises. Above all, maximum field-of-view was sought within the available space. Secondarily, best-available sensitivity was an initial design parameter. Depth-of-field was not a constraint, and turned out to be rather broad in conventional terms (40 cm). This exemplifies how some parameters inevitably give way to others in the lens-and-grid schlieren system design process.

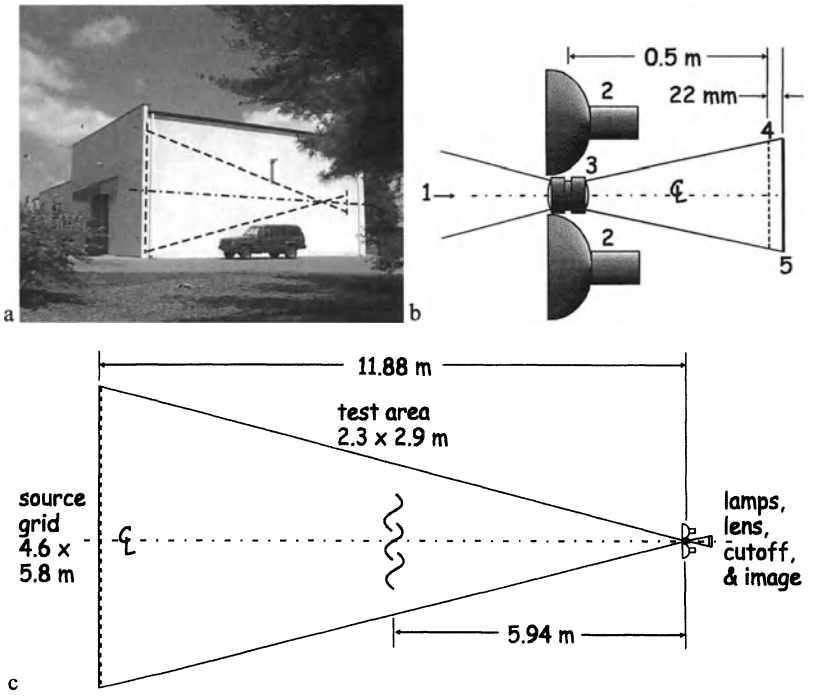

Fig. 4.13. **a** Controlled Atmosphere Storage Building of the Penn State College of Agriculture, now home to the Full-Scale Schlieren System (optical path roughly inscribed to show scale). **b** Close-up diagram showing 1: returning beam from retroreflector, 2: floodlamps, 3: camera lens, 4: cutoff grid, 5: image plane. **c** Top view of optical layout, revealing that it is essentially a single-reflector coincident schlieren system as described in Chap. 3.

The source grid indicated in Fig. 4.13c is a large front-lit retroreflective panel mounted against one wall of the building. Opposite this, a large-format camera lens produces a cutoff-grid size of 20x25 cm (8x10 inches) and an image plane only slightly larger than this (dictated by the available size of photographic film). The nominal test area of the schlieren system is a rectangle 2.3 m high by 2.9 m wide, or about 7.5 x 9.5 feet, which is 8.5 times larger than the field-of-view of

Penn State's mirror-based 1-m coincident schlieren system described in Sect. 4.1.3. This test area normally lies midway between the source grid and lens and is centered 2.4 m above the concrete floor. Other choices of test area location along the optical axis are also possible, though, yielding either larger field at reduced sensitivity or the converse.

The first (1995) embodiment of the Full-Scale Schlieren System used a beam-splitter to fold the optical axis parallel to the shorter building wall, thus extending the axis by several meters [111]. Altho ugh it succeeded after a fashion, this ill-conceived design was plagued by alignment problems and field non-uniformities. In 1998 the beamsplitter – by then recognized as the root of all evil – was abandoned in favor of the shorter, simpler in-line system shown in Fig. 4.13.

Likewise, the initial lens of the system [111] was a 10-cm-diameter f/6 flat-field aerial camera lens of post-WWII vintage. Though of impressive dimensions, it lacked the benefit of modern lens design and coating techniques. This was manifest in both its resolution and its color correction. When funds became available, it was replaced by the biggest large-format camera lens then on the market: a Schneider-Optics 5.7-cm-diameter f/8.4 Apo-Symmar. This modern 6-element coated lens yielded a notable improvement in chromatic fidelity, resolution, and resulting schlieren sensitivity.

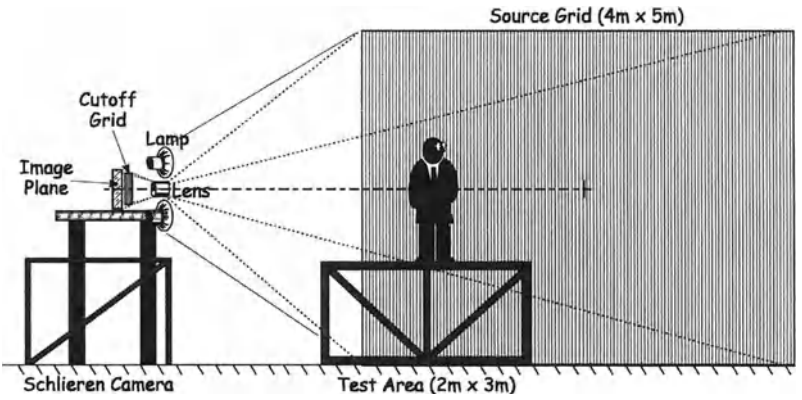

Fig. 4.14. Overall elevation sketch of the Penn State Full-Scale Schlieren System.

In addition to the lens, the key element of the Full-Scale Schlieren System – and its third major challenge – is the front-illuminated source grid. It is made of white 3M retroreflective highway-sign material Type 3970-G. [5] This plastic sheet is mounted to 12 1.2 x 2.4 m x 2.5 mm aluminum sign panels that are assembled

[5] I thank the 3M Corporation for the donation of this retroreflective material.

on a frame. Upon the retroreflective material are silk-screened 5.08-mm-wide vertical black gridlines spaced 5.08 mm apart. The desired accuracy went beyond normal highway-sign silk-screening practice, and was eventually achieved using a special direct-emulsion photographic silkscreen process based on a precise 1.2 x 2.4 m gridline template on photographic film [111]. The 5.08-mm (0.2 inch) spacing was chosen early in the design process as a best compromise between the image resolution and banding criteria discussed earlier.

Source-grid illumination comes from four Calumet Series 2 studio flash heads arranged symmetrically about the camera lens (Figs. 4.13b and 4.14). These each have 24-cm-diameter reflectors and are all driven by a single 3 kW PS4N power supply. 60-125 Joules of flash energy is usually required for schlieren photographs, but setup and video are done using the continuous 250 W modeling lamps in each flash head. Oblique front-lighting of objects in the test area is further done by two additional flash heads driven by a separate power supply.

Special illumination is needed to freeze the motion of high-speed events, however. The studio flashes are about 1 ms in duration, during which interval a shock wave could traverse 1/3 m or more. For such experiments [166] the source grid is illuminated by a Viewstar Inc. Model 955-5 high-speed triple-flash light source similar to that described in [241]. Each Xenon flashtube discharges 5-10 Joules in about 5 μsec through dichroic filters designed to separate the three flashes via red, blue, and green exposures on a single color photograph. In cases where only a single illuminating flash is desired, the second and third flashes of the Viewstar light source are disabled and the color filter pack is removed.

The schlieren image plane was originally observed visually on a ground-glass viewing screen with continuous lighting, or was flash-photographed using a Polaroid 20 x 25 cm film back. Videography was later done from the ground glass with the aid of a Fresnel lens. Polaroid photos have been made using 20 x 25 cm Type 809 color film (ISO 80) or Type 803 black-and-white film (ISO 800) and the studio-flash illumination described above.

The Viewstar high-speed light source, however, emits insufficient luminance to expose 20 x 25 cm Polaroid film. Instead, a Fresnel relay lens of 24 cm focal length is placed near the schlieren image plane, creating an image of the camera-lens aperture at its back focus that is accepted by the 105 mm f/2.4 lens of a Pentax 67 medium-format camera. 120-size roll film at ISO 3000 speed is thus exposed for high-speed still images such as those shown in Color Plates 12 and 48. The Fresnel lens has the worst optical quality of any element in the schlieren system, but sharp photographs are nonetheless obtainable. Such Fresnel relay lenses need a fine pitch interval [159] – better than the usual 0.5mm if available.

The length of the building containing the Full-Scale Schlieren System – minus adequate working space beyond the image plane – dictated a length L (Fig. 4.9) of 11.88 m. Locating the test area nominally at $\ell = L/2$, the thin-lens formula with f = 0.48 m (App. A.3.3) yields the distances $L' = 0.50$ m and $\ell' = 0.522$ m. As shown in Fig. 4.13c, this leads to a highly-foreshortened schlieren analyzer assembly, with only F = 22 mm between the cutoff grid and the image plane.

The demagnification of the cutoff grid with respect to the source grid is $L'/L = 0.042$, while that of the schlieren image with respect to the test area is $\ell'/\ell = 0.088$.

But, since one is practically limited to 20 x 25 cm photographic materials, this constrains the maximum size of the cutoff grid and the image plane. As a result, the full 4.6 m height but not the full 7.2 m width of the source grid is usable. In fact, only 5.8 m of source-grid width is presently used. The test-area dimensions of 2.3 x 2.9 m follow directly from this.

Given the source-grid constant of 5.08 mm, cutoff gridlines are demagnified to a width of b = 0.213 mm or n = 2.34 line-pairs/mm. At 50% cutoff, Eqn. 4.12 yields a sensitivity of about 9 arcseconds. This is not very good, but 50% is not the most sensitive setting. Modulation transfer function information for the Apo-Symmar camera lens (www.schneideroptics.com) claims a resolution of at least 75 line-pairs/mm, so a = 27 μm or at least 87% cutoff is justified. In this case Eqn. 4.12 yields ε_{min} = 2.3 arcseconds, and indeed, by comparison with Schardin's standard (Figs. 3.12 and 3.13), the best sensitivity of the Full-Scale Schlieren System is in the 2-arcsecond range. It is limited by the cutoff-grid extinction ratio, evenness of cutoff across the field-of-view, and chromatic aberration. Despite modern computerized apochromatic lens design, some residual chromatic aberration remains in this demanding application for a camera lens. Dull green and red shades are the result in the schlieren image near full cutoff.

Eqn. 4.8 yields ϕ = 2.8, thoroughly violating Weinstein's [110] criterion for avoiding image banding. This is an inevitable result of the short separation distance between the cutoff and image planes – a concession to size and sensitivity – but it is amazingly not a noticeable problem. Weak vertical bands can be seen with about 0.3-mm spacing in the 20 x 25 mm image plane: so fine and low-contrast that they are usually unnoticeable unless deliberately sought.

According to Eqn. 4.7, the size of a resolvable object in the image plane at λ = 0.51 μm is slightly over 1 mm. Resolving 1 mm in a 2 x 3-m test area yields razor-sharp images, borne out by the results shown below.

Maintaining a high-quality cutoff grid is imperative to achieving the performance just described. A recently-exposed grid is required since, over time, various small thermal expansions and misalignments eventually spoil the match between the cutoff grid and the source image. A 20 x 25 cm sheet of Kodalith film is held firmly between glass plates for exposure, then developed and re-installed approximately. Bolt heads on the source-grid panels serve as alignment reference marks. A Viewstar 4-axis micropositioner provides vernier control of x, y, and z cutoff-grid position and rotation in the x,y-plane. The first version of the schlieren system [111] lacked this important feature, making uniform manual cutoff adjustment a hit-or-miss ordeal.

Examples of images from the Full-Scale Schlieren System are shown in Figs. 9.9a and 9.15, and in Color Plates 10-13 and 48. Four additional examples are shown in Fig. 4.15 below. They show new applications now possible at full scale, the general sensitivity and resolution of the image, and front-lit human subjects.

The front-lighting of the test area, covered more thoroughly in Chap. 7, is done from the direction of the camera lens according to the studio principles of key and fill lighting. Lamp locations are restricted, though, to those off-axis positions where no specular reflections from the source grid appear in the schlieren image.

Further, since the schlieren illumination is itself slightly off-axis, some slight shadowing is usually seen around opaque objects in the test area.

Potential applications abound for a schlieren system large enough to accommodate full-scale equipment and people. Some of these, especially leak detection, explosions, and ventilation, are covered later in Chap. 9. Future projects for the Full-Scale Schlieren System include fume hood isolation flows and human interactions, agricultural airflows in greenhouses, room air currents in indoor air quality and the dispersion of room deodorizers, cold-air isolation in grocery display freezers, external ballistics imaging, and the interaction of the human thermal plume with insect pests and the ambient breeze. A variety of industrial customers with problems ranging from HVAC airflows to motorcycle mufflers is also served.

Fig. 4.15. Full-scale schlieren images of **a** blackjack table, dealer, and players, **b** commercial air curtain (courtesy Mars Air Door, Inc.), **c** commercial kitchen ventilation with spillage of cooking fumes from exhaust hood [175,232,236], and **d** supermarket chest freezer with frozen pizza being removed. Models are H. A. Gowadia, L. J. Dodson, and J. D. Miller.

4.4 Large-Field Scanning Schlieren Systems

4.4.1 Scanning Schlieren Systems for Moving Objects

Schardin [2] mentioned scanning schlieren methods in passing, but did not pursue the concept. It then lay undeveloped for more than 50 years. The idea is to scan the eye or camera in Schardin's schlieren method no. 1 (Fig. 4.4), so that the distant light/dark boundary traces the schlieren features across an entire test area rather than just a single line of sensitivity. Alternatively, the optics may remain fixed while the schlieren object traverses the field-of-view if moving photographic film or other recording media are used. Weinstein patented such a schlieren system for moving objects in 1996 [242], as illustrated in Fig. 4.16.

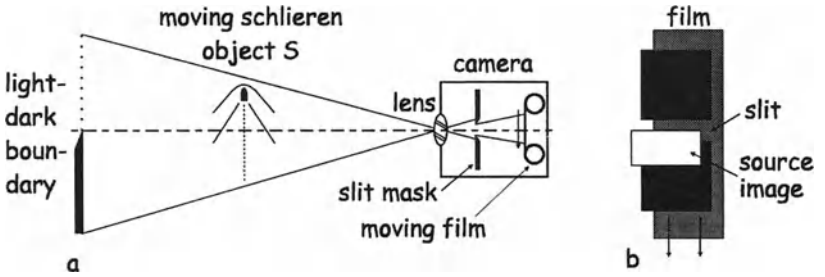

Fig. 4.16. Diagram of Weinstein's [242] schlieren method for moving objects. **a** Overall layout. **b** Detail showing light-source image, cutoff by slit mask, and moving filmstrip.

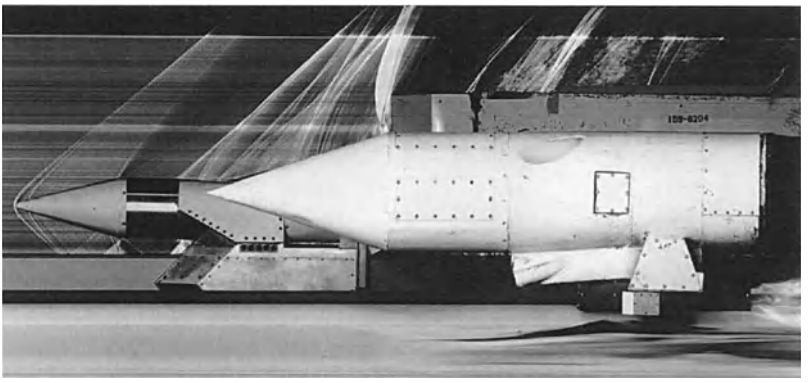

Fig. 4.17. Holloman AFB high-speed test track Maglev model, Mach 1.8 [113] (US Govt. photo courtesy Leonard M. Weinstein).

In this device the film transport speed is arranged so that the moving image of the schlieren object is rendered stationary with respect to the film. Meanwhile the image of the fixed light/dark boundary, being partially cut off by the slit aperture, produces an instantaneous line of schlieren sensitivity which sweeps out an entire two-dimensional schlieren image on the film during its exposure. Dramatic results have been obtained in rocket-sled test track experiments, Fig. 4.17 [113], and the full-scale flight experiments described below. Industrial uses, e.g. production and assembly lines, are a promising but untried application.

The size of the field-of-view of this schlieren system is limited only by the size of the distant light/dark boundary. If the horizon, the Sun, or the Moon are used, then fields of enormous size may be examined by schlieren. Such is the case in the preferred embodiment of Weinstein's invention, known as "Schlieren for Aircraft in Flight" [111,112,224,242-245].

Schlieren for Aircraft in Flight was already described briefly in Chap. 1. Its operating principle follows Fig. 4.16, except that the single lens shown becomes telescopic optics, and the light/dark boundary is the Sun's disk.

In Fig. 4.18a, a 16 mm streak camera records the schlieren image and provides the necessary scanning of the line of schlieren sensitivity across the image. The schlieren stop is a mask, shown in Fig. 4.18b, mounted inside the telescope at the Sun's image plane. It has a curved slit that matches the edge of the Sun. The amount of cutoff is varied by positioning this slit with respect to the Sun's image.

The telescope drive maintains the Sun's image fixed with respect to the mask while an aircraft is flown across the Sun as seen by the telescope. The distance from telescope to aircraft is pre-arranged so that the latter will be sharply focused on the film plane. The motion of the film is in the direction of flight of the aircraft, and is adjusted to maintain the image of the aircraft fixed while scanning the masked edge of the Sun across it to record the schlieren field.

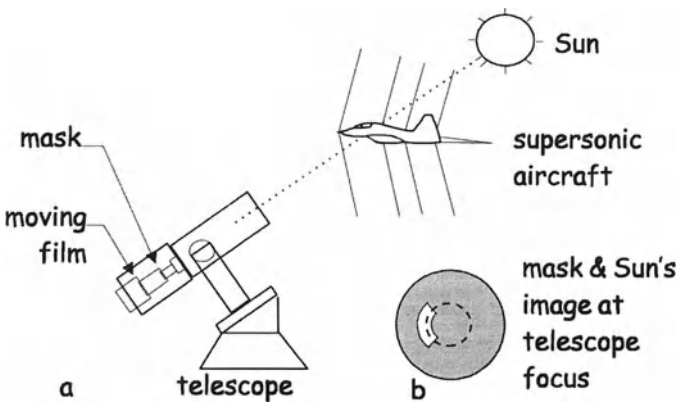

Fig. 4.18. Schlieren for Aircraft in Flight. **a** General optical arrangement. **b** Mask at Sun's image plane providing schlieren cutoff. (Re-drawn from [112].)

The practicality of this approach was demonstrated by Weinstein in 1993 [112], when he photographed a NASA T-38 aircraft flying across the Sun at Mach 1.1 and 9.75 km range from his specially-fitted 20 cm f/10 telescope. The resulting image was shown earlier as Fig. 1.24b. Since then, several high-speed aircraft including the F-18 and SR-71 have been imaged in sonic boom studies using this full-scale outdoor schlieren method [224]. Just as in wind tunnel testing at model scale, Schlieren for Aircraft in Flight reveals the location of shock waves, boundary-layer transition, the extent of flow separation, vortical-flow details, etc. A version with airborne optics is planned, as is the imaging of the Space Shuttle Orbiter during reentry into the atmosphere.

Several limitations occur due to the use of film as a recording medium in a streak camera. A newer version of the schlieren camera for full-scale aircraft imaging uses an improved electronic camera instead [243]. This camera operates on a "time-delay integration" principle [246], where a moving image is effectively tracked by scanning sequential rows of pixels perpendicular to the direction of motion. Since the scan rate is variable, it can be adjusted to match the motion of the aircraft image across the schlieren image plane.

4.4.2 Schlieren Systems with Scanning Light Source and Cutoff

Alternatively, one may consider scanning the light/dark boundary and the schlieren mask in cases where the schlieren object remains stationary. While this scheme may appear inefficient at first, it has certain advantages for large fixed fields-of-view. Moreover, it has features and components in common with flatbed image scanners and copy machines. A diagram is shown in Fig. 4.19.

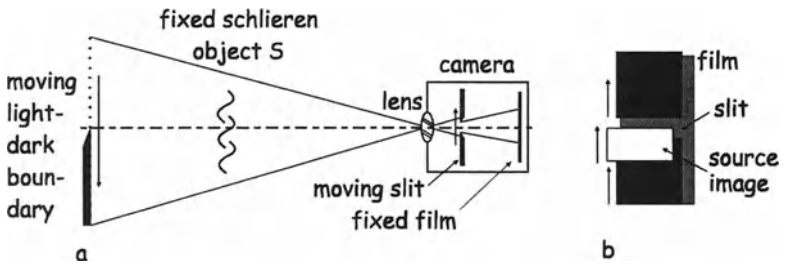

Fig. 4.19. Diagram of a scanning schlieren method with moving light source and cutoff. **a** Overall layout. **b** Detail showing moving source image, moving slit mask, and fixed film.

This is not precisely what Schardin had in mind [2] when he suggested rotating both the light/dark boundary and the slit mask about the center of the lens. For large fields-of-view, however, independent planar motion of the light source makes more sense. Arranging for the slit to track the light source motion and maintain a constant schlieren cutoff is not difficult with modern electronics.

Such a schlieren system has never been assembled as of this writing. The idea originated with L. M. Weinstein and the author in 1997 as a way to obtain outdoor schlieren images for gas-leak detection with simple portable apparatus (see [237] and Chaps. 7 and 9). A practical optical system is sketched in Fig. 4.20.

This is intended to be a portable schlieren instrument involving equipment that can be carried around in a few suitcase-sized containers. It can be set up in a few minutes to less than an hour, operated on battery power for remote locations, and used to image schlieren objects anywhere within its roughly 1x3 m field-of-view. Once the instrument is set up, this field-of-view can be moved around to inspect different pieces of equipment, for example, requiring only a brief readjustment time after each move. Alternatively, the instrument can be set up in a fixed location where it can observe full-sized schlieren objects.

The light source is a battery-powered linear fluorescent tube that scans between two portable masts on taut wire supports. It is necessary that the schlieren object, if not completely steady, at least changes little during the scan time. Localized convective heat transfer, natural-gas leaks, and many other interesting phenomena satisfy this requirement well enough to allow useful imaging with scan times on the order of one second.

Aimed at the test area and the background is a tripod-mounted schlieren camera. Inside the camera, a lens focuses an image of the scanning light source upon a scanning schlieren cutoff (slit mask) that is electronically driven in sync with the light source. A digital camera acquires the schlieren image and displays it on the screen of a laptop computer. Alternatively, a digital flatbed scanner pickup can be synchronized to acquire the image by following the scanned line of schlieren sensitivity in the image plane.

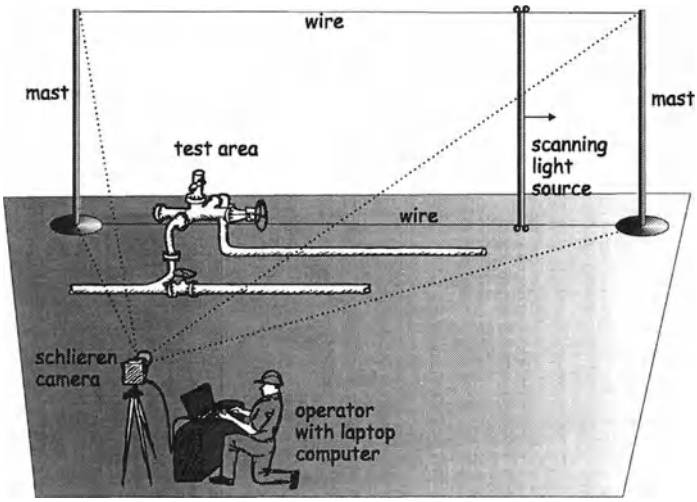

Fig. 4.20. Diagram of a scanning-light-source schlieren system for large fields-of-view.

The automatic adjustment features of this portable full-scale schlieren instrument avoid a tedious alignment procedure during setup, and thus make it require little operator training. The approach does require a clear optical path, however, and sufficient space on either side of the test area. A prototype demonstration instrument is planned.

4.5 Moiré-Fringe Methods

The scientific use of moiré patterns is traceable to Lord Rayleigh more than a century ago [247]. Moiré fringes have appeared since then in so many different schlieren adaptations that one must distinguish them carefully. In this case we consider a variant of the lens-and-grid method with grids on either side of the schlieren object, arranged and sized to coincide in the image producing fringes. In this case large fields-of-view require only large transparent grids, but the method is inferior in some respects to the lens-and-grid methods described earlier.

Schardin [2] first suggested, with reference to his schlieren method no. 2 (Fig. 4.5), that a negative of the undisturbed source-grid image could be made and superimposed with the schlieren image plane, emulsion-to-emulsion, in order to mask the stripes. This fails to provide a uniform schlieren field, but does at least remove the background stripes in cases where they are distracting.

Fromme [248] next considered the deliberate use of moiré patterns in a twin-grid schlieren apparatus. His work was followed by that of Bampfield [249], Waddell [216] and Dalziel et al. [250-252]. The general optical arrangement of all these works is shown in Fig. 4.21a, where the imaging of an illuminated grid 1 through grid 2 is diagrammed. A similar effect can be obtained by projecting grid 2 onto grid 1 using a light source in place of the camera in the figure [216,249,253] (see Sect. 10.4.4). It is clear from this figure that the large-field features described earlier for lens-and-grid methods apply here as well.

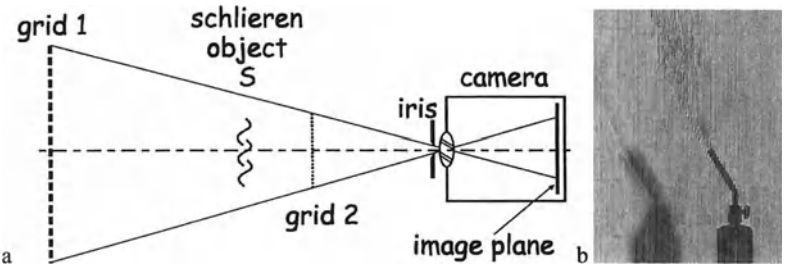

Fig. 4.21. **a** Diagram of a twin-grid moiré-fringe schlieren instrument. **b** "Synthetic schlieren" image of the thermal plume of a propane torch.

Sharp-focusing is another story. To achieve moiré effects, the grids and the schlieren object must all be simultaneously in focus. This implies a small lens aperture and a correspondingly-large depth of field.

Dalziel et al. contributed to this method by realizing that grid 2 could be simulated electronically in the image capture device [250,251,254]. A video image of grid 1 is first obtained without the schlieren object present. This is stored and then subtracted from the image of grid 1 plus the schlieren object, effectively removing the grid from the image by optical processing. An example is shown in Fig. 4.21b. Dalziel et al. [254] admit that the chief drawback of this approach is reduced spatial resolution compared to standard schlieren methods. On the other hand, the potential to use the brick wall of a building as a background grid promises a very large field-of-view (yet to be actually realized). The background-oriented schlieren method, covered in Sect. 10.3.5, involves a related approach.

Two associated methods deserve mention in closing. Weinberg's full-scale optical fire research method [255] is actually a large-area infinitesimal-shear interferometer with a laser light source. However, the shadowgram-like result is formally equivalent to the distorted shadow of a fine grid, and moiré readout techniques are used. The method of Giglio et al. [256] is similar to the large-field optics discussed earlier in this Chapter. However, a double-exposure specklegram rather than a schlieren image is recorded. The schlieren image only appears later during post-processing, when a converging readout beam and knife-edge are applied. Despite these issues, Giglio et al. [256] show a 70-cm schlieren image obtained without the use of expensive, large-diameter precision optics.

4.6 Holographic and Tomographic Schlieren

Even though laser interferometry and holography are outside the scope of this book, such methods deserve at least a brief mention when related to large-scale and focusing schlieren,. Since Gabor's original work [257], holography has promised three-dimensional imaging and has generally delivered. Hologram reconstruction of schlieren phase objects, yielding both the amplitude and the phase of the original light beam, was demonstrated repeatedly [258-263]. Holographic multiple-source schlieren systems have also been built: Buzzard's system [264] used lenticular lenses to break the input laser beam into several spatially-separated sources for sharp-focusing. A similar approach embodying Weinstein's contributions to focusing schlieren is given by Doggett and Chokani [265].

Tomographic schlieren methods began with the work of Lamplough [266], who devised elaborate "rangefinder" and shock-wave plotting methods. A parallel schlieren beam was rotated perpendicular to the optical axis to map the tangential elements of the curved shock wave on a swept wing. In the 1950's – the early days of transonic aerodynamics – this method revealed the 3-D shapes of shock waves on swept wings. Results were shown from both wind tunnel and flight tests. After Lamplough, though, this approach was apparently never used again.

Related experiments using tomographic views to derive complex shock-wave shapes are described by Winkelmann and Feldhuhn [267], Larcombe [268], Agrawal et al.[269], Curell and Belford [270], and Skews [271]. The theoretical background required to extract the refractive-index distribution from complex schlieren images using multiple beam paths is given by Vasiliev [102], Tanner [272], Sedel'nikov and Chernov [273], and Watt [274]. A computational example is given by Cianfrini et al. [275] and the application to flames is discussed by Schwarz [276].

5 Specialized Schlieren Techniques

> Genius is nothing more than knowing the use of tools, but there must be tools for it to use.
>
> *Samuel Johnson*

> The result of the experiment depends on the nature and the quality of the tools, not on the ideology of the experimenter.
>
> *Freeman Dyson, in* 'The Sun, the Genome, and the Internet'

The users of schlieren techniques since Toepler's time have been a prolific group. Eager to add their own touch, they have invented, published, and re-invented dozens of adaptations and changes, grouped here into a few general categories. This diversity may be due in part to the lack of standardized commercial schlieren instruments; users having to build their own naturally add improvements and variations along the way. In any case the trend continues right up to the present, revealing that schlieren techniques still constitute a healthy theme of optics and experimental physics. A few specialized techniques not covered in this Chapter are instead included in Chap. 10 on Quantitative Evaluation.

5.1 Special Schlieren Cutoffs

The most popular variation on the schlieren theme has been the specialized cutoff, or source/cutoff pair, aimed at emphasizing certain features of the schlieren image. All those involving color are covered in Sect. 5.2, but many others remain. Some are trivial: for example the L-shaped cutoff of Speak and Walters [126] and the arrowhead cutoff of Taylor and Waldram [133], both being equivalent to an ordinary knife-edge set at an angle. Indeed the simple, time-honored knife-edge and rectangular slit source remain by far the most-used source/cutoff combination in all of schlieren imaging. Vasiliev and Otmennikov [277] point out that nearly any possible values of schlieren sensitivity can be obtained by such a simple source/cutoff pair, concluding that "there is no reason to use diaphragms with complicated shapes." Other reasons will arise in this Chapter nevertheless.

G. S. Settles, *Schlieren and Shadowgraph Techniques*

5.1.1 Graded Filters

Invented by R. J. North [93] in 1952, the graded filter is a simple expedient to extend the range and lessen the diffraction effects of the knife-edge cutoff at some cost in sensitivity, as illustrated in Fig. 5.1.

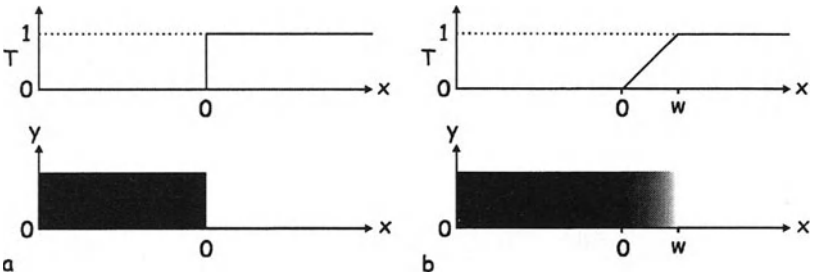

Fig. 5.1. A comparison of the transmission function T and the actual appearance of **a** the vertical knife-edge, and **b** the vertical graded filter schlieren cutoff.

Whereas the knife-edge produces an abrupt half-plane cutoff, the graded filter spreads the cutoff linearly[1] over an arbitrary width w in the schlieren cutoff plane. Recalling the geometric theory of schlieren sensitivity from Chap. 3, the role of "*a*," the partial height of the light-source image unobscured by the knife-edge, is here replaced by w. Assuming a 5% contrast-detection threshold, the smallest test-area refraction angle ε_{min} visible in the graded-filter schlieren image is given by:

$$\varepsilon_{min} = 10313 \cdot w / f_2 \qquad \text{(arcseconds)} \tag{5.1}$$

Commercially-available graded filters in the form of "fuzzy" photomasks can be had from DSC Laboratories (see App. D) in widths w = 1.5, 4, 6.5, 9, and 11 mm. For the tabletop example schlieren system of Chap. 8, with f_2 = 864 mm, the corresponding ε_{min} values range from 18 to 131 arcseconds. The same optical system with a 95% knife-edge cutoff of a source image 1.5 mm wide is capable of 1 arcsecond sensitivity. Candle-flame schlieren images are shown in Fig. 5.2 to illustrate this sensitivity range.

Clearly, the knife-edge is preferred over the graded filter in almost all applications where sensitivity is paramount, but sensitivity is not always paramount. Applications like high-speed wind tunnel testing, with strong refractions due to shock

[1] Linearity is shown in Fig. 5.1 and is assumed here for convenience. But in fact, nonlinear graded filters can be made and used, and even an honest attempt to fabricate a linear graded filter can result in partial nonlinearity [283].

waves, suffer when high sensitivity and its attendant narrow measuring range are used (see Fig. 3.20). Better schlieren images are had in such cases when a graded filter allows reduced – but still adequate – sensitivity along with a broader measuring range and less vibration sensitivity. A good example of such an image was shown earlier in Fig. 1.21.

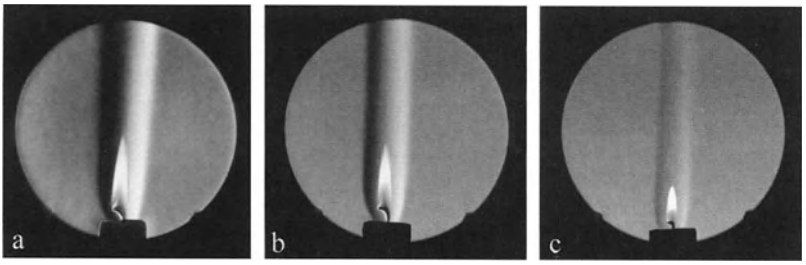

Fig. 5.2. **a** Knife-edge schlieren image of candle flame with approximately 95% cutoff of a 1.5-mm-wide light-source image at $f_2 = 86.4$ cm, **b** graded-filter cutoff with gradation width $w = 1.5$ mm, **c** graded-filter cutoff with $w = 11$ mm. All images are adjusted to a common tone balance. Note that the candle wick burned down during the sequence. Photos by Heather Ferree.

In such cases the use of a graded filter in place of a knife-edge imparts a number of advantages [84,98]. The diffraction halo disappears (see Fig. 5.2) and the other effects of diffraction, described in Section 3.6, are ameliorated. Sharper images with better spatial resolution result. Broad graded filters can be used to extend the measuring range without limit, save for the limit imposed by inadequate sensitivity. Reduced sensitivity also carries with it a reduction in susceptibility to mechanical vibration, as discussed further in Chap. 7.

An additional degree of flexibility is also provided by the graded filter cutoff that the knife-edge lacks: the sensitivity, range, and cutoff direction can be varied without having to change the light source size or orientation. Thus, for example, both schlieren and shadowgraph images can be obtained from the same apparatus without requiring a compromise on light-source dimensions.

Kean [146] asserted that the beneficial effects of the graded filter result, at least in part, from its linearization of the schlieren system sensitivity. [2] Exact linearity and a precisely-inverse relationship between sensitivity and range are benefits of the use of a linear graded-filter cutoff [66,154]. For most purposes, tho ugh, this distinction is too subtle to be of much concern.

[2] It was noted by some [130,146,154] that the knife-edge schlieren system is not strictly linearly-sensitive to phase gradients from the Fourier-optics standpoint (see App. B), as it is when based purely on geometric optics (see Chap. 3). Zakarin and Stricker [1013] found geometric-optical behavior with incoherent light but not with coherent light.

A serious concern arises, however, with use of a laser as a schlieren light source [100]. The same knife-edge that works well with extended white-light sources is too harsh for use with coherent illumination, as demonstrated in App. B. Here the graded filter plays a crucial role, to be illustrated and discussed further in Chap. 7.

The Neutral-Density Knife-Edge. Closely allied with the graded filter is the partially-transmitting neutral-density knife-edge, which has a sharp edge like a razor blade but transmits a certain fraction of the light that the razor blade blocks. Its utility, like that of the graded filter, arises on those occasions when knife-edge cutoff is too harsh, or when diffraction effects can stand improvement at the cost of some image contrast. This is principally the case for coherent illumination, where the truncation of the DC component and one whole sideband of the Fourier spectrum in the cutoff plane leaves insufficient remaining information to form a good image (see App. B and [171]). Fig. 5.3 shows an example.

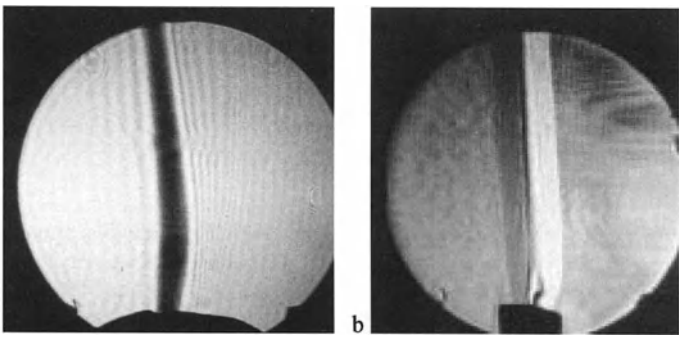

Fig. 5.3. **a** Helium-neon laser-illuminated schlieren image of a candle plume using a razor-blade knife-edge cutoff. **b** A neutral-density knife-edge with about 30% transmission replaces the razor blade. While image a is binarized and almost useless, image b is a more-reasonable schlieren image despite some coherent artifact noise. See Chap. 7 and App. B for more on lasers as schlieren light sources. Photos by T. C. Hanson and Heather Ferree.

Curiously, the partially-transmitting knife-edge has almost never been used before in schlieren imaging *per se*. It is used in microscopy [278,279], however, and is supplied as an add-on to standard microscopes under the trade name of Hoffman Modulation Contrast [280-282] (see Sect. 9.4.7).

Fabrication of graded filters and neutral-density knife-edges is usually either photographic [93,98,283] or is done by sputtering a metallic coating upon a glass substrate [284]. The former method is simple and suitable for all uses except coherent light, where the film grain leads to unwanted image speckle. At the time of this writing, photomasks suitable as graded filters can be bought cheaply (see [285] and App. D). A clear Estar film base is used, and the center transmission of the

graded zone is claimed to be 50%. Even in the high-tech 21 st Century, however, simple neutral-density knife-edges can still be made easily the old way, by taping a glass slide, sooting it in a candle flame, then peeling off the tape. Such an edge was used to obtain Fig. 5.3b. According to Wilska [278]: "The background of the...image appears in an agreeable sepia tone, often giving the illusion of sky-illuminated objects on the sand floor of a shallow sea."

In summary, while neutral-density knife-edges are new to schlieren optics, graded filters find frequent use in allowing the schlieren range and sensitivity to be matched to a particular phenomenon. A set of graded filters of various widths, w, is an important accessory to any Toepler schlieren system.

5.1.2 Exponential Cutoffs and Source Filters

A curved cutoff in place of a straight knife-edge was first suggested by D. D. Maksutov of telescopy fame [101]. His arrangement, sketched in Fig. 5.4a, promotes simplified data reduction since ε is directly proportional to the optical density of the schlieren photo. This is thoroughly covered by Vasiliev [102] with emphasis on photometric methods for quantitative evaluation of schlieren images. That issue is also taken up in Chap. 10, but here the emphasis remains qualitative.

Why one would wish to use a curved rather than straight cutoff or source filter was addressed briefly in Chap. 3, where it was noted that the human eye and photographic film both have an approximately-logarithmic response to the illuminance of the schlieren image. To achieve a linear visual or photographic response, then, one must then employ a source slit or cutoff with an exponential contour. Kean [146] discusses this at length.

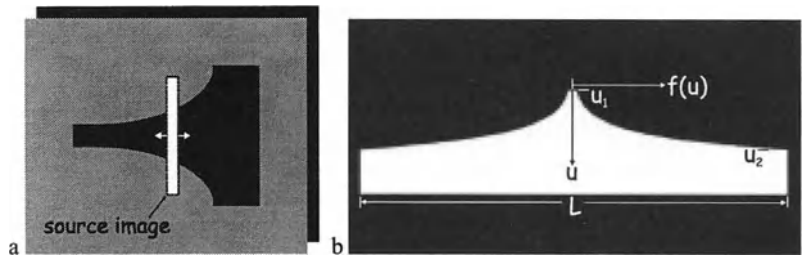

Fig. 5.4. **a** Maksutov's curved schlieren cutoff [101,102]. **b** Kean's exponential light-source slit [146] oriented for horizontal knife-edge cutoff.

Briefly, Kean chose to introduce the curvature in the entrance slit rather than the cutoff, though this choice is largely innocuous. More importantly, the exponential shape (Fig. 5.4b) linearizes the schlieren system response for the eye or film at a modest cost in ultimate sensitivity. The advantage is identical to that of a

linear graded filter, which accomplishes the same purpose. However, Kean notes that the exponential source filter covers a small measuring range at higher sensitivity, while the graded filter naturally covers a broader range at lower sensitivity [146]. Because the sensitivity of neither method depends on the unobstructed source image height, a, as does the Toepler knife-edge and slit, both methods may be described by the term "constant sensitivity." This has advantages in reduced vibration susceptibility, the amelioration of diffraction errors, better tolerance of poor optical components, and the preservation of detail visibility across the entire measuring range. Further, the quantitative evaluation of schlieren images is significantly supported when the system sensitivity is constant with respect to refraction angle ε.

Kean's significant work on this and related topics suffered from appearing only in an obscure government report [146], while the curved cutoff of Maksutov [101,102] never made it outside the former Soviet Union. North's graded filter [93] fared better in terms of popularity, and is still used. In fact, tho ugh, these methods are all complimentary and of similar utility.

Curved cutoffs and source slits are best made by photographing artwork onto high-contrast film or plates at a suitable scale reduction. The formula for the curved portion of Kean's L = 6 mm exponential source slit, shown in Fig. 5.4b, is

$$f(u) = \pm ae^{ku} \tag{5.2}$$

where k = 5, $u_1 = \ell n(k)/k = 0.32$ mm, $u_2 = L/k = 1.2$ mm, and $a \approx 7.5$ mm.

5.1.3 Matched Spatial Filters at Source and Cutoff

> It does not seem to be generally recognized that the search for a particular phenomenon can be greatly facilitated by designing a marking aperture on the basis of a known deflection field.
>
> *F. J. Weinberg* [66]

> Of special interest are diaphragm pairs which are similar to each other, like circle and circle, slit and slit, edge and edge,...so that the second diaphragm is superimposed upon the image of the first if the (test) object is absent.
>
> *H. Wolter* [119]

Weinberg and Wolter attest to the central, unique feature that schlieren optics shares with optical processing: the ability to examine subjects using a matched pair of spatial filters in the conjugate source and cutoff planes. This usually requires incoherent, extended light sources and sometimes "white light" as well.

According to Meyer-Arendt [286], spatial filtering is the process of enhancing or suppressing certain features of an image in an optical system (optical processor, microscope, schlieren system). Often the reason for it involves detecting a desired signal in the presence of noise. A good physical description of the Fourier-optics approach to matched filtering in optical processing is given by Kelsey [129].

In order to classify and compare methods of matched spatial filtering in a schlieren system, a diagram of the type first used by Maddox [287,288] is shown in Fig. 5.5. A simple schlieren system with an extended white-light source is shown, with matched-filter pairs arrayed below it in the conjugate source and cutoff planes. The first source-cutoff pair shown is simply the Toepler slit and knife-edge, since they absolutely qualify as a matched pair of spatial filters [289]. This pair enhances features (e.g. filaments) that are roughly parallel to the knife-edge direction while de-emphasizing those perpendicular to it [289].

Next come dark- and bright-field illumination, obviously inherited from microscopy. The slit-type darkfield approach, Fig. 5.5b, was first used for schlieren in the 1930's [98,133,290,291] and is illustrated by way of a candle-plume schlieren image in Fig. 5.6b. Townend's [290] reflective darkfield cutoff was a silvered plastic strip salvaged from a Christmas decoration.

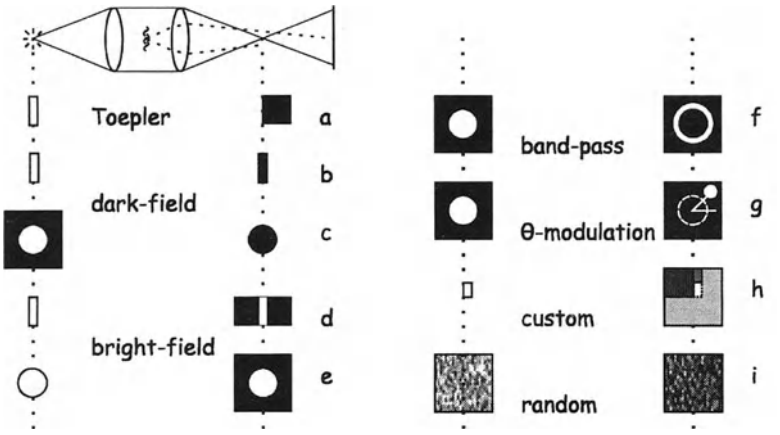

Fig. 5.5. Classification diagram of matched spatial filter pairs for schlieren imaging. **a** Toepler's slit and knife-edge, **b** slit-type darkfield illumination, **c** symmetric darkfield illumination, **d** slit-type brightfield illumination, **e** symmetric brightfield illumination, **f** annular band-pass filtering, **g** θ-modulation, **h** a custom matched pair using color filters, **i** matched random filters.

From the Fourier-optics standpoint, darkfield methods block the zero th-order or DC component of the spatial frequency spectrum in the cutoff plane (see App. B). This produces bright higher-order features against a dark field. Brightfield methods do the opposite, Figs. 5.5d and e, passing the DC component and blocking the higher-frequency information. Examples of brightfield schlieren images are shown in Figs. 2.4a and 5.6a. Both bright- and dark-field yield symmetric schlieren images, unlike the antisymmetric illumination of Toepler's method. In the case of circular matched filters, Figs. 5.5c and e, radial symmetry in all directions perpendicular to the optical axis is achieved [292,293].

Unfortunately neither bright- nor dark-field illumination is especially suited for the kind of general schlieren work handled so well by Toepler's knife-edge method. In Chap. 3 we saw that optimum schlieren sensitivity occurs with limited background illumination: not dark and certainly not bright. The image symmetry touted by some as an advantage rarely proves so in routine schlieren work, where the directional asymmetry of Toepler illumination is familiar and accepted (see Sect. 2.6). It is plainly more difficult to vary the sensitivity of dark- and bright-field schlieren images than it is to adjust the Toepler knife-edge (for example, in the case of Fig. 5.5c, sensitivity must be adjusted by way of an iris in the light-source plane). Astigmatism further limits the use of circular filter pairs in off-axis mirror systems. Finally, as illustrated in App. B, both dark- and bright-field images are susceptible to spurious imaging when coherent illumination is used.

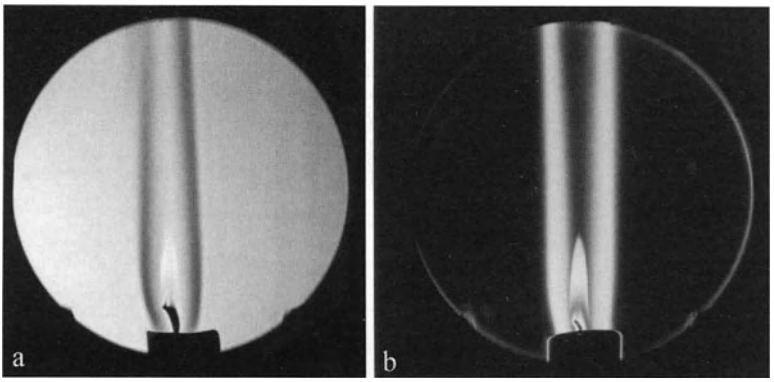

Fig. 5.6. **a** bright-field and **b** dark-field schlieren images of a candle plume according to the matched spatial filter pairs of Fig. 5.4d and b, respectively. Photos by Heather Ferree.

The band-pass filtering scheme of Fig. 5.5f is actually a special case of dark-field illumination. It exemplifies, however, an important element of matched spatial filtering: dividing the radially-symmetric spatial frequency spectrum into discrete passbands. Many such passbands at different radii from the axis can be used if they are marked by color in a white-light system (see Sect. 5.2).

θ-modulation [71], Fig. 5.5g, makes use of the other available cylindrical dimension in the cutoff plane: azimuth angle. ∇n is a vector in x,y,z, of course, and even if we restrict ourselves to the x,y cutoff plane, standard schlieren techniques lack the ability to distinguish all radial vector components. One does this by θ-modulation. For example, it is illustrated in Fig. 5.5g by passing light in the cutoff plane only in a particular radial direction. Many directions can be so marked, but distinguishing them usually requires the added dimension of color.

As a specific example, the custom pair of matched filters shown in Fig. 5.5h was designed by North and Cash [125] to mark specific features of transonic air-

foil flows according to the azimuthal direction of light refracted in a wind tunnel test section. Shock waves are shown in red and expansion fans in blue against a green background [95]. Color is required, but the underlying principle involves designing the matched filter pair specifically to reveal a known general deflection field. Weinberg [66] remarked upon the infrequent use of this powerful approach in 1963, but the intervening decades have brought few additional examples of its use. To use it, one first examines the *polar diagram* of deflected light in the knife-edge plane using a point light source. Different phenomena produce different polar diagrams, which can be distinguished in the schlieren image by clever use of color bands or segments in the cutoff filter [66].

Kelsey [129] suggested a matched filter pair, Fig. 5.5i, based on a random pattern such as an array of variously-sized round spots. Experimental results were shown, indicating a superior noise-rejection capability at reduced sensitivity. Once again, no one seems to have found a subsequent use for this approach.

Finally, in terms of practical issues, note that large matched filters generally require large light sources, such as the multi-filament tungsten lamps used in slide- and cinema-projectors. To prevent the detailed features of the source from propagating through the optical system, the new technology of light-shaping diffusers can be applied [294].

5.1.4 Phase Contrast

> Although the phase contrast technique has proved to be extremely useful in microscopy, its value in optical testing seems to be limited.
>
> *J. Ojeda-Castañeda* [153]

Fritz Zernike won the Nobel Prize in physics in 1953 for the phase contrast method, which improved upon dark-and bright-field microscopy by making weak phase objects visible. Zernike believed this would replace traditional methods like schlieren [295]. But, although the schlieren principle is seldom used nowadays in microscopy (see Sect. 9.4.7), likewise phase contrast plays a relatively-minor role in the broader context of this book, for reasons described below.

Phase contrast accomplishes a partial de-phasing of the light beam in the schlieren cutoff plane. It relies more on interference than on spatial amplitude filtering, and is thus not strictly within the present scope. On the other hand, it uses the same optical equipment but for replacing the schlieren knife-edge by an appropriate phase plate. In that sense, phase contrast may be considered a schlieren-type method using a special cutoff. The distinction is further blurred when the de-phasing is accompanied by reduced transmission, combining pure phase shift with the neutral-density knife-edge method covered in Section 5.1.1.

Phase contrast is well-described by Merzkirch [82], to whom the reader is referred. Coverage is also found especially in [119] and [295], as well as in [98], [102], and [296]. Accordingly, only limited detail is given here.

Zernike's [295] original phase-contrast method involves placing a "phase spot" on the optical axis in the cutoff plane, shifting the phase of the central diffraction order (DC component, or undisturbed light) by ¼ of the light wavelength, λ, and

also attenuating it by 90-99%. The result is part dark-field due to the attenuation, and part interference of the phase-shifted DC component with the higher diffraction orders. For weak schlieren objects, causing roughly $\lambda/4$ phase change, the resulting phase-contrast image is a null-fringe interferogram. It resembles a schlieren image, but has higher sensitivity and characteristic diffraction halos, as illustrated in Fig. 5.7. For stronger schlieren objects of more than 1 λ phase change, the image locally resembles a finite-fringe interferogram.

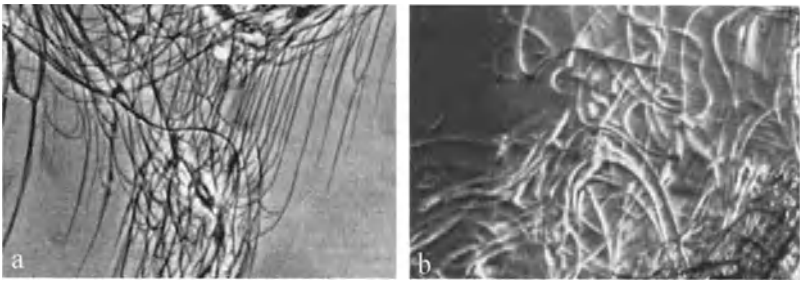

Fig. 5.7. **a** Phase-contrast image of soda-lye soap mixing with water (from Wolter [119], reproduced by permission of Springer-Verlag). **b** Schlieren image of sugar mixing with water (photo by author).

Wolter [119] suggested an alternative to Zernike's phase spot: the $\frac{1}{2}\lambda$ "phase knife" method. Here the phase plate consists of a half-plane, $\frac{1}{2}\lambda$ phase-shift with its straight edge centered on the optical axis. It mimics the knife-edge in terms of attenuation while simultaneously shifting the phase of the attenuated half the Fourier spectrum by 180° [297]. This avoids having to specify a phase-spot diameter, thus gaining some versatility [298]. A computer simulation of the Wolter phase knife is shown and compared with the standard knife-edge cutoff for weak schlieren in App. B.

In monochromatic light the phase shift and interference phenomena just described are unambiguous, but with white-light illumination the fixed phase plate causes a different phase shift for each color. Thus in microscopy [296] a green filter is often used to limit the spectrum width. On the other hand, color phase contrast effects are possible using means described by Wolter [119]: in essence, he combines phase contrast for the smallest, weakest features of the test object with color schlieren, discussed below in Section 5.2.

Phase contrast imaging has the advantage of high sensitivity to small, weak phase disturbances that are beyond the limit of normal schlieren sensitivity. For these objects a 4-to-10-fold contrast enhancement is possible [128]. The limitations of phase contrast, however, are severe outside the realm of microscopy.

While phase contrast improves the visualization of phase objects, it makes amplitude objects less distinct. It thus works best for fine-structured phase distur-

bances like polishing defects in glass, but not so well for the majority of larger-scale phenomena accessible to standard schlieren methods [119]. Its images also suffer from characteristic diffraction halos at sharp opaque edges. Also, a specialized phase plate is needed in the cutoff plane, compared to the ubiquitous razor blade of the schlieren technique.

Further, while commercial phase condensers and objectives are available for microscopy [296], phase filters for schlieren use are not sold commercially. Special-order phase plates are expensive, and need to be specified carefully (e.g. [299]). Methods of making your own phase plate are described in [257,300-302]. These include mica, varnish, or clear tape on a microscope slide, etching the slide with hydrofluoric acid, and bleaching photographic film. Trials of some of these methods show that successful homemade phase plates are not an easy proposition.

Aside from Figs. 5.7 and B.9, another example of phase contrast in microscopy is shown in the discussion of that topic surrounding Fig. 9.34. Phase contrast applied to rarefied hypersonic flows is shown in [297], to small-scale gas-dynamic flows in [299], and to weak natural-gas jets in air in [303].

5.1.5 Photochromic and Photorefractive Cutoffs

Photochromic materials react to illumination by changing their optical density. Specially-formulated glass and the organic compound *bacteriorhodopsin* exhibit this property. Typically, patterns may be "written" in these materials with light of a certain color and "erased" by light of a different color. A popular example is found in eyeglasses that darken automatically upon encountering sunlight.

Photochromic cutoffs were first tried in schlieren systems in the 1970's [304,305]. Initially the idea was to improve upon Toepler's method by using a cutoff that adapted to and cancelled unwanted changes in the undisturbed source image, e.g. due to vibration, thermal expansion, etc. This seems to work, though requiring the added complexity of two separate colors of illumination to write the cutoff and then read the schlieren image.

More recently [306,307] this has been tried with traditional focusing schlieren equipment of the type described in Section 4.2. The results are admittedly not as good as those with the usual fixed photographic cutoff, but advantages are cited in terms of adaptivity and ease of alignment.

This approach shares a common goal with "synthetic schlieren" (Sect. 4.5), the outdoor applications covered in Sect. 9.4.10, and the background-oriented methods described in Sect 10.3.5, namely, the use of large natural outdoor backgrounds for full-scale schlieren illumination. It has not yet been realized with photochromic cutoffs, however. Suitable photochromic materials may not be readily available, and research has not progressed beyond the demonstration stage. Nonetheless, some innovative thinking is called for here. Matched spatial filters (Sect. 5.1.3) using photochromic material at the cutoff might yield a significant new schlieren technique.

Photorefractive materials respond to illumination by a change in refractive index. Examples include barium titanate and lithium niobate crystals. The optics of coherent four-wave mixing in such crystals is complicated, but there is a host of new-age nonlinear-optical applications. One of the least of these – but still significant – is the photorefractive cutoff for a laser schlieren system [308-310]. It provides a temporal rather than spatial schlieren cutoff, thus responding to the frequency of changes in the schlieren object. Sato et al. [308] dubbed it a "dynamic schlieren system."

Some practical examples are shown in Ref. [309]. Uses of photorefractive schlieren include the study of turbulent flows, where it is doubtless more effective than the time-honored method of examining schlieren photos with different exposure times for image smearing. On the other hand, this is much more sophisticated than just a change of cutoff: an entire optical system is needed for photorefractive imaging, and the disadvantages of coherent illumination apply (see Chap. 7).

5.2 Color Schlieren Methods

> I can't imagine why anyone would take a color schlieren photo, other than to hang it on the wall.
>
> *Hans W. Liepmann* (to the author, Feb. 1980)

I reviewed color schlieren techniques in 1980 [311] and again in more detail in 1985 [127]. Here that material is briefly repeated and updated to include developments over the last 15 years.

Color schlieren has been very popular, with hundreds of references since Toepler and more than 60 since my 1985 review. If monochrome schlieren images are aesthetically appealing (Sect. 2.6), color schlieren images are usually even more so. 48 Color Plates at the end of this book amply illustrate the possibilities.

5.2.1 Reasons for Introducing Color

There are several advantages of adding color to the monochrome schlieren image [98]. *Color coding* is useful in studies where additional data (such as n-gradient magnitudes and directions) are required. Wolter [119,312] notes that the gray-scale can only represent a scalar in schlieren imaging, while the vector displacement and angle in the cutoff plane require the extra dimension of color. In certain cases the hue, saturation, and intensity of color are used in quantitative analyses of schlieren images. *Color contrast* is similarly useful in distinguishing the features of the schlieren field from one another and from the black silhouettes of opaque objects. The advantage of the perceived contrast of a color scale [313,314] versus that of a gray-scale gives added sensitivity (if not offset by the sensitivity loss inherent in some color schlieren techniques). The colors also make it easier to refer

to features of the image, and they sometimes help reconcile the conflicting requirements of high sensitivity and broad measuring range. A color schlieren image is usually more evenly-illuminated than a black-and-white image. And finally, the aesthetic value of color schlieren makes it useful for teaching, demonstration, and a range of possibilities beyond those of a pure diagnostic tool.

One must balance these advantages against the disadvantage of some added optical complexity, the slightly-higher cost of color image recording, and the extra cost of color printing (now giving way to digital publishing and the Internet).

The justification for color in schlieren images has been a subject of continuing debate. Some argue that it serves little real purpose other than showmanship, while others claim that it has powerful technical utility. The truth appears to be closest to the latter argument: color serves the same purpose here as in computer graphics, microscopy, satellite imagery, and many other scientific tools: It provides an extra dimension, where required, for coding the features and enhancing the contrast of displayed information. Its concomitant aesthetic value and mass appeal nevertheless invite the criticism of some who disdain the qualitative and always take their technology very seriously.

5.2.2 Conversion from Monochrome to Color Schlieren

Color schlieren imaging requires an extended "white" light source, as described in Sect. 2.5.2 and, in more practical terms, in Sect. 7.1.1. The color temperature of the source and the type of photographic film affect the balance of color in the final image, though this is only critical in quantitative work. The wide range of commercially-available color photographic film is gradually giving way to electronic imaging, where color balance is traditionally somewhat more subjective. The standard discussion of schlieren sensitivity and range, given in Chap. 3, still holds with some additional considerations for the effect of color. The color filter fabrication itself is covered in Sect. 7.1.3

5.2.3 Classification of Color Schlieren Techniques

Overall, adding color to Toepler's schlieren system continues the line of reasoning begun in Sect. 5.1.3 on matched spatial filters. Another Ma ddox-type classification diagram is accordingly given in Fig. 5.8 for this purpose. One sees from it immediately that most color schlieren methods involve a round aperture or slit in the source plane and a 1-D or 2-D colored spatial filter at the cutoff. These matched filters can be interchanged in principle, yielding the same effect except for minor practical issues.

As noted in Chap. 1, Toepler [40] observed chromatic-aberration colors in his schlieren image but Rheinberg [67] was the true inventor of color schlieren. His two-color cutoff filter is the first example given in Fig. 5.8 [315-319]. It produces an image equivalent to the standard black-and-white schlieren, except the gray

scale is now replaced by a two-color-mixture scale. Some sensitivity is gained from color contrast, while some may be lost to diffraction and scattering at the filter. A good color-combination suggestion is lemon-yellow and medium blue, providing decent contrast and a pleasant olive-colored background (see, e.g., Color Plates 3, 14, and 30).

Rheinberg [67] foresaw a century ago, in terms of microscopy, much of what now forms the basis of color schlieren methods. His ring-lattice (bullseye) filter, Fig. 5.8b, produces a symmetric image with respect to the refraction direction in the x,y-plane, while coding the refraction magnitude in color [66,102,119,320-324]. Variations on this theme are nowadays much more popular in schlieren imaging [212,325-332] than they are in microscopy [296]. Similarly, Rheinberg's sector filter color-codes refraction angle but not magnitude [67,333-336]. Wolter [119,312,323,333] devised a sector filter with enough contrasting colors to code both quantities: the refraction magnitude via color saturation and the direction via hue. He developed a theory of this approach and found a novel way to make the sector filter from a birefringent quartz plate and crossed polarizers.

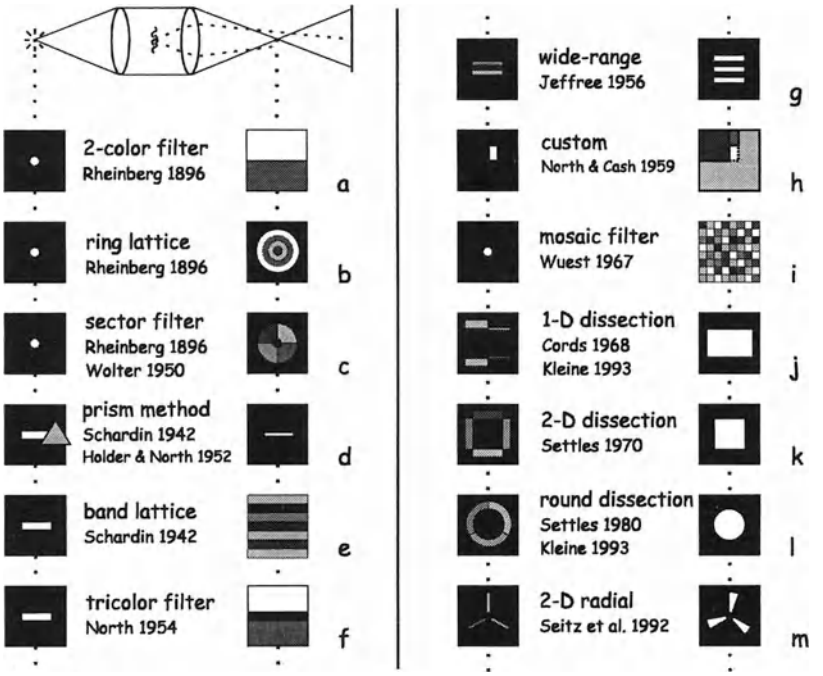

Fig. 5.8. Classification diagram of matched spatial filter pairs for color schlieren imaging. (Colors are represented by gray shades in this diagram).

The prism method due to Schardin [2] and Holder and North [337] uses a prism to spread the light beam into a spectrum, forming the effective light source of the schlieren system. Part of the spectrum image is then blocked by a slit in the cutoff plane. Light refractions in the test area shift elemental images of the spectrum with respect to the slit, causing contrasting colors to appear in the image. Care is required to avoid image resolution loss due to diffraction at the narrow cutoff slit. [3]

Nevertheless this early color schlieren technique has seen many successful applications [66,82,98,102,109,119,132,284,320-322,338-347]. A typical arrangement of the optical components is shown in Fig. 5.9. Vasiliev [102] also shows a prism attachment for the Soviet-made IAB-451 schlieren instrument that allows variable spectral dispersion. A color schlieren photo made by this instrument is shown in Color Plate 15, and Schardin's prism-method photo of a lighted match appears in Color Plate 2.

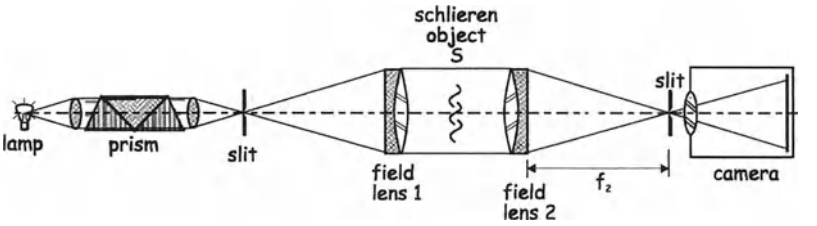

Fig. 5.9. Optical layout of a prism-type color schlieren system employing lenses as field elements and a direct-view prism that does not bend the optical axis, after [344].

Similar in principle is Schardin's band-lattice-cutoff method [2], Fig. 5.8e. It suffers the same resolution restrictions on cutoff slit width, but is simpler than the prism method [102,109,119,320,340,348-357]. Moreover, lattice bands of known width lead to a simple means of estimating refraction magnitudes from the observed image colors (See Chap. 10 and [2,119,288,320,351,356,358-361]). This method is at its best when high sensitivity is not required, and quantitative measurements are practical only when the schlieren object is basically two-dimensional. Vasiliev [102] notes that the source-slit image size should correspond closely to the lattice constant of the color bands, lest the schlieren image lack sensitivity or color contrast. Color Plates 16-18, 39-42, and 47 exemplify band-lattice color schlieren photos of various phenomena.

The tricolor filter technique of R. J. North [94,98], Fig. 5.8f, is almost the same in principle, but has only two colors separated by a central band that gives the image background a third, contrasting color. This technique has been very popular for qualitative studies [82,258,336,338,339,350,362-373]. It yields images that

[3] See Eqn. 4.7. A method is also given by Hosch and Walters [171] to estimate the size of a slit or other limiting aperture in the cutoff plane for a certain image resolution.

are easy to interpret and involves only a trivial modification to an existing schlieren system (replacing the knife-edge by the color filter). Its utility is showcased in the famous Shell film "Schlieren" [95]. One of North's tricolor images of supersonic flow is shown in Color Plate 3.

The compromise between sensitivity and measuring range (Sect. 3.3) prompted the development of several wide-range color schlieren techniques [194-196,359,374,375]. Jeffree's [374] approach involves a color-band source mask and multiple slits in the cutoff plane, Fig. 5.8g. The color cycle is thus repeated several times in the image for strong refractions, effecting an extension of the measuring range without an accompanying decrease in sensitivity to weak refractions. Of course, the coding of refraction magnitudes by specific colors is no longer unique in this case. Maddox [287,288,376] used a diffraction grating to produce a source spectrum and a diffuse, semi-transparent cutoff slit array to extend the range while partially alleviating the diffraction effects. Surget [375], Phillips [359], and Rotem et al. [194,196] also used similar range-extending schemes. Extended light sources in these wide-range techniques provide the schlieren apparatus with a reduced depth of focus in the object space, as described in Chap. 4, that is sometimes advantageous.

The techniques diagrammed in Fig. 5.8a, d, e, f and g are all one-dimensional (1-D): they can only display the refraction vector components normal to the orientation of the color bands in the x,y cutoff plane. As in black-and-white schlieren methods, two orientations of the matched filter pair may thus be required to see all the features of a given schlieren object. This restriction does not hold for the two-dimensional color schlieren techniques of Fig. 5.8b and c, or for those described next.

The custom pair of matched filters designed by North and Cash [125] to mark specific features of transonic airfoil flowfields, shown before in Fig. 5.5h, is shown again in Fig. 5.8h. It is an example of what can be done by applying color schlieren to a specific problem and exercising a little ingenuity.

Wuest [350] suggested a "mosaic" filter, Fig. 5.8i, that codes both 2-D refraction magnitude and direction explicitly by arbitrary rectangular colored segments in the cutoff mask. This approach is strongly limited by diffraction at the mosaic filter, and by the difficulty of specifying dozens of distinct color segments. It could be useful for strong schlieren objects, but apparently it has not found any applications to date.

An important development in color schlieren techniques was published by Cords [213] in 1968. His one-dimensional "dissection" method [377-380] separates the color bands in the source mask by a few mm, so a narrow cutoff slit is no longer required to gain high sensitivity. Instead, the sensitivity is controlled by the degree of cutoff of the image of each color band, while the spacing between the bands (and thus the aperture of the cutoff mask) may be arbitrarily large. By this means the sensitivity and resolution of color schlieren images were brought into parity with the best black-and-white results for the first time. Such a color schlieren photo, from Hypersonic Wind Tunnel No. 9 of the now-defunct US Naval Ordnance Lab, is shown in Color Plate 19.

I worked with Paul Cords briefly in 1967, and became fascinated by the quality of the color schlieren images he produced. It occurred to me later that the dissection principle could be extended to 2-D schlieren imaging, Fig. 5.8k, and this idea succeeded [381-384]. It has been used by various investigators over the last 30 years, and has been popular in the mass media as well [127,237,378,385-396]. Examples are shown in Color Plates 4-8, 14, and 20-32.

A square array of color bands forms the source mask of this 2-D dissection method, and an adjustable square aperture serves as the cutoff mask. The colors in the image match the refraction directions via a polar diagram, as in the sector filtering scheme above, but the available sensitivity and image resolution are much improved by way of Cords' dissection principle. Since four colors are required, good color contrast was achieved with opposing yellow-blue and red-green pairs in the horizontal and vertical directions, respectively. One can assess this method by comparing the monochrome horizontal- and vertical-knife-edge schlieren images of Fig. 5.10 with the corresponding 2-D dissection color schlieren image shown in Color Plate 4.

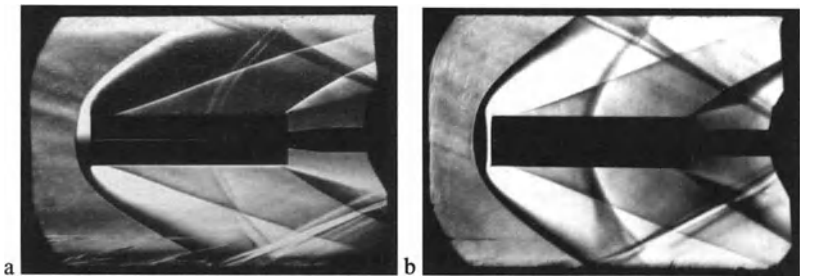

Fig. 5.10. Mach 3 airflow over a blunt cylindrical test model in a supersonic wind tunnel, **a** horizontal knife-edge, **b** vertical knife-edge. Compare with corresponding 2-D dissection color schlieren image shown in Color Plate 4 (photos by author).

This works well for qualitative imaging but violates good colorimetry by mixing a secondary hue with the three primaries. One can overcome this objection by way of a round annular source filter, Fig. 5.8l, and a variable iris diaphragm in the cutoff plane [127,311,378,397-400]. Using 120° color sectors, only the three primary colors are needed. The benefits of 2-D dissection still apply so long as the iris aperture is at least a few mm in diameter.[4] Kleine [401] calls this "the most illustrative and graphic color schlieren method of all."

Seitz et al. [402,403] recently proposed an alternate 3-color 2-D scheme, shown in Fig. 5.8m. Radial color slits at 120° intervals form the source filter. The pie-

[4] All the dissection techniques, Figs. 5.8j-l, are characterized by relatively-large apertures in the schlieren cutoff plane to avoid image resolution loss due to slit diffraction.

shaped apertures in the cutoff plane equally cut off each of the colored source image bands as the cutoff filter is rotated about the optical axis. One must insure that the pie-segments are broad enough to avoid slit diffraction effects.

Although the above constitute the main color schlieren schemes, there are some other schemes that deserve mention, e.g. Schardin's large-colored-grid-background method, already discussed in Section 4.3.3 (Refs. [212,320,404] and Color Plate 9). Meyer-Arendt [132,405,406] added a colored background to a microscope image using a wedge interference filter in the optical train ahead of the back focal plane of the objective. This produced striking results in the microscope, but is suitable only for visualizing strong refractions in an ordinary schlieren system.

When schlieren objects create their own spectral dispersion, a color schlieren image of the prism type can be had simply by using a slit source and cutoff. This occurs, for example, due to diffraction in ultrasonic beams (Sect. 9.2.4), or to strong refractions in stratified liquids [407,408].

The oldest and least useful color schlieren technique, due to chromatic aberration of the field lenses [3,37,40,320,409,410], arises from the same prism principle. Toepler liked it, but it is now generally regarded as a nuisance rather than an advantage, and is termed "involuntary color schlieren" by Weinberg [66].

Finally, note that multi-colored schlieren-like images arise in certain white-light interferometers, especially the Wollaston-prism differential-interferometer, which is covered in Section 5.4.1 and illustrated in Color Plates 36 and 37.

5.2.4 Recent Developments

Color schlieren continues to be popular since last reviewed in 1985 [127]. Significant advances in personal computing, color imaging and videography, color reproduction in digital publications, and the Internet have made this and all color scientific imaging methods more accessible.

"Rainbow" and "bullseye" color schlieren methods, for example, have seen significant recent use [269,325,331,332,357-361,411-414]. They are adaptations of Rheinberg's ring lattice and Schardin's band lattice in which a continuous bullseye or linear spectrum is produced on a color transparency, subsequently used as a schlieren cutoff. Instead of producing separate colored image bands or isochromes, these methods produce a continuous change of hue with increasing schlieren refraction, as in the original prism method. Some impressive quantitative schlieren measurements have been made [269,358,360,361] by digitizing and quantifying the color attributes of the resulting images. For more on these new-age, digital-color computerized schlieren methods, see Sect. 10.2.1.

New light sources have also become available recently for color schlieren imaging. These include sub-microsecond spark sources [400,415], a 3-color multi-flash unit for imaging high-speed events [218,241], and ganged xenon tubes or "gliding sparks" to better accommodate the large source shapes used, for example, in the dissection color schlieren methods [397].

Undoubtedly the leading contributor to color schlieren in the 1990's was Harald Kleine [378,393,396,398-400,416,417], beginning with his Ph.D. thesis on improving the optical methods of gas dynamics [400]. Cords' dissection technique proved valuable for shock tube flows, and Kleine improved it by adding 5 narrow color bands on either side of the wide central gap (see Fig. 5.8j). These colors mix in the schlieren image with progressively-stronger schlieren refractions, until the strongest appear almost white in hue. A calibration is shown [400] in which flow-field $\partial\rho/\partial x$, over the range of 0-100 kg/m^4, is indicated by six successive colors.

Kleine also applied direction-indicating color schlieren to shock-tube flows, finding that vortex cores reveal themselves by displaying the polar diagram characterizing the chosen color scheme. Using the round dissection approach (Fig. 5.8l), Kleine [400] made the inner annulus of his color source filter slightly out-of-round in order to shade the schlieren background in one of the three primary colors. He also found, in z-type mirror optics corrected for astigmatism by a cylindrical lens according to Sect. 3.1.2 and [147], that one must distort the source-filter shape deliberately in order to gain a round color source image in the cutoff plane. Kleine's striking vortex and shock-wave images have set a high standard for resolution, sensitivity, and color contrast (see examples reproduced in Color Plates 33-35).

Finally, some new applications arose quite recently. By tradition, color schlieren techniques are most useful in the qualitative study of complex refractive fields where either black-and-white schlieren is confusing or additional information is needed to aid the interpretation. This applies, of course, to many of the possible subjects for schlieren examination. Particular application is found in cases of strong refraction, refraction over a wide range, highly 3-D phenomena, self-luminous or semi-transparent phenomena, and cases where a quantitative evaluation is assisted by color-coding. While the broad applications of schlieren and shadowgraphy are covered in detail in Chap. 9, some of these recent, novel color-schlieren applications are tabulated below.

Table 5.1. Recent novel applications of color schlieren techniques.

Topic	Reference Number
Microgravity	[329,418,419]
Electrophoresis	[318,420]
Water table or liquid waves	[134,212,330,408,421]
Flatness testing of computer disks	[326]
Color television projection	[422]
Shock waves and shock tubes	[378,393,396,398,399]
Holography	[423,424]
Leak detection	[124,237]
Laser-tissue interaction	[331,332]
Art and entertainment	[391,425,426]

5.3 Stereoscopic Schlieren

> To see in relief is to receive by means of each eye the simultaneous impression of two distant images of the same object.
>
> *Euclid, 280 BC*

Ordinary schlieren images show 3-D objects as flat pictures, with all depth features integrated. For complex 3-D test subjects this is often not very useful [98]. Such schlieren images lack depth, it is impossible to determine feature locations along the optical axis, and in the particular case of shock waves, only a cross-section of the flow in the plane normal to the optical axis appears.

Sharp-focusing and tomographic methods around this difficulty were discussed in Chap. 4. In addition to these methods, we can get often get a qualitative 3-D picture of such objects by the simple expedient of stereoscopic schlieren.

The background of binocular vision and stereoscopy [427,428] is briefly covered in Sect. A.5 and cited references. Most attempts to obtain stereo schlieren images use twin schlieren beams crossed at an angle of 10 °-15° [429,430], since this allows simultaneous left- and right-eye views. Occasionally a single beam is used, able to rotate about an axis perpendicular to its optical axis [102]. Simplest of all, for static test objects, one rotates the object in the schlieren beam between exposures, with typical results shown in Fig. 5.11 below.

Glass figurines make excellent examples for this purpose, while a flame or an aerodynamic flow would likely change between sequential exposures. In Fig. 5.11a the photography was as described earlier in Fig. 4.6 for schlieren objects seen against an illuminated background (Schardin's [2] schlieren method no. 3). The refractions are very strong at the glass-air interface, obscuring most internal detail in the figurine. A second figurine was immersed in a cell with optical-glass windows that was filled with Wesson™ cooking oil for a better refractive-index match. While invisible to the unaided eye, the weaker internal refractions of the figurine become visible in Fig. 5.11b under standard knife-edge schlieren illumination in the small Toepler schlieren system described in Chap. 8. In both cases the figurines and their refractions are seen in full 3-D relief when the image pairs are viewed with a simple stereo viewer (see App. D.6).

Other examples of background-distortion stereo schlieren are given in [431] for 3-D supersonic interacting flows and in [319] for the background-oriented stereo schlieren imaging of helicopter rotor wakes (Sect. 10.3.5). Stereo schlieren pairs are also shown by Weinberg [66], depicting a flame, by Nevskii et al. [432], depicting a supersonic wind tunnel test, and by Struth [433], depicting a ballistic projectile.

The largest-scale stereo schlieren system ever attempted was set up to shoot footage for the IMAX stereo movie "The Hidden Dimension" [425,428,434]. It was done using the 0.76 m z-type schlieren system of the Penn State Gas Dynamics Lab, described earlier in Section 4.1.2. From the outset, limited parallax was recognized as a problem: the 120 kg refrigerator-sized IMAX stereo camera [434] has only a 72.4 mm interocular distance, but had to be positioned more than 7.5 m

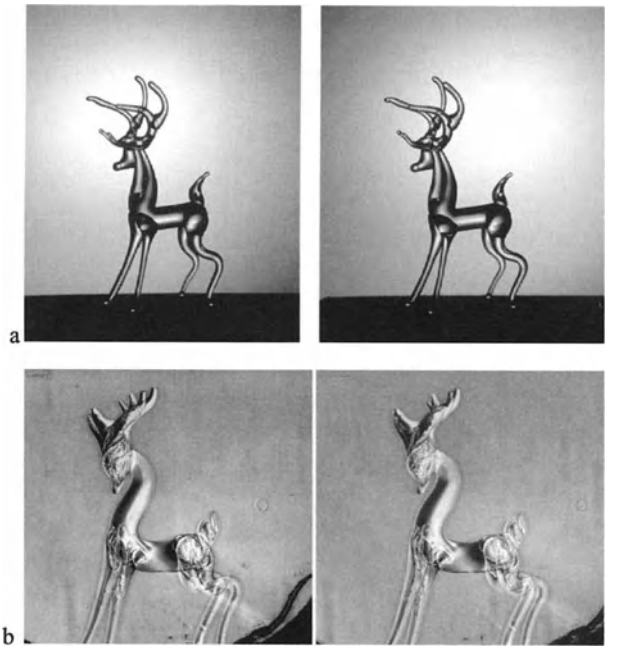

Fig. 5.11. **a** Stereo image pair of a crystal glass figurine, imaged by Schardin's [2] schlieren method no. 3. **b** Stereo pair of a similar figurine immersed in cooking oil and imaged by a z-type Toepler schlieren system. A stereo viewer is needed to see these images in 3-D. Experiment and photos by Heather Ferree.

Fig. 5.12. Single frame from 70mm stereo schlieren image pair, from the IMAX stereo movie "The Hidden Dimension". The star of the movie, Elly (played by actress Charlotte Sullivan) is shown in bed just before waking. Her body heat and thermal plume are revealed in color and in 3-D. The movie depicts Elly's exploration of the world around her using scientific imagery. A stereo schlieren sequence showing the lighting of a candle is also included.

from the schlieren test area. Instead of the typical 10 °-15° parallax angle, this afforded a mere ½°. Nevertheless, early trials showed some visible stereo effect so the project proceeded. Twin halogen lamps with condensers and slits spaced at

the interocular distance provided the schlieren illumination. Twin color cutoffs of the 2-color (yellow and blue with a central dark band) variety were used. Despite the parallax issue, excellent results were obtained and two stereo schlieren segments were included in the final movie edit (Fig. 5.12).

5.4 Schlieren Interferometry

While interferometry is excluded from the scope of this book *per se*, a few interferometric schemes, like the phase contrast method covered in Section 5.1.4, come arbitrarily close to specialized schlieren techniques. Thus a brief account of these "schlieren interferometry" methods is called for.

5.4.1 The Wollaston-Prism Shearing (Differential) Interferometer

The idea of a polarization refractor goes back to Jamin [435] in 1868, but Francon [436,437] and Nomarski [438] share credit for adapting this principle to microscopy, where it has been very successful.[5] The conversion of schlieren systems to differential-shear interferometers was quickly adapted for optical flow visualization in the 1950's [439-441], when rocketry and high-speed flight were proliferating according to Chap. 1. Notable references since that time include [82], [98], and [442-445]. Merzkirch [82] covers this topic more thoroughly than present space allows.

In principle, a laser or spatially-coherent white-light source is used in a schlieren apparatus with the knife-edge replaced by a birefringent Wollaston prism between crossed polarizers, as shown in Fig. 5.13. Such a prism splits the light beam into two beams with perpendicular polarization and a small divergence angle ε between them. Phase differences between these beams subsequently lead to interference phenomena in the image. There is no schlieren cutoff, so this method is strictly a shearing interferometer masquerading as a schlieren system.

For a masquerade, though, it does a nice job. It can yield results much more like schlieren images than interferograms. Due to the lateral shear between the two beams, it is the gradient $\partial n/\partial x$ or $\partial n/\partial y$ that determines the image illumination, not n itself as in traditional interferometry. Further, if the prism is carefully centered upon the second focus of the optical system, infinite-fringe interference yields a uniform image background, just like schlieren (Fig. 5.14b). Finally, weak

[5] In fact, Nomarski Differential Interference Contrast, which yields colored microscope images, is credited [296] with replacing Rheinberg illumination for that purpose. The opposite holds true in schlieren imaging, however: Rheinberg-type color schlieren methods (Sect. 5.2) are dominant and differential interferometry is seldom-used in comparison.

disturbances in the test area lead to sub-fringe intensity distributions that can appear almost identical to schlieren images [446]. When a white light source is used, the image appears in Newton's ring colors and rivals color schlieren (see Color Plates 36 and 37).

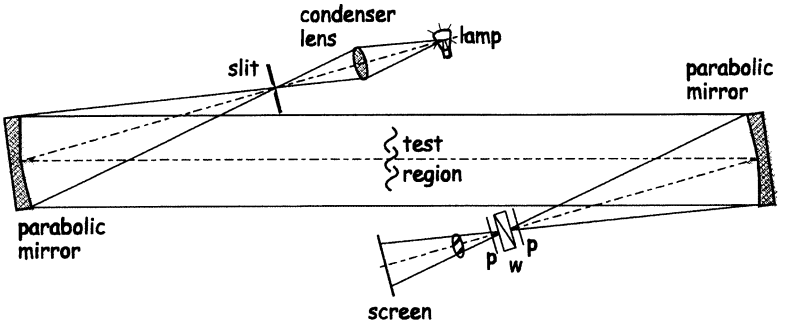

Fig. 5.13. Diagram of a z-type schlieren system modified for differential interferometry by replacing the knife-edge with a Wollaston prism w between crossed polarizers p.

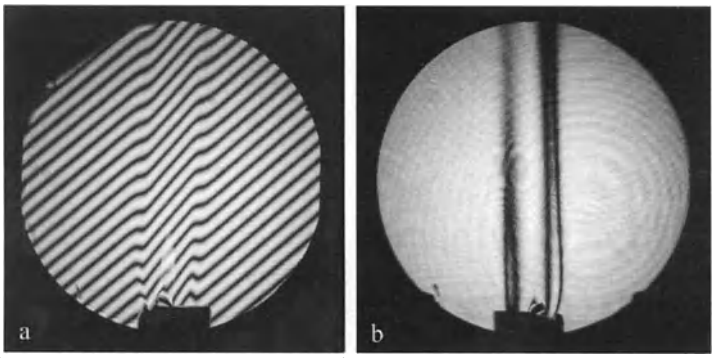

Fig. 5.14. **a** Finite-fringe differential interferogram of candle flame. **b** infinite-fringe differential interferogram. Images obtained with the optics diagrammed in Fig. 5.13, where λ = 0.633 μm, ε_{prism} = 3 arcminutes, f_2 = 86.4 cm, and d = 10.8 cm. Photos by Heather Ferree.

Displacement of the Wollaston prism from the beam focus causes finite fringes to appear in the image, Fig. 5.14a. These fringes then become shifted in proportion to refractive index gradients in the test region. This has been popular for heat transfer studies, since the convective heat transfer coefficient is proportional to $\partial T/\partial x$ or $\partial T/\partial y$ normal to a heating or cooling surface, which is measured directly by the fringe shift if certain conditions are met. Quantitative heat transfer evaluations are thus facilitated [443,445,447,448].

Edge doubling can occur in the images of solid objects in the test area due to the lateral offset of the interfering light beams. If the divergence angle ε of the prism is kept small, however (e.g. a few minutes of arc), then the doubling is too small to be noticeable.

Differential interferometry is championed by Oertel, Smeets, Seiler, George and Srulijes of the French-German Institut Saint-Louis, ISL [83,444,446,449,450]. They use twin Wollaston prisms at the conjugate foci of the optics, rather than the single prism advocated by Merzkirch [442]. Of many fine images, one of their best is reproduced here in Fig. 5.15. This interferogram of a supersonic jet is roundly mistaken for a schlieren image, and even its originators call it "schlieren-like" [450]. There is, however, a crucial difference: this image was obtained by dual complementary exposures, during one of which there was no flow. Features common to both exposures – like window flaws – do not cause interference and thus do not appear. This unique capability is had at the expense of extra optical equipment and effort, but is beyond the capacity of ordinary schlieren imaging.

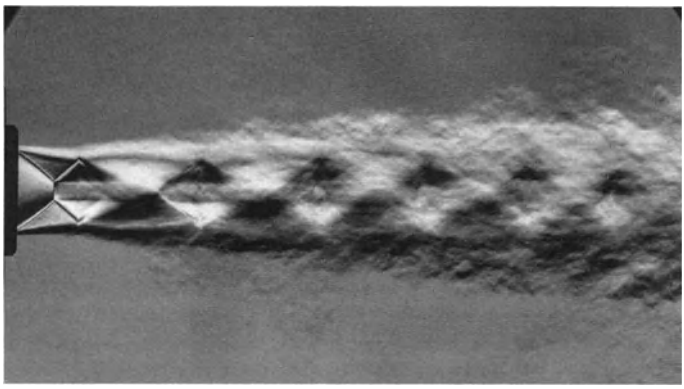

Fig. 5.15. Schlieren-like differential interferogram of an overexpanded supersonic jet [449]. Reproduced by courtesy of the French-German Institut Saint-Louis, ISL.

At its best, the Wollaston-prism schlieren interferometer takes advantage of both schlieren optics and common-path interferometry, making it much easier to align and much less vibration-sensitive than the classical Mach-Zehnder interferometer. It's implementation in the present demonstration schlieren system (Chap. 8) was trouble-free. On the other hand, Wollaston prisms can be rather expensive (currently several $100US; see App. D).

5.4.2 Diffraction-Based Schlieren Interferometers

In 1934, Maksutov [101] first suggested the use of a fine wire or filament in place of Foucault's knife-edge for optical shop testing. In 1949, Gayhart and Prescott

[451] observed that, with partially-coherent schlieren illumination and either a standard knife-edge or a filament cutoff, fringes are seen in boundary layers perpendicular to the cutoff orientation due to the interference of direct and cutoff-diffracted light. They built a quantitative schlieren approach from this observation, demonstrating that these are functionally the same fringes one obtains in a standard interferometer, yielding the optical path difference directly, not the schlieren refraction angle. Interferometers, like the Mach-Zehnder device, were painful to use in the mid-20th Century due to vibration sensitivity, poorly-coherent lamps, and overall clumsiness. A quantitative interferometer based on a simple modification to a robust schlieren apparatus was thus appealing, and it caught on quickly [139,452-454].

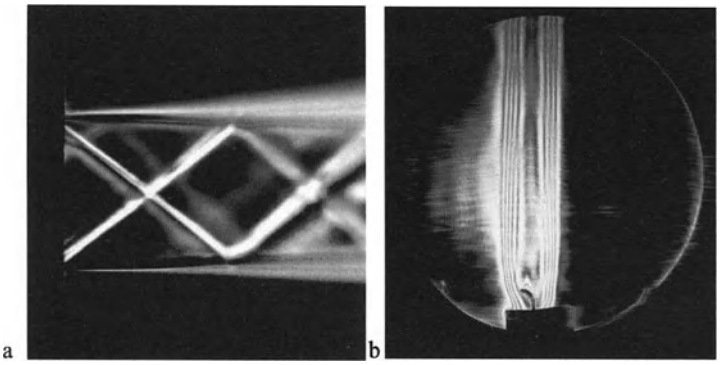

Fig. 5.16. **a** Interference fringes appear in the horizontal free shear layers bounding a rectangular supersonic jet (partially-coherent illumination near full knife-edge cutoff). **b** dark-field, vertical-focal-filament schlieren interferogram of a candle plume (λ = 0.633 μm). Photos by the author and Heather Ferree.

Temple [452] provided the Fourier-optical background for this approach. He showed that, by inserting a small absorbing object in the focal plane of a schlieren system and blocking the central maximum of the Fourier spectrum, one causes diffraction at the cutoff that spreads the background illumination into the disturbance area near heated objects, for example. The resulting interference produces fringes that can be used for quantitative evaluation, as in an interferometer. The interference region is of limited extent near solid boundaries, however, and lends itself best to boundary layers rather than whole-field interferometry.

Temple derived a useful criterion for the focal filament diameter D:

$$D \leq 1.2\lambda f / \pi d \tag{5.3}$$

where λ is the illumination wavelength, f is the lens or mirror focal length, and d is the width of the schlieren object of interest in the test-area x,y-plane. Bracken-

ridge and Peterka [454] later concluded that the fringe meaning is unclear if this criterion is not met.

Several quantitative examples of convective-flow schlieren interferometry followed in the literature [102,139,453,454]. Brackenridge and Gilbert [139], for example, used a laser source and 75-μm-diameter circular obstacle to block the DC component of the source image (see the example of darkfield illumination in App. B.4). Dodd [455] adapted this schlieren-interferometry approach to microscopy.

A complementary approach was suggested by Erdmann [456] in 1951: instead of the focal filament, a narrow transmitting line is scribed or etched on a partially-absorbing plate in the schlieren cutoff plane. This "field-absorption" method is similar to the example of bright-field coherent illumination given in App. B, and is also a diffraction-based schlieren interferometer.

After the 1960's, robust laser interferometers became readily available and diffraction-based schlieren-interferometry methods fell into relative disuse.

5.5 Computer-Simulated Schlieren

> ...in real life mistakes are likely to be irrevocable. Computer simulation, however, makes it economically practical to make mistakes on purpose.
>
> *J. McLeod & J. Osborn,* 'Natural Automata & Useful Simulations,' 1966

Modern computational fluid dynamics (CFD) methods are able to solve, on supercomputers, the equations of motion for inviscid flows and some viscous flows by numerical calculations. Unfortunately, in the broad category of turbulent flows, such solutions are approximate and are likely to be wrong if not guided and validated by experiments. But given sufficient validation, the CFD results can be taken as a good representation of what actually occurs in nature. In that case, one has essentially all flow properties at hand in the CFD output: velocity, pressure, temperature, and the entire density field. A comparatively-simple exercise in post-processing of the output can then extract the gradient of flowfield density, integrate it along an "optical axis," and display it by amplitude or color using computer graphics: a computed or computational schlieren image.

The computational power to do this became available by the 1980's, especially including graphics hardware and software, and early examples appeared in the literature [128,457-459]. Key papers of the 1990's included Yates [460], who showed several fine examples, Brown et al. [461], and Shenoy et al. [361], who took "rainbow" color schlieren images of jets and flames and compared them with computed color schlieren results. Other examples can be found in [332,462-465]. At least one commercial post-processing code (see App. D.6) currently includes utilities to construct computed schlieren images and interferograms from CFD solutions. An example of computed schlieren imaging is shown below in Fig. 5.17.

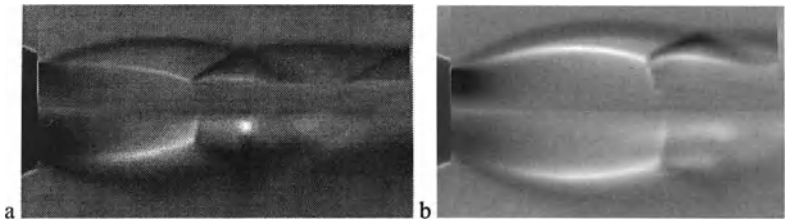

Fig. 5.17. Comparison of computed and time-averaged experimental schlieren images of the jet from a sonic nozzle at pressure ratios of **a** 2.5 and **b** 8.0. The top halves of both frames are computed, while the bottom halves are experimental. The Mach disk location is one measure of the comparison. Images courtesy of J. W. Naughton, et al. [465].

Apart from CFD, a different approach uses Fourier optics to generate computed schlieren images from input phase distributions, truncating the spatial frequency spectrum in the schlieren cutoff plane by way of a "computational knife-edge" or Hilbert transform. Examples are found in [198-200,461], and a detailed example is given in App. B.3. Fiadeiro and Emmony [466] reversed this procedure by separately imaging both the schlieren image plane and the cutoff plane, iterating to reconstruct the experimental phase distribution, then constructing various computed schlieren images from the combined measurements and computations.

As noted by Yates [460], comparisons like the one given in Fig. 5.17 are comprehensive tests, not only of the governing-equation solver but also of the experimental data. They are meta-comparisons, weighing forest against forest rather than tree against tree. Before they became available, CFD code validation was done by comparing many individual profile plots of flow quantities. In contrast, when comparing computed and experimental schlieren images, the overall level of agreement is much easier to judge.

Is this the wave of the future for schlieren imaging? One of them, certainly. As CFD improves, more computed schlieren images are bound to appear. Schlieren is a paradigm of scientific visualization by which such results can be displayed succinctly for human consumption, no matter how they originated. To put it another way, computed schlieren images do not compete with schlieren images, they *are* schlieren images. Nonetheless, the analog optical way of obtaining these images will continue to see vigorous use in the foreseeable future.

5.6 Various Specialized Techniques

To conclude this Chapter, we briefly consider several minor-but-interesting specialized schlieren techniques.

5.6.1 Resonant Refractivity and the Visualization of Sound

> He goes but to see a noise that he heard.
>
> *Shakespeare,* A Midsummer Night's Dream

Certain unusual gases, e.g. sodium vapor in air, may absorb light in the visible range if it is near their molecular resonant frequencies. When such absorption occurs, the gas refractivity $(n - 1)$ can become orders of magnitude higher than usual [82]. The principle was first used in low-density ballistics experiments to magnify the schlieren sensitivity [467]. Barrekette [468] achieved a 5-fold sensitivity increase, while Blendstrup et al. [469] aimed for 2 orders of magnitude. Unfortunately, sodium vapor is reactive and disagreeable even in weak concentrations, so this never became a practical flow visualization method.

Despite that, it raises an example that answers the often-asked question [1]: "Can one use the schlieren method to see sound?" The late Prof. D. Bershader of Stanford University championed resonant refractivity, and gave the following answer [470]: a simple calculation shows that a schlieren system with 0.2 arcseconds sensitivity (quite good, per Fig. 3.12) cannot render 1 kHz sound visible at less than a 122 dB under normal conditions. 122 dB is a painful and dangerous sound pressure level requiring ear protection. In this range the distinction between sound waves and weak shock waves becomes blurred. With 0.1 molar percent of sodium vapor in the air, however, Bershader and Prakash [470] reckoned that one might observe normal conversation at 61 dB by schlieren. This experiment has apparently never been tried, thus the answer to the question remains "no" for practical purposes. Ripple-tank experiments and similar analog methods must continue to suffice for the experimental visualization of true (linear) sound [5,471-473].

5.6.2 Anamorphic Schlieren Systems

Anamorphic optics magnify one dimension of the observed field differentially with respect to the other [98]. This can become important in cases where the field of interest is laterally thin [474], or where the schlieren beam is distorted by reflection from a curved aerodynamic surface [475,476]. Similar beam distortions can occur in the curved windows and cylindrical test sections of some aero- and hydrodynamic test facilities [82,477,478]. To the extent that these factors distort the schlieren beam solely in one direction, a compensating cylindrical lens can often be used to restore the proper image aspect ratio.

5.6.3 Schlieren Observation of Tracers

Schardin [1,2] took a special interest in schlieren methods applied to low-speed flows, where no inherent change in refractive index occurs naturally. His work (with J. Pohl, see Fig. 5.18) improved upon the original work of Ludwig Mach in

1896, who to built a low-speed wind tunnel with schlieren observation of heated air filaments used as streamline tracers [479].

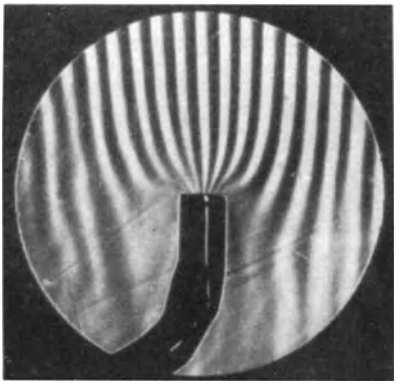

Fig. 5.18. Visualization of airflow streamlines in a low-speed wind tunnel, using electrically-resistive wires located just above the field-of-view to heat filaments visualized by the schlieren method. A compressed-air injector is shown drawing in air at a rate of 5 liters/s from a uniform downward flow at 1.5 m/s. An upstream straightener helps provide uniform flow. Photo by H. Schardin and J. Pohl [2], reproduced by courtesy of Springer-Verlag.

This approach was championed in the 1930's by British investigator H. C. H. Townend [64,480]. He used not only continuous heated filaments but also "hot spots" generated by firing small spark gaps in the flow. After a while the heated spark gaps project visible filaments of warm air with regularly-spaced "knots" where the sparks have fired. Cinematography of such flows yields quantitative flow data (see Sect. 10.3 on quantitative image velocimetry) as well as qualitative visualizations. By synchronizing the illuminating spark of the schlieren system with his spark gaps and camera, Townend produced stroboscopic movies that revealed aerodynamic phenomena with unparalleled clarity.

One of the leading aerodynamicists of his day, Townend used this method to explore and illustrate many concepts of early aircraft design. He found that warming his test models contributed to the visualization by revealing the boundary layer flow. He also discovered the drag-reducing benefits of a cowl, or "Townend ring," around a radial-piston aircraft engine [480].

Modern uses of thermal filaments in schlieren observation of low-speed flows include Shimizu et al. [481] and Kanazawa et al. [482], who studied the airflow over silicon wafers without the particle contamination inherent in smoke. Indeed the "thermal tuft" schlieren method [483], using an electrical resistive element on the end of a long wand, is similarly important for airflow studies in clean rooms, or anywhere that airborne particles are forbidden.

With only a handful of modern attempts to its credit, this bit of early-20 th Century ingenuity deserves more use. It is cleaner and less objectionable than smoke and its filaments are less susceptible to disruption as airspeed increases [480]. A modern adaptation also appears in Weinstein's vaporizing-particle interferometer [484], where dust or smoke particles are the receptors of massive laser-beam energy, "writing" hot spots in a flowing gas that are then observed by schlieren imaging. Both airspeed and temperature data can be extracted.

Gases of different refractive index can also be used, as well as heated filaments, to render low-speed streamlines visible. Ideally one wants a gas with the same density as the air, but the density difference – even that of helium in air – is not usually a problem unless the flow speed is low enough to be comparable to that of the buoyant motion. CO_2, ether, and acetylene have also been suggested [2], but the latter two are too hazardous to use.

5.6.4 Two-View Schlieren

Townend also first suggested modifying a schlieren system to yield two simultaneous views of the test subject. This oddity has been attempted a few times, both to yield simultaneous horizontal- and vertical-knife-edge images [485,486] and to give two views of the test subject from orthogonal directions [487,488]. In both cases it seems to be more trouble than it is worth in general, though some particularly-trying applications might make good use of it. In any case the need for simultaneous horizontal- and vertical-cutoff images never really materialized, and has been superceded by the directional color schlieren methods described in Sect. 5.2.

5.6.5 Immersion Methods

Although immersion refractometry is beyond the present scope, it was shown earlier in Fig. 5.11 that it is sometimes necessary to overcome the strong exterior refractions of a schlieren object in order to observe its internal detail. For crystals, glass, and acrylic objects, immersion in a tank of refractive-index matching fluid can accomplish this. The tank itself must be of good optical quality or it will contribute unwanted features to the visualization.

A variety of resources is available on index-matching fluids. For glass, with $1.4 \leq n \leq 1.8$ depending upon composition, hydrocarbon matching fluids are tabulated in [489]. Pyrex glass, with $1.43 \leq n \leq 1.48$, can be accurately matched by solutions of sodium iodide [490]. Merzkirch [82] lists additional hydrocarbons to cover the typical clear-acrylic range of $1.48 \leq n \leq 1.53$, and an aqueous solution of zinc iodide can also be formulated to cover this range [491].

Most of the applications in the literature involve shadowgraphy [492-494], but the immersion technique is equally useful for schlieren imaging. In addition to Fig. 5.11, another schlieren example is shown below in Fig. 5.19.

5.6.6 Infrared Schlieren

Recall the Gladstone-Dale relationship (Eqn. 2.1): $n - 1 = k\rho$. Since k increases with the illumination wavelength, λ, it follows for a given schlieren object that the refractivity, $n - 1$, increases as well. To produce a significant effect, however, one

must shift the illumination right out of the visible spectrum and into the infrared. Since excellent IR detectors are available, it remains feasible to work in the IR and then upshift a visible schlieren image to a suitable readout device.

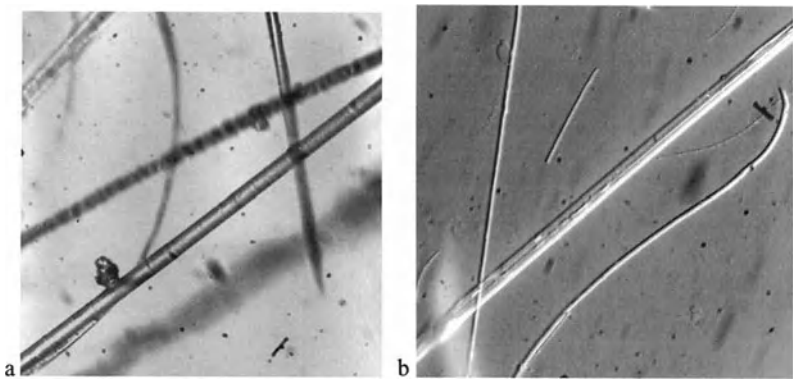

Fig. 5.19. Microscope images of glass fibers, ~500X magnification. **a** brightfield image of fibers in air, **b** fibers in an index-matching oil as seen by Hoffman Modulation Contrast [280] (a schlieren method for the microscope). Although the match is not perfect, internal and surface fiber details are visible in b but not in a. Micrograms by Heather Ferree.

Glasser et al. [495] tried this in order to better measure the electron density of a plasma, while Wilkerson et al. [496] showed that an infrared analog of the standard schlieren method can visualize gases that absorb the IR. Even more noteworthy was the compact Japanese commercial schlieren system "Elmex SSC-610," which was claimed to have 4 times the sensitivity of a visible-light system due to its IR semiconductor-laser source. Apparently it is no longer sold.

Overall, infrared schlieren illumination buys extra sensitivity at the cost of added complexity, difficulty of alignment, and a possible loss of ultimate resolution compared to standard visible-light methods. It may be useful in specific cases, but it is not a technique of broad appeal.

6 Shadowgraph Techniques

> Shadow is the means by which bodies display their form.
>
> *Leonardo da Vinci,* Notebooks

> This method of observation is absolutely new, and I invite all physicists to try it. I believe it will lead to new discoveries in certain branches of physics.
>
> *J. P. Marat* [28]

> In many cases where this method is employed there is a certain element of risk for the film, if not for the photographer.[1]
>
> *W. F. Hilton* [122]

6.1 Background

The history of shadowgraphy was covered in Chap. 1, with more depth given below. The theory of light refraction by a schlieren object, underlying both schlieren and shadowgraphy, is given in Chap. 2 and Sect. A.6. In Sect. 2.3 a distinction was drawn between schlieren and the more-rudimentary approach of shadowgraphy, while in Sect. 2.4 the simple "direct" shadowgraph principle was stated. Here the various shadowgraph methods are covered in detail, naturally dividing them into "direct" and "focused" methods and a collection of lesser miscellany.

6.1.1 Historical Development

As already noted, shadowgraphy is very ancient. It has even worked its way into evolution: certain oceanic predators detect their transparent prey by way of its

[1] This comment by aerodynamicist William F. Hilton (1912-1997) refers to traditional "direct" shadowgraphy's need for close proximity of the film to the test subject in the dark, which can sometimes be dangerous (e.g. explosions, propellers, and bullets in flight).

shadow [114]. The term "shadowgraph" is shared with several other things, including x-rays (absorption shadowgrams), hand-shadow plays cast on a wall, photograms by the 20th-Century artists Moholy-Nagy and Man Ray, and even some of the essays of Kierkegaard [497].

The recorded history of optical shadowgraphy begins with Wiesel [11], Hooke [14,22] and Marat [28]. It was finally established by Dvorák [23], Boys [62], Townend [64] and Schardin [1,2] (see Chap. 1). Schardin [2] was the first to analyze the sensitivity and resolution of the method, but his analysis was incomplete and contained some errors. Further analysis by Hannes [173], Weinberg [66], and Kessler and Hebenstreit [498] now provides a more-complete theoretical framework. In addition to the standard geometric-optics approach, several authors have also treated shadowgraphy in terms of Fresnel diffraction [498-501].

6.1.2 The Role of Shadowgraphy

A role was gradually staked out for shadowgraphy, independent of schlieren imaging, beginning with Dvorák [23]. Simpler and less accurate than schlieren, shadowgraphy nonetheless excels at many tasks. Schardin [1] first defined shadowgraphy's role by assigning it the visualization of gross or coarse schlieren objects (Table 6.1). It is suitable for strong gradients creating sharp changes in screen illumination, not for mild gradients or quantitative evaluation. Its setup is quick and simple, even in adverse situations. Shadowgraphy is "rough and ready."

Table 6.1. The customary applications of shadowgraph techniques, each with a few representative references.

Topic	Reference Number
Glass technology	[2,321,502]
Shock waves, explosions, ballistics, and supersonic flows	[1,2,62,202,203,503-505]
Liquids and liquid surfaces	[506-509]
Turbulence	[510-512]
Flames	[28,66,513]
Solid fracture mechanics	[514,515]
Helicopter rotor aerodynamics	[516-521]
Outdoor refractive visualizations	[522]

Further, because it reveals the Laplacian of the refractive field, thin, sharp-edged inhomogeneities are best shown. Shadowgraphy thus conveys an impression of the "skeleton" of a complex phenomenon, clearly indicating its salient features without the schlieren method's emphasis on the details [122].

6.1.3 Advantages and Limitations

The great advantage of shadowgraphy is its extreme simplicity. It is also adaptable to large fields-of-view. Unlike schlieren, here the optical quality requirements can often be relaxed (single-element lenses, Fresnel lenses, inexpensive mirrors, etc.). Shadowgrams may be cast on photographic film, on ground-glass or projection screens, or on any reasonably-flat, diffusely-reflecting surface such as a wall, sandy soil, or snow. When he specified a paperboard screen painted with the white pigment of the Carmelite Friars, Marat [28] was clearly being too picky.

If the lateral scale of schlieren-object features is small, shadowgraphy gains the further advantage of high sensitivity. Thus shock waves and turbulence show up well in supersonic gas flows, but gradual phenomena like expansion fans do not (Fig. 6.1 and [42]). For these, the schlieren technique is usually required.

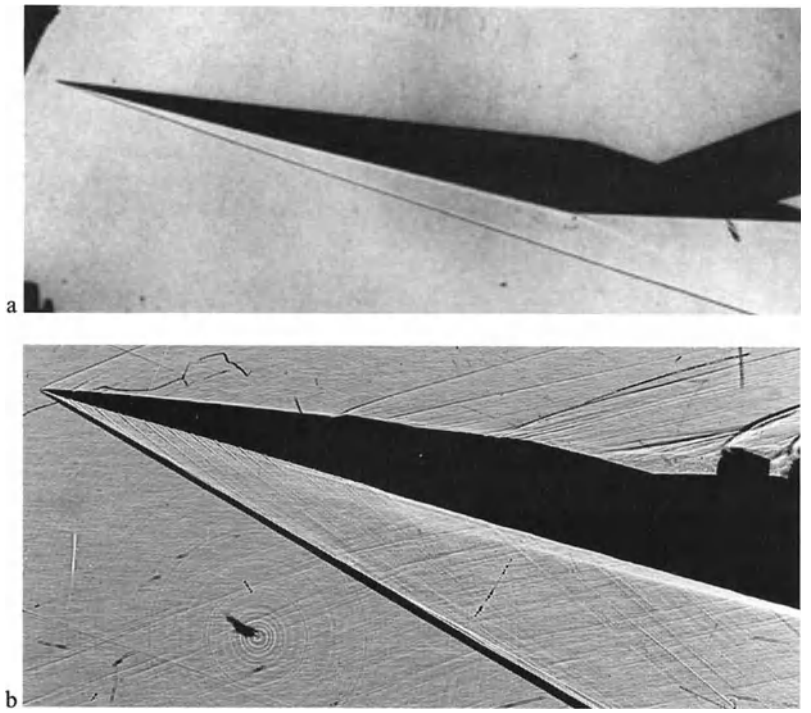

Fig. 6.1. **a** Shadowgram of hypersonic flow over an all-body flight vehicle. The oblique shock wave is obvious, but the expansion fan that follows it is barely visible. No features are visible in the low-density flow above the vehicle (NASA photo AC87-0104-a).
b "Contact" shadowgram of supersonic airflow over a delta wing at angle of attack [523]. Bright band adjacent to flat lower surface is light refracted by boundary layer.

Most of the drawbacks of shadowgraphy stem from its essential ambiguity: *A shadowgram is not an image; it is a shadow*. There is no 1:1 correspondence between the object and its shadow (as there is between object and image in schlieren optics, where a lens generates an optically-conjugate relationship between the two). Thus shadowgrams are not true-to-scale in general. Only the dark regions of a shadowgram can yield an undistorted representation of the schlieren object, since they mark where the deflected rays originate [66]. The bright zones mark where these rays end up, which is shown in Figs. 6.2a and b to be potentially misleading. Light rays can overlap, cross, and intersect before forming a shadowgram if the screen distance is large enough, thus forming *caustics*.

For example, Fig. 6.2c is an oscillating-airjet shadowgram taken with a distance of almost 7 times the field diameter between object and film. This reveals sound waves and turbulence well, but the cellular structure of the jet itself is hopelessly blurred and distorted by caustics. (The jet structure of this example is shown properly in a companion short-distance shadowgram in [524].)

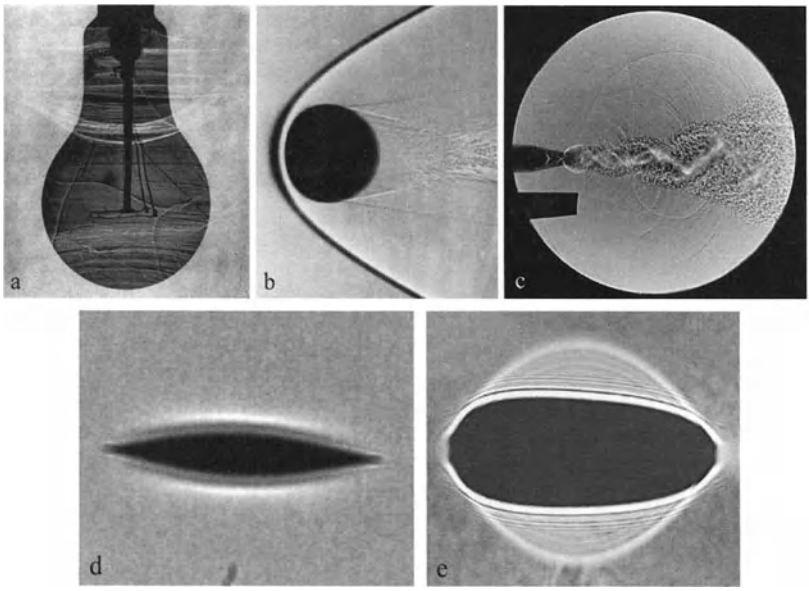

Fig. 6.2. Examples of shadowgraph errors. **a** Schardin's [2] shadowgram of a clear incandescent bulb, showing the dark bulb outline and the bright caustic patterns generated by strong refractions in the glass (reproduced by courtesy of Springer-Verlag). **b** shadowgram of a ballistic sphere in air. The dark band shows the bow-shock-wave position, but the front of the sphere shadow is distorted by the displaced bright light (US government photo by A. C. Charters, Army Ballistic Research Lab). **c** shadowgram of an oscillating underexpanded sonic airjet, (from Hammitt [524], reproduced by courtesy of the Princeton University Gas Dynamics Lab). **d** small- and **e** large-displacement shadowgrams of an air bubble in an antique-glass window pane (shadowgrams by Heather Ferree).

To emphasize this point still further, Fig. 6.2d is a shadowgram of an eye-shaped air-bubble inclusion in glass. The distance from object to shadow was on the order of a few cm. Thus the shadowgram, though not a focused imaged, nevertheless gives a good representation of the bubble. Upon increasing the distance to several meters, however (Fig. 6.2e), the bubble is no longer recognizable. The lesson of this example is that one must minimize the distance between object and shadow if a faithful object representation is desired in the shadowgram.

Similarly, objects of significant extent along the optical axis in diverging-light shadowgraphy suffer different magnifications of their near and far features in the shadowgram. An inversion of normal perspective occurs [122], in that the nearer an object is to the film plane, the smaller is its magnification. The resulting shape distortion is a problem if angular measurements are needed [42], e.g. the body and shock-wave angles in Fig. 6.1. A calculation by Melton et al. [499] shows a resulting shock angle error of 1° in a particular example. They recommend that the light source lie on a line through the model apex and perpendicular to the film plane in order to minimize this error.

Semi-quantitative measurements of the positions and angles of shadowgram features can still be made if such precautions are observed. In general, though, shadowgraphy is not well-suited to quantitative evaluation of refractive index, since a double integration is required [82]. Having said that, a few quantitative examples are nonetheless given in Sect. 10.4.

Finally, the formation of caustics in shadowgrams is a particular disadvantage when the caustics become confused with some other phenomenon. For example, a boundary layer can act as a cylindrical lens, focusing light into a bright line or band adjacent to a solid surface in a shadowgram [82,98,340,525,526]. Depending on object-to-film distance, this line can lie at, within, or outside the apparent boundary-layer thickness. Since it does not indicate the boundary-layer thickness, though, it leads to confusion. For example, in Fig. 6.1b the bright band falsely suggests that the boundary layer becomes thinner with distance downstream. Sometimes this phenomenon is confused with the bright reflection line that runs parallel to misaligned polished surfaces (Sect. 7.2.3). Hauf and Grigull [340] discuss this issue further under the heading "the boundary layer as a schlieren lens."

6.2 Direct Shadowgraphy

> The (direct) shadowgram is not produced by optical imaging, but rather by partially-coherent projection.
>
> *Kessler & Hebenstreit* [498]

Direct shadowgraphy was defined and discussed briefly in Sect. 2.4. In its simplest (diverging-light) form, only a small bright light, a schlieren object, and a suitable surface upon which to cast the shadowgram are required. A more-refined

version first collimates the light, projecting a parallel beam through the schlieren object to form the shadowgram. Both forms are considered in what follows.

6.2.1 Direct Shadowgraphy in Diverging Light

The direct shadowgraph in diverging light is the time-honored method of Marat [28], Dvorák [23], and Boys [62]. It's geometric-optical theory [2,66] follows the notation shown in Fig. 6.3. The schlieren object S of height d is located at distance g from the plane of the shadowgram. Illuminated by a "point" source of light L at distance h from that plane, the schlieren object casts a shadow of height d′. The magnification of the shadowgram with respect to the schlieren object is then given simply by

$$m = h/(h-g) \tag{6.1}$$

In the special case of h = 2g, the shadowgram appears at twice full-size.

Now consider the light ray c, originally straight, which suffers a refraction through angle ε at the edge of the schlieren object. Following its new path, the refracted ray c′ strikes the screen a distance Δa from the original position of c, thus redistributing the light in the shadowgram.

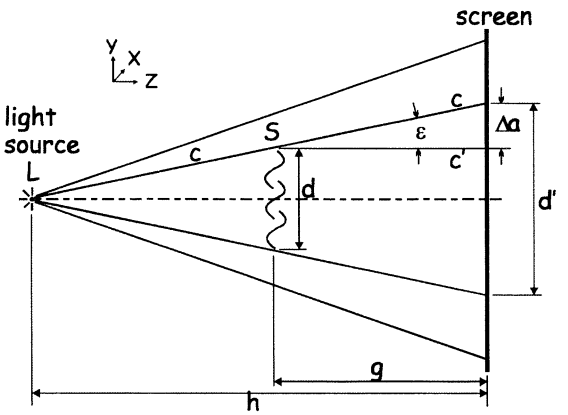

Fig. 6.3. Diagram of the direct shadowgraph technique with diverging light.

This refraction of incident light through angle ε, yielding displacement Δa at distance g, is the essential principle upon which shadowgraphy is based [430]:

$$\varepsilon \cdot g = \Delta a \tag{6.2}$$

It is, of course, basically the same principle already cited in Eqn. 2.6 for schlieren techniques, but its consequences are manifested differently in shadowgraphy.

Sensitivity. The contrast of the direct shadowgram in diverging light, according to Schardin [2], is equal to the ray displacement relative to the size of the shadow,

$$\frac{\Delta E}{E} = \frac{\Delta a}{d'} = \frac{\varepsilon}{d} \cdot \frac{g(h-g)}{h} \tag{6.3}$$

but since ε/d characterizes only the schlieren object, the term g(h-g)/h represents the entire effect of optical geometry on sensitivity. Differentiating with respect to g, this term is found to have a maximum at g/h = ½. Schardin thus stated two principles for high sensitivity in direct diverging-light shadowgraphy: 1) make h as large as possible, and 2) locate the schlieren object halfway between the light source and the screen.

Schardin loved to test such simple analyses against reality, and did so here using a glass windowpane with many flaws and striations. As shown in Fig. 6.4, the shadowgraph contrast rises quickly from g = 0, but then less quickly as g/h approaches ½. Another example shown by Schardin [2], not reproduced here, proves that the contrast actually does decrease for g > h/2, per Eqn. 6.3.

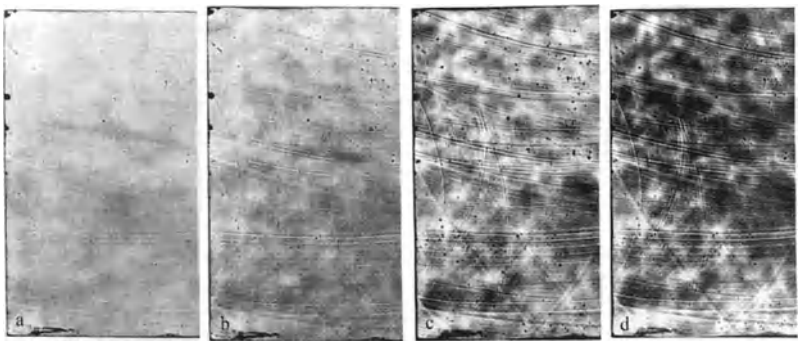

Fig. 6.4. Schardin's [2] shadowgrams of a glass windowpane illustrate the sensitivity change over the range $0 \le g/h \le ½$. **a** g/h = 0.05, **b** g/h = 0.1, **c** g/h = 0.4, to **d** g/h = 0.5 (reproduced by courtesy of Springer-Verlag).

Hannes [173], a student of Schardin, argued that the strength of the refraction in the schlieren object, ε/d in Eqn. 6.3, should be written instead as $\delta\varepsilon/\delta y$ or $\partial\varepsilon/\partial y$, where y is perpendicular to optical axis z in Fig. 6.3. This notation clarifies that it is not the refraction angle, $\varepsilon \propto \partial n/\partial y$, that is sensed by shadowgraphy, but rather its spatial derivative $\partial\varepsilon/\partial y \propto \partial^2 n/\partial y^2$. Hence, while the schlieren method reveals the refractive-index gradient $\partial n/\partial y$, it is the second spatial derivative (Laplacian) $\partial^2 n/\partial y^2$ that we observe with shadowgraphy. Restating contrast in these terms:

$$\frac{\Delta E}{E_0} = \frac{\partial \varepsilon}{\partial y} \cdot \frac{g(h-g)}{h} \tag{6.4}$$

Of course, the same holds for $\partial\varepsilon/\partial x$ in the plane perpendicular to the optical axis, and the effect of the geometric factor g(h-g)/h remains unchanged.

Weinberg [66] warns, however, that this relationship oversimplifies the difficulty of representing an object by its shadow. Eqn. 6.4 is approximately true, at best, only for those portions of a shadowgram illuminated by rays that traverse just one part of the test area. Once superposition of light from different regions occurs, the difficulties shown in Fig. 6.2 disqualify the shadowgram from any simple interpretation. Weinberg also gives an elegant method of testing for superposition using an inclined slit in the test area.

Geometric Blur. Next we consider the resolving power of shadowgraphy, and what is meant by a "point" light source. One can make the source diameter, D, small with respect to g and h, but not precisely zero. There is consequently an aperture angle, D/h, associated with the finite source size, that leads directly to a circle of confusion of diameter gD/(h-g) in the shadowgram (Fig. 6.5). When shadowgraphy is arranged for maximum sensitivity with g = h/2, the light source diameter equals that of the circle of confusion per geometric optics [66].

On the other hand, where sensitivity is secondary (as in glass and shock-wave testing), sharp shadowgrams can be had no matter how large the light source if g tends to zero. This encourages *contact shadowgraphy*, in which the photographic plate or film is placed directly against the schlieren object (Fig. 6.4a) or the wind tunnel window (Fig. 6.1b). The contact shadowgram shown in Fig. 6.1b reveals a wealth of flowfield detail as well as scratches and concentric grinding rings on the glass window. The original is a 20 x 25 cm sheet-film negative that loses some of its detail and clarity when reproduced at a smaller scale here. Edgerton [44] used the same principle to expose tiny aquatic creatures in a thin layer of water lying directly upon a sheet of film. Contact shadowgraphy, where feasible, minimizes both blur and geometric distortion by minimizing the distance g. Hilton's quote at the beginning of this Chapter applies especially to contact shadowgraphy.

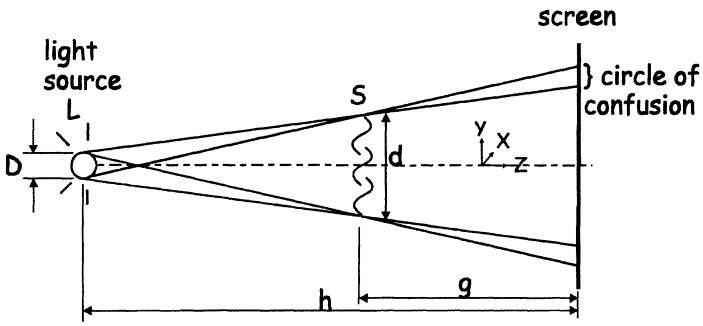

Fig. 6.5. Diagram illustrating geometric blur in direct shadowgraphy with divergent light.

Schardin [2] and others [66,173,498] recognized that the tolerable level of blur in a shadowgram depends upon the size, δ, of the smallest feature one needs to resolve. Dividing the geometric circle-of-confusion diameter by the shadowgram magnification, one obtains a relative blur size gD/h, whence the light source diameter equals twice that of the circle of confusion at peak sensitivity. Put another way, if one must resolve schlieren-object features of true size δ in the shadowgram, then g must be maintained less than δh/D. The corresponding maximum usable sensitivity [66] is:

$$\frac{\Delta E}{E_0} = \frac{\partial \varepsilon}{\partial y} \cdot \frac{\delta h}{2D} \tag{6.5}$$

Diffraction Blur. Despite these geometric considerations, the wave nature of light cannot be neglected in any discussion of optical resolution. The previous geometric theory suggests that both resolution and sensitivity can be increased indefinitely by reducing the light-source diameter D. The error in this approach is shown in Fig. 6.6. As the size of the source is systematically reduced, a limit is reached (frame c) beyond which further reduction fails to improve the shadowgram resolution because diffraction fringes appear. Diffraction thus sets an ultimate limit on the resolution attainable in a shadowgram. Kessler and Hebenstreit [498] further show that the source diameter has more effect than the spectral width on this limit. Even so, monochromatic light is undesirable for shadowgraphy since it exacerbates diffraction fringing and mimics the effect of a too-small light source [66].

Schardin [2] first attempted to apply diffraction theory to shadowgraph resolution, but did not fully succeed. Later attempts were made by Melton et al. [499], Hannes [173], Wolter [119], Weinberg [66], and Kessler and Hebenstreit [498]. The pertinent theory is worked out in laborious detail in some of these references, and is thus not repeated here.

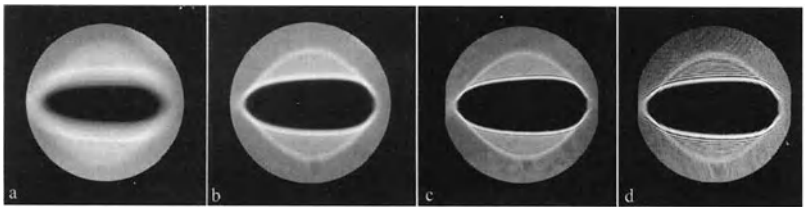

Fig. 6.6. Shadowgrams of an air bubble in an antique-glass window pane. **a** D = 1.5 mm white-light source. **b** D = 0.5 mm white-light source. **c** D = 0.2 mm white-light source. **d** λ = 0.6328 μm laser source with spatial filter (photos by Heather Ferree).

Briefly, recalling Eqn. 3.12, note that there is an unsharpness angle ε_u associated with diffraction blur. At a fixed light wavelength it varies inversely with the feature size δ that one wants to observe. In order for the feature δ to become visi-

ble, the refraction angle ε in the schlieren object must exceed the unsharpness angle ε_u associated with it. Thus, as in schlieren methods, shadowgram resolution depends not only on the size of the feature but also on the strength of its refraction.

Following this line of reasoning, Weinberg [66] derived an expression for the minimum refraction angle ε_{min} resolvable above the diffraction blur:

$$\varepsilon_{min} = 1.33\sqrt{\lambda h / g(h-g)} \tag{6.6}$$

where λ, the wavelength of illumination, was taken to be monochromatic in the analysis for the sake of simplicity. Similarly the smallest feature of the schlieren object resolvable in the shadowgram is given by:

$$\delta_{min} = 1.33\sqrt{\lambda g(h-g)/h} \tag{6.7}$$

and finally, the minimum useful light-source diameter, evaluated at the onset of diffraction fringing in the shadowgram, is:

$$D_{min} = 1.33\sqrt{\lambda h(h-g)/g} \tag{6.8}$$

Schardin [2] summarized shadowgram sensitivity and the effects of diffraction and geometric blur in a handy plot, repeated here with some modifications in Fig. 6.7. The sensitivity function is shown to change little over the range $0.3 < g/h < 0.7$, so it is not necessary to position the schlieren object exactly at h/2 for high sensitivity. Diffraction blur unfortunately also peaks in this range,[2] while geometric blur simply rises linearly with the distance g between the schlieren object and the shadowgram. Contact shadowgraphy is indicated in the narrow range of $g \approx 0 - 0.05$. The high end of the g/h scale is not recommended for practical shadowgraphy due to low sensitivity and large geometric blur.

6.2.2 Direct Shadowgraphy in Parallel Light

> The parallel-beam (shadowgraph) system is superior to the divergent one on almost every consideration.
>
> *F. J. Weinberg* [66]

Building on what was learned, we now let the distance h between light source and shadow in Figs. 6.3 and 6.5 approach infinity [66,82,98,173,527]. The magnification thus becomes unity and the light beam is rendered parallel, as if it originated from a star. Of course, the practical way to accomplish this within limited space is by way of a lens or mirror, as illustrated in Figs. 2.2 and 6.8, respectively.

[2] Schardin [2] erroneously showed this peak at g/h = 0.25, not 0.5. The mistake was later corrected by Weinberg [66] and Kessler and Hebenstreit [498].

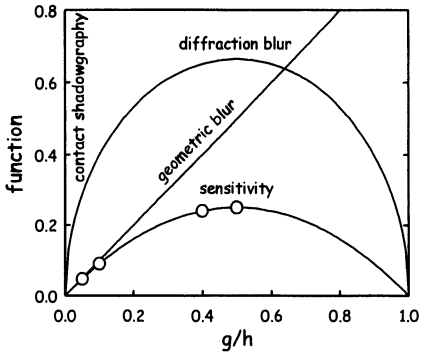

Fig. 6.7. Plot of sensitivity and blur functions vs. g/h for direct shadowgraphy in divergent light. The sensitivity function is (g/h)(1-g/h), the geometric blur function is simply g/h, and the diffraction blur function, based on Eqn. 6.7, is $1.33[(g/h)(1-g/h)]^{½}$. The open symbols represent the conditions of the four shadowgrams of Schardin [2] shown in Fig. 6.4.

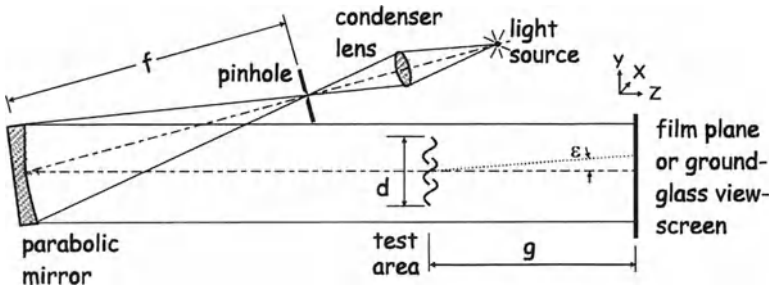

Fig. 6.8. Diagram of a parallel-light direct-shadow setup using half the optics of a z-type schlieren system to collimate the light beam.

Sensitivity. The contrast of the direct shadowgram in parallel light, according to Schardin's [2] definition, now becomes simply

$$\frac{\Delta E}{E_0} = \frac{\Delta a}{d} = \frac{\varepsilon \cdot g}{d} \tag{6.9}$$

In the more-rigorous form advocated by Hannes [173], this is written

$$\frac{\Delta E}{E_0} = \frac{\partial \varepsilon}{\partial y} \cdot g \tag{6.10}$$

By comparing Eqn. 6.10 for parallel illumination with its more general form for diverging light, Eqn. 6.4, and recalling that the maximum sensitivity in the latter

case occurred at g = h/2, it is clear that the contrast of the latter is exactly half that of the former [66]. Thus twice the sensitivity is available from parallel-light shadowgraphy for the same distance g, making it the technique of choice except for cases where unreasonably-large collimating elements are required. Parallel light further avoids the shadow distortion mentioned earlier, and better matches the sort of 2-D phenomena often studied in wind tunnels [122].

Geometric Blur. The aperture angle due to finite source size, formerly D/h, now becomes D/f for the parallel-light arrangement. The corresponding circle-of-confusion diameter in the shadowgram is gD/f. To minimize geometric blur, then, one wants a long-focus collimator and a small light source, bearing in mind that an excessively-small source is no advantage due to diffraction fringing. If one must resolve schlieren-object features of true size δ in the shadowgram, then g must be kept less than $\delta f/D$. The corresponding maximum usable sensitivity [66] is:

$$\frac{\Delta E}{E} = \frac{\partial \varepsilon}{\partial y} \cdot \frac{\delta f}{D} \tag{6.11}$$

Diffraction Blur. Weinberg's [66] expressions for the minimum resolvable refraction angle, ε_{min}, the smallest feature δ_{min} of the schlieren object resolvable in the shadowgram, and the minimum useful light-source diameter D_{min} now become:

$$\varepsilon_{min} = 1.33\sqrt{\lambda / g} \tag{6.12}$$

$$\delta_{min} = 1.33\sqrt{\lambda g} \tag{6.13}$$

$$D_{min} = f\sqrt{\lambda / g} \tag{6.14}$$

Here and in Eqns. 6.6-6.8 the factor 1.33 comes from an arbitrary definition of diffraction blur: the distance by which the first bright diffraction fringe protrudes beyond the geometric shadow edge [66]. These formulae should therefore not be interpreted as accurate to within 1%, but rather as general guidelines.

The confusion over the location of a shock wave caused by diffraction fringing is illustrated in Fig. 6.9, where the coherent Fraunhofer diffraction pattern due to a step-function phase disturbance is simulated by computation. High interest in shock waves has generated several papers on the interpretation of their shadowgrams and their diffraction phenomena [283,528-531].

As noted earlier, "white" light sources of small diameter have an advantage over monochromatic light in shadowgraphy, since the fringe patterns of the different wavelengths overlap, making fringing less obvious compared to the desired geometric effects. Despite this, broad-spectrum sources of small diameter are still partially-coherent, and spatial coherence alone is sufficient to produce obvious diffraction effects, as shown in Fig. 6.10.

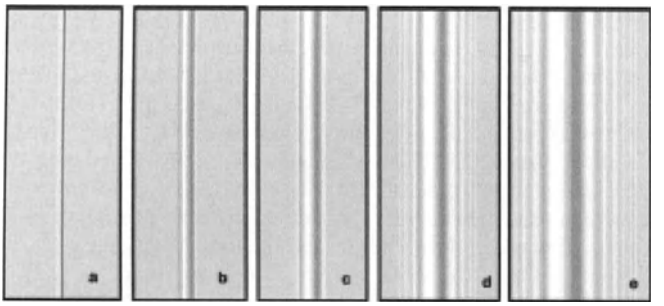

Fig. 6.9. Computed Fraunhofer diffraction patterns due to a λ/10 phase step-function at distances g = **a** 2 cm, **b** 11 cm, **c** 20 cm, **d** 40 cm, and **e** 80 cm. Parallel coherent light with λ = 0.6328 μm was applied in a simulation using GLAD 4.6 (see Apps. B and D). A weak shock wave (Mach 1.01) in standard air is simulated. The width scale of frame **a** is 3 mm.

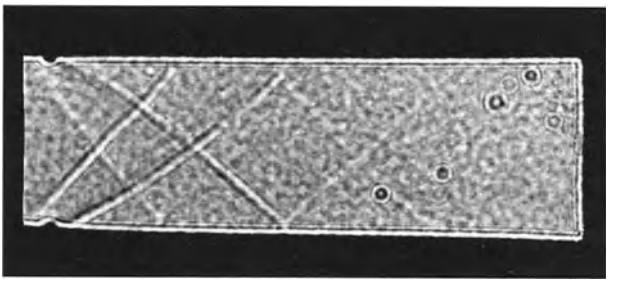

Fig. 6.10. White-light "point source" shadowgram taken in a small supersonic wind tunnel. Diffraction fringing is incipient in the oblique shock wave shadows, but is more obvious at the test section walls and window-spot flaws. Photo by the author ca. 1964 [532].

Illuminance of the shadowgram is inversely proportional to magnification in the divergent-light case. For parallel-light shadowgraphy, however, it is the same as the illuminance in the test area of a parallel-beam schlieren system (Eqn. 3.2). In present terms,

$$E_0 = \pi BD^2 / 4f^2 \tag{6.15}$$

6.3 "Focused" Shadowgraphy

6.3.1 Principle of Operation

The so-called "focused" shadowgraph method is diagrammed in Fig. 6.11. It is parallel-light shadowgraphy with one or more additional optical elements inter-

posed between the test area and the shadowgram. A parallel-light shadowgram would appear at plane M, lying distance g beyond the schlieren object S, if a screen were placed there. Instead, a second field lens is used to bring the beam to a focus, as in schlieren optics without a knife-edge, and a third (focusing) lens is used to image shadowgram plane M onto the screen at M*. Since M and M* are conjugate optical planes, the "primary" shadowgram at M is projected by these lenses to form a real shadowgram at M*. These two shadowgrams may be imaged at the same size, or else non-unity magnification can occur, depending upon focusing-lens choice. Except for magnification and illuminance differences in that case, though, the theory of the previous section applies here unaltered.

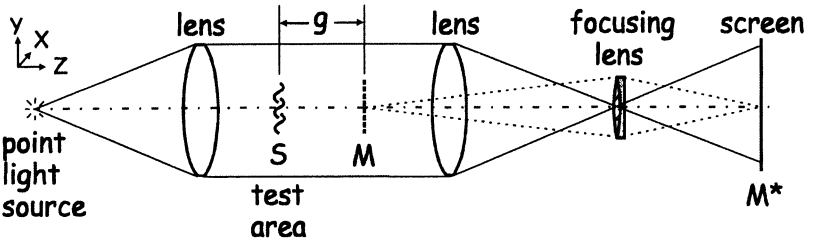

Fig. 6.11. Diagram of a lens-based optical arrangement for "focused" shadowgraphy.

6.3.2 History and Terminology

"Focused" shadowgraphy began, strictly speaking, with the Cranz-Schardin camera in 1929 (Ref. [6] and Sect. 7.3.3). When used without knife-edges, it produces a series of high-speed "focused" shadowgrams. The terminal-ballistic images of Schardin and Struth [533] were clearly made this way. Winckler's detailed study [534] of the 1890's-vintage Mach-Zehnder interferometer later revealed a shadowgram superimposed upon the focused interferogram image due to the finite extent of the test area along the optical axis. Hannes [173] was the first to study this "focused" shadowgram in its own right.

Like a child with an unfortunate name, "focused" shadowgraphy is troubled with needless controversy. This is because focusing is antithetical to shadowgraphy, in that focusing the schlieren object S upon the screen in Fig. 6.11 would eliminate the possibility of a shadowgram.[3] But, since the shadowgram plane M is focused at M* and not the schlieren object S, the objection is purely semantic.

Hannes [173] advocated "focused" shadowgraphy, on account of certain advantages described below, while Weinberg [66] objected to it strongly. Holder and

[3] Recall from Chap. 2 that a light ray passing through the forward focal plane of a lens - regardless of the ray angle – is returned to its same relative location at the back focus.

North [98] were decidedly lukewarm, but did give it mention, whereas Merzkirch [82] accepted it without question.

A sensible present approach is to recognize that the technique has value and is used. The terminology is thus accepted here with the enclosure of "focused" in quotes. (Perhaps we should rather call it "almost-focused" shadowgraphy?)

6.3.3 Advantages and Limitations

Advantages. A clear advantage of "focused" shadowgraphy is that it allows variable magnification of the shadowgram [66,173]. Film larger than 20 x 25 cm is not readily available for shadowgraphy, especially in an age where photographic materials are being replaced by small digital sensors. The ability to demagnify the shadowgram to a convenient size is important in light-starved applications as well.

Recalling Hilton's [122] comment on the risk to film and photographer, the ability to distance the shadowgram from the schlieren object is likewise advantageous. One may still do "contact shadowgraphy" with focusing optics, even when actual contact is inadvisable or impossible. In this case the field and focusing lenses after the schlieren object are relay lenses, and a change in magnification can also occur.

"Focused" shadowgraphy uses identically the same optics – whether lenses or mirrors – as a schlieren system, but without the knife-edge. Weinberg [66] saw the advantage of being able to take shadowgrams with a schlieren instrument, but not of assembling so many optical elements purely for the purpose of shadowgraphy.

Finally, another advantage lies in the ability to adjust the shadowgraph sensitivity and resolution simply by focusing a lens while observing the shadowgram, rather than having to vary the distance g. Magnification and sensitivity are thus decoupled by a proper choice of focusing lens [173].

Limitations. The field-of-view of "focused" shadowgraphy is limited by the field-lens or mirror diameter, just as in parallel-light shadowgraphy. One must also beware of a too-small focusing-lens aperture, lest refracted rays are cut off and a schlieren image appears instead of the expected shadowgram. Due to finite lens depth-of-focus, the "focused" shadowgram represents not just the plane M, but a focal zone surrounding it. Similarly, for schlieren objects that are broader than this zone, a shadowgram appears superimposed upon the expected schlieren image in routine schlieren work. The close similarity of the apparatus used for schlieren and "focused" shadowgraphy can even lead to some apparent confusion between the two.[4]

[4] Occasionally, in thousands of references, schlieren is promised but a shadowgram is actually delivered. Aside from ignorance and the discrepancy in translating "shadow methods" from the Russian (noted earlier), the only other explanation is that the schlieren cutoff is either ineffectual or missing altogether. What then remains is the superimposed "focused" shadowgram, e.g. [1016].

6.3.4 Magnification, Illuminance, and the Virtual Shadow Effect

The shadowgram illuminance in parallel light, Eqn. 6.15, must now be proportioned by the magnification m. Since it often happens that the primary shadowgram at M in Fig. 6.11 is demagnified to fit the recording medium at M*, the value of m is then less than unity. The background illuminance of the "focused" shadowgram is

$$E_0 = \frac{\pi B D^2}{4 f^2 m^2} \tag{6.16}$$

where any amplitude losses through the lenses have been ignored. Thus the demagnified shadowgram at M* grows brighter in proportion to its area reduction, even while the sensitivity and resolution are held constant by appropriate lens focus. The ability to do this is unique in shadowgraphy [173]. One must only be sure that the smallest shadowgram feature of interest, δ, remains larger than the resolution of the recording medium.

Finally, in all previous shadowgraph methods the shadowgram occurs unequivocally *after* the schlieren object in the progression of events along the optical path. However, in Fig. 6.11 it is entirely possible to adjust the lens focus so that plane M lies *before* the schlieren object, rather than after it as shown.

Why do this? Hannes [173] examined the issue, concluding that the *virtual shadowgram,* occurring at negative values of g, can be useful in some circumstances. Schlieren objects that focus the light in a "normal" (real) shadowgram will diverge it in the corresponding virtual shadowgram, and vice versa. Depending upon the schlieren object, occasionally the virtual shadowgram gives the better representation. Fig. 6.12 shows an example.

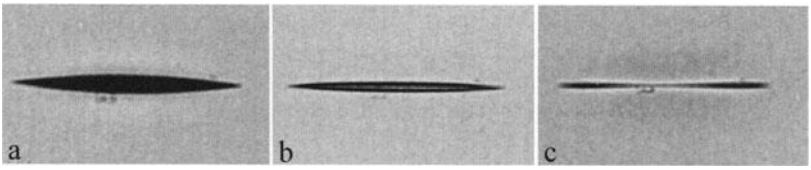

Fig. 6.12. a "focused" shadowgram of a stretched air-bubble inclusion in a glass window, g = 3 cm, **b** bubble sharply focused at g = 0 (note fine white line center line), **c** virtual shadowgram at g = - 3.5 cm. Photos by Heather Ferree.

6.3.5 "Focused" Shadowgraphy in Ballistic Ranges

A frequent use of "focused" shadowgraphy is in ballistic testing: the sensitivity of schlieren is unnecessary, the robustness of shadowgraphy is required, and the usual type of "contact shadowgraphy" with high-speed projectiles is deadly. Or-

dinary lens or mirror systems – of schlieren type without the cutoff – are used to relay the shadowgram to a safe film location at a reasonable magnification [209,433,537-539]. Even so, the potential for damage to the optics is high. Thus shadowgraphy's tolerance of relaxed optical quality is invoked by using large, cheap Fresnel-lens or metallic-reflector field elements near the ballistic trajectory [535,540,541].

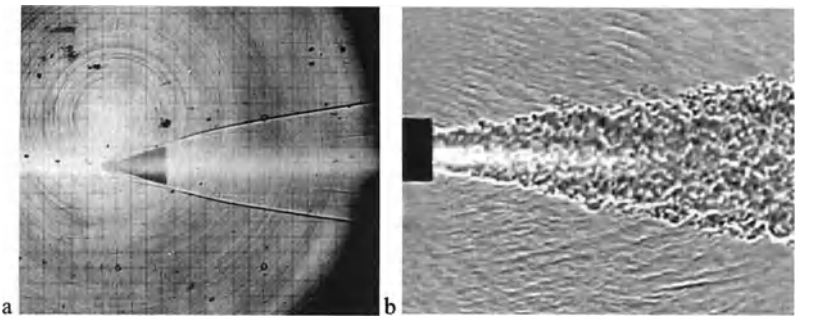

Fig. 6.13. Examples of "focused" shadowgrams: **a** self-luminous ballistic cone at 5365 m/s, US Air Force photo [535] **b** Hot turbulent exhaust from a high-velocity oxy-fuel thermal spray torch [536], taken with the optics of Sect. 4.1.3 minus the schlieren cutoff. ("Focused" shadowgrams cannot normally be distinguished from ordinary shadowgrams.)

Fig. 6.13a [535,540] exemplifies the use of a large plastic Fresnel lens as the main field element of a "focused" shadowgraph station in a large government ballistic range. The projectile passes in front of the Fresnel lens and the shadowgram is cast upon it from a distant point light source. The Fresnel lens serves to collect and converge the shadowgraph beam, so that it can be accepted by a small camera. As a consequence of focusing this camera on the Fresnel lens, its pitch interval appears in the form of concentric rings in the shadowgram. Black splotches in Fig. 6.13a indicate ballistic damage to the Fresnel lens, which needs occasional replacement.

6.4 Specialized Shadowgraph Techniques

6.4.1 Large-Scale Shadowgraphy

To some extent, direct shadowgraphy in divergent light (discussed earlier) is inherently large-scale. Not only is it amenable to sizable schlieren objects without sizable optics, but also its shadowgrams are always bigger-than-life. Nonetheless it was Harold E. Edgerton (1903-1990), the inventor of the electronic flash and

stroboscope, who first produced truly-large-scale shadowgrams [44,542]. He cast his shadowgrams outdoors on a 1.2 x 1.8 m black Scotchlite ™ screen, imaging them in a view-camera by way of reflected light. One of his strobe lamps was the light source for an optical setup much like the retroreflective schlieren methods described in Chap. 4, but without cutoff. This retroreflective shadowgraphy scheme has been widely used since then, especially in ballistics. Edgerton took several spectacular shadowgrams this way, two of which are shown in Fig. 6.14.

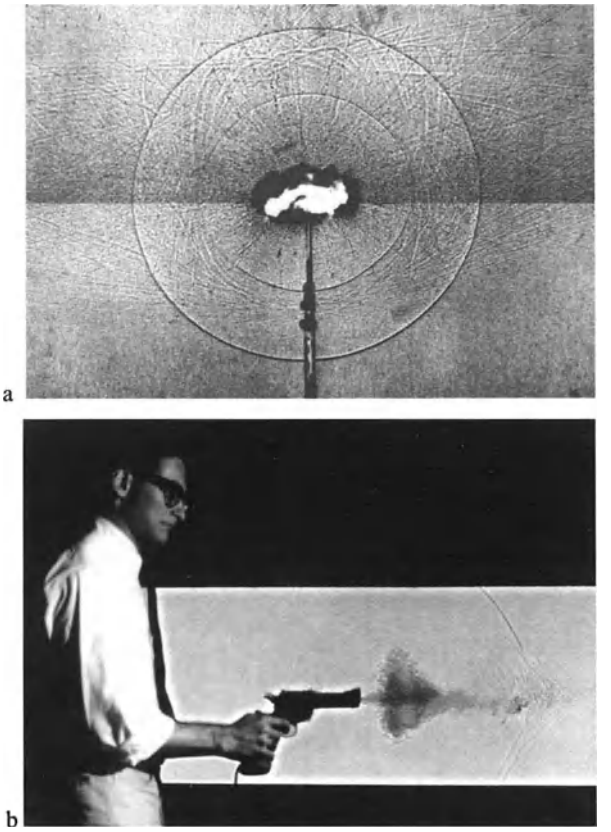

Fig. 6.14. **a** Shadowgram of dynamite cap explosion in open daylight, but with Sun behind the screen. **b** Shadowgram of Barry Rosoff firing a blank cartridge. © The Harold E. Edgerton 1992 Trust, courtesy of Palm Press, Inc.

The remaining examples of large-scale shadowgraphy are similarly oriented outdoors. Weinberg and Wong [255] developed a large-area infinitesimal-shear

interferometer with a laser light source and a shadowgram-like result. They proposed that an outdoor movie-theater screen could be appropriated for full-scale fire research. An ingenious solar-powered shadowgraph was also reported by Winn and Morin [543] for flammability studies. Large outdoor shadowgrams cast by the Sun are further considered in Sect. 9.4.10.

6.4.2 Microscopic, Stereoscopic, and Holographic Shadowgraphy

Microscopic Shadowgraphy is not usually so-called, but rather is termed "defocusing." In microscopic immersion testing (Sect. 5.8.5) a slight amount of defocus is enough to bring out the lines of strong second derivatives in transparent subjects [492,494]. By focusing just above or below the best-focus position, one sees the real and virtual shadowgrams described above under "focused" shadowgraphy. In the special case of objects like crystals, with sides parallel to the illuminating beam, the bright-dark bands due to shadowgraphy are called "Becke lines" [492].

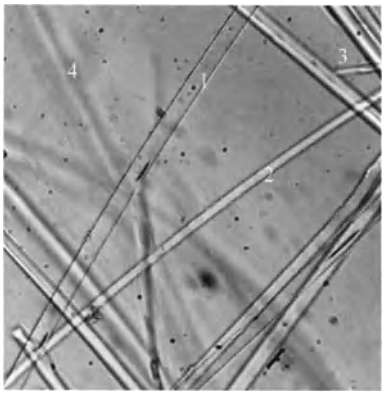

Fig. 6.15. Microscopic shadowgram of glass fibers immersed in Wesson™ cooking oil at about 500X magnification. The fiber labeled 1 is near best focus, while fiber 2 shows some convergence of light toward its center. Fibers labeled 3 in the upper right corner are still further defocused, displaying strong bright and dark lines. Some fibers, e.g. 4, are so far out of focus that they almost disappear. Microgram by Heather Ferree.

Stereoscopic Shadowgraphy was popularized by McCutchen [544-546], but has seen less use than the stereoscopic schlieren method of Sect. 5.3. The optical principles are very similar. McCutchen used stereo shadowgraphy to watch fish swimming in a temperature-stratified aquarium. Wake turbulence, one of the specialties of shadowgraphy, was photographed behind the fish. Kersh and Miller [547] also applied the technique to visualize shock waves.

Holographic Shadowgraphy was introduced by Denis Gabor, the inventor of holography, and his colleagues in an early seminal paper on phase imaging of reconstructed optical wavefronts [257]. It later became popular in aerodynamic testing to reconstruct shadowgrams, schlieren images, and interferograms from holographic records obtained with pulsed laser exposures [209,260]. After-the-fact

flexibility is gained in holographic shadowgraphy, since a number of different shadowgrams could be had from a single hologram by varying the focus of the reconstructing optics. A certain loss of shadowgram clarity inevitably occurs, though, due to coherent artifact noise in the illumination.

6.4.3 Computed Shadowgraphy

Predating computed schlieren, this topic began with an amazing computation in 1945 [115,548,549]. Undoubtedly arising from atomic weapons development in that early day of computing, synthetic shadowgrams allowed the strength of an explosion-generated shock wave to be inferred.

Clearly before its time, this precedent was not surpassed for more than 40 years. By then, however, computed shadowgraphy could be done routinely with much better graphics. Shock waves, one of shadowgraphy's strong points, were once again a subject of interest [550]. High-speed flow [460], convective mass transfer [551,552], and vortex [553] shadowgrams were also computed. In most cases these were compared with experimental shadowgrams.

Samtaney and Zabusky [554] review algorithms to generate images from computational fluid dynamics. They consider only one of many possible example flows, applying various edge-detection methods to simulate schlieren and shadowgraphy. They also propose the novel idea of using the Laplacian of pressure as well as that of density to discriminate shock waves from contact surfaces in unsteady flows. (Density can change across both, but pressure cannot change across a contact surface.) While this is computationally straightforward, no analog optical method can display the pressure Laplacian. These authors state a concise reason for such computed images: to reduce massive computational data sets to their essential mathematical-physical entities.

6.4.4 Conical Shadowgraphy

Many of the schlieren objects illustrated in this book have planar 2-D symmetry that is exploited to best advantage if the optical axis points in the direction of no change. Likewise other schlieren objects are fully 3-D, needing tomographic optical methods (Sect. 4.6) to completely reveal them. But where any type of symmetry exists, it always invites optical exploitation.

This is the case for a class of high-speed gas flows governed by a "hyperbolic" partial differential equation that admits conical solutions [555,556]. Included are supersonic flows about sharp streamlined bodies, where the flow properties are constant along conical rays from a common vertex. Shadowgrams of such flows, if taken from any random direction, will likely be confused or unrevealing. But by projecting the shadowgraph beam with a focus at the vertex and diverging light along the conical rays of the flow, a natural correspondence occurs between the flow symmetry and the beam symmetry. The resulting conical shadowgram then reveals all features of the conical flow in its simplest projection.

This method was pioneered by Love and Grigsby [557] and Pierce and Treadgold [558] for supersonic wind tunnel testing. It was then used by Zubin and Ostapenko [559] to produce the first revealing optical projection of the swept interaction of a shock wave and a boundary layer. Further work [493,505,560,561] proved that such interactions of high-speed aerodynamics are truly quasi-conical rather than fully 3-D, as was previously thought.

Most recently a method was proposed [562] to produce a light source for shadowgraphy by the electrical breakdown of the air due to an intense focused laser beam. With this, illumination can be introduced at the vertex of a conical flow even if that vertex lies at an otherwise-inaccessible point inside the airstream.

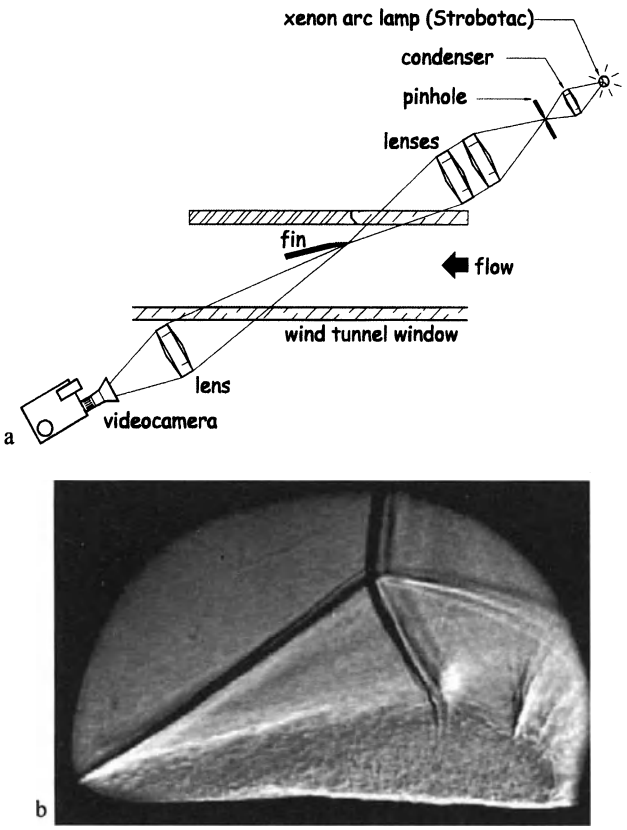

Fig. 6.16. **a** Diagram of conical shadowgraphy optics for supersonic wind tunnel studies of swept conical flows. **b** conical shadowgram of the swept interaction of an oblique shock wave, generated by a sharp fin at an angle of 20°, and a turbulent boundary layer flowing from left to right at Mach 3, from [505,560,561].

7 Practical Issues

It is apparently of the rudest possible construction...

C.V. Boys [62], *referring to his spark shadowgraph setup*

7.1 Optical Components

7.1.1 Light Sources

Of course nowadays all respectable experiments must employ a laser; you can hardly walk down the street without one.

Sir Brian Flowers, in Proc. 11th Intl. Congr. on High-Speed Photography

Light sources have improved tremendously since Hooke's first candle-illuminated schlieren system. Combustion lamps eventually gave way to electric sparks, arcs, and filaments, which were then supplemented by coherent and solid-state devices. There is now an expansive literature on the topic that needs no thorough review here. Instead some key references are cited, followed by a brief treatment of the important lamp types for schlieren and shadowgraphy.

Holder and North [98] and Hyzer [168] give detailed but dated reviews of the pertinent light sources. Früngel's work [563] is more recent, and includes early laser technology. Edgerton's classic book on the electronic flash [44] is highly recommended. A more-theoretically-oriented treatment is given by Hugenschmidt and Vollrath [564], and Fuller [565] gives a brief recent overview.

Schlieren vs. Shadowgraph Light Sources. As noted in Chap. 3, a rectangular light source with overall dimensions of a few mm is most suitable for schlieren imaging according to sensitivity and measuring-range considerations. Approximate spatial coherence, on the other hand, is a key requirement for sharp shadowgrams, since geometric blur grows linearly with light-source diameter (Sect. 6.2). Such small circular shadowgraph light sources do not make good schlieren

G. S. Settles, *Schlieren and Shadowgraph Techniques*

sources, however; when the traditional knife-edge cutoff is used, the measuring range is insufficient. Holder and North [98] therefore recommend the use of a graded-filter cutoff in such cases, effectively decoupling the measuring range from the source size.

In fact, all the appropriate light sources are relatively small, usually a few mm at most. High luminous exitance, measured in lux (formerly "brilliance;" see App. A.1), is thus an important lamp characteristic in order to insure sufficient illuminance in the final image or shadow [42,98,104]. Holder and North [98] reckon that 50 lux is needed on a ground-glass viewing screen, so the source exitance should be at least 100 lux for a schlieren system at ½ cutoff. Except for occasional cases of high image magnification, modern schlieren light sources have no difficulty meeting this requirement.

The duration of intermittent light sources is a further issue if one wants to stop motion, as discussed in more detail below. Spectral content, though, is usually a secondary concern except for some color schlieren work [397,400].

Incandescent Lamps are continuous-wave (CW) light sources not well-suited for short-duration use. They have a long history of service for schlieren illumination, but are not normally employed for shadowgraphy due to their filament size. Automotive headlamp bulbs without reflectors [104,133] have been diverted for use as schlieren lamps since the dawn of the automobile. Modern tungsten-halogen lamps [566], intended for various automotive uses, still head the list of inexpensive schlieren sources. Examples include the GE 9006 low-beam headlight bulb (12V, 1 x 5 mm coil filament, about $10US) and the GE halogen H3 or H3-55 fog-lamp bulb, about $6US. These modest lamps are cheap, stable, and dependable. They also outperform lasers for general-purpose schlieren illumination, as elaborated below.

Several projector bulbs similarly fit the requirements for schlieren illumination. Particularly useful are lamps with a rectangular multi-filament array designed to evenly-illuminate the frame of a movie or slide projector. These can be used – with suitable diffusers – to illuminate comparatively-large source filters of the sort described in Sects. 5.1 and 5.2.

Tungsten-halogen bulbs can produce high luminous exitance, though still one or two orders of magnitude less than an arc lamp. Given the low cost of the automotive bulbs, they can be operated at 15-17 V for higher exitance at the expense of reduced lifetime. Their color temperature is in the 3000 K range, producing "white" light with a yellowish cast.

These lamps have tightly-wound coil filaments. They can be used directly at the forward focus of a schlieren system, but better source definition and higher sensitivity are obtained with the use of a condenser and slit (covered later on in Sect. 7.1.4). Even so, the illumination over the source slit may not be perfectly uniform, which matters only if quantitative results are needed. In that case an expensive ribbon-filament bulb might be a better choice, or else a light-shaping diffuser to avoid hot spots [294].

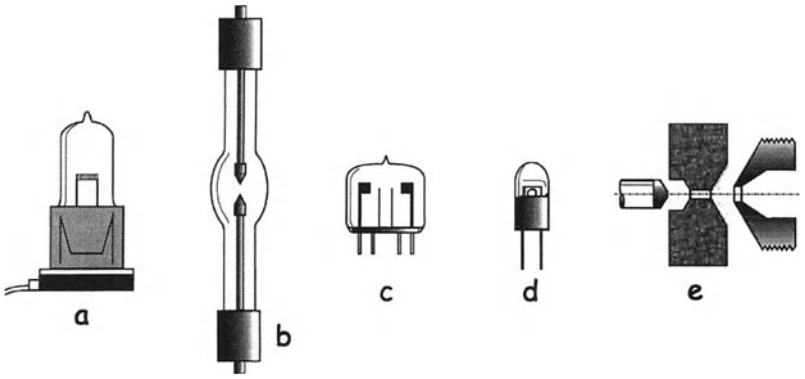

Fig. 7.1. Types of light sources for schlieren and shadowgraphy: **a** tungsten-halogen automotive lamp, **b** compact arc lamp, **c** xenon flash tube, **d** light-emitting diode, **e** constrained "point-source" spark gap after French Army Gen. Paul Libessart [499] (exploded view).

Compact-Arc Lamps strike a small arc between electrodes confined in a glass bulb, emitting light from the plasma thus produced [567]. They are 10-100 times higher in luminous exitance than tungsten-filament lamps. This makes them more suitable for schlieren and shadowgraph applications where light is at a premium, for example in high-speed cinematography. Many arc lamps can be operated in either CW or pulsed mode, with pulse durations in the microsecond range or less.

The archetype of this light source in the mid-20th Century was the high-pressure mercury arc lamp, specifically the GE air-cooled BH-6 [65,138]. It produced a line source 1 mm wide by several mm long, and operated in either CW or microsecond-pulse mode [65,98,138]. It has since been replaced by compact high-pressure mercury-arc lamps with an arc size of about 0.2 mm and the highest luminous exitance of any light source for schlieren and shadowgraphy. Though prejudiced toward the blue-green end of the spectrum, these lamps make excellent shadowgraph sources (see Figs. 6.2d and e and 6.6c for typical results). Mercury-arc lamps also emit dangerous UV radiation and have some risk of bulb explosion.

Xenon arc lamps have a better white-light color balance than mercury arcs, mimicking the Sun's color temperature of 6000 K. Their luminous exitance is less by about an order of magnitude, though, and the effective source dimensions are often larger. Ceramic xenon arc lamps with integral parabolic reflectors eliminate the need for a separate condenser lens [567].

Electronic Flashtubes. Edgerton [44] wrote "Studio photography, especially of children, has been tremendously benefited by electronic flash." This equally applies to many scientific applications that likewise refuse to stand still. But the millisecond-range studio flash or camera flash of today is not fast enough to stop ballistic phenomena or shock waves. Edgerton [44] and Früngel [563] review a variety of flashtubes that do operate in the μsec range or faster.

As an example, consider the xenon flashtube depicted in Fig. 7.1c. It is incorporated in the "Strobotac" stroboscope/tachometer manufactured by Quadtech Genrad (see App. D). The roughly-rectangular arc is about 2 x 10 mm in size, and is suited to illuminate a schlieren source slit by way of a condenser lens. The flash repetition rate can be set to 30 Hz line synchronization for quasi-CW setup and video illumination (RS-170/NTSC). Three intensity settings yield single-flash exposure times of 0.8 - 3 μsec. The high color temperature of the flash gives white light with a slight bluish cast. Though intended for tachometry, the Model 1531AB Strobotac makes an excellent and versatile schlieren light source that can also be adapted for shadowgraphy [44,568]. At this writing it costs about $4500US.

Xenon flashtubes can also be ganged together for multi-flash applications [166,241,563]. This approach provides a few separate high-speed flashes at a high repetition rate: one relatively-inexpensive way to tackle the problem of high-speed imaging (see also Sect. 7.3.3). Before xenon flashtubes, the approach was pioneered using spark gaps [98].

Spark Gaps are the oldest intermittent light sources for schlieren and shadowgraphy. Examples of their key role in illuminating the experimental physics of Toepler and Mach are given in Chap. 1. Typically of 0.1-1 μsec duration, they require several-kilovolt power supplies and large capacitors.

The Libessart gap, Fig. 7.1e, was popular during the first half of the 20th Century [98,499], and was used to take schlieren images such as Fig. 3.20b and shadowgrams such as Fig. 6.1b. Powered by a large capacitor, its exposed electrodes could kill careless users, requiring that it eventually be made into a self-contained, hazard-free system.

Fischer [569] discovered how to close-couple the components to minimize spark duration, which he reduced to the nanosecond range. The Fischer Nanolite [563] served to freeze motion in white-light-illuminated shadowgrams and schlieren images before nanosecond pulsed lasers became available, and it is still sold commercially (see App. D). Modern Nanolites have durations of 8-18 nanoseconds, outputs of tens of milliJoules, and kHz repetition rates. As many as 10 Nanolite spark gaps can be ganged together for short-burst high-speed imaging at MHz frame rates. Many examples of such multi-spark applications are found in the literature on shock tubes and ballistic ranges [6,98,210,503,570,571].

Finally, color schlieren imaging needs illumination across the visible spectrum, which lasers cannot provide but sparks can. Along with xenon flashtubes, spark gaps are important for illuminating color schlieren images of high-speed events [377,386,397,398,400,415].

Lasers and Laser Diodes. There is a tendency for novices to reason that, if a $6 tungsten-halogen lamp makes a good schlieren light source, then a $60,000 laser must be a lot better. This logic is generally false. The reason was stated by M. McDonnell in SPIE Vol. 120: "Coherent light is not good for imaging, particularly where a small-aperture system like the human eye is used for viewing the image." Excess coherence in shadowgraphy was also discussed in the previous chapter.

But this is not to discount lasers altogether for present purposes. All readers interested in this topic should read Oppenheim, Urtiew, and Weinberg [100]. The paper is unfortunately misnamed, and ought to be titled "On the use of laser light sources in shadowgraph, schlieren, and schlieren-interferometer systems." In some sense it is an update of Weinberg's 1963 *Optics of Flames* [66] to account for the advent of laser light sources. The authors describe three difficulties of lasers for schlieren and shadowgraphy: 1) the geometric-optical description of the results breaks down, 2) a very-small focal spot is produced at the schlieren cutoff, and 3) high energy density burns the optics in the cutoff plane.

As a result, laser illumination with an ordinary knife edge fails to yield a recognizable schlieren image. Instead, a binary cutoff occurs and fringes appear due to diffraction (see Fig. 5.3a for an example). In effect, all schlieren systems with coherent laser light sources thus become schlieren-interferometers.

A graded-filter-cutoff solution to this problem is given by Oppenheim et al. [100] for laser-illuminated schlieren imaging. As described fully in App. B, Figs. B.5 and B.6, a knife-edge cutoff is too harsh for good schlieren imaging with coherent light. A graded filter (Fig. 7.2) or a partially-transmitting knife-edge (Fig. 5.3) does a much better job of revealing phase gradients through amplitude changes. Examples of bad laser schlieren images with improper cutoffs abound in the literature, e.g. in Ref. [572], but there is no excuse for them.

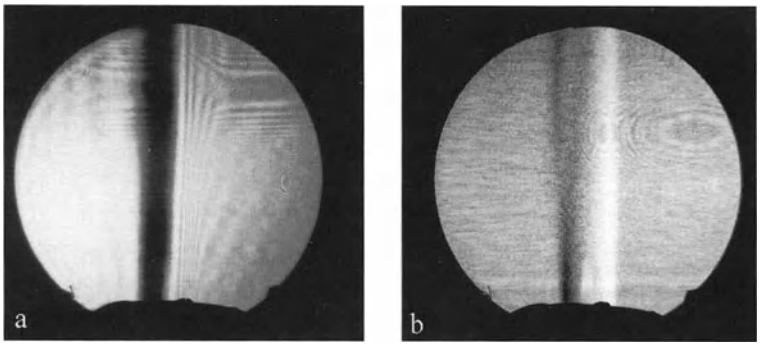

Fig. 7.2. **a** Candle plume schlieren image with $\lambda = 0.6328$ μm laser illumination and knife-edge cutoff. **b** knife-edge replaced by a graded filter. Some graininess appears due to the photographic-film grain of the graded filter. Photos by Thomas C. Hanson.

Geometric optics also breaks down in coherent-lit shadowgraphy, as discussed in Chap. 6. Hannes [173] first demonstrated that this happens when the light-source size falls below a certain useful limit. For such excessively-coherent illumination, poor shadowgrams result with fringes occupying the traditional bright band caused by a schlieren object (Fig. 6.6d). Here, however, one may still proceed to use a laser shadowgraph source so long as the consequences are kept in mind during shadowgram interpretation.

Similar principles apply in optical image processing [573], where white-light illumination has the recognized advantages of better signal-to-noise ratio and a broader spectral range than coherent illumination. Broad-spectrum "white" light smoothes over the fringing that occurs with monochromatic light. Lasers are intense and spatially coherent, but diffraction and coherent artifact noise degrade the resulting image. Clean, high-quality, scratch-free optics are needed. The laser, almost a true point source, also lacks the redundancy of an extended source (see App. B). Finally, lasers tend to be much more expensive than white-light sources.

On the other hand, laser illumination offers the advantages of evading chromatic aberration effects, pulsing in 1 or 2 nanoseconds, and providing an intense light emission. The coherence of laser illumination has been reduced for microscopy using a phase randomizer [574], and a novel fiber-optic ball [575] has been suggested as a point-source laser illuminator for shadowgraphy.

Light-Emitting Diodes (LEDs) are modern semiconductor light sources (Fig. 7.1d) that have found application in both pulsed and CW schlieren and shadowgraph illumination [563,576-581]. Originally monochromatic, LEDs are now available with white-light emission as well. One has even found commercial application as a miniature pocket flashlight [582]. LEDs are compact and very inexpensive, but have a relatively-low light output compared to sparks and flashtubes. A typical LED for shadowgraphy has a few mW output at 8000 K color temperature, but 200 mW output or more is on the horizon. Its beam originates from 0.25 x 0.25 mm effective source dimensions and diverges at a 20 ° half-angle through an integral molded lens. This makes a good replacement for the now-defunct zirconium concentrated-arc lamp, except for its low power rating. LEDs can be pulsed in the sub-μsec range, though, making them useful for high-speed imaging [578,579].

7.1.2 Mirrors

> We are forced to use what the astronomers have already developed for us...
> *W. F. Hilton,* [122]

Parabolic Mirrors are discussed in Chaps. 3 and 4 as field elements for coincident and z-type schlieren systems up to a meter in diameter or more. Cost, availability, and aberrations arising from their off-axis use are covered there and in App. D. Astronomical telescope mirrors continue to make the best-available field elements for traditional schlieren systems, the accuracy requirements being similar for both applications.

Spherical Mirrors are ideal for single-mirror coincidence schlieren systems, but not for parallel-beam systems. However, at f/10 or higher the difference between a spheroid and paraboloid is within λ/2 [98,126], making the two indistinguishable for schlieren use. Spherical primary mirrors with correctors are used in some telescopes, and in some commercial schlieren instruments discussed in Sect. 7.4.

Plane First-Surface Folding Mirrors for shortening the length of a schlieren setup are discussed in Chap. 3. They are subject to the same high standards of optical quality (i.e. flatness) as schlieren field elements. A great advantage in cramped quarters, they nonetheless exacerbate the chore of optical alignment.

Cleaning First-Surface Mirrors must be approached with great care, since it is easy to damage the aluminized coating. Greasy fingerprints are insidious, and at least one wind tunnel lab tells a horror story involving a large parabola, a janitor, and some steel wool. A clean, dry airjet or can of "Dust-Off" removes dust and anything else not strongly adherent. Lens tissue can also be used locally and carefully, but the recommended cleaning procedure [98] involves spraying the mirror with water containing a mild detergent. Spray bottles do not damage the mirror, but a final rinse in distilled water is needed to avoid spotting.

7.1.3 Schlieren Cutoffs and Source Filters

New single-edged razor blades have always made excellent schlieren knife-edges. Lord Rayleigh [172] preferred Gillettes, but in fact any brand will do.

More-sophisticated cutoffs and source filters, such as those described in Chap. 5, must be made to order. This is achievable with simple materials and tools, given a little experience. Care is needed to preserve the optical quality of anything placed in the schlieren cutoff plane, since the beam waist there contains all the information needed to form a sharp schlieren image, but is susceptible to distortion and disruption. Ragged edges, narrow slits, and poor color filters take their toll.

Color filter manufacture is discussed by North and colleagues [94,125], who always give their readers practical fabrication advice, and by Stong and Settles [385]. Cords [213] advocates making a high-contrast photographic negative of an opaque mask as a background for the color filters of his "dissection" color schlieren method. Similar methods for Rheinberg microscope filters are described by Vetter [583].

Two example color schlieren filters are drawn in Fig. 7.3 to illustrate these fabrication methods. In both cases a 35 mm slide-cover glass serves as a substrate.

In Fig. 7.3a, Kodak Wratten gelatin filters are used to produce a 2-color cutoff. Wratten filters are traditional for this purpose, having much-better optical quality than the usual plastic filters and gels. They can be cut to size carefully using a new razor blade and a metal ruler, but even so it is hard to get edges clean enough to butt together precisely. For that reason the junction can then be covered by a narrow opaque band trimmed from black vinyl electrical tape. This band should almost match the width of the light-source image in the cutoff plane, but should not be narrower than 1 mm or so on grounds of diffraction resolution loss. Schlieren sensitivity is then varied by adjusting the source-slit width while keeping the source image centered on the opaque band. This affords higher sensitivity than the case without the opaque band, due to lower background illuminance in the image.

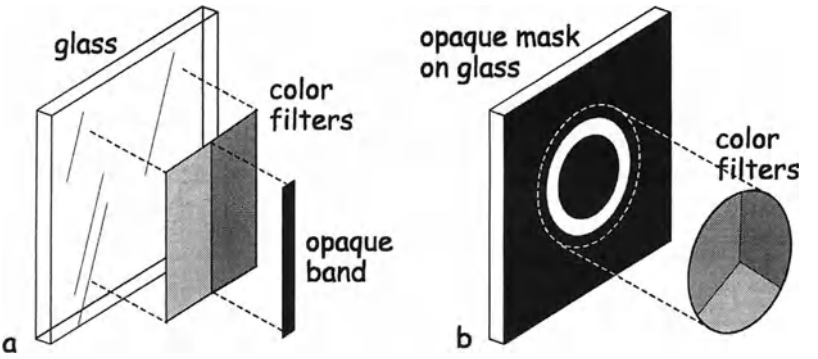

Fig. 7.3. Fabrication details of **a** two-color schlieren cutoff filter, **b** source filter for a round 2-D dissection-type color schlieren system.

In Fig. 7.3b a photographically-made clear ring in an opaque mask serves to define the shape of the source filter, while three 120° pie-shaped segments of Wratten color filters (typically the primary colors, red, green, and blue [400]) provide the color contrast. In this case any slight gaps where the color segments adjoin are of little consequence.

Several other filter fabrication methods can serve as well as those just described. For example, black vinyl electrical tape and drafting tapes are often used to lay down rectangular masks upon a glass substrate; circular masks like Fig. 7.3b are more difficult to cut accurately, and one must beware not to melt the tape with too much focused illuminance. Metal foil can also be cut to form masks that can withstand this problem better, since they reflect unused illumination. Beyond a certain level of mask complexity, though, one should prepare an enlarged black-and white version on paper and reduce it photographically.

Finally, this same photographic approach can be applied to make entire color source and cutoff filters using color transparency film [325,377,411]. It is tricky to get color saturation approaching that of Wratten filters, though, and North [94] cautions about diffraction effects that can occur at the dye-layer boundaries of color transparencies. But, in the almost-half-century since his original work on this topic, color films have matured and the problem no longer seems serious.

7.1.4 Condensers and Source Slits

The illustrations of various schlieren arrangements in Chap. 3 show lamp illumination focused by a condenser lens upon a "source slit," Fig. 7.4. This effectively crops the irregular intermediate image of the source in order to produce a regular, usually rectangular, approximately-uniform effective light source. The idea originated with Toepler [37], who used it to improve the schlieren sensitivity. He recognized that the shape of the source aperture is actually unimportant, so long as it has one straight edge corresponding to the knife-edge cutoff. Recalling

has one straight edge corresponding to the knife-edge cutoff. Recalling Fig. 2.6, sensitivity is related directly to the unobscured source-image height a in the schlieren cutoff plane. But if the source edge is ill-defined, then small a-values approaching the diffraction limit of sensitivity cannot be had. The effect is similar to that of replacing the knife-edge by a graded filter. One can always do that, of course, in the cutoff plane, but a sharply-defined effective source is universally recognized as a good idea.

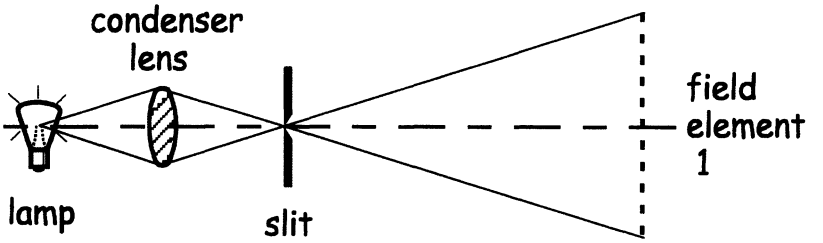

Fig. 7.4. Diagram of typical light source, condenser, source slit, and first field element (lens or mirror) of a schlieren system.

Note especially that the width of the source slit – and thus of its image in the cutoff plane – affects the measuring range of the schlieren system but not either the sensitivity or the background illuminance of the image; these depend only on the amount of cutoff. There are restrictions, however, on source-slit width. Obviously it should be less than the width of the source image focused upon it by the condenser, in order to define the effective source sharply as just described. For the example of a tungsten-halogen lamp, the filament image superposed upon an appropriate source slit is sketched in Fig. 7.5a. Though cr opping the filament image to produce sharp edges, the condenser-slit combination cannot render the illumination perfectly uniform over the entire area of the slit. As noted earlier, this is not a problem except when quantitative results are needed, in which case a ground-glass or light-shaping diffuser [294] can be used directly before the slit.

The lower limits on source-slit width arise from too-narrow measuring range, inadequate light level, and condenser aberrations. Any spherical aberration in the condenser prevents a sharp focus of the source image upon the slit, and can lead to uneven illumination downstream. A sheet of matte white paper held in the beam before the position of the first field element will reveal this immediately. Nonuniform patterns like that shown in Fig. 7.5b indicate the inability of the condenser to pass a Foucault knife-edge test. A better condenser can be substituted, the light-shaping diffuser strategy mentioned above can be invoked, or else the source slit can be widened until the illumination regains its uniformity.

Returning to Fig. 7.4, the f/number of the condenser and that of the first schlieren field element are shown to be identical. This provides the best match of illumination, exactly filling the schlieren field. From a practical standpoint, though, it is unwise. Schardin [1] notes that the finite size of the source slit leads

to reduced illumination near the periphery of the schlieren field in this case. Vasiliev [102] recommends that the effective condenser f/number be 1.5 to 2 times smaller than that of the first field element in order to fill the latter uniformly (never mind the spillage of light). Thus aberration-free condensers of large diameter and small focal length are favored for light collection efficiency.

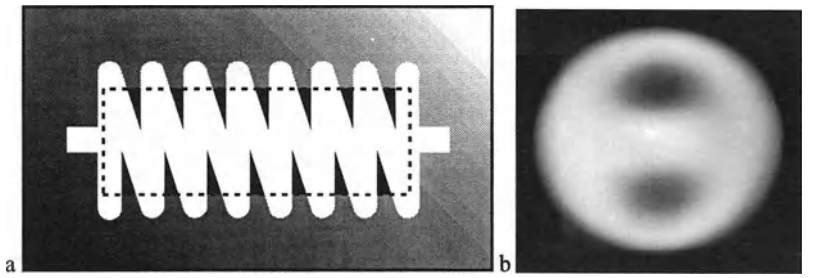

Fig. 7.5. **a** image of lamp filament superposed upon a horizontal source slit, **b** uneven illumination pattern projected through schlieren system by the combination of a condenser with spherical aberration and an excessively-narrow horizontal source slit.

In most cases there is ample radiated luminance from the source and some spillage of light due to excess beam diameter at the first field element is taken in stride. A ground-glass diffusing screen before the slit spreads the outgoing beam, and is thus costly in terms of collection efficiency. Even at best the condenser can accept only a small fraction of the total light radiated through 2π steradians by the source. Further commentary on the general issue of lamp-condenser collection efficiency in projectors is given by Dewey [584].

Similarly one can magnify or reduce the source image size at the slit by various combinations of source-to-condenser and condenser-to-slit distances [98]. Magnification can be used to increase the schlieren measuring range, but it interplays directly with the light collection efficiency issue just mentioned.

Ideally, the condenser lens should be free of both spherical and chromatic aberrations as well as internal defects [98,104]. Practically, some compromise is usually necessary in the interest of economy. Single-element aspheric condensers are inexpensive and efficient at light collection (see App. D). Multi-element objective lenses from cinema projectors [133], large eyepiece lenses from surplus military optics, and fast camera lenses can also serve effective condenser duty.

7.1.5 The Required Optical Quality

Parabolic and spherical mirror quality requirements for schlieren optics were already discussed in detail in Sect. 3.1.2. These requirements are very severe, and

having met them at some expense, one cannot then allow a poor window or lens to spoil the instrument.

Lenses, especially including the focusing lens and the field elements of lens-type systems, face stringent requirements of accurate surface figure, internal quality, and aberration correction. These requirements were discussed earlier in Sect. 3.1.1. As an example, cheap single-element lenses are entirely inappropriate for schlieren field lenses. If they were used, the quality of the source image in the cutoff plane would be so corrupted by aberrations that no uniform cutoff could be had, and only the strongest of schlieren objects could even be seen.

Chromatic aberration is corrected at two separate wavelengths in (expensive) achromatic doublets made of crown and flint glass. Even so, schlieren systems with white-light illumination are seldom entirely free of chromatic dispersion. In the most-serious cases the schlieren image appears split into red and blue half-circles [410]. Toepler [40] took delight in these "magnificent colors." Nowadays, though, color schlieren ought to be voluntary.

Windows. Since 0.1-arcsecond refractions are visible in the best schlieren systems, windows in the field-of-view are severely challenged to rise above the level of the schlieren objects under observation. Once again, surface flatness and interior quality are equally important, making windows several times as expensive as mirrors of the same diameter. One should therefore avoid windows if possible, but in wind tunnel or combustion work, for example, they are a necessity.

BK-7 glass is often chosen for schlieren windows, though fused silica also serves at a much-higher cost. In fact, specifying "schlieren grade" is guaranteed to drive up the cost of any window to a breathtaking level. Even a century ago, large schlieren-quality windows proved too expensive for Ludwig Mach, who pioneered the use of schlieren imaging in his early low-speed wind tunnel [479].

To avoid this expense, one can pre-screen glass in a schlieren system and mark the clear areas for window fabrication. Even commercial plate glass can make acceptable schlieren windows if the tin-bath direction is kept parallel to the knife-edge. Occasionally even acrylic windows are found suitable under limited circumstances, especially when annealed to relieve internal strains.

Large monolithic wind-tunnel windows were once made from poured blanks, causing pouring-ring striations to appear in the finished product under schlieren observation (see the concentric rings in Color Plates 6-8, taken in the former NASA-Ames 6x6 supersonic wind tunnel.) At least a few striations are hard to avoid in wind tunnel windows, as illustrated in Fig. 7.6.

Holder and North [98] specify $\lambda/2$ per 25 mm surface flatness for wind tunnel windows, and give window mounting advice as well. Volluz [109] has a substantial section on the design of wind tunnel test section windows to withstand pressure loads. Special care is required to avoid cracking due to thermal constriction of the glass edge by its metal window-frame. Modern windows in large government wind tunnels sometimes use segmented glass with "prison-bar" su pports for window strength.

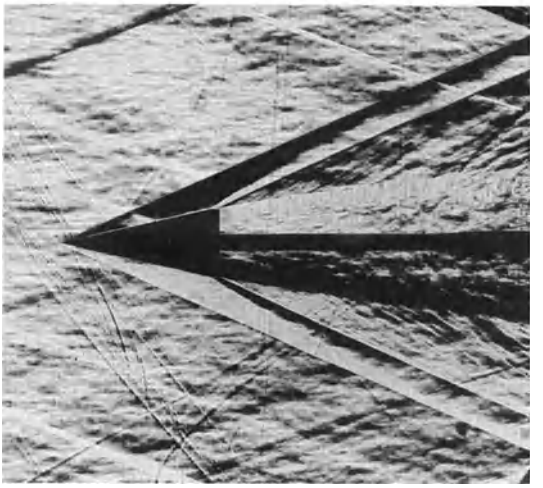

Fig. 7.6. Schlieren image of supersonic airflow over a cone model, shot through windows containing striations. A trained eye can easily distinguish the striations, which are either vertical or at about a -50° angle, from the shock waves that are more steeply inclined with respect to the horizontal. Photo courtesy of the Princeton University Gas Dynamics Lab.

7.2 Equipment Fabrication, Alignment, and Operation

7.2.1 Schlieren System Design Using Ray Tracing Codes

Until recently, schlieren system layout and component specification was done entirely by hand. This is still mainly so, but modern optical computer-aided design (CAD) programs can now assist in this task. In fact, ray-tracing software is able to design much-more-complicated optics than any schlieren system discussed thus far. These capabilities include, for example [585], the design of optical systems with several mirrors or lenses, system evaluation and optimization, ray tracing and spot diagrams, imaging performance assessment, and stray-light analysis.

Precedents for the use of such software in schlieren-system design include Hosch and Walters [171], who use ray-tracing to assess image resolution, Buchele and Griffin [414], and Collicott [586], who analyzed a multiple-source system. Thompson et al. [206] extracted quantitative schlieren data by ray-tracing, as did Verdaasdonk et al. [332]. Ojeda-Castañeda saw computed spot diagrams of the Foucault knife-edge test as a useful training exercise for optical-shop students.

Ray tracing [587] calculates the aberrations of an optical system using a collection of individual rays. The resulting distortion of the image of a source spot is an index of optical system performance [588]. Ray tracing is geometric, tho ugh, and cannot include the diffraction effects that are important in schlieren imaging (except as an add-on in a few codes). In particular, spatial filtering relies on physical optics (see [589] and App. B).

As a brief, simple example, one of the current ray-tracing codes (OSLO LT, see App. D.6) was used to analyze a single-mirror coincident schlieren system in poor

alignment. As shown in Fig. 7.7a, some lateral offset is allowed for practical reasons, between point-source and focus, as well as a small focal-distance offset. The resulting spot diagram shows the distortion of the point-source image due to astigmatism and spherical aberration. (Actually, though, the worst practical effect of these misalignments is likely to be a doubling of the schlieren image, Sect. 3.1)

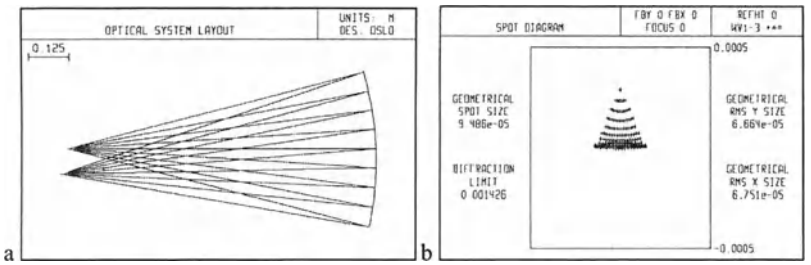

Fig. 7.7. **a** ray-tracing diagram, and **b** spot diagram for a misaligned single-mirror coincident schlieren system.

The upshot of this topic is: computational ray tracing is probably overkill for simple schlieren setups, but for specialized systems, added optical complications, or very cramped quarters, it can be quite useful.

7.2.2 Fabrication of Apparatus

Since few schlieren instruments can be bought ready-made, there is strong precedent to do-it-yourself. This frustrates some, but is good for the soul of the yo ung investigator. Few scientific discoveries were made by appliance operators.

Holder and North took a decidedly build-it-yourself approach in their book on schlieren methods [98]. To a lesser extent so did Vasiliev [102]. The next chapter of this book likewise describes the fabrication of a small z-type schlieren system. Other resources includes Strong's *Procedures in Experimental Physics* [301], a charming but dated introduction to building one's own apparatus. Fabrication of modular units [590], use of off-the-shelf telescope components [414], and even optical mounts made of LEGO blocks [591] prove that the resourceful experimenter still survives, at least in a few isolated pockets. The authors of Ref. [591] acknowledged the president of their institute, who caught them playing with LEGO blocks and believed the explanation that they were actually working.

Having said all that, it is still entirely possible to buy essentially every optical component you need for a schlieren system without having to build anything; you only have to assemble it. Optical mounts are readily available – see Apps. C and D – but they can be expensive. Examples include stands, mounting rods, rod holders and bases, magnetic bases, lens-, filter-, and ground-glass-holders, irises,

mirror mounts, pinholes, adjustable slits, laser mounts, positioners, stages, and lamphouses. Some typical examples are shown in Fig. 7.8

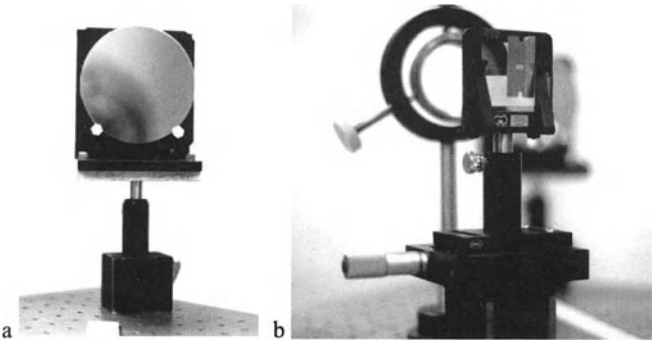

Fig. 7.8. **a** 10.8 cm diameter parabolic schlieren field mirror rod-mounted to a magnetic base. **b** razor-blade knife-edge in filter holder with micrometer x-drive (focusing lens in a ring-mount is in the background). Photos by Heather Ferree.

As shown in the figure, an optical breadboard or table with magnetic mounts can be used to advantage for small schlieren instruments. Larger ones, especially in-line lens setups, should employ optical benches or beams instead. Toepler [37] used the time-honored Zeiss v-beam bench, still available today (see Figs. 3.5b and 4.12) and not improved upon by the various modern lathe-bench schemes. In any case the open optical bench is definitely preferred, for ease of adjustment, to enclosed pre-set schlieren systems like those described by Vasiliev [102].

Holder and North [98] commented on such open optical-bench schlieren setups and emphasized the need for dust covers to protect the optics when not in use. This holds especially in view of the constant threat of greasy fingerprints on first-surface mirrors.

Most of the optical components require some facility for adjustment, but the only fine (vernier) adjustment one usually needs is at the knife-edge (a 1 thread/mm lead screw is suggested). In special cases, though, more fine adjustments may be needed. For example, a 3-axis-translation plus 1-axis-rotation micropositioner is required for the cutoff of the Penn State Full-Scale Schlieren System, Sect. 4.3.5.

Further discussion of the fabrication of schlieren and shadowgraph apparatus, including windows, cutoffs, and optical mounts, can be found in Refs. [65,104,138,301,592-595].

7.2.3 Setup, Alignment, and Adjustment

Beginning with Toepler [40], several authors have given instructions for setting up a schlieren instrument once all the components are on hand [65,98,102,126,592].

Toepler gave an 8-10 minute procedure to set up and align his in-line, lens-type apparatus "from scratch." His time estimate is good for an experienced hand, but the novice might need an extra minute or two.

Holder and North [98] briefly cover the setup procedure for a z-type schlieren system, introducing the basic alignment "tool": a white card or clean sheet of white paper. This can be held in the schlieren beam at any point to observe the beam profile, e. g. immediately after knife edge to adjust the cutoff amount, or after the source slit to judge the uniformity of illumination (Fig. 7.5b). Holder and North also note that weak reflections from plane glass windows in the parallel schlieren beam can be traced back to the source to check the window alignment.

Other than the sheet of white paper, a few other props are similarly helpful in setting up schlieren instruments. Some use a laser beam to mark the optical centerline during setup, but this is not really necessary. Novices seem to have inordinate trouble focusing the schlieren image sharply upon the test area, in part because a small source and resultant large depth-of-field makes sharp-focusing difficult. In this case it helps to place a threaded bolt, glass stirring rod, light bulb, or candle flame in the test area to focus upon. Self-luminous objects produce diverging light from the test area that focuses sharply upon the schlieren image. The glass stirring rod focuses incident parallel light on its centerline, causing a fine bright line to appear in the schlieren image at critical focus, Fig. 7.9a.

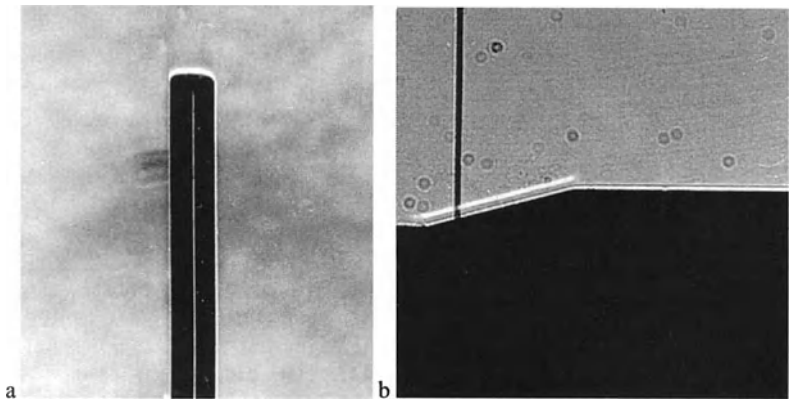

Fig. 7.9. **a** sharply-focused schlieren image of a glass stirring rod, showing the characteristic central hairline (photo by Rossana Quiñones). **b** shadowgram of a wind-tunnel model with no airflow, showing the offset bright band from a ramp that indicates horizontal misalignment of the light beam with respect to the planar model surface.

A similar bright band also appears near reflecting planar surfaces that are misaligned with the parallel schlieren beam [98]. Unlike the usual diffraction fringing, this band stands away from the surface and marks rays that have reflected from it. In Fig. 7.9b a test model is aligned with the beam vertically but mis-

aligned in the horizontal plane, thus the telltale band is obvious only next to an inclined surface. Rotating the beam into proper alignment in the horizontal plane merges the bright band with the edge of the model silhouette, and the band disappears. Vasiliev [102] suggests placing a prism on the surface to gauge such misalignment, but this is only necessary if the surface is non-reflecting.

The Alignment of a Z-Type Schlieren System. Vasiliev [102] has 10 worthwhile pages of discussion and recommendations on the alignment of a commercial z-type schlieren system. From that source and the author's experience, the following brief procedure is given.

One begins by presetting all optical elements to a common centerline elevation, e.g. above the plane of an optical table or bench. Armed with a white card or sheet of white paper, now dim the room lights and proceed to set up the light source, condenser, and source slit according to Sect. 7.1.4. This task is accomplished when the source image is focused upon the slit and cropped to a sharp rectangle, Fig. 7.5a, and the emerging beam observed on the sheet of paper is uniform without the anomalies shown in Fig. 7.5b.

Next aim the light beam emerging from the source slit at the first parabolic field mirror and position the slit at its focus to produce a collimated beam. An incorrect focal length leads to a non-parallel beam reflected from the mirror. Here it often helps to stop down the source slit temporarily to perhaps 0.5 x 0.5 mm in order to better approximate a point, since a finite source slit causes some beam spreading even when placed at the proper mirror focus. Check the beam diameter at various distances using the sheet of white paper and a ruler: the diameter should be constant and equal to that of the first mirror, and it should just fill second mirror. Vasiliev says $\pm$ 3 mm is an acceptable tolerance on the first focal length setting.

According to Sect. 3.1.2 and Fig. 3.6, now minimize the offset angle 2θ between the centerline of the source-condenser-slit illuminator and the centerline between the field mirrors. This minimizes astigmatism and coma when done in concert with an equal offset angle on the other side of the system. In practice, the light source never can be located right at the edge of the parallel beam due to the size of the slit and condenser mounts. Common practice, though, allows no significant clearance between those mounts and the edge of the beam.

Next insure that the second parabolic field mirror lies on a common centerline with the first, so that the parallel beam just fills the second mirror. Any mismatch here crops the field-of-view into an oval. The distance between field mirrors is immaterial in principle, but should be long enough that the test area in the middle remains free from interference with the illuminating and analyzing beams. When that much space is not available, plane beam-folding mirrors are called for.

Now aim the second field mirror to focus on the opposite side of the parallel beam from the illuminator, but with the same (minimum) angle 2θ between centerlines. Position the knife-edge near the focus of the second mirror and visually examine the source image projected upon the knife-edge. Set the knife-edge parallel to the long edge of source image, usually either vertical or horizontal, depending on the phenomenon one wishes to observe.

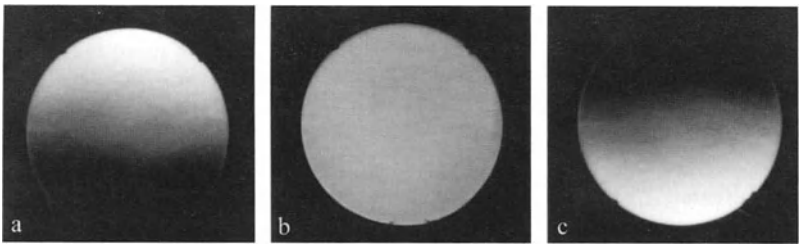

Fig. 7.10. Effect on the schlieren image of knife-edge displacement along the optical axis for a horizontal knife-edge entering the beam from below. **a** knife-edge too close to mirror, **b** correct adjustment, **c** knife-edge too far from mirror. Photos by Rossana Quiñones.

Placing your white-paper screen beyond the knife-edge, run the knife-edge in to cut off part of the source image. If the screen spot darkens non-uniformly from one side, note the side. If it is the same side as knife-edge, increase the axial distance of the knife-edge from the second mirror and try again. If it is opposite the knife-edge, decrease the axial distance. The knife-edge position is correct when the screen darkens uniformly, as shown in Fig. 7.10b.

Focus the viewing-screen schlieren image sharply upon the test area by adjusting the focusing lens, located immediately after the after the knife-edge (see Sect. 3.7.1). One of the props mentioned earlier (stirring rod, candle flame, etc.) marks the center of the test area for this purpose. If no sharp focus is possible, the screen may be too close or too far away from the focusing lens along the optical axis. Choose a different screen position or different focusing lens and try again until a sharply-focused image is obtained. The focus can be checked further, if necessary, by the disappearance of the shadowgraph effect when observing the thermal plume from a candle with no knife-edge.

The final step in the schlieren system setup is adjusting the percent of knife-edge cutoff in order to obtain the desired sensitivity. Schardin [2] suggests using several standard thermal test objects to gauge the schlieren sensitivity after alignment: a match or lighter, a candle, a light bulb, and one's hand. The latter two are shown in Figs. 3.12 and 3.13 for several knife-edge settings, with sensitivity levels indicated. Rhodes et al. [596] placed a light meter in an unused corner of their schlieren image, yielding a real-time monitor of cutoff and system alignment.

Further comments on setup and alignment are given in Chap. 8 as part of the description of a small do-it-yourself z-type schlieren system.

7.2.4 Vibration and Mechanical Stability

Toepler [37] recognized at the outset the importance of a vibration-free lab for schlieren imaging. Ideally, one looks for a concrete floor above earth, not an upstairs lab with wooden floors. Stuck with the latter, Reichenbach [597] said: "Once the schlieren knife had been adjusted with great difficulty, nobody was allowed to move until the picture was taken."

Next one wants sturdy, massive, vibration-free optical mounts [65,104,138]. Two such approaches for large z-type schlieren systems are shown in Figs. 1.19 and 3.5a, namely either a self-contained framework linking all components rigidly, or else heavy pedestal mounts on casters with tripod screws to lift the casters off the floor. Earlier granite-slab optical tables and sandboxes have been replaced by modern honeycomb optical tables supported by regulated pneumatic isolators [598], much to the chagrin of the lab cat.

Commercial schlieren instruments from the former Soviet Union, discussed later in this Chapter, embody similar design principles for rigidity. Vasiliev [102] describes rubber straps used to hold down the illuminator and analyzer tubes of the IAB-451 mount, as well as fixing both illuminating and analyzing optics to the same rigid beam to prevent independent motion. He further notes the related problem of thermal deformation misalignment in parts of the instrument.

Vasiliev [102] also pointed out the chief reason for schlieren vibration problems: the unwanted motion of the source slit image with respect to the cutoff. Regular vibration from adjacent heavy machinery, for example, tends to cause "coning" of the light beam leaving the second mirror, wherein the source image describes a circular motion in the x,y cutoff plane. At two points during each cycle the degree of cutoff will be instantaneously correct, but it is maddening to use such an instrument. In one case where coning was unavoidable [599], a light meter and a knife-edge servo controller were installed in order to maintain a constant schlieren cutoff. A much-cruder approach is to videotape the schlieren image, then save only those frames in which the correct cutoff occurs.

In any case note that schlieren vibration problems directly affect the desired level of sensitivity [102,600]. For a typical instrument with $f_2 = 1$ m, in order to register a schlieren refraction of 1 arcsecond the source image must not move more than 1 μm during the exposure. If the sensitivity can be deliberately reduced, either by less cutoff or by replacing the knife-edge with a graded filter, vibration errors are ameliorated. In some shaky wind tunnel labs, then, graded filters are used for reasons having little to do with extending the schlieren measuring range.

But even at worst, the schlieren technique is not nearly so vibration-sensitive as interferometry, where motion of a fraction of one λ can be devastating [600,601]. Modern common-path interferometers are less sensitive to this than the early Mach-Zehnder instrument, since both beams now move in tandem, but vibration is still a serious issue. Schlieren, on the other hand, depends primarily on geometric- rather than wave-optics, making it superior to any form of interferometry in its resistance to shock and vibration. Shadowgraphy, lacking the cutoff problem mentioned above, is far less vibration-sensitive even than schlieren.

Finally, there is the issue of portable instruments required to function in hostile environments. Horst Herbrich is the modern expert on this topic, having done many on-site industrial jobs [602]. Not even a "solid" concrete floor avoids these problems in a printing plant, for example, with massive machines generating low-frequency vibrations. Thus portable instruments must draw from all of the isolation schemes already mentioned, plus inner-tube dampers, counterweights, and the use of alternating-layered soft-foam and hard plates underneath the optical ele-

ments to damp vibrations. Linking the illuminating and analyzing optics to a rigid frame is especially important. According to Herbrich [602], "80% of portable schlieren applications involve a struggle against all manner of vibrations."

7.2.5 Stray Light, Self-Luminous Events, and Secondary Images

Toepler [40] anticipated many of the practical issues covered in this Chapter, including the need to block stray light from encroaching upon the optical path. According to Kean [146], the schlieren image illuminance should be written $E + E^*$, where E^* is the component not due to geometric ray deflection by a schlieren object. E^* is composed of flare, scattering, other stray light, and the diffracted light that was discussed in Sect. 3.6. Not much can be done about the latter, but stray light can certainly be minimized in order to make the actual image illuminance agree better with the sensitivity theory of Chap. 3.

Stray light problems can arise, for example, when ambient room light strikes the schlieren image or shadowgram. Another mode arises from stray illumination from the light-source itself, that has followed some path other than the intended one. Weak secondary images usually result from reflections from transmissive glass surfaces along the optical train. Self-luminous events generate their own light: more diffuse than the schlieren or shadowgraph beam, but nonetheless competing with it in the image.

Examples of self-luminous events include flames, visible radiation following strong shock waves, and luminosity from heated solid objects in the field-of-view [535,603-606]. An example of shadowgram fogging due to a glowing ballistic projectile was shown earlier in Fig. 6.13a. Vasiliev [102] makes a strong distinction between short-duration spark- or flash-illumination and the much-longer time period over which a self-luminous event can affect the image. Increasing the distance from the self-luminous event to the second schlieren mirror reduces the aperture angle of extraneous light captured by the optical system [98]. Capping shutters are also sometimes used to reduce such extraneous exposures. Another strategy involves using a laser light-source and a narrow "notch" filter at the laser frequency. The filter admits the direct laser light but excludes most of the broad-frequency self-luminosity from the image.

General strategies for reducing stray light depend on high collimation of the schlieren or "focused"-shadowgraph beam. Masking is used to block stray rays oblique to this collimation. A stray-light mask or stop is most effective at a beam waist [133], namely at the source slit and especially in the cutoff plane. Beware, though, not to stop down the beam so severely as to block refracted rays or even the schlieren illumination itself, or to degrade the image resolution by slit-diffraction effects. Front-lighting, discussed later in Sect. 7.3.4, is deliberate stray light that is incompatible with such a narrow cutoff-plane mask.

Finally, the experience of lens designers [167] can be bro ught to bear in stubborn cases, such as schlieren systems that must function in areas of high ambient illumination. Systems of glare stops and baffles are used in camera lenses, binoculars, and some telescopes. Auxiliary stops are located at images of the primary stops to cut stray light, and the optical path is enclosed in a tube with

stops to cut stray light, and the optical path is enclosed in a tube with internal surfaces scored or threaded and painted flat black.

7.2.6 Interference from Ambient Airflows

Astronomers have grappled with the ambient-airflow issue for centuries (see Fig. 1.6): not just with upper-level meteorology, but also with local thermals due to temperature differences between their instruments, the environment, and themselves. For sensitive schlieren and shadowgraph systems the situation is better, since these are usually housed indoors and some control over ambient airflows is assumed.

The first line of defense is to turn off the room ventilation. Next, look for and eliminate drafts and warm-air sources beneath the optical beam or cold air above it. Human motion stirs up the ambient air causing currents, so everyone present needs to find a spot and sit or stand still during sensitive schlieren work.

Next comes shielding from air currents in the form of tubes or hanging draperies. This is an extreme measure that should not usually be necessary in a dedicated lab if the previous suggestions work. On the other hand, tube-enclosed schlieren beams are common in wind-tunnel labs, for instance, where many other activities generate air currents and not all of them can be controlled. As an example, the Penn State 1-m coincident schlieren system (Sect. 4.1.3), with very high sensitivity and an open optical path length of 10 m, has seldom required shielding when ventilation and people-motion constraints were enforced. The exceptions include experiments [191] that showed extraordinary sensitivity to air currents, where cloth draperies around the test area with an opening for the light beam proved effective.

Sometimes, despite all measures, it becomes necessary to have a witch-hunt for an elusive source of troublesome hot or cold air. If the schlieren light source is small, a convection current along the parallel beam cannot be localized optically. Enlarging the source sometimes allows enough focusing to localize the culprit. Disturbances near the light-source or cutoff, on the other hand, betray their locations by appearing large and out-of-focus in the schlieren image. A candle flame (by now an old friend; buy them by the case) is sensitive to drafts and can be moved along the optical path to locate them.

7.3 Capturing Schlieren Images and Shadowgrams

With so much information available on photography, cinematography, digital imaging, and videography, this Section could easily get out of hand. Instead, only the aspects of these topics unique to schlieren and shadowgraphy are covered.

7.3.1 Photography and Cinematography

The issue of image capture is changing rapidly in the digital age, but the resolution afforded by photographic emulsions has yet to yield to any digital process. Thus we still consider schlieren *photography* to be important and relevant. Basic references include Hyzer [168] and Strong [301], among many others that treat scientific photography.

Background. By way of brief review, note once again that the Weber-Fechner curve for the human eye and the Hurter-Driffield curve for photographic film both show a logarithmic sensitivity to a light stimulus. This is why photographs of familiar objects look natural to us [301]. Similarly schlieren and shadowgram photos resemble their respective images observed directly by eye, but there is no natural standard against which to judge them [98]. This holds for color schlieren as well, where true color rendition is not nearly so crucial as in, say, wedding photography. Within broad limits, then, schlieren and shadow photos are what they depict, and only experience with the equipment and phenomena can distinguish the "good" ones from the "bad."

Holder and North [98] wrote an extensive section on photographing the schlieren image. Having surveyed many typical schlieren images, they find that the ratio of maximum to minimum illuminance seldom exceeds 10. Ordinary portrait or landscape photography often reaches higher illuminance ratios than this. Thus Holder and North conclude that schlieren is distinguished from ordinary photography by its relatively-low contrast. Nonetheless, by choosing appropriate films, exposing for an optical density of at least 0.25 (preferably 0.5) in the negative, and printing when necessary with a γ greater than one, results with good contrast can still be obtained.

Of course, Holder and North did not have current digital image processing technology at their disposal. Even with this, though, one still wants to capture the best-possible original schlieren and shadow photographs. Afterwards, of course, the range of possibilities to enhance the result is much broader now than it was in 1963, as discussed earlier in Sect. 3.2.4.

Holder and North [98] also found schlieren photography to be further set apart from ordinary photography by its frequent need for short exposure times: not just the millisecond exposures of camera and studio flash units, but often microsecond exposures or even, in some cases, nanoseconds. This adds a low-light-level problem to the low-contrast problem just discussed. Fortunately, since the 1960's some new, fast, high-power light sources have become available, especially xenon flashtubes and pulsed lasers.

Metering and Exposure. Expressions for the background illuminance of a schlieren image were developed in Chap. 3, e.g.,

$$E = \frac{\beta \cdot B \cdot b \cdot a}{m^2 f_1 f_2} \tag{7.1}$$

which can be used to find the image illuminance in lux as a function of system constants and the unobstructed source-image height *a*. The same holds for "focused" shadowgraphy if *a* is replaced by the full source-image height h. The factor β is included in Eqn. 7.1 to account for reflection and transmission losses at glass surfaces in the optical path; β obviously varies with each optical setup.

In reality, though, one seldom works from the lamp luminance and system constants to figure a photographic exposure. Instead, a light meter simply reads the schlieren image illuminance E directly, and the exposure of photographic film in lux-seconds (lumen-sec/m^2) is found simply from E·t, where t is the exposure time.

Some practical details of this procedure bear elaboration, though. If the sensor of a lux-meter is held in the plane of the image, then E is read directly within the accuracy of the meter. Unfortunately most photographic light meters do not read out in lux, but rather in EV (exposure value), for which the conversion is:

$$\text{lux} = 2.5 \cdot 2^{EV} \tag{7.2}$$

Further, it is sometimes not possible to meter incident illuminance directly in the schlieren image plane, either due to lack of access if a camera is mounted there, or due to the characteristics of the meter itself. In that case one can handily meter the light transmitted by the ground-glass viewing screen upon which the image is cast, invoking another loss factor that is usually taken to be about 50% or one f/stop.

In fact, most single-lens-reflex cameras in 35mm and medium formats have electronic through-the-lens meters to handle this chore automatically. These usually succeed for ordinary photography, but the schlieren image can deceive them because it differs from the usual case for which they are calibrated. Schlieren and shadowgram backgrounds lie within a definite grayscale range: A survey of many examples reproduced in this book (including the classic photos by Schardin) shows almost no backgrounds lighter than 20% or darker than 50% gray, with the majority falling between 30% and 40%. Since camera light meters assume the image features average to 18% gray, their readings often lead to overexposed schlieren images and shadowgrams. Experience thus shows that through-the-lens meter readings are not to be trusted outright for schlieren and shadow photography, and should be bracketed at least by exposures of +1 and -2 f/stops from the metered indication.

Alternatively, one can use a spot-meter to read schlieren image illuminance directly from the ground-glass as described above. By metering both the schlieren background and the highlights, one gains a better impression of the illuminance range that the film exposure must accommodate. This range is broadest when a wide light-source image is mostly cut off by the knife-edge for high sensitivity, but strong refractions nonetheless occur in the schlieren object. In that case the challenge is to accommodate both the schlieren background and highlights within the latitude of the photographic film. Once again, exposure bracketing is needed.

A further difficulty arises regarding what f/number to use for schlieren photography. Light meters and camera computers allow the interplay of four parameters in establishing an exposure: light-meter reading (EV), shutter speed, film speed,

and lens aperture f/number. The schlieren image, however, is projected onto the film plane by an external optical system. One can stop down the focusing-lens aperture, but this does not change the effective f/number of the exposure. (It merely vignettes the beam, which is no help at all.) One workable solution to this problem is to ignore the standard exposure calculation altogether, and work only with the metered light level, film speed and shutter speed. Test images, often on Polaroid film, will indicate a combination of these parameters that yields a good exposure. Then, except for extremes in exposure time, the reciprocity law can be used freely to choose different combinations of film speed and exposure time, or to adjust these parameters to changes in metered light level.

Of course, for microsecond- or nanosecond-range exposures, even less information is at hand. Commercial flash meters exist, but do not respond usefully in the microsecond range or below. On this account, high-speed-flash schlieren and shadowgraph photography is done almost entirely by trial-and-error, using Polaroid film to get quick results. Once achieved, a good Polaroid photo is an approximate guide to the proper exposure of other film materials such as negative film or transparencies.

High-speed schlieren and shadowgraph photography [98] is further plagued by low light levels. Choosing a light source of greater luminous exitance is not usually an option, and simply opening the focusing-lens aperture is again no help for reasons just described. One can use a shorter focusing lens for a smaller image size, or improve the light-collection efficiency of the schlieren illuminator (Sect. 7.1.4). Fast photographic films (up to ISO 3000 at this writing) are readily available, and even these can be push-processed by two stops without significant loss of quality. Finally, reciprocity-law failure can occur at pulsed-laser exposure times, adding some additional frustration. All this makes high-speed schlieren and shadowgraph photography a matter of experience and patience.

Camera and Lens. Schlieren focusing-lens issues were discussed earlier in Sect. 3.7.1. A separate focusing lens and film back can be used, effectively constituting a camera if connected by a bellows or used separately in the dark. Likewise commercial cameras, ranging from 35 mm reflex to large-format view cameras, are routinely applied to schlieren and shadowgraphy. The special requirements of accepting a projected image dictate the aperture and focal length of the lens, as already discussed. Lens-extender rings or a bellows attachment are sometimes required to bring a schlieren image of appropriate size to focus on the film plane. Lens-mounted shutters tend to vignette the schlieren beam, whereas a focal-plane shutter is very useful to isolate the film during setup. It may not be fast enough to regulate the exposure, but it can be used in "bulb" or "time" mode with a cable release and a flash light-source. Mechanical shutters are slower than 1 ms speed, but opto-electronic shutters like the Kerr cell can be much faster [168,563,607].

One should resist the temptation to take a schlieren photo or shadowgram by aiming a camera at a ground-glass viewing screen. The light intensity, image contrast, and resolution all suffer when this is done. Instead, remove the screen and focus the image directly upon the photosensitive material for superior results.

Cinematography. Schlieren cinematography was pioneered by Schrott [608] and Schardin [1]. North, Cash, and Holder [98,125] established color-schlieren cinematography with the excellent 1956 Shell Film "Schlieren" [95], still well worth seeing[1]. North and Cash [125] also describe the details of wind-tunnel schlieren cinematography, including 16mm focusing and mounting the movie camera on an optical bench.

Otherwise, cinematography gets short shrift. Except for large-format feature films (e.g. Sect. 5.3 and Ref. [425]), it is all but replaced by videography, covered next. The Penn State Gas Dynamics Lab gets several requests yearly to shoot television, documentary, and advertising schlieren footage, but the last one shot on film was in 1979 [609]. Cinematography is still important, though, for high-speed imaging above 1000 frames/sec, as discussed in [168] and [610].

7.3.2 Videography

Since about 1980, simple, cheap color video equipment designed for the home-entertainment market has become available to scientific imaging worldwide. This equipment is easily adaptable to schlieren imaging in most cases, and the videotape is so low-cost that large archives of video footage have been built up. The chief drawback, of course, is poor image resolution: only about 525 x 384 pixels for the RS-170/NTSC standard (see Sect. 3.5). But this is adequate for many purposes, and individual frames can even be digitized and processed to yield reasonable medium-resolution schlieren images (e.g. Fig. 4.1b). Of course the chief advantage of videography, compared to cinematography, is real-time imaging.

Inoué and Spring [170] provide an excellent primer for anyone interested in scientific videography: fundamentals, standards, resolution, fields, frames, and synchronization are all covered.

Modern video imaging arrays are more sensitive than photographic film, but may have less dynamic range [159]. Nevertheless the 8-bit video grayscale yields 256 shades of gray (plus chroma); more than enough if fully utilized. As in the still-image case discussed in Sect. 3.2.4, contrast stretching, histogram equalization, and unsharp masking can all be used to improve the contrast sensitivity of schlieren video and also to adjust its brightness. In-line electronic processors are also available to accomplish this processing in real time.

As in photographic cameras, the chief roadblock in adapting a videocamera to a schlieren system is the lens. Video lenses are designed to focus a scene onto an imaging array, not to accept a projected beam from an external optical system. Consequently the usual video lens, with a small internal aperture that vignettes the beam, is inappropriate for schlieren and "focused" shadowgraphy. The free aperture of a schlieren focusing lens must always admit the entire beam, especially those rays undergoing large deflections.

[1] Contact Jane Poynor, Exhibitions and Video Producer, Shell Film and Video Unit, Visual Media Services, Shell International Ltd., Shell Centre, London SE1 7NA, phone +44 (0)20 7934 3318, fax +44 (0)20 7934 4095, email Jane.J.Poynor@SI.Shell.com.

The solution is to replace the standard video lens with an outboard lens of appropriate aperture and focal length. (As before, the focusing-lens iris is not usable and should be set wide-open.) As a result of this, none of the videocameras with integral, non-removable lenses are suitable for present purposes. Only on rare occasions these have been forced to cooperate successfully with schlieren imaging.

In routine schlieren videography the focusing lens is either mounted separately on the optical bench, or else a C-mount adapter is used to mount a wider-aperture 35 mm fixed-focus camera lens or zoom lens to the videocamera body. The average camera-to-schlieren-object distance often demands a long-focal-length lens in order to size the image appropriately, thence 35-mm zoom lenses in the 50-300 mm focal-length range find frequent application.

Continuous illumination principles are the same for videography as for photography. Pulsed light, however, must synchronize with the 30 Hz (RS-170/NTSC) video frame rate. This was once a problem, causing annoying scan-line anomalies to float across the screen. Now, however, strobe lamps such as the 1431AB Strobotac (Sect. 7.1.1 and App. D) are automatically synchronized with videocameras via the power-line frequency. In some stubborn cases a hard-wired synchronization through a video "sync stripper" may still be needed.

The recently-introduced digital video technology poses no additional problems for schlieren videography, and has important advantages of reproducibility and multimedia use, e.g. [611]. Progressive-scan videocameras should eliminate the interlaced-scan-line anomalies that sometimes plague schlieren videography of rapidly-changing subjects. Also on the horizon is High-Definition Television, which promises to bring photographic image resolution to videography.

7.3.3 High-Speed imaging

Edgerton says "High-speed photographic methods serve as extensions of our eyesight" [44]. So do schlieren and shadowgraphy. When combined, these methods further extend our eyesight to include invisible events that are also too fast to see. Beginning with Toepler and Mach, the strong historical flavor of high-speed imaging was already conveyed in Chap. 1. Several references give a broad overview of the topic [44,168,210,563,612,613].

High-Speed Single-Frame Imaging. Often a single image of sufficiently-short exposure time provides the necessary critical insight. Mach's famous bullet schlieren photo (Fig. 1.12) and the shadowgrams of Brown and Roshko (Fig. 1.23) are prime examples, but many more are also reproduced in this book.

Exposure time plays a central role in determining what is seen, whether it is desired to "freeze" all motion or to allow some intentional motion blur. High-speed aerodynamics offers a ready example of this [157,614], since long exposures average out turbulence and reveal weak stationary phenomena while short-enough exposures stop all motion, turbulence included (Fig 7.11). Thus the limit of schlieren sensitivity, discussed in Sect. 3.2.3, depends to some extent upon expo-

sure time as well as the other cited factors. Strobe-illuminated videography, mentioned in the previous section, offers a compromise in the form of an animated ensemble of instantaneous images: it can be examined piecemeal, or else played at various speeds in order to see the range of unsteady motion in the observed phenomenon.

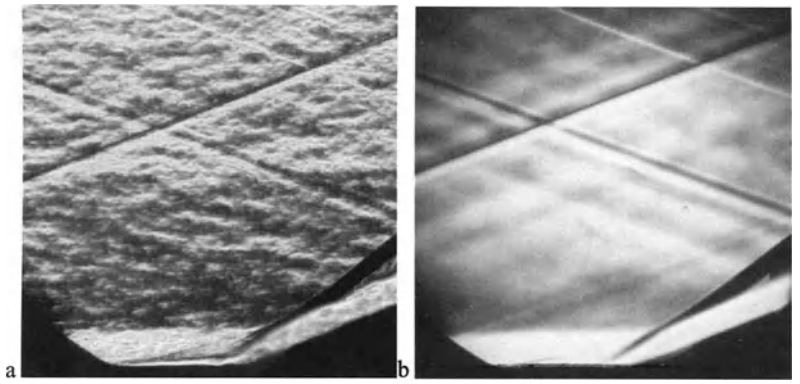

Fig. 7.11. **a** Microsecond-exposure spark-schlieren image of a shock wave/boundary-layer interaction at a 2-D compression corner at Mach 3. **b** the same flow exposed at about 0.01 second. The turbulence seen in frame a is mostly optical noise from wind-tunnel sidewall boundary layers, and is completely averaged out in frame b. Photos by the author [614].

Hyzer [168] discusses the calculation of exposure time Δt to minimize motion blur, concluding that

$$\Delta t = \frac{\ell_b}{mV\cos\theta} \tag{7.3}$$

where ℓ_b is the blur length, m is the image magnification, V is the speed of the phenomenon observed, and θ is the angle between the direction of motion and the image plane. For example in Fig. 7.11a, $\theta = 0$, m = 0.4 and V has a maximum value of 570 m/s. For $\Delta t = 1$ μs, ℓ_b is found to be about 0.2 mm, a negligible value compared to the 150 mm field-of-view shown. On the other hand, Fig. 7.11b has $\ell_b = 2$ m, so any flow features traveling at even a fraction of the freestream speed are hopelessly smeared. That degree of blur averages out all moving features, revealing the underlying schlieren image of the stationary-wave pattern.

The Cranz-Schardin Camera [6] was introduced in Chap. 1 as one of the key contributions to high-speed photography in the 20th Century. Shown schematically in Fig. 7.12, it uses multiple sparks to expose several shadowgraph or schlieren images on a single sheet of photographic film. The framing rate is controlled electronically, not by moving parts, and can thus be as much as 1 MHz or

more. This opened new vistas of high-speed physics [514,533,563,612,615], and is still an important instrument more than 70 years after its introduction.

The troublesome multiple-spark gaps of the original Cranz-Schardin camera are now often replaced by more-dependable LEDs [579-581] or laser diodes [616]. In one ultra-high-speed example [617], seven different flash times are obtained by optical delay lines from a single laser pulse.

Until recently, an 8-spark commercial version of the Cranz-Schardin camera, known as the "Chronolite 8" [618], was available from the company founded by F. Früngel (now High-Speed Photo Systeme, see App. D). While these can no longer be bought, it is still very realistic to build your own system, e.g. [580,619,620]. Helpful optical design principles are given in [581]. Eventually, the Cranz-Schardin camera may be replaced by advances in high-speed digital imaging [210,621], but the digital imaging still has a long way to go.

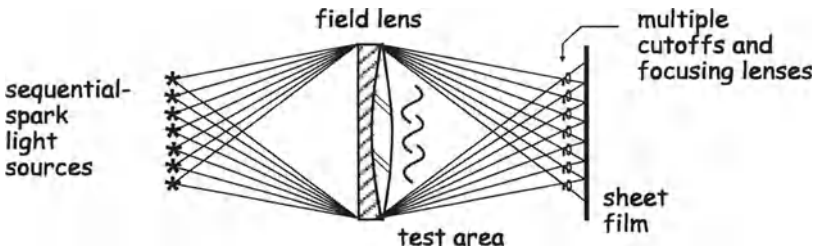

Fig. 7.12. Diagram of the Cranz-Schardin camera, actually a multiple-source schlieren system with sequentially-fired spark sources. Each image depicts the schlieren object from a slightly-different angle.

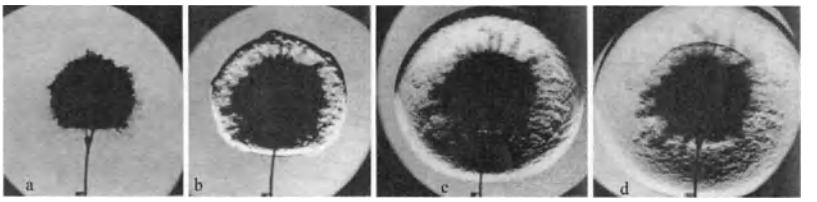

Fig. 7.13. Four frames from a Cranz-Schardin schlieren sequence of the explosion of 1 gram of lead azide. Schardin's photos [2] reproduced courtesy of Springer-Verlag.

Stroboscopy. Repetitive-flash light sources, like the Quadtech/Genrad Model 1531AB Strobotac mentioned earlier, can be used quite easily to observe periodic phenomena [44,568]. In such cases the motion is effectively "frozen" by the illumination and the result is observed by eye or by an ordinary camera. Toepler [37] and Wood [48,74,622] pioneered this by synchronizing their illuminating spark

with another spark that generated a "sound wave" (weak shock). Examples of stroboscopic schlieren studies of periodic flows, ultrasonics, and intense sound fields are found in [240,476,623-625].

Prism, Drum, Rotating-Mirror, And Streak Cameras are used to record high-speed schlieren images and shadowgrams, usually with continuous illumination. General references include [168,563,564,610,626,627]. High-speed rotating-prism cinema cameras like the Hycam II shoot 16 mm film up to about 11,000 frames/sec. Beyond that speed, cinematography in the usual sense is no longer possible. Neither the drum camera (up to about 200,000 frames/sec) nor the rotating-mirror camera (beyond 1 MHz) produces a projectable movie. The resulting series of still frames (typically several hundred) can be animated, however, to produce a movie or a videotape with a lot of effort.

Streak cameras [168,626] do not yield ordinary images of a schlieren object in x and y, but rather write records of motion in one space dimension vs. time. The film motion in a drum camera is set perpendicular to a narrow slit in the schlieren field-of-view, or else a modern electronic streak camera is used. Such records are very useful in ballistics [203,626] and wave motion studies [628-630], for example, and are analogs of the wave-diagrams or x-t-diagrams used to teach and analyze unsteady one-dimensional flows. Figs. 1.24b and 4.17 are, in principle, streak-schlieren photos depicting fast-moving objects.

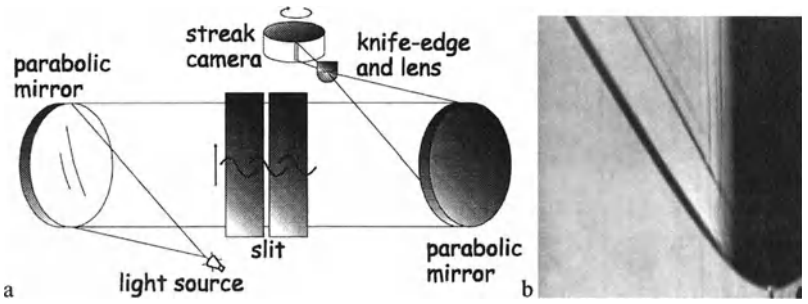

Fig. 7.14. **a** Z-type schlieren system with a slit in the test area, set up to record the position of moving test-area refractions vs. time in a streak-camera record, after Holder and North [98]. **b** Schardin's [2] streak schlieren record of a lead-azide pellet explosion, reproduced courtesy of Springer-Verlag (compare with still-frames of the same schlieren object in x and y in Fig. 7.13).

Lighting and Triggering High-Speed Images. Beyond what was said of pulsed and repetitive light sources earlier in this Chapter, see also [98,168] and especially [565] for more on high-speed-imaging light sources.

Triggering is a special concern for rapid events like explosions, where both the event and the schlieren/shadowgraph light source may need to be sequenced properly with microsecond accuracy. One of the simplest triggering schemes uses a microphone to pick up the shock wave from an explosion, gunshot, etc. The microphone signal initiates an immediate trigger of a fast light source to take a schlieren photo in a darkened lab, with the film shutter open and ready for exposure. The distance of the microphone from the event then determines the trigger timing. Color Plates 5, 23-26, 28 and 29, depicting such rapid events, were taken this way with a Quadtech/Genrad Model 1431AB Strobotac as a light source. Holder and North [98] and Hyzer [168] discuss triggering further, and a thoro ugh modern review of the topic is given by Fuller [631].

High-Speed Videography [632] was originally done by speeding up analog video equipment, and was not very satisfactory. Recent digital systems, such as the Kodak Ektapro 1000 HRC, produce cleaner results and are much more user-friendly, though very expensive. Frame rates, however, do not currently exceed a few thousand frames/s. Faster rates with a correspondingly-limited number of frames can be had from CCD cameras that write several frames to one large focal mosaic [210,633,634]. As with standard video, no particular difficulty is had adapting such systems to schlieren or shadowgraphy, except that outboard or c-mount lenses are usually required.

7.3.4 Front-Lighting

Schardin [1,2] first pointed out that front-lighting solid objects in the schlieren test area can be useful, and is independent of the primary schlieren illumination. It makes the schlieren image more comprehensible and clearer, especially for complicated objects. Stolzenburg [371] applied this to wind-tunnel models that are often confusing when appearing only in silhouette (e. g. Fig. 7.15).

Front-lighting is secondary illumination, a deliberate form of stray light. It's luminance, color temperature, distance from the test area, duration, and timing can all be chosen at will. The efficiency of reflection from opaque objects in the test area must always be considered, however.

Often strong front-lighting by floodlamps or flashlamps is needed to register the reflected features of test models, people, etc. in the schlieren image. Front-lighting must come from the direction of the schlieren analyzer, not the illuminator, and it should be as nearly axial as possible: large angles of incidence cause most of the reflected light to leave the optical path. Of course, floodlamps for front-lighting should never be allowed to block the schlieren beam or to interfere with it by way of their thermal plumes.

The reflected secondary front-illumination that gets as far as the knife-edge plane appears in a diffuse halo around the schlieren source image. The knife-edge inevitably blocks some of it, but most of the focusing-lens aperture can be shifted to the free side of the knife-edge in order to accept this diffuse halo. On the other hand, a narrow slit aperture in the cutoff plane will frustrate even the strongest

front-lighting, according to the stray-light-reduction principles discussed earlier. The f/no. of the focusing lens also affects the front-light but not the direct schlieren beam: stopping-down thus shifts the illumination balance in favor of the latter.

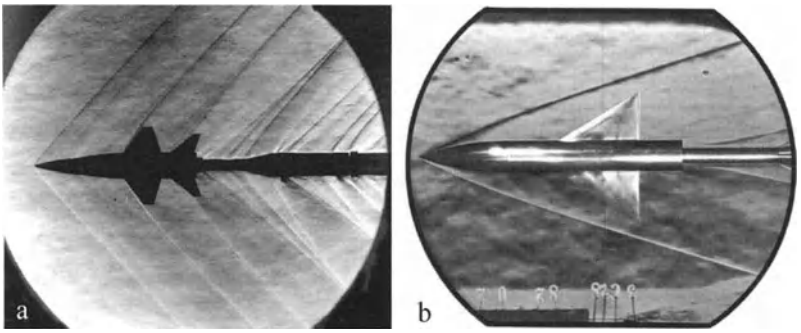

Fig. 7.15. **a** Schlieren image of X-15 wind tunnel model undergoing test without front-lighting. **b** Front-lighting applied to a missile model at Mach 4. NASA photos from Langley Research Center and the Jet Propulsion Laboratory.

How should these two illumination sources be properly balanced in the final image? Experience shows that too much front-light overpowers a schlieren image, calling attention to opaque-object features and detracting from the visualization. Muted front-lighting, however, emphasizes the visualization though still revealing the important features of opaque objects. The routine underexposure of front-lit objects by ½ to 1 stop is therefore recommended.

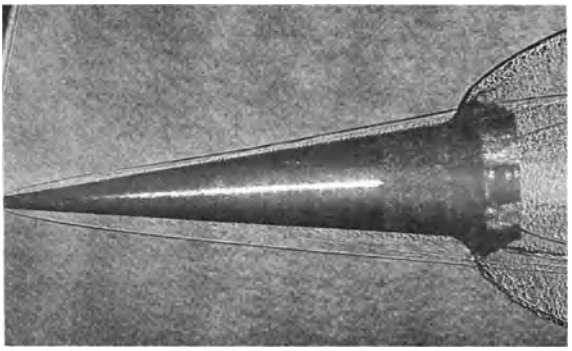

Fig. 7.16. Pulsed-ruby-laser front-lit "focused" shadowgram of a hypersonic ballistic projectile in the AEDC ballistic range G (US Government photo from [538]).

Usually the front-lighting and the schlieren beam expose the image simultaneously. This is required in cinema and videography, since the exposure times are the same for both light sources [98]. But in still photography of stationary objects one may expose sequentially, with a longer front-light exposure if need be.

Special schlieren methods sometimes cause special front-lighting problems. A color cutoff filter, for example, changes the color balance of the front-light as well as that of the schlieren beam [635]. This plays havoc with skin tones if there are front-lit people in the field of view. Multiple-source schlieren systems, on the other hand, typically have large effective camera apertures that admit considerable stray light, including front-light. Even ordinary room lights may then be enough to give a front-lit schlieren image.

Many front-lit schlieren examples are shown in this book. See especially Schardin's images in Figs. 3.12-3.14 and the full-scale schlieren images in Fig. 4.15. "Focused" shadowgrams can be front-lit too, as illustrated by Fig. 7.16.

7.4 Commercial and Portable Schlieren Instruments

> We do not invent, we take ready-made from capitalism.
>
> *V.I. Lenin*

There are few schlieren instruments commercially-available in the world today, so this Section is appropriately short. There were once more, though, and those bygone instruments are still interesting to discuss. Why there are fewer now, since scientific instruments of all sorts are very big business, is a difficult question.

Actually there never were many commercial schlieren instruments in the West; it has always been a build-it-yourself proposition. Some grand old workhorse instruments were once mass-produced in the East, but the rise of laser interferometry, the end of the Cold War, and unknown factors brought them down. It may be that there was simply never enough demand for commercial schlieren instruments to succeed under capitalism. On the other hand, untold thousands of expensive microscopes and telescopes are sold each year, and interferometers are currently offered from stock by dozens of corporations worldwide. I cannot explain all this, but it has certainly influenced the nature of this book.

7.4.1 Soviet Instruments

Lenin's ill-considered boast, quoted above, does not apply at all to schlieren instruments, for none of consequence have ever been produced commercially by capitalism. But at least one Soviet-made instrument has become ubiquitous and famous in the East: the venerable IAB-451 can be found in research labs all over the former Soviet Union and the People's Republic of China.

The IAB-451 is a massive, self-contained z-type schlieren instrument of 230 mm aperture, thoroughly discussed by Vasiliev [102]. Its twin field mirrors are spherical, and are ground off-axis to avoid astigmatism. Spherical aberration is corrected by a meniscus plate after Russian telescope pioneer D. D. Maksutov [101,636]. While no western schlieren instrument was ever made this way, the IAB-451 is nonetheless evidently a fine optical system that can sense refractions of 2 arcseconds and resolve 4-10 lines/mm in its test area [169]. Its vibration- and draft-conscious designer enclosed it in twin tubes (illuminator and analyzer) with a total weight of 150 kg.

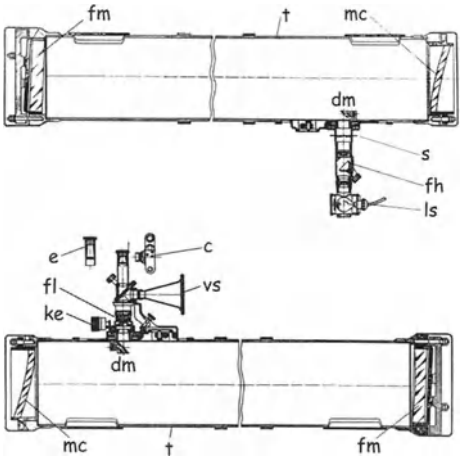

Fig. 7.17. Drawings of the IAB-451 illuminator unit (top) and analyzer unit (bottom), courtesy of I. V. Ershov. c: camera, dm: diagonal mirror, e: eyepiece, fh: filter holder, fl: focusing lens, fm: field mirror, ke: knife-edge vernier knob, ls: light-source, mc: meniscus corrector, s: source slit, t: tube, vs: viewing screen.

Vasiliev [102] gives a very detailed and involved alignment procedure, and claims "The original IAB-451 is a limited-purpose instrument and is unsuitable for applications with many of the methods." This is due to the encapsulated nature of its components, inviting no modifications. Yet modifications were made, including a color schlieren attachment with a source prism and cutoff slit to replace the original detachable source and imaging units.

The former Soviet literature is full of schlieren examples using the IAB-451 [102,169,354,488,637-641]. A color schlieren IAB-451 photo is reproduced here in Color Plate 15 as an example.

Notwithstanding such broad use, the IAB-451 and its cousins were criticized by Legu et al. [590], who claim that it is "expensive and cumbersome" compared to

what is done "abroad." At this writing the Russian manufacturer of the IAB-451 lists it as "temporarily out of production" [642] (see App. D).

Other Soviet Instruments include the IAB-453 and the 150-mm aperture TE-19. Both are reviewed by Vasiliev [102], but neither is still manufactured. The defunct TE-19 was apparently dreadful enough to earn Vasiliev's stinging criticism: "Due to the complexity of the instrument and the large number of optical components, it is beyond the user's power to align the instrument, as he was able to do with the IAB-451. Furthermore the instrument goes frequently out of alignment and needs servicing by authorized technicians."

Evidently, however, a range of IAB-designated schlieren instruments is still produced at the Kazan State Technical University TechnoPark [642], or was produced until recently. These range from the IAB-471, a 70 mm-aperture lens-type system, to the 800-mm-aperture IAB-467 (see App. D).

Additional modern Russian schlieren instruments for wind-tunnel use, with apertures up to 500 mm in portable equipment and up to 1 m in stationary installations, are described in [643]. These are designated as the IT-144 and IT-228 instruments, but nothing is known of their current availability.

Carl Zeiss Jena, the world-famous optical fabricator, produced schlieren systems in the mid-20th Century as described by Thiele [644] and Nebe [645], and in Zeiss-Jena brochures [646,647]. Their 1954 80-mm "Schlieren Camera 80" was a small commercial system that found considerable use [352,648].

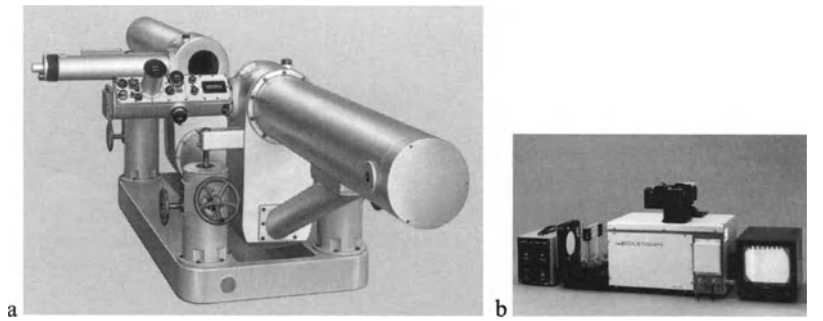

Fig. 7.18. **a** The 1948 Zeiss "Schlierengerät 300" instrument (photo by courtesy of W. Wimmer, Carl Zeiss Jena GmbH). **b** Schlierograph EDS-100 (photo by courtesy of H. Kubota and K. Arita, ATTO Corp., Tokyo).

In 1948 Carl Zeiss Jena marketed an impressive 300-mm-aperture z-type schlieren system that was built like the very proverbial brick outhouse (Fig. 7.18a). Completely enclosed above a massive floorplate, with its own control panel, it seems only to lack a plush seat for the operator. This was certainly the

high-water mark of commercial schlieren instruments. Regrettably, Carl Zeiss Jena ceased all production of schlieren equipment some years ago.

7.4.2 Western Instruments

What the West offers is paltry by comparison. Rudimentary 108 and 152-mm-aperture z-type schlieren systems, comprised of a lamp, twin parabolic mirrors and a knife-edge, have been available in the US from Edmund Industrial Optics for years. The US Companies Aerolab and NK Biotechnical and British TecQuipment Ltd. supply schlieren systems as part of larger wind-tunnel apparatus for educational use. The Optison Schlieren System, made by Intec Research, is a 50-120-mm-aperture specialty instrument for ultrasonic diagnostics [649].

In Japan, the ATTO Schlierograph EDS-100 (Fig. 7.18b) is a folded, compact double-pass coincident color schlieren system designed specifically for gel electrophoresis (Sect. 9.4.2). It is not available for export. Mizojiri Optical Ltd. in Tokyo makes schlieren systems up to 1 m aperture, but these instruments likewise do not appear to be available outside Japan. The Elmex Ltd. SSC-610 infrared schlieren system, described in Sect. 5.8.6, is no longer being produced.

Contact information for these companies is provided in App. D. Several optical houses in the US and abroad also list schlieren optics as a capability, but do not offer any stock instruments for sale.

7.4.3 Portable Schlieren Apparatus

Sometimes newcomers to this field expect a sort of camera that one can take outdoors to photograph heat rising from buildings. In fact, schlieren systems are not generally portable, owing to their delicate adjustments and their vibration sensitivity. Reasons to try to make them portable include live demonstrations (e.g. in the classroom or TV studio), on-site industrial uses, and the rare application that actually does demand going outdoors.

Early schlieren demonstrations used direct projection of the image onto a screen [133,192]. Technology has now overtaken this, and a videocamera at the image plane, plus a monitor or video projector, avoids the need for a large directly-projected schlieren image.

An early portable schlieren system at MIT [42] had a 125 mm aperture and a folded optical beam, and was arranged to roll around on casters in a single unit.

Horst and Liselotte Herbrich of Industriefilm in Germany have developed two portable schlieren systems for on-site industrial use [602,650]. The smaller of these is a folded parallel-beam lens-type system entirely enclosed in a box that one person can carry. The larger system is a single-mirror coincident setup based on a 300 mm f/10 spherical mirror. It fits in three ordinary suitcases and a camera bag, and travels widely by posing as normal luggage. Color Plate 38 was made with this system. A similar instrument is described in Ref. [651].

Viewstar Inc., Newport News, VA makes portable focusing schlieren systems following the lens-and-grid principle of Sect. 4.3.4. These offer fields-of-view on the order of 1 m without requiring large, expensive mirrors.

The concept of a portable scanning schlieren instrument, involving equipment that can be carried around in a few suitcase-sized containers, was described earlier in Sect. 4.4.2.

Finally, Fig. 7.19 shows a 320 mm-aperture f/6 z-type portable schlieren system built by the author for IBM in 1986. The beam-folded illuminator and analyzer sections were separately mounted on heavy-duty rolling pedestals. This system is interesting to compare with the definitely-not-portable Zeiss-Jena 300-mm-aperture system shown in Fig. 7.18a. The difference in design philosophy is stark, the former being open and lightly-built compared to the latter's massive rigidity. Surprisingly, though, the portable system suffered few vibration problems in on-site use in an IBM clean room, [483,652] and Fig. 7.19.

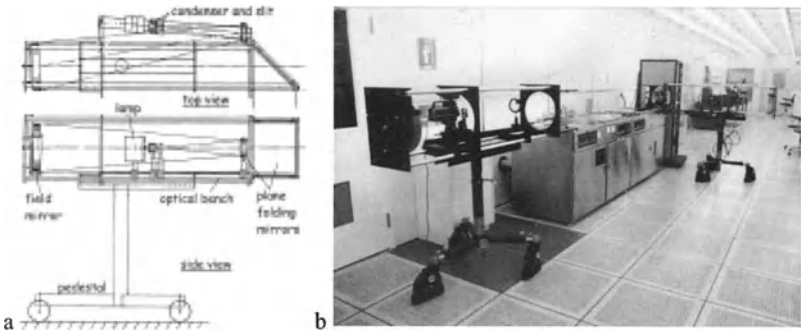

Fig. 7.19. 320 mm f/6 z-type portable schlieren system built for IBM. **a** drawing of illuminator unit. **b** system set up to study the airflow above a silicon-wafer-processing bench in a clean room [483], with analyzer unit shown in left foreground.

8 Setting Up Your Own Simple Schlieren and Shadowgraph System

> The operation of this instrument can at first glance seem inconvenient, but in practice it is very easy.
>
> *August Toepler* [37]

> I would ask those readers who have grown up...to remember that the lectures were meant for juveniles...
>
> *C.V. Boys* [653]

In some sense this is a stand-alone Chapter. It describes a modest schlieren system that should be within the financial and technical means of just about anyone who has read this far. Variations of this optical system were built as science-fair projects by several generations (see Stong [344,385,386,532]), and that is, in fact, how your author got his humble start in schlieren imaging at age 16 [385,532]. The optical setup suffices for both schlieren and shadowgraphy, the latter by either direct parallel-light or in the "focused" shadowgraph mode. It deliberately evokes *Scientific American* magazine's Amateur Scientist section in its heyday, when C. L. Stong's text and Roger Hayward's splendid artwork helped convince amateurs that it was both fascinating and fun to build the simple – and sometimes not-so-simple – apparatus described there. The same schlieren system is now used as a learning tool by students of the Penn State Gas Dynamics Laboratory. So, despite the science-fair flavor, professionals who are new to schlieren and shadowgraph techniques can equally benefit from this exercise.

8.1 Designing the Schlieren System

For generality and economy, choose a z-type mirror-based schlieren system. A more-expensive lens-based system is simpler to align, but then for present purposes it becomes altogether too simple. With a mirror-based system you get to experience all the joys of optical alignment and the off-axis aberrations too. This is valuable practice for using larger "professional" schlieren equipment.

G. S. Settles, *Schlieren and Shadowgraph Techniques*

Economy depends on using telescope mirrors intended for the amateur astronomy market, as described in earlier chapters. A wide variety of small telescope mirrors is available (see App. D), from which a pair of 108 mm-diameter, f/8, $\lambda/8$ parabolas has been selected (available from Edmund Industrial Optics). F/10 parabolas are also available, but f/8 avoids excessive system length.

This z-type schlieren system is simple enough that the selection of its field mirrors already specifies much of the design. The remaining design issues follow the principles laid out in Chap. 3, keeping frills to a minimum. Ray-tracing computer codes, etc., discussed in the previous chapter, are unnecessary here.

According to Fig. 3.6, one next finds the minimum mirror tilt angle θ, which has the same magnitude but opposite sign for each of the two field mirrors. A little trigonometry quickly shows that $\theta_{min} = 1.8°$ when the foci of the mirrors just coincide with the edges of the parallel beam. This is impractical, though, as well as unnecessary: give yourself enough room to work while still keeping the beam angles small. A better compromise is $\theta = 3°$, yielding incoming and outgoing beam angles of $2\theta = 6°$, well within the astigmatism guidelines of Chap. 3.

The only remaining significant design issue is the overall schlieren-system length, which is immaterial from an optical viewpoint but nonetheless of practical consequence. If it is too short, there is no useful working space in the test area; too long, and the system can no longer be mounted on a single table. To provide at least 10 cm of unencumbered parallel-beam length for the test area, an overall system length of 1.5 m is chosen here. In the Penn State Gas Dynamics Lab, this optical setup just fits diagonally on a 91 x 122 cm (3 x 4 foot) optical table. In other cases, to save space, both the incoming and outgoing beams are sometimes folded using plane mirrors. But in the interest of keeping this example simple, beam-folding is not considered further.

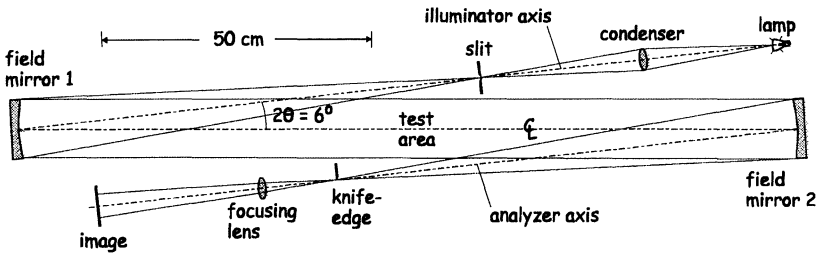

Fig. 8.1. Scaled layout of a simple z-type schlieren/"focused" shadowgraph system based on twin 108 mm f/8 parabolic mirrors, with beam entrance and exit angles of $2\theta = 6°$.

A layout drawing, or top view, of this schlieren system is given in Fig. 8.1. Although the condenser illumination is shown as f/8 to match the f/number of the first field mirror, in practice a shorter-focus condenser is used and some light spillage is allowed at the first field mirror according to Sect. 7.1.4. Typical condensers are much "faster" than f/8 for better optical collection efficiency.

8.2 Determining the Cost

There was once a time when the optical components needed to build a schlieren system were hard to find. Amateur astronomers ground their own mirrors, and so did a handful of amateur strioscopists. Nowadays these components can all be ordered from optical catalogs, if one is willing to pay the price.

Beginning with the twin field mirrors, their cost as of this writing is about $111US each. They will only grow more expensive,[1] but even so this is a modest price (lenses of comparable diameter and quality can cost 10 times as much). The condenser lens is in the $30 range, and a high-quality achromatic-doublet focusing lens of 200-300 mm focal length (see Sect. 3.7.1) can be had for about $50. Thus the key optical components are available for around $300 total. If need be, everything else can be homebuilt at a cost that is trivial in comparison.

Assuming therefore that cost is a concern, a tungsten-halogen automotive bulb makes a fine light source for a few dollars (see Sect. 7.1.1). It can be battery-powered or, somewhat better, operated from the AC line through a variable transformer that is adjustable in the 0-20 V range. Without involving cameras at this point, a piece of ground-glass for a schlieren-image viewing screen costs only a few dollars. Both the source slit and knife-edge are easily made from single-edged razor blades.

That accounts for everything except the table and the optical mounts. Most any solid table or workbench of sufficient size will do for this purpose. The optical mounts, however, could easily become the biggest expense of all if bought commercially. Current prices from optical suppliers total around $1200 for a set of adequate-but-not-fancy optical mounts for this schlieren system. (If the word "laser" appears in the mount description, double the cost estimate). The obvious alternative, with a lot more effort but comparatively-trivial expense, is to make your own optical mounts (see Sect. 7.2.2).

Most of the optical components require only mounts with a coarse height adjustment, their horizontal position and orientation being accomplished by moving the mount about the table. Rod mounts with thumbscrew locks, like those depicted in Figs. 7.8, 8.2, and 8.3, can be bought or built from scratch. The schlieren field mirrors additionally require a vertical tilt adjustment: homemade mirror mounts serving this purpose are described, for example, in [301] and [654]. Only the knife-edge warrants a vernier adjustment, and then only in the direction of the cutoff, though a two-axis adjustment is handy when the cutoff orientation is changed. Micrometer drives like the one shown in Fig. 7.8b and 2-axis optical mounts can cost several hundred dollars each, but the design of an alternative, homegrown 3-axis drive for a schlieren cutoff is given in Ref. [385].

[1] My first schlieren mirrors in the 1960's were slightly smaller (75 mm diameter), but they only cost about $8 each at the time [532].

A brief parts list for this simple schlieren/shadowgraph system is also given, with current prices, in App. C. Photos of the actual setup, as implemented in the Penn State Gas Dynamics Lab, are shown in Figs. 8.2 and 8.3 below.

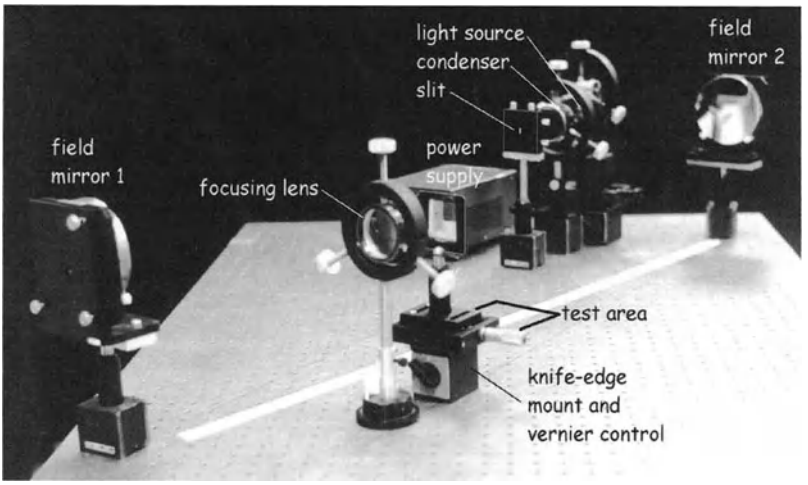

Fig. 8.2. Photo of the implementation of a simple z-type schlieren/"focused" shadowgraph system based on twin 108 mm f/8 parabolic mirrors. Distances are compressed by perspective and the viewing screen is omitted for clarity. Photo by Heather Ferree.

8.3 Choosing a Setup Location

First find a solid wooden or metal table or workbench big eno ugh to accommodate the 1.5 m minimum length of the schlieren system. Next find an appropriate room in which to set it up. A caution was already given in Chap. 7 about upstairs rooms and rickety floors. The basement is a much-better location for a schlieren setup, so long as enough space is available for the table and access around it. Basement accommodations also automatically satisfy the need to darken the room for stray-light elimination. Not to be too particular, though, almost any location can be adapted to the present purpose with some ingenuity.

One must be able to shut down or block off the room ventilation and to tame any stray air currents during sensitive experiments. The familiar candle flame located in the test area will reveal these problems right away when they occur. Pedestrian traffic and doors opening and closing are especially noticeable. Even with such airborne disturbances, though, some of the best schlieren images are obtained in time-honored fashion by patience and by seizing the right moment.

8.4 Aligning the Optics

The alignment procedure for a z-type schlieren system was discussed earlier in Sect. 7.2.3. The comments that follow are additional and specific to the schlieren system described here.

Begin by leveling the table and chocking the legs to prevent any motion. (A rickety-legged bench should be fixed or replaced at this point before proceeding.) Next choose an appropriate height of the horizontal optical centerline plane above the tabletop. Every optical component must be centered in this plane, else vertical misalignments will certainly cause frustration.

Prepare the key schlieren alignment tool: a plain white sheet of paper with an inscribed 108-mm circle corresponding to the field mirror diameter. Smooth white cardboard without printing also does a fine job.

Place the two field mirrors at either end of the table. A spacing of 1.5 m is a minimum for this system, but longer is better if available. Draw a centerline on the table connecting the centers of the field mirrors, or else mark this line with tape. Halve the distance between the mirrors and mark the test area there, a square of about 10 cm size (shown in Fig. 8.2).

Now assemble the light-source, condenser, and slit to form the schlieren illuminator, and aim it at the first field mirror. A line on the tabletop at a 6 ° angle to the centerline between the mirrors helps to locate the illuminating optics upon their axis according to Fig. 8.1. A hash-mark on this line indicates the 864 mm focal length of the first field mirror, where the slit should be located. The illuminator is acceptably set up when the illuminance across the first mirror is uniform and the reflected beam just fills the 108 mm circle on the paper, irrespective of its distance from the mirror.

The rotation and tilt controls of the first mirror are now adjusted to render the parallel beam horizontal above the optical centerline. It should just fill the second mirror. A corresponding line on the tabletop at a 6 ° angle to the centerline between the mirrors now helps to locate the analyzing optics on their axis. Measure once again 864 mm out along this line and place the knife-edge there. The rotation and tilt controls of the second mirror are now adjusted to bring the light-source image to bear upon the knife-edge, which should then be retracted far enough to let the entire beam pass.

For now, locate the focusing lens immediately after the knife-edge. Place a focusing prop (stirring rod, bolt, etc.) in the parallel beam above the test-area "box," and adjust the position of the ground-glass viewing screen along the analyzer axis to bring the silhouette of the prop into sharp focus. Anything handy can be used to support focusing props and objects of study in the test area.

Cranking the knife-edge back into the beam, a darkening of the screen is observed. With the knife-edge parallel to the long side of the source slit, follow the detailed discussion associated with Fig. 7.10 in order to achieve a uniform cutoff over the entire schlieren image. The schlieren system is now ready to use for visual observations.

8.5 Troubleshooting

At this stage I get a lot of questions from new schlieren users who have run into difficulty. Few of these problems are serious, but here is some further general troubleshooting advice based on experience with them.

Alignment. Use your sheet of paper to trace the light beam from the source to the schlieren image. Look for deviations from the layout shown in Fig. 8.1. Uneven illuminance of the spot on the paper often comes from the illuminator problems discussed in Sect. 7.1.4 and illustrated by Fig. 7.5b. Don't expect a splendid schlieren image right away after only a rough alignment, or with huge incoming and outgoing beam angles. Instead, take the time to set the system up carefully at the outset. The universal sign of poor alignment is no nuniform illuminance across the schlieren image, but this can certainly be corrected, as Figs. 3.11 and 7.10b attest.

Fig. 8.3. Rossana Quiñones prepares to light a candle in the test area of the simple z-type schlieren/"focused" shadowgraph system described in this Chapter. On the right is the illuminator section and one field mirror. On the left is an old Speed Graphic camera being used without a lens for Polaroid photography.

Focusing the schlieren image is sometimes one of the novice's worst problems. Either an inappropriate focusing lens is chosen (sometimes the one that comes on a film or video camera), or else the viewing screen is placed too close or too far

away from the knife-edge and nailed down. Whatever the problem, a sharp image cannot be found no matter what, and there is aggravation and disappointment.

The solution to this problem is to proceed with a few logical steps. First, place a focusing prop in the test area as previously described. Second, note the distance from the test area to the second field mirror. Usually, as in Fig. 8.1, this distance is less than the mirror focal length, so no real image of the test area is formed by the schlieren system without a proper focusing lens. Nevertheless the sheet of white paper, if held in the beam 20 or 30 cm after the knife-edge, reveals a fuzzy schlieren image. The task of the focusing lens is to bring this into sharp focus.

Note the focal length of your focusing lens. It can be found crudely by using the lens to focus the room lights onto your sheet of paper and noting the distance from the lens to the paper. According to the calculation of Sect. 3.7.1, a 260 mm focal length is needed to size the schlieren image appropriately for 35 mm photography. For viewing the image directly on a screen, use a long-focus single-element lens of 750 or 1000 mm focal length. It should be clear that an ordinary camera lens, with a focal length of 50 mm or less, will produce a schlieren image too small for most purposes when used with the optical system described here.

Having secured an appropriate lens, place it shortly after the knife-edge (say 5 cm). Now use your sheet of paper after the lens, moving the paper farther away along the optical axis until the image of the focusing prop comes into sharp focus upon it. Mark that location on the table and mount your viewing screen or camera there. If the focus is found in thin air off the edge of the table, then the focal length of the lens is too long. Obviously, a selection of focusing lenses or a zoom lens meant for 35 mm photography is handy to have available.

Additional effects helpful in focusing the optical system were mentioned in earlier chapters. The direct light from a candle flame in the test area, as well as the diffraction halo around any opaque object at full knife-edge cutoff, come very sharply into focus when the adjustment is correct. Likewise the shadowgraph effect from a candle plume disappears when sharply focused with no knife-edge.

Other Problems include astigmatism, especially when it is misunderstood. Read about astigmatism in Chap. 3 and be on the lookout for it. It is not serious in this schlieren system if a single knife-edge is used and is properly positioned. Recall that the knife-edge position along the optical axis for uniform cutoff depends on edge orientation (i.e. vertical or horizontal) when astigmatism is present.

Referring to Fig. 8.1, ample room has been provided for the test area, but no more than that. Sometimes a large schlieren object gets into the illuminator or analyzer beam as well as the parallel test beam. This causes double-imaging, with the false image oversized and out of focus. The solution is to get the schlieren object out of the beam in which it does not belong, or else to lengthen the optical system and thus generate more free space around the test area.

The effects of an extended light-source, e.g. a slit rather than a point, also sometimes cause confusion. With an extended source the schlieren beam will not appear perfectly sharp when it falls on the white-paper screen. It will instead have a fuzzy boundary and will be oblong in the direction of the long slit axis. These natural consequences of finite light-source size are not a cause for concern.

Finally, questions like "how can the screen darken uniformly as the knife-edge cuts off the source image?" betray a lack of understanding of the composite source image concept. The answer is to be found in Sect. 2.5.2.

8.6 Recording the Schlieren Image or Shadowgram

After some initial visual observations, almost everyone who builds this optical system will want to take schlieren pictures. Ernst Mach became famous for doing that, so maybe the potential is still there.

The quickest – but not the cheapest – way to begin schlieren photography is with Polaroid film or a digital camera. In the case of Polaroid, one needs not only the film and "film back" (the holder in which the film is exposed and later developed), but also a camera with a removable lens, a shutter with an aperture big enough to accept the schlieren beam, and a ground-glass screen on which to focus the schlieren image. Commercial studio or scientific view cameras with focal-plane shutters are ideal for this, but are also quite expensive.

As for digital cameras, unfortunately the cheaper ones have integral short-focus lenses that are not compatible with schlieren imaging for reasons described earlier. Please don't try to take a schlieren image by pointing such a camera at the ground-glass screen. On the other hand, if you can get a digital camera with a removable lens, focus the schlieren image directly on the camera's sensor plane and instantly you're in the digital schlieren imaging business.

The same goes for videocameras. Some have integral lenses that are unusable here. A few will accept the schlieren beam directly into the lens in telephoto mode without vignetting it. If the lens comes off, disable all the automatic controls and focus the schlieren image on the camera sensor plane. This can be tricky, since the sensor is often only a cm wide or so. In this case a focusing lens in the f = 50-100 mm range will produce an image filling the video screen. Beware not to focus too much light into your videocamera and thus damage it; turn down the lamp voltage at first, then slowly bring it back up while observing the video image.

If you have more patience than the digital crowd, 35mm photography is still the best way to take high-resolution schlieren images, especially in color. Most of the Color Plates at the end of this book were shot on Kodak Ektachrome 35 mm transparencies. The automatic features of newer 35 mm cameras can get in the way, but the older manual ones are great for this purpose. Most are reflex cameras with focal-plane shutters, so they can function well with outboard focusing lenses and provide film isolation even with the lens off. Taking the lens off, however, is not usually necessary if you mount a telephoto zoom lens with a 300 mm focal-length range to the camera. For best results, though, note the comments on through-the-lens metering of schlieren exposures given in Sect. 7.3.1.

8.7 Conclusion

Now that you've built your own modest schlieren system, the question is: what to do with it? The next chapter surveys the broad range of applications of schlieren and shadowgraphy known thus far, but many more applications are possible.

Fig. 8.4 below shows two schlieren images from my 75 mm schlieren system of the 1960's. The present system is better, having a larger field-of-view. Up to this point in the book, more than 30 images illustrating all sorts of schlieren and shadowgraph concepts were photographed using this modest example of a tabletop schlieren system: it is no toy. On the other hand, it is a toy! Have fun with it.

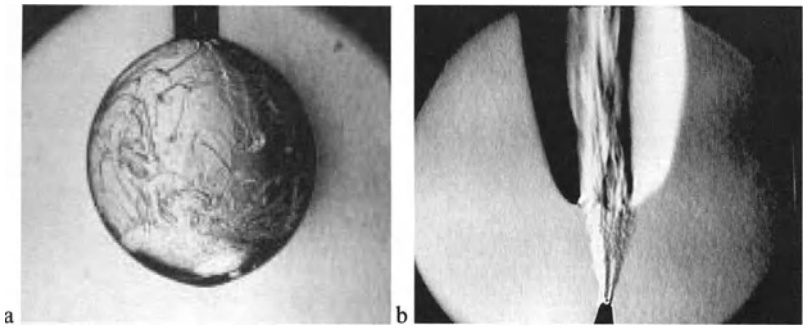

Fig. 8.4. Images from the author's 1960's-vintage 75 mm z-type schlieren system [385,532]. **a** propane-filled soap bubble, in which the soap film appears to have a curious reaction to the propane. **b** "lifted" diffusion flame, wherein propane is injected into the air under pressure, undergoing turbulent mixing before the flame front occurs. See also a direct shadowgram taken using this system and shown earlier in Fig. 6.10.

9 Applications

> Until now, schlieren methods were generally considered applicable only to a few cases.
>
> *Hubert Schardin* [2]

> That field has the most merit which contributes most heavily to, and illuminates most brightly, its neighbouring scientific disciplines.
>
> *Alvin M. Weinberg*

Schlieren and shadowgraphy are paradigms of scientific visualization that permeated the fabric of science and technology during the 20th Century. Both Schardin [2] and Holder and North [98] surveyed this broad range of applications thoroughly. Though technical journals have mushroomed since then, computerized databases and the Internet allow me to continue that tradition here. I make no attempt to cite every reference, but give special attention to the several new and unusual applications that turned up. Of many possible classification schemes, grouping schlieren that occur in solid, liquid, and gaseous states seems the most natural.

9.1 Phenomena in Solids

9.1.1 Glass Technology

> ...the Veins in polish'd Plates of Glass did also cast the like broad Shadows
>
> *Sir Isaac Newton,* Opticks

Glass is an amorphous mixture of substances with great optical clarity. It is one of our most basic materials since antiquity, and it is the premier schlieren object in solid form. Schlieren and shadowgraph systems made of glass are used to inspect glass, as already shown in over a dozen figures and several of the Color Plates.

Hooke, Newton, and Huygens all visualized glass flaws using rudimentary schlieren and shadowgraph techniques. Observing schlieren in glass was a point of departure for Toepler's later elaboration of the schlieren instrument [40]. Ernst Abbe took an interest in glass, and had a special schlieren system built by Carl

G. S. Settles, *Schlieren and Shadowgraph Techniques*

Zeiss for the purpose [47]. Schardin and his colleague G. Stamm [2,320-322] became experts on the topic, writing with great authority. All of this history occurred before the recent invention of the float-glass process, fiber optics, gradient-index lenses, and flat-panel displays. Much of glass technology changed in the last few years, and is still changing.

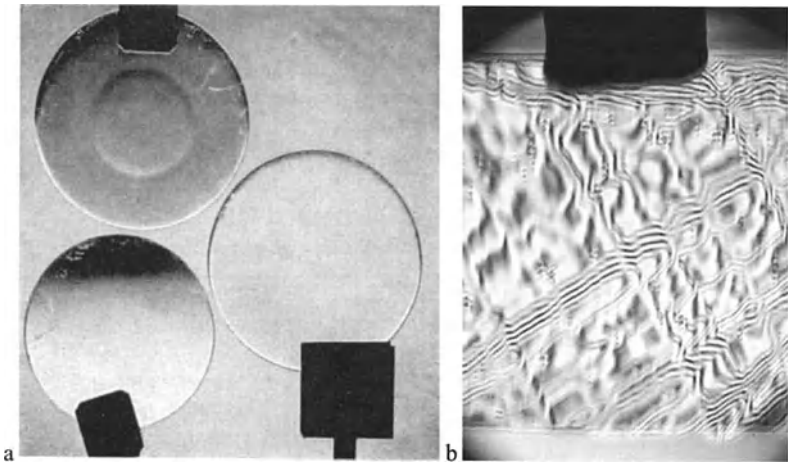

Fig. 9.1. **a** Schardin's [2] schlieren photo of three polished glass disks. The top disk has a grinding ring and the lower left disk has a spherical error. The third disk is defect-free within the limits of the schlieren sensitivity shown here (reproduced courtesy of Springer-Verlag). **b** Ronchi-grid schlieren image of a sample cut from an antique windowpane (photo by author).

For additional background, note that true schlieren arise from the irregular mixing of the glass melt, but thickness variations and surface waviness also show up in the schlieren image. According to Vasiliev [102], schlieren imaging of commercial glass enabled the causes of these defects to be studied. In plate-glass testing [2,320], true striations are distinct from wedge errors, surface ripple, internal strains, blisters or bubbles (seed), and solid inclusions (stones). If the glass (or any transparent solid) has internal temperature gradients, these are also visible by schlieren [655].

The plate glass industry is enormous: residential, commercial, and automotive uses consume 0.4-0.5 million m^2/year in US alone, and worldwide sales total more than $40 billion each year. Schlieren techniques once played a much larger role in this industry, though, than they do today.

Schardin's background-grid-distortion schlieren methods [2], Sects. 4.3.2 and 4.3.3, still see use, however, and are re-invented in several recent patents [204,207,208]. These so-called "zebra" methods benefit from simplicity and large field-of-view but are not very sensitive. One rotates auto windshields and CRT

screens before a striped background and finds the "zebra angle" at which striations become visible [656]. Grid- and lattice-cutoff schlieren methods are better ([2], Fig. 9.1b, and Sect. 10.2), but are no longer used.

Instead, flying-spot laser scanners have superceded traditional schlieren methods [656,657] in recent years. Automatic optical inspection by scanning lasers now routinely tests both float glass and glass containers. These systems are costly, but they detect 0.5 mm commercial defects in float-glass ribbons that move by at about 0.25 m/s. They do most of the job adequately, but fail to reveal distortional faults that can ruin an automobile windshield, for example. Even today these are still routinely inspected visually [204,657,658]. Exactly why laser scanners replaced white-light-illuminated schlieren imaging is unclear, but lasers are sexier than white light and new technology replaces old.

Tempered automotive glass [2,659] is a special case: it is trending toward thinner sheets, with supersonic airjets providing the necessary rapid cooling for tempering. Here lies a rare confluence of two prime candidates for schlieren observation: the airjets, and the resulting optical quality of the glass itself.

Overall, this field is ripe for renewed schlieren applications. At full-scale, using line-scanning optics and a TDI camera (Sect. 4.4.2), scanning schlieren is ideal for this purpose. No speckle or coherent artifact noise occurs with white-light illumination, and a sensitive physical picture of the glass defects results – much more intuitive than a laser-spot readout or an interferogram.

Non-scanning large-field schlieren systems (Sect. 4.3) can also play a useful role in modern plate-glass and automotive-glass testing. More on this general topic is found in Sect. 10.2 on quantitative deflection mapping, Ronchi methods, and moiré deflectometry.

9.1.2 Polymer-Film Characterization

Many of the above comments apply equally to polymer sheets and films. Schlieren imaging makes the characterization of polymer film imperfections simpler and less expensive, as described in a little-known paper by McCallum [660]. The types of observable optical inhomogeneities are: refractive differences due to incomplete mixing of the components, film thickness variations, birefringence due to shear in the forming process, and gas bubble inclusions.

The commercial appeal of thin transparent polymer films, for example, depends upon their optical and mechanical properties. These require on-line testing during manufacture. Quite recently, producers of commercial clear food-wrap films made of PVC were still searching for cost-effective ways to monitor film quality and uniformity. They should consider schlieren methods (Fig. 9.2a).

Other schlieren applications in polymer science are discussed by McCallum [660] and illustrated in Fig. 9.2. Often the polymer-film feature sizes of interest require that schlieren imaging be combined with microscopy, as discussed further in Sect. 9.4.7.

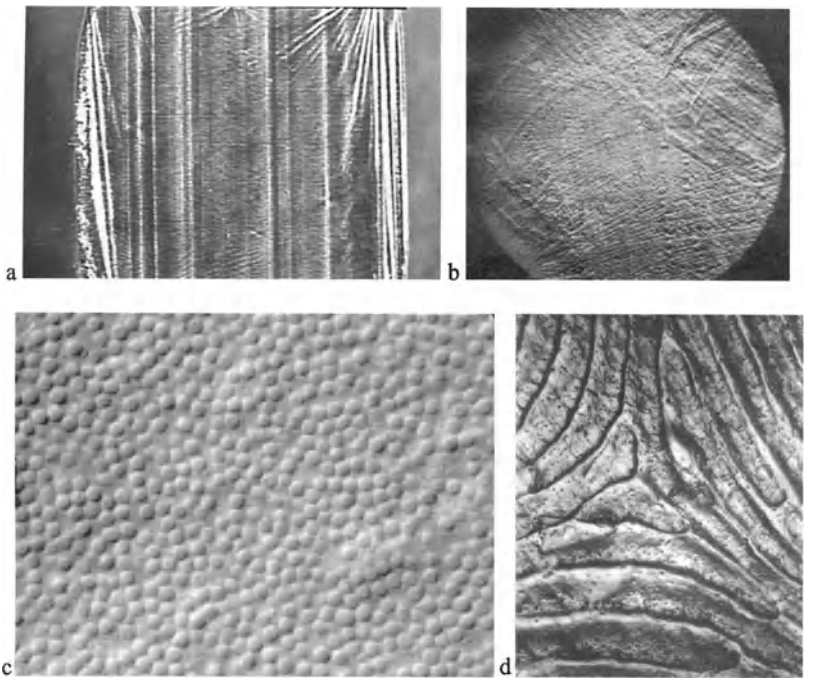

Fig. 9.2. **a** Schlieren image of a commercial clear plastic food-wrap film (some of the vertical streaks represent film "bunching," but other defects of various types are also visible). **b** 3-mm-thick PMMA sheet, showing both surface and internal striations. **c** micrographic schlieren image of a PVC plastisol, with a width scale of about 35 μm. **d** schlieren microgram of a polymer-film replica of a human fingerprint. Images b-d courtesy William H. McCallum [660].

9.1.3 Fracture Mechanics and Terminal Ballistics

Shadowgraphy is used extensively to study high-speed failure of solids by crack propagation [514,533,661,662]. A key modern reference is Beinert [514], who surveys the field. Elastic stresses change the refractive index and surface shape of transparent solid bodies, often made of acrylic. From the form and magnitude of the resulting shadowgram caustics, one determines the wave-field strength. Cranz-Schardin cameras, Sect. 7.3.3, play a significant role [533,663,664]. High sensitivity is unnecessary, but schlieren techniques nevertheless see some use to supplement the shadowgraphy [665].

Terminal ballistic studies involve firing high-speed projectiles into transparent solid samples, e.g. Fig. 9.3 [666]. Upon impact, fracture mechanics becomes important. Terminal ballistic studies in liquids are covered later in Sect. 9.2.5.

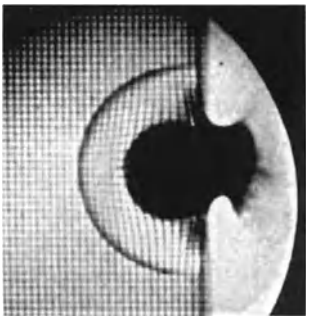

Fig. 9.3. Impact of a polycarbonate cylinder with a PMMA block containing an imbedded grid. At 4.59 μs after impact, the photo shows cratering of the plastic and a spherical shock wave propagating through the material. Both shadowgraphy and background distortion are involved. This study arose from an interest in hypervelocity micrometeor impact with spacecraft. NASA-Langley photo L-70-8001.

9.1.4 Specular Reflection from Surfaces

Pioneered by Nadai [667] at Prandtl's suggestion, schlieren observation of reflecting surfaces became well-known by Schardin's time [1,2]. It does not require transparency, and the reflection angle of the incident beam, ε, is simply twice the local surface inclination angle. Applications include lacquered-surface flaw detection [221] and inspections of magnetic tape quality [668]. This method also allows polished wind-tunnel and water-tunnel models to act as reflective optical elements [205,463,475,669-672] in both schlieren and shadowgraph systems. It has been superceded in some cases by retro-reflective holographic interferometry. See also reflection from liquid surface waves in Sect. 9.2.2.

9.2 Phenomena in Liquids

> Adequate data on flow patterns is a necessary condition in all good fluid mechanics work, and usually the cheapest, quickest and most effective way to obtain them is by visual studies
>
> *S. J. Kline* [673]

The density of a liquid as a function of refractive index is not given by a simple rule like the Gladstone-Dale Law for gases, but rather directly by measurement [116]. Moreover the refractivity, $n - 1$, is orders of magnitude greater for liquids than for gases. Thus, as noted in Chap. 2, strong refractions are likely [82], and schlieren and shadowgraph techniques do not usually need or want high sensitivity.

9.2.1 Convective Heat and Mass Transfer

This topic is a key part of a basic technical education in the thermal sciences. It is crucial in a variety of engineering processes too broad to list here. Schlieren and

shadowgraph techniques have played an important role in imaging convection for many years [82,674].

Convective Boundary Layers in liquids are observed, for example, by setting the schlieren knife-edge parallel to the surface of the body bearing the boundary layer. Examples are found in [315,343,672,675,676]. For best results the knife-edge is oriented to show a light boundary layer against an opaque body [164].

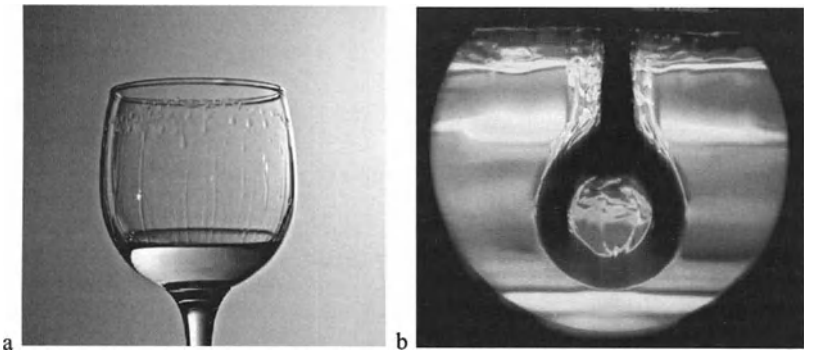

Fig. 9.4. **a** "Wine tears," formed by alcohol evaporation and condensation [653], and imaged by Schardin's schlieren method no. 3 (Sect. 4.3.3). Photo by Heather Ferree. **b** an electric immersion-coil heater in water, original color schlieren photo by Horst Herbrich.

Mixing and Instability in liquid convective systems are observed due to both forced motion and natural convection [370,677-679]. In particular, unsteady thermal plumes are induced when an instability is created by heating the fluid from below [680].

Concentration Boundary Layers occurring in electro-deposition cells, chemical reactors, materials processors and the like [681,682] are amenable to schlieren or shadowgraph observation when clear liquids and high-quality cell windows are employed.

Double-Diffusive Convection [683,684] occurs in laminar liquid systems due to opposing gradients of, say, temperature and salinity. It is popularly visualized by shadowgraphy [506-508,683-687], and is discussed further in this Chapter under the special topic of geophysical studies, Sect. 9.4.4.

Rayleigh-Bénard and Marangoni Convection are important fundamental fluid phenomena. Rayleigh-Bénard convection is the gravity-driven, thermally-unstable flow of a horizontal fluid layer. It occurs inside the Earth's mantle and atmos-

phere, and near the surface of the Sun [688]. More fundamentally, it also provides a framework to observe the onset of transition to turbulence and chaos. Examples of its visualization by schlieren and shadowgraphy are found in [551,678,688-690] and Fig. 9.5. Berg et al. [691] also show many fascinating schlieren images.

Marangoni convection is similar, but has an upper surface-tension boundary. Toepler observed and sketched it [37,41] using his original schlieren system. This observation has been forgotten, however, and due to strong refractions, shadowgraphy is more often used today. Examples are found in [688] and [692]. Okhotsimskii and Hozawa [693] show many striking images, and their paper is a good example of how schlieren and shadowgraphy reveal, even today, new vistas and a wealth of visual detail in phenomena that are normally invisible.

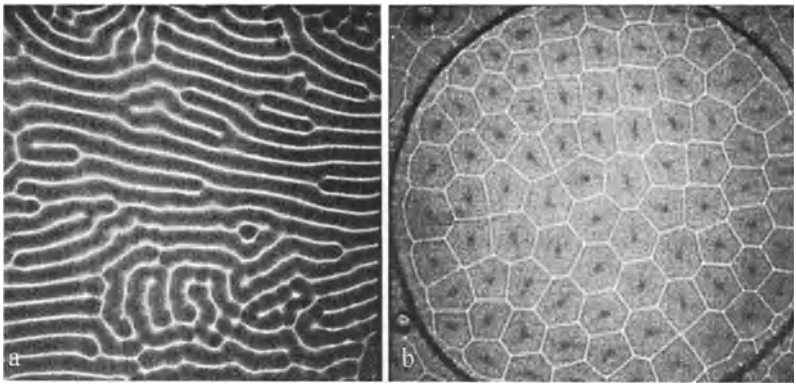

Fig. 9.5. **a** Shadowgram of Rayleigh-Bénard convection. **b** shadowgram of Marangoni convection. Photos courtesy J. A Whitehead [688], Woods Hole Oceanographic Institute.

Shadowgraphy of other convective flows in liquids includes cryogenic helium [694], porous media [690,695], and convection due to the freezing of water [696]. Schlieren optics is used to observe crystal growth [697] and the boundary layers of swimming fish [315,544]. In fact, marine biologists also use schlieren to observe the water flow produced by fish eating zooplankton [698] and thermal flows through mollusks [699].

9.2.2 Liquid Surface Waves

Faraday pioneered the study of liquid surface waves in 1831 [700], and Lord Rayleigh used schlieren to observe ripples and measure the surface tension of water in 1890 [701]. Jeffree [702] patented light-modulating devices to image ripples on liquid surfaces in 1939. Schardin [2] took color schlieren images of liquid surface waves and used them to reveal wave propagation. Wolter [119] found that

surface waves are ideal for shadowgraphy, so long as one remains aware of the focusing effect of the waves in adjusting their distance from the viewing screen. Jenny [703], Flournoy [704], and Settles [391] attempted to set these waves to music (see further discussion in Sect. 9.4.1 and Color Plates 39 and 40). Faraday waves, in which the fluid oscillates in the same direction as the gravity vector, are still very interesting to modern fluid physics, e.g. [705].

From these precedents it is clear that the confluence of liquid surface waves with schlieren and shadowgraphy has born fruit in the ability to measure surface-wave slopes, and in useful apparatus like ripple tanks and water-table analogies.

Surface-wave slopes can be determined either from reflected or transmitted light if the fluid is transparent [134,706]. Marangoni cells, having a distorted free surface, are quite amenable to such studies [707,708]. In shadowgraphy, strong refractions quickly form caustic patterns as familiar as the local swimming pool. Such caustics also appear in shadowgrams of turbulence, Fig. 6.13b and [511]. In schlieren imaging the illuminance is proportional to the surface wave slope, and both hue and saturation are also available to encode information in the image [2,134]. Almost all of these studies concern liquid pools, but Nosoko et al. [509] also observed surface waves on a falling liquid film.

Ripple tanks have been around since at least the early 19 th Century, are used for demonstrating wave motion and interference, and were once offered commercially as educational apparatus. A shallow stationary layer of water on a glass plate is illuminated from below, and shadowgraphy does the rest. The water-table hydraulic analogy with high-speed gas flow is more recent, however; it was suggested by Jouget in 1920 [709] and developed in the period leading up to World War II [710]. The wave patterns upon a thin water-channel flow become visible either by shadowgraphy or background-distortion schlieren, but they are so strong that only a casual application of these techniques is necessary. Skews [212] applied color schlieren somewhat more rigorously, with a result shown in Color Plate 41. The water-table analogy is still used occasionally to simulate supersonic gas flows [330,711].

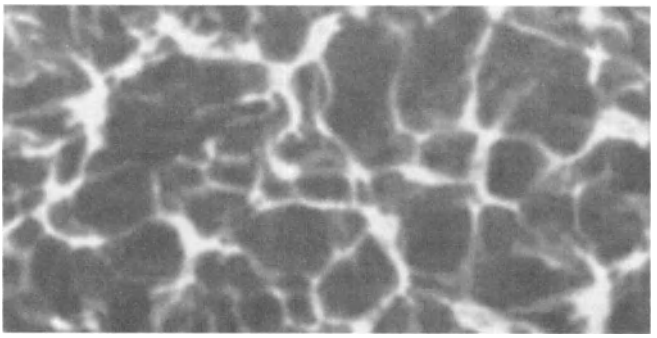

Fig. 9.6. Caustic shadowgram pattern formed by projecting light through a disturbed liquid surface onto the flat bottom of the containing vessel: "swimming-pool caustics."

9.2.3 Liquid Atomization and Sprays

Fraser and Dombrowski [712] describe various lighting techniques to image the breakup of a clear liquid sheet. These include direct shadowgraphy and several adaptations of background-distortion schlieren per Schardin's method no. 3 (Sect. 4.3.3). One, in particular, reflects either a diffuse or collimated light beam from the liquid sheet into a camera, where the camera aperture acts as a schlieren cutoff (as does the iris of the eye, when observing visually). This illustrates once again that *de facto* schlieren imaging is sometimes done without a deliberate knife-edge, and sometimes even without the awareness of the investigator.

Liquid atomization for materials processing is revisited in Sect. 9.4.5.

9.2.4 Ultrasonics

Modern ultrasonic medical diagnostics and non-destructive testing use acoustic beams in water tanks. Based on the work of Raman and Nath [713] on light diffraction by an ultrasonic beam, schlieren optics traditionally images these underwater activities. The grating-like beam produces diffraction, but there is a superposed ordinary schlieren effect as well [104]. This application is important enough to spawn a rare commercial schlieren instrument, the Intec Research Corp. Optison Schlieren System [649], described earlier in Sect. 7.4.2.

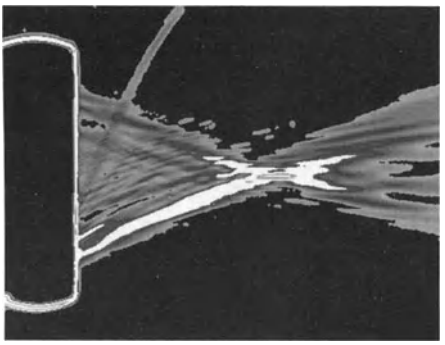

Fig. 9.7. Schlieren image of a focused ultrasonic beam propagating left-to-right underwater from the transducer on the left. A defect has caused the wave that leaves the image at the top. The application is high-intensity focused ultrasound for medical therapeutic use. Original color image courtesy of C. I. Zanelli, Intec Research Corporation, www.intec.com.

Reviews of schlieren imaging of underwater acoustics are given by Neubauer [714], Darius [715], Hennige [716], and Brezeale [717]. Korpel et al. [718] questioned the role of diffraction, Bucaro and Dardy [719] considered the sensitivity, and Moore and Bucaro [720] compared schlieren to acoustic holography. Porter [721] proposed a quantitative real-time system, while Pitts et al. [722] performed schlieren tomography and compared shadowgraph and schlieren images of ultrasonic phenomena.

Schlieren imaging in medical diagnostic ultrasonics is used, for example, in ophthalmology [723], gallstone surgery [724], and imaging through the human

skull [725]. Medical therapeutic ultrasound, [726] and Fig. 9.7, focuses an intense ultrasonic beam into the body, e.g. for the treatment of Meniere's disease [727].

Ultrasonic non-destructive-testing uses the schlieren method [625,728] to observe, for example, submerged plates [729,730] and composite de-laminations [731]. A unique example comes from railway research, where the design of a "wheel probe" for ultrasonic track inspection is observed by schlieren imaging using glass cross-sections of rails [732].

9.2.5 Water Tunnel Testing and Terminal Ballistics

Schlieren is sometimes used in water-tunnel testing [154,733-736], where either thermal marking by small temperature differences or chemical marking provides the necessary variation of refractive index. Peters et al. [737] give a fine example of the latter, reproduced here in Fig. 9.8a. Optical distortion of the schlieren beam occurs through cylindrical water-tunnel test sections, but is correctable using a cylindrical lens [477]. Liquid boundary layers, Sect. 9.2.1, are closely related to this topic, especially in Allan's color schlieren investigation of boundary layers on swimming fish [315].

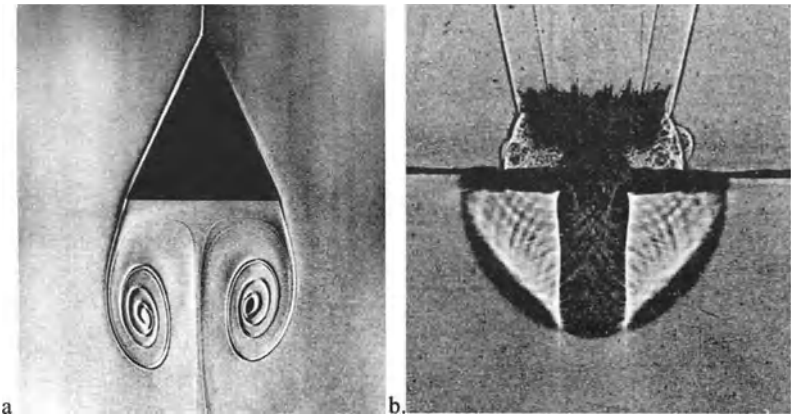

Fig. 9.8. **a** "Sugar schlieren" image of vortices behind a wedge in a downward water-tank flow (sugar strongly alters the refractive index of water but diffuses slowly in it). Photo courtesy F. Peters [737]. **b** terminal-ballistic shadowgram of a Mach 6.1 sphere impacting an air/water interface. US Navy photograph by J. H. McMillen [738].

Terminal ballistics of projectiles in water generates both military and forensics interest. Sometimes direct photographs at high speed make use of the background-distortion schlieren effect, but otherwise shadowgraphy is most applicable in view of the strong refractions that occur [2,738].

9.3 Phenomena in Gases

> ...one cannot arrange the subject of fluid mechanics in any linear fashion.
>
> *M. Van Dyke* [739]

> p is the pressure but **p** is the momentum; V is the volume but **V** is the velocity. One must keep one's wits about one in order to keep track of that.
>
> *R. Feynman,* lecture on kinetic theory of gases

The connection between refractive index, gas density, and gas temperature was discussed in Sect. 2.1. Schardin [1,2] gives considerable background on this, tabulating and discussing various flow properties vs. Δn. For example, starting with "standard" air at 273 K and about 1 bar pressure, $\Delta n = -0.00001$ corresponds to a temperature increase of 10 K, a pressure drop of 36 millibars, a 3.5% decrease in density, or an increase of 88 m/s in airspeed. Similarly a shock wave with $\Delta n = 0.00001$ across it in standard air travels at a Mach number of only 1.02, such as one might experience within a meter or so of a spark discharge or a small firecracker explosion [166]. Yet this same Δn yields a refraction of over 4 arcseconds according to the simple refraction model given in Sect. 3.4, so all of the above phenomena are visible in a sensitive schlieren image.

In other words, schlieren and shadowgraph observation works well for many phenomena in gases. Since Toepler's time a very broad range of applications has therefore arisen, as described below.

9.3.1 Agricultural Airflows

> Schlieren photography soon taught me that the air near the surface of a leaf is never really still.
>
> *D. M. Gates* [740]

Toepler pioneered the schlieren observation of convection from plants in 1864 [3]. Then nothing more happened for a century, until David Gates [123,740] conducted a fascinating schlieren study of heat transfer from leaves. Briefly, solar heating, re-radiation, transpiration, and convective cooling are all important to plant-life's ability to manage its heat load and avoid environmental stress. Gates measured the convective contribution from schlieren images and used it to improve a theoretical model of the process. He found that leaf size and shape, orientation, and ambient wind are central to convective heat loss from leaves.

Better aero-environmental load management means better crop health, a potential that evolution has already explored in various ways.[1] Genetic engineering of

[1] "Skunk cabbage," for example, has a central wand that heats up to discharge a thermal plume. This plume bears a scent that attracts insects for pollination.

crops may yield further improvements to help feed the world. Since Gates, however, no additional work with schlieren methods is found.

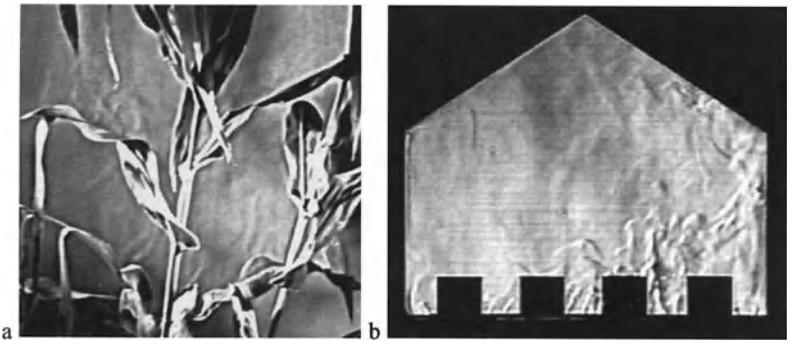

Fig. 9.9. Schlieren imaging of agricultural airflows. **a** convection from a live corn plant, observed using the Penn State Full-Scale Schlieren System. **b** airflow in a model greenhouse with solar gain from above left and convection from crop rows [186].

Doi [741] reviews the general topic of flow visualization in agriculture. Related topics include the optical imaging of airflows in greenhouses [186] and convective flow about farm animals [742]. These are linked to larger topics, indoor airflows and biomedical applications, that are taken up later in this Chapter.

9.3.2 Aero-Optics

> There are nights when the upper air is windless and the stars in heaven stand out in their full splendor round the bright moon.
>
> *Homer,* The Illiad

Astronomy, meteorology, and military applications all demand that we understand atmospheric distortions of optical beam propagation. The topic is reviewed by Roggemann and Welsh [743] with a historical background that cites Newton, but neglects to mention Hooke's *Micrographia*.

Somewhat more recently, Douglass [36] described the form of atmospheric disturbances seen through his telescope a century ago. He was the first to take shadowgrams outdoors for atmospheric observation (Fig. 9.10). Deitz and Wright [744] did similar experiments with a laser source and a brightfield schlieren cutoff, while Eaton et al. [745] took their mirror-type schlieren system outdoors. These experiments revealed stark variations in beam distortion patterns near the ground, depending on the time of day and weather conditions.

Modern military aero-optical investigations are more concerned with high altitudes, high speeds, and laser-beam propagation through turbulent shear layers

[746]. They use coherent light and holographic or non-imaging diagnostics, though schlieren and shadowgraphy are still sometimes applied, e.g. [747].

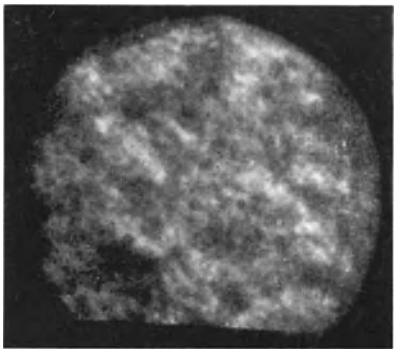

Fig. 9.10. Shadowgram of thermal disturbances in the atmosphere, taken by Douglass [36] in 1900 at the Lowell Observatory in Flagstaff AZ. Sunlight was focused through a small telescope, producing a parallel beam that traversed 1500 m before being brought to a focus by a concave mirror. After the focus a photographic plate received the shadowgram. (This could be a shadowgram, alluded to earlier, that shows schlieren effects due to a restrictive aperture at the focus.) See also Fig. 9.36.

9.3.3 Architectural Acoustics

Soun is naught but air y-broken,
And every speche that is spoken
Loud or preve, foul or fair,
In his substance is but air;
For as flaumbe is but lighted smoke,
Right so soun is air y-broke

Geoffrey Chaucer

Down through human history there was always a consistent and fundamental need to gather in public places to see and hear theater and music. Those public places must strive to give all listeners a satisfactory visual and aural experience, a principle recognized ever since the classical Greek theater [748].

Shadowgraphy played an influential role in this process about a century ago. Toepler [3] introduced the idea of "seeing sound," followed by similar visualizations of Dvorák [23], Wood [48], Boys [62], and Foley and Souder [779]. Their publications inspired Wallace C. Sabine, a pioneer of architectural acoustics and the acoustician of Boston's Symphony Hall. He built models of concert halls, fired sparks, and sent weak shock waves reverberating around them [5,471]. These weak shocks, almost sound waves, revealed themselves in direct shadowgrams like the example shown in Fig. 9.11.

Others also adopted this 2-D optical approach to theater and concert-hall design and acoustic diagnosis [472], but eventually it seems to have run its course. No reference to schlieren or shadowgraphy in architectural acoustics is found since 1967 [749], and today computer methods strive – not always successfully – to provide 3-D visualizations of sound propagation in theaters and concert halls [750].

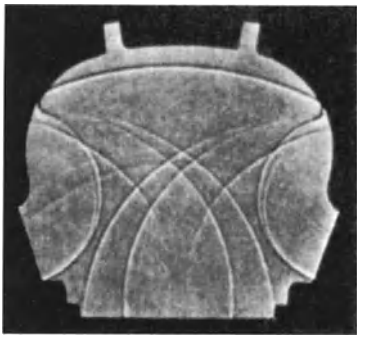

Fig. 9.11. Sabine's shadowgram of wave motion in a model of the New Theatre of New York City, ca. 1900 [471]. A horizontal plane through the theater is shown. Curved walls create focusing that leads to objectionable echoes. For this reason, modern theaters and concert halls assume, instead, the form of a rectangular shoebox.

9.3.4 Boundary Layers

> ...consider the boundary layer as a "Schlieren lens" whose focal length is dependent on the distance from the wall. *Hauf and Grigull* [340]

Ludwig Prandtl's brainchild, the boundary layer, permeates all of fluid dynamics. Being thin and hugging solid surfaces, boundary layers delimit the challenging zones of viscous shear and allow us to make the crucial assumption of simpler inviscid flow almost everywhere else. When marked by density changes, boundary layers are readily visible to schlieren and shadowgraph observation. Examples were already shown in Figs. 1.21, 3.13c, 6.1, 6.16, and 7.11, and are present but not so obvious in several other figures.

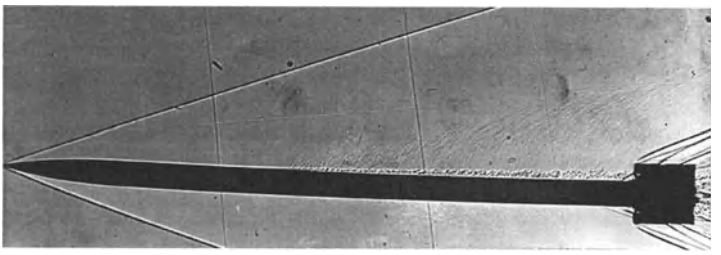

Fig. 9.12. Shadowgram showing laminar-boundary-layer transition on a ballistic "pencil" at Mach 3.5. Note sound radiation from turbulence. US Govt. photo, NACA [751].

Sometimes quantitative boundary-layer measurements are made by schlieren [638,752], but usually the observations are qualitative, e.g. "is the boundary layer attached or separated?" This application is so popular that the number of references in which schlieren and shadowgraphy are routinely used in boundary-layer studies is beyond citing here.

9.3.5 Convective Heat and Mass Transfer

Continuing this topic from Sect. 9.2.1, thermal convection in gases – notably air – has been visualized by schlieren and shadowgraphy since the early work of Hooke [17] and Marat [28]. Toepler [37] conducted somewhat-more-formal convection studies, and Schmidt [526] concentrated on the topic. Schardin reviewed the issue thoroughly [1,2]. Modern studies include [196,357,448,674], to list just a few. Merzkirch [82] notes that the Wollaston-prism schlieren interferometer (Sect. 5.4.1) is very attractive for heat transfer studies, since the heat-transfer coefficient is proportional to $\partial T/\partial y$, measured directly by the interference fringe shift.

Examples shown here include Figs. 1.4a, 1.6, 3.12, 3.13, 3.18, 4.1b, and 4.15 given earlier, and Fig. 9.13 shown below.

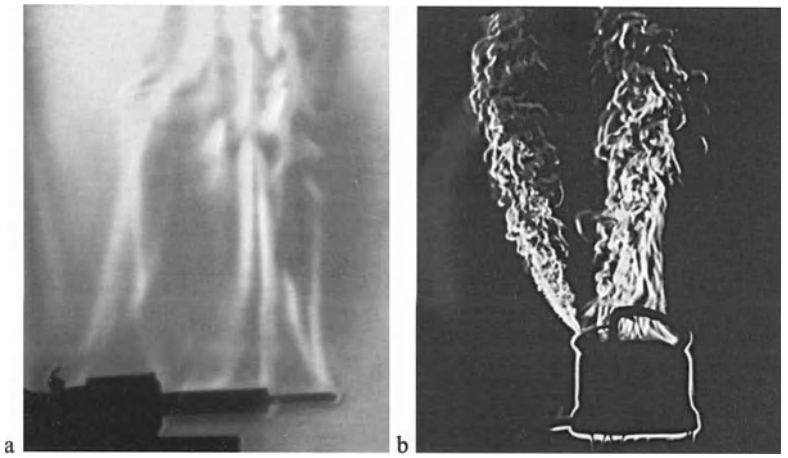

Fig. 9.13. **a** Schlieren image of the free-convection plume from a soldering iron (after the candle and the human hand, probably the third most popular convecting schlieren object). **b** darkfield schlieren image of the steam and convection plumes from a hot teakettle (a better teakettle design places the handle off to the right side).

In addition to general references on this subject, several detailed quantitative analyses of free-convective plumes were conducted using color schlieren techniques of the band- or ring-lattice type, Sect. 5.2 and Chap. 10. Color Plate 18 depicts free convection about a heated horizontal cylinder, where a vertical band-lattice constituted the source filter with a slit cutoff [356].

All these free-convection flows are scaled by non-dimensional parameters, especially the Grashof no.,

$$Gr \equiv \frac{\ell^3 \rho^2 g \beta_T \Delta t}{\mu^2} \tag{9.1}$$

where β_T is the fluid coefficient of thermal expansion in K^{-1}. Schardin [2] remarks: "It is inconvenient that the characteristic length is raised to the third power. If one scales down the flow by 50%, the temperature difference ΔT must increase by a factor of 8." Such scaling issues naturally introduce the next topic.

9.3.6 Heating, Ventilation, and Air-Conditioning

> A man has to keep his head, not breathe the hot air, and stay out of the draft.
> *Harry S. Truman*

The motion of indoor air currents due to heating, ventilation, and air-conditioning (HVAC) ought to be one of the likeliest applications of schlieren and shadowgraphy, but for the large scales involved. For many years this has dictated that only scale-model studies could be observed optically, e.g. Fig. 9.9b and Fig. 9.14 below. Schardin [1,63] and Phillips [359] showed schlieren images of small air-filled room and mine models, but recognized problems with dynamic similarity. Proper scaling requires matching the Grashof number, defined above, or its cousin the Rayleigh number [187,753,754], without which the laminar model flow may poorly represent the actual case of turbulent flow at full scale (Fig. 9.14a). By substituting water for air, the ρ^2 term in Eqn. 9.1 compensates enough for reduced length to allow conveniently-sized model experiments at 1/6 scale or even smaller [328,755]. Some of these model tests also produced quantitative results [328,359,756]. But model testing never has satisfied the need for full-scale HVAC flow visualization.

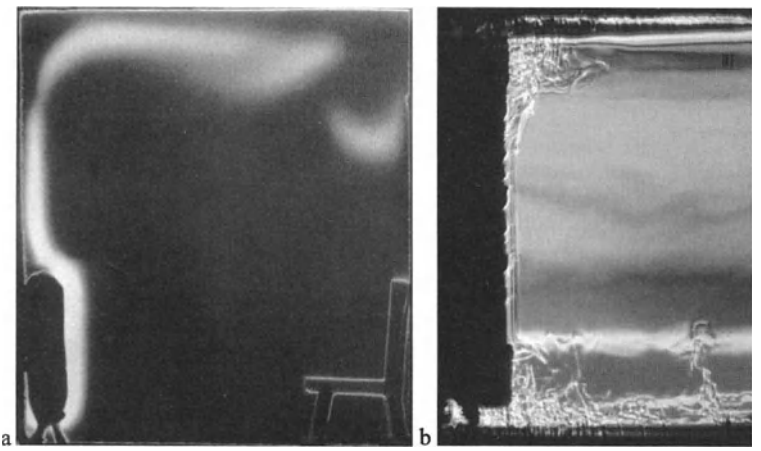

Fig. 9.14. **a** Dark-field schlieren image of a laminar heating current of air in a scale-model room. **b** liquid model of a room with a solar heater, maintaining proper scaling and revealing both turbulence and strong temperature stratification from floor to ceiling [328].

Tracers such as smoke or $TiCl_4$ are often used in full-scale HVAC studies. Much was learned from this, especially by Daws [757], but tracers tag only the air currents into which they are introduced; they fail to yield an overall picture of thermal motion. Thus the continuing need for direct visualization of air currents at full scale became an incentive to develop the Penn State Full-Scale Schlieren facility [111,236], Sect. 4.3.5. Example full-scale schlieren images of HVAC airflows were shown earlier in Fig. 4.15, and additional examples are shown below in Fig. 9.15 and in Color Plates 10 and 13.

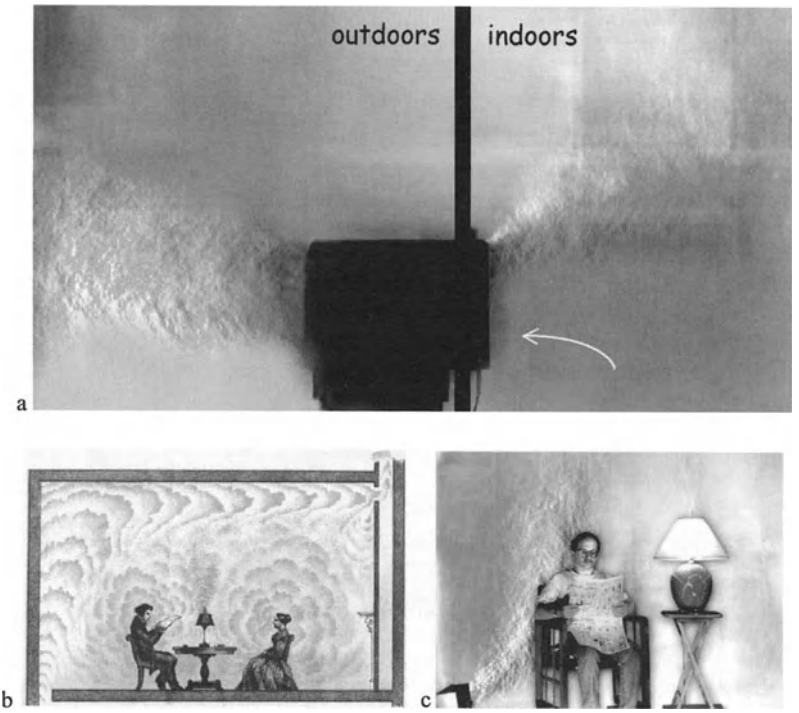

Fig. 9.15. **a** Full-scale schlieren photo of a room air-conditioner discharging its waste heat outdoors and its cooled airstream to the upper right (isothermal room air input from the lower right does not appear, but is shown by an arrow). **b** drawing of room ventilation according to Leeds [758], reproduced courtesy of the Rare Books Room, the Pennsylvania State University Libraries. **c** Full-scale schlieren photo of a domestic scene with a 1 kW space heater and a 100 W table lamp (modeled by J. D. Miller; see also Fig. 3.18).

Lewis W. Leeds [758] gives us a fascinating look at conceptual HVAC flow visualization from the 19th Century. Leeds used water models and sketches to illustrate the sad state of building ventilation at the time. In Fig. 9.15b, for exam-

ple, warm fresh air enters a residential room at bottom left, but short-circuits the living space and exits at top right, leaving residents bathed in their own pollution. Leeds underestimated the strength of the human thermal plume and made some other errors, but most of his reasoning was solid. Aside from the period costumes, his sketches bear a striking resemblance to the present-day full-scale schlieren images of Figs. 4.15a, 9.15c, and Color Plate 10. Leeds' contribution to HVAC is long forgotten, and it took more than a century to finally visualize the real thing at full scale [111,236,757]. Building ventilation is still in a sad state, tho ugh.

Within the field of HVAC are many specialized applications. Commercial kitchen ventilation [175,232,236] was illustrated earlier in Fig. 4.15c, and has become a major energy-conservation issue. Likewise industrial ventilation for hazardous fume removal can benefit from schlieren observation [759], as can the design of airflow patterns and equipment for hospital operating rooms [760]. Microelectronics manufacturing in clean rooms is a particle-sensitive application where schlieren imaging is especially valuable, e.g. [187,482,483,652,761], Color Plate 29, and Fig. 7.19.

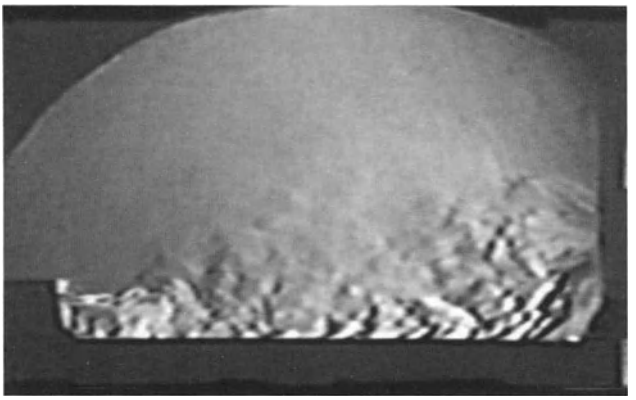

Fig. 9.16. a Push-pull ventilation from left to right for fume removal from a hot volatile industrial cleaning tank [759] (from video shot using the 0.76 m schlieren system described in Sect. 4.1.2).

9.3.7 Gas Leak Detection

The pipeline industry needs better gas leak detection systems. Similar needs occur in other industries, including chemicals and paper, metals, manufacturing, utilities, microelectronics, and military/aerospace. Leak rates in these various applications range from liters/year to dozens of m^3/hour. Some of the high-tech solutions proposed to date include acoustic detection, electrochemical sensing, laser light absorption, and various kinds of sniffers. Schlieren and shadowgraphy have seen very little use in this application, but they deserve to see more.

Schardin mentions it [1], but claims the schlieren field-of-view is too small. Vasiliev [102] also mentions it in the context of industrial applications. Yamauchi et al. [762] patented a schlieren method to detect gas leakage from fiber bundles, and Herbrich [602] applied schlieren to observe inert-gas filling of reed relays in 1962. Leak detection is further mentioned as one of the applications of moiré deflectometry [763], "zebra" schlieren [231], and a bacteriorhodopsin-based adaptive schlieren cutoff [307].

The issue was addressed most recently by Settles [237]. A full-scale schlieren image of natural-gas leak detection from [237] is reproduced in Color Plate 11, while Color Plate 31 shows a much-smaller propane leak from a rubber hose. Finally, a portable scanning schlieren approach to industrial leak detection was described in Sect. 4.4.2.

Almost any leaking gas can be detected and visualized by schlieren and shadowgraphy. O_2 and N_2 are hard to image in air, but hydrocarbon gases and vapors from volatile liquids are easy to see. So are helium, hydrogen and chlorofluorocarbons, some denser and others less dense than the surrounding air. Schlieren images not only locate such leaks, but also provide information to estimate the leak rate and indicate the leak dispersion pattern as well. This information helps to position fixed sensors near potential leak sources.

As a further example, consider the escape of gasoline fumes while filling an automobile fuel tank [764], currently an international air pollution issue. Horst Herbrich studied this fume leakage problem using his portable 300 mm single-mirror coincident schlieren system (Sect. 7.4.3). One of his results is reproduced here as Color Plate 38.

9.3.8 Electrical Breakdown and Discharge

Basic research on the electrical breakdown across a high-voltage spark gap has identified precursor phenomena (leaders and filaments) prior to the onset of the actual spark [630,765]. These precursors are relatively non-luminous, so schlieren and shadowgraphy can image their refractive fields. (Marat, in fact, first observed these by shadowgraphy in the 18th Century [30].) One must often isolate the light beam from the direct self-luminosity of the spark, e.g. by using a laser source with a narrow bandpass filter (see [605,766] and Sect. 7.2.5). Similar phenomena, including electro-convection and streamers, are seen in the breakdown of liquid dielectric insulators [767-770]. Waters [771] reviews the general topic of diagnostic methods for such discharges and plasmas.

A related application is found in the high-voltage electrical switchgear and circuit breakers of commercial power companies. Breakers interrupting tens-of-kA currents use SF_6 gas to assist in interrupting and cooling the resulting arcs. Thus the electrical phenomena are coupled with gas dynamics, and together they are best observed by schlieren optics [766,772-776]. The University of Sydney produced an award-winning color film in which high-speed schlieren cinematography visualizes such circuit-breaker arcs [777].

9.3.9 Explosions, Blasts, Shock Waves, and Shock Tubes

> Shock wave photography resembles ordinary photography in that it is partly an art and partly science.
>
> *W. F. Hilton* [122]

> A physical experiment which makes a bang is always worth more than a quiet one.
>
> *G. C. Lichtenberg*

Beginning with the strong precedent set by Toepler [40,41,135] and Mach et al. [55,56,778], visualizing moving shock waves has always been one of the most robust applications of schlieren and shadowgraphy. Explosions, blasts, and moving shock waves have peaceful as well as destructive uses, both of which were imaged extensively in many studies. Examples were shown earlier in Figs.1.9b, 1.11a, 1.17b, 1.18b, 6.14, 7.13, and 7.14b. Several more are shown in Fig. 9.17 below, and in Color Plates 5, 12, 23-25, 33-35, and 48.

The early investigators, per Chap. 1, also included Boys [62], Wood [48,74], and Foley and Souder [779]. Schardin [2,615,780] pioneered high-speed schlieren and shadow cinematography in the shock tube [781], followed by Glass [628,629] and several more-recent investigators [83,378,393,397,449,612]. Key references include Lighthill's popular lecture [782], Glass's *Shock Waves and Man* [628], the textbook by Lewis and von Elbe [513], and the reviews of shock and blast flow visualization by Dewey and McMillin [202,210].

The classical problems of shock motion, much observed by schlieren and shadowgraphy, include shock-wave diffraction [416,783] and Mach reflection [202,550,784,785]. Shocks in porous or layered media are also studied optically [786,787]. Recent work includes laser-driven shock waves [617,788,789] with applications, for example, in living tissue ablation [790]. While nuclear weapons development in the late 20th Century prompted many outdoor blast studies, the rise of international terrorism has now triggered new investigations of blast effects, shock motion, and scaling inside buildings and aircraft: [166,597,791-793] and Color Plates 12 and 48.

Further, the optical properties of a blast wave itself are quite interesting [529]. Mair [164] notes that a strong shock wave in glancing light can act as a mirror, causing a mirage effect [795]. Burton et al. [42] also observe that, since shock waves are exceptionally thin, glancing light rays are usually refracted completely out of them. Strong shocks can refract light through as much as 2000 arcseconds, causing ray displacements of several centimeters in the schlieren cutoff plane and leading to image measuring-range anomalies described earlier in Sect. 3.3.

Usually the schlieren image or shadowgram only reveals the envelope of a shock-wave-bounded region, where the light glances the wave. Examples are shown in Figs. 1.11a, 2.7a, 6.13a, 6.14a, and 7.15, depicting flowfields that are actually spherical or conical, though only the projected shock envelope is actually seen. Diffraction of light by shock waves, illustrated in Fig. 6.9, is further discussed in [528-531].

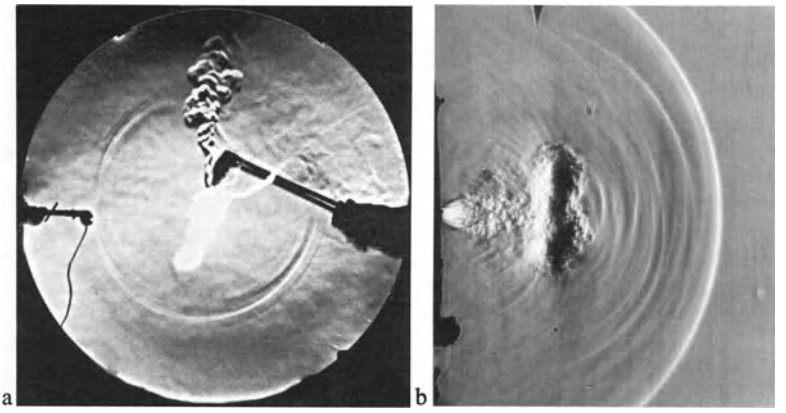

Fig. 9.17. **a** The explosion of oxygen and acetylene causes a weak shock wave when a cutting torch is turned off improperly (photo by author). **b** an expanding gas jet generates a head wave and a compressible vortex ring [794], photo courtesy A. Choulmeister.

9.3.10 Ballistics

> You may be disposed to say now, it is all very pretty and interesting to observe a projectile in its flight, but of what practical use is it? It is true, I reply, one cannot *wage war* with photographed projectiles.
>
> *Ernst Mach* [9]

> A well-trained eye can immediately read the appropriate flight velocity from the schlieren image
>
> *Hubert Schardin* [2]

Ballistics is central to our centuries-old need to hurl things through the air, usually at one another. Many examples were already shown in various contexts, including Figs. 1.12, 1.18a, 2.7, 4.5d, 6.2b, 6.13a, 6.14b, 7.16, 9.8b, and 9.12. A few more are included here and in Color Plates 23-25 for completeness (or maybe overkill).

Mach and Salcher set the precedent for high-speed optical ballistics [4], followed by the lifelong effort of Cranz [78] and then his student, Schardin [1,2]. This historical path was summarized in Chap. 1 and is covered in more detail by Kutterer [80]. Schardin, a military ballistician in his early career, adds the fascinating historical note that transonic projectile drag-rise was uncorrelated with Mach number until after World War I. "Sufficient attention to the schlieren images would thus have considerably improved precision firing during the war" [2].

Ballistic ranges flourished during and after World War II as free-flight analogs of the wind tunnel. Typically, a test model encased in a protective *sabot* is fired from a gun down a long tube, filled with air and having a number of high-speed instrumentation ports. The sabot peels off upon exiting the gun muzzle. At the end of the range the model strikes a barrel of sand and is destroyed. Between the

muzzle and the sand, in a few milliseconds, shadowgrams are taken and – with luck – something useful is learned. "Focused" shadowgraphy is most often used for this, as described earlier in Sect. 6.3.5. The higher sensitivity of the schlieren method seldom overrides shadowgraphy's robust simplicity for this application.

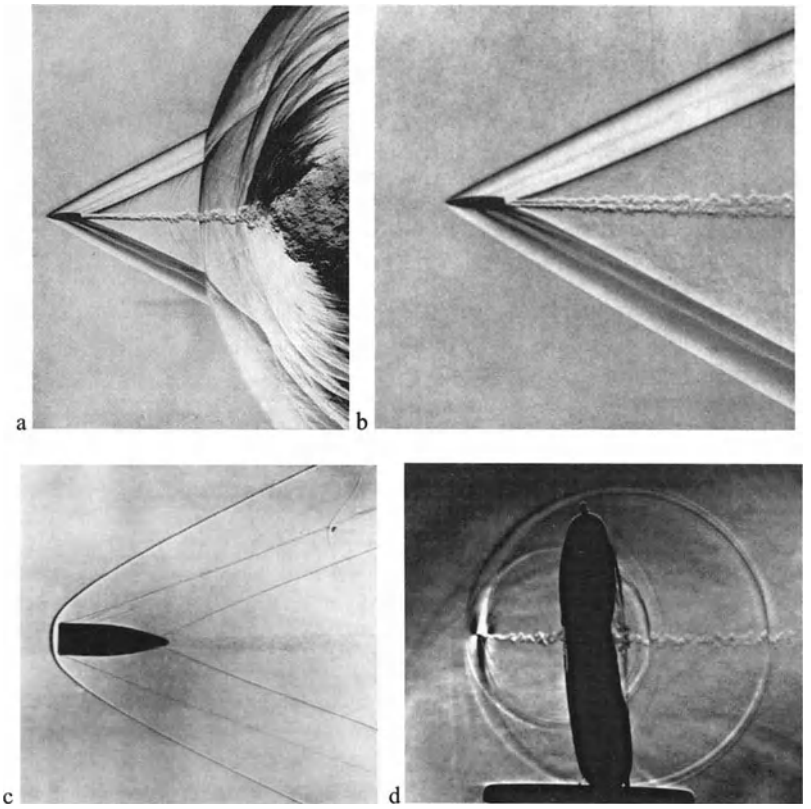

Fig. 9.18. **a** A supersonic bullet overtakes its own muzzle-blast wave. **b** closeup of a supersonic bullet. **c** a startling shadowgram of a supersonic bullet flying backwards. **d** a toy balloon is burst twice by the same transonic bullet. Schlieren photos a and b from Schardin [2] and shadowgram c from Cranz [78] are reproduced by courtesy of Springer-Verlag. Schlieren photo d was taken by the author.

Such ballistic-range tests have the advantages of clear air and no support interference. Their obvious disadvantages lie in the destruction of the model and the severe limits placed upon its instrumentation. In fact, the foremost type of data obtained is usually quantitative trajectory data derived from shadowgrams. These

shadowgrams must obviously be fast and well-timed. Qualitative data on shock-wave and shear-layer positions, boundary-layer separation, etc. also result.

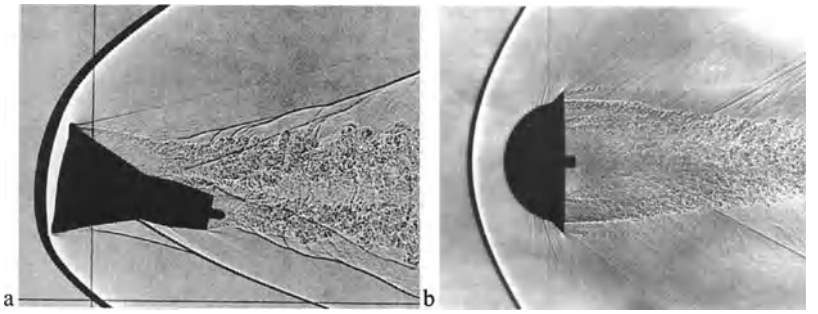

Fig. 9.19. **a** Gemini capsule model in simulated hypersonic reentry into the atmosphere. **b** ballistic shadowgram of a finned hemispherical model. US Govt. photos (NASA-Ames).

Fuller [203], Mishin [796], and Dementjev et al. [148] surveyed high-speed photography in ballistics. Recent reviews of NASA [797] and Japanese [798] ballistic-range facilities show that shadowgraphy remains important. Replacing the traditional photographic film by an electronic shadowgraph camera is receiving current attention [633,634].

9.3.11 Gas Dynamics and High-Speed Wind Tunnel Testing

> Tunnel windows, like tunnel models, are often expendable items, and if one breaks in use, the other usually breaks in sympathy.
>
> *W. F. Hilton* [122]

Probably more than half of all the publications ever written on schlieren and shadowgraphy are in this application area. Schlieren optics have long been standard equipment for high-speed wind tunnels, and more was learned of the flow behavior from schlieren and shadowgraph observations than from any other diagnostic method. It is a very broad application, merely abstracted here with no attempt at thoroughness.

Mach and Salcher [60] invented the high-speed wind tunnel as described in Chap. 1. Prandtl's research group [75] established the underlying theory and built practical apparatus for testing, leading eventually to the first large supersonic wind tunnels at Peenemünde [85]. Historical and practical references on optical flow visualization in high-speed wind tunnels include Schardin [2], Stack [88], Hilton [122], Holder and North [98,99], Mair [164], and Volluz [109]. An essential reference is *High-Speed Wind Tunnel Testing* by Pope and Goin [799], and two ex-

cellent, though dated, films are available [95, 800]. The former-Soviet-Union perspective is given by Vasiliev [102] and Skotnikov [638], while miniature home-built tunnels are described by Stong [532] and Pantalos [801]. Recent publications [128,224,400,802] prove that the topic is still evolving.

Many illustrations were shown in previous chapters, including Figs. 1.16, 1.19, 1.21, 3.16, 3.17, 3.20, 4.5c, 5.10, 5.17, 6.1, 6.10, 6.16, 7.6, 7.11, 7.15, and several of the Color Plates. Additional Color Plates 42-44 show a horizontal band-lattice color schlieren photo of a shock wave/boundary-layer interaction [614], 2-D supersonic flow over a planar wedge, and an early prism-method image of a supersonic missile test [345], respectively. Four more images are given below to further exemplify the many flow phenomena that one typically observes in high-speed wind-tunnel testing.

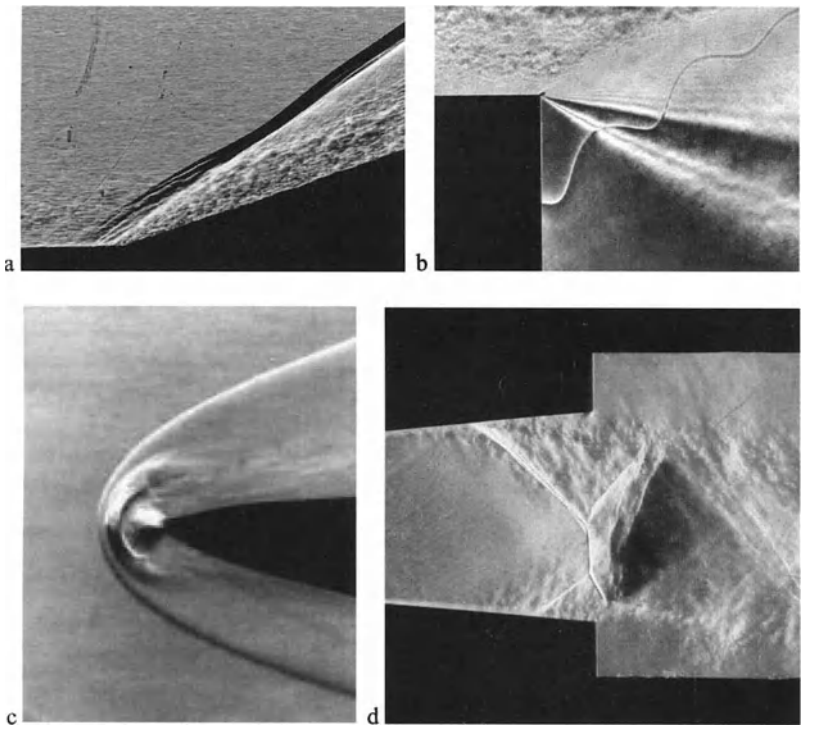

Fig. 9.20. **a** Contact shadowgram of Mach 3 shock wave/turbulent boundary-layer interaction at a compression corner [614]. **b** Wollaston-prism schlieren-interferogram of Mach 3 turbulent boundary-layer re-laminarization though a Prandtl-Meyer expansion fan at a backstep (from [803] by permission of R. H. Page). **c** counter-flow injection of high-pressure gas at the nose of a body in Mach 7 flow, NASA-Langley photo EL-1997-00053. **d** asymmetric separation at the exit of a 2-D supersonic nozzle, μsec image by the author.

Fig. 9.20 illustrates Prandtl-Meyer expansions, turbulent boundary layers, plane and curved shock waves, and flow separation. These phenomena, along with slip lines and laminar boundary layers, comprise some of the "building blocks" of complex compressible flows through channels and over flight vehicles and projectiles. Mair [164] notes that a nearly-2-D shock wave usually appears in a schlieren image as a fan-shaped region of small included angle (e.g. Fig. 9.20d), since it is unlikely ever to be exactly parallel to the light beam.

Supersonic and hypersonic wind tunnels are routinely fitted with high-quality schlieren windows, while subsonic tunnels normally need only plate-glass windows for smoke or oil-flow visualization purposes when insufficient refraction is present. Transonic tunnels [799] are a special case, since the need for slotted or perforated test-section walls precludes ordinary schlieren windows. The multiple-source schlieren arrangements discussed in Chap. 4 have had some success in this difficult testing regime [215,238].

Qualitative information gleaned from schlieren and shadowgraphy in high-speed wind tunnels includes shock-wave shapes and locations, the positions of boundary-layer separation and vortex cores, and regions of wave interference. Sonic-boom research also depends upon such qualitative cues [243]. Semi-quantitative data on shock-wave angles, transition locations, and the extent of separation (when it occurs) are likewise routinely extracted from the optical visualizations. Quantitative density data are obtained much less often, and are covered in Chap. 10.

Special shear-layer wind tunnels sprang up late in the 20th Century for compressible turbulent mixing research [7,804-809]. Schlieren and shadowgraphy not only played their traditional qualitative role in identifying large-scale structures (see Fig. 1.23), but also provided quantitative velocimetry data [220,620].

Flight testing is even more expensive than wind tunnel testing, but is essential for some purposes. Schlieren and shadowgraphy have occasionally gone along for the ride ever since the 1950's [112,243,266,810-814].

9.3.12 Supersonic Jets and Jet Noise

With jet propulsion comes jet noise, a major headache for aero-acousticians, jet-engine manufacturers, and people who live near airports. Decades of research have revealed various modes of noise production in high-speed jets, including the interaction of shock waves and turbulence, jet oscillations, and feedback phenomena. From the outset, when Mach and Salcher [60] first visualized supersonic jets, schlieren and shadowgraphy have played a key role in revealing the physics of jet noise. Stroboscopic illumination is especially helpful in capturing jet oscillations that can lead to discrete, directional noise emissions.

Salcher's original supersonic jet is shown in Fig. 1.13b. Steady jets are depicted in Figs. 5.15, 5.16a, and 5.17, while a noisy, oscillating jet is shown in Fig. 6.2c [524]. Other jet schlieren and shadowgram examples can be found in Refs. [226,239,240,319,449,504,815-818] and Color Plates 21 and 22.

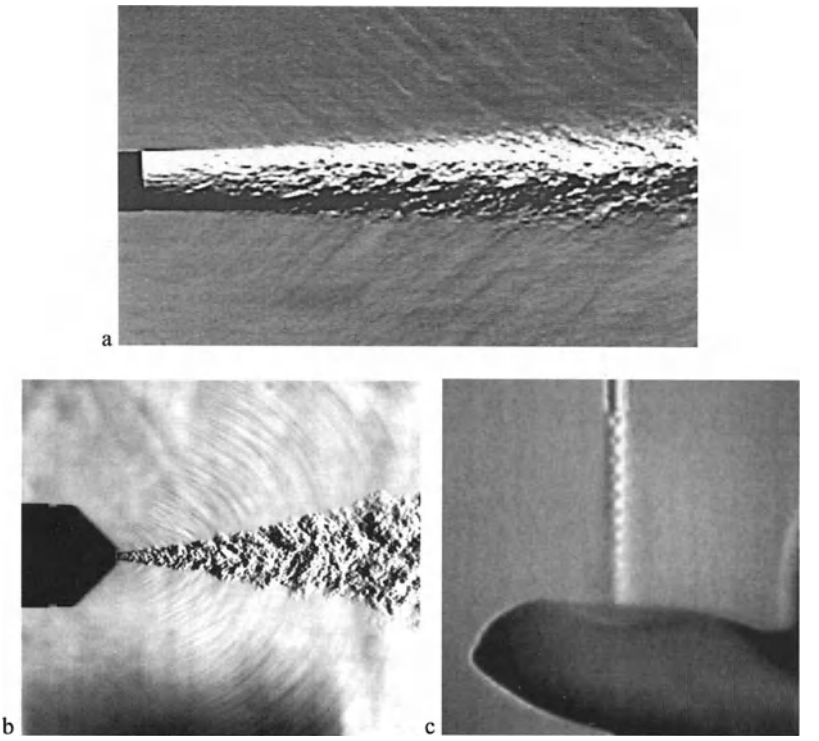

Fig. 9. 21. **a** Schlieren image of a Mach 3 axisymmetric turbulent free-jet, μsec exposure showing acoustic radiation [808,819]. **b** jet noise is directed in a forward cone in this cold-flow image of a cutting-torch nozzle by H. Herbrich [124], reproduced by courtesy of Messer Griesheim GmbH, Industriegase Deutschland, a member of the Hoechst Group. **c** a supersonic microjet dimples the author's fingertip, observed by focusing schlieren [818].

9.3.13 Turbomachinery and Rotorcraft

In the special case of the rotating axial-flow compressors and turbines of jet engines, specular reflection from blades was used in one schlieren investigation [475]. More commonly, though, fixed cascade flows are imaged [330,820-822], and color schlieren is popular.

In rotorcraft research, the wakes and tip vortices of rotor blades are visible by refraction and much can be learned from this. Large, rapidly-spinning helicopter rotors are one of those applications where the robust simplicity and large field-of-view of direct shadowgraphy rules [516-520,553,823,824]. A new contender, though, is the background-oriented schlieren system described further in Sect. 10.3.5 [812,814,825]. Trivial by comparison, an ordinary window fan still reveals a beautiful tip vortex in Color Plate 20 [386,387].

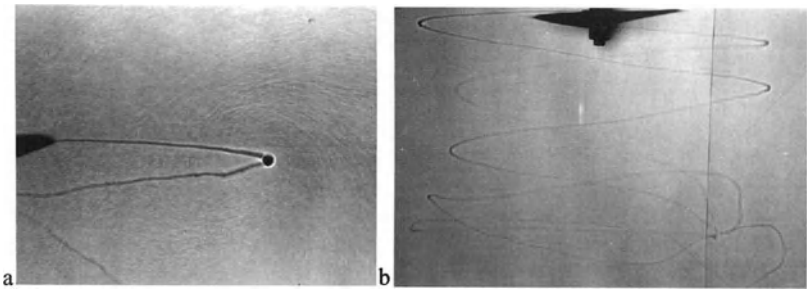

Fig. 9.22. Shadowgrams of rotor wakes **a** Close-up of the tip-vortex trailing from a helicopter rotor blade. **b** two-bladed propeller operating in the static thrust condition. Note the onset of wake instabilities well downstream of the rotor, appearing in the form of interactions between adjacent vortex filaments. Photos courtesy of J. G. Leishman, University of Maryland [223,519,520,553].

9.4 Other Applications

Despite the ordered classification of schlieren applications in solid, liquid, and gaseous matter just given, some topics demand special consideration. They are grouped in this Section in alphabetical order.

9.4.1 Art and music

> I have written only one masterpiece. That is the *Bolero*. Unfortunately, it contains no music.
>
> *Maurice Ravel*

Few readers will get this far without realizing the aesthetic aspects of schlieren and shadowgraph pictures. The stone-carving bas-relief effect of a schlieren image was pointed out in Sect. 2.6, and many of the images shown so far were singled out for their beauty. Part of this arises from the natural symmetry and abstraction of the phenomena observed, while another part comes from the schlieren photographer himself, who, in the spirit of Schardin and Edgerton, is much more than just a technician operating the equipment.

Art and scientific illustration have been inseparable since Leonardo da Vinci. Toepler, Schardin, Holder, and North all appreciated the artistic side of their images. Though he said little about it, Schardin evidently made a h obby of taking spectacular and beautiful schlieren photographs. Why else fire supersonic bullets in tandem (Fig. 9.23a below) or through candle flames (Fig. 1.18a)? R. J. North's

color schlieren photos (Color Plate 3) were exhibited at the 1952 International Exhibition of the Photographic Society of America. Howes [411] noted the artistic effects of "rainbow" schlieren, and Davies [635] observed that attractive schlieren photographs might open up many new applications in commercial art, advertising, and special effects. Kleine [826] is the most recent author to consider the artistic side of flow visualization.

Schlieren images display recognizable forms (candles, people, bullets, etc.) to the public in the unfamiliar context of scientific photography, thus exciting curiosity and fascination. Some of my color schlieren images have appeared hundreds of times in popular books, magazines, newspapers and television programs around the world for this reason, e.g. [389,827-830]. The most popular of all these is "the human cough" (Color Plate 28), especially sought after during influenza season.

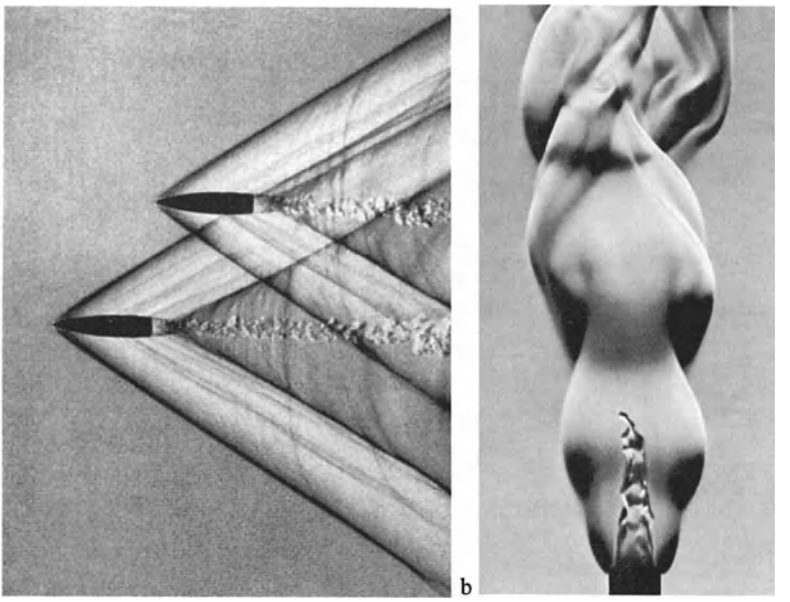

Fig. 9.23. Deliberately- and accidentally-artistic schlieren photos: **a** twin supersonic bullets flying almost abreast, from Schardin [2] courtesy Springer-Verlag. **b** "The Lady in the Flame," from Keagy, Ellis, and Reid [136,592] courtesy Battelle.

Despite all this, it appears that only one professional artist has ever incorporated schlieren or shadowgraph images directly in his work. Brazilian artist Mario Ramiro creates art in which "changes in dimensions that are invisible to us resonate in and can be made visible in the material world" [426]. His first works of this type were "thermal sculptures" whose convected heat was visualized by laser shadowgraphy. Changing the visible sculptures caused corresponding changes in

their normally-invisible thermal plumes, symbolizing fire without actual combustion and recalling the ghost of Marat. In Ramiro's later works, insubstantial human figures confront their own more-tangible images in a large schlieren mirror, suggesting themes of opposition and duality (see [426] for an example).

That such deliberate use of schlieren and shadowgraphy in serious art has only been attempted once indicates the almost-untouched artistic potential of these techniques. For some young M. C. Escher, equally at home in art and science, here lies a grand opportunity.

Music has two main junctures with schlieren and shadowgraphy: the optics are used to image tone generation in musical instruments, and they provide a potential means to render the music itself visible through some mechanism of translation.

Schardin [2] reports on various uses of schlieren imaging to visualize tones created by gas flows, especially edge tones and Aeolian tones due to Kármán vortex shedding. In the former, a stream of gas is directed against a sharp edge, causing regular vortex shedding at an audible frequency. Though this was first observed in the early 20th Century, Krüger and Casper [831] first defined a Strouhal number for the shedding process based on darkfield schlieren observations in 1936. Recent work by A. Hirschberg and colleagues of Eindhoven Technical University, the Netherlands, applies schlieren observation to edge-tones in woodwind instruments [832-835]. These investigators point out that woodwinds are much more complex, physically, than stringed instruments due to fluid dynamics. Using glass-walled instruments blown with CO_2 for refractive contrast, they produced the examples shown in Fig. 9.24 below. Having gained a better understanding of the fluid physics of woodwind instruments, Hirschberg et al. note that the instruments behave overall like simple global oscillators, but the actual music is produced by flow details at much-smaller-than-global scales.

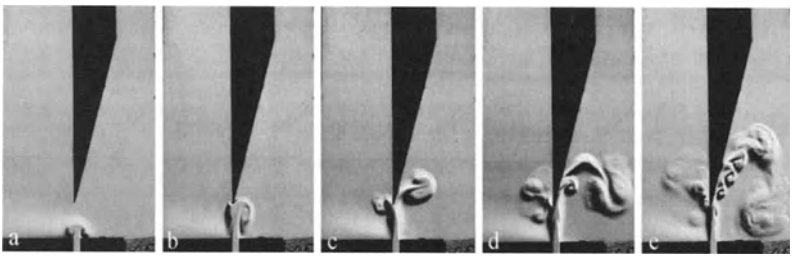

Fig. 9.24. Edge-tone generation in a small flue-organ pipe with a geometry typical of a recorder flute. A close-up of the mouth of the instrument is shown with a flue (slit) width of 1 mm and a distance from flue exit to labium (sharp edge) of 4 mm. The stagnation pressure of CO_2 exiting the flue is 200 Pa above atmosphere, and the time delay between adjacent frames is approximately 1 ms. Schlieren images courtesy A. Hirschberg [835].

In related work [834], Hirschberg et al. have also observed shock waves at the mouths of trombones played at fortissimo levels, causing a "bright metallic" sound

quality. Similar results are expected for trumpets. Thus the gas dynamics of wind instruments has become one of the latest new, non-traditional applications of schlieren imaging.

Rendering the music itself visible, on the other hand, is a much-tougher pr oposition than observing the gas dynamics of music-making. There is no Rosetta Stone for the translation of 1-D audio signals into 2-D visual patterns, though this has not stopped hardy inventors who have built and patented "color music display" devices for centuries [836,837] with varying degrees of success. Good examples are found in Disney's *Fantasia* (1940), and some laser light shows [838].

A few of these color music displays use fluid effects and even schlieren or shadowgraph principles. Boys [653], for example, recounts Glew's use of sunlight shadowgraphy to observe vibrations of thin soap films, revealing the combined motion and color effects produced by music. Forkner's [839] light display instrument similarly visualizes the vibrations of a stretched membrane-mirror by way of color schlieren optics.

Hans Jenny [703] invented his "tonoscope" in the 1960's to visualize sound and music by way of vibration-induced liquid-surface-wave patterns. In this he invoked the original work of Faraday [700] and Rayleigh [701]. The topic is very close to that of Sect. 9.2.2, but the goal is now the artistic presentation of a color music display, not the scientific measurement of wave patterns.

Jenny's rudimentary schlieren observation of music-driven surface waves was expanded upon by Flournoy and Settles [391,704] using a stroboscopic color schlieren beam reflected from a pool of mercury driven vertically by a loudspeaker. Faraday waves on the mercury surface were excited by musical tones, producing the abstract color patterns shown in Color Plates 39 and 40. However, like many of its predecessors, this device succeeded only partially: when driven directly by music, it produced disjointed, frenetic, even irritating visual patterns.

The lesson having been learned once again that music does not translate literally into visual patterns, Flournoy and Settles [391,704] then discovered that they could drive the surface waves and the visual display with an auxiliary sound track of simple tones timed to coincide with the actual music. The driving-tone frequency determines the scale and apparent rhythmic motion of the resulting wave patterns, while its amplitude establishes which colors come into play in the band-lattice schlieren cutoff. By this artificial means a successful color music display became possible. This particular device, however, as well as the general topic of schlieren and shadow effects in music representation, belong to a very incomplete field of endeavor.

9.4.2 Biomedical Applications

A broad panoply of biomedical applications has opened up for schlieren and shadowgraphy in the latter half of the 20th Century. These are grouped below in four general categories. One topic, ultrasonic medical imaging, was already discussed in Sect. 9.2.4. The expansive topic of microscopy is covered later, and certain non-imaging ultracentrifuge applications are outside the scope of this book.

Medical Diagnostic uses of schlieren and shadowgraphy begin in 1649 with ophthalmology as practiced by Johannes Wiesel (1583-1662), the very first historical record yet found [11]. 3½ centuries later the human eye is still a subject for schlieren and shadowgraph examination [723,840-843]. An example image is shown in Fig. 9.25a.

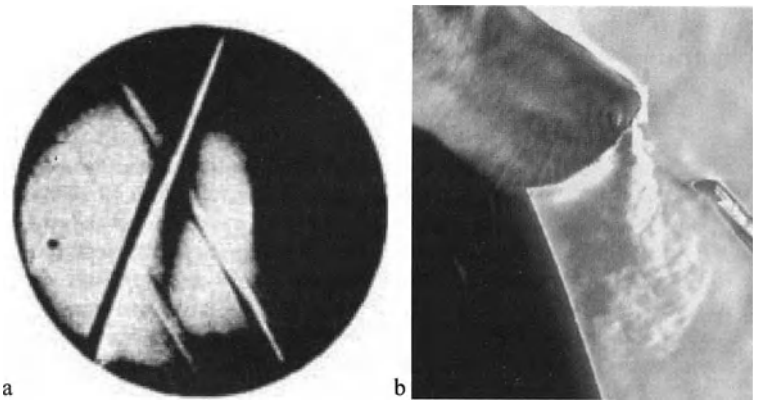

Fig. 9.25. **a** Schlieren image of vitreous strands in the human eye, from Winthrop [841]. **b** air exhaled from canine nostrils is vectored downward and to the sides [190].

Davies [844] suggests the use of schlieren imaging in speech therapy, where abnormalities in the escape of air from the lungs and mouth are related to certain speech problems. An even-larger application area is sleep apnea, a serious condition wherein breathing ceases during sleep. The advantage of schlieren imaging in these applications is its non-intrusiveness, suitable even for sleeping patients. Yet these opportunities remain entirely unexplored.

A good example of the possibilities, however, is found in a study of the aerodynamics of canine olfaction by Kester et al. ([190] and Fig. 9.25b). Dogs were observed non-intrusively by schlieren optics while sniffing, revealing that their nostrils function as variable-geometry aerodynamic samplers. Nostril motion produces separate pathways for the inhaled and exhaled air, the latter being directed rearward and to the sides by flaring the nostril side slits.

Conventional medical diagnostic x-ray images, still the main way of looking inside the human body, are not usually associated with schlieren and shadowgraphy. They are, in fact, shadowgrams of a different sort: absorption rather than refraction. Nonetheless x-rays do refract, and recent work [845,846] utilizes this by applying schlieren and shadowgraph principles to better distinguish different kinds of soft tissue. In mammography at x-ray energies of 15-25 keV, for example, refraction is orders of magnitude larger than absorption. Cancer cells contain more protein than normal cells, altering their density and refractive index and making them visible. Striking results are obtained, including a radiogram on the cover of *Physics Today* that bears the unmistakable likeness of a schlieren image [845].

Laser Pulses and Shocks Waves are important in certain medical treatments. Laser tissue ablation produces shocks that are observed by schlieren in several studies [790,847]. Similarly the thermal response of tissue has been examined [331,332]. Laser lithotripsy and extracorporeal shock wave lithotripsy break up kidney stones and gallstones by focusing a shock wave upon them, as imaged by schlieren and shadowgraphy in Refs. [724,848-855].

Gel Electrophoresis is a biochemical method of protein separation that got an early start with schlieren imaging in 1937 (Tiselius [856]). Protein zones in electrophoretic gels are difficult to locate or stain, but show strong refractivity under schlieren or shadow observation. The 60-year-plus history of this is well described by Takagi and Kubota [420], including several color schlieren images and the description of a rare commercial schlieren instrument (see Sect. 7.4.2). Related work is found in [318,394,857-859].

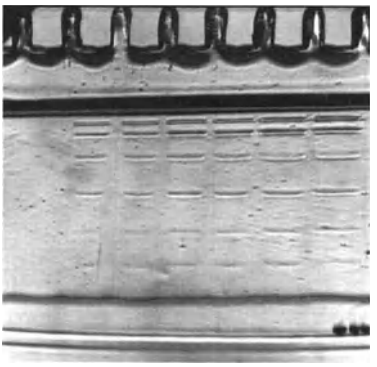

Fig. 9.26. Schlieren image of protein bands in gel electrophoresis [420]. The six columns show the effect of increasing concentration of the initial protein solution (left to right), while the vertical distance between bands is the electrophoretic separation of the six proteins in the solution. From an original color schlieren image taken using the Schlierograph EDS-100 instrument, reproduced by courtesy of H. Kubota and K. Arita, ATTO Corp., Tokyo.

The Human Thermal Plume, though invisible, is alluded to more richly in the general literature than in all the technical journals. Examples include:

> Here he this instant stood; I stand in his air, - but I'm alone.
>
> *Herman Melville,* Moby Dick

> That woman has left damp fingerprints in the air.
>
> *Sinclair Lewis,* Main Street

> The warmth of her couched body rose in the air.
>
> *James Joyce,* Ulysses

Further to the point, the first shadowgraphy of the human thermal plume occurred at a strange and hilarious path-crossing of the great historical figures Franklin and Marat, as described earlier in Chap. 1. Since no image was recorded at the time – over two centuries ago – I have dared to sketch an impression of it in Fig. 9.27a. I imagine that the event was accompanied both by laughter and astonishment.

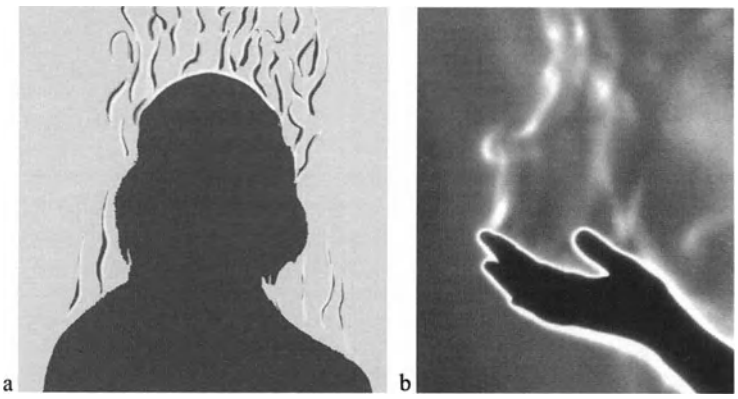

Fig. 9.27. **a** Sketch recreating the first optical observation of the human thermal plume: Benjamin Franklin offers his bald head as a subject for Marat's shadowgraph (see Sect. 1.2). **b** the thermal plume and boundary layer of a human hand (photo by author).

A century later, Toepler [3] first described the optical visualization of the human thermal plume in detail. Though he showed no images, he discussed the plume from the hand, body heat transfer through thick clothing, and the overall thermal plume rising from a person.

No one took notice again for another century, until medical doctors H. E. Lewis and R. P. Clark [373,860-863] stumbled afresh upon schlieren visualization of the human plume while on a tour of wind tunnel facilities in the UK National Physical Laboratory. At long last, they explored the topic comprehensively.

Many images of the human thermal plume are already shown here in Figs. 1.6, 3.12, 4.1, 4.15, 5.12, 9.15, 9.16, and Color Plates 10 and 29. It is instructive to compare one more schlieren image of the plume from a human hand, Fig. 9.27b, with Draper's [35] sketch, Fig. 1.6, and Schardin's examples, Fig. 3.12.

A few subsequent studies of clothing effects [864], hospital operating rooms [760], mosquito homing mechanisms [865], and the plumes of animals [742] have certainly not exhausted the potential of this application. Settles et al. have studied it most recently [111,127,187,188,236,652]. Key developments from this work lie in ventilation [236,761] and the portal detection of trace signals from the human body [188,189,866].

I cannot quit this subject without at least mentioning the "human aura." The publication of human-thermal-plume schlieren images like those shown here has elicited many inquiries about a possible connection with the alleged energy field or "aura" of the human body [867]. One enthusiast suggested that the a red zone at the lower back of a human subject one of my color schlieren photos indicates serious back problems. Having looked into the matter, however, I can state conclusively that there is no such connection: while the human aura is a paranormal concept of questionable legitimacy, the human thermal plume is certifiably known to be nothing but hot air.

9.4.3 Combustion

> "Look not too long into the face of the fire, O Man! Never dream with thy hand on the helm!"
>
> *Herman Melville*, Moby Dick

Hooke [14,21] and Marat [28] pioneered the study of combustion by schlieren and shadowgraphy (see Chap. 1). Toepler carried out many schlieren flame observations as well [3,40,41]. While each of these investigators had a century to himself, the 20th Century saw schlieren and shadowgraphy become everyone's favorite means of combustion observation. Combined with the direct inspection of luminous flames [868], optical methods nowadays provide a unique view of the convective aspects of burning phenomena.

No other publication covers this topic better than Weinberg's *Optics of Flames* [66], still a thorough and essential reference after almost 40 years. [2] Weinberg points out, for example, the salient difference between the refractive fields of combustion phenomena, where 40 arcseconds is a small beam deflection, and those of aerodynamic phenomena where deflections may be 100 times smaller.

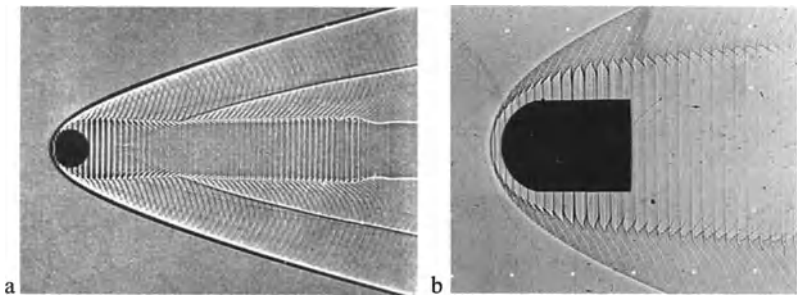

Fig. 9.28. **a** Struth's [433] shadowgram of a projectile fired at Mach 4.75 into a reactive H_2/air mixture. **b** similar photo by Lehr [869], revealing cyclic detonation behind the bow shock, the cause of the regular flow striations. Flame-front distances measured from such photos make it possible to define the ignition delay time. Both shadowgrams of ballistic combustion are reproduced by courtesy of the French-German Institut Saint-Louis, ISL.

Previously-shown examples include Figs. 2.4, 8.4b, and 9.17a, and more candle-flame images than can be conveniently listed. Two additional examples of ballistic combustion are given in Fig. 9.28 as well. Oppenheim expounds on the beauty of combustion fields observed by color schlieren [877], and many fine

[2] Written before the laser, *Optics of Flames* should now be considered along with a later paper by Oppenheim, Urtiew, and Weinberg on the laser as a schlieren light source [100].

schlieren and shadowgraph images of combustion are reproduced in the classic textbook by Lewis and von Elbe [513].

Among the topics well-represented in the literature is fire safety research, where scaling is once again a problem and large optical fields-of-view are often required [143,255,870,871]. Much more could be done on this topic with the large-scale methods described in Chaps. 4 and 6.

Self-luminosity, already covered in Sect. 7.2.5, becomes a problem for highly-luminous flames, as in solid-propellant combustion studies [368,604]. Also the flame temperature itself has been inferred from schlieren images in several instances [276,872,873].

Internal combustion engines for research use are traditionally fitted with quartz windows through which a schlieren beam can pass [327,874]. Other types of combustion chambers are also amenable to schlieren [481,875] and shadowgraph [876] observation. Cylinder-charging swirl and fuel droplet evaporation are observed by schlieren, and the fractal dimension of flames has been determined [121].

9.4.4 Geophysics

Surprisingly, even large-scale geophysical phenomena of the atmosphere, ocean, and earth can be modeled successfully in the laboratory. Optical imaging is important in these studies, including salt fingers in the ocean, magma convection in the earth's mantle, and seismic phenomena. Turner [687] gives an excellent recent summary, including several shadowgrams.

Salt fingers result from double-diffusive convection (Sect. 9.2.1) when warm salty water overlies colder, fresher water in a stratified tank or ocean environment [506,507,684,878]. Salt fingers were predicted theoretically and observed in the laboratory [685,687] before they were first detected in the ocean using shadowgraphy [879,880].

Convection also dominates the flow of magma in the earth's mantle. Unlike the case of the ocean, no direct observation is possible, but both schlieren and shadowgraphy reveal the relevant flow patterns in laboratory-scale experiments [687-690,881-884]. Rayleigh-Bénard convection, transverse rolls, bimodal convection, highly-viscous flow, magma chambers, and crystallization have all been observed and studied.

Finally, 2-D transparent gel or acrylic models have also been used to study elastic wave propagation in the earth's crust, including faults, layered models, and liquid-solid models [637,639,885-893]. J. Kozák and colleagues led this work at the Geophysical Institute of the Czech Academy of Sciences in the 1970's, using one of the time-honored IAB-451 schlieren instruments described in Sect. 7.4.1. Both qualitative and quantitative results were obtained in this work. Since seismic waves in solids travel at km/sec speeds, high-speed imaging was required. In summary of this research, Prof. Kozák states that "the schlieren measurements can be understood as one step up the long staircase of human progress in seismic wave propagation study [894]." An example IAB-451 schlieren image is shown in Fig. 9.29b.

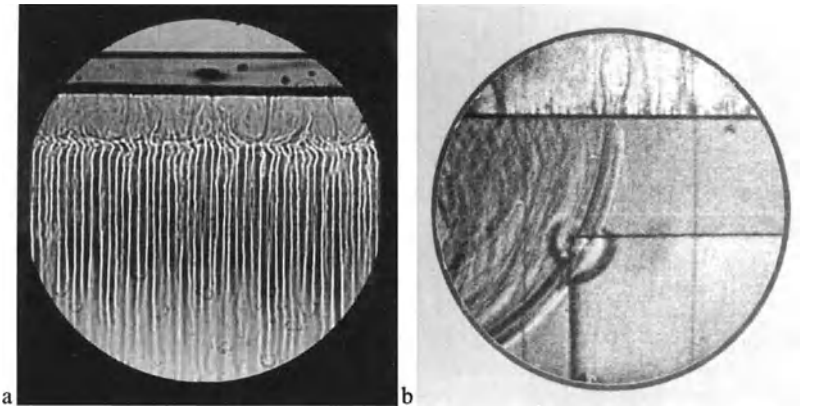

Fig. 9.29. **a** Laboratory salt fingers observed using the small optical system of Chap. 8 (experiment and shadowgram by Heather Ferree). **b** high-speed schlieren image of elastic waves in a seismic gel model [885] (photo reproduced by courtesy of Prof. J. Kozák).

9.4.5 Industrial Applications

The experts on this topic are Horst and Liselotte Herbrich of Industriefilm, Kelkheim, Germany, http://www.schlierenoptics.de, whose firm meets a broad range of industrial needs for flow visualization [124,602,650]. Several of the present topics spring significantly from their experience. Unfortunately, many of these studies were never formally published.

Automotive applications of schlieren and shadowgraphy include both interior and exterior airflows, engine combustion and cooling, window-glass testing (Sect. 9.1.1) and assembly-line issues such as the evaporation of solvent following auto body painting. Imaging the fume escape from the fuel tank was discussed in Sect. 9.3.7 and is illustrated in Color Plate 37.

Domestic Appliances and Products present broad opportunities for schlieren and shadowgraphy. Hair dryers, hair sprays, space heaters (Fig. 9.15c), stoves, immersion heaters (Fig. 9.4b), plastic wrap (Fig. 9.2a), and room deodorizers (Fig. 9.30a) are but a few examples. Convection about light fixtures (Fig. 3.18) is both a domestic and a commercial issue, especially in cleanrooms and hospitals [760].

Other Applications include abrasive blasting (Fig. 9.30b), leak detection (Sect. 9.3.7), railways [732], commercial kitchen ventilation [232,236] (Fig. 4.15c), printing, melt-blowing of fibers and non-woven fabrics, the texturing of man-made fibers, heat exchangers, boilers, silicon wafer inspection, electrochemical deposition [682], air knives, spray nozzles, thermal management of electronics, water-jet cutting, oxygen lances in steel-making [898], injection molding [899],

and pharmaceuticals [900]. Xu et al. have surveyed some of this industrial flow visualization [901]. The closely-related field of materials processing is also considered next.

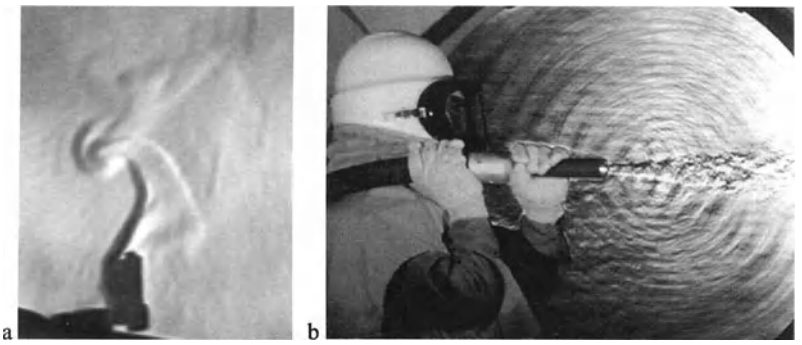

Fig. 9.30. **a** Convective plume from a plug-in air freshener. **b** abrasive blasting at a stagnation pressure of 6 atmospheres, a rich source of jet noise [895-897]. Photos by author.

9.4.6 Materials Processing

Thermal cutting began with the oxy-acetylene torch, studied by schlieren methods beginning in the 1930's [1,124,902,903], Figs. 2.4, 3.5b, and 9.21b. Plasma-arc cutting is a relative newcomer [904], and laser cutting is the most recent of all [905-908]. Examples of the latter two applications are shown in Fig. 9.31. Note that thermal cutting processes are strongly self-luminous.

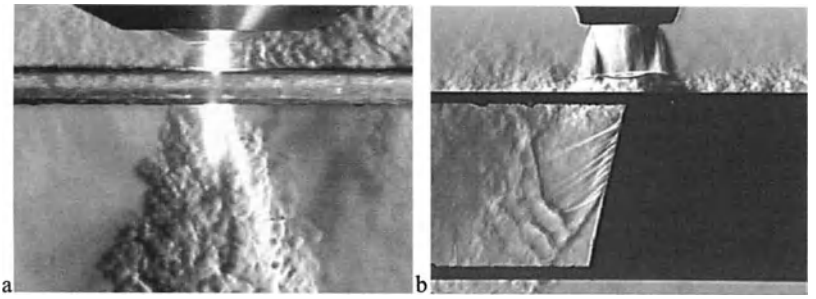

Fig. 9.31. **a** Schlieren image of a plasma torch cutting a steel plate [904] (research sponsored by the Hypertherm Corp.). **b** cold-flow glass-sidewall model of a supersonic laser-cutting assist-gas jet and its separation from the kerf leading edge [908].

Welding is another application where self-luminosity must be overcome for successful schlieren or shadowgraphy [606,909,910]. The deposition of metal droplets, the surrounding thermal field, and the shield gas stream are all worthy subjects of investigation.

Thermal Spray Technology uses a combustion or plasma torch to heat and accelerate particles toward a target, where they fuse to form a coating. A schlieren image of the combustion case is given in Color Plate 26, while a plasma spray torch is illustrated in Fig. 9.32a. Related references include [235,536,911-913].

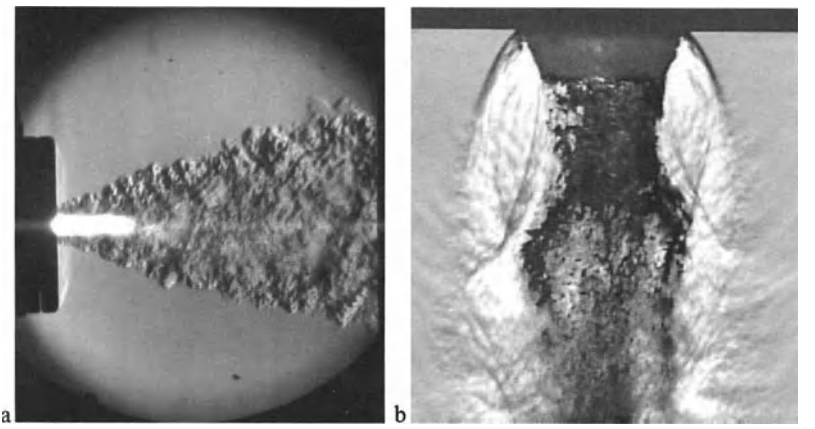

Fig. 9.32. **a** Schlieren image of the plume from a plasma thermal spray torch used to deposit thermal barrier coatings on engine components, exposure time 300 ms (courtesy S. P. Mates, NIST). **b** the atomization of molten tin by a coaxial supersonic inert-gas stream; fine-scale tin breakup occurs at and below the bottom of the image [914-916].

Liquid Metal Atomization feeds the multi-$billion powder metallurgy industry. Much of it is done by supersonic inert gas streams issuing from coaxial nozzles like the one shown in Fig. 9.32b. This has generated several optical studies [711,914-919]. Mates and Settles [914-916] found, in part by schlieren observation, that nozzle geometry is secondary to gas stagnation pressure in determining the resulting metal-powder size distribution.

Microgravity materials processing, along with fluids and combustion studies, figures prominently in plans for manned space flight by the US National Aeronautics and Space Administration (NASA). In principle, by removing gravity-based convection, one can grow larger crystals, produce higher-quality materials, and advance the basic knowledge of combustion. This has spawned several schlieren and shadowgraph studies, some of which have flown in microgravity aircraft flights and in orbit [329,418,419,572,697,921-928]. Some of these instruments

are marvels of light weight, compactness, and remote control, and one of them – discussed in Sect. 10.2.1 – is important beyond the microgravity field. The Fluids and Combustion Facility that is to become a part of the International Space Station (ISS) in 2003 will also include the capability of schlieren observations.

Not everyone believes in this, though. To the difficulties and dangers of manned spaceflight, one must add the current cost of roughly $22,000US/kg of material hefted into orbit. Microgravity research has been used to rationalize the development of the horrifically-expensive ISS with only questionable justification of its payback in terms of new knowledge. In orbit, a candle flame no longer even yields enough light to read by. Nicolaas Bloembergen of Harvard University is credited with saying "Microgravity is of microimportance."

9.4.7 Microscopy

> Nature composes some of her loveliest poems for the microscope and telescope
>
> *Theodore Roszak*

> Any projection-type schlieren method can be readily applied to the microscope
>
> *Hans Wolter* [119]

The thread of microscopy is interwoven with the present subject all the way back to Hooke's *Micrographia* [11,17]. Much was already said about microscopic schlieren and shadow methods in Chaps. 1, 5, and 6. The goal of this Section is not to repeat that material, but rather to briefly summarize, show some further illustrations, and attempt to define a trend for the future.

Toepler [45] made the first competent application of the schlieren principle to microscopy. He recognized that the common method of de-centering the light source to achieve "oblique illumination" was actually a crude means of schlieren microscopy – lacking, however, the ability to produce a uniform cutoff. He then added a simple schlieren diaphragm in the back focal plane of the microscope objective, Fig. 9.33, and achieved a proper, uniform schlieren cutoff. He thus produced microscopic schlieren images having the striking 3-D effect of bas-relief.

Toepler reported that this application of his schlieren principle in microscopy was "inexpensive and convenient even for the novice" [45]. In older microscopes it amounts to a simple tube modification, though expensive modern microscopes sometimes thwart this simplicity by limiting access to the back focal plane of the objective [660].

Shortly following Toepler, Rheinberg [67] developed optical color contrast, effectively inventing color schlieren methods by introducing them into the microscope (Fig. 9.33). Though Toepler's knife-edge schlieren microscopy had not caught on, this approach did. It became the premier method for the "optical staining" of transparent objects in early-20th-Century microscopy. Rheinberg [67] also simultaneously invented "θ-modulation," or encoding information in the direction perpendicular to the optical axis (see Sect. 5.1.3).

Since Rheinberg, the theme of schlieren imaging has followed a path in microscopy parallel to its "mainstream" development in flow diagnostics, but there was much cross-fertilization between these paths. In addition to Rheinberg's work, both phase contrast and differential interferometry began in microscopy and subsequently spread to macroscopic fluid dynamics and heat transfer studies. Dark- and bright-field schlieren illumination are similarly inherited from microscopy, while graded-filter techniques appear to have migrated in the opposite direction. Most surprisingly, the simple schlieren methods that are robust and active in many fields covered in this chapter have declined in microscopy, in favor of more-recent, higher-technology methods like Nomarski differential interference contrast.

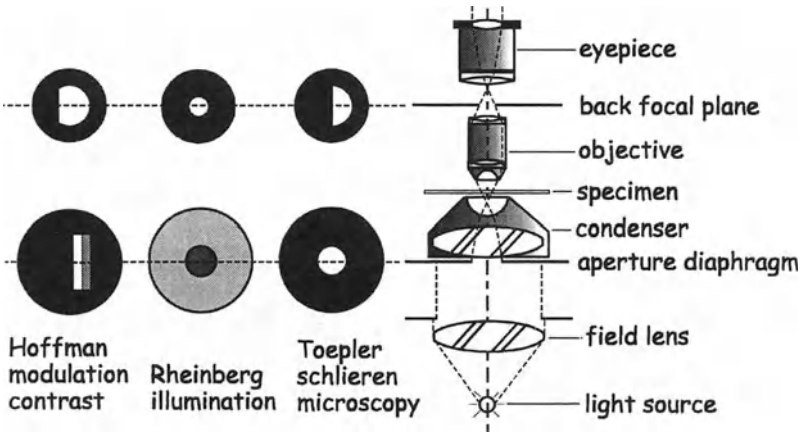

Fig. 9.33. Schematic diagram of a compound microscope illustrating the conjugate optical planes (aperture diaphragm and back focal plane of the objective) where schlieren processing occurs. While Toepler's [45] approach uses a classical knife-edge cutoff, Rheinberg [67] first introduced color schlieren methods to the microscope (see Fig. 5.8). Hoffman Modulation Contrast [280,282] is a modern adaptation of schlieren microscopy.

Several of the old and newer methods of microscopic illumination are well-illustrated by the comparison of diatom images given by Smith [929] and reproduced here in Fig. 9.34. Detailed reviews of all these methods can be found, for example, in [296] and [930].

Other pioneers of schlieren microscopy include Schardin, who wrote a key paper [322] on its application to glass technology. Wolter's [119,312,323,333] contribution to the topic was the quantification of Rheinberg's color methods. One of his micrograms is reproduced here in Color Plate 45. Unfortunately, Schardin's and Wolter's methods are no longer used.

Glass-fiber micrograms were used earlier to illustrate bright-field illumination, Hoffman Modulation Contrast [280-282], and shadowgraphy in the microscope

(Figs. 5.19 and 6.15). Several of McCallum's [660] schlieren micrograms were shown in Fig. 9.2. Two more examples are also shown in Fig. 9.35 below.

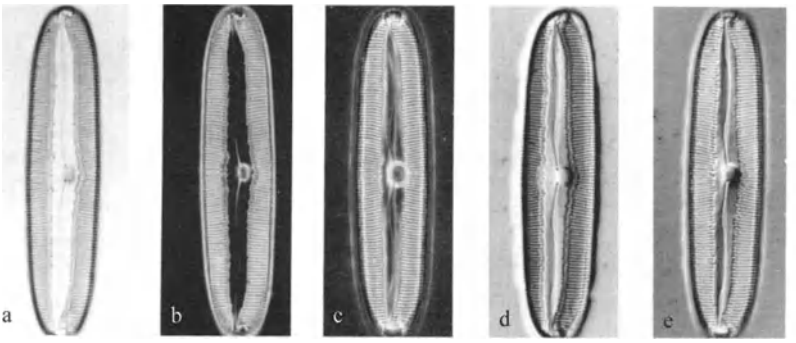

Fig. 9.34. Comparative study of the same diatom by five different methods of microscopic illumination: **a** brightfield, **b** darkfield, **c** phase contrast, **d** oblique (schlieren), **e** Nomarski interference. While frames d and e are similar, oblique illumination holds a slight resolution advantage. Reproduced from Smith [929] by permission of CRC Press.

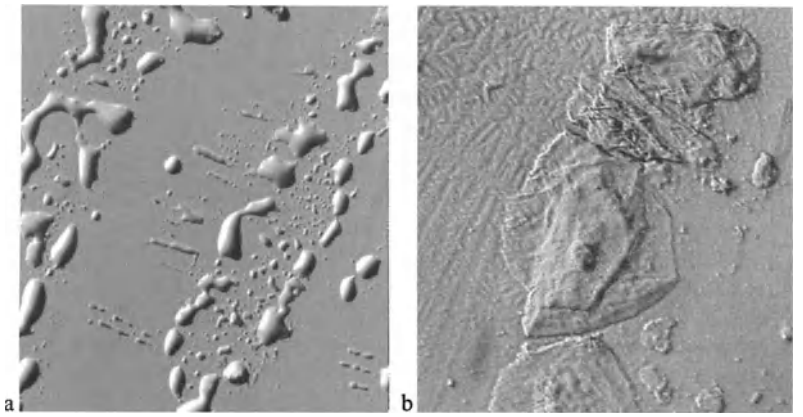

Fig. 9.35. **a** Toepler schlieren microgram of a fingerprint on a glass slide, 100X, showing the oily imprint of two ridges. **b** human-cheek epithelial cells, 500X, revealing cell nuclei and crystallized saliva. Micrograms by the author and Heather Ferree.

Today, oblique illumination (the "poor man's schlieren" or the "penniless man's Nomarski") remains the prevalent microscopic schlieren method due to its extreme simplicity [45,931-933]. Almost any microscope can be made to perform in the oblique mode, usually without additional apparatus.

Both oblique illumination [933] and Toepler's microscopic schlieren [279,934] are occasionally re-discovered by modern investigators. Toepler's role is forgotten, though, and sometimes schlieren microscopy gets a newer, less-elegant name, like "single-sideband edge-enhancement microscopy" [279].

One of these re-discoveries is significant, however, because it spawned a viable commercial product: Hoffman Modulation Contrast [280-282] employs a slit aperture with a stepwise gradation in the plane of the aperture diaphragm below the condenser (Fig. 9.33). A corresponding knife-edge is mounted in the back focal plane of the objective. The central band of the slit filter transmits a fraction of the incident light (variable by way of polarizers), producing a graded-filter-like effect that extends the measuring range of microscopic schlieren observation with some loss of ultimate sensitivity. This is combined with oblique illumination to create a striking schlieren effect (see Fig. 5.19b, Color Plate 46, and several fine examples in Ref. [282]). It may be called modulation contrast, but it is certainly also schlieren microscopy.

To get this, the buyer of a modern microscope specifically requests that it be fitted for Hoffman Modulation Contrast. A special rotary aperture diaphragm and custom objectives are then provide at extra cost (see App. D). Clearly there is a market for it, proving that schlieren microscopy is not completely dead. Moreover, recent patent activity (Takaoka [935]) gives a good indication for the future.

In fact, schlieren microscopy is poised for a comeback. It is straightforward and its 3-D bas-relief effect is almost as compelling as that of the enormously-popular scanning electron microscope. Even in the age of entirely new microscope types (atomic force, confocal, etc.), the time-honored technique of schlieren microscopy still deserves its rightful place. Microscopists, use the schlieren method!

To conclude this section, note that both schlieren and shadowgraph principles work successfully in transmission electron microscopy as well, e.g. [936]. Also, readers of German will enjoy Rienitz's recent book [937], where the history of optical instruments is traced from binoculars through telescopes and microscopes to holography, especially including schlieren and shadowgraphy.

9.4.8 Optical Processing

> The close relationship between digital and optical processing suggests hybrid approaches for flow visualization
>
> *L. Hesselink* [161]

This is a proto-application: mostly imagined at this point, but full of latent potential. Like microscopy, optical image processing is an oft-repeated theme in this book. Indeed, the optics of a schlieren system and of a Fourier processor [72,129,130] are very similar. Matched spatial filtering (Sect. 5.1.3) is central to both systems. Likewise the mathematical treatment (App. B) is the same and, finally, digital schlieren and shadowgram processing (Sect. 3.2.4) can be done optically as well. Apparently these optical systems differ mostly in their applications.

Optical processors have been tasked with pseudocolor-encoding grayscale images, recognizing patterns and texture in aerial imagery or radiography, and rejecting noise using white-light illumination. Abbe [938] and Rheinberg [67], both microscopists, laid the groundwork for this field. Armitage and Lohmann [492], Indebetouw [573], Bescos and Strand [69], Glaser [939], and Yu [72] all made important contributions. Hesselink [161,500] points out that optical image processing has a great speed advantage over digital processing: it is massively-parallel processing of a simultaneous array of image points, a true analog computing application in the digital 21st Century.

But to get to the point, can we make better use of the schlieren system's image-processing nature to observe and measure transparent phenomena? For example, Bernal et al. [940] used (digital) image analysis of a mixing-layer shadowgraph movie to characterize the coherent structures of the flow. Yao and Lee [941] suggested spatial filters to integrate image features, and to take other spatial derivatives such as $\partial^2 n/\partial x \partial y$. Kelsey's [129] matched random filter pair, Fig. 5.5i, deserves more investigation of its noise-rejection capability. In short, the possibilities of matched filters are plainly not exhausted by those few shown in Fig. 5.5, and a careful study of the optical image processing literature might well yield improved systems and new uses for schlieren and shadowgraphy.

9.4.9 Optical Shop Testing

> The Foucault test may be considered the first optical shop test, from which many others were developed.
>
> *J. Ojeda-Castañeda* [153]

Beginning with Christiaan Huygens and Leon Foucault, optical shop testing is one of the oldest applications of schlieren and shadowgraphy. It is closely related to glass technology, and excellent general references are available [151,153,654] as well as key historical accounts [101,942]. Laser interferometry is outside the present scope, but moiré fringe methods are included as a subset of the general schlieren technique [247,942-944].

Of course, optical shop testing of telescopic parabolas remains an important application of the schlieren principle, for example the botched null test of the Hubble Space Telescope primary mirror that required a costly retrofit in space. No better example could be shown than Bowen's [945] starlight Foucault test of the Hale Telescope Mirror at Mt. Palomar, Fig. 9.36. It simultaneously illustrates four key themes that run through this book: optical shop testing, atmospheric optics, telescopic optics, and optics on a magnificent scale.

The initial Foucault knife-edge tests of the 5.08 m (200 inch) Hale Telescope mirror were done with the light of the star Sirius. 1/20-sec exposures, however, revealed only broad-scale schlieren due to atmospheric turbulence and masked the mirror figure (Figs. 9.36a and b). A subsequent test with a faint star source and a 20-80 sec exposure time-averaged the turbulence and revealed the mirror figure,

Fig. 9.36c. Additional polishing to remove a raised edge eventually yielded the almost-perfect Foucault test result shown in Fig. 9.36d.

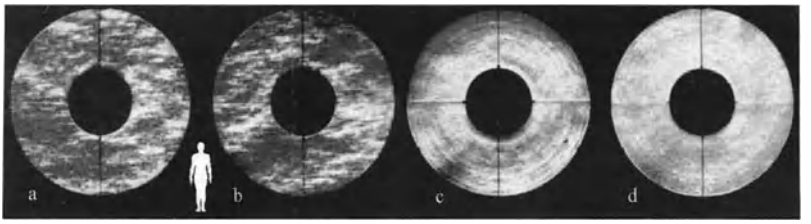

Fig. 9.36. Starlight-illuminated Foucault test results of the 5.08 m (200 inch) diameter Hale Telescope Mirror at Mt. Palomar (see text for details). The relative size of a person 1.83 m (6 feet) tall is indicated between frames a and b. This figure originally appeared in the Publications of the Astronomical Society of the Pacific, Bowen [945]. Copyright © 1950, Astronomical Society of the Pacific; reproduced with permission of the Editors.

9.4.10 Outdoor Schlieren and Shadowgraphy

I reviewed this topic in detail in 1999 [522], apparently for the first time. A succinct version of that review[3] is given here with selected illustrations from [522] and two additional examples.

Throughout this book, by tradition, shadowgraph and schlieren methods have been treated as items of laboratory apparatus. The few exceptions include the outdoor scanning schlieren systems of Sect. 4.4, Edgerton's daylight shadowgraph setup (Fig. 6.14a), some aero-optics (Sect. 9.3.2), and salt finger observations in the ocean, Sect. 9.4.4. Yet schlieren and shadowgraph effects can be seen outdoors on almost any day, as Robert Hooke initially observed [17], if one knows where and how to look for them.

Ernst Mach, for example, mentioned several outdoor shadowgraph and schlieren visualizations in his *Popular Scientific Lectures* [9]. These included convection from hot objects and the blast wave from a dynamite explosion (as related to him by C. V. Boys). Mach further tells of the French artillerist Journée, who claimed to have seen by eye certain waves trailing from a high-speed projectile that he followed telescopically. Schardin [2] likewise remarked upon the schlieren he saw in windowpanes and above hot railroad tracks.

The sum of these anecdotes amounts to more than just open-air curiosity on a sunny day. There is potential value here as well, not only in a better understanding of natural phenomena through flow visualization, but also in the possibility that new techniques and visualizations may arise from such considerations.

[3] Copyright © 1999, Proc. 2nd Pacific Symp. on Flow Vis. and Image Proc., PSFVIP-2.

In all cases, outdoor shadowgraphy occurs in direct sunlight or moonlight and outdoor schlieren effects arise from simple background distortion. These two effects are discussed separately in what follows.

Sunlight Shadowgraphy is direct shadowgraphy with the Sun serving as a light source and any convenient surface (often the ground) as a projection screen. A sketch of an example was given earlier in Fig. 1.14b, while the general optical diagram is that of Fig. 6.5.

Referring to the latter, note that the Sun subtends an angle of about ½ ° (31 minutes of arc) at our average distance from it, so it always fails the primary criterion for good shadowgraphy: that of a "point" light source.[4] Nevertheless the Sun excels for shadowgraphy in most other respects, being sufficiently intense and readily available to cast shadowgrams on an enormous scale if required.

In Fig. 6.5, denote the circle of confusion due to finite light-source size by δ. Then

$$\delta / g = \tan\left(1/2^{\circ}\right) = 0.009 \tag{9.2}$$

Thus the blur δ is linearly proportional to the object-to-screen distance g, which must always be minimized if a sharp shadow is desired.

The sensitivity of sunlight shadowgraphy to a ray deflection angle ε by the schlieren object S is related to the change in illumination thus caused on the screen. If Δa denotes the ray displacement on the screen due to this deflection, then $\Delta a = g \tan\varepsilon$. We can compare this ray deflection with the circle of confusion as follows

$$\frac{\Delta a}{\delta} = \frac{\tan\varepsilon}{\tan(1/2^{\circ})} \approx \frac{\varepsilon}{1/2^{\circ}} \tag{9.3}$$

revealing that, regardless of standoff distance g, ray deflections by the schlieren object must always compete with a substantial blur angle in order to be visible. Weak disturbances, like human thermal convection, therefore have little chance of being seen by sunlight shadowgraphy, since the deflection-to-blur ratio $\Delta a/\delta$ of Eqn. 9.3 tends to zero in these cases. Strong convective plumes, defects in glass, and shock waves in air have finite values of $\Delta a/\delta$, rendering them easily visible.

Two sunlight shadowgrams reenacting Hooke's original candle-flame observation were shown earlier in Fig. 1.3, and swimming-pool caustics in sunlight were shown in Fig. 9.6. Two additional examples are given in Fig. 9.37.

Cooper and Rathert [946] first used sunlight shadowgraphy to reveal shock wave locations on high-speed aircraft wings. The topic was later addressed by Crowder [811] and most recently by Fisher et al. [813], Fig. 9.37a. The effect may be seen often in commercial jet travel when the Sun is roughly overhead.

---

[4] Sunlight shadowgrams are sharper on the more-distant planets.

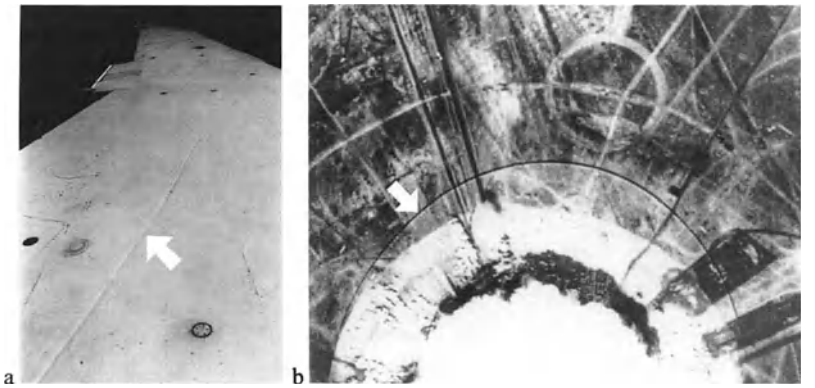

Fig. 9.37. **a** Sunlight shadowgram of shock wave on L-1011 jet transport wing at transonic cruise [813] (US Govt. photo by Carla Thomas, NASA Dryden Research Center). **b** aerial view of the sunlight shadowgram of a spherical shock wave generated by 500-ton TNT explosion "Operation Snowball," courtesy J. M. Dewey [202,210]. (White arrows indicate the shock wave shadows in both frames.)

Background-Distortion Schlieren observation can occur outdoors when the background provides one or more light-dark boundaries. The optical principles involved are those of Schardin's schlieren method no. 1, as described in Sect. 4.3.1 and illustrated in Fig. 4.4. Of itself, the human eye lacks the capability for schlieren processing, but it can serve as the analyzer section of a schlieren apparatus if the proper light source is naturally provided. The horizon or the Sun most often serve this purpose, though several other natural and artificial out door light-dark boundaries are also available.

Despite the natural occurrence of this schlieren technique, however, its sensitive field-of-view is severely limited as discussed in Sect. 4.3.1. In the outdoors, moving the eye or camera may allow one to scan this narrow range of visibility across a sizable schlieren object. Usually, though, it helps to open the lens aperture enough to defocus the distant light/dark boundary somewhat in the schlieren image. This extends the working range in the direction perpendicular to the boundary at the expense of the peak sensitivity, like replacing the knife-edge by a graded filter in the classical Toepler schlieren system.

Many fine examples of this outdoor optical effect are aviation-related, including the shock waves about high-speed aircraft and their exhaust plumes. For example, Fig. 9.38a shows an F-15E fighter exhaust by background distortion of the distant trees. The exposure time was short enough to "freeze" turbulence in the exhaust, which appears sharply focused against a less-distinct background. In Fig. 9.38b an F-111 fighter is shown in transonic flight at low altitude, with oblique shock waves and exhaust clearly seen against the background light/dark boundary of a mountain ridge. In Fig. 9.38c the transonic shock wave above the wing of an L-1011 jet transport, corresponding to the sunlight shadowgram shown above, is

seen against a background of scattered clouds over the Pacific Ocean. Unlike the shadowgram, this view is almost never available on commercial flights. It was necessary to bank the aircraft steeply during a flight test [813] to provide the background. Finally, Fig. 9.38d shows a jet aircraft taking off against an enlarged telephoto image of the Sun, revealing the refraction of the jet exhaust. Striking images like this are very popular in travel advertisements, where they s uggest taking off into a serene sunset for places unknown. They never suggest the reality of losing a night's sleep in a claustrophobic metal cylinder.

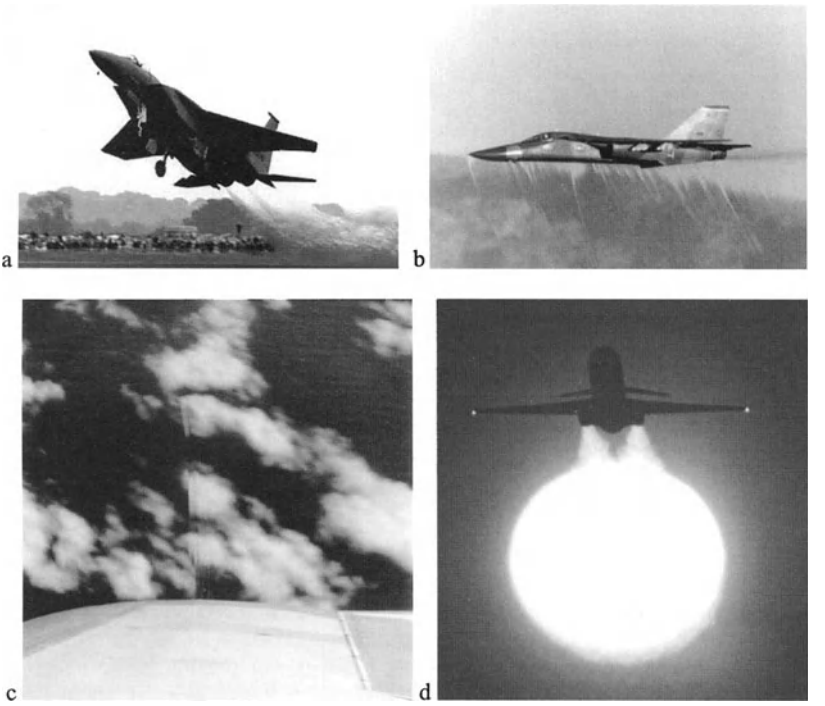

Fig. 9.38. **a** An F-15E Eagle takes off at a 1998 air show in this photo by Peter Steehouwer, http://www.steehouwer.com/, reproduced by permission. **b** transonic F-111 fighter (US Govt. photo by Sandia National Laboratories, courtesy D. McBride). **c** Shock wave on L-1011 wing (US Govt. photo by Carla Thomas, NASA Dryden Research Center). **d** a DC-9 takes off against the setting Sun, © David Nunuk, Photo Researchers.

The Sun serves as well to provide the background for outdoor schlieren heat transfer observations like that of Fig. 9.39a, first described by Robert Hooke in 1665 [17]. Likewise Sun-warmed metal surfaces often reveal their thermal

boundary layers, Fig. 9.39b, when viewed against an appropriate background. The reverse curvature of the gridlines in the car roof boundary layer is the result of a light refraction component toward the left, where the air density increases in this example. Even certain phenomena of solar physics [947] can be observed by background-distortion schlieren against the "limb" of the Sun itself.

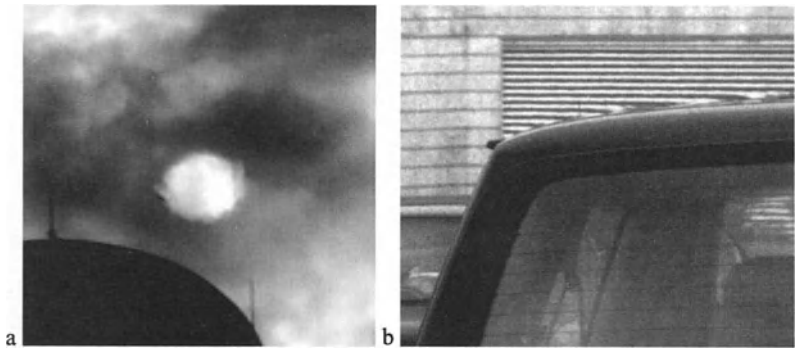

Fig. 9.39. **a** Distortion of the Sun's disk by the hot-air plume of a smokestack. **b** Thermal boundary layer on hot car roof, seen by distortion of a background grid pattern.

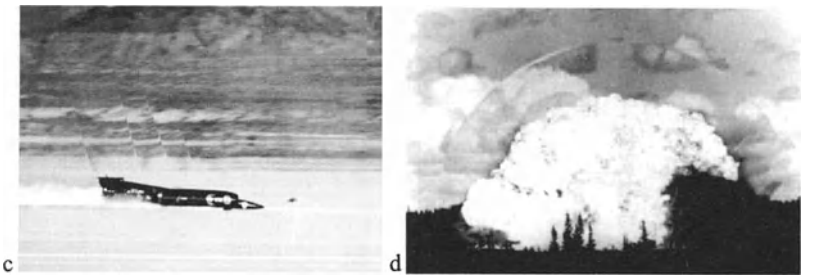

Fig. 9.40. **a** Transonic flow about the *Thrust SSC* car. Photo by Chris Rossi, © 1997, reproduced by permission (http://www.supersoniccars.com). **b** large chemical explosion (US Govt. photo by Defense Special Weapons Agency).

In 1997 two jet-powered cars vied to "break the sound barrier" for the first time, and one of them, called *Thrust SSC*, succeeded. Despite considerable media coverage, only one still image by astute photographer Chris Rossi managed to capture the attendant shock wave phenomena, Fig. 9.40a. Four oblique shock waves are clearly visible above the vehicle via background distortion of the desert. Less obvious but certainly also present is the bow shock wave, about ½ vehicle length ahead and normal to the direction of motion. The Mach number of the car in this photo is 1.02.

Some experiments can only be performed outdoors, where the usual optical apparatus is unavailable. This was so in Dewey's sunlight shadowgram, Fig. 9.37b, and is also the case in the background-distortion schlieren observation of a very large chemical explosion, Fig. 9.40b. Following the above-ground nuclear test ban treaty, it still remains possible to approximate nuclear blast effects using very large conventional chemical explosions. The scale of this example is shown by the trees at bottom center, dwarfed by the giant fireball. The hemispherical shock wave reveals itself by distortion of the cloudy background sky.

Finally, atmospheric conditions sometimes allow extraordinary visualizations. Of all the rocket launches ever filmed, only one is known to have provided a natural schlieren visualization, shown here in Fig. 9.41. Layered clouds at dusk offered a natural background grid with which to observe the oblique shock waves streaming back from a supersonic missile launch.

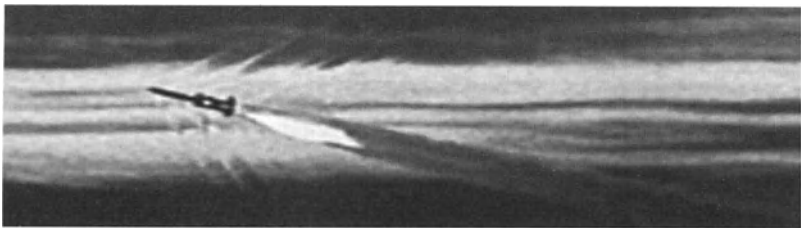

Fig. 9.41. Naturally-visible oblique shock waves about a missile, observed by the background-distortion schlieren effect. From the 1959 Shell Film *Approaching the Speed of Sound*, Part 1 of *High-Speed Flight*, reproduced courtesy of the Shell Film and Video Unit.

9.4.11 Plasma Dynamics

Plasma, an ionized gas at very high temperatures, is often referred to as the fourth state of matter. It is frequently observed by schlieren and shadow methods [948]. Examples of plasma jets used for thermal cutting and thermal spraying were given earlier in Sect. 9.4.6, while others concerning electrical breakdown and discharge plasmas were discussed in Sect. 9.3.8.

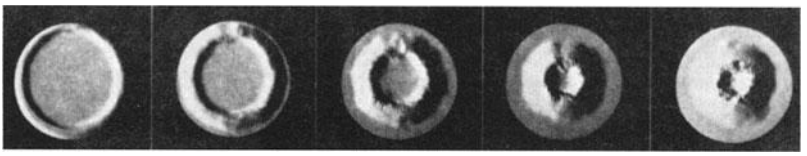

Fig. 9.42. Sequence of the development of a hydrogen θ-pinch, from Lovberg [952]. The elapsed time from the left to the right image is 0.8 μsec. Vertical-knife-edge schlieren images reveal the plasma electron density.

Research on thermonuclear fusion focuses on magnetic plasma confinement in θ-pinch and tokamak reactors, and more recently in laser fusion experiments [457,462,949,950]. Plasmas exhibit high refractivity, as noted in Chap. 2 [82,951], so one can measure free-electron concentration and infer temperature by schlieren methods [102,495,912]. A 1960's schlieren example from plasma propulsion [952] reveals a θ-pinch experiment in Fig. 9.42

9.4.12 Television Light Valve Projection

> In the broad sense, these (light-valve projectors) are all schlieren optical systems.
>
> *A.G. Dewey* [584]

The Fischer *Eidophor* system [953], invented in 1940 and mentioned in Schardin's review of schlieren techniques [2], uses a schlieren system as an integral component of a large-screen television projector. In it, an electron gun "writes" the TV picture onto an oil film that becomes dimpled by the deposited electrostatic charges as a result. The modulated oil film – one type of spatial light modulator or "light valve" – then becomes the schlieren object of an optical system illuminated by an arc lamp. Light diffracted by the oil film is focused upon a lattice-type schlieren cutoff with clear bands matching the spacing of the diffraction orders in the cutoff plane. The opaque lattice bands block undiffracted light in this dark-field schlieren arrangement. Optically, it is similar to Schardin's [2] schlieren method no. 4, the precursor of the modern lens-and grid focusing/large-field schlieren system (Sect. 4.3.4). Nevertheless, instead of a single lens, a separate field lens and focusing lens are used in Fischer's Eidophor.

The Eidophor system has been very successful for large, bright projection TV displays. Other light valve types were developed, including liquid crystals, deformable-membrane mirrors and addressable-mirror-matrix arrays, but in all cases some form of schlieren projector is used, typically with a lattice, circular, or cruciform cutoff. These devices effectively separate the functions of the cathode-ray tube and the powerful projector required for a large display, amplifying the TV image many fold by way of the schlieren principle.

References describing various adaptations of the schlieren-light-valve TV projector include [70,954-956]. Most of these studies emphasize the light valve, not the schlieren projector, but the latter is featured in a few cases [584,957,958]. Color TV projections are required, of course, and to this end three separate or integrated light valves in the three primary colors are frequently used. All three component images must be carefully registered in the final color schlieren image (e.g. [422]).

It seems likely that flat-panel displays of various types will eventually supercede this projection technology, but even in the last ten years schlieren TV projectors are still going strong.

9.4.13 Turbulence

> Turbulence is one of those phenomena which are difficult to describe, but easy to recognize once seen
>
> *Peter Bradshaw*

The subject of turbulence is impossible to avoid in fluid flows; it is immensely important and equally difficult. 20th-Century attempts to understand and deal with it have produced limited success and unlimited disappointment. Yet schlieren and shadowgraph techniques have had a significant positive impact, revealing turbulence non-intrusively and globally by way of its refractive field. Almost every chapter of this book contains several illustrations of turbulent flows. The topic is closely aligned with boundary layers, jets and wakes, aero-optics, and – by way of the turbulent mixing of fuel and oxidizer – with combustion.

Shadowgraphy has been a favorite method of revealing turbulence for at least a century, given its simplicity and sensitivity to the Laplacian of refractive index in turbulent eddies (see Sects. 2.3 and 6.12). A few of these shadowgrams, especially Fig. 1.23 by Brown and Roshko [7], though qualitative, were central to achieving a better understanding of turbulence. Many studies, however, have also involved attempts to extract quantitative turbulence measurements from shadowgrams.

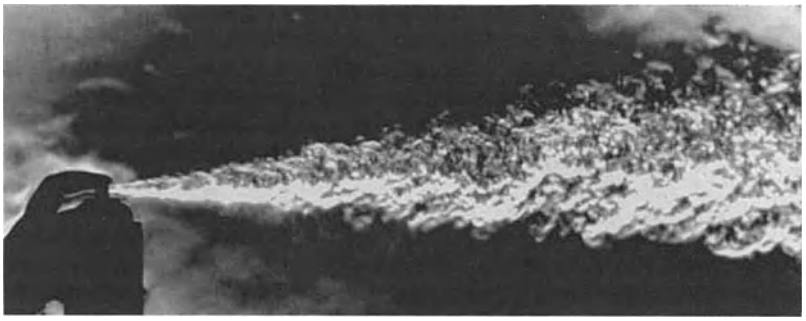

Fig. 9.43. Axisymmetric turbulent jet from an aerosol can, revealing large-scale mixing structures (from an original color schlieren photo by the author.)

Uberoi and Kovasznay pioneered this approach in 1955 [959], followed by Taylor [510,960] and Hesselink and White [161,511]. In some cases a statistical analysis of shadowgram intensity is related to turbulent density fluctuation levels and spectra, yielding quantitative results. The recent availability of powerful desktop computers prompted several such studies within the last decade, examining turbulent wakes [512,961], aero-optical flows [747,962], and supersonic shear layers [963]. Quantitative shadowgraphy is also discussed in Sect. 10.4.

Schlieren investigations of turbulence began with Townend [964], who analyzed movies of turbulent pipe flow with no help at all from computers in 1934. There followed several quantitative studies [816,965-967] in the 1960's and 1970's. Jagoda and Weinberg [948] extracted quantitative data from schlieren images of plasma-jet mixing in 1980. With the help of modern computers, quantitative turbulent flow measurements from schlieren images have continued in recent years [121,500,968,969]. Some of this work was prompted by late-20th-Century interest in high-speed mixing [620,804,805,808,970,971], and some of it involved schlieren velocimetry of turbulent structures [191,620,805,808,971], also discussed further in Sect. 10.3.

An outstanding concluding example of the contribution schlieren imaging has made to turbulent flows lies in the work of Hibberd [972] and Riediger [973]. Polymer additives in turbulent shear layers are known to reduce drag, but the physics of this has often evaded simple explanations. Nevertheless, schlieren images of such flows reveal one powerful physical reason: small-scale turbulent motion is dramatically suppressed by the polymer additive. Given enough additive, in the schlieren results of Riediger [973], even the largest turbulent scales all but disappear (Fig. 9.44).

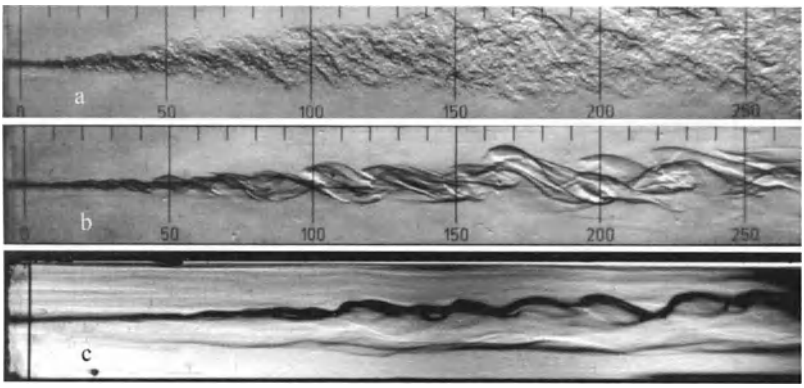

Fig. 9.44. Schlieren photos of a mixing layer in **a** water only, **b** water + 50 ppm polyacrylimide, **c** water + 900 ppm $C_{14}TASI$. Images courtesy S. Riediger [973].

10 Quantitative Evaluation

> 'Counting': Ounce, dice, trice, quartz, quince, sago, serpent, oxygen, nitrogen, denim.
>
> *Alastair Reid*

When the schlieren publication rate ballooned to hundreds of papers per year after World War II, about 10% of them involved quantitative evaluations: This fell dramatically in the 1970's when laser interferometry, a more-directly-quantitative optical tool, took precedence. Still, a few percent of present-day schlieren publications remain quantitative and some interesting possibilities still exist, especially now that digital image processing eases much of the drudgery [357].

Let us first define what we mean by *quantitative*: the measurement of gas density or temperature – and recently velocity – from schlieren images or shadowgrams. On the other hand a *qualitative* judgment of refraction angles can be had merely by inspecting a schlieren photo [2,42], and geometric data from schlieren images are at least *semi-quantitative*. For example, shock-wave angles are measurable even when density data are not forthcoming [146].

Schardin [1,2] and Vasiliev [102] devoted substantial chapters to quantitative schlieren density measurements, and Skotnikov wrote a whole book on it [638]. His book covers only gas dynamics applications, tho ugh, and few of the methods he treats are still practiced for the reasons discussed earlier. But, instructive examples of supersonic boundary layers and optical shock-wave strength measurements are given. A chapter is devoted to the calculation of radial refractive-index gradient profiles in axisymmetric flows, and an approximate method to solve Abel's integral is presented. There is no English translation, though, so most of us are left to struggle with the Cyrillic and peruse the figures.

The Wollaston-prism schlieren-interferometer (Sect. 5.4.1) is mainly for quantitative use, as is the exponential schlieren source/cutoff of Sect. 5.1.2.

Some quantitative schlieren methods are overlooked in what follows because they are non-imaging or little-used. For example Schmidt's technique [526], later Schardin's schlieren method no. 12 [2], meets both these rejection criteria.

Finally, quantitative density methods are covered only briefly here because the emphasis of this book remains on qualitative and semi-quantitative visualization. The present goal is quite distinct from Skotnikov's [638].

G. S. Settles, *Schlieren and Shadowgraph Techniques*

10.1 Quantitative Schlieren Evaluation by Photometry

Formerly, the photometry of schlieren photographic negatives was done by hand using a microdensitometer. Scores of young people were hired to acquire these data and tabulate them on paper spreadsheets. The data were reduced by hand too, using a mechanical calculator. Those days are gone forever, and no regrets.

Every image in this book was either digital at the outset or was scanned from a photograph. The scanning process is imperfect, but the results can be adjusted according to Sect. 3.2.4. Once digitized, the gray-scale pixel values of the image provide automatic photometry, given an appropriate calibration standard.

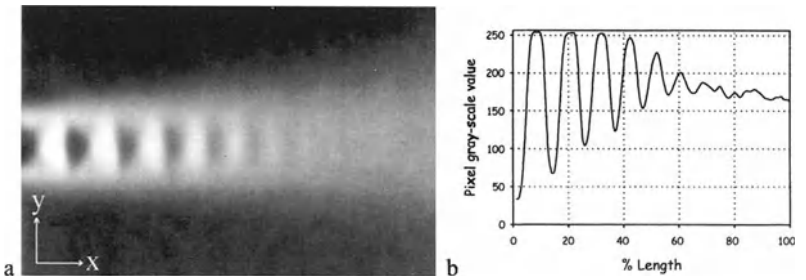

Fig. 10.1. **a** Vertical-knife-edge schlieren image of a planar 2-D supersonic air jet flowing left-to-right along the x-axis. **b** Plot of pixel gray-scale values on the jet centerline.

For example, consider Fig. 10.1. The simple 8-bit gray-scale schlieren image shows visually that "shock diamonds" in a supersonic jet cause alternating bright and dark zones. Quantitative pixel values along the jet centerline tell more of the story: the full contrast range is not used, since the darkest pixel already has a value of 33. Likewise there is some clipping of the highest values in the first two or three bright zones. Except for that, the intensity variation is quite sinusoidal over 6 or 7 complete diamonds, before turbulent mixing finally has its way. There is no calibration with this example, but if there was, one could use it to associate pixel gray-scale values with source-image displacement values Δa (see Fig. 2.6). Knowing the schlieren-system focal length f_2, one could then find the jet-centerline distribution of deflection angle ε (Eqn. 2.6), and from that the distribution of $\partial n/\partial x$ (Eqn. 2.5). Invoking the Gladstone-Dale Law (Eqn. 2.1) and forging ahead without concern for any clipping errors, optical errors, or departures from two-dimensionality, we then have an expression for the density gradient along the jet axis:

$$\frac{\partial \rho}{\partial x} \cong \frac{\Delta a}{kLf_2} \tag{10.1}$$

where L is the depth of the flowfield along the optical axis (normal to the page). Finally we integrate this in x to obtain the jet centerline density distribution $\rho(x)$, assuming the flow density ρ_{ref} at a reference point (the surrounding air) is known:

$$\rho(x) \cong \frac{1}{kLf_2} \int_{x_1}^{x_2} \Delta a(x) dx + \rho_{ref} \tag{10.2}$$

This conveys the essence of quantitative schlieren image evaluation, all done automatically by the desktop computer if you like. It is certainly much faster and easier than in the old days, and the previous subjectivity of evaluation is mostly avoided. There are pitfalls, of course, to be described below. Laser interferometry suffers the same set of pitfalls, but is simpler because the integration step is unnecessary.

Quantitative schlieren-image evaluation by photometry is approached in two different ways, depending upon whether or not a calibration standard is included in the image [2,102]. None was included in the example just given: such cases, called absolute photometry, are considered further in the next section.

10.1.1 Absolute Photometric Methods

In absolute photometry the schlieren image illuminance E directly indicates the light refraction by the schlieren object. Connecting these values then yields a map of refractive-index (density, or temperature) variations within the schlieren object, according to the above scheme, provided the set of assumptions is fulfilled.

Absolute photometry yields the best sensitivity of all the quantitative schlieren methods: therefore use it especially where high sensitivity is needed.

It relies on the geometric-optical schlieren theory introduced in Sect. 3.2.1. One must know k, L, f_2, the image magnification m, the source luminance B (candela/m^2), the source width h, and the fraction a of source height not cut off.

Step 1 in quantitative schlieren-image evaluation associates pixel gray-scale values with source-image displacement values Δa. For this purpose a schlieren calibration curve like Fig. 2.6 must be determined using a micrometer knife-edge adjustment and a suitable photocell, PIN diode, or photomultiplier tube. All optics must be in place for this, including windows, etc., but no schlieren object.

This calibration alone does not insure accuracy, however, since various quantitation errors can occur. One such error happens when a ray is bent out of the disturbance that refracts it while it is still within the test area. Shock waves, being strong, thin optical disturbances, cause this sort of error and quantitation usually breaks down across them. But since they are thin, it can continue elsewhere.

According to Speak and Walters [126], such quantitative schlieren studies demand parallel light, lest they become hopelessly complicated. Similarly no 3-D flows need apply unless one is willing to resort to the tomographic methods discussed in Sect. 5.5.2.

Diffraction effects limit the applicability of the geometric theory, and they are not readily calculable. This weighs against quantitative photometry at high schlieren sensitivity settings, where the light-source image is almost entirely cut off. Thus there is a tradeoff between schlieren sensitivity and quantitative accuracy, and a compromise must be established in order to proceed.

Here the nonlinearity of the recording medium, mentioned earlier, also comes into play. Photographic film yields an optical density proportional to the logarithm of the incident illuminance when exposed within the proper range. Kean [146] suggests that photometry is more practical with a linear schlieren system response, and also notes that one should avoid the vicinity of 0% and 100% knife-edge cutoff, where the response is inherently nonlinear (e.g. Fig. 3.10). Curved-stop methods, Sect. 5.1.2, and graded-filter methods, Sect. 5.1.1, can be used to linearize the system response.

Alternatively, one can use a linear detector instead of photographic film. A good example is given by Garg et al. [974]. This has advantages, including constant sensitivity regardless of the value of Δa, and automatic *tare* (no-flow) subtraction. 50% cutoff is used for best management of the available measuring range: a good idea even though not the most sensitive setting. This also minimizes diffraction, but 3-D errors still remain.

Schardin [1] gives an example of the quantitative evaluation of a schlieren image based on pure photometry. Other examples can be found in [752] and in [822], where video gray levels are quantified after subtraction of a tare image, and higher-resolution results than laser-Doppler velocimetry are shown.

In addition to planar 2-D phenomena, axisymmetric phenomena can also be analyzed quantitatively by photometry. The procedure is more complex, and generally requires an inverse Abel transform [975]. (For fully 3-D objects the inverse Radon transform is required.) Schardin [1] gives an approximate method for axisymmetric flows, as do Refs. [102,104,138] and [638]. Schwarz [276] performed tomographic schlieren imaging of flames, derived quantitative temperature profiles photometrically, and coined the interesting term "Gladstone-Dale Pyrometry"

10.1.2 Standard Photometric Methods

Unlike pure photometry, these methods include a "standard" refractive object – the *standard schliere* – in the field of view for calibration purposes. This calibration object contains one or more known refractions as benchmarks for quantitative evaluation. Doing this relaxes some of the stringent requirements on absolute photometry and eliminates some of the resulting errors.

Unfortunately, other errors remain. Diffraction effects are not completely accounted for [98], and uniformity of cutoff across the schlieren field of view becomes very important. Overall, Vasiliev [102] claims that standard methods have little advantage over pure methods of photometry, but most others disagree.

The standard schliere is often placed in an unused corner of the frame and imaged along with the schlieren test field. Schardin [1] gives an example of a standard lens and a bullet in flight. To quantify the results, one matches a schlieren-

lens and a bullet in flight. To quantify the results, one matches a schlieren-object point with a point of the same illuminance in the standard schliere, where the refraction ε is known [1]. Small test objects, however, may not correspond with a large standard schliere due to the varying diffraction effect with size [171].

Of several possible types of standard schlieren, Schardin [1,2] recommends a weak plano-convex lens. The refraction at the lens edge should be more than the strongest schlieren object to be observed, i.e. typically several hundred arcseconds. Since the refraction at the lens center is zero, a broad measuring range is covered. Evaluation is accomplished by way of the simple relation $\varepsilon = r/f$, where r is the radius from lens center and f is the lens focal length [102]. Unfortunately, small high-quality lenses with focal lengths of several meters are hard to find. There is also a loss of about 8% of the light incident upon the standard, due to reflection and absorption [102], that must be accounted for in quantitation.

Various other interesting standard schlieren have been suggested. For example, an infinitely-variable lens combination [976] and a standard glass wedge. Both of these are adjustable, the wedge by rotating it with respect to the schlieren cutoff direction. NASA-Langley uses a 5-arcsecond rotating wedge, which yields any refraction between 0 and 5 arcseconds depending on its rotation angle.

Other approaches include helium-filled soap bubbles [138], CO_2-filled soap bubbles [977], and a gas-filled "air lens" [2]. Greenberg et al. [358] used a gas-filled wedge and Lindsey [978] used a line of prism pairs.

Perhaps the easiest standard schliere is a simple flat glass plate [979]. Rotated about an axis perpendicular to the optical axis, such a glass flat offsets the incident parallel light beam by a distance:

$$\delta = t \cdot \sin\theta \left[1 - \sqrt{\frac{1-\sin^2\theta}{n^2-\sin^2\theta}} \right] \tag{10.3}$$

where t is the plate thickness, θ is its rotation angle from the normal to the optical axis, and n is the glass refractive index. Such an offset acts through the focal length f_2 as a schlieren refraction according to Eqn. 2.6, causing a displacement at the knife-edge and a corresponding illuminance change in the image.

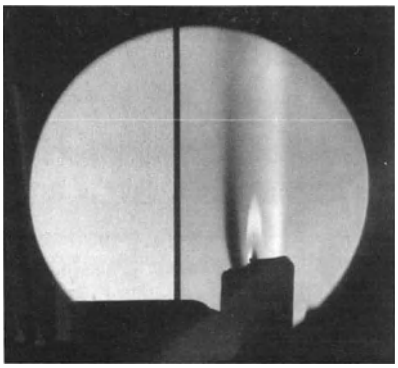

Fig. 10.2. Schlieren image of candle plume with 3 mm-thick glass plate (left) at 45° to the optical axis, serving as a standard schliere. At the horizontal white line the pixel gray-scale value in the standard averages 192, while the schlieren background averages 171. Correcting for glass reflection and absorption, the standard corresponds to the brightest candle-plume point, where $\varepsilon \sim 260$ arcseconds. The schlieren setup of Chap. 8 is used with 50% cutoff, h = 2 mm, f_2 = 864 mm, and n = 1.5.

A specific example is shown in Fig. 10.2. However, no detailed quantitative evaluation is attempted due to candle-plume axisymmetry, a vertical background gradient, and the non-linearity inherent in the photographic image.

10.2 Grid-Cutoff Methods

Schlieren methods using a grid, lattice, or bullseye cutoff filter indicate Δa directly in the image, providing a simpler means of quantitative evaluation than photometric methods [146]. Since $\Delta a = f_2\varepsilon$ according to Eqn. 2.6, this method essentially maps the refraction angle ε directly [82]. Ronchi [942,980] first tested lenses this way in 1925, and Schardin [1,2] later adapted the technique to schlieren imaging.

Grid methods are less-involved than photometry, rapid, simple, and also notably less sensitive. They are inherently quantitative, having little other justification for their existence. Originally intended to relieve the drudgery of quantitative photometry, they served the purpose well in the mid-20th Century. Although labor-saving methods of the pre-computer age have now lost some of their relevance, these methods still deserve note.

10.2.1 Focal Grids

In the focal-grid method the grid, lattice, *Gitterblende,* Ronchi ruling, or bullseye cutoff filter is located exactly at the focus in the schlieren cutoff plane as shown in Fig. 10.3a. If a is the grid bandwidth, then the lattice constant is generally $2\,a$, although opaque and clear bands of different widths are also usable. The light-source image width h is set about equal to a.

For small refractions in the test area, this method works just like Toepler's method, Chap. 3. But for sufficiently-strong refractions, light can be deflected across several grid bands, leading to discrete fringe-like *isophotes* in the schlieren image. Isophotes look like interference fringes, but are actually fringes of $\partial n/\partial y$ or $\partial n/\partial x$ rather than n itself. They are curves of constant illuminance and constant ε in the schlieren image, automatically handling the calibration issue. The boundary conditions must still supply the constant of integration, but a rapid and simple quantitative evaluation is now possible at modest sensitivity ($\varepsilon_{min} \sim 30$ arcseconds) without any photometry. Convective heat transfer, glass testing, and similar applications were once popular with these focal-grid methods. They have largely fallen into obscurity since the 1970's, except for one modern computerized adaptation to be described later.

Schardin [1] introduced focal grids for quantitative measurement, number seven in his epic explication of schlieren methods [2]. Prominent users included Darby [981], Speak and Walters [126], Didion and Oh [982], and Vasiliev [102], and

several more users of colored grids mentioned below. Also, Cornejo-Rodriguez [944] reviewed the Ronchi test from which all these methods originally sprang.

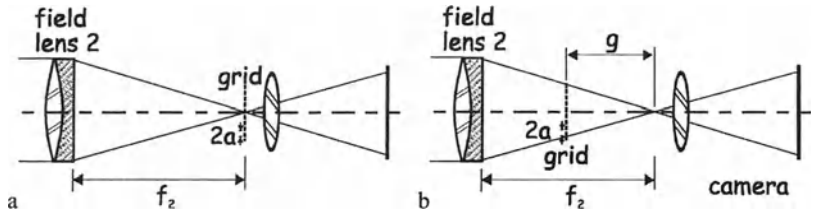

Fig. 10.3. **a** Focal grid method. **b** defocused grid method.

In principle, focal-grid schlieren eliminates many quantitative errors, but a few remaining errors must still be dealt with. Chief among these is the old resolution-sensitivity tradeoff once again: one wants a fine grid for high sensitivity, but this acts as a diffraction grating and smears the image resolution. This topic arose before in Sect. 3.6, Fig. 3.22c, and Sect. 4.3.4; an excellent discussion of it is given by Hosch and Walters [171].

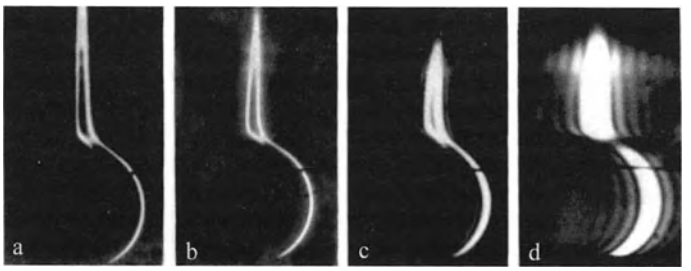

Fig. 10.4. Two isophotes from a focal-grid schlieren image of a heating pipe seen end-on. The grating slit width is: **a** 3.27 mm, **b** 1.60 mm, **c** 0.75 mm, and **d** 0.38 mm. Reproduced from Schardin [2] by courtesy of Springer-Verlag.

Schardin [2] illustrated this embodiment of the diffraction problem nicely with a focal-grid schlieren image of a 2-D horizontal heating-pipe flowfield, Fig. 10.4, where all but one dark grid band and the two adjacent clear bands were masked off. As the grid constant narrows in frames 10.4a-d, diffraction eventually smears the two resulting isophotes together until they become indistinguishable. When this happens, as it also did in Fig. 9.1b, quantitative evaluation is no longer possible. Thus the optimum grid constant a yields the narrowest *resolvable* isophotes in the schlieren image, since one wants the maximum number of usable isophotes

for best quantitation accuracy and sensitivity. To some extent, this best choice of grid constant and source-slit width also depends upon the strength and nature of the schlieren object under test.

Schardin appreciated the end-on horizontal heating-pipe flowfield as a prime example of a 2-D thermal flow amenable to parallel-light schlieren. It was often used as a test case, and it deserves continued use as a benchmark for new optical methods. Here, briefly, is Schardin's quantitation example [1,2] based on this flowfield.

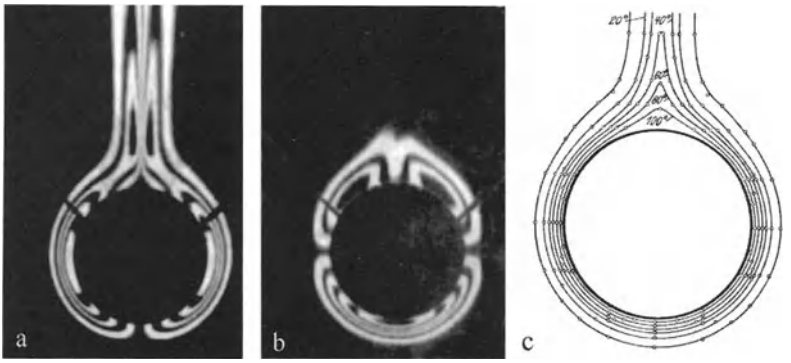

Fig. 10.5. Quantitative focal-grid schlieren evaluation of a horizontal heating-pipe flow by Schardin [1,2]. **a** vertical-grid image. **b** horizontal-grid image. **c** resulting temperature distribution (the pipe temperature was 140°C). Reproduced courtesy of Springer-Verlag.

Figs. 10.5a and b show two of Schardin's focal-grid schlieren images of a 4-cm-diameter, 30-cm-long heating pipe in parallel light. In both cases the light-source image is blocked by an opaque grid band, yielding darkfield exposures. To extract the entire temperature distribution, both horizontal and vertical grid orientations are required. The isophotes yield values of ε_x and ε_y throughout the flowfield, whence the quantitation proceeds using the formula $\varepsilon = 2ja/f_2$, where j is the ordinal number of the clear grid band corresponding to a given isophote. Details of the calculation are given in [1] and the resulting free-convection temperature distribution is shown in Fig. 10.5c.

Colored grids can be used when doubt arises about the ordinal number j of the isophotes. Each clear grid band is given a contrasting color using glass or gelatin filter material, and the resulting *isochromes* in the schlieren image are recorded in color. This is, in fact, Schardin's color band-lattice method, illustrated in Fig. 5.8 and discussed in the corresponding text. Several examples are shown in the Color Plates, and more can be found in [2,119,288,320,351,356,359].

Rainbow and Bullseye Schlieren are the new names taken on by the color-band-lattice and ring-lattice methods in the 1980's. Howes [325,411,412] introduced

color-transparency cutoff filters featuring continuous rather than discrete lattice bands. This improved the sensitivity of traditional band-lattice methods at some cost in resolution. More importantly, it ushered in a modern role for a technique on the verge of disuse, offering quantitative evaluation of suitable schlieren objects by simple calculations from the recorded hue, rather than from gray-scale values.

Given the computing power now available, some very nice quantitative rainbow schlieren studies have recently been published [358,360,361]. Continuously-graded, computer-generated rainbow filters are now a clear improvement upon the discrete bands of old [357], recovering much of the sensitivity lost by Schardin's band-lattice method. In fact, Howes [412] and Greenberg et al. [358] mustered enough sensitivity to beat laser interferometry at its own game.

The comparison of rainbow schlieren results with flow computations [361] and probe measurements [269,360] shows excellent agreement. Agrawal et al. [269] even succeeded with a 3-D tomographic adaptation. In short, computerized quantitative rainbow schlieren is definitely an issue for the future, maybe even for a new commercial schlieren instrument.

10.2.2 Defocused Grids

Now displace the grid a distance g to one side or the other of the schlieren focus, as shown in Fig. 10.3b. Given a small-enough light source, shadows of the gridlines immediately appear in the schlieren image with spacing inversely proportional to g. These straight shadows – fringes, if you like – are distorted by the refraction of a schlieren object in the test area. Such a "deflection mapping" approach [66] avoids all concern for photometry, image uniformity, or visualization quality in favor of measuring the gridline displacement. Simplicity of evaluation follows, since ε is proportional to displacement divided by f_2, as before. For simple schlieren objects, the displacement is obvious from a single image and no "tare" image is required. In many respects this method is a lower-sensitivity counterpart to classical finite-fringe interferometry [983].

Following Ronchi [980], subsequent investigators have refined the defocused-grid schlieren method [66,98,126,316,981,984]. Meyer-Arendt and Shettle [985] combined it with a lens-type standard schliere, obtaining a line ratio for calibration use. Vasiliev [102] devotes 25 pages to this topic, and is clearly the authority.

Since the fringe shift does not depend on the number of fringes, fine grids can be used for detailed work. Diffraction smearing limits this, however, as it did for the focused grid: 4 lines/mm is considered a practical limit [981]. Too much diffraction confuses the number of gridlines and confounds the analysis.

A sensitivity level of a few arcseconds is feasible with a defocused grid, but the method is most-often used to measure rather large deflections. Vasiliev [102] gives the analytical relations for sensitivity, range, and evaluation in more detail than is warranted here.

For the quantitative measurement of complicated schlieren objects, one must generally identify points in the image corresponding to points on the grid in both

"tare" and working images. Even so, the gridline shadows can become sufficiently confused that color-coding is also called for.

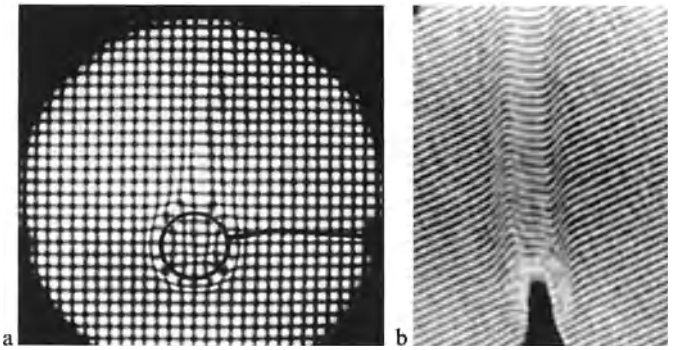

Fig. 10.6. Defocused-grid images by Weinberg [316]. **a** horizontal heating pipe imaged with a defocused wire screen having a 1.5 mm pitch. **b** "bat's-wing" flame viewed edge-on with a grating of 2.4 lines/mm. The deflection magnitude is evident from the distortion of the otherwise-straight gridlines. (US Government photographs.)

Vasiliev [102] discusses screen grids and circular-point grids for measuring simultaneous displacements in mutually-perpendicular directions. He finds these very diffraction-prone, but able to yield both deflection magnitude and direction. He also gives a good point-grid example of the horizontal heating-pipe flowfield.

10.2.3 Defocused Filament Cutoff

For completeness, consider next a defocused grid consisting of only a single opaque gridline. This resembles the focal-filament method already covered in Sect. 5.4.2, but here the filament is defocused and often at an angle to the schlieren object. Once again a simple estimate of beam deflection magnitude is the goal, and the proper visualization of most of the schlieren field is sacrificed in order to attain it.

The defocused-filament method was first suggested at about the same time by Taylor and Waldram [133] and Maksutov [101] in the 1930's. Several later investigators have used it [104,451,452,986-989] for quantitative work. Useful mainly for steady processes, it requires a survey of the image plane with two mutually-perpendicular filaments in order to map all of a general schlieren object. The method is not highly-sensitive, but is especially useful to determine heat transfer coefficients in boundary layers [357]. Vasiliev [102] gives quantitative examples of horizontal heating pipe and 2-D supersonic airfoil flows, and claims an accuracy of 1.5% to 10%, depending on conditions.

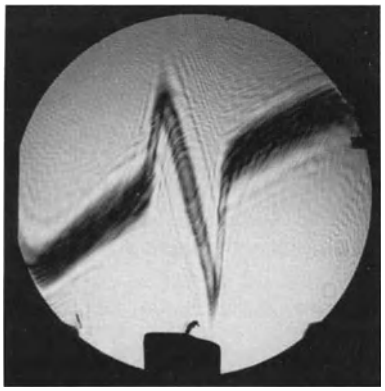

Fig. 10.7. Defocused-filament schlieren image of a candle plume with helium-neon laser illumination. The filament was a human hair defocused by several mm and rotated to the angle indicated by its shadow. The shadow distortion across the plume is a direct indication of ray deflection magnitude, which could be used to extract a quantitative temperature profile across the plume in this particularly-simple example. Photo by the author and Heather Ferree.

10.3 Quantitative Image Velocimetry

10.3.1 Background

While quantitative schlieren density measurements are well-known, no one until recently has tried schlieren velocimetry except for the hardy Townend [480]. His method, described earlier in Sect. 5.6, followed warm-air tufts from heated spark electrodes recorded in movies. The data analysis must have been painful in 1936.

More recently, Weinberg and Wong [255] analyzed infinitesimal-shear interferograms by consecutive frame analysis to get flow velocities, but the details are sketchy. Also Amman [874] reviewed combustion diagnostics, including eddy tracking in high-speed schlieren movies. These early attempts lacked a firm theoretical background and the digital hardware needed for practicality.

The theoretical background came in the 1990's. Image correlation velocimetry, wherein scalar image pairs are digitally analyzed for feature motion, was established by Tokumaru and Dimotakis [990] in 1995. Similar but independent work was published by Smith and Dutton [991] in 1999. Neither of these studies considered schlieren images specifically, but the approach serves generally for any type of imaging process.

At about the same time, Weinstein [484] patented a vaporizing-particle flow velocimeter in which dust or smoke particles are vaporized by a laser beam, creating hot-spots that convect downstream under the view of a schlieren instrument. The growth of these spots may yield temperature data as well.

Always an eclectic mix of the old and the new, schlieren imaging has taken this useful quantitative turn only within the last decade. Velocimetry is a big deal in flow diagnostics, where laser-Doppler velocimetry has recently given way to whole-field particle-image velocimetry (PIV). That approach requires particle seeding, of course, but schlieren imaging does not. The particles are always troublesome, so here the schlieren technique hold a clear advantage.

10.3.2 Multiple-Exposure Eddy and Shock Velocimetry

With high-speed cameras, turbulent eddy convection can be followed even in supersonic flows. Following Townend's original lead [480], Papamoschou [620] and McIntyre and Settles [808] used this approach to measure convection speeds in supersonic shear layers from consecutive high-speed schlieren images. The approach is simple and slightly subjective, in that corresponding structures are identified by eye before Δx and Δt are obtained to compute the velocity. Smith and Dutton [991] studied similar flows, but used laser scattering rather than schlieren images and applied an objective computerized approach. Kharitonov and Ershov [992], Seitz et al. [241] and Settles et al. [166] similarly clocked shock-wave motion in consecutive high-speed schlieren frames. An example from McIntyre's work is shown in Fig. 10.8.

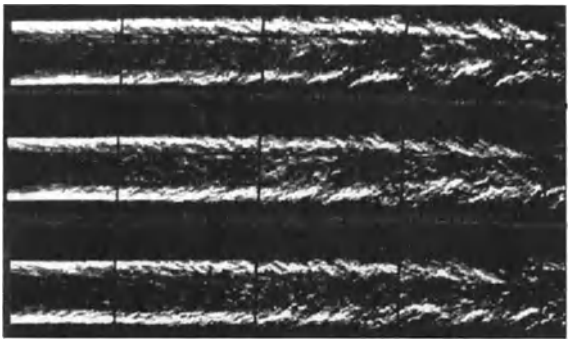

Fig. 10.8. Three consecutive Cranz-Schardin-camera schlieren images of the Mach 3 axisymmetric turbulent air-jet shown earlier in Fig. 9.21a [808,819]. Darkfield cutoff renders the larger turbulent shear-layer structures more evident. The elapsed time between frames is 8 μsec. With only a little imagination, a structure can be chosen and followed as it convects and evolves downstream.

10.3.3 Schlieren Image Correlation Velocimetry

Fu and Wu [993] accomplished schlieren velocimetry by digital image analysis of the plume from a flame in 1998. Fu et al. [994] later extended this work to lens-and-grid schlieren images of gas jets and convective plumes.

Kegerise and Settles [191] applied schlieren image-correlation velocimetry to an axisymmetric turbulent convective plume, checking their results against the velocity field obtained from planar laser scattering. This approach stops short of that advocated by Tokumaru and Dimotakis [990], making no attempt to comply with the equations of fluid motion. Instead, it merely determines the displacement field between two successive images based on the cross-correlation between translated image windows. The analysis is computationally-intensive but within the

range of a desktop computer. Clear working and tare schlieren images of the flow are required, and the Δt between images must be chosen so that a motion correlation actually exists between them.

The convective plume spreading rate and centerline velocity decay are accurately indicated by both schlieren and smoke images when analyzed this way. Path-integration in the schlieren measurements did not cause any error, apparently due to the broadly-counteracting effect of differentiation perpendicular to the schlieren cutoff (Davis and Li [121]).

This encourages a lot more schlieren image-correlation velocimetry in the future. Unfortunately the working and tare images require special attention, so one may not usually extract velocities from most of one's archived schlieren footage.

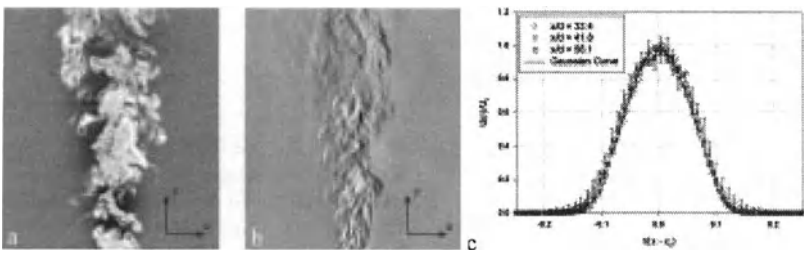

Fig. 10.9. Axisymmetric turbulent convective plume imaged by **a** planar laser scattering from smoke particles, and **b** schlieren imaging. **c** comparison of schlieren-image-correlation velocity profiles with a Gaussian curve. From Kegerise and Settles [191].

10.3.4 Focusing Schlieren Deflectometry

Focusing schlieren deflectometry was proposed in 1991 by McIntyre, Stanewsky, and Settles [808,971] and improved in 1993 by Alvi, Settles, and Weinstein [219] to combine the advantages of focusing schlieren and the high-speed two-point digital correlation of turbulent flows. The schlieren system images the flow in a plane sufficiently narrow to isolate individual turbulent structures, Fig. 10.10. Twin fiberoptic pickups and photomultiplier tubes sense the illumination at two points in the schlieren image, and these channels are digitized at high speed and analyzed. No attempt is made to do standard photometry, and in fact the amplitude of the two signals is ignored in favor of their frequency content. This makes the instrument uniquely suited for statistical turbulent flow measurements and velocimetry.

The focusing schlieren deflectometer was used to investigate the structure of a two-dimensional, adiabatic, Mach 3 wind tunnel wall boundary layer in [220]. Good agreement was found with hot-wire-anemometer data, and the distributions of broadband convection velocity of large-scale structures through the boundary later were measured. These results showed better resolution than previous data from intrusive probes.

Thus the focusing schlieren deflectometer deserves further use in turbulence research. It is unique among similar approaches in showing a real image of the flow under study, making fiberoptic probe placement less ambiguous. The approach was also extended to conventional photometric evaluation by Garg et al. [974].

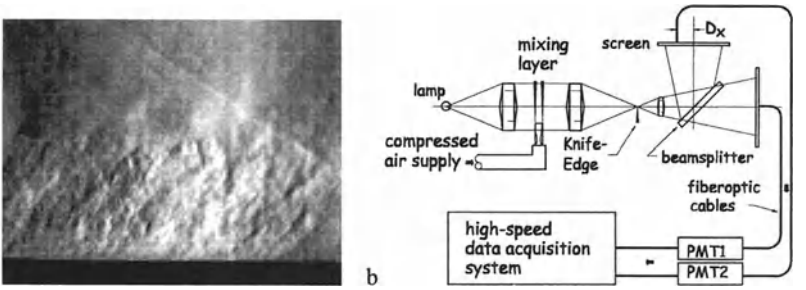

Fig. 10.10. **a** Microsecond focusing schlieren image of a Mach 3 turbulent boundary layer, showing individual inclined turbulent structures about 2 cm high [220]. A weak oblique shock wave is also seen in the upper right. **b** schematic diagram of the schlieren deflectometer, here shown with Toepler rather than focusing-schlieren optics [808,971].

10.3.5 The Background-Oriented Schlieren System

Raffel, Richard, Meier and associates at DLR Göttingen, Germany have recently suggested yet another simple new-age schlieren method [319,812,825]: a time-dependent optical field is viewed against a detailed background, along the lines first discussed in Sect. 4.3.2. Here, however, quantitative analysis is performed. The distortion of the background is recorded and standard computerized PIV methods are applied to extract the displacement field. The results can be used for velocimetry or for the measurement of the refractive-index-gradient distribution.

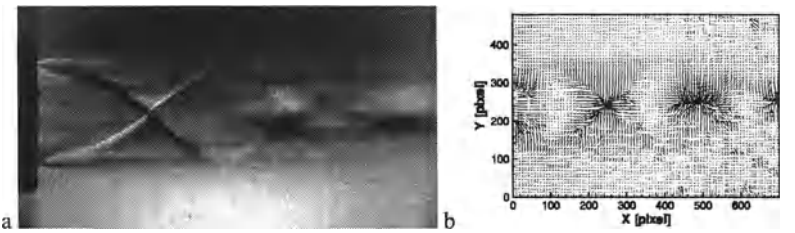

Fig. 10.11. **a** schlieren image of supersonic jet. **b** corresponding background-oriented schlieren displacement data. From [825], reproduced by courtesy of M. Raffel, DLR.

A noteworthy application of this method is in full-scale helicopter-rotor flowfield analysis (see also Sect. 9.3.13). The mottled appearance of the concrete helicopter pad was used as a background [814] and stereoscopic views were obtained.

10.4 Quantitative Shadowgraphy

10.4.1 Double Integration of $\partial^2 n/\partial y^2$

The double integration of $\partial^2 n/\partial y^2$ or $\partial^2 n/\partial x^2$ to extract quantitative refractive-index data has seldom been tried. Conventional pre-computer wisdom [98] held that it stretched things too far, and many restrictive assumptions were required. The level of effort is relieved by modern computer methods, but the basic question remains: why attempt it? Anyone who tries should be mindful of Weinberg's [66] warning about superposition, Sect. 6.2.1. An example is given by Lewis et al. [995].

10.4.2 Turbulence Research

As noted in Sect. 9.4.13, quantitative shadowgraphy has played a role in turbulence research beginning with Uberoi and Kovasznay in 1955 [959], followed by Taylor [510,960] and Hesselink and White [161,511]. The statistical analysis of shadowgram intensity variations is related to turbulent density fluctuation levels and spectra, yielding useful results [512,747,961-963].

10.4.3 Shock-Wave Strength Quantitation

In Sect. 6.4.3 on computed shadowgraphy, synthetic shadowgrams for shock-wave strength quantitation were noted as early as 1945 [115,252,548,549]. Undoubtedly arising from atomic weapons research, this method allows the strength of an explosion-generated shock wave to be inferred. More recent applications [460,550-553] similarly compare experimental shadowgrams with computed maps of $\partial^2 n/\partial y^2$ for the purpose of quantitation.

10.4.4 Grid Shadowgraphy Methods

Again, as described in Sect. 6.2.1, shadowgrams are very susceptible to ambiguity whenever light superposes on a point in the shadow from two different regions of the test area [66]. It helps to resolve this ambiguity by tagging and tracking the history of individual light rays, for example by imposing a grid or screen upon the

initial light beam [2]. The optical arrangement for direct shadowgraphy in diverging light is diagrammed in Fig. 10.12a, and an example is shown in Fig. 10.13. Schardin [2] remarked that the "evaluation is naturally very tedious," but nowadays computers can bear the brunt of this.

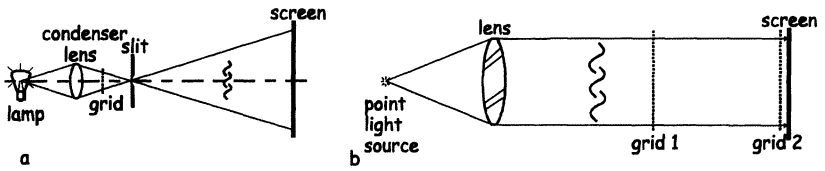

Fig. 10.12. **a** Diagram of direct shadowgraphy with grid projection [2]. **b** diagram of the moiré deflectometry process [118,600,996-998].

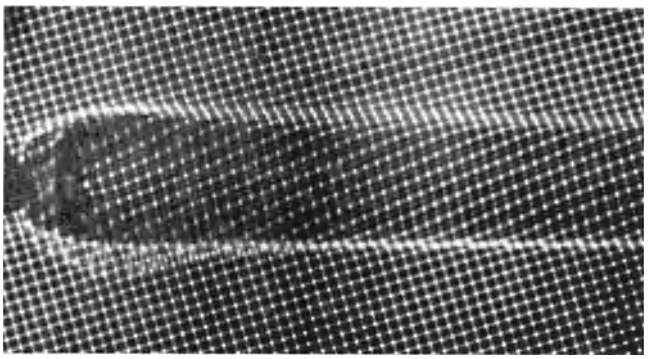

Fig. 10.13. Grid-projection shadowgram of a "bat's-wing" flame. From Weinberg [316], rotated 90° for convenience. US Government photograph.

Moiré Deflectometry, a popular optical method, is classified here as grid shadowgraphy because no conjugate image of the schlieren test area is produced. Instead, a grid near the test area is shadow-projected upon a like grid at the viewing screen position, Fig. 10.12b. The method has antecedents in Fromme [248], Nishijima and Oster [247] and Bampfield [249], where moiré patterns generated between two grids indicate subtle distortions in the optical wavefront. Investigators Kafri, Glatt, Kreske, Keren, and Stricker explored a wide variety of applications for this in the 1980's [118,326,600,601,763,872,943,996-1000]. Rotlex Ltd., an Israeli high-tech company, patented the technology. Rotlex now seems to concentrate solely upon the application of moiré deflectometry to ophthalmic measuring instruments (http://www.israel.net/rotlex).

11 Summary and Outlook

New glimpses through the old holes.

> I made the journey to knowledge like dogs who go for walks with their masters, a hundred times forward and backward over the same territory; and when I arrived I was tired.
>
> *G. C. Lichtenberg*

Throughout the writing of this book I expected to gain a new perspective on the time-honored techniques considered here: approaches not tried before, clues to important new applications, and a broader appreciation of the role schlieren and shadowgraphy – the optics of inhomogeneous media – play in science and technology. Now comes the moment of truth.

11.1 Summary

11.1.1 Perceptions Outside the Scientific Community

One of the present goals is to clarify some misconceptions. Some examples were mentioned already: confusion over the strange word *schlieren*, and over the "human aura." Some even confuse the present topic with Kirlian photography, which is a very different thing indeed. Also, those unfamiliar with laboratory optics often expect to see a special point-and-shoot "schlieren camera," or even a unique filter placed over an ordinary camera lens in order to take schlieren photos. Photographers want to know what special backdrop was used (none of the answers: "the lamp filament," "the mirror surface," or "there is no backdrop" satisfies). Most often schlieren is mistaken for infrared thermography, which outnumbers it at least 10:1 in both the technical literature and in movie special effects.

Unfamiliar views of recognizable things grab the public attention. Not-too-abstract scientific images thus have a lot of appeal. Color is an important part of this appeal, too [602]. Nowadays, even though the public is inundated with all sorts of pseudo-scientific imagery, good images that tell a story are still important.

G. S. Settles, *Schlieren and Shadowgraph Techniques*

But of course, they must also be *new*. The media like to show schlieren images that are striking, appealing, and scientifically-flavored, but when I tell them about Robert Hooke it turns them off. This same fixation is responsible, I think, for the disuse of some perfectly-good schlieren methods: something newer and sexier just happened along (in glass testing and microscopy, for example). I believe this was unwise, and schlieren methods are ripe to re-emerge.

11.1.2 Other Lessons Learned

I began this book convinced that quantitative schlieren methods were obsolete. Clearly I was wrong, since a couple of computerized quantitative methods have sprung up in the last decade with good justification. Likewise I felt that lasers were inappropriate schlieren light sources; not so, just use the proper cutoff.

Some of the other lessons learned were equally surprising: computer searches of databases like Medline and Agricola turned up many new applications, swelling Chap. 9 far beyond expectation. I also found several interesting and useful ideas buried in the literature, evidently never used since their introduction. That may be the nature of the scientific enterprise, but exhuming and examining these old ideas on occasion is quite instructive.

Schlieren and shadowgraph methods are rather unique in science and technology, in that they are used regularly but have almost no commercial presence. In Toepler's day a scientist built all his own apparatus, but now an amazing range of scientific instruments is available off-the-shelf. The paucity of commercial schlieren instruments and the failure of earlier examples remains hard to understand, but somehow they simply never grew up in this respect. As always, we just continue to build our own; it helps prevent us from becoming appliance operators.

Partly due to the necessity of building-our-own, schlieren users have shown boundless inventiveness and no small amount of re-inventiveness. I see that partly as an educational activity: for every professional monograph on this topic there are several theses, papers, and Web pages on "building my own schlieren system."

Of its siblings, the present topic is closer to microscopy than to telescopy. True, its large parabolic mirrors are inherited from telescopes, but much else, including many spatial filtering schemes, came originally from microscopy. [1] So, to become a master of the schlieren arts, know your microscopy, but also think like an astronomer: think in arcseconds.

Finally, schlieren and shadowgraphy established themselves in the 20 th Century as visualization tools that are useful without having to steal the show. Almost everyone writes about what they saw with these techniques, but comparatively few write about the techniques themselves. As a result, more so than either telescopy or microscopy, schlieren and shadowgraphy live almost entirely through their applications. Horst Herbrich [602] thinks we have collectively "undersold" these

[1] Oblique illumination, Toepler's microscopic schlieren, Rheinberg illumination, Zernike's phase contrast, differential interferometry, and Hoffman Modulation Contrast.

techniques to the public, so the techniques emerge for awhile in new fields only to go dormant again (the *Sleeping Beauty Effect*). To avoid another trance, he recommends published examples in the trade press, affordable proven commercial instruments, and a modern book!

11.1.3 Further Comments on Historical Development

A reasonably-complete appreciation of this topic's fascinating history, given in Chap. 1, is only quite recent. Before 1975 [14], schlieren was simply ascribed to Toepler and shadowgraphy to Dvorák, with Foucault mentioned occasionally by Francophiles. The true historical path is much more contorted, halting, and beset with apparent dead-ends than that. Media technologist James Burke, author of the popular historical *Connections* series, claims that many technical fields developed along such non-linear, non-sequitur paths.

Toepler is the key historical figure in schlieren imaging, being directly responsible for its popularization and growth in the 19th and 20th Centuries. Next in importance is Schardin, who was the first to provide a unified view. Thanks to them, the reputation and applications of schlieren and shadowgraphy blossomed in the last century. Schlieren images and shadowgrams became paradigms of visualization that permeated the fabric of science and technology. Once you know them, you cannot even thumb through a magazine or take a walk out doors without seeing an inadvertent shadowgram or a background-distortion schlieren image.

11.1.4 Further Comments on Images and Visualization

> Only in half-shadows could I make some phenomena visible.
>
> *August Toepler* [40]

> It is sufficient for images to resemble objects in but a few ways, and even that their perfection frequently depends on their not resembling them as much as they might.
>
> *René Descartes,* 4th Discourse on Optics, 1637

Previous chapters repeatedly point to the unique beauty of a schlieren image, like a relief sculpture or the play of light and shadow on a sand dune. Here lies the charm of the entire topic, of course: that it not only allows us to see the invisible, but also to see it in an elegant, even artistic manner. The few "ugly" schlieren images or shadowgrams found in the literature result from a neglect of this principle, from regarding the optical methods as purely utilitarian and peripheral to the topic at hand, and from having no feeling for aesthetics.

Images appeal to us on many levels [8,1001-1004]. In fact all of visualization, not just schlieren and shadowgraphy, depends upon a background of ideas from art history and perceptual and cognitive psychology. Visualization requires right-brain activity: seeing spatial relationships, recognizing patterns and what they rep-

resent, thinking in pictorial terms [1004]. In this sense, schlieren images and shadowgrams are high-level forms of data presentation [1003], portraying the information visually for immediate conscious analysis based on our knowledge and experience. These images convey technical concepts directly to the brain.

So, when you examine the images of various phenomena in this book, allow yourself to see not just gray-scale or color maps of optical phase, but rather the actual phenomena themselves, observed directly through "schlieren eyes," through the window of the page. Unlike photographs of people, schlieren images cannot be compared directly with their schlieren objects in order to judge accuracy. They do not pretend to be what they are not [1001], rather they stand in place of what they portray. Kafka said: "Photography concentrates one's eyes on the superficial" [1005]. Not schlieren and shadowgraphy, though: they let you see clear through.

Icons help to reinforce this point. These familiar little pictograms reduce an image to its bare essentials, conveying instant visual concept recognition in a few pen strokes and transcending language barriers [1001]. Six "schlieren icons" are shown in Fig. 11.1, drawn from some of the actual images presented earlier. They stand for the various phenomena described in the caption, although naming them should not really be necessary. More broadly, they convey concepts that would require a lot of explanation if not for images: heat rises, heavy vapors fall, the air about us is rather turbulent, two streams mix by organized vortical motion, shock waves propagate spherically, and supersonic projectiles leave their sound behind.

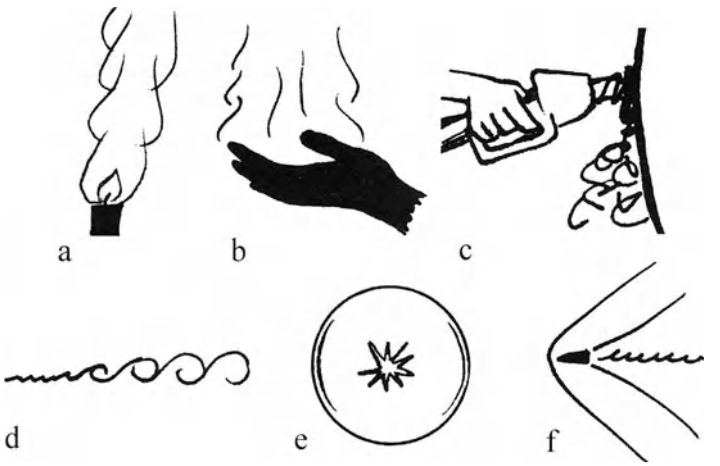

Fig. 11.1. Schlieren icons: **a** a turbulent candle plume, **b** convection from a human hand, **c** vapor leak while filling a fuel tank, **d** Kelvin-Helmholtz vortices in a planar mixing layer, **e** the spherical shock wave from an explosion, **f** a supersonic bullet.

These interpretations are all well-known, but for a new or a complicated phenomenon, the interpretation of schlieren and shadowgraphy is not always so sim-

ple. As a very young man in 1967, I got to show one of my early schlieren images to Walter F. Lindsey, a seasoned NASA researcher. I told him what I thought I saw in it, but he saw something different. When I objected, he pointed out that he was a lot older than me, and that he was interpreting schlieren pictures before I was born. Beyond the hubris of youth, this illustrates that a schlieren image or shadowgram can often have a variety of interpretations. The ability to make a correct one calls for experience. There is no substitute for it, but the images and interpretations in this book are intended to give the reader some guidance.

For the fluid dynamicist, further principles of visualization are stated and exemplified in important papers by Kline [673] and Roshko [1006], and in Van Dyke's splendid Album [739]. Flow visualization is useful in basic fluids research for discovery, exploration, qualitative insight, and quantitative measurement. The nature of the governing equations admits multiple flow patterns for a single set of boundary conditions, and even today's powerful computers cannot generally say which patterns may occur in practice. Visualization is thus the cheapest, quickest, and most direct route to flow patterns, which are the very fabric of fluid dynamics.

Finally, Stephens [1001] notes that images also have the power to upset the status quo. Muybridge's historic galloping-horse sequence, for example, revealed a reality at variance with expectations and upset a lot of people. Mach's supersonic-bullet schlieren image (Fig. 1.12), on the other hand, served to settle a theoretical argument by force of direct visual evidence. I try to warn potential industrial clients that, although schlieren may show them what is there, it may not turn out to be what they hope and expect to see.

11.1.5 Renewed Vitality

In the 58 years since Schardin's epic monograph on schlieren methods and their applications [2], these methods saw rapid growth followed by a slower period once lasers came on the scene. I am pleased to observe, though, that schlieren and shadowgraphy now show renewed vitality. Laser interferometry never really replaced them, and computers have been brought on-board in several useful ways.

The 1990's saw significant growth of new methods and applications. Inspired by Leonard Weinstein, focusing schlieren became a popular technique and several large-scale schlieren systems were built on the lens-and-grid principle, now finally mature. Background-distortion schlieren methods, for years a Schardin curiosity, now flourish outdoors [112,522] as well as in the lab. Scanning schlieren methods are largely yet to be exploited, but have important industrial applications ready and waiting for them.

Videography and digital imaging have been integrated fully into schlieren and shadowgraphy since 1980, encouraging some new methods to develop. [2] Digital image post-processing and contrast enhancement prompted the first significant

[2] e.g. "synthetic" schlieren [250,251,254].

revision of schlieren sensitivity principles in 60 years (Sect. 3.2.4). The link with optical image processing still remains essentially unexplored.

Computers have changed schlieren and shadowgraphy in several useful ways. Computational fluid dynamics (CFD) yields computed schlieren images and shadowgrams to compare with the experimental kind. This teaches everyone some basic scientific visualization, and reminds us that clever scientific experiments must not disappear merely because computers have arrived.

Ray-tracing optical design codes now allow us to design schlieren and shadowgraph systems much more complex than the simple ones shown here. This can be important for compact systems intended to fly in orbit, or – for a real challenge – new commercial schlieren instruments here on Earth.

Quantitative schlieren and shadowgraphy have staged a comeback very recently, thanks to the computer for relieving the drudgery of data acquisition and reduction. Now, not only the flow density but also the velocity field can be extracted from images once regarded as essentially qualitative.

Finally, more new applications arose than old ones declined in the late 20 th Century. This promising trend relies on new technology developments elsewhere, and reminds us to be always on the lookout for new opportunities. All considered, the popularity of schlieren and shadowgraphy is definitely growing.

11.2 Outlook: Issues for the Future

11.2.1 Predictions

Predicting the future is pretty scary. Hooke made no attempt to say where he thought his newly-discovered techniques were headed, but Marat boldly predicted new physics discoveries from shadowgraphy. Toepler saw the wave of the future in spark-illuminated schlieren images of high-speed events, and he was right. Dvorák got off on the wrong foot by trying to make shadowgraphy an adversary of schlieren. Schardin saw lens-and-grid schlieren, for example, as a quantitative method for strongly-refracting schlieren objects, missing its modern focusing and large-field uses. He also mentioned scanning systems only in passing without exploring their potential. These omissions are minor, though, for someone who saw so much.

50 years ago, Burton [104] doubted any great advances in schlieren imaging because "the design limitations seem to come from the properties of light itself." No one then foresaw the lasers, digital imaging, and computers that we have today. Burton's own focusing schlieren innovation, required almost 50 years to mature. Similarly Fish and Parnham [106] believed that 30 cm was the practical size limit for a schlieren source grid (the largest nowadays, Sect. 4.3.5, is almost 6 m).

North [84] claimed that Schardin's works on schlieren methods "could hardly be improved upon if they were rewritten now, but since times have changed, it is unlikely that this task will ever be attempted." Here I am attempting it, 60 years later, in part because times *have* changed, and good reasons to do so have emerged: Fourier optics, lens-and-grid systems, digital post-processing, computed schlieren images, many new applications, and so forth.

So, where does it all go from here? I see no farther through a brick wall than anyone else, but I will hazard a few guesses.

The ground covered in this book still has many ill-explored pathways. Multi-pass, high-sensitivity schlieren and resonant refractivity are two examples. Some of these paths deserve more exploration, others do not. The future of schlieren microscopy and the tie-in with optical image processing are especially promising, and I hope to see them pursued.

I expect to see new light sources arise that will augment and extend schlieren and shadowgraphy. Likewise new digital image sensors at high resolution and video at much-higher speeds are likely. The consequent demise of special photographic films, however, will probably eliminate some of the useful methods discussed here.

New commercial schlieren instruments with the breadth of those once manufactured (Sect. 7.4) are not likely according to historical perspective. Specialty instruments like the Intec Optison and the ATTO Schlierograph, though, seem to follow different rules. More instruments of this type are probable.

I expect to see increased activity in plastic and glass testing applications, and in all manner of applications for focusing and full-scale schlieren imaging. Portable lens-and-grid schlieren setups are already on the rise, and scanning systems have similar potential. Quantitative computerized schlieren imaging also seems ripe for further development. An opportunity for a new commercial schlieren instrument might even lie here.

Fusions of schlieren and shadowgraphy with other technologies have flourished in recent years. Thus schlieren + particle-image velocimetry yields background-oriented schlieren, schlieren + video processing yields "synthetic" schlieren, and schlieren + image processing yields schlieren velocimetry. Horst Herbrich [620] sees a potential for schlieren + thermography in materials-processing applications. Look for even more fusions of this sort.

Traditional applications, on the other hand, show few signs of fading. Supersonic wind tunnels have given some ground to computers, but ballistics, heat transfer and combustion applications are robust and will continue to be so.

By all accounts the lasers and computers associated with the present topic will see advances hardly predictable now. In fact, the brave new world of modern optics and photonics has already swept past the niche occupied by the optics of inhomogeneous media. Look for advances in micro-electromechanical systems (MEMS), like mega-mirror micro-arrays that could become either programmable schlieren objects or programmable cutoffs.

What about the traditional rivalry between schlieren methods and laser interferometry? I think schlieren will always outperform interferometry at qualitative visualization, being more sensitive and intuitive, and lacking the discrete fringes.

Laser interferometry will continue to dominate the quantitative applications, but will give some way to computerized quantitative schlieren methods.

Desktop physical-optics codes already allow the simulation of a schlieren system with the all-important diffraction terms included (App. B). Better handling of extended polychromatic light sources is still needed, but soon such codes will allow a realistic virtual schlieren-system simulation. Coupled with CFD, for example, this will not only yield computed schlieren images, but also will let one adjust the sensitivity and range, choose among a variety of cutoffs, and even add color.

Finally, this book is written in an era when many traditional technologies are becoming obsolete. For example, some fluid dynamicists expect that someday – not anytime soon – CFD will completely eliminate the need for experiments in fluids, including traditional schlieren images. n/ y will still be extracted from these solutions, of course, and will be displayed as computed schlieren for human consumption. Believing in the great tradition of scientific experimentation, I doubt this scenario.

Will schlieren and shadowgraphy pass into obscurity like the slide rule, the planimeter, and the mathematical method of steepest descent? No; not unless microscopes and telescopes suffer the same fate.

11.2.2 Opportunities

Several opportunities for the future were mentioned earlier. These opportunities lie in the use of certain new or neglected schlieren and shadowgraph methods, and in the pursuit of certain applications summarized below.

Quantitative Opportunities, covered in detail in Chap. 10, arise from computers having relieved the drudgery of schlieren data analysis, and because laser interferometry has lost its first blush of novelty. Rainbow quantitative schlieren is well-represented in the literature [269,325,358,360,361,411,412], but background-oriented methods [319,812,825], schlieren deflectometry [219,220,808,971,974], and schlieren velocimetry [191,993,994] are newer and need further exposure.

Current-Application Opportunities include schlieren microscopy, which is poised for a comeback. It is straightforward and its pseudo-3-D images are as compelling as scanning electron micrograms. Even in this age of new atomic-level microscopes, countless traditional optical microscopes still see daily use. The revealing beauty of Rheinberg illumination ought to be used more often in this routine microscopic work.

Plate-glass testing using scanning schlieren systems has enormous market potential, as described in Sects. 4.4 and 9.1.1. In some cases, like glass tempering by cold supersonic jets, multiple opportunities exist.

Another opportunity lies in exploiting the almost-untouched artistic implications of schlieren and shadowgraphy, sect. 9.4.1. Some of the more aesthetic images generated by these techniques can literally be framed and hung as art. Scien-

tific art, to be sure, but that is a refined art form that carries a visual message directly from the Shop of Nature.[3] There is no shame in this for any scientist or engineer motivated enough and capable of doing it. Carl Sagan (1934-1996) and M. C. Escher (1898-1972) were both criticized by their peers for crossing the boundaries between science, art, and popularization. I forget the names of those critical peers, though.

Weinstein's Schlieren for Aircraft in Flight (Sect. 4.4.1) promises a considerable advantage over wind tunnel testing. It was already used for sonic boom studies, but its broader potential lies in full-scale transonic flight imaging, where wind tunnels are least accurate. The necessary resolution comes from optics mounted in a "chase" plane that follows the test aircraft and looks across it at the Sun.

Educational uses of the present techniques represent a similar opportunity, and another window into the Shop of Nature that is seldom used for this purpose. Holder and North [95] and Coles [800] knew just how to do it, but their films have become dated. My colleagues and I made a more-recent attempt using multimedia [611]. One of our schlieren examples, the video counterpart of Fig. 4.1b, can also be found on a commercial educational CD-ROM [1007].

New-Application Opportunities can be found in such topics as porous-media flows [690,695], where focusing schlieren or shadowgraphy could lend a crucial advantage. Turbid materials, especially human flesh, may become accessible to schlieren and shadow observation after the application of refractive-index-matching agents to reduce light scattering.[4] Also speech therapy, sleep apnea, and related medical applications (Sect. 9.4.2) are opportunities almost untouched by schlieren and shadowgraphy. A broad panoply of untouched industrial applications awaits schlieren equipment robust, portable, and vibration-resistant enough (Sect. 7.4.3) to leave the laboratory and venture out into the world.

Opportunities Due to Other Technology Developments include, for example, large, light telescope mirrors intended for astronomy [137,176-182,1008], and commercial kitchen ventilation [232,236]. Ventilation engineers recently lacked a way to visualize the capture and containment of cooking fumes. When schlieren imaging fulfilled this need, it was written into an ASTM Standard [175].

The close ties between schlieren imaging and Fourier optics were covered in Sect. 9.4.8. New, better spatial filtering schemes represent a special opportunity, since matched spatial filters are an underdeveloped theme of schlieren imaging. Weinberg's [66] powerful principle of designing the matched filter pair specifically to reveal a certain deflection field is almost never used.

Can we use the image-processing nature of the schlieren system to observe or measure new things? For example, can we do schlieren "character recognition" to reveal specific features of a schlieren object? Can we make better use of photochromic and photorefractive cutoffs? What about spatial filters for unusual derivatives like $^{2}n/ x y$, or the optical integration of the schlieren image [941]?

[3] Great art and great photography often manage to illustrate or even tell stories [1001].

[4] Members of my generation will fondly recall the "Visible Man" and "Visible Woman."

rivatives like $^2n/ x y$, or the optical integration of the schlieren image [941]? Some innovative thinking about this might produce significant new schlieren methods and applications.

The revolution in schlieren sensitivity due to digital image processing can also yield new opportunities [161]. Though some image enhancements are rather obvious (Sect. 3.2.4), what about special algorithms tailored for this specific application, e.g. a detector of bas-relief illumination, or a Mach number filter based on wave angle?

The intersection of the present methods with computed solutions of the governing equations for various phenomena is an endless source of future opportunities. Computed schlieren and shadowgraphy (Sects. 5.5 and 6.4.3) no doubt constitute one wave of the future. As computations improve, more computed schlieren images are bound to appear, providing meta-views of large datasets. They don't compete with schlieren images, they *are* schlieren images. Let us accept them as such; the experimental variety will not fade away on that account.

Can we put our strong visual experience with schlieren and shadowgraphy to use at other wavelengths? The sensitivity advantage of infrared schlieren was discussed in Sect. 5.8.6, but more drastic excursions than that are possible. Microwave schlieren has been attempted, for example, and the present principles certainly still work in transmission electron microscopy [937] and x-ray radiography [845,846]. Neutron shadowgraphy was demonstrated most recently [1009], though the misleading name "phase contrast" was applied. Our experience in visible-light schlieren and shadowgraphy ought to be helpful to our colleagues, who are only now discovering these techniques at other wavelengths.

Finally, modern optical design programs (ray-tracing codes) offer opportunities for optical systems more sophisticated than the simple examples given here. The same can be said for electronics and electro-optics, which are under-utilized for chores like knife-edge tracking for constant background illuminance and automatic adjustment of the schlieren measuring range.

11.2.3 Recommendations

Much of the above can be condensed into a few simple recommendations for the future of schlieren and shadowgraphy: fertile directions to take, based on a survey of the state-of-the-art.

In schlieren imaging, work at the minimum sensitivity level for the phenomenon you want to visualize. This means less vibration sensitivity, less diffraction, and less distracting background noise. Schardin understood this very well. Nowadays, though, the sensitivity often gets cranked up too high.

For this purpose use a graded filter instead of a razor-blade cutoff. Graded filters are quite easy to obtain and use (Sect. 5.1.1), but few use them these days.

Use laser light sources for schlieren and shadowgraphy whenever they yield an advantage, but not ever with a razor-blade knife-edge cutoff. Instead, a graded filter or a neutral-density knife-edge does a much-better job (Sect. 7.1.1).

Use color schlieren and "focused" shadowgraphy without reluctance. Critics of these useful methods have missed the point.

A host of other powerful specialized optical methods is available but underused: Weinberg's polar-diagram method to design matched spatial filters, stereoscopic schlieren, the Cranz-Schardin camera, computed schlieren, and schlieren streamline tracers. Take advantage of the many opportunities for schlieren and shadowgraphy outdoors. Above all, use schlieren microscopy, focusing schlieren, and full-scale schlieren and shadowgraphy. The best wizards know how to reach deeply into their bags of tricks.

Finally, I recommend that less-experienced readers build and use the simple z-type schlieren system of Chap. 8. It's a great learning experience.

11.3 Closing Remarks

From the historical outset, it has been clear that schlieren and shadowgraphy are not ordinary scientific instruments, not machines that go "beep." The broad visual range of their applications comes from broad dissemination of knowledge about them, starting a long time ago. This book attempts to consolidate that knowledge in one place, and to make it even more widely available.

Though they are time-honored techniques, schlieren and shadowgraphy can never grow old in the sense of being replaced by more modern methods, thus falling into disuse. Like the microscope and the telescope, they are too basic and too broadly applicable for that. Important new developments in the optics of inhomogeneous media will continue so long as fertile minds survive in the tradition of Toepler, Mach, Schardin, and Weinstein.

The examples in this book show the key role these optical techniques have played in the progress of science and technology. They provide a way to see – a window into the Shop of Nature – that is unique, useful, and elegant. To fully appreciate and exercise them, the technician and scientist need a touch of the artist and poet as well. Schlieren and shadowgraph techniques, relatively-simple but powerful visual tools, help us satisfy our insatiable curiosity.

References

1. Schardin, H. Das Toeplersche Schlierenverfahren: Grundlagen für seine Anwendung und quantitative Auswertung. *VDI-Forschungsheft No. 367*, **5**(4):1-32, 1934.
2. Schardin, H. Die Schlierenverfahren und ihre Anwendungen. *Ergebnisse der Exakten Naturwissenschaften*, **20**:303-439, 1942. English translation available as NASA TT F-12731, April 1970 (N70-25586).
3. Toepler, A. *Beobachtungen nach einer neuen optischen Methode - Ein Beitrag zur Experimentalphysik*. M. Cohen & Son, Bonn, 1864.
4. Mach, E. and P. Salcher. Photographische Fixierung der durch Projectile in der Luft eingeleiteten Vorgänge. *Sitzungsb. Akad. Wiss. Wien*, **95** :764-780, 1887.
5. Sabine, W. C. Theatre acoustics. *American Architect*, **104**:257ff, 1913.
6. Cranz, C. and H. Schardin. Kinematographie auf ruhendem Film und mit extrem hoher Bildfrequenz. *Zeitschrift für Physik*, **56**:147-183, 1929.
7. Brown, G. L. and A. Roshko. On density effects and large structure in a turbulent mixing layer. *J. Fluid Mech.*, **64**(4):775-816, 1974.
8. Clark, K. *Looking at pictures*. Holt, Rinehart & Winston, NY, 1960.
9. Mach, E. On some phenomena attending the flight of projectiles. *Popular Scientific Lectures*, ed. T. J. McCormack. Open Court Pub. Co., IL, ed. 5, pp. 309-337, 1943.
10. Reese, W. E. *The Settle-Suttle family*. ed. F. L. C. Fisher. Thomasson Printing Co., Carrolton, GA, http://people.mw.mediaone.net/gbs00/index.htm., 1974.
11. Rienitz, J. Optical inhomogeneities: schlieren and shadowgraph methods in the seventeenth and eighteenth centuries. *Endeavor*, **21**(2):77-81, 1997.
12. Krehl, P. and S. Engemann. August Toepler - the first who visualized shock waves. *Shock Waves*, **5**:1-18, 1995.
13. Ershov, I. V. Private communication. Feb. 1, 2000.
14. Rienitz, J. Schlieren experiment 300 years ago. *Nature*, **254**(5498):293-295, 1975.
15. Andrade, E. N. d. C. Robert Hooke. *Sci. Am.*, **194**:94-98, 1954.
16. Montagu, M. F. A. A spurious portrait of Robert Hooke. *Isis*, **33**:15-17, 1941.
17. Hooke, R. *Micrographia*. J. Martyn & J. Allestry, London, 1665.
18. Simpson, A. D. C. Robert Hooke and practical optics. *Robert Hooke: New Studies*, ed. M. Hunter and S. Schaffer. Boydell Press, NH, pp. 33-61, 1989.
19. Morgan, J. R. Robert Hooke (1635-1703). *Sci. Progress*, **25**:282-294, 1930.
20. Moore, D. T. Gradient-index optics: a review. *App. Optics*, **19**(7):1035-1038, 1980.
21. Birch, T. *The history of the Royal Society of London*. Vol. 3. London, 1757.
22. Hooke, R. *Lampas*. J. Martyn, London, 1677.
23. Dvorák, V. Über eine neue einfache Art der Schlierenbeobachtung. *Wiedemanns Annalen der Physik und Chemie*, **9**(3):502-511, 1880.
24. Bennett, J. A. Robert Hooke as Mechanic and Natural Philosopher. *Notes and Records of the Royal Society*, **35**:33-48, 1980.

25. Hooke, R. *The diary of Robert Hooke, M.A., M.D., F.R.S., 1672-1680.* ed. H. W. Robinson and W. Adams. Taylor & Francis, London, 1935.
26. Huygens, C. *Oeuvres completes de Christiaan Huygens*. Vol. 21. Martinus Nijhoff, La Haye, Holland, ed. 1, 1944.
27. Gottschalk, L. R. *Jean Paul Marat - A Study in Radicalism*. B. Blom, New York, 1927.
28. Marat, J. P. *Recherches physiques sur le feu*. Cl. Ant. Jombert, Paris, 1780.
29. Asimov, I. *Asimov's biographical encyclopedia of science and technology*. Avon Books, New York, ed. 2, 1972.
30. Conner, C. D. *Jean Paul Marat: scientist and revolutionary*. Humanities Press Intl., Atlantic Highlands, NJ, 1997.
31. Foucault, L. Mémoire sur la construction des télescopes en verre argenté. *Annales de l'Observatoire Impérial de Paris*, **5**:197-237, 1859.
32. Foucault, L. *Recueil des travaux scientifiques de Leon Foucault*. ed. C. M. Gariel. Gauthier-Villars, Paris, pp. 554-558, 1878.
33. Ellison, W. F. A. Testing; Foucault shadow testing. Chap. 3 of *Amateur Telescope Making, Book 1*, ed. A. G. Ingalls. Scientific American, NY, ed. 4, pp. 82-84, 1980.
34. Porter, R. W. Mirror making for reflecting telescopes. Chap. 1 of *Amateur Telescope Making, Book 1*, ed. A. G. Ingalls. Scientific American, NY, ed. 4, pp. 1-19, 1980.
35. Draper, H. On the construction of a silvered glass telescope 15.5" in aperture, and its use in celestial photography. *Smithsonian Contribns. Knowledge*, **14**, pp. 1-19, 1864.
36. Douglass, A. E. Atmosphere, telescope, and observer. *Amateur Telescope Making, Book 2*, ed. A. G. Ingalls. Scientific American, New York, ed. 4, pp. 585-605, 1980.
37. Toepler, A. Optischen Studien nach der Methode der Schlierenbeobachtung. *Poggendorfs Annalen der Physik und Chemie*, **131**:33-55, 1867.
38. Witting, A. *Notes on "Beobachtungen nach der Schlierenmethode" by A. Toepler. Ostwald's Klassiker exacten Wiss.*, Vol. 158. W. Engelmann, Leipzig. pp. 95-102, 1906.
39. Mach, E. *The science of mechanics*. Open Court Pub., IL, ed. 6, p. 148,1960.
40. Toepler, A. *Beobachtungen nach einer neuen optischen Methode - Ein Beitrag zur Experimentalphysik. Ostwald's Klassiker der exakten Wissenschaften,* ed. A. Witting. Vol. 157. W. Engelmann, Leipzig, 1906.
41. Toepler, A. *Beobachtungen nach der Schlierenmethode. Ostwald's Klassiker der exakten Wissenschaften,* ed. A. Witting. Vol. 158. W. Engelmann, Leipzig, 1906.
42. Burton, R. A., D. Z. Bailey, F. W. Barry, L. A. deFrate, and E. P. Neumann. Optical measuring techniques. Chap. 9 of *Aerodynamic Measurements*, ed. R. C. Dean, Jr. MIT Gas Turbine Lab, Cambridge, MA, pp. 167-184, 1953.
43. Talbot, W. H. F. On the production of instantaneous images. *Phil. Mag.*, **34**(1):73-77, 1852.
44. Edgerton, H. E. *Electronic flash, strobe*. MIT Press, ed. 3, 1970.
45. Toepler, A. Über die Methode der Schlierenbeobachtung als mikroskopisches Hilfsmittel, nebst Bemerkungen zur Theorie der schiefen Beleuchtung. *Poggendorfs Annalen der Physik und Chemie*, **127**:556-580, 1866.
46. Toepler, A. and L. Boltzmann. Uber eine neue optische Methode, die Schwingungen tönender Luftsaulen zu analysieren. *Poggendorfs Annalen der Physik und Chemie*, **141**:321-352, 1870.
47. Czapski, S. Einige neue optische Apparate von Prof. Abbe. *Zeitschrift für Instrumentenkunde*, **5**(4):117-121, 1885.
48. Wood, R. W. Photography of Sound-Waves by the "Schlieren-Methode". *Phil. Mag.*, **48**:218-227, 1899.
49. Toepler, M. Objektive Sichtbarmachung von Funkenschallwellen nach der Schlierenmethode mit Hilfe von Gleitfunken. *Wiedemanns Annalen der Physik und Chemie*, **14**:838-842, 1904.

50. Merzkirch, W. Mach's contribution to the development of gas dynamics. *Ernst Mach - Physicist and Philosopher*, ed. R. S. Cohen and R. J. Seeger. D. Reidel Pub., Dordrecht, Holland, pp. 42-59, 1967.
51. Reichenbach, H. Contributions of Ernst Mach to fluid mechanics. *Ann. Rev. Fluid Mech.*, **15**:1-28, 1983.
52. Dvorák, R. Contribution of Ernst Mach to gas dynamics. In *Ernst Mach and Contemporary Physics*, Prague, 1988.
53. Dvorák, R. Prague's contribution to the science of flow visualization. In *Flow Visualization V*, ed. R. eznícek. Hemisphere Pub., NY, pp. 4-8, 1989.
54. Riemann, G. F. B. Über die Fortpflanzung ebener Luftwellen von endlicher Schwingungsweite. *Abhandl. Göttinger Gesellschaft Wissenschaft*, **8**:43, 1860.
55. Mach, E. and J. Sommer. Über die Fortpflanzungsgeschwindigkeit von Explosionsschallwellen. *Sitzungsb. d. k. Acad. d. Wiss. Math. Naturw. Cl. Wien*, **75**:101-130, 1877.
56. Mach, E. and J. Wentzel. Ein Beitrag zur Mechanik der Explosionen. *Sitzungsb. Akad. Wiss. Wien*, **92**:625-638, 1885.
57. Ackeret, J. Der Luftwiderstand bei sehr grossen Geschwindigkeiten. *Schweizerische Bauzeitung*, **24**:179-183, 1929.
58. Melsens, M. Sur les plaies produits par les armes a feu. *Soc. Royale d. Sciences Medicales,* Brussels, 1872.
59. Mach, E. and L. Mach. Weitere Ballistisch-Photographische Versuche. *Sitzungsb. Akad. Wiss. Wien*, **98**:1310-1326, 1889.
60. Mach, E. and P. Salcher. Optische Untersuchung der Luftstrahlen. *Sitzungsb. Akad. Wiss. Wien*, **98**:1303-1309, 1889.
61. Krehl, P. Private communication. Nov. 1, 1996.
62. Boys, C. V. On electric spark photographs; or, photography of flying bullets, etc., by the light of the electric spark. *Nature*, **47**(1218):415-421, 1893.
63. Schardin, H. Die Anwendung der Schlierenmethoden zur Untersuchung von Problemen aus der Wärmetechnik. *Heiz. und Lüft.*, pp. 167-172, Dec. 1932.
64. Townend, H. C. H. On rendering airflow visible by means of hot wires. ARC R&M 1349, British Aeronautical Research Council, 1931.
65. Barnes, N. F. and S. L. Bellinger. Schlieren and shadowgraph equipment for air flow analysis. *JOSA*, **35**(8):497-509, 1945.
66. Weinberg, F. J. *Optics of flames: including methods for the study of refractive index fields in combustion and aerodynamics*. Butterworths, London, 1963.
67. Rheinberg, J. On an addition to the methods of microscopical research, by a new way of optically producing colour-contrast between an object and its background, or between definite parts of the object itself. *J. Roy. Microsc. Soc.,* Ser. 2, **16**(8):373-388, 1896.
68. Delly, J. G. Rheinberg differential color illumination in biomedical photography. *Biomedical Photography,* Pub. N-19, Eastman Kodak, Rochester, NY, pp. 3-16, 1976.
69. Bescos, J. and T. C. Strand. Optical pseudocolor encoding of spatial frequency information. *App. Optics*, **17**(16):2524-2531, 1978.
70. True, T. T. Color television light valve projection systems. In *Proc. Intercon 73*, IEEE, Vol. 5, Session 26, 1973.
71. Armitage, J. D. and A. W. Lohmann. Theta modulation in optics. *App. Optics*, **4**(4):399-404, 1965.
72. Yu, F. T. S. *White-light optical signal processing.* Wiley, NY, ed. 1, 1985.
73. Rheinberg, L. The history of Graticules Ltd. *Microscopy: the Journal of the Quekett Microscopical Club*, **33**(2):348-357, 1978.
74. Wood, R. W. Photography of sound-waves, and the kinematographic demonstration of the evolutions of reflected wave-fronts. *Phil. Mag.*, **50**(7):148-156, 1900.
75. Prandtl, L. Neue Untersuchung über die strömende Bewegung der Gase und Dämpfe. *Physicalische Zeitschrift* , **8**(1):23-30, 1907.

76. Meyer, T. *Über zweidimensionale Bewegungsvorgänge in einem Gas, das mit Überschallgeschwindigkeit Strömt.* Ph.D. Thesis, Göttingen University, 1908.
77. Magin, E. *Optische Untersuchung über den Ausfluss von Luft durch eine Laval-Düse.* Ph.D. Thesis, Göttingen University, 1908.
78. Cranz, C. *Lehrbuch der Ballistik.* Vol. 3, Springer-Verlag, Berlin, 1927.
79. Reichenbach, H. Hubert Schardin (1902-1965) - his life and work. In *Proc. 20th Intl. Congr. on High-Speed Photography and Photonics*, ed. J. M. Dewey and R. G. Racca. SPIE, Vol. 1801, pp. 2-9, 1993.
80. Kutterer, R. E. Zur ballistischen elektrischen Momentphotographie - der Weg von E. Mach über C. Cranz zu H. Schardin. *Wehrtech. Monatshefte*, **63**(11):25-33, 1966.
81. Schardin, H. C. Cranz. Chap. 1 of *Beiträge zur Ballistik und technischen Physik*, ed. H. Schardin. J. A. Barth, Leipzig, pp. 1-8, 1938.
82. Merzkirch, W. *Flow visualization.* Academic Press, New York, ed. 2, 1987.
83. Oertel, H. 33 years of research by means of shock tubes at the French-German Research Institute at Saint-Louis. In *Proc. 14th Intl. Symp. on Shock Tubes and Shock Waves*, New South Wales Univ. Press, pp. 3-13, 1983.
84. North, R. J. A brief review of some recent schlieren, schlieren-interferometer, and interferometer methods. *Wehrtechnische Monatshefte*, **63**(7-supple-ment):174-187, 1966.
85. Wegener, P. P. *The Peenemünde wind tunnels: a memoir.* Yale University Press, New Haven, CT, pp. 22-33, 1996.
86. Dornberger, W. *V-2.* Viking Press, ed. 1, 1954.
87. Becker, J. V. The high-speed frontier; case histories of four NACA programs, 1920-1950. NASA SP-445, 1980.
88. Stack, J. Compressible flows in aeronautics, the 8th Wright Brothers lecture. *J. Aero. Sci.*, **12**(2):127-148, 1945.
89. Rogers, E. W. E. Private communication. July 20, 1996.
90. Pearcey, H. H. Private communication. June 18, 1996.
91. North, R. J. Private communication. Aug. 20, 1996.
92. Young, A. D., R. C. Pankhurst, and D. L. Schultz. Douglas William Holder (1923-1977). *Biographical Mem. of Fellows Royal Soc.*, **24**:223-244, 1978.
93. North, R. J. Schlieren systems using graded filters. ARC Report 15,099, British Aeronautical Research Council, 1952.
94. North, R. J. A colour schlieren system using multicolor filters of a simple construction. NPL Aero Report 266, British National Physical Laboratory, 1954.
95. de Normanville, P. *Schlieren*, 16mm film. Shell Film & Video Unit, London, 1956.
96. Pearcey, H. H. A method for the prediction of the onset of buffeting and other separation effects from wind tunnel tests on rigid models. Report 20,631, British Aeronautical Research Council, 1958.
97. Pearcey, H. H. The aerodynamic design of section shapes for swept wings. Chap. 3 of *Adv. in Aero. Sci.*, Pergamon Press, NY, pp. 277-322, 1962.
98. Holder, D. W. and R. J. North. *Schlieren methods,* NPL notes on applied science no. 31. Her Majesty's Stationery Office, London, 1963.
99. Holder, D. W. and R. J. North. Optical methods for examining the flow in high-speed wind tunnels; Part 1: Schlieren methods. AGARDograph 23, NATO, 1956.
100. Oppenheim, A. K., P. A. Urtiew, and F. J. Weinberg. On the use of laser light sources in schlieren-interferometer systems. *Proc. Roy. Soc. A*, **291**:279-290, 1966.
101. Maksutov, D. D. *Tenevye metody issledovaniya opticheskikh sistem (Schlieren methods in the study of optical systems).* Problems in Advanced Physics, Vol. 23. GTTI Izdatel'stvo, Leningrad, 1934.
102. Vasiliev, L. A. *Schlieren methods* . ed. A. Baruch. Israel Program for Scientific Translations, New York, 1971.
103. Ershov, I. V. Private communication. Dec. 15, 1999.

104. Burton, R. A. *The application of schlieren photography in fluid flow and heat transfer analysis*. M.S.M.E. Thesis, University of Texas, 1951.
105. Kantrowitz, A. and R. L. Trimpi. A sharp-focusing schlieren system. *J. Aero. Sci.*, **17**:311-319, 1950.
106. Fish, R. W. and K. Parnham. Focussing schlieren systems. Report CP-54, British Aeronautical Research Council, 1950.
107. Burton, R. A. A modified schlieren apparatus for large areas of field. *JOSA*, **39**(11):907-908, 1949.
108. Burton, R. A. Notes on the multiple source schlieren system. *JOSA*, **41**(11):858-859, 1951.
109. Volluz, R. J. Flow visualization. Navord Report 1488, Vol. 6, Sec. 20, US Navy Bureau of Ordnance, pp. 303-322, 1961.
110. Weinstein, L. M. Large-field high-brightness focusing schlieren system. *AIAA J.*, **31**(7):1250-1255, 1993.
111. Settles, G. S., E. B. Hackett, J. D. Miller, and L. M. Weinstein. Full-scale schlieren flow visualization. In *Flow Visualization VII*, ed. J. P. Crowder. Begell House, NY, pp. 2-13, 1995.
112. Weinstein, L. M. An optical technique for examining aircraft shock wave structures in flight. NASA CP-3279, pp. 1-17, 1994.
113. Weinstein, L. M. and D. Minto. Focusing schlieren photography at the Holloman high speed test track. In *Proc. of 22nd Intl. Congr. on High-Speed Photography and Photonics*, SPIE Vol. 2869, pp. 865-873, 1996.
114. Johnsen, S. Transparent animals. *Sci. Am.*, **282**(2):80-89, 2000.
115. Weyl, F. J. Analytical methods in optical examination of supersonic flow. Navord Report 211-45, US Navy Bureau of Ordnance, 1945.
116. Goldstein, R. J. and T. H. Kuehn. Optical systems for flow measurement - shadowgraph, schlieren, and interferometric techniques. Chap. 8 of *Fluid Mechanics Measurements*, Springer-Verlag, Berlin, pp. 377-397, 1983.
117. Jebsen-Marwedel, H. "Schlieren" als Wort, Gebilde und Begriffe. *Glastechniche Berichte*, **33**(12):475-477, 1960.
118. Kafri, O. Noncoherent method for mapping phase objects. *Optics Letters*, **5**(12):555-557, 1980.
119. Wolter, H. Schlieren, Phasencontrast, und Lichtschnittverfahren. *Fundamentals of Optics, Handbuch der Physik Vol. 24*, Springer-Verlag, Berlin, pp. 555-645, 1956. (English translation available as NTIS AD-833177.)
120. Davis, M. R. Determination of turbulent flow properties by a penetrating beam dynamic shadowgraph method. *J. Physics E*, **20**(10):1271-1277, 1987.
121. Davis, M. R. and H. L. Li. Evaluation of fractal dimension for mixing and combustion by the schlieren method. *Expts. Fluids*, **21**(4):248-258, 1996.
122. Hilton, W. F. *High-speed aerodynamics*. Longmans & Green, NY, 1951.
123. Gates, D. M. and C. M. Benedict. Convection phenomena from plants in still air. *American Journal of Botany*, **50**(7):563-573, 1963.
124. Herbrich, H. Die Schlierenphotographie - ein optisches Diagnoseverfahren. *Sensor*, (3):5-9, 1990.
125. North, R. J. and R. F. Cash. Colour schlieren photography in high-speed wind tunnels. NPL Aero Note 383, British National Physical Laboratory, 1959.
126. Speak, G. S. and D. J. Walters. Optical considerations and limitations of the schlieren method. ARC R&M 2859, British Aero. Research Council, 1950.
127. Settles, G. S. Colour-coding schlieren techniques for the optical study of heat and fluid flow. *International Journal of Heat & Fluid Flow*, **6**(1):3-15, 1985.
128. Philbert, M., J. Surget, and C. Veret. Shadowgraph and schlieren. Chap. 12 of *Handbook of Flow Visualization*,. Hemisphere Pub., Washington, ed. 1, pp. 189-217, 1989.

129. Kelsey, J. F. Image formation in optical systems that use amplitude and phase masks in the Fourier image plane. Report TR-13 (AD-470297), Ultrasonics Lab, Michigan State Univ. Phys. Dept. 1965.
130. Goodman, J. W. *Introduction to Fourier optics*. McGraw-Hill, NY, 1968.
131. Shulman, A. R. Principles of optical data processing for engineers. NASA Technical Report R-327, 1970.
132. Meyer-Arendt, J. R. *Introduction to classical and modern optics*. Prentice-Hall, Englewood Cliffs, NJ, ed. 4, 1995.
133. Taylor, H. G. and J. M. Waldram. Improvements in the schlieren method. *J. Sci. Inst.*, **10**(12):378-389, 1933.
134. Zhang, X., D. Dabiri, and M. Gharib. Optical mapping of fluid density interfaces: concepts and implementations. *Rev. Sci. Instr.*, **67**(5):1858-1868, 1996.
135. Toepler, A. Die vom elektrischen Funken in Luft erzeugte Welle. *Poggendorfs Annalen der Physik und Chemie*, **131**:180-215, 1867.
136. Keagy, W. R., Jr., H. H. Ellis, and W. T. Reid. Schlieren techniques for the quantitative study of gas mixing. Report R-164, Rand Corp., 1949.
137. Carbone, F. Innovations make large-segment mirror telescopes more affordable. *Laser Focus World*, **34**(8):229-238, 1998.
138. Keagy, W. R., Jr. and H. H. Ellis. The application of the schlieren method to the quantitative measurement of mixing gases in jets. In *Proc. 3rd Intl. Symp. on Comb., Flame, Explosion Phenom.*, Combustion Inst., pp. 667-674, 1948.
139. Brackenridge, J. B. and W. P. Gilbert. Schlieren interferometry. An optical method for determining temperature and velocity distributions in liquids. *App. Optics*, **4**(7):819-821, 1965.
140. Gayhart, E. L. and E. A. Bunt. Use of schlieren optics with low gas pressures. Report CF-2817, Applied Physics Lab, Johns Hopkins Univ., 1959.
141. Simorsen, J. M. Extensions and limitations of schlieren and shadowgraph methods. In *Symp. on Flow Visualization*, ASME, 1960.
142. Zobel, T. W. Schlieren apparatus of improved optical quality. US Patent 2,642,770, June 28, 1953.
143. Butler, C. P. Schlieren system for fire spread studies. *J. Fire Flam.*, **5**(1):4-15, 1974.
144. Albe, F. L'astigmastisme dans le montage strioscopique. Report T49/68, Institut Saint-Louis, 1969.
145. Walker, B. H. *Optical engineering fundamentals*. McGraw-Hill, NY, 1995.
146. Kean, L. A contribution to the theory of schlieren sensitivity and quantitative evaluation. USAF Systems Command Report ASD-TDR-62-924, 1962.
147. Prescott, R. and E. L. Gayhart. A method of correction of astigmatism in schlieren systems. *J. Aero. Sci.*, **18**:69, 1951.
148. Dementjev, I. M., I. A. Kamalov, V. A. Komissaruk, A. N. Mikhalev, and S. G. Tomson. Ballistic range optical equipment. In *Flow Visualization V*, ed. R. eznícek. Hemisphere Pub., NY, pp. 549-555, 1990.
149. Shafer, H. J. Physical optic analysis of image quality in schlieren photography. *Journal of the SMPE*, **53**(11):524-544, 1949.
150. Dall, H. E. A null test for paraboloids. *Amateur Telescope Making, Book 3*, ed. A. G. Ingalls. Scientific American, New York, ed. 4, pp. 149-153, 1980.
151. Offner, A. and D. Malacara. Null tests using compensators. Chap. 12 of *Optical Shop Testing*, ed. D. Malacara. Wiley, NY, ed. 2, pp. 427-454, 1991.
152. Hall, L. S. High sensitivity schlieren technique. *Rev. Sci. Instr.*, **37**:1735-1736, 1966.
153. Ojeda-Castañeda, J. Foucault, wire, and phase modulation tests. Chap. 8 of *Optical Shop Testing*, ed. D. Malacara. Wiley, NY, ed. 2, pp. 265-288, 1991.
154. Lopez, C. A. Numerical simulation of a schlieren system from the Fourier optics perspective. AIAA Paper 94-2618, 1994.

155. Blackwell, H. R. Contrast thresholds of the human eye. *JOSA*, **36**:624-643, 1946.
156. Hyzer, W. G. The Role of the Eye in High-Speed Motion Analysis. In *Proc. 22nd Intl. Congr. on High-Speed Photography and Photonics,* ed. D. L. Paisley and A. M. Frank. SPIE Vol. 2869, pp. 38-43, 1997.
157. North, R. J. and C. M. Stuart. Flow visualization and high-speed photography in hypersonic aerodynamics. NPL Aero Report 1029, 1962.
158. Merzkirch, W. Sensitivity of flow visualization methods at low-density flow conditions. *AIAA J.*, **3**(4):794-795, 1965.
159. Weinstein, L. M. Designing and using focusing schlieren systems. Private communication, April 1, 1997.
160. Holder, D. W. and R. J. North. The Toepler schlieren apparatus. ARC R&M 2780, British Aeronautical Research Council, 1950.
161. Hesselink, L. Digital image processing in flow visualization. *Annual Review of Fluid Mechanics*, **20**:421-485, 1988.
162. Russ, J. C. *The image processing handbook.* CRC Press, Boca Raton, 1992.
163. Weinstein, L. M. Private communication. Feb. 15, 2000.
164. Mair, W. A. The sensitivity and range required in a Toepler schlieren apparatus for photography of high-speed airflow. *Aeronautical Quarterly*, **4**(8):19-50, 1952.
165. John, J. E. A. *Gas Dynamics.* Prentice-Hall, ed. 2, 1984.
166. Settles, G. S., A. D. Brandt, and J. D. Miller. Full-scale schlieren imaging of shock waves for aviation security research. In *Proc. 8th Intl. Symp. on Flow Visualization,* Sorrento, Italy, ed. G. M. Carlomagno, Paper no. 30, 1998.
167. Smith, W. J. *Modern optical engineering.* McGraw-Hill, New York, 1966.
168. Hyzer, W. G. *Engineering and scientific high-speed photography.* The Macmillan Company, New York, ed. 1, 1962.
169. Ershov, I. V. Metrological characteristics of schlieren instruments. *Sov. J. Opt. Tech.*, **57**(3):182-185, 1990.
170. Inoué, S. and K. R. Spring. Video signal fundamentals. Chap. 5 of *Video Microscopy*, Plenum Press, New York, ed. 2, pp. 189-231, 1997.
171. Hosch, J. W. and J. P. Walters. High spatial resolution schlieren photography. *App. Optics*, **16**(2):473-482, 1977.
172. Lord Rayleigh (Strutt, J. W.). On the theory of small optical retardations. *Phil. Mag.*, **33**:161-178, 1917.
173. Hannes, H. Über die Eigenschaften des Schattenverfahrens. *Optik*, **13**(1):34-48, 1956.
174. Avila, F. and R. T. Olvera. Private communication. Mar. 1, 2000.
175. Standard test methods for performance of commercial kitchen ventilation systems. Standard F 1704-99, ASTM, West Conshohocken, PA, 1999.
176. Chen, P. Telescope mirrors successfully lose weight. *Laser Focus World*, **34**(10):69-72, 1998.
177. Semenov, A. P., V. E. Patrikeev, A. V. Samuylov, and Y. A. Sharov. Computer-controlled fabrication of large-size ground and space-based optics from glass ceramic Sitall CO-115M. In *Proc. Conf. on Optomechanical Design & Engrg.,* Denver, SPIE Vol. 3786, pp. 474-479, 1999.
178. Burge, J., B. Cuerden, S. Miller, B. Crawford, H. Dorth, D. Sandler, and R. Wortley. Manufacture of a 2-m mirror with glass membrane facesheet and active rigid support. In *Proc. Conf. on Optical Manuf. & Testing III*, SPIE Vol. 3782, pp. 123-133, 1999.
179. Waddell, P. Laser moiré-schlieren system of variable sensitivity. In *Proc. Conf. on Industrial Apps. of Laser Tech.* SPIE Vol. 398, pp. 200-207, 1983.
180. King, W., P. Waddell, and T. Raptodimos. Holographic testing of stretchable concave imaging mirrors. In *Proc. Conf. on Optics in Engineering Measurement*, Cannes, SPIE Vol. 599, pp. 80-87, 1986.

181. McKay, S., S. Mason, L. S. Mair, P. Waddell, and S. M. Fraser. Stereoscopic display using a 1.2-m diameter stretchable membrane mirror. In *Proc. 6th Stereo. Displays & Virtual Reality Sys.*, SPIE Vol. 3639, pp. 122-131, 1999.
182. McKay, S., S. Mason, L. S. Mair, P. Waddell, and S. M. Fraser. Membrane mirror based display for viewing 2D and 3D images. In *Proc. Projection Displays Conference V,* San Jose, SPIE Vol. 3634, pp. 144-155, 1999.
183. Waddell, P., M. Stickland, S. Mason, S. McKay, and L. S. Mair. Fluid flow analysis by a sharp focusing moiré-schlieren system. In *Proc. 1st Pacific Symp. on Flow Vis. & Image Proc.,* ed. S. Mochizuki, pp. 580-585, 1997.
184. Mendonsa, R. A. High-speed imaging helps study spacecraft re-entry. *Photonics Spectra*, **32**(1):132-134, 1998.
185. Davies, T. P. Schlieren photography. *Photomethods*, **29**(7):21, 1986.
186. Settles, G. S. Airflow visualization in a model greenhouse. In *Proc. 15th Intl. Congr. for Plastics in Agriculture, Hershey, PA*, pp. 88-98, 2000.
187. Settles, G. S. Indoor environments. Chap. 37 of *Handbook of Flow Visualization*, ed. W.-J. Yang. Hemisphere Pub., Washington, pp. 619-626, 1989.
188. Settles, G. S., H. A. Gowadia, S. B. Strine, and T. E. Johnson. The natural aerodynamic sampling of trace explosives from the human body. In *Proc. 2nd FAA Symp. on Explosives Detec. & Aviation Security Tech.,* ed. W. H. Makky, FAA, pp. 65-70, 1996.
189. Settles, G. S. Chemical trace detection portal based on the natural airflow and heat transfer of the human body. US Patent 6,073,499, June 13, 2000.
190. Kester, D. A., G. S. Settles, and L. J. Dodson-Dreibelbis. The aerodynamics of canine olfaction. *Journal of Experimental Biology*, 2001 (submitted for publication).
191. Kegerise, M. A. and G. S. Settles. Schlieren image-correlation velocimetry and its application to free-convection flows. In *Proc. 9th Intl. Symp. on Flow Visualization,* ed. G. M. Carlomagno and I. Grant, Paper no. 380, 2000.
192. Mortensen, T. A. An improved schlieren apparatus employing multiple slit-gratings. *Rev. Sci. Instr.*, **21**(1):3-6, 1950.
193. Dixon-Lewis, G. and G. L. Isles. Sharp-focusing schlieren systems for studies of flat flames. *J. Sci. Inst.*, **39**:148-151, 1962.
194. Rotem, Z., E. G. Hauptmann, and L. Claassen. Semifocusing color schlieren system for use in fluid mechanics and heat transfer. *App. Optics*, **8**(11):2326-2328, 1969.
195. Sabersky, R. H. and E. G. Hauptmann. Forced convection heat transfer to carbon dioxide near the critical point. *Intl. J. Heat & Mass Trans.*, **10**:1499-1508, 1967.
196. Rotem, Z. and L. Claassen. Natural convection above unconfined horizontal surfaces. *J. Fluid Mech.*, **39**:173-192, 1969.
197. Collicott, S. H. and T. R. Salyer. Quantification of noise reduction in multiple-source schlieren systems. AIAA Paper 94-0279, 1994.
198. Hanenkamp, A., W. Merzkirch, and F. Peters. A Fourier approach to the sharp focusing schlieren system. In *Proc. 9th Intl. Symp. on Flow Visualization,* ed. I. Grant and G. M. Carlomagno, Paper no. 120, 2000.
199. Serafino, G. *Visualizzazione di immagini di fase: elaborazione ottica in luce bianca con sorgente estesa codificata.* Engineer's Degree Thesis Thesis, Dept. di Elettrotecnica, Elettronica e Informatica, University of Trieste, 2000.
200. Serafino, G. and P. Sirotti. Phase image visualization with incoherent light sources. In *Proc. 9th Intl. Symp. on Flow Visualization*, Paper no. 454, 2000.
201. Dugger, P. H. and J. W. Hill. A new dimension in front-light laser photography. *AIAA J.*, **10**(11):1544-1546, 1972.
202. Dewey, J. M. and D. J. McMillin. Visualization of shock and blast wave flows. In *Proc. 1st Intl. Symp. on Flow Visualization*, Hemisphere, pp. 279-284, 1977.
203. Fuller, P. W. W. High speed photography in ballistics. In *Proc. 8th Intl. Congr. on Instrum. in Aerospace Sim. Facilities, ICIASF'79 Record*, IEEE, pp. 112-123, 1979.

204. Genco, L. E. and H. L. Task. Field test unit for windscreen optical evaluation. US Patent 4,310,242, Jan. 12, 1982.
205. Settles, G. S. The state of the art of conventional flow visualization techniques for wind tunnel testing. NASA CP-2243, pp. 9-26, 1982.
206. Thompson, P. A., Y.-G. Kim, and G. E. A. Meier. Flow visualization of a shock wave by simple refraction of a background grid. In *Optical Methods in Dyn. of Fluids & Solids*, ed. M. Pichal. Springer-Verlag, pp. 225-231, 1985.
207. Ringlien, J. A. Inspection of transparent containers. US Patent 5,243,400, Sept., 1993.
208. Okugawa, S. Method of and apparatus for detecting defect of transparent sheet as sheet glass. US Patent 5,452,079, Sept. 19, 1995.
209. Trolinger, J. D. Flow visualization holography. *Opt. Engrg.*, **14**(5):470-481, 1975.
210. Ray, S. F., ed. *High speed photography and photonics*. Focal Press, 1997.
211. Swezey, K. M. How to photograph glass. *Popular Science*, **152**(11):216-219, 1948.
212. Skews, B. W. Colour encoded visualization applied to the hydraulic analogy for supersonic flow. In *Proc. 8th Intl. Symp. on Flow Visualization,* Sorrento, Italy, ed. G. M. Carlomagno, Paper no. 31, 1998.
213. Cords, P. H., Jr. A high resolution, high sensitivity color schlieren method. *SPIE Journal*, **6**:85-88, 1968.
214. Boedecker, L. R. *Analysis and construction of a sharp focusing schlieren system.* MS Thesis, Dept. of Aeronautics & Astronautics, MIT, 1959.
215. Bowker, A. NAE multi-source schlieren apparatus for 5-foot x 5-foot trisonic wind tunnel. *NRC Quarterly Bulletin* (Canada), (3):27-49, 1970.
216. Waddell, P. A large field retroreflective moiré-schlieren system. In *Proc. Electro-Optics/Laser International Conf. '82, Brighton, UK*, ed. H. G. Jerrard. Butterworth Scientific, pp. 74-82, 1982.
217. Gardner, A. P. A low-cost method of large field schlieren photography. *J. Audiovisual Media in Medicine*, **9**(4):144-146, 1986.
218. Weinstein, L. M. An improved large-field focusing schlieren system. In *Proc. AIAA 29th Aerospace Sciences Mtg.*, AIAA Paper 91-0567, 1991.
219. Alvi, F. S., G. S. Settles, and L. M. Weinstein. A sharp-focusing schlieren optical deflectometer. AIAA Paper 93-0629, 1993.
220. Garg, S. and G. S. Settles. Measurements of a supersonic turbulent boundary layer by focusing schlieren deflectometry. *Expts. Fluids*, **25**(3):254-264, 1998.
221. Marguerre, H. Ein neues inkohärentes Schlierenverfahren mit Retroreflektor. *Optik*, **71**(3):105-112, 1985.
222. Heineck, J. T. Retroreflection focusing schlieren system. US Patent 5,515,158, 1996.
223. Winburn, S., A. Baker, and J. G. Leishman. Angular response properties of retroreflective screen materials used in wide-field shadowgraphy. *Expts. Fluids*, **20**(3):227-229, 1996.
224. Weinstein, L. M. Large field schlieren visualization - from wind tunnels to flight. In *Proc. VSJ-SPIE98*, Vis. Soc. of Japan, Paper AB124, 1998.
225. Levey, B. S. *An experimental investigation of a supersonic vortical flow.* Ph.D. Thesis, George Washington Univ., 1991.
226. Ponton, M. K., J. M. Seiner, L. K. Mitchell, J. C. Manning, B. J. Jansen, and N. T. Lagen. A wind tunnel application of large-field focusing schlieren. In *Proc. 14th DGLR/AIAA Aeroacoustics Conf.*, Vol. 1, pp. 169-176, 1992.
227. Davidhazy, A. How to build a basic focusing schlieren system. *Opt. Engrg. Reports*, (2):11-14, 1999.
228. Kothari, R. D. and Y. J. Wu. Visualization and image analysis of temperature distribution using a positive-negative grid Schlieren system. In *High-Speed Imaging & Sequence Analysis*, SPIE Vol. 3642, pp. 149-155, 1999.

229. Cutler, A. D. and B. S. Levey. Vortex breakdown in a supersonic jet. AIAA Paper 91-1815, 1991.
230. Cook, S. P. and N. Chokani. Quantitative results from the focusing schlieren technique. AIAA Paper 93-0630, 1993.
231. Peale, R. E. and P. L. Summers. Zebra schlieren optics for leak detection. *App. Optics*, **35**(22):4518-4521, 1996.
232. Schmid, F. P., V. A. Smith, and R. T. Swierczyna. Schlieren flow visualization in commercial kitchen ventilation research. In *Proc. 1997 Annual Meeting*, ASHRAE, Vol. 103, Part 2, pp. 937-942, 1997.
233. Chun, K., W. J. Ratvasky, C. M. Lee, and R. J. Locke. Focused schlieren flow visualization studies of multiple venturi fuel injectors in a high pressure combustor. AIAA Paper 94-0280, 1994.
234. Pellett, G. L., W. L. Roberts, L. G. Wilson, W. Humphreys, S. M. Bartram, L. M. Weinstein, and K. M. Isaac. Structure of hydrogen-air counterflow diffusion flames obtained by focusing schlieren, shadowgraph, PIV, thermometry, and computation. AIAA Paper 94-2300, 1994.
235. Raghu, S. and G. Goutevenier. Visualization of a high-speed, luminous plasma jet using a focusing schlieren technique. *Expts. Fluids*, **19**(2):136-138, 1995.
236. Settles, G. S. Visualizing full-scale ventilation airflows. *ASHRAE Journal*, **39**(7):19-26, 1997.
237. Settles, G. S. Imaging gas leaks by using schlieren optics. *Pipeline and Gas Journal*, **226**(9):28-30, 1999.
238. Gartenberg, E., L. M. Weinstein, and E. E. Lee, Jr. Aerodynamic investigation with focusing schlieren in a cryogenic wind tunnel. *AIAA J.*, **32**(6):1242-1249, 1993.
239. Raman, G. H. and R. Taghavi. Visualization of the multiple supersonic jet oscillations by swept focused strobed schlieren technique. In *Proc. Techfest 20,* AIAA, Wichita State Univ., 1994.
240. Taghavi, R. and G. Raman. Visualization of supersonic screeching jets using a phase conditioned focusing schlieren system. *Expts. Fluids*, **20**(6):472-475, 1996.
241. Seitz, M. W., P. A. Seitz, and B. W. Skews. Three-color common-axis light source suitable for shock wave studies. *Opt. Engrg.*, **33**(9):2903-2906, 1994.
242. Weinstein, L. M. Schlieren system and method for moving objects. US Patent 5,534,995, Feb. 1995.
243. Weinstein, L. M. An electronic schlieren camera for aircraft shock wave visualization. In *Proc. High-Speed Research Program Sonic Boom Workshop*, NASA, Vol. 1, pp. 244-258, 1996.
244. Weinstein, L. M., K. Stacy, G. J. Vieira, E. A. Haering, Jr., and A. H. Bowers. Imaging supersonic aircraft shock waves. *J. Flow Vis. Image Proc.*, **4**(3):189-199, 1997.
245. Weinstein, L. M., W. Culliton, and R. Rivers. Visualization of transonic flow over a T-38 aircraft. In *Proc. 8th Intl. Symp. on Flow Visualization,* Sorrento, Italy, ed. G. M. Carlomagno, Paper no. 80, 1998.
246. Asundi, A. K. and M. R. Sajan. Digital drum camera for dynamic recording. *Opt. Engrg.*, **35**(6):1707-1713, 1996.
247. Nishijima, Y. and G. Oster. Moiré patterns: their application to refractive index and refractive index gradient measurements. *JOSA*, **54**(1):1-5, 1964.
248. Fromme, T. The moiré-schlieren method. In *Proc. 3rd Intl. Congr. on High-Speed Photography*, pp. 276-278, 1956.
249. Bampfield, J. F. A Moiré pattern technique for the detection of shockwaves. Report NOLTR 67-57, US Naval Ordnance Lab, White Oak, MD, 1968.
250. Dalziel, S. B., G. O. Hughes, and B. R. Sutherland. Synthetic schlieren. In *Proc. 8th Intl. Symp. on Flow Visualization,* ed. G. M. Carlomagno, Paper no. 62, 1998.

251. Sutherland, B. R., S. B. Dalziel, G. O. Hughes, and P. F. Linden. Visualization and measurement of internal waves by 'synthetic schlieren'. Part 1. Vertically oscillating cylinder. *J. Fluid Mech.*, **390**:93-126, 1999.
252. Keenan, P. C. The measurement of densities in shock waves by the shadowgraph method. Report 86-46, US Navy Ordnance Bureau, Washington, 1946.
253. Sakai, S. Visualisation of internal gravity waves by moiré method. *Kashika-Joho*, **10**:65-68, 1990.
254. Dalziel, S. B., G. O. Hughes, and B. R. Sutherland. Whole-field density measurements by `synthetic schlieren'. *Expts. Fluids*, **28**(4):322-335, 2000.
255. Weinberg, F. J. and W. Y. Wong. Optical studies in fire research. In *Proc. 16th Intl. Symp. on Combustion*, Combustion Inst., pp. 799-807, 1976.
256. Giglio, M., S. Musazzi, and U. Perini. White light speckle schlieren technique. *Optics Comm.*, **36**(2):117-120, 1981.
257. Gabor, D., G. Stroke, D. Brumm, A. Funkhouser, and A. Labeyrie. Reconstruction of phase objects by holography. *Nature*, **208**(5016):1159-1162, 1965.
258. O'Hare, J. E. and J. D. Trolinger. Holographic color schlieren. *App. Optics*, **8**:2047-2050, 1969.
259. Tsuruta, T. and Y. Itoh. Hologram schlieren and phase-contrast methods. *Japanese J. App. Phys.*, **8**(1):96-103, 1969.
260. Havener, A. G. Holographic applications in shadowgraph, schlieren, and interferometry analyses of heat transfer and fluid flow test subjects. Report ARL 70-0270, USAF Aerospace Research Lab, Wright-Patterson AFB, 1970.
261. Belozerov, A. F. and N. M. Spornik. The production of shadowgrams during reconstruction of holographically recorded wavefront in white light. *Sov. J. Opt. Tech.*, **38**(3):138-140, 1971.
262. Belozerov, A. F. and N. M. Spornik. Obtainment of color shadowgraphs in the study of a wave front reconstructed from a hologram. *Geodeziia i Aerofotos'emka*, **1**:139-141, 1974.
263. Kurtz, R. L. and L. M. Perry. A holographic optical schlieren system /HOSS/. *Opt. Engrg.*, **18**(3):243-248, 1979.
264. Buzzard, R. D. Description of three-dimensional schlieren system. In *Proc. 8th Intl. Conf. on High-Speed Photography,* Wiley, NY, pp. 335-340, 1968.
265. Doggett, G. P. and N. Chokani. Large-field laser holographic focusing schlieren system. *J. Spacecraft Rockets*, **30**(6):742-748, 1993.
266. Lamplough, F. E. Shock-wave shadow photography in tunnel and in flight. *Aircraft Engineering*, (4):94-103, 1951.
267. Winkelmann, A. E. and R. H. Feldhuhn. How to analyze 2-D schlieren photographs to obtain the density gradient structure of 3-D flow fields. Report NOLTR 69-80, US Naval Ordnance Laboratory, White Oak, MD, 1969.
268. Larcombe, M. J. A numerical procedure for constructing shock-wave envelopes around conical bodies using data from schlieren photographs. ARC-CP-1143, British Aeronautical Research Council, 1970.
269. Agrawal, A. K., N. K. Butuk, and S. R. Gollahalli. Three-dimensional rainbow schlieren tomography of a temperature field gas flows. *App. Optics*, **37**:479-485, 1998.
270. Curell, P. C. and D. R. Belford. Three dimensional imaging using tomography with conventional schlieren images. *AIAA Student J.*, **34**(3):10-13, 1996.
271. Skews, B. W. Oblique imaging for visualization of three-dimensional supersonic flows. In *Proc. 9th Intl. Symp. on Flow Visualization,* ed. I. Grant and G. M. Carlomagno, Paper no. 282, 2000.
272. Tanner, L. H. The application of Berry-Gibbs theory to phase objects, using interferometry, holography or schlieren methods. *J. Physics E – Sci. Instr.*, **3**:987-993, 1970.

273. Sedel'nikov, A. I. and E. I. Chernov. Tomographic determination of the density field in a supersonic jet behind a nozzle with a slanted exit section. *AN SSSR. Sibirsk. Otd., Izvestiia, Ser. Tekh. Nauki*, 77-80, 1990.
274. Watt, D. W. Fourier-Bessel expansions for tomographic reconstruction from phase and phase-gradient measurements: Theory and experiment. In *Proc. Fluids Engrg. Div. Summer Mtg., FEDSM'97*, ASME, Part 13, 1997.
275. Cianfrini, C., M. Corcione, and D. M. Fontana. Reconstruction of 3-D thermal fields by tomographic schlieren methods. In *Heat transfer 1998, Proc. 11th IHTC,* Kyongju, Korea, Vol. 4, pp. 89-96, 1998.
276. Schwarz, A. Multi-tomographic flame analysis with a schlieren apparatus. *Measurement Science and Technology*, 7:406-413, 1996.
277. Vasiliev, L. A. and V. N. Otmennikov. Studies of high-velocity gas flows by a shadow photometric method using visualizing diaphragms of complicated shapes. *Sov. J. Opt. Tech.* , **43**(8):457-459, 1976.
278. Wilska, A. A new method of light microscopy. *Nature*, **171**(4357):353, 1953.
279. Ellis, G. W. Advances in visualization of mitosis in vivo. *Cell reproduction: in honor of Daniel Mazia*, Academic Press, New York, pp. 465-476, 1978.
280. Hoffman, R. and L. Gross. Modulation contrast microscope. *App. Optics*, **14**(5):1169-1176, 1975.
281. Hoffman, R. Variable background intensity apparatus for imaging systems. US Patent 4,062,619, 1975.
282. Hoffman, R. The modulation contrast microscope: principles and performance. *Journal of Microscopy*, **110**(3):205-222, 1977.
283. Ahlborn, B. and A. J. Barnard. Velocity measurement by Doppler effect. *AIAA J.*, **4** (6):1136-1137, 1966.
284. Kent, J. C. Fabrication of graded filters for knife-edge replacement in laser schlieren optical systems. *App. Optics*, **8**(10):2148-2149, 1969.
285. DSC Laboratories, http://www.dsclabs.com/.
286. Meyer-Arendt, J. R. Microscopy as a spatial filtering process. *Adv. Optical & Electron Microscopy, Vol. 8*, Academic Press, London, pp. 11-14, 1982.
287. Maddox, A. R. *Flow studies with an improved diffraction grating interferometer and a new color schlieren method for quantitative analysis*. Ph.D. Thesis, Mechanical Engrg. Dept., Univ. of Southern CA, 1968.
288. Maddox, A. R. and R. C. Binder. New dimension in the schlieren technique - flow field analysis using color. *App. Optics*, **10**(3):474-481, 1971.
289. Naumov, B. V. and O. G. Shakhrai. Visualization features of random inhomogeneities by a schlieren instrument having a Foucault knife edge. *Sov. J. Opt. Tech.*, **52**(3):131-133, 1985.
290. Townend, H. C. H. Improvements in the schlieren method of photography. *J. Sci. Inst.*, **11**(6):184-187, 1934.
291. Stolzenburg, W. A. The double knife-edge technique for improved schlieren sensitivity in low-density hypersonic aerodynamic testing. *SMPTE J.*, **74**(8):654-659, 1965.
292. Edmonson, R. B., E. L. Gayhart, and H. L. Olsen. Radial symmetry in a schlieren image. *JOSA*, **42**:984-985, 1952.
293. Alekhin, V. A. and Y. P. Gushcho. Calculation of the value of the luminous efficiency when reproducing relief recordings by schlieren optics with circular irises. *Optics and Spectroscopy (USSR)*, **43**(5):578-581, 1977.
294. Weiss, R. J. Efficiency shines in LSDs. *Optical Engrg. Reports*, (1):8, 1996.
295. Zernike, F. Beugungstheorie des schneidenverfahrens und seiner verbesserten form, der phasenkontrastmethode. *Physica*, **1**(44):689-704, 1934.
296. Abramowitz, M. *Contrast methods in microscopy: transmitted light.* Microscope Basics and Beyond, Vol. 2, Olympus Corp., Melville, NY, 1995.

297. Royer, H. A new method of visualizing and measuring hypersonic wakes: a schlieren arrangement using amplitude subtraction. In *Proc. 9th Intl. Congr. on High Speed Photography,* SMPTE, Paper no. 94, 1970.
298. Ojeda-Castañeda, J. Edge filters for phase contrast imagery 1:Theoretical design. *App. Optics*, **18**(14):2355-2357, 1979.
299. Bradfield, W. S. and J. J. Jr. Sheppard. Microschlieren - A technique for the study of details in compressible flow. *Aero/Space Engrg.*, (5):37-56, 1959.
300. Stong, C. L. The Amateur Scientist: two methods of microscope lighting that produce color. *Sci. Am.*, **217**(4):125-129, 1966.
301. Strong, J. D. *Procedures in experimental physics*. Prentice-Hall, NY, 1944.
302. Bortolussi, G. L. and P. Sirotti. Optical processing for flow visualization. In *Proc. 25th AIAS Natl. Conf.,* Lecce, Italy, pp. 737-744, 1996.
303. Bouyer, R. and C. Chartier. Application of phase contrast to the study of high-speed gas jets. In *Proc. 3rd Intl. Congr. on High Speed Photography*, pp. 271-275, 1956.
304. Baranov, V. K., V. N. Stasenko, and V. A. Tsekhomskiy. Use of photochromic glasses as the visualizing diaphragm of a shadowgraph. *Sov. J. Opt. Tech.*, **41**(2):104-105, 1974.
305. Stasenko, V. N. Parameters of a photoelectric shadowgraph equipped with a visualizing diaphragm of photochromic glass. *Sov. J. Opt. Tech.*, **41**(3):129-131, 1974.
306. Downie, J. D. Application of bacteriorhodopsin films in an adaptive-focusing schlieren system. *App. Optics*, **34**(26):6021-6027, 1995.
307. Peale, R. E., B. Ruffin, J. Donahue, and C. Barrett. White light schlieren optics using bacteriorhodopsin as an adaptive image grid. *App. Optics*, **36**(19):4446-4450, 1997.
308. Sato, T., H. Kojima, O. Ikeda, and Y. Odai. Two-dimensional, optical temporal bandpass filter using four-wave mixing in a BSO crystal: dynamic schlieren imaging System. *App. Optics*, **26**(10):2016-2019, 1987.
309. Siahmakoun, A. and T. Harrer. Dynamic photorefractive schlieren system. *App. Optics*, **32**(35):7281-7284, 1993.
310. Siahmakoun, A. and P. W. Southard. Real-time detection of laser damage threshold of AR coating of high-power optics. In *Proc. Opt. Engrg. Midwest '95*, ed. R. P. Guzik. SPIE Vol. 2622, pp. 73-78, 1995.
311. Settles, G. S. Color schlieren optics - A review of techniques and applications. In *Flow Visualization II*, ed. W. Merzkirch. Hemisphere, pp. 187-197, 1981.
312. Wolter, H. Zweidimensionale Farbschlierenverfahren. *Ann. Phys.,* Series 6, **8**(1-2):1-10, 1950.
313. Carter, E. C. and R. C. Carter. Color and conspicuousness. *JOSA*, **71**(6):723-729, 1981.
314. Carter, R. C. and E. C. Carter. High-contrast sets of colors. *App. Optics*, **21**(16), pp. 2936-2939, 1982.
315. Allan, W. H. Boundary-layer photography of swimming fish. In *Proc. 6th Intl. Congress on High Speed Photography*, pp. 229-234, 1962.
316. Weinberg, F. J. A versatile apparatus for the study of refractory index fields in gases. Report ARL 63-45, USAF Aeronautical Research Lab, 1963.
317. Abraham, M., III and D. W. Netzer. Nonmetallized solid propellant combustion in standard and high acceleration environments. *Comb. Sci. Tech.*, **11**(1-2):75-83, 1975.
318. Takagi, T., P. F. Rao, and H. Kubota. Real-time monitoring of polyacrylamide gel electrophoresis by schlieren optics. *J. Biochem. (Tokyo)*, **102**(4):681-684, 1987.
319. Carpenter, T. W. The analysis of thrust vectored nozzles using schlieren photography. In *Proc. 9th Intl. Symp. on Flow Visualization,* ed. I. Grant and G. M. Carlomagno, Paper no. 47, 2000.
320. Schardin, H. and G. Stamm. Prüfung von Flachglas mit Hilfe eines farbigen Schlierenverfahrens. *Glastechniche Berichte*, **20**(9):249-258, 1942.

321. Schardin, H. Glastechnische Interferenz- und Schlierenaufnahmen. *Glastechniche Berichte*, **27**(1):1-12, 1954.
322. Schardin, H. Das Schlierenmikroskop und seine Anwendung in der Glastechnik. *Glastechniche Berichte*, **27**(3):70-79, 1954.
323. Wolter, H. Zur Abbildung von Amplituden-, Phasen- und Polarisationsobjekten in einem einzigen farbigen Bilde. *Ann. Phys.*, Series 6, **9**(2-4):57-65, 1951.
324. Bayer, M. and J. R. Meyer-Arendt. Farbschlierenphotographie in der Mikroskopie. *Photographie und Wissenschaft*, **4**(3):19-20, 1955.
325. Howes, W. L. Rainbow schlieren. NASA TP-2166, 1983.
326. Kafri, O. and K. Kreske. Flatness analysis of hard disks. *Opt. Engrg.*, **27**(10):878-882, 1988.
327. Oren, D. C., R. P. Durrett, and C. R. Ferguson. Bullseye color schlieren flow visualization. *Expts. Fluids*, **6**(6):357-364, 1988.
328. Carlson, A. B., D. T. Harrje, and G. S. Settles. An optical study of thermal convection in a passive solar heated room. In *Proc. Century 2 Solar Energy Conference,* San Francisco, ASME Paper 80-C2/SOL-1, 1980.
329. Poteet, W. M. and R. B. Owen. Compact field color schlieren system for use in microgravity materials processing. *Opt. Engrg.*, **25**(7):841-845, 1986.
330. Farmer, C. S. and S. Fleeter. Flow visualization and analysis of aerodynamically detuned supersonic rotors. *Expts. Fluids*, **6**:145-155, 1988.
331. Verdaasdonk, R. M. and C. Borst. Optical technique for color imaging of temperature gradients in physiological media: A method to study thermal effects of cw and pulsed lasers. In *Proc. Laser-Tissue Interaction IV*, SPIE Vol. 1882, pp. 355-365, 1993.
332. Verdaasdonk, R. M., Lodder.R., C. F. Van Swol, and M. C. Grimbergen. Thermal imaging of laser-tissue interaction using color schlieren techniques quantified by ray-tracing simulation. In *Proc. Laser-Tissue Interaction X: Photochemical, Photothermal, and Photomechanical*, SPIE Vol. 3601, pp. 156-165, 1999.
333. Wolter, H. Phase contrast, schlieren and interference microscopy. *Microscopica Acta*, **77**(1):2-25, 1975.
334. Becker, B. A schlieren-optical method for visualization and differentiation of density gradients of arbitrary direction. *Arch. Tech. Mess. Indus. Mess.*, **5** (144-7):21-22, 1972.
335. Schmidt, U. Über Auswertungsmöglichkeiten bei einem zweidimensinalen Farbschlierenverfahren. *Ann. Phys.*, Series 7, **1**(7):203-218, 1958.
336. Kameda, M., H. Abe, H. Chinju, M. Konno, Y. Watanabe, and F. Higashino. Flow visualization of a ballistic range by color schlieren methods. In *Proc. 1st Pacific Symp. on Flow Vis. & Image Proc., PSFVIP-1*, ed. S. Mochizuki. pp. 379-382, 1997.
337. Holder, D. W. and R. J. North. A schlieren apparatus giving an image in color. *Nature*, **169**:466, 1952.
338. Hyzer, W. G. Color schlieren. *Research/Development*, **25**(10):28-32, 1974.
339. Waddell, J. H. and J. W. Waddell. A new technique for color schlieren. *Research/Development*, **21**(3):30-32, 1970.
340. Hauf, W. and U. Grigull. Optical methods in heat transfer. *Advances in Heat Transfer*, ed. J. P. Hartnett and T. F. Irvine. Academic Press, NY, Vol. 6, pp. 133-366, 1970.
341. Creel, T. R., Jr. and J. L. Hunt. Photographing flow fields and heat-transfer patterns in color simultaneously. *Astronautics and Aeronautics*, **10**(4):54-55, 1972.
342. Holder, D. W. and R. J. North. Colour in the wind tunnel. *The Aeroplane*, **82**:16-19, 1952.
343. Kraus, W. Die Verwendung der Farbschlieren-Photographie zur Sichtbarmachung von Misch- und Rührvorgangen. *Photographie und Wissenschaft*, **3**(3):3-8, 1954.
344. Stong, C. L. The Amateur Scientist: how to photograph air currents in color. *Sci. Am.*, **210**(2):132-136, 1964.

345. Westkaemper, J. C. Supersonic flow visualization in color. OAL Memorandum 67, US Army Ordnance Aerophysics Laboratory, Daingerfield, TX, 1954.
346. Schnerr, G. H. and J. Zierep. Airfoils in supersonic source and sink flows. *Zeitschrift für Flugwissenschaften und Weltraumforschung*, **13**(5):281-290, 1989.
347. Philpott, D. R. A variable sensitivity and orientation colour schlieren system. *Expts. Fluids*, **29**:42-44, 2000.
348. Salamandra, G. D. Vibrational flame propagation in a tube. *High-Temp. Properties of Gases*, ed. A. S. Predvoditelev. Izdatel'stvo Nauka, Moscow, pp. 148-152, 1969.
349. Nakamura, Y. and T. Tsuno. Measurement of density gradient by pseudo-colored schlieren method. In *Proc. Intl. Congress on High-Speed Photography and Photonics*, SPIE Vol. 1032, pp. 1046-1049, 1988.
350. Wuest, W. Sichtbarmachung von Strömungen IV. Das Schlierenverfahren. *Arch. Tech. Mess. Indus. Mess.*, **5**(144-5):81-86, 1967.
351. Apashev, M. D., I. F. Belyayeva, and V. D. Mikhaylenko. The use of a color screen for quantitative investigations of schlieren by the Toepler optical method. In *Proc. Engine Institute, Academy of Sciences, USSR*, Izdatel'stvo Nauka, 6, 1962.
352. Brauer, H. Schlierenoptische Beobachtungen bei der Wärmeübertragung. *Chemie-Ingeneur-Technik*, **34**(2):73-78, 1962.
353. Kaspar, J. Colour in high-speed photography by modified schlieren apparatus. In *Proc. 8th Intl. Conf. on High-Speed Photography*, Wiley, NY, pp. 357-358, 1968.
354. Salamandra, G. D. Obtaining color schlieren photographs of rapid processes using the IAB-451 instrument. *High-Temperature Properties of Gases*, ed. A. S. Predvoditelev. Akademiya Nauk SSSR, pp. 153-156, 1969.
355. Oguni, Y., M. Sato, H. Kanda, S. Sakakibara, and H. Miwa. The schlieren observation system installed in the NAL two-dimensional high- Reynolds number transonic wind tunnel and attempts to improve it. Report NAL-TR-964, National Aerospace Laboratory, Japan, 1988.
356. Settles, G. S. A new quantitative schlieren technique for use in heat transfer and gas dynamics. In *Proc. Region IV Student Conf.*, ASME, pp. 18-39, 1971.
357. Tanda, G. Application of the schlieren technique to convective heat transfer measurements. Electronic publication http://dau.ing.univaq.it/omhat, 1999.
358. Greenberg, P. S., R. B. Klimek, and D. R. Buchele. Quantitative rainbow schlieren deflectometry. *App. Optics*, **34**(19):3810-3813, 1995.
359. Phillips, H. A three-colour quantitative schlieren system. *J. Sci. Instr. Ser. 2.*, **1**:413-416, 1968.
360. Al-Ammar, K., A. K. Agrawal, S. R. Gollahalli, and D. Griffin. Application of rainbow schlieren deflectometry for concentration measurements in an axisymmetric helium jet. *Expts. Fluids*, **25**(2):89-95, 1998.
361. Shenoy, A. K., A. K. Agrawal, and S. R. Gollahalli. Quantitative evaluation of flow computations by rainbow schlieren deflectometry. *AIAA J.*, **36**(11):1953-1960, 1998.
362. Cash, R. F. and A. M. Catley. Separation measurements on a delta wing in a shock tunnel at M=8.6 using monochrome and colour-schlieren photography. British NPL Aero Note 1097 (ARC 32,399), 1970.
363. Kessler, T. J. and W. G. Hill. Schlieren analysis goes to color. *Astronautics and Aeronautics*, **4**(1):38-40, 1966.
364. Kessler, T. J. and W. G. Hill. A color schlieren system. *Photo. Apps. Sci. Tech. Med.*, **9**(1):22-34, 1974.
365. Kessler, T. J. and A. A. Kuebler. Film study of high-velocity gas flow phenomena. *SMPTE Journal*, **75**(8):742-744, 1966.
366. Kozhushko, A. A. and V. I. Miroshnichenko. Streak photography with a color schlieren system. *Soviet Technical Physics Letters*, **1**(4):177-178, 1975.

367. Murphy, J. L. and D. W. Netzer. Ammonium perchlorate and ammonium perchlorate-binder sandwich combustion. *AIAA J.*, **12**(1):13-14, 1974.
368. Netzer, D. W. and J. R. Andrews. Schlieren studies of solid-propellant combustion. Chap. V-1 of *Experimental Diagnostics in Combustion of Solids,* Vol. 63, Progress in Astronautics and Aeronautics, ed. T. L. Boggs. AIAA, NY, 1978.
369. Page, R. H., T. J. Kessler, and A. A. Kuebler. Color schlieren studies of transient flows with high speed motion picture photography. In *Proc. of the 4th Space Congr., Cocoa Beach*, Canaveral Council of Tech. Societies, Part 1, Paper no. 4, 1967.
370. Smith, L. L. and J. H. Waddell. Techniques of colored schlieren. In *Proc. 9th Intl. Congr. on High Speed Photography*, Denver, SMPTE, Paper no. 86, 1970.
371. Stolzenburg, W. A. Optical flow visualization instrumentation: quantitative color schlieren. Report SM-41397-9, Douglas Aircraft Co., El Segundo, CA, 1963.
372. Clark, R. P., T. D. Preston, D. C. Gordon-Nesbitt, S. Malka, and L. Sinclair. The size of airborne dust particles precipitating bronchospasm in house dust sensitive children. *Journal of Hygiene*, **77**(3):321-325, 1976.
373. Clark, R. P. and R. N. Cox. An application of aeronautical techniques to physiology. 1. The human microenvironment and convective heat transfer. *Medical and Biological Engineering*, **12**(3):270-274, 1974.
374. Jeffree, H. A wide range Schlieren system. *J. Sci. Inst.*, **33**:29-30, 1956.
375. Surget, J. Strioscopie Quantitative a Grille Coloree et Fente d'Entree Multiple. *La Recherche Aérospatiale*, **97**(6):37-42, 1963.
376. Maddox, A. R. Observations on the backward-facing step with an improved diffraction grating interferometer and a new color schlieren technique. In *Proc. 5th Aerodynamics Testing Conf.*, AIAA Paper 70-571, 1970.
377. Doyon, P. High sensitivity color schlieren photography of hypervelocity models at DREV hypersonic range 5. Report DREV-TN-1948/71, Defense Research Establishment Valcartier (Canada), 1971.
378. Kleine, H. and H. Groenig. Color schlieren methods in shock wave research. *Shock Waves*, **1**(1):51-63, 1991.
379. Arbuzov, V. A. and Yu. N. Dubnishchev. Real-time coloured visualization of phase flows by the schlieren method. *Optics and Laser Technology*, **23**(2):118-120, 1991.
380. Hsieh, T., A. B. Wardlaw, Jr., and T. J. Birch. Vortical flows about a long cylinder at M = 3.5 and alpha = 18 deg. AIAA Paper 91-1808, 1991.
381. Settles, G. S. A direction-indicating color schlieren system. *AIAA J.*, **8**(12):2282-2284, 1970.
382. Settles, G. S. A four color schlieren techique with sensitivity in all directions. *Tennessee Engineer*, (12):4-9, 1970.
383. Settles, G. S. A two-dimensional color schlieren technique. *Image Technology*, **14**:19-23, 1972.
384. Clark, R. P. and J. Hill. Safety cabinets and product protection. *Journal of Clinical Pathology*, **34**(12):1404, 1981.
385. Stong, C. L. The Amateur Scientist: schlieren photography is used to study the flow of air around small objects. *Sci. Am.*, **224**(5):117-123, 1971.
386. Stong, C. L. The Amateur Scientist: an air flash lamp advances color schlieren photography. *Sci. Am.*, **231**(8):104-109, 1974.
387. Vandiver, J. K. and H. E. Edgerton. Color schlieren photography of short duration transient events. In *Proc. 11th Intl. Congr. on High Speed Photography,* Chapman & Hall Ltd., London, pp. 398-403, 1975.
388. Baroth, E. C. and M. Holt. Investigation of supersonic separated flow in a compression corner by laser doppler anemometry. *Expts. Fluids*, **1**:195-203, 1983.
389. Settles, G. S. Hidden frenzy. *Science Digest*, **89**(8):44-49, 1981.

390. Settles, G. S. Schlieren photography: a versatile means of making invisible phenomena visible. *Technical Photography*, **14**(2):35-41, 1982.
391. Settles, G. S. Moving beyond light shows: a new concept in color music displays. *Mix Magazine*, **9**(10):48-53, 1985.
392. Chen, R. Y. and Z. F. Ge. Color schlieren system using square color filter and its application to aerofoil test in transonics. In *Proc. 18th Intl. Congr. on High Speed Photography and Photonics*, Xian, PRC, SPIE Vol. 1032, pp. 845-849, 1989.
393. Kleine, H. and H. Groenig. Colour schlieren experiments in shock tube and tunnel flow. In *Strong Shock Waves, Proc. Intl. Workshop*, Chiba, Japan, pp. 41-48, 1992.
394. Meyer-Arendt, J. R. *Selected papers on schlieren optics*. SPIE Milestone Series MS 61, Bellingham, WA, 1992.
395. Wu, X. Y. A new color schlieren system of adjustable sensitivity. In *Proc. 2nd China-Japan Symp. on Visualization*, Academic Press Intl., Vol. 2, pp. 111-114, 1992.
396. Kleine, H. and H. Groenig. Visualization of transient flow phenomena by means of color schlieren and shearing interferometry. In *Proc. 20th Intl. Congr. on High Speed Photography and Photonics*, SPIE Vol. 1801, pp. 410-416, 1993.
397. Krehl, P., S. Engemann, and P. Neuwald. Flash lighting instrumentation for color schlieren shock wave photography. *Shock Waves*, **5**(4):195-207, 1995.
398. Takeishi, K., M. Matsuura, H. Kleine, and S. Miyashiro. Application of new color schlieren methods to shock tunnel. *J. Japn. Soc. Aero. Space Sci.*, **44**(509):15-20, 1996.
399. Kleine, H. Development of simultaneous holographic interferometer/color schlieren system for the investigation of compressible flows. In *Proc. 9th Intl. Symp. on Flow Visualization*, ed. I. Grant and G. M. Carlomagno, Paper no. 168, 2000.
400. Kleine, H. *Verbesserung optischer methoden für die gasdynamik*. Ph.D. Thesis, RWTH Aachen, 1993.
401. Kleine, H. Private communication. Aug. 24, 2000.
402. Seitz, M. W., D. M. Scott, and B. W. Skews. Two-dimensional color schlieren system with adjustable sensitivity. In *Proc. 20th Intl. Congr. on High Speed Photography and Photonics*, ed. J. M. Dewey and R. G. Racca. SPIE Vol. 1801, pp. 410-416, 1993.
403. Seitz, M. W., D. M. Scott, and B. W. Skews. Color schlieren photographic system. *Opt. Engrg.*, **33**(9):2907-2910, 1994.
404. Salamandra, G. D., N. M. Venttsel, and O. I. Luneva. Color images of inhomogeneous transparent media. In *Proc. 12th Intl. Congr. on High Speed Photography and Photonics,* Toronto, SPIE Vol. 97, pp. 49-51, 1977.
405. Meyer-Arendt, J. R., L. M. Montes, and W. S. Muncey, Jr. A color schlieren system without image degradation. *SPIE Journal*, **9**(11):18-21, 1970.
406. Meyer-Arendt, J. R. and H. Appelt. Microscopy using a new type of color schlieren technique. *Microscopica Acta*, **80**(2):111-114, 1978.
407. Chashechkin, Y. D. Colour schlieren method. In *Optical Methods in Dynamics of Fluids and Solids*, ed. M. Pichal. Springer-Verlag, Berlin, pp. 275-282, 1985.
408. Chashechkin, Y. D. Schlieren and colour schlieren visualization of a stratified flow. *Journal of Visualization*, **1**(4):329-404, 1999.
409. Mowbray, D. E. The use of schlieren and shadowgraph techniques in the study of flow patterns in density stratified liquids. *J. Fluid Mech.*, **27**(Part 3):595-608, 1967.
410. Hays, G. E. A color schlieren system for high-speed photography. *SMPTE Journal*, **66**(6):355-356, 1957.
411. Howes, W. L. Rainbow schlieren and its applications. *App. Optics*, **23**:2449-2460, 1984.
412. Howes, W. L. Rainbow schlieren vs Mach-Zehnder interferometer - a comparison. *App. Optics*, **24**:816-822, 1985.
413. Howes, W. L. Optical elements formed by compressed gases: Analysis and potential applications. NASA TP-2555, 1986.

414. Buchele, D. R. and D. W. Griffin. Compact color schlieren optical system. *App. Optics*, **32**(22):4218-4222, 1996.
415. Miyashiro, S., H. Kleine, and H. Groenig. Short-duration spark source for color schlieren methods. In *Proc. 20th Intl. Congr. on High Speed Photography & Photonics*, ed. J. M. Dewey and R. G. Racca, SPIE Vol. 1801, pp. 248-257, 1993.
416. Kleine, H., E. Ritzerfeld, and H. Groenig. Shock wave diffraction - new aspects of an old problem. In *Shock Waves at Marseilles IV*, ed. R. Brun. Springer-Verlag, Berlin, pp. 117-122, 1995.
417. Kleine, H. Flow Visualization. Chap. 5.1 of *Handbook of Shock Waves*, ed. G. Ben-Dor, O. Igra, and E. Elperin. Academic Press, Boston, ed. 1, 2001.
418. Trolinger, J. D., R. B. Lal, C. S. Vikram, and W. K. Witherow. Compact spaceflight solution crystal-growth system. In *Proc. Crystal Growth in Space and Related Optical Diagnostics*, San Diego, SPIE Vol. 1557, pp. 250-258, 1991.
419. Kamei, S., T. Hanyu, and M. Ishikawa. Color schlieren optical device for airplane experiment and observation of flow under gravity modulational field. *J. Japan Soc. Microgravity App.*, **12**(4):3-14, 1995.
420. Takagi, T. and H. Kubota. The application of schlieren optics for detection of protein bands and other phenomena in polyacrylamide gel electrophoresis. *Electrophoresis*, **11**:361-366, 1990.
421. Ivey, G. N. and R. I. Nokes. Vertical mixing due to the breaking of critical internal waves on sloping boundaries. *J. Fluid Mech.*, **204**:479-500, 1989.
422. Gerhard-Multhaupt, R., W. Brinker, H. J. Ehrke, W. D. Molzow, H. Roeder, T. Rosin, and R. Tepe. Viscoelastic spatial light modulators and schlieren-optical systems for HDTV projection displays. In *Proc. Large-Screen Projection Displays II*, SPIE Vol. 1255, pp. 69-78, 1990.
423. Rodriguez-Vera, R., A. Olivares-Perez, and A. A. Morales-Romero. Holographic pseudocoloring of schlieren images. In *Holographic Optics III: Principles and Applications*, the Hague, SPIE Vol. 1507, pp. 416-424, 1991.
424. Spornik, N. M. Holographic color schlieren method of flow visualization. In *Flow Visualization VI*, ed. J. Tanida, Springer-Verlag, Berlin, pp. 667-671, 1992.
425. Cox, P., director. *The hidden dimension, an IMAX 3-D film,* 39 mins. IMAX Corp., 1997. http://www.imax.com/films/distribution/hidden_dimension.html.
426. Ramiro, M. Between form and force: connecting architectonic, telematic and thermal spaces. *Leonardo*, **31**(4):247-260, 1998.
427. Norling, J. A. The stereoscopic art - a reprint. *SMPTE Journal*, **60**(3):268-308, 1953.
428. *IMAX®, the 15/70 filmakers manual.* Available from www.imax.com, 1999.
429. Hett, J. H. A high-speed stereoscopic schlieren system. *SMPTE Journal*, **56**(2):214-218, 1951.
430. Veret, C. La strioscopie stéréoscopique. *La Recherche Aéronautique*, **29**:3-7, 1952.
431. Settles, G. S. and H. Y. Teng. Flow visualization methods for separated 3-D shock wave/turbulent boundary-layer interactions. *AIAA J.*, **21**:390-397, 1983.
432. Nevskii, L. B., A. D. Frolova, and V. A. Yakovlev. Visualization of gas flows through use of IT-144 interferometer. *Soviet J. of Optical Technology*, **47**(5):312-313, 1980.
433. Struth, W. Kurzeitaufnahmen von Schüssen mit Hyperschallgeschwindigkeit in reagierende Gase. In *Proc. 6th Intl. Congr. on High Speed Photog.*, pp. 443-449, 1963.
434. Harris, G., W. Shaw, M. Dean, M. Hendriks, M. Omidvar, H. Murray, and K. Baker. 3D for the nineties - A wide field stereo IMAX camera. In *Proc. 135th SMPTE Technical Conference*, Los Angeles, SMPTE Preprint 135-23, 1993.
435. Jamin, J. Sur un réfracteur differential pour la lumière polarisée. *Comptes Rendus*, **67**:814, 1868.
436. Françon, M. Interférences par double réfraction en lumière blanche. *Revue d'Optique*, **31**:65-80, 1952.

437. Françon, M. Polarization apparatus for interference microscopy and macroscopy of isotropic transparent objects. *JOSA*, **47**(6):528, 1957.
438. Nomarski, G. Remarques sur le fonctionnement des dispositifs interférientiels à polarisation. *J. Phys. Radium*, **17**:15-35, 1956.
439. Chevalerias, R., Y. Latron, and C. Veret. Methods of interferometry applied to the visualization of of flow in wind tunnels. *JOSA*, **47**:8, 1957.
440. Philbert, M. Applications metrologiques de la strioscopie interférentielle. *Revue d'Optique*, **37**(12):598, 1958.
441. Philbert, M. Emploi de la strioscopie interférentielle en aérodynamique. *Recherche Aerospatiale*, **65**:19-27, 1958.
442. Merzkirch, W. A simple schlieren interferometer system. *AIAA J.*, **3**(10):1974-1976, 1965.
443. Small, R. D., V. Sernas, and R. H. Page. Single beam schlieren-interferometer using a Wollaston prism. *App. Optics*, **11**:858-862, 1972.
444. Smeets, G. Observational techniques related to differential interferometry. In *Proc. 11th Intl. Congr. on High Speed Photog.*, Chapman & Hall, UK, pp. 283-288, 1975.
445. Sernas, V. Interferometric methods in heat transfer research. In *Flow visualization III*, ed. W.-J. Yang. Hemisphere Pub., Washington DC, pp. 753-767, 1985.
446. Srulijes, J., K. Runne, and F. Seiler. Flow visualization on spike-tipped bodies. In *Proc. 9th Intl. Symp. on Flow Visualization,* Paper no. 284, 2000.
447. Sernas, V. and L. S. Fletcher. A schlieren interferometer method for heat transfer studies. *Journal of Heat Transfer, Transactions ASME*, **92**(2):202-204, 1970.
448. Oertel, H., Jr. and K. Bühler. A special differential interferometer used for heat convection investigations. *Intl. Journal of Heat and Mass Transfer*, **21**:1111-1115, 1978.
449. Oertel, H. Jet noise research by means of shock tubes. In *Proc. 10th Intl. Shock Tube Symposium,* Kyoto, ed. G. Kamimoto. Shock Tube Research Soc., pp. 488-495, 1975.
450. Smeets, G. Interferometry. Report CO-214/90, Institut Saint-Louis, 1990.
451. Gayhart, E. L. and R. Prescott. Interference phenomenon in the schlieren system. *JOSA*, **39**(7):546-550, 1949.
452. Temple, E. B. Quantitative measurement of gas density by means of light interference in a schlieren system. *JOSA*, **47**(1):91-100, 1957.
453. Reisman, E. and P. M. Sutton. Measurement of air temperature distributions with the schlieren interferometer. *App. Optics*, **4**(1):144-145, 1965.
454. Brackenridge, J. B. and J. Peterka. Criteria for quantitative schlieren interferometry. *App. Optics*, **6**(4):731-735, 1967.
455. Dodd, J. G. Interferometry with schlieren microscopy. *App. Optics*, **16**(2):470-472, 1977.
456. Erdmann, S. F. A new simple interferometer for obtaining quantitatively-evaluable flow patterns (translated as NACA TM 1363). *App. Sci. Research*, **B.2**:149ff, 1951.
457. Noll, R., G. Herziger, C. R. Haas, and B. Weikl. Computer simulation of schlieren images of rotationally symmetric plasma systems - A simple method. *App. Optics*, **25**:769-774, 1986.
458. Schnerr, G. H. Digital image interpretation for optical flow measurement methods: System description and preliminary application examples. In *Proc. DGLR Conf. on 2-D Measuring Techniques*, pp. 93-104, 1988.
459. Tamura, Y. and K. Fujii. Visualization for computational fluid dynamics and the comparison with experiments. AIAA Paper 90-3031, 1990.
460. Yates, L. A. Images constructed from computed flowfields. *AIAA J.*, **31**(10):1877-1884, 1993.
461. Brown, D., T. Cole, B. Peters, J. P. Wilson, and A. G. Havener. CFI- shadowgraph/schlieren photography for aerodynamic applications. AIAA Paper 94-2616, 1994.

462. Decker, G., R. Deutsch, W. Kies, and J. Ryback. Computer-simulated schlieren optics. *App. Optics*, **24**(6):823-828, 1995.
463. Donohoe, S. R., E. M. Houtman, and W. J. Bannink. A high-speed surface reflective visualization system for the study of vortex breakdown over a delta wing. AIAA Paper 94-248, 1994.
464. Zhang, X., A. Rona, and J. A. Edwards. An observation of pressure waves around a shallow cavity. *J. Sound Vibration*, **214**(4):771-778, 1998.
465. Naughton, J. W., E. Venkatapathy, and D. G. Fletcher. Combined computational/experimental flow field imaging for efficient testing. In *Flow Visualization VII*, ed. J. P. Crowder. Begell House, NY, pp. 832-837, 1995.
466. Fiadeiro, P. T. and D. C. Emmony. Phase retrieval in computer generation of schlieren images. In *Proc. of Conf. on Optical Techniques in Fluid, Thermal, and Combustion flow,* SPIE Vol. 2546, pp. 331-340, 1995.
467. Leonard, D. A. and J. C. Keck. Schlieren photography of projectile wakes using resonance radiation. Report 130, Avco Everett Research Laboratory, 1962.
468. Barrekette, E. S. Real time optical information processing. In *Applications of Holography*, Plenum Press, NY, pp. 309-322, 1971.
469. Blendstrup, G., D. Bershader, and P. W. Langhoff. Recent results of resonant refractivity studies for improved flow visualization. In *Proc.12th Intl. Symp. on Shock Tubes and Waves*, Magnes Press, Jerusalem, pp. 258-265, 1980.
470. Bershader, D. and S. G. Prakash. Improved flow visualization by use of resonant refractivity. AIAA Paper 76-71, 1976.
471. Sabine, W. C. Architechtural acoustics. *Journal of the Franklin Institute*, Jan. 1915.
472. Davis, A. H. and G. W. C. Kaye. *The acoustics of buildings*. G. Bell & Sons Ltd., London, 1927.
473. Kock, W. E. *Seeing Sound*. Wiley-Interscience, New York, 1971.
474. Buchele, D. R. and H. R. Goosens. Lens system producing unequal magnification in two mutually perpendicular directions. *Rev. Sci. Instr.*, **25**:262, 1954.
475. Fertin, G. Recording of schlieren pictures for flow visualization in rotating machines. In *Proc. 11th Intl. Congr. on High-Speed Photography*, ed. P. J. Rolls. Chapman & Hall, London, pp. 374-379, 1975.
476. Philbert, M. and G. Fertin. Schlieren systems for flow visualization in axial and radial flow compressors. *J. Engrg. Power, Trans. ASME*, **97**(2):254-260, 1975.
477. Vikram, C. S. and M. L. Billet. Modifying tunnel test sections for optical applications. *Opt. Engrg.*, **25**(12):1324-1326, 1986.
478. Costen, R. C., D. B. Rhodes, and S. B. Jones. Schlieren system for flow studies in round glass pipes. *App. Optics*, **30**(3):271, 1991.
479. Mach, L. Sichtbarmachung von Luftstromlinien. *Zeitschrift für Luftschiffahrt und Physik der Atmosphäre*, **15**(6):129-139, 1896.
480. Townend, H. C. H. A method of airflow cinematography capable of quantitative analysis. *J. Aero. Sci.*, **3**(10):343-352, 1936.
481. Shimizu, S., K. Wakai, and M. Sonobe. Simple method to visualize a transient flow of urburnt gas in a chamber. *JSME Intl. Journal, Series II*, **32**(1):121-126, 1989.
482. Kanazawa, S., T. Ohkubo, T. Adachi, M. Inokuchi, and A. Shibuya. Flow visualization of a particle deposition on silicon wafers in clean rooms. In *Proc. Industry Apps. Soc. Ann. Mtg.*, IEEE, Part 1, pp. 640-645, 1991.
483. Settles, G. S. and G. G. Via. A portable schlieren system for clean-room airflow analysis. *J. Environmental Sci.*, **30**(5):17-21, 1987.
484. Weinstein, L. M. Vaporizing particle velocimeter. US Patent 5,153,665, Oct. 6, 1992.
485. Barry, F. W. and G. M. Edelman. An improved schlieren apparatus. *J. Aero. Sci.*, **15**:364-365, 1948.

486. Owen, R. B. and W. K. Witherow. Dual laser optical system and method for studying fluid flow. US Patent 4,391,518, 1983.
487. Rudinger, G. and L. M. Somers. A simple schlieren system for two simultaneous views of a gas flow. *SMPTE Journal*, **62**(10):107, 1957.
488. Golub, V. V., A. I. Kharitonov, I. L. Sharov, and A. M. Shulmeister. Two-direction visualization of vortex rings emerging in the course of formation of the supersonic jet. In *Flow visualization V*, ed. R. Řeznícek. Hemisphere Pub., NY, pp. 556-561, 1990.
489. Lide, D. R. ed. *CRC handbook of chemistry and physics*. ed. 77, pp. 10-265,1996.
490. Narrow, T. L., M. Yoda, and S. I. Abdel-Khalik. A simple model for the refractive index of sodium iodide aqueous solutions. *Expts. Fluids*, **28**:282-283, 2000.
491. Hendriks, F. and A. Aviram. Use of zinc iodide solutions in flow research. *Rev. Sci. Instr.*, **53**:75-78, 1982.
492. Chamot, E. M. and C. W. Mason. Determination of refractive indices in liquids and solids. Chap. 11 of *Handbook Chem. Micros.*, Wiley, NY, ed. 3, pp. 311-334, 1958.
493. Schmidt, M. C. and G. S. Settles. Alignment and application of the conical shadowgraph flow visualization technique. *Expts. Fluids*, **4**(2):93-96, 1986.
494. Vlad, V. I., N. Ionescu-Pallas, and F. Bociort. New treatment of the focusing method and tomography of the refractive index distribution of inhomogeneous optical components. *Opt. Engrg.*, **35**(5):1305-1310, 1996.
495. Glasser, J., R. Viladrosa, and J. Chapelle. Diagnostic of dense plasmas by infrared schlieren and absorption techniques. *J. Phys. D. Appl. Phys.*, **11**(12):1703-1707, 1978.
496. Wilkerson, T. D., J. M. Lindsay, and G. F. Frazier. Development of an infrared schlieren system. Rpt. 122-5, AFOSR-TR-78-1451, Versar Inc., Springfield, VA, 1978.
497. Kierkegaard, S. *Either/or: a fragment of life*. 1843.
498. Kessler, S. and J. Hebenstreit. Theoretical Investigations of the shadow method, Part I: general properties. *Experimentelle Technik der Physik*, **37**(5):413-423, 1989.
499. Melton, B. S., R. Prescott, and E. L. Gayhart. A working manual for spark shadowgraph photography. Bumblebee Report 90, Applied Physics Lab, Johns Hokins University, Silver Spring, MD, 1948.
500. Hesselink, L. Optical image processing. *Handbook of Flow Visualization*, ed. W.-J. Yang. Hemisphere Pub., Washington DC, ed. 1, 1989.
501. Sirotti, P. Phase images in non-destructive evaluation. In *Proc. 6th Intl. Conf. on Image Processing & Applications*, IEEE, Vol. 2, pp. 717-721, 1997.
502. Hoegerl, K. and G. F. West. Homogeneity of fluoride glasses. *Glass Tech.*, **36**(4):135-138, 1995.
503. Brabham, C. Multispark shadowgraph system for a free flight aeroballistic range. In *ICIASF '77 Record*, IEEE, pp. 177-181, 1977.
504. Umeda, Y., H. Maeda, and R. Ishii. Hole tone generated from almost choked to highly choked jets. *AIAA J.*, **26**(9):1036-1043, 1988.
505. Alvi, F. S. and G. S. Settles. Structure of swept shock wave/boundary-layer interactions using conical shadowgraphy. AIAA Paper 90-1644, 1990.
506. Linden, P. F. The formation of banded salt finger structure. *Journal of Geophysical Research*, **83**(C6):2902-2912, 1978.
507. Turner, J. S. Double-diffusive intrusions into a density gradient. *Journal of Geophysical Research*, **83**(C6):2887-2901, 1978.
508. Beckermann, C. and R. Viskanta. Experimental study of solidification of binary mixtures with double-diffusive convection in the liquid. In *Proc. 1988 Natl. Heat Transfer Conf.*, ASME Paper HTD-96, pp. 67-79, 1988.
509. Nosoko, T., T. Nagata, T. Shinzato, K. Oyakawa, T. Ohmija, and M. Nagai. Image analysis of a shadowgram visualizing surface waves on a falling liquid film. In *Proc. 6th Intl. Symp. Trans. Phen. Thermal Engrg.*, Begell House, NY, pp. 1417-1422, 1993.
510. Taylor, L. S. Analysis of turbulence by shadowgraph. *AIAA J.*, **8**:1284-1287, 1970.

511. Hesselink, L. and B. S. White. Digital image processing of flow visulaization photographs. *App. Optics*, **22**(10):1454-1461, 1983.
512. Dykstra, P. C. and J. D. Kuzan. A method of investigating scales of motion in a turbulent wake. Report BRL-MR-3922, US Army Ballistic Research Lab, MD, 1991.
513. Lewis, B. and G. von Elbe. *Combustion, flames, and explosions of gases*. Academic Press, Orlando, ed. 3, 1987.
514. Beinert, J., J. F. Kalthoff, U. Seidelmann, and U. Soltesz. Das Schattenoptische Verfahren und seine Anwendung in der Bruchmechanik. *VDI- Berichte*, **297**:15-25, 1977.
515. Bourne, N. K., Z. Rosenberg, and J. E. Field. High-speed photography of compressive failure waves in glasses. *J. App. Phys.*, **78**(6):3736-3739, 1995.
516. Norman, T. R. and J. S. Light. Rotor tip vortex geometry measurements using the wide-field shadowgraph technique. *J. American Helicopter Soc.*, **32**(2):40-50, 1987.
517. Parthasarathy, S. P., Y. I. Cho, and L. H. Back. Wide-field shadowgraphy of tip vortices from a helicopter rotor. *AIAA J.*, **25**(1):64-70, 1987.
518. Light, J. S., T. R. Norman, and A. A. Frerking. Application of the wide-field shadowgraph technique to helicopters in forward flight. In *Proc. 46th AHS Annual Forum,* American Helicopter Soc., Vol. 2, pp. 1207-1220, 1990.
519. Bagai, A. and J. G. Leishman. Improved wide-field shadowgraph set-up for rotor wake visualization. *J. American Helicopter Soc.*, **37**(3):86-92, 1992.
520. Leishman, J. G. and A. Bagai. Challenges in understanding the vortex dynamics of helicopter rotor wakes. *AIAA J.*, **36**(7):1130-1140, 1996.
521. Panov, I. U. and A. I. Shvets. Separation of a Turbulent Boundary Layer in a Supersonic Flow. *Soviet Applied Mechanics*, **2**:58-61, 1966.
522. Settles, G. S. Schlieren and shadowgraph imaging in the great outdoors. In *Proc. PSFVIP-2*, ed. S. Mochizuki, Paper PF302, 1999.
523. Settles, G. S. and F. K. Lu. Conical similarity of shock/boundary-layer interactions generated by swept and unswept fins. *AIAA J.*, **23**:1021-1027, 1985.
524. Hammitt, A. G. The oscillation and noise of an overpressure sonic jet. *J. Aero. Sci.*, **28**(9):673-680, 1961.
525. Pearcey, H. H. The indication of boundary-layer transition on aerofoils in the NPL 20 inch by 8 inch high speed tunnel. Report ARC CP 10, British Aero. Res. Council, 1950.
526. Schmidt, E. Schlierenaufnahmen des Temperaturfeldes in der Nähe wärmeabgebender Körper. *Forschung auf dem Gebiete des Ingenieurwesens*, **3**(4):181-189, 1932.
527. Glass, I. I. and J. G. Hall. Optical methods -schlieren and interferometry. Navord Report 1488, Vol. 6, Sec. 18, US Navy Bureau of Ordnance, pp. 532-573, 1959.
528. Pfeifer, H. J., H. D. vom Stein, and B. Koch. Mathematical and experimental analysis of light diffraction on plane shock waves. In *Proc. 9th Intl. Congr. on High-Speed Photography,* SMPTE, pp. 423-426, 1970.
529. Adamovsky, G. Optical techniques for shock visualization and detection. In *Proc. Optical Techniques in Fluid, Thermal, and Combustion Flow,* SPIE Vol. 2546, 1995.
530. Panda, J. Wide Angle Light Scattering in Shock-Laser Interaction. *AIAA J.*, **33**(12):2429-2430, 1995.
531. Panda, J. Shock Detection Technique Based on Light Scattering by Shock. *AIAA J.*, **33**(12):2431-2432, 1996.
532. Stong, C. L. The Amateur Scientist: how to build a wind tunnel that achieves supersonic speeds with a vacuum system. *Sci. Am.*, **215**(4):120-125, 1966.
533. Schardin, H. and W. Struth. Hochfrequenzkinematographische Untersuchung der Bruchvorgänge im Glas. *Glastechniche Berichte*, **16**(7):219-227, 1938.
534. Winckler, J. The Mach interferometer applied to studying an axially symmetric supersonic airjet. *Rev. Sci. Instr.*, **19**(5):307-322, 1948.
535. Henderson, W. F., G. W. Robertson, and J. W. Hill. Investigation of shadowgraphs for use with highly ablating, self-luminous, ballistic projectiles. Report AEDC-TR-71-225.

536. Hackett, C. M., G. S. Settles, and J. D. Miller. On the gas dynamics of HVOF thermal sprays. *Journal of Thermal Spray Technology*, **3**(3):299-304, 1994.
537. Slattery, R. E., W. G. Clay, and A. P. Ferdinand. High speed photographic techniques in a ballistic range. In *Proc. 8th Intl. Congr. on High-Speed Photography,* Wiley, NY, pp. 351-356, 1968.
538. Bock, O. H. Focused shadowgraph visualization of boundary-layer transition in aeroballistic range studies. *Opt. Engrg.*, **13**(2):143-146, 1974.
539. Berger, A. G., P. H. Cords, Jr., and N. W. Sheetz, Jr. Temperature-control techniques and instrumentation for viscous flow investigations in a ballistics range. AIAA Paper 68-384, 1968.
540. Clemens, P. L. and R. E. Hendrix. Developments of instrumentation for the VKF 1000-ft hypervelocity range. In *Advances in Hypervelocity Techniques*, ed. A. M. Krill. Plenum Press, NY, pp. 245-277, 1962.
541. Lankford, J. L. Application of laser and flash X-ray techniques in hypervelocity ablation/erosion investigations in a hyperballistics range. In *Proc. 9th Intl. Congr. on High-Speed Photography,* SMPTE Preprint 28, 1970.
542. Edgerton, H. E. Shockwave photography of large subjects in daylight. *Rev. Sci. Instr.*, **29**(2):171-172, 1958.
543. Winn, R. C. and C. R. Morin. Low cost shadowgraph technique for flammable vapor visualization. In *Proc. IECEC-97,* Honolulu, AIChE, Vol. 1, pp. 642-647, 1997.
544. McCutchen, C. W. Flow visualization with stereo shadowgraphs of stratified fluid. *Journal of Experimental Biology*, **65**(1):11-20, 1976.
545. McCutchen, C. W. Fluid dynamic phenomena can be demonstrated with stereo shadowgraphs of stratified fluid. *American J. Phys.*, **44**(10):981-983, 1976.
546. Walker, J. The Amateur Scientist: easy ways to make holograms and view fluid flow, and more about funny fluids. *Sci. Am.*, **262**(2):158-172, 1980.
547. Kersh, P. T. and K. A. Miller. A stereo synchroballistic shadowgraph system. In *Proc. 9th Intl. Congr. on High-Speed Photography,* SMPTE Preprint 114, 1970.
548. Keenan, P. C. Shadowgraph method of determining the strength of a shock wave. *Physical Review*, **69**:677, 1946.
549. Weyl, F. J. Analysis of optical methods. Chap. A.1 of *Physical Meas. in Gas Dynamics and Combustion,* Vol. 9, ed. R. W. Ladenburg. Princeton University Press, Princeton, NJ, pp. 3-25, 1954.
550. Hisley, D. M. BLAST2D computations of the reflection of planar shocks from wedge surfaces with comparison to SHARC and STEALTH results. Report BRL-TR-3147, US Army Ballistic Research Lab, Aberdeen Proving Ground, MD, 1990.
551. Thess, A. and S. A. Orszag. Surface-tension-driven Bénard convection at infinite Prandtl number. *J. Fluid Mech.*, **283**:201-230, 1995.
552. Schöpf, W., J. C. Patterson, and A. M. H. Brooker. Evaluation of the shadowgraph method for the convective flow in a side-heated cavity. *Expts. Fluids*, **21**(5):331-340, 1996.
553. Bagai, A. and J. G. Leishman. Flow visualization of vortex structures using density gradient techniques. *Expts. Fluids*, **15**:431-442, 1993.
554. Samtaney, R. and N. J. Zabusky. Visualization, feature extraction and quantification of numerical visualizations of high gradient compressible flows. Chap. 12 of *Flow Visualization Techniques and Examples*, ed. A. J. Smits and T. T. Lim. Imperial College Press, London, pp. 317-344, 2000.
555. Shapiro, A. H. *The Dynamics and Thermodynamics of Compressible Fluid Flow.* Vols. 1 & 2. Ronald Press, New York, 1953.
556. Liepmann, H. W. and A. Roshko. *Elements of gasdynamics*. Wiley, NY, 1957.
557. Love, E. S. and C. E. Grigsby. A new shadowgraph technique for the observation of conical flow phenomena in supersonic flow. NACA TN 2950, 1953.

558. Pierce, D. and D. Treadgold. Some examples of the use of a conical shadowgraph technique. TN Aero 2955, British Royal Aeronautical Establishment, 1964.
559. Zubin, M. A. and N. A. Ostapenko. Structure of flow in the separation region resulting from interaction of a normal shock wave with a boundary layer in a corner. *Fluid Dynamics*, **14**(3):365-371, 1979.
560. Alvi, F. S. and G. S. Settles. Physical model of the swept shock wave/boundary-layer interaction flowfield. *AIAA J.*, **30**(9):2252-2258, 1992.
561. Settles, G. S. Swept shock/boundary-layer interactions: scaling laws, flowfield structure, and experimental methods. AGARD Report 792, Advisory Group for Aernautical Research and Development, NATO, Brussels, Belgium, pp. 1.1-1.40, 1993.
562. Zakharin, B., J. Stricker, and G. Toker. Laser-Induced spark schlieren imaging. *AIAA J.*, **37**(9):1133-1135, 1999.
563. Früngel, F. B. A. *High speed pulse technology Vol. IV: sparks and laser pulses.* Academic Press, New York, 1980.
564. Hugenschmidt, M. and K. Vollrath. Light sources and recording methods. Chap. 8 of *Methods of experimental physics, Vol. 18B: Fluid Dynamics*, ed. R. J. Emrich. Academic Press, New York, pp. 687-753, 1981.
565. Fuller, P. W. W. Lighting for cine and high-speed photography. Chap. 2 of *High Speed Photography and Photonics*, Focal Press, Oxford, UK, pp. 29-47, 1997.
566. Muehlemann, M. Tungsten halogen. *The Photonics Design & Applications Handbook*, Laurin Pub., Pittsfield, MA, ed. 46, pp. H-264-267, 1999.
567. Harp, J. Short-arc lamps. *The Photonics Design & Applications Handbook*, Laurin Pub., Pittsfield, MA, ed. 46, pp. H-259-263, 1999.
568. O'Neel, W. E. *Handbook of high-speed photography.* Form 3100-A, General Radio Co., West Concord, MA, 1963.
569. Fischer, H. Simple submicrosecond light source with extreme brightness. *JOSA*, **47**(11):981-984, 1957.
570. Patzke, H. G. Combi spark. In *Proc. 12th Intl. Congr. on High Speed Photography & Photonics,* SPIE Vol. 97, pp. 478-485, 1976.
571. Patzke, H. G. and F. B. A. Früngel. Microsecond and nanosecond sparks for photographic techniques. In *Proc. Photogrammetria Noise, Shock and Vibr. Conf.*, Monash Univ., Victoria, Australia, pp. 305-334, 1974.
572. Owen, R. B. and R. L. Kroes. Holography on the Spacelab 3 mission. *Optics News*, **11**(7):12-16, 1985.
573. Indebetouw, G. Production of color coded equidensities using nonlinear filtering. *App. Optics*, **16**(7):1951-1954, 1977.
574. Ellis, G. W. A fiber-optic phase randomizer for microscope illumination by laser. *Journal of Cell Biology*, **83**(11):303a, 1979.
575. Parks, R. E. and R. E. Sumner. Bright inexpensive pinhole source. *App. Optics*, **17**(16):249, 1978.
576. Hutchings, I. M. and D. R. Andrews. Light-emitting diodes as short-duration light sources. In *Proc. 13th Intl. Congr. on High-Speed Photography & Photonics*, 1979.
577. Haley, R. F. and P. R. Smy. An inexpensive light source for high-speed schlieren photography. *J. Phys. E Sci. Instr.*, **21**(12):1172-1174, 1988.
578. Stasicki, B., W. J. Hiller, and G. E. A. Meier. Light pulse generator for high speed photography using semiconductor devices as a light source. *Opt. Engrg.*, **29**(7):821-827, 1990.
579. Stasicki, B. and G. E. A. Meier. Miniaturized semiconductor light source system for Cranz-Schardin applications. In *Proc. 19th Intl. Congr. on High-Speed Photography and Photonics,* SPIE Vol. 1358, pp. 1222-1227, 1990.
580. Bretthauer, B., G. E. A. Meier, and B. Stasicki. An electronic Cranz-Schardin camera. *Rev. Sci. Instr.*, **62**(2):364-368, 1991.

581. Lu, F. K. and X. J. Liu. Optical design of Cranz-Schardin cameras. *Opt. Engrg.*, **36**(7):1935-1941, 1997.
582. Allen, D. M. Pocket flashlight. US Patent D375,372, Nov. 5, 1996.
583. Vetter, J. P. The production and use of Rheinberg color differential filters. *J. Biological Photographic Assoc.*, **31**(1):15-18, 1963.
584. Dewey, A. G. Projection systems for light valves. *IEEE Trans. on Electron Devices*, **ED-24**(7):918-930, 1977.
585. Weiss, S. A. Optical design: software serves nonexperts. *Photonics Spectra*, **32**(12):134-136, 1998.
586. Collicott, S. H. Evaluation of options for improved large grid multiple-source schlieren systems. AIAA Paper 94-2301, 1994.
587. Strong, J. D. *Concepts of classical optics*. W.H.Freeman, San Francisco, CA, 1958.
588. Lawrence, G. N. Introduction to GLAD: Laser and physical optics analysis. Applied Optics Research, www.aor.com, 1997.
589. Lawrence, G. N. and S. H. Hwang. Beam propagation in gradient refractive-index media. *App. Optics*, **31**(25):5201-5210, 1992.
590. Legu, L. Y., L. T. Mustafina, A. Y. Smolyak, R. V. Fedot'yeva, and V. I. Yanichkin. Shadow and interference systems made from modular units. *Sov. J. Opt. Tech.*, **39**(9):581-583, 1972.
591. Quercioli, F., B. Tiribilli, A. Mannoni, and S. Acciai. Optomechanics with LEGO. *App. Optics*, **37**(16):3408-3416, 1998.
592. *Schlieren photography*. Pamphlet P-11, Eastman Kodak Co., Rochester, NY, 1960.
593. Ahmad, A. *Handbook of optomechanical engineering*. CRC Press, Boca Raton, FL, pp. 151-252, 1997.
594. Moore, J. H., C. C. Davis, and M. A. Coplan. *Building scientific apparatus*. Addison-Wesley, Reading, MA, ed. 2, 1989.
595. Newport Corp. Understanding performance. *The Photonics Design & Applications Handbook*, Laurin Pub., Pittsfield, MA, ed. 46, pp. H-424-427, 1999.
596. Rhodes, D. B., J. M. Franke, S. B. Jones, and B. D. Leighty. Simple schlieren light meter. *NASA Tech Briefs*, **16**(1):23, 1992.
597. Reichenbach, H. In the footsteps of Ernst Mach - a historical review of shock wave research at the Ernst-Mach-Institut. *Shock Waves*, **2**:65-79, 1992.
598. Barrett, R. M. An introduction to vibration control. *The Photonics Design & Applications Handbook*, Laurin Pub., Pittsfield, MA, ed. 46, pp. H-428-432, 1999.
599. Wells, C. B. Knife-edge controller for a schlieren system. *App. Optics*, **4**(7):815-818, 1965.
600. Glatt, I. and O. Kafri. Moiré deflectometry - ray tracing interferometry. *Optics and Lasers in Engineering*, **8**(3-4):277-320, 1988.
601. Keren, E. Immunity to shock and vibration in moiré deflectometry. *App. Optics*, **24**(18):3028-3031, 1985.
602. Herbrich, H. Private communications. Dec. 15, 1999 and Jan. 28, 2001.
603. Siddon, O. J. and J. M. Webster. A laser-schlieren technique to take kine films of gas flows within a highly luminous, transient arc. *J. Photographic Sci.*, **17**:25-31, 1969.
604. Andrews, J. R. and D. W. Netzer. Laser schlieren for study of solid-propellant deflagration. *AIAA J.*, **14**(3):410-412, 1976.
605. Mathews, S. E., T. M. Niemczyk, and J. P. Walters. Schlieren system for time and space resolved photography of self-luminous electrical discharges. *Applied Spectroscopy*, **34**(2):200-206, 1980.
606. Allemand, C. D., R. Schoeder, D. E. Ries, and T. W. Eagar. Method of filming metal transfer in welding arcs. *Welding Journal*, **64**(1):45-47, 1985.
607. Steel, G. B. High-speed schlieren photography using a Kerr cell modulated laser light source. *AIAA Student J.*, **4**(3):82-86, 1966.

608. Schrott, C. Schlieren cinematography. *Die Kinotechnik*, **12**:40, 1930.
609. *Patterns*, 16mm film, from the series *The Search for Solutions*. Playback Associates Inc./Phillips Petroleum, 1979.
610. Rendell, J. T. and J. Honour. High speed cine systems. Chap. 4 of *High Speed Photography and Photonics*, ed. S. F. Ray. Focal Press, Oxford, UK, pp. 68-80, 1997.
611. Miller, J. D., G. S. Settles, and L. J. Dodson-Dreibelbis. Hypermedia flow visualization for compressible flow instruction. *Amer. Phys. Soc. Bulletin*, **45**(9):183, 2000.
612. Vollrath, K. and G. Thomer. *Kurzzeitphysik*. Springer-Verlag, Berlin, 1967.
613. Paisley, D. L. *Selected papers on scientific and engineering high-speed photography*. SPIE Milestone Series MS 109, Bellingham, WA, 1995.
614. Settles, G. S. *An experimental study of compressible turbulent boundary layer separation at high Reynolds numbers*. Ph.D. Thesis, Princeton University, 1975.
615. Schardin, H. High-frequency cinematography in the shock tube. In *Proc. 3rd Intl. Congr. on High-Speed Photography*, pp. 365-369, 1956.
616. Cross, L. A. Photographic applications of pulsed semiconductor lasers. In *Proc. 6th Intl. Congr. on HS Photog. Videog. & Photonics*, SPIE Vol. 981, pp. 272-280, 1988.
617. Zakharenkov, Y. A. and A. S. Shikanov. Multiframe ultrahigh-speed schlieren photography in a ruby laser beam. *Instrum. Exp. Tech.*, **17**(5.2):1445-1448, 1974.
618. Thorwart, W., F. Suarez, and H. G. Patzke. Chronolite 8 versatile multiple high-speed spark camera. *Explosivstoffe*, **17**(3):49-57, 1968.
619. Conway, J. C. An Improved Cranz-Schardin High-Speed Camera for Two-Dimensional Photomechanics. *Rev. Sci. Instr.*, **43**(8):1172-1174, 1972.
620. Papamoschou, D. I. A two-spark schlieren system for very-high velocity measurement. *Expts. Fluids*, **7**(5):354-356, 1989.
621. Honour, J. Electronic Camera Systems Take the Measure of High-Speed Events. *Laser Focus World*, **30**(10):121-127, 1994.
622. Wood, R. W. *Physical optics*. MacMillan, New York, ed. 3, 1934.
623. Lawrence, L. F., S. F. Schmidt, and F. W. Looschen. A self-synchronizing stroboscopic schlieren system for the study of unsteady air flows. NACA TN 2509, 1951.
624. Kadlac, R. A. and S. S. Davis. Visualization of quasi-periodic unsteady flows. In *Proc. 19th AIAA/ASME Struct. Dynamics & Matls. Conf.*, pp. 275-281, 1978.
625. Andrews, D. R. Study of wavefronts in acoustic diffraction patterns using a stroboscopic schlieren technique. In *Proc. 15th Intl. Congr. on High Speed Photography and Photonics*, SPIE Vol. 348, Part 2, pp. 565-570, 1983.
626. Swift, H. F. Smear and streak photography. Chap. 7 of *High Speed Photography and Photonics*, ed. S. F. Ray. Focal Press, Oxford, UK, 1997.
627. Parker, V. C. and C. Roberts. Rotating mirror and drum cameras. Chap. 10 of *High Speed Photography and Photonics* , ed. S. F. Ray. Focal Press, Oxford, UK, 1997.
628. Glass, I. I. *Shock waves and man*. Univ. of Toronto Press, Toronto, Canada, 1974.
629. Glass, I. I. Aerodynamics of blasts. Inst. of Aeronautical Sci. Paper 60-100, 1960.
630. Domens, P., J. Dupuy, A. Gibert, R. Diaz, B. Hutzler, J. P. Riu, and F. Ruehling. Large air-gap discharge and schlieren techniques. *J. Phys. D Appl. Phys.*, **21**(11):1613-1623, 1988.
631. Fuller, P. W. W. Synchronization and triggering. Chap. 3 of *High Speed Photography and Photonics*, ed. S. F. Ray. Focal Press, Oxford, UK, 1997.
632. Balch, K. High speed videography. Chap. 6 of *High Speed Photography and Photonics*, ed. S. F. Ray. Focal Press, Oxford, UK, 1997.
633. Snyder, D. R. and F. M. Kosel. Applications of high resolution still video cameras to ballistic imaging. In *Proc. Ultrahigh- & High-Speed Photography, Videography, Photonics, and Velocimetry '90*, SPIE Vol. 1346, pp. 216-225, 1990.
634. Lake, D. W. A four-million pixel camera for ballistic shadowgraph applications. In *Proc. U.- & HS Photog., Videog., Photon. Mtg.*, SPIE Vol. 1757, pp. 194-202, 1993.

635. Davies, T. P. Colour schlieren photography. In *Proc. 16th Intl. Congr. on High Speed Photography and Photonics,* SPIE Vol. 491, pp. 809-811, 1985.
636. Maksutov, D. D. *Izgotovlenie i issledovanie astronomicheskoi optiki.* Nauka, Moscow, pp. 151-182,1984.
637. Kozák, J. and L. Waniek. Schlierenoptische untersuchungen an seismischen Gelmodellen mit photometrischer Auswertung des Wellenfeldes. *Journal of Geophysics = Zeitschrift für Geophysik*, **36**:175-192, 1970.
638. Skotnikov, M. M. *Quantitative schlieren methods in gas dynamics.* Izdatelt'zvo Nauka, Moscow, USSR, ed. 1, 1976.
639. Waniek, L. A schlieren study of elastic waves passing through a stress-concentration region. *Doklady USSR. Acad. Sci.: Earth Science*, **210**(1-6):10-12, 1974.
640. Golub, V. V., I. M. Naboko, and A. M. Shulmeister. An investigation of impulse jet outflowing from multi-nozzle blocks by means of the schlieren installation. In *Optical Mtds. Dyn. of Fluids and Solids*, ed. M. Pichal. Springer-Verlag, pp. 357-363, 1985.
641. Ershov, I. V. and V. N. Otmennikov. Color shadow TV-filming of nonstationary gas flow. In *Proc. Conf. Illum. Source Engrg.,* SPIE Vol. 3428, pp. 28-32, 1998.
642. Gabaydullin, M. R. Private communication. Feb. 3, 2000.
643. Dukhopel, I. I. and V. A. Yakovlev. Multifunction set of optical research equipment for wind tunnel experiments. In *Proc. 23rd Intl. Congr. on High-Speed Photography and Photonics*, SPIE Vol. 3516, pp. 186-195, 1999.
644. Thiele, W. Schlierengeräte und ihre Anwendungen. *Jena Nachr.*, **8**(2):75-100, 1958.
645. Nebe, W. 100 Jahre Schlieren-methode nach Toepler. *Jenaer Rundschau*, **9**(5):223-229, 1964.
646. Zeiss Schlierengeräte. Pamphlet 32-280-1, Carl Zeiss, Jena, 1946.
647. Schlierengeräte. Pamphlet 64-280-d, Carl Zeiss, Jena, 1964.
648. Řeznícek, R. Flow visualization: optical methods of analyzing flows. NASA TTF-15,236, 1974.
649. Hanafy, A. and C. I. Zanelli. Quantitative real-time pulsed schlieren imaging of ultrasonic waves. In *Proc. Ultrasonics Symp.*, IEEE, pp. 1223-1227, 1991.
650. Herbrich, H. Advances in the practical application of schlierenphotography in industry. In *Proc. 19th Intl. Conf. on High-Speed Photography and Photonics*, ed. P. W. W. Fuller. SPIE Vol. 1358, pp. 24-28, 1991.
651. Postasy, R., L. I. Kiss, and L. Banhidi. Development of a new, mobile, large-field-of-view schlieren device. *Meres es Automatika*, **37**(2):82-85, 1989.
652. Settles, G. S., B. C. Huitema, S. S. McIntyre, and G. G. Via. Visualization of clean room flows for contamination control in microelectronics manufacturing. In *Flow Visualization IV*, ed. C. Veret. Hemisphere Pub., Washington, pp. 833-838, 1987.
653. Boys, C. V. *Soap bubbles.* Dover Pub. Inc., NY, 1959.
654. Ingalls, A. G. *Amateur Telescope Making.* Vols. 1-3. Scientific American, New York, ed. 4, 1980.
655. Naparin, Iu. A. and V. I. Shakhurdin. On the use of the schlieren method in the study of temperature fields in solids. *Heat Transfer - Soviet Research*, **4**(2):55-59, 1972.
656. Potts, T. A. In-situ inspection of high quality films. *Vac. & Thinfilm*, (4):32-35, 1999.
657. Slabodsky, F. B. Automatic inspection of glass. *Sensor Review*, **10**(2):79-83, 1990.
658. Bettley, W. and D. D. Ross. Float glass inspection. *Glass Tech.*, **35**(5):193-195, 1994.
659. Aratani, S., H. Ojima, and K. Takayama. Holographic interferometric investigation of supersonic jet impingement on a plate. In *Proc. 21st Intl. Congress on High-Speed Photography and Photonics*, SPIE Vol. 2513, pp. 366-373, 1994.
660. McCallum, W. H. How to characterize polymer films optically. *SPE Journal*, **28**(5):39-43, 1972.
661. Beinert, J. Schlierenoptical stress analysis of short duration pulses in elastic plates. *J. Appl. Mech. Trans. ASME*, **42**:5-8, 1975.

662. Häusler, E. and J. Pollok. Shadow optical measurement techniques for investigating dynamic stress states. *Forschung im Ingenieurwesen*, **35**(5):133-139, 1969.
663. Schirrer, R. and R. Pixa. The limits of the use of the ultra high speed Cranz-Schardin camera, direct shadow visualization of a fracture. *Intl. J. Fracture*, **11**(12):1003-1009, 1975.
664. Fortner, M. L. and G. R. Hough. Application of pulsed laser shadow photography to terminal ballistic investigations. In *Proc. High Speed Photography, Videography, and Photonics IV,* SPIE Vol. 693, pp. 156-160, 1986.
665. Nakamura, Y., K. Yabu, S. Kubota, and Y. Kiritani. Visualization of dynamic behavior of stress waves and cracks in blasting processes by high-speed videography. In *Proc. 9th Intl. Symp. on Flow Visualization,* Paper no. 222, 2000.
666. Kassel, P. C., Jr. and J. D. DiBattista. An ultra-high-speed photographic system for investigating hypervelocity impact phenomena. NASA TN D-6128, 1971.
667. Nadai, A. The phenomenon of slip in plastic materials. *Proc. ASTM*, **31**(Part II):11-46, 1931.
668. Optical device for online assessment of magnetic tape surface quality. *IBM Technical Disclosure Bulletin*, **28**(10):4235-4237, 1986.
669. Moseley, G. W., J. B. Peterson, and A. L. Braslow. An investigation of splitter plates for the aerodynamic separation of twin inlets at Mach 2.5. NASA TND-3385, 1966.
670. Klein, E. J. A planview shadowgraph technique for boundary-layer visualization. *AIAA J.*, **8**:963-965, 1970.
671. Donohoe, S. R. and W. J. Bannink. Surface reflective visualizations of shock-wave/vortex interactions above a delta wing. *AIAA J.*, **35**(10):1568-1573, 1997.
672. Zuercher, E. J., J. W. Jacobs, and C. F. Chen. Experimental study of the stability of boundary-layer flow along a heated, inclined plate. *J. Fluid Mech.*, **367**:1-25, 1998.
673. Kline, S. J. The importance of flow visualization. In *Symposium on Flow Visualization*, ASME, pp. 1.1-1.9, 1960.
674. Grigull, U. Visualisation of heat transfer. In *Proc. 4th Intl. Heat Transfer Conference,* Versailles, Elsevier Pub. Co., Amsterdam, 1971.
675. Karwe, M. V. *Thermal transport between a continuously moving heated plate and a quiescent ambient medium.* Ph.D. Thesis, Rutgers University, NJ, 1987.
676. Tanda, G. and F. Devia. Application of a schlieren technique to heat transfer measurements in free-convection. *Expts. Fluids*, **24**(4):285-290, 1998.
677. Davidhazy, A. Photographic techniques for phenomena in liquids. *Phot. Sci. Engrg.*, **10**(3):160-170, 1966.
678. Davidhazy, A. Applications of photography in distillation research. *Photo. Apps. Sci. Tech. Med.*, **4**(9):27-31, 1969.
679. Turnbull, R. J. Electroconvective instability with a stabilizing temperature gradient. II - Experimental results. *Phys. Fluids*, **11**:2597-2603, 1968.
680. Mollendorf, J. C., H. Arif, and E. B. Ajiniran. Developing flow and transport above a suddenly heated horizontal surface in water. *Intl. J. Heat Mass Transfer*, **27**(2):273-289, 1996.
681. Pawliszyn, J. Concentration gradient detection based on schlieren optics. *Spectrochimica Acta Review*, **13**(4):311-354, 1990.
682. Barkey, D. Morphology selection and the concentration boundary layer in electrochemical deposition. *J. Electrochemical Soc.*, **138**(10):2912-2917, 1991.
683. Huppert, H. E. and J. S. Turner. Double-diffusive convection. *J. Fluid Mech.*, **106**:299-329, 1981.
684. Tanny, J. and A. B. Tsinober. Double-diffusive convection. Chap. 31 of *Handbook of Flow Visualization*, ed. W.-J. Yang. Hemisphere, ed. 1, pp. 513-529, 1989.
685. Shirtcliffe, T. G. L. and J. S. Turner. Observations of the cell structure of salt fingers. *J. Fluid Mech.*, **41**(4):707-719, 1970.

686. Bergman, T. L., F. P. Incropera, and R. Viskanta. Interaction of external and double-diffusive convection in linearly salt-stratified systems. *Expts. Fluids*, **5**(1):49-58, 1987.
687. Turner, J. S. Development of geophysical fluid dynamics: the influence of laboratory experiments. *Applied Mechanics Reviews*, **53**(3):R11-R22, 2000.
688. Whitehead, J. A., Jr. Cellular convection. *American Scientist*, **59**(4):444-451, 1971.
689. Weinstein, S. A. and P. Olson. Planforms in thermal convection with internal heat sources at large Rayleigh and Prandtl numbers. *Geophys. Research Letters*, **17**(3):239-242, 1990.
690. Howle, L. E., R. P. Behringer, and J. G. Georgiadis. Visualization of convective fluid flow in a porous medium. *Nature*, **362**(6417):230-232, 1993.
691. Berg, J. C., M. Boudart, and A. Acrivos. Natural convection in pools of evaporating liquids. *J. Fluid Mech.*, **24**(Part 4):721-735, 1996.
692. Wierschem, A., M. G. Velarde, H. Linde, and W. Waldhelm. Interfacial wave motions due to Marangoni instability. *J. Colloid & Interface Science*, **212**(2):365-383, 1999.
693. Okhotsimskii, A. and M. Hozawa. Schlieren visualization of natural convection in binary gas-liquid systems. *Chemical Engineering Science*, **53**(14):2547-2573, 1998.
694. Sullivan, T., R. E. Ecke, and V. Steinberg. Low-temperature flow visualization of thermally-convecting liquid helium. In *Proc. 8th Oregon Conf. on LT Physics*, 1991.
695. Howle, L. E., R. P. Behringer, and J. G. Georgiadis. Convection and flow in porous media. Part 2. Visualization by shadowgraph. *J. Fluid Mech.*, **332**:247-262, 1997.
696. Liu, J., L. Arnberg, N. Backstrom, H. Klang, and S. Savage. Fluid flow behaviour and solidification studies during ultrasonic gas atomization. *Matls. Sci. Engrg.*, **98**:43-46, 1988.
697. Pusey, M., W. K. Witherow, and R. Naumann. Preliminary investigations into solutal flow about growing tetragonal lysozyme crystals. *J. Crystal Growth*, **90**(1-3):105-111, 1988.
698. Coughlin, D. J. and J. R. Strickler. Zooplankton capture by a coral reef fish: an adaptive response to evasive prey. *Environmental Biology of Fishes*, **29**(1):35-42, 1990.
699. Westphal, J. A. Schlieren technique for studying water flow in marine animals. *Science*, **149**(3691):1515-1516, 1965.
700. Faraday, M. On a peculiar class of acoustical figures; and on certain forms assumed by groups of particles upon vibrating elastic surfaces. *Philos. Trans. Royal Soc. London*, **121**:299-340, 1831.
701. Lord Rayleigh (Strutt, J. W.) On the tension of water surfaces, clean and contaminated. *Phil. Mag.*, **30**:386, 1890.
702. Jeffree, J. H. Light modulating device. US Patent 2,155,661, Apr. 25, 1939.
703. Jenny, H. *Cymatics - the structure and dynamics of waves and vibrations*. Basilius Presse AG, Basel, Switzerland, 1967.
704. Flournoy, R. D. *The schlieren audio-visual pattern transducer and its application to music*. B.S. Honors Thesis, Mechanical Engrg., Pennsylvania State University, 1985.
705. Simonelli, F. and J. P. Gollub. Surface wave mode interactions: effects of symmetry and degeneracy. *J. Fluid Mech.*, **199**:471-494, 1989.
706. Sellin, R. H. J. A technique based on the schlieren principle for studying the free surface of a liquid. *J. Sci. Inst.*, **40**(7):355-357, 1963.
707. Kayser, W. V. and J. C. Berg. Surface relief accompanying natural convection in liquid pools heated from below. *J. Fluid Mech.*, **57**(4):739-752, 1973.
708. Özbelge, H. O., E. N. Lightfoot, and E. E. Miller. Reflectance-schlieren technique for measurement of free liquid surface perturbations. *J. Phys. E Sci. Instr.*, **14**(12):1381-1385, 1981.
709. Jouget, E. Quelques problèmes d'hydrodynamique générale. *Journal de Mathématiques Pures et Appliquées*, **8**(3):1-63, 1920.

710. Shapiro, A. H. Free surface water table. Chap. H,1 of *Physical Measurements in Gas Dynamics and Combustion, Vol. 9*, ed. R. W. Ladenburg. Princeton University Press, Princeton NJ, pp. 309-321, 1954.
711. Anderson, I. E. and R. S. Figliola. Observations of gas atomization process dynamics. In *Proc. Intl. Powder Metallurgy Conf.*, APMI, pp. 205-223, 1988.
712. Fraser, R. P. and N. Dombrowski. The dependence of interpretation on photographic technique in fluid kinetics research. In *Proc. 3rd Intl. Conf. on High-Speed Photography*, pp. 376-384, 1956.
713. Raman, C. V. and N. S. N. Nath. The diffraction of light by high-frequency sound waves: part 1. *Proceedings of the Indian Academy of Science*, **2**:406-412, 1935.
714. Neubauer, W. G. Observation of acoustic radiation from plane and curved surfaces. Chap. 2 of *Physical Acoustics*, Academic Press, New York, p. 61, 1973.
715. Darius, J. Visions of sound; acoustic field visualization by schlieren color photography. *New Scientist*, **62**:408-414, 1974.
716. Hennige, C. W. Schlieren optical system for visualizing ultrasonic waves. *Materials Evaluation*, **47**(5):496-499, 1989.
717. Breazeale, M. A. Schlieren photography in physics. In *Acousto-Optics and Applications III*, SPIE Vol. 3581, pp. 41-47, 1998.
718. Korpel, A., T. T. Yu, H. S. Snyder, and Y. M. Chen. Diffraction-free nature of schlieren sound-field images in isotropic media. *JOSA A*, **11**(10):2657-2663, 1994.
719. Bucaro, J. A. and H. D. Dardy. Sensitivity of the schlieren method for the visualization of low-frequency ultrasonic waves. *J. Acoustical Soc. Am.*, **63**(3):768-773, 1978.
720. Moore, W. E. and J. A. Bucaro. Measurement of acoustic fields using schlieren and holographic techniques. *J. Acoustical Soc. Am.*, **63**(1):60-67, 1978.
721. Porter, B. Quantitative real-time schlieren system for ultrasound visualization. *Rev. Sci. Instr.*, **55**(2):216-221, 1984.
722. Pitts, T. A., J. F. Greenleaf, J. Y. Lu, and R. R. Kinnick. Tomographic schlieren imaging for measurement of beam pressure and intensity. In *Proc. Ultrasonics Symposium*, IEEE, Part 3, pp. 1665-1668, 1994.
723. Bronson, N. R. An inexpensive schlieren apparatus. *Ultrasonics*, **7**:67-70, 1969.
724. Gonzalez, L. and W. J. MacIntyre. Acoustic shadow formation by gallstones. *Radiology*, **135**(1):217-218, 1980.
725. Smith, S. W. and F. L. Thurstone. Schlieren study of pulsed ultrasound transmission through human skull. *J. Clin. Ultrasound*, **2**(1):55-59, 1974.
726. Schaetzle, U., T. Reuner, J. Jenne, and A. Heilingbrunner. Quality assurance tools for therapeutic ultrasound. *Ultrasonics*, **36**(1-5):679-682, 1998.
727. Croot, C. F. and R. Robbins. Schlieren photography of an ultrasonic beam. *Med. Biol. Illus.*, **17**(3):202-207, 1967.
728. Bar-Cohen, Y. Schlieren visualization of acoustically imaged defects. *Materials Evaluation*, **41**(1):88-93, 1983.
729. Dragonette, L. R. and W. G. Neubauer. Detection of flaws on plates by schlieren visualization. *Materials Evaluation*, **32**(10):218-222, 1974.
730. Richards, R. T. *Quantitative schlieren analysis of acoustic interaction with submerged plates*. Ph.D. Thesis, Pennsylvania State University, 1980.
731. Bar-Cohen, Y., B. Ben-Joseph, and E. Harnik. Schlieren ultrasonic visualization of delaminations in composite materials. *Ultrasonics*, **17**(1):9-10, 1979.
732. Hall, K. G. Visualization techniques for the study of ultrasonic wave propagation in the railway industry. *Materials Evaluation*, **42**(7):922-929, 933, 1984.
733. Golovkin, V. A., et al., Optical flow visualization in a hydraulic tunnel. *Uchenye Zapiski TsAGI*, **11**(5):1-6, 1980.
734. Fiedler, H., K. Nottmeyer, P. P. Wegener, and S. Raghu. Schlieren photography of water flow. *Expts. Fluids*, **3**(3):145-151, 1985.

735. Rodriguez, O. Three-dimensional wake visualization in water tunnel by a selective large scale structures thermal marking. In *Flow Visualization V*, ed. R. Řeznícek. Hemisphere Pub., NY, pp. 331-337, 1990.
736. Rodriguez, O. Base drag reduction by control of the three-dimensional unsteady vortical structures. *Expts. Fluids*, **11**:218-226, 1991.
737. Peters, F., T. Kuralt, and J. Schniderjan. Visualization of water flow by sugar schlieren. *Expts. Fluids* , **12**:351-352, 1992.
738. McMillen, J. H. Impact shock waves in water. Report NOLR-1135, US Naval Ordnance Laboratory, pp. 83-98, 1950.
739. Van Dyke, M. *An album of fluid motion*. Parabolic Press, Stanford, CA, 1982.
740. Gates, D. M. Heat transfer in plants. *Sci. Am.*, **211**(12):76-84, 1965.
741. Doi, J. Agriculture. Chap. 38 of *Handbook of Flow Visualization*, ed. W.-J. Yang. Hemisphere Pub., Washington, ed. 1, pp. 627-636, 1989.
742. Stephens, D. B. and I. B. Start. Schlieren photography of the piglet's microenvironment. *Cornell Veterinarian*, **62**(1):20-26, 1972.
743. Roggemann, M. C. and B. Welsh. *Imaging through turbulence*. CRC Press, Boca Raton, FL, 1995.
744. Deitz, P. H. and N. J. Wright. Saturation of scintillation magnitude in near-earth optical propagation. *JOSA*, **59**(5):527-535, 1969.
745. Eaton, F. D., W. A. Peterson, J. R. Hines, J. J. Drexler, D. B. Soules, A. H. Waldie, and J. A. Qualtrough. Morphology of atmospheric transparent inhomogeneities. In *Proc. 3rd Mtg. Propagation Engrg.*, SPIE Vol. 1312, pp. 134-146, 1990.
746. Sutton, G. W. Aero-optical foundations and applications. *AIAA J.*, **23**(10):1525-1537, 1985.
747. Haight, J. S., B. R. Peters, D. A. Kalin, L. C. Brooks, and J. M. Kinser. Experimental investigation of simultaneously recorded shadowgraphs and images through a high-velocity turbulent flow. In *Inv. Probs. Scat. Imag.*, SPIE Vol. 1767, pp. 326-333, 1992.
748. Shankland, R. S. The development of architectural acoustics. *American Scientist*, **60**(2):201-209, 1972.
749. Kesner, Z. and J. Polasek. Die Formgestaltung eines Saales und ihr Einfluss auf die Zeitfolge der ersten Rückwürfe. *Acustica*, **19**:257-263, 1967.
750. Rosen, J. Shaping the sound of concert halls. *Mech. Engrg.*, **108**(8):48-55, 1986.
751. James, C. S. Observations of turbulent burst geometry and growth in supersonic flow. NACA TN 4235, 1958.
752. Hannah, B. W. Quantitative schlieren measurements of boundary layer phenomena. In *Proc. 11th Intl. Congr. on High Speed Photography*, ed. P. J. Rolls. Chapman & Hall, London, pp. 539-545, 1975.
753. Baturin, V. V. *Fundamentals of industrial ventilation*. Pergamon Press, New York, ed. 3, pp. 12-24, 1972.
754. Winter, E. F. Flow visualization techniques. *Progress in Combustion Sci. & Tech.*, ed. J. Ducarme, M. Gerstein, & A. Lefebvre. Pergamon Press, NY, pp. 1-36, 1960.
755. Cooper, P. and P. F. Linden. Natural ventilation of an enclosure containing two buoyancy sources. *J. Fluid Mech.*, **311**:153-176, 1996.
756. Chou, X., Y. Z. Li, and J. Z. Shu. Flow visualization in the model of a solar house by means of a differential interferometer. In *Flow Visualization IV*, ed. C. Veret. Hemisphere Pub., Washington, pp. 691-695, 1987.
757. Daws, L. F. Movement of airstreams indoors. *Journal of the Institution of Heating and Ventilation Engineers*, **37**(2):241-253, 1970.
758. Leeds, L. W. *A treatise on ventilation*. John Wiley & Son, New York, 1871.
759. Heinsohn, R. J., S. T. Yu, C. L. Merkle, G. S. Settles, and B. C. Huitema. Viscous turbulent flow in push-pull ventilation systems. In *Proc. 1st Intl. Symp. for Contamination Control*, ed. H. D. Goodfellow, Elsevier, Amsterdam, Vol. 24, pp. 529-566, 1986.

760. Whyte, W. and B. H. Shaw. The effect of obstructions and thermals in laminar-flow systems. *Journal of Hygiene*, **72**(3):415-423, 1974.
761. Settles, G. S. I sistema schlieren visuatizzazione in scala reale di flussi d'aria indotti dalla ventilazione. *Condizion. d. Aria Riscald. Refridg.*, **43**(1):27-32, 1999.
762. Yamauchi, K., T. Tanaka, and S. Kawai. Method and apparatus for detecting leaks in hollow fiber membrane modules. US Patent 4,188,117, Feb. 12, 1980.
763. Kreske, K., E. Keren, and A. Livnat. New applications blossom for moiré deflectometry. *Photonics Spectra*, **23**(11):101-103, 1989.
764. So gefährlich ist das Tanken. *Hörzu*, **44**:20-21, 1992.
765. Kurimoto, A., O. Farish, and D. J. Tedford. Schlieren studies of impulse breakdown in air gaps. *Proc. Inst. Electr. Engrs. (London)*, **125**(8):767-769, 1978.
766. Kogelschatz, U. and W. R. Schneider. Quantitative schlieren techniques applied to high current arc investigations. *App. Optics*, **11**(8):1822-1832, 1972.
767. Weber, K. H. and G. H. Halsey. Free convection in electric fields. In *Proc. Heat Transfer and Fluid Mechanics Inst.*, Stanford Univ. Press, CA, pp. 97-110, 1953.
768. Qureshi, M. I. and W. G. Chadband. On the relation between current pulses and discharges. *IEEE Transactions on Electrical Insulation*, **23**(4):715-722, 1988.
769. Ohgaki, S. and Y. Tsunoda. Propagation characteristics of positive surface discharge in insulating oil. *Electr. Engrg. Japan*, **103**(6):1-8, 1983.
770. Nakao, Y., H. Nagasawa, Y. Suzuki, H. Itoh, Y. Hamada, and Y. Sakai. Investigation of prebreakdown phenomena in dielectric liquids with various molecular structures by using high-speed schlieren photography. In *Proc. 22nd Intl. Congr. on High-Speed Photography & Photonics,* ed. D. L. Paisley. SPIE Vol. 2869, pp. 740-745, 1997.
771. Waters, R. T. Diagnostic techniques for discharges and plasmas. *NATO ASI Series B: Physics, Vol. 89b*, Plenum Press, New York, pp. 203-265, 1983.
772. Mentel, J. Schliereninterferometric investigations of the gas flow occurring in high-voltage SF_6 switchgear. *Siemens Forsch. Entwick. Res. Dev. Rep.*, **4**(6):380-388, 1975.
773. Kobayashi, A., S. Yanabu, S. Yamashita, and Y. Ozaki. Experimental investigation on arc phenomena in SF_6 puffer circuit breakers. *IEEE Trans. on Plasma Science*, **8**(4):339-343, 1980.
774. Kopplin, H., H. Motschmann, K. P. Rolff, and K. Zueckler. Study of the arc and of the interaction between arc and operating mechanism in SF_6 puffer breakers. *IEEE Trans. on Plasma Science*, **8**(4):331-338, 1980.
775. Stokes, A. D., S. Manganaro, M. Giglio, and E. Colombo. SF_6 puffer circuit breaker: schlieren visualisation of hot circulation following fault interruption. *Energia Elettrica*, **61**(6):275-280, 1984.
776. Iwamoto, K. Study of supersonic flow fields through nozzles used in gas circuit breakers. *Trans. Japan Soc. Mechanical Engrs.*, Part B, **60**(578):3388-3391, 1994.
777. Anon. Circuit breaker arcs, 16mm film. University of Sydney, Australia, 1978.
778. Mach, E. and L. Mach. Über die Interferenz der Schallwellen von Grosser Excursion. *Sitzungsb. d. k. Acad. d. Wiss. Math. Naturw. Cl. Wien*, **98**:1333-1336, 1889.
779. Foley, A. L. and W. H. Souder. A new method of photographing sound waves. *Physical Review*, **35**(5):373-386, 1912.
780. Schardin, H. Modellversuche für Explosionsvorgänge. In *Proc. 4th Intl. Congr. on High-Speed Photography*, pp. 142-150, 1958.
781. Krehl, P. History of shock tubes. *Handbook of Shock Waves*, ed. G. Ben-Dor, O. Igra, and E. Elperin. Academic Press, Boston, ed. 1, 2001.
782. Lighthill, M. J. Shock waves. *M&P Manchester Lit. Phil. Soc.*, **101**(1):1-16, 1958.
783. Skews, B. W. The perturbed region behind a diffracting shock wave. *J. Fluid Mech.*, **29**(Part 4):705-719, 1967.
784. Glass, I. I. Some aspects of shock-wave research. *AIAA J.*, **25**(2):214-229, 1987.

785. Ben-Dor, G., O. Igra, and E. Elperin, eds. *Handbook of shock waves*. Academic Press, Boston, ed. 1, 2001.
786. Reichenbach, H. Visualization of shock waves in layered media. In *Proc. 18th Intl. Congr. on High Speed Photog. & Photon.,* SPIE Vol. 1032, Part 2, pp. 837-844, 1989.
787. Sharov, I. L., Yu. P. Lagutov, and L. G. Gvozdeva. Optical method to investigate the interaction of shock waves with porous compressible materials. In *Flow Visualization VII*, ed. J. P. Crowder, Begell House, NY, pp. 2-13, 1995.
788. Giulietti, A., M. Vaselli, and F. Giammanco. Shadowgraphic detection of spherical implosive shock fronts produced by laser pulses. *Optics Comm.*, **33**(3):257-261, 1980.
789. Amiranoff, F., R. Fedosejevs, R. F. Schmalz, R. Sigel, and Y. Teng. Laser-driven shock-wave studies using optical shadowgraphy. *Physical Review A - General Physics, 3rd Series*, **32**(12):3535-3546, 1985.
790. Bor, Z., B. Hopp, B. Racz, G. Szabo, I. Ratkay, I. Suveges, A. Fust, and J. Mohay. Plume emission, shock wave and surface wave formation during excimer laser ablation of the cornea. *Refractive Corneal Surgery*, **9**(Suppl. 2):S111-S115, 1993.
791. Neuwald, P., H. Klein, and H. Reichenbach. Unsteady flows inside structures: high-speed visualization as a tool for numerical modeling and code validation. In *Proc. 22nd Intl. Congr. High-Speed Photog. Photon.,* SPIE Vol. 2869, pp. 798-806, 1997.
792. Kleine, H., J. M. Dewey, K. Ohashi, T. Mizukaki, and K. Takayama. Characteristics of blast waves generated by milligram charges of silver azide. *Shock Waves*, **11**, 2001.
793. Settles, G. S., B. T. Keane, B. W. Anderson, and J. A. Gatto. Shock waves in aviation security. In *Proc. 23rd Intl. Symp. on Shock Waves,* Arlington TX, ed. F. K. Lu. 2001.
794. Choulmeister, A. M., T. V. Bazhenova, V. V. Golub, and D. A. Nikitin. The dynamics of supersonic vortex rings in hot and cold impulsive jets. In *Proc. 9th Intl. Symp. on Flow Visualization*, ed. I. Grant and G. M. Carlomagno, Paper no. 57, 2000.
795. Fraser, A. B. and W. H. Mach. Mirages. *Sci. Am.*, **255**(1):102-112, 1976.
796. Mishin, G. I. Optical methods of ballistic research. In *Proc. 16th Intl. Congr. on High Speed Photography and Photonics,* SPIE Vol. 491, Part 1, pp. 426-432, 1985.
797. Strawa, A. W., G. T. Chapman, J. O. Arnold, and T. N. Canning. Ballistic range and aerothermodynamic testing. *Journal of Aircraft*, **28**:443-449, 1991.
798. Nonaka, S. and K. Takayama. Overview of the ballistic range program at Tohoku University. In *Proc. 20th Ground Testing Conf.,* AIAA Paper 98-2604, 1998.
799. Pope, A. Y. and K. L. Goin. *High-speed wind tunnel testing*. Wiley, New York, 1965.
800. Coles, D. *Channel flow of a compressible fluid*, 16mm film. National Committee for Fluid Mechanics Films, distr. Encyclopaedia Britannica Educ. Corp., 1985.
801. Pantalos, G. M. Mach 3 for $2.99; miniature supersonic wind tunnel construction. *AIAA Student J.*, **14**(Summer):34-38, 1976.
802. Settles, G. S. Aerospace and wind tunnel testing. Chap. 25 of *Handbook of Flow Visualization*, ed. W.-J. Yang. Hemisphere Press, Washington, pp. 395-408, 1989.
803. Page, R. H. and V. Sernas. Apparent reverse transition in an expansion fan. *AIAA J.*, **8**(1):189-190, 1970.
804. Papamoschou, D. I. and A. Roshko. The compressible turbulent shear layer - an experimental study. *J. Fluid Mech.* , **197**:453-477, 1988.
805. Papamoschou, D. I. Structure of the compressible turbulent shear layer. *AIAA J.*, **29**:680-681, 1991.
806. Goebel, S. G. *An Experimental Investigation of Compressible, Turbulent Mixing Layers*. Ph.D. Thesis, Illinois Univ. at Urbana-Champaign, 1990.
807. Clemens, N. T., Mungal, M. G., Berger, T. E., and Vandsburger, U. Visualizations of the structure of the turbulent mixing layer under compressible conditions. AIAA Paper 90-0500. 1990.
808. McIntyre, S. S. and G. S. Settles. Optical experiments on axisymmetric compressible turbulent mixing layers. AIAA Paper 91-0623, 1991.

809. Elliott, G. S., M. Samimy, and S. A. Arnette. A study of compressible mixing layers using filtered Rayleigh scattering. AIAA Paper 92-0175, 1992.
810. Cooper, G. E. and R. S. Bray. Schlieren investigation of the wing shock-wave boundary-layer interaction in flight. NACA RM A51G09, 1951.
811. Crowder, J. P. Flow visualization techniques applied to full-scale vehicles. In *Proc. AIAA Atmospheric Flight Mechanics Conf.,* Monterey, CA, pp. 164-171, 1987.
812. Raffel, M., H. Richard, and G. E. A. Meier. On the applicability of background oriented optical tomography for large scale aerodynamic investigations. *Expts. Fluids*, **28**:477-481, 2000.
813. Fisher, D. F., E. A. Haering, Jr., G. K. Noffz, and J. I. Aguilar. Determination of sun angles for observations of shock waves on a transport aircraft. NASA TM 1998-206551, 1998.
814. Raffel, M., C. Tung, H. Richard, Y. Yu, and G. E. A. Meier. Background oriented stereoscopic schlieren (BOSS) for full-scale helicopter vortex characterization. In *Proc. 9th Intl. Symp. on Flow Visualization,* Paper no. 450, 2000.
815. Lighthill, M. J. The bakerian lecture, sound generated aerodynamically. *Proc. Roy. Soc. A*, **267**(1329)1962.
816. Davis, M. R. Quantitative schlieren measurements in a supersonic turbulent jet. *J. Fluid Mech.*, **51**:435-447, 1972.
817. Umeda, Y. and R. Ishii. Hole tone generated from highly choked jets. *J. Acoust. Soc. Am.*, **94**(2):1058-1066, 1993.
818. Scroggs, S. D. and G. S. Settles. An experimental study of supersonic microjets. *Expts. Fluids*, **21**(6):401-409, 1996.
819. McIntyre, S. S. *Optical experiments and instrument development for compressible turbulent mixing layers.* PhD Thesis, M. E. Dept., Pennsylvania State Univ., 1994.
820. Stastny, M. and K. Pekarek. Flow visualization in a steam turbine profile cascade using a colour schlieren method. In *Optical Methods in Dynamics of Fluids and Solids*, ed. M. Pichal. Springer-Verlag, Berlin, pp. 267-273, 1985.
821. Nagashima, T. and Y. Tanida. Synchronized schlieren method for vortex shedding in cascade during acoustic resonance. *J. Sound Vibration*, **110**:351-355, 1986.
822. Bell, R. F. and L. Fottner. Schlieren method with quantitative evaluation by digital image processing. In *Proc. 12th Symp. on Measuring Techniques for Transonic and Supersonic Flows in Cascades and Turbomachines,* Prague, 1994.
823. Swanson, A. A. Application of the shadowgraph flow visualization technique to a full-scale helicopter rotor in hover and forward flight. AIAA Paper 93-3411, 1993.
824. Leishman, J. G. *Principles of helicopter aerodynamics.* Cambridge Univ. Press, 2000.
825. Richard, H., M. Raffel, M. Rein, J. Kompenhans, and G. E. A. Meier. Demonstration of the applicability of a Background Oriented Schlieren (BOS) method. In *Proc.10th Intl. Symp. Appl. Laser Techniques to Fluid Mechanics,* p. 15.1.1-15.1.10, 2000.
826. Kleine, H. The artistic side of flow visualization. In *Proc. 24th Intl. Congr. on High-Speed Photography and Photonics*, SPIE Vol. 4183, 2001.
827. Caudron, S. Du laser a la thermographie. *Science et Vie*, **97**(12):116-131, 1971.
828. Ghisoni, M. Schlieren photography. *Amateur Photographer*, 57-59, 1990.
829. Cover photo, *The Pharmaceutical Journal*, **245**(6611), 1990.
830. Iannotta, B. Scramble for space. *New Scientist*, **86**:38-40, 1998.
831. Krüger, F. and H. Casper. Über die Wirbelbildung bei Schneidentönen. *Zeitschrift für Technische Physik*, **17**:417, 1936.
832. Fabre, B., A. Hirschberg, and A. P. J. Wijnands. Vortex shedding in steady oscillation of a flue organ pipe. *Acta Acustica*, **82**(6):863-877, 1996.
833. Hirschberg, A., X. Pelorson, and J. Gilbert. Aeroacoustics of musical instruments. *Meccanica*, **31**(2):131-141, 1996.

834. Hirschberg, A., J. Gilbert, R. Msallam, and A. P. J. Wijnands. Shock waves in trombones. *J. Acoustical Soc. Am.*, **99**(3):1574, 2000.
835. Verge, M. P., B. Fabre, W. E. A. Mahu, A. Hirschberg, R. R. van Hassel, A. P. J. Wijnands, J. J. de Vries, and C. J. Hogendoorn. Jet formation and jet velocity fluctuations in a flue organ pipe. *J. Acoustical Soc. Am.*, **95**:1119-1132, 1994.
836. Whitney, J. H. *Digital harmony: on the complementarity of music and visual art.* Byte Books, McGraw-Hill, Peterborough, NH, 1980.
837. Pellegrino, R. *The electronic arts of sound and light.* Van Nostrand Reinhold, New York, 1983.
838. Walker, J. The Amateur Scientist: dazzling laser displays that shed light on light. *Sci. Am.*, **262**(8):158-167, 1980.
839. Forkner, J. F. Light display instrument. US Patent 3,580,126, May 25, 1971.
840. Ward, B. Schlieren photography of the lens capsule. *Amer. J. Optometry & Archives of the Amer. Academy of Optometry*, **43**(2):107-111, 1966.
841. Winthrop, J. T., R. F. Van Ligten, and K. C. Lawton. Apparatus and method for detecting and viewing transparent objects in the vitreous humor. US Patent 3,850,527, Nov. 26, 1974.
842. Friberg, T. R., Y. Tano, and R. Machemer. Streaks (schlieren) as a sign of rhegmatogenous detachment in vitreous surgery. *Amer. J. Ophthalmology*, **88**(5):943-944, 1979.
843. Walker, J. The Amateur Scientist: "floaters": visual artifacts that result from blood cells in front of the retina. *Sci. Am.*, **264**(4):150-161, 1982.
844. Davies, T. P. Schlieren photography- a tool for speech research. *Acoustics Letters*, **3**(3):73-75, 1979.
845. Fitzgerald, R. Phase-sensitive x-ray imaging. *Physics Today*, **53**(7):23-26, 2000.
846. Nugent, K. A., T. E. Gureyev, D. F. Cookson, D. Paganin, and Z. Barnea. Quantitative phase imaging using hard x-rays. *Phys. Rev. Letters*, **77**(14):2961-2964, 1966.
847. Pratisto, H., M. Frenz, M. Ith, V. Romano, D. Felix, R. Grossenbacher, H. J. Altermatt, and H. P. Weber. Temperature and pressure effects during erbium laser stapedotomy. *Lasers in Surgery and Medicine*, **18**(1):100-108, 1996.
848. Tidd, M. J., J. Webster, H. C. Wright, and I. R. Harrison. Mode of action of a surgical electronic lithoclast - high speed pressure, cinematographic and schlieren recordings following an ultrashort underwater electronic discharge. *Bio. -Med. Eng. (London)*, **11**(1):5-11, 24, 1976.
849. Marlinghaus, E. H., O. J. Wess, and J. Katona. A new pressure wave generator for extracorporeal lithotripsy. *Biomed. Tech. (Berlin)*, **35**(Suppl 3):235-236, 1990.
850. Kolacek, K., V. Babicky, J. Preinhaelter, P. Sunka, and J. Benes. Pressure distribution measurements at the shock wave focus in water by schlieren photography. *J. Phys. D. Appl. Phys.*, **21**(3):463-469, 1988.
851. Isuzugawa, K., M. Horiuchi, and Y. Okumura. Focusing of shock waves in water and its observation by the schlieren method. SPIE Vol. 1801, pp. 1003-1010, 1991.
852. Carnell, M. T., R. D. Alcock, and D. C. Emmony. Optical imaging of shock waves produced by a high-energy electromagnetic transducer. *Phys. Med. Biol.*, **38**(11):1575-1588, 1993.
853. Carnell, M. T. and D. C. Emmony. A schlieren study of the interaction between a lithotripter shock wave and a simulated kidney stone. *Ultrasound Med. Biol.*, **21**(5):721-724, 1995.
854. Carnell, M. T., T. P. Gentry, and D. C. Emmony. The generation of negative pressure waves for cavitation studies. *Ultrasonics*, **36**(1-5):689-693, 1998.
855. Shaw, S. J., W. P. Schiffers, T. P. Gentry, and D. C. Emmony. A study of the interaction of a laser-generated cavity with a nearby solid boundary. *J. Phys. D. Appl. Phys.*, **32**(14):1612-1617, 1999.

856. Tiselius, A. A new apparatus for electrophoretic analysis of colloidal mixtures. *Trans. Faraday Society*, **33**:524-531, 1937.
857. Elliott, A. The instantaneous monitoring of polyacrylimide gels during electrophoresis. *Biochemical Journal*, **159**:743-748, 1976.
858. Fries, E. Visualization of protein zones in preparative electrophoresis and carrier ampholyte zones on isoelectric focusing in gel slabs by two light refraction methods. *Analytical Biochemistry*, **70**:124-135, 1976.
859. Takagi, T., H. Kubota, and S. Oishi. Application of schlieren optics to real-time monitoring of protein electrophoresis in crosslinker-free linear polyacrylamide solution. *Electrophoresis*, **12**(6):436-438, 1991.
860. Lewis, H. E. Colour photography of the convecting air next to the skin. *Journal of Physiology*, **188**(2):6P-7P, 1967.
861. Lewis, H. E., A. R. Foster, B. J. Mullan, R. N. Cox, and R. P. Clark. Aerodynamics of the human microenvironment. *Lancet*, **1**(7609):1273-1277, 1969.
862. Clark, R. P. and N. Toy. Natural convection around the human head. *J. Physiology (London)*, **244**(2):283-293, 1975.
863. Clark, R. P. and O. G. Edholm. *Man and his thermal environment*. E. Arnold, London, 1985.
864. Weiner, L. I. Evaluation of comfort factors in clothing design. Materials R&E Report C/OM-MR/E-64-7, US Army Natick Labs, 1964.
865. Wright, R. H. Why mosquito repellents repel. *Sci. Am.*, **233**(7):104-111, 1975.
866. Gowadia, H. A. *The natural sampling of airborne trace signals associated with the human body*. Ph.D. Thesis, M. N. E. Dept., Pennsylvania State University, 2000.
867. Kilner, W. J. *The human aura*. University Books Inc., NY, 1965.
868. Dunn-Rankin, D. & F. J. Weinberg. Location of the schlieren image in premixed flames-axially symmetric refractive index fields. *Comb. Flame*, **113**(3):303-311, 1998.
869. Lehr, H. F. Experiments on shock-induced combustion. *Astronautica Acta*, **17**(4 & 5):589-596, 1972.
870. Xie, Y. S. and C. C. Hwang. Effect of base board orientation on flame propagation along matchstick arrays. In *Flow Visualization III*, Hemisphere, pp. 787-791, 1985.
871. Ishida, H. Initiation of fire growth on fuel-soaked ground. *Fire Safety Journal*, **18**(3):213-230, 1992.
872. Keren, E., E. Bar-Ziv, I. Glatt, and O. Kafri. Measurements of temperature distribution of flames by moiré deflectometry. *App. Optics*, **20**:4263-4266, 1981.
873. Tabei, K. and H. Shirai. Temperature and/or density measurements of asymmetrical flow fields by means of the Moiré-Schlieren method. *JSME Intl. Journal, Series II*, **33**(5):249-255, 1990.
874. Amman, C. A. Classical combustion diagnostics as applied to diesel engines. *Automotive Engineering*, **93**(4):72-77, 1985.
875. Hall, J. L. *An experimental investigation of structure, mixing, and combustion in compressible turbulent shear layers*. Ph.D. Thesis, CalTech, 1991.
876. Indebetouw, G. Color coding of spatial frequencies using incoherent optical processing. *App. Optics*, **18**(24):4206-4209, 1979.
877. Oppenheim, A. K. The beauty of combustion fields and their aerothermodynamic significance. In *Dynamics of Reactive Systems*, AIAA, Vol. 1, pp. 3-13, 1986.
878. Hendricks, P. J. Fine structure and turbulence in the deep ocean. Report WHOI-77-21, Woods Hole Oceanographic Institute, 1977.
879. Williams, A. J. Salt fingers observed in the Mediterranean outflow. *Science*, **185**:941-943, 1974.
880. Kerr, R. A. Fingers of salt help mix the sea. *Science*, **211**(9):155-158, 1981.
881. Davies, P. A. Laboratory modeling of mantle flows. In *NATO Adv. Study Inst. on Mech. of Cont. Drift & Plate Tectonics*, Acad. Press, London, pp. 225-244, 1980.

882. Tritton, D. J. and P. A. Davies. Convection of a very viscous fluid heated from below. In *NATO Adv. Study Inst. on Mech. of Cont. Drift & Plate Tectonics*, Academic Press, London, pp. 267-287, 1980.
883. Carrigan, C. R. Multiple-scale convection in the earth's mantle: a three-dimensional study. *Science*, **215**(19 Feb. 1982):965-968, 1982.
884. Sparks, R. S. J., H. E. Huppert, and J. S. Turner. The fluid dynamics of evolving magma chambers. *Proc. Roy. Soc. A*, **310**:511-534, 1984.
885. Kozák, J. Contemporary possibilities of the schlieren-method in the study of seismic boundary phenomena. *J. Geophysics = Zeits. für Geophysik*, **38**(3):595-608, 1972.
886. Rahman, A. A new type of wave discovered in the schlieren photographs. *Zeitschrift für Geophysik*, **31**:146-158, 1965.
887. Behrens, J., J. Kozák, and L. Waniek. Investigation of wave phenomena on corrugated interfaces by means of the schlieren method. In *Proc. 12th General Assembly, European Seismological Commission*, pp. 1-5, 1970.
888. Cervený, V., J. Kozák, and I. Psencík. Refraction of elastic waves into a medium of lower velocity-psuedospherical waves. *Pure and App. Geophys.*, **92** (9):115-132, 1971.
889. Cervený, V. Experimental evidence and investigation of pseudospherical waves. *Journal of Geophysics = Zeitschrift für Geophysik*, **38**(3):617-626, 1972.
890. Waniek, L. Model studies of wave propagation in low velocity layers with sharp boundaries. *Journal of Geophysics = Zeitschrift für Geophysik*, **38**(3):647-658, 1972.
891. Kozák, J. Colour schlieren representation of compressional-stress fields with respect to focal zone study. *Studia Geophysica et Geodetica*, **17**:314-320, 1973.
892. Kozák, J. Wave phenomena of blocks; a schlieren model study. *Studia Geophysica et Geodetica*, **19**(4):350-357, 1975.
893. Niewiadomski, J., M. Gorski, and J. Kozák. Tensional crack development in physical models with inhomogeneities under load. *Stud. Geophy. Geodet.*, **24**:373-381, 1980.
894. Kozák, J. Private communication. Oct. 12, 1999.
895. Settles, G. S. and S. Garg. A scientific view of the productivity of abrasive blasting nozzles. *J. Protective Coatings & Linings*, **12**(4):28-102, 1995.
896. Settles, G. S. and S. T. Geppert. Redesigning blasting nozzles to improve productivity. *J. Protective Coatings & Linings*, **13**(10):64-72, 1996.
897. Settles, G. S. Supersonic abrasive iceblasting apparatus. US Patent 5,785,581, July 28, 1998.
898. Smith, G. C. Multiple-jet oxygen lances - theoretical analysis and correlation with practice. *Journal of Metals*, **18**(7):846-851, 1966.
899. Wimberger-Friedl, R. Assessment of orientation, stress and density distributions in injection-molded amorphous polymers by optical techniques. *Progress in Polymer Science (Oxford)*, **20**(3):369-401, 1995.
900. Hill, E. A. Visualization of airflow inside blow fill seal machinery using schlieren imaging. *BFS News*, (Autumn):8-12, 1999.
901. Xu, Y. R., N. G. Zhang, and W.-J. Yang. Industrial applications of optical flow visualization. In *Proc. WAM-91*, ASME, Vol. 132, pp. 137-144, 1991.
902. Zobel, T. W. Erhöhung der Schneidegeswindigkeiten beim Brennschneiden durch neue Düsenformen. VDI-Verlag Gmbh, Berlin, 1936.
903. Matsunawa, A., T. Nakai, and I. Okamoto. Interaction between supersonic jet and burning iron wall in oxygen cutting (Part I) - Shock wave behaviour and combustion phenomena. *Trans. Japanese Welding Research Inst.*, **14**(1):45-54, 1985.
904. Bemis, B. L. and G. S. Settles. Visualization of liquid metal, arc, and jet interactions in plasma cutting of steel sheet. In *Proc. 8th Intl. Symp. on Flow Visualization,* Sorrento, Italy, ed. G. M. Carlomagno, Paper 108, 1998.
905. Matsunawa, A. and S. Katayama. High speed photographic study of yag laser materials processing. In *Proc. ICALEO '85*, Laser Inst. of America, pp. 41-48, 1986.

906. Leidinger, D. and D. Schuoecker. Investigations on the gas flow of conic-cylindrical and supersonic nozzles in a laser cut kerf. In *Proc. 10th Intl. Symp. on Gas Flow and Chemical Lasers,* Friedrichshafen, Germany, SPIE Vol. 2502, pp. 577-582, 1995.
907. Man, H. C., J. Duan, and T. M. Yue. Behaviour of supersonic and subsonic gas jets inside laser cut kerfs. In *Proc. ICALEO '97*, LIA, Part 1, pp. B27-B36, 1997.
908. Brandt, A. D. and G. S. Settles. Effect of nozzle orientation on the gas dynamics of inert-gas laser cutting of mild steel. *J. Laser Applications*, **9**(6):269-277, 1997.
909. McClure, J. C., G. Garcia, H. Hou, and A. C. Nunes. Gas flow observation during VPPA welding using a shadowgraph technique. NASA CR-204347, 1993.
910. Bálsamo, P. S. S., L. O. Vilarinho, M. Vilela, and A. Scotti. Development of an experimental technique for studying metal transfer in welding: synchronized shadowgraphy. *Journal of Metals*, 2001 (In Press).
911. Hackett, C. M. and G. S. Settles. The High-Velocity Oxy-Fuel (HVOF) thermal spray - materials processing from a gas dynamics perspective. AIAA Paper 95-2207, 1995.
912. Tabei, K., H. Shirai, F. Takakusagi, and S. Oikawa. Temperature measurements of atmospheric argon plasma free jets using Moiré-Schlieren and spectroscopy methods. *Heat Transfer - Japanese Research*, **18**(1):45-56, 1989.
913. Hackett, C. M. *The gas dynamics of high-velocity oxy-fuel thermal sprays.* Ph.D. Thesis, Mechanical Engrg. Dept., Pennsylvania State University, 1996.
914. Mates, S. P. and G. S. Settles. Flow visualization study of the gas dynamics of liquid metal atomization nozzles. In *Advances in Powder Metallurgy & Particulate Matls.*, Metal Powder Industries Fed., Vol. 1, pp. 15-29, 1995.
915. Mates, S. P. and G. S. Settles. High-speed imaging of liquid metal atomization by two different close-coupled nozzles. In *Advances in Powder Metallurgy & Particulate Matls.*, Metal Powder Industries Fed., Vol. 1, pp. 67-80, 1996.
916. Mates, S. P. *Gas atomization of molten metal.* Ph.D. Thesis, Mechanical Engrg. Dept., Pennsylvania State University, 1999.
917. Ünal, A. Influence of gas flow on performance of 'confined' atomization nozzles. *Metallurgical Transactions B* , **20**(6):833-843, 1989.
918. Ünal, A. Flow separation and liquid rundown in a gas-atomization process. *Metallurgical Transactions B*, **20**(5):613-622, 1989.
919. Biancaniello, F. S., P. I. Espina, G. E. Mattingly, and S. D. Ridder. Flow visualization study of supersonic inert gas-metal atomization. *Matls. Sci. & Engrg. A*, **119**(1-2):161-168, 1989.
920. Espina, P. I. and U. Piomelli. Numerical simulation of the gas flow in gas-metal atomizers. In *Proc. Fluids Engrg. Div. Summer Mtg.*, ASME Paper FEDSM98-4901, 1998.
921. Owen, R. B. and M. H. Johnston. Laser shadowgraph and schlieren studies of gravity-related flow during solidification. *Optics & Lasers in Engrg.*, **2**(2):129-146, 1981.
922. Hart, J. E., J. Toomre, A. E. Deane, N. E. Hurlburt, G. A. Glatzmaier, G. H. Fichtl, F. Leslie, W. W. Fowlis, and P. A. Gilman. Laboratory experiments on planetary and stellar convection performed on Spacelab 3. *Science*, **234**:61-64, 1986.
923. Owen, R. B. and M. H. Johnston. Laser schlieren crystal monitor. US Patent 4,681,437, 1987.
924. van den Assem, D., R. H. Huijser, and J. P. B. Vreeburg. On the development of an optical diagnostic instrument for fluid-physics research in microgravity. *J. Phys. E. Sci. Instr.*, **20**(8):992-1000, 1987.
925. Ecker, A., D. O. Frazier, and J. Alexander. Fluid flow in solidifying monotectic alloys. *Metallurg. Trans. A Phys. Metallurgy & Matls. Sci.*, **20A** (12):2517-2527, 1989.
926. Spaan, F. H. and A. J. Kramer. Analysis of the alignment of a Schlieren system for tele-operation. In *Proc. 8th European Symp. on Materials & Fluid Sciences in Microgravity*, European Space Agency, Vol. 1, pp. 435-440, 1992.

927. Jin, W. Q., Z. L. Pan, N. Cheng, and H. Yuan. Application of schlieren-differential interference microscope to the in situ direct observation of the growth process of a crystal in microgravity. In *Proc. 47th Intl. Astronautical Congr.*, IAF Paper 96-J409, 1996.
928. Dubois, F., L. Joannes, O. Dupont, J. L. Dewandel, and J. C. Legros. An integrated optical set-up for fluid-physics experiments under microgravity conditions. *Measurement Science and Technology*, **10**(10):934-935, 1999.
929. Smith, R. F. *Microscopy and photomicrography - a working manual.* CRC Press, Boca Raton, FL, 1990.
930. Inoué, S. and K. R. Spring. Microscope image formation. Chap. 2 of *Video Microscopy*, Plenum Press, New York, ed. 2, pp. 13-91, 1997.
931. Rienitz, J. Kritik des Positiv-Negativ-Verfahrens und der mikroskopischen Reliefverfahren (schiefe Beleuchtung, Schlierenmikroskopie und Shearing-interferenzmikroskopie). *Mikroskopie*, **22**(7):169-193, 1968.
932. Smith, R. F. Oblique illumination. *Industrial Photography*, (8):14-15, 1994.
933. Kachar, B. Asymmetric illumination contrast: a method of image formation for video light microscopy. *Science*, **227**:766-768, 1985.
934. Axelrod, D. Zero-cost modification of bright field microscopes for imaging phase gradient on cells: Schlieren optics. *Cell Biophysics*, **3**(2):167-173, 1981.
935. Takaoka, H. Optical microscope which has optical modulation elements. US Patent 5,969,853, Oct. 19, 1999.
936. Chapman, J. N. The investigation of magnetic domain structures in thin foils by electron microscopy. *J. Phys. D App. Phys.*, (4):623-647, 1984.
937. Rienitz, J. *Historical and physical lines of development of optical instruments: from magic to partial coherence.* Pabst Science Publishers, Lengerich, Germany, 1999. (ISBN 3-934252-13-3. In German.)
938. Abbe, E. Beitrage zur Theorie des Mikroskops und der mikroskopischen Wahrnehmung. *Arch. für Mikr. Anat.*, **9**:413-468, 1873.
939. Glaser, I. Optical texture pseudocoloring. *J. Optics (Paris)*, **11**(4):215-217, 1980.
940. Bernal, L. P., M. A. Hernan, and V. Sarohia. Characterization of coherent structures in a turbulent mixing layer by digital image analysis. In *Flow Visualization III*, ed. W.-J. Yang. Hemisphere Pub., Washington, pp. 274-278, 1985.
941. Yao, S. K. and S. H. Lee. Spatial differentiation and integration by coherent optical-correlation method. *JOSA*, **61**(4):474-477, 1971.
942. Ronchi, V. Forty years of history of a grating interferometer. *App. Optics*, **3(4)**:437-451, 1964.
943. Kafri, O. and I. Glatt. Moiré deflectometry - a ray deflection approach to optical testing. *Opt. Engrg.*, **24**(6):944-960, 1985.
944. Cornejo-Rodriguez, A. Ronchi test. Chap. 9 of *Optical Shop Testing*, ed. D. Malacara. New York, Wiley & Sons, ed. 2, pp. 321-365, 1991.
945. Bowen, I. S. Final adjustments and tests of the Hale telescope. *Pubs. of the Astronomical Soc. of the Pacific*, **62**(365):91-97, 1950.
946. Cooper, G. E. and G. A. Rathert. Visual observations of the shock wave in flight. NACA Report RM A8C25, 1948.
947. Ohman, Y. Can mirage phenomena be traced on the sun? *Solar Physics*, **96**(3):209-212, 1985.
948. Jagoda, I. J. and F. J. Weinberg. Optical studies of plasma jets. *J. Phys. D. Appl. Phys.*, **13**:551-561, 1980.
949. Rye, B. J., J. W. Waller, A. S. V. McKenzie, and J. Irving. Schlieren photography in the first half-cycle of a theta pinch discharge. *Brit. J. App. Physics*, **16**(9):1404, 1965.
950. Sigel, R., A. G. M. Maaswinkel, and G. D. Tsakiris. High-speed diagnostics in laser fusion experiments. In *Proc.16th Intl. Congr.on High Speed Photography & Photonics*, SPIE Vol. 491, Part 2, pp. 814-824, 1985.

951. Alpher, R. A. and D. R. White. Optical refractivity of high temperature gases. I. Effects resulting from dissociation of diatomic gases. *Phys. Fluids*, **2**(2):153-161, 1959.
952. Lovberg, R. H. Investigation of current-sheet microstructure. *AIAA J.*, **4**(7):1215-1222, 1966.
953. Baumann, E. The Fischer large-screen projection system. *SMPTE Journal*, **60**(4):344-356, 1953.
954. Glenn, W. E. Principles of simultaneous-color projection television using fluid deformation. *SMPTE Journal*, **79**(9):788-794, 1970.
955. van Raalte, J. A. A new schlieren light valve for television projection. *App. Optics*, **9**(10):2225-2230, 1971.
956. Good, W. E. Recent advances in the single-gun color television light-valve projector. In *Simulators & Simulation* , SPIE Vol. 59, pp. 96-99, 1975.
957. Hayes, J. D., G. G. Hart, and R. M. Bobbe. The projection and viewing of transparent image storage materials. *SPIE Journal*, **2**(Aug.-Sept.):242-246, 1964.
958. Fritsch, M. W. Schlieren optical system using liquid crystral phase gratings for large screen projection. *Displays*, **13**(1):45-60, 1992.
959. Uberoi, M. and L. S. G. Kovasznay. Analysis of turbulent density fluctuations by the shadow method. *J. App. Phys.*, **26**(1):19-24, 1955.
960. Taylor, L. S. Twinkling range of turbulence layers. *JOSA*, **59**:113-114, 1969.
961. Gerber, N. and R. Sedney. Study of wake optical properties. *AIAA J.*, **29**(6):1005-1006, 1991.
962. Haight, J. S., B. R. Peters, and D. A. Kalin. Application of an ultra-high-speed framing camera to aero-optic investigations. In *Atmospheric Propagation and Remote Sensing II*, SPIE Vol. 1968, pp. 841-848, 1993.
963. Bowersox, R. D. W., J. A. Schetz, and R. W. Conners. Digital analysis of shadowgraph images for statistical index of refraction (density) turbulent fluctuation properties in high-speed flow. *Measurement: J.Intl. Meas. Confed.*, **15**(3):201-209, 1995.
964. Townend, H. C. H. Statistical measurements of turbulence in the flow of air through a pipe. *Proc. Roy. Soc. A*, **145**:180-211, 1934.
965. Thompson, L. L. and L. S. Taylor. Analysis of turbulence by schlieren photography. *AIAA J.*, 7:2030-2031, 1969.
966. Davis, M. R. Measurements in a subsonic turbulent jet using a quantitative schlieren technique. *J. Fluid Mech.*, **46**:631-656, 1971.
967. Ivanov, V. G. Possible use of the schlieren method to measure characteristics of turbulence. *Soviet Physics - Technical Physics*, **19**(9):429-431, 1974.
968. Deron, R. and J. P. Faleni. Estimation of the turbulent spectral densities of the mass-density using two-dimensional Fourier transform of digitized schlieren pictures. ONERA TP No. 1990-110, 1990.
969. Gumennik, I. V. and B. S. Rinkevichius. The flow visualization by schlieren methods with fuco knife and scanning light beam. In *Flow visualization V*, ed. R. Řeznícek. Hemisphere Pub., NY, pp. 113-118, 1990.
970. Hall, J. L., P. E. Dimotakis, and H. Rosemann. Experiments in non-reacting compressible shear layers. *AIAA J.*, 31(12):2247-2254, 1993.
971. McIntyre, S. S., E. Stanewsky, and G. S. Settles. An optical deflectometer for the quantitative analysis of turbulent structures. In *ICIASF '91 Record*, pp. 34-42, 1991.
972. Hibberd, M. F. Study of a turbulent mixing layer in drag-reducing fluids using schlieren photography. In *Flow Visualization III*, ed. W-J Yang, pp. 615-619, 1985.
973. Riediger, S. *Examination of a turbulence structure in a plane mixing layer and behind a channel enlargement for the flow of two non Newtonian fluids.* Ph.D. Thesis, Fachbereich Chemietechnik, Dortmund Univ., Germany, 1989.

974. Garg, S., L. N. Cattafesta, III, M. A. Kegerise, and G. S. Jones. Quantitative schlieren measurements of coherent structures in planar turbulent shear flows. In *Proc. 8th Intl. Symp. on Flow Visualization,* Sorrento, Italy, ed. G. M. Carlomagno, paper 237, 1998.
975. Vest, C. M. Formation of images from projections: Radon and Abel transforms. *JOSA*, **64**(9):1215-1218, 1974.
976. Legu, L. Y., A. K. Beketova, and R. K. Biktagirov. Standard phase inhomogeneity. *Sov. J. Opt. Tech.*, **45**(1):59, 1978.
977. Murray, W. L. The sensitivity of a black and white single-mirror schlieren apparatus. *Journal of Photographic Science*, **15**:191-196, 1967.
978. Lindsey, W. F. Device for evaluating the sensitivity of an optical system ultilizing the Foucault knife edge test. US Patent 2,777,355, Jan. 15, 1957.
979. Avramenko, A. S., E. Y. Durovich, and B. V. Naumov. Measurement of sensitivity of shadowgraphic instruments with spherical autocollimating mirror. Report JPRS-UEQ-84-001, Joint Publications Research Service, Arlington, VA, pp. 57-58, 1984.
980. Ronchi, V. *La prova dei sistema ottici.* Nicola Zanichelli, Bologna, 1925.
981. Darby, P. F. The Ronchi method of evaluating schlieren photographs. Navord Report 74-46, US Navy Bureau of Ordnance, pp. 31-32, 1946.
982. Didion, D. A. and Y. H. Oh. A quantitative schlieren-grid method for temperature measurement in a free convection field. Report no. 1, Dept. of Mechanical Engineering, Catholic Univ. of America, Washington, DC, 1966.
983. Reid, G. T. Moiré fringes in metrology. *Optics & Lasers in Engrg.*, **5**(2):63-93, 1984.
984. Weibel, E. E. A new quantitative optical method applied to fluid flow problems. In *Proc. 1st US Natl. Congr. App. Mech.*, J.W. Edwards, Ann Arbor, pp. 693-698, 1952.
985. Meyer-Arendt, J. R. and E. P. Shettle. Calibration of schlieren systems. *App. Optics*, **4**(6):757, 1965.
986. Knoos, S. Boundary-layer structure in a shock-generated plasma flow part 2. experiments using a new quantitative schlieren technique. *J. Plasma Phys.*, **2**(Part 2):243-255, 1968.
987. Sukhorukikh, V. S. Diffraction theory of schlieren methods. In *Proc. 8th Intl. Conf. on High-Speed Photography, Stockholm*, Wiley, NY, pp. 341-345, 1968.
988. Gubchik, A. A., E. P. Kazandzhan, and V. S. Sukhorukikh. Detection of strong and weak discontinuity surfaces in gasdynamic flows from optical experiment data. *Izvestiya AN SSR, Mekh. Zhidkosti i Gaza*, **5**(1):169-173, 1970.
989. Devia, F., G. Milano, and G. Tanda. Evaluation of thermal field in buoyancy-induced flows by a schlieren method. *Experimental Thermal and Fluid Science*, **8**:1-9, 1994.
990. Tokumaru, P. T. and P. E. Dimotakis. Image correlation velocimetry. *Expts. Fluids*, **19**:1-15, 1995.
991. Smith, K. M. and J. C. Dutton. A procedure for turbulent structure convection velocity measurements using time-correlated images. *Expts. Fluids*, **27**:244-250, 1999.
992. Kharitonov, A. I. and I. V. Ershov. Optoelectronic technique for measuring phase object speed by displacing visualization field images. In *Flow Visualization V*, ed. R. Řeznícek. Hemisphere Pub., NY, pp. 119-124, 1990.
993. Fu, S. and Y. Wu. Quantitative analysis of velocity distribution from schlieren images. In *Proc. 8th Intl. Symp. on Flow Visualization*, Paper no. 233, 1998.
994. Fu, S., Y. Wu, R. D. Kothari, and H. Xing. Flow visualization using the negative-positive grid schlieren system and its image analysis. In *Proc. 9th Intl. Symp. on Flow Visualization,* ed. I. Grant and G. M. Carlomagno, Paper no. 324, 2000.
995. Lewis, R. W., R. E. Teets, J. A. Sell, and T. A. Seder. Temperature measurements in a laser-heated gas by quantitative shadowgraphy. *App. Optics*, **26**(17):3695-3704, 1987.
996. Stricker, J. and O. Kafri. Moiré deflectometry, a new method for density gradient measurements in compressible flows. Report TAE-436, Aerospace Engrg. Dept., Technion, Haifa, Israel, 1981.

997. Kafri, O., A. Livnat, and E. Keren. Infinite fringe moiré deflectometry. *App. Optics*, **21**(21):3884-3886, 1982.
998. Stricker, J. and O. Kafri. A new method for density gradient measurements in compressible flows. *AIAA J.*, **20**(6):820-823, 1982.
999. Stricker, J., E. Keren, and O. Kafri. Axisymmetric density field measurements by moiré deflectometry. *AIAA J.*, **21**(12):1767-1769, 1983.
1000. Kreske, K., E. Keren, and O. Kafri. Insights on moiré deflectometry. *Lasers & Optronics*, **7**(10):63-66, 1988.
1001. Stephens, M. *The rise of the image, the fall of the word.* Oxford Univ. Press, New York, 1998.
1002. Freedberg, D. *The power of images.* Univ. of Chicago Press, Chicago, IL, 1989.
1003. Friedhoff, R. M. and W. Benzon. *Visualization: the second computer revolution.* Harry N. Abrams, NY, 1989.
1004. Edwards, B. *Drawing on the right side of the brain.* J. P. Tarcher Inc., CA, 1989.
1005. Janouch, G. *Conversations with Kafka.* New Directions, NY, ed. 2, 1971.
1006. Roshko, A. Flow visualization as a basic research tool. In *Flow Visualization VII*, ed. J. P. Crowder. Begell House, NY, pp. 983-994, 1995.
1007. Homsy, G. M., H. Aref, K. S. Breuer, S. Hochgreb, J. R. Koseff, J. R. Munson, K. G. Powell, C. R. Robertson, and S. T. Thoroddsen. *Multi-media fluid mechanics CD-ROM.* Cambridge University Press, Cambridge, UK, 2000.
1008. Marzwell, N. and M. Dragovan. Inflatable membrane reflectors for multi-purpose applications. *NASA Tech Briefs*, **23**:69, 1999.
1009. Allman, B. E., P. J. McMahon, K. A. Nugent, D. Paganin, D. L. Jacobson, M. Arif, and S. A. Werner. Phase radiography with neutrons. *Nature*, **408**:158-159, 2000.
1010. Lovell, D. J. The legacy of Joseph Fourier. *App. Optics*, **19**(5):SR-143-Sr-146, 1980.
1011. Porter, A. B. On the diffraction theory of microscope vision. *Phil. Mag.*, **11**:154-166, 1906.
1012. Lord Rayleigh (Strutt, J. W.) On the theory of optical images, with special reference to the microscope. *Phil. Mag.*, **42**(5):167, 1896.
1013. Zakharin, B. and J. Stricker. Fourier optics analysis of schlieren images. In *Proc. 9th Intl. Symp. on Flow Visualization*, ed. I. Grant and G. M. Carlomagno. Paper no. 386, 2000.
1014. Yu, F. T. S. *Optical information processing.* Wiley, NY, ed. 1, 1983.
1015. Barakat, R. General diffraction theory of optical tests, from the point of view of spatial filtering. *JOSA*, **59**(11):1432-1439, 1969.
1016. Santiago-Rosanne, M., M. Vignes-Adler, and M. G. Velarde. Dissolution of a drop on a liquid surface leading to surface waves and interfacial turbulence. *Journal of Colloid and Interface Science*, **191**:65-80, 1997.
1017. Lowenthal, S. and Y. Belvaux. Observation of phase objects by optically processed Hilbert transform. *Applied Physics Letters*, **11**(2):49-51, 1967.
1018. Ojeda-Castañeda, J. and L. R. Berriel-Valdos. Classification scheme and properties of schlieren techniques. *App. Optics*, **18**(19):3338-3341, 1979.
1019. Muller, R. and J. Marquard. The Hilbert transform and its generalization in optics and image processing. *Optik*, **110**(2):99-109, 1999.
1020. Ojeda-Castañeda, J. and E. Jara. Isotropic Hilbert transform by anisotropic spatial filtering. *App. Optics*, **25**(22):4035-4038, 1986.

Appendix A Optical Fundamentals

This Appendix does not pretend to cover the optical fundamentals comprehensively, since that coverage is available in many other fine sources. Instead, only a brief account is given of some selected issues in support of the main text. A good recent textbook on optics is Meyer-Arendt [132]. More detail on such issues as photographic optics and scientific imaging, though somewhat dated, can be found in Hyzer [168] and Smith [167].

A.1 Radiometry and Photometry

> "Both (radiometry and photometry) have been cursed with a jungle of often-bewildering terminology"
>
> *W. J. Smith* [167]

Radiometry is the measurement science of radiant quantities, e.g. in units of Watts/m^2. Photometry is similar, but specific to the visible spectrum. It has its own set of SI units: the candela, lumens, and lux. A full discussion can be found, for example, in Chap. 21 of [132].

To minimize confusion only the SI photometric units system is used here. The *candela* is the basic SI unit of luminous intensity, given in lumens/steradian. The *lumen* is the unit of luminous power, i.e. energy/time. An extended light source is characterized by its *luminous exitance*, i.e. the radiant power density in *lux* (lumens/m^2) of its surface area. Because of its exitance, the light source radiates *luminance* into the space around it, measured in candela/m^2. When this light strikes a surface it produces *illuminance*, also measured in lux. The illuminance distribution of an image is a key issue in the Chap. 3 discussion of schlieren sensitivity, and is assigned the symbol E.

Only a few additional issues bear mentioning here. The efficiency or efficacy of a light source is given in lumens/watt, a measure of how well its power consumption is used in generating light. For intermittent sources the total light output over a period of time is measured in lumen-seconds. The lux-second (see [168]),

or lumen-sec/m^2, is useful for photographic exposures. The term "illumination" is not a photometric quantity, rather a method of delivering light. Terms like "brightness" and "brilliance" in the older schlieren and shadowgraphy references have given way to luminous exitance, though "intensity" is still used when referring to a point source.

Finally the *color temperature* of a light source (from colorimetry) relates the color content of the light to that radiated by a blackbody radiator at a certain Kelvin temperature. It is a consideration in color schlieren imaging, and any time faithful color reproduction is required.

A.2 Refraction Angle ε

A.2.1 Small Optical Angles and Paraxial Space

By analogy with telescopy, arcsecond measure is used here for the schlieren refraction angle ε. Even for large refractions like 200 arcseconds, no attempt is made to use alternate units, e.g. 3 1/3 arcminutes. For reference, one degree of arc equals 3600 arcseconds and 1 radian equals 206264.8 arcseconds. A μradian is thus about 0.2 arcsecond.

Since ε is a very small angle, when expressed in radians it is essentially equal to sinε or tanε by trigonometric approximation. Similarly $\cos\varepsilon \cong 1$. Thus in Eqn. 2.6, for example, $f_2 \cdot \varepsilon_y$ is used in place of the mathematically-correct $f_2 \cdot \tan\varepsilon_y$.

Paraxial space is the space close enough to the optical axis that the small-angle approximation applies, as assumed throughout this book. The optics of paraxial space is called Gaussian optics.

A.2.2 Huygens' Principle and Refraction

According to Huygens' Principle, points on an optical wavefront serve as new sources of spherical wavelets, whence the propagation of the wavefront may be determined. The wavefront always propagates at the local speed of light. Applied to refractions in inhomogeneous media, the wavefront at the boundary between one optical medium and another of higher refractive index is skewed toward the normal to the interface between the two. Light rays, always normal to the local wavefront, are thus bent toward the zone of higher refractive index. In gases this is equivalent to the zone of higher density. Huygens' Principle therefore determines the direction of the refraction angle ε at such an interface, which is the elemental boundary of a schlieren object.

A.3 Optical Components and Devices

A.3.1 Conjugate Optical Planes

As described in Chap. 2, the front and back foci of a lens or concave mirror constitute conjugate optical planes bearing a 1:1 relationship to one another. In a schlieren system the light-source and knife-edge planes, as well as the test-area and screen planes, form sets of conjugate optical planes. These two sets bear reciprocal Fourier-transform relationships to one another (see App. B). Thus an accurate image of the light source is focused upon the knife-edge, and an accurate image of the schlieren object appears upon the viewing screen. These pairs of conjugate optical planes are central to understanding the schlieren effect.

A.3.2 Lens f/number

The f/number is the focal ratio of a lens or mirror, f/d, where f is the lens focal length and d is the lens diameter. Photographic lenses usually have built-in iris diaphragms by which means the f/no. can be varied from its minimum value (wide open) to it maximum (smallest available aperture for a fixed focal length). Lenses with small f/numbers, including condenser lenses and some camera objectives, are known as "fast" lenses because of their light-gathering ability.

F/stops are fixed detents on a lens iris corresponding to equal increments of its clear aperture. Thus f/1.7, 2.8, 4, 5.8, 8, 11, 16, and 22, for example, each represent an aperture setting at which the illuminance reaching the film is reduced to half its previous value. Within the range of the reciprocity law for photographic film, a one-stop decrease in aperture can be compensated by doubling the exposure time, e.g. from 1/60 to 1/30 sec. Experienced photographers can visually judge the over- or under-exposure of a test photograph in f/stops, then adjust the lens aperture or shutter speed to obtain a correct exposure on the next trial. Negative films have more exposure *latitude* than color transparencies, but generally about ± 3 stops is sufficient to render a photograph irrecoverably over- or under-exposed.

A.3.3 The Thin-Lens Approximation

In Chaps. 3 and 4, schlieren image magnification and focusing calculations used the standard thin-lens-formula, Refs. [66,98,132,167] and [592]. Here the axial thickness of a lens is neglected compared to its focal length, yielding:

$$\frac{1}{o}+\frac{1}{i}=\frac{1}{f}$$

where o is the object distance, i is the image distance, and f is the lens focal length.

A.3.4 Viewing Screens and Ground Glass

Schlieren images and shadowgrams are often projected upon screens for viewing [167]. The sheet of matte white paper, recommended as an optical alignment tool in Chap. 7, broadly reflects 70-80% of the incident light. Only a small fraction of this reaches the viewer, though. Instead, a ground-glass rear-projection viewing screen is much more efficient. It transmits about 75% of the incident light in a directional pattern along the optical axis. As already noted in Chap. 7, one should resist the temptation to take a schlieren photo or shadowgram by aiming a camera at a white-paper or ground-glass viewing screen.

A.3.5 Optical Density

Optical-glass or gelatin neutral-density (ND) filters are very useful in schlieren and shadowgraphy for attenuating an optical beam without either stopping down the aperture or degrading the optical quality. These filters obey the formula:

$$\text{Optical Density} = \log_{10}(E_i / E_o)$$

where E_i and E_o are the incident and transmitted beam illuminance values. Thus an ND filter transmitting 75% of the incident light (a ½-stop attenuator) has an optical density of 0.125, a 1-stop attenuator has an optical density of 0.3, and so forth.

A.4 Optical Aberrations

Optical aberrations *coma* and *astigmatism* are introduced in Sect. 3.1.2 regarding off-axis mirror-type schlieren systems using mirrors figured for on-axis use. Both aberrations lead to errors in the faithful production of the light-source image in the cutoff plane, and thus to uneven schlieren-image background illuminance. Coma occurs when the direction of light reflected from a mirror depends on the position of the point of reflection. It spreads a point focus into a line. Astigmatism arises from differences in path length along the optical centerline and the mirror periphery due to off-axis tilt, and results in stretching the image of a point into two perpendicular lines spaced along the optical axis. In z-type mirror schlieren systems these aberrations are minimized by restricting the offset angles θ to their minimum practical values and using mirrors with f/numbers of 6 or greater

Spherical aberration is less likely to be a problem than coma or astigmatism, since it is not involved in mirror tilt. Instead, if a poor-quality lens with spherical aberration were used as a schlieren field lens, parallel rays passing through the outer zones of the lens would not focus at the same point as rays nearer the optical axis. Again, a non-uniform schlieren background results. Camera lenses and re-

fracting-telescope objectives are usually well-corrected for spherical aberration, but this factor makes lens-type schlieren systems expensive at larger apertures.

A simple single-element lens with spherical aberration figures prominently in the Dall null corrector, Sect. 4.1.3, which allows one to use a single parabolic mirror in a double-pass coincident optical system.

Chromatic aberration results from the prism-like variance of glass refraction with wavelength of light. In simple lenses, this causes the effective focal length to vary along the optical axis with light wavelength. If simple lenses are used as schlieren field lenses, the resulting color anomalies in the image ("involuntary color schlieren," first observed by Toepler) interfere with the schlieren sensitivity. Compound achromatic lenses correct this problem at two different wavelengths, but are never entirely free of chromatic aberration across the visible spectrum. For example, the highly-engineered large-format camera lens used in the Penn State Full-Scale Schlieren System (Sect. 4.3.5) still suffers residual chromatic errors at high schlieren sensitivity settings.

A wealth of information on these and other optical aberrations can be found in many optical texts, including [132,145,167,587].

A.5 Light and the Human Eye

Throughout this book, three general types of image sensors are considered: electronic sensors, photographic film, and the human eye. The latter two respond logarithmically to changes in incident illuminance, but each of them is unique in many ways. Since photography and digital imaging were discussed in several earlier chapters, a brief review of the characteristics of the eye is given here for completeness. Additional coverage is found in [156] and [167].

As a camera, the eye has a focal length of 15.9 mm and an aperture range between f/2 and f/8. Its contrast sensitivity threshold plays a key role in the Chap. 3 definition of schlieren sensitivity. The best contrast sensitivity occurs for luminance values between 100 and 10,000 cd/m^2. The equivalent exposure index of the eye is about ISO 2000 [156].

The eye's temporal resolution is not very impressive at only about 1/10 sec, though, and it can handle a data rate of only 1000-10000 bits/second. Comparing this with modern high-speed cameras at up to a trillion bits/sec, it becomes clear that the unaided eye could never explore high-speed physics. Its best velocity discrimination occurs at angular speeds of only 1-10 deg/sec; very slow by high-speed imaging standards. Thus, when observing turbulence on the schlieren screen, for example, individual turbulent eddies are seldom visible under continuous lighting.

The resolution of the eye, however, is outstanding. The retina contains about 10^8 photoreceptor cells, compared with only about 10^5 pixels in a standard television or computer screen. Wavelengths from 0.38 to 0.74 μm are visible, and are

interpreted by the brain as the rainbow colors. Many other colors are also visible by color mixing, as displayed on the CIE chromaticity chart [131,167].

Stereoscopic vision covers about a 130° circular field-of-view. The interocular distance averages 6.5 cm and the parallax viewing angle for best depth perception is 10-15° [427]. However, stereo vision interpreted by the brain can perceive depths from a few cm to a km or more.

A.6 Geometric Theory of Light Refraction by a Schliere

In Eqn. 2.3, the curvature of a refracted light ray is expressed as a function of the refractive-index gradient through which it passes. The derivation of this is too involved to present in Chap. 2, but is important enough not to be omitted. It can be found in various forms in Schardin [1,2], Speak and Walters [126], Weyl [115], Burton [104], Goldstein and Kuehn [116], and Vasiliev [102], who develops it all the way from Maxwell's Equations. The present version is thus kept appropriately brief, following Burton.

Of course, the geometric theory of refraction is only an approximation to the more-complete physical optics approach, but is sufficient for present purposes. We further assume parallel illumination of a planar 2-D schlieren object in x and y, with no change along the principle direction (optical axis) z. Finally, within the schlieren object itself, the displacement of a light ray from its original rectilinear path is assumed negligible.[1]

In Fig. A.1, for simplicity, we assume a negative vertical refractive-index gradient $dn/dy < 0$, and no gradient in the x- or z-directions. A planar wavefront of light is initially vertical upon passing through z_1, and is thus normal to the horizontal optical centerline z. As this wavefront propagates through the schlieren object from z_1 to z_2, it covers the differential distance Δz in differential time Δt and is refracted[2] through the differential angle $\Delta\varepsilon$. Since light rays always point normal to their wavefronts, the horizontal ray originally passing though z_1 is likewise refracted through differential angle $\Delta\varepsilon$.

[1] This is a good assumption except for strong refractions [82], like those caused by shock waves in gases. Even so, the assumption is only violated locally. Strong refractions in solids and liquids, however, may be serious enough to invalidate this approach.

[2] Since n_2 at y_2 is less than n_1 at y_1 because dn/dy is negative, the wavefront is skewed through a clockwise angle $\Delta\varepsilon$ toward the region of higher n per Huygens' Principle, Sect. A.2.2.

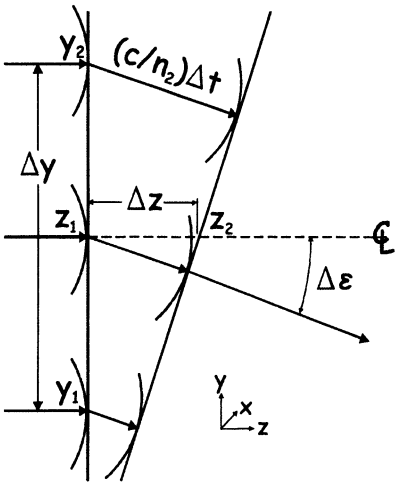

Fig. A.1. Diagram of elemental light refraction by a refractive-index gradient dn/dy.

By definition $n = c_o/c$, so the local value of the light speed c is c_o/n, where c_o is the speed of light in a vacuum. From the figure we can write:

$$\Delta\varepsilon = \frac{(c_0/n_2 - c_0/n_1)}{\Delta y}\Delta t$$

The differential time Δt can further be expressed as:

$$\Delta t = \Delta z \frac{n}{c_0}$$

Combining these expressions,

$$\Delta\varepsilon = \frac{n}{c_0}\frac{(c_0/n_2 - c_0/n_1)}{\Delta y}\Delta z$$

and simplifying terms,

$$\Delta\varepsilon = \frac{n}{n_1 n_2}\frac{(n_1 - n_2)}{\Delta y}\Delta z$$

The term n/n_1n_2 in this equation can be simplified to $1/n$ in the limit as Δy tends to zero. Letting all the finite differences approach zero, then, we obtain

$$\frac{d\varepsilon}{dz} = \frac{1}{n}\frac{dn}{dy}$$

But since ε is a very small angle, it is approximately equivalent to dy/dz, the slope of the refracted ray, according to Sect. A.2.1. Implementing this and writing the total derivatives as partials to account for the general case in which other refractive-index gradients are present, one obtains

$$\frac{\partial^2 y}{\partial z^2} = \frac{1}{n}\frac{\partial n}{\partial y}$$

which relates the curvature of the refracted ray to the magnitude of the responsible refractive-index gradient. The similar expression

$$\frac{\partial^2 x}{\partial z^2} = \frac{1}{n}\frac{\partial n}{\partial x}$$

can also be written for the other component, ∂n/∂x, of a general 2-D gradient field.

Appendix B The Schlieren System as a Fourier Optical Processor

> ...a body of data may simply not be in a form compatible with a human observer, and a linear transformation of the data may place it in compatible form.
>
> *J. W. Goodman* [130]

> The purist may note that I have taken some liberties in expressing the Fourier series. Pshaw.
>
> *D. J. Lovell* [1010]

The foundations of the diffraction theory of optical imaging were laid by Hermann Helmholtz (1821-1894) and Ernst Abbe (1840-1905) in terms of microscopy. They recognized that image formation and resolution could not be explained by geometric optics, but that the wave nature of light (physical optics) was required. The famous Abbe-Porter experiments [938,1011] demonstrated that microscope images result from diffraction by the grating-like structures of the microscopic specimens. Others [295,1012] also contributed to this approach, realizing that a microscope objective or a focusing lens performs a Fourier transform upon the light distribution presented by the object that it images. (A Fourier transform decomposes a complex function – the incoming light distribution – into a collection of simpler complex-exponential functions [130]). The inverse Fourier transform of the illumination in front of the lens then yields the image of the object produced by the lens. An optical image is thus regarded as the result of two successive Fourier transforms [132].

This view of image formation is general and powerful. If the light distribution at the lens focus is now modified, e.g. by a knife-edge cutoff, then it provides the theoretical background for everything we have learned about schlieren techniques.

Following the work of the early pioneers just mentioned, 20th-Century optics developed strong ties with communication theory and electrical engineering [130]. The heavy computational burden of three-dimensional Fourier transforms was first relieved by mainframe computers in the mid-20th Century, and now by the desktop PC. One must admire the several pre-computer-era investigators, led by Lord Rayleigh [66,102,126,149,172,452], who laboriously worked out examples of Fourier schlieren optics by hand.

No attempt is made to do that here. Optical modeling, with its lengthy calculations and large memory requirements, is a child of the computer age [588]. Geometric ray-tracing codes, discussed in Chap. 7, are useful for optical design and can express the aberrations of a z-type schlieren system, for example, but they cannot describe the key role of diffraction in the formation of the schlieren image. Instead, modern physical-optics codes conveniently handle the numerics and free the user to see the process in an overall view. Specifically, one such commercial program called GLAD 4.6 [588,589], available from Applied Optics Research (www.aor.com), is used in the example that follows. While most previous analyses treated only one space dimension normal to the optical axis for simplicity, GLAD 4.6 allows us the luxury of computing authentic-looking 2-D schlieren images. Considering this, and realizing that there are several other analyses of physical schlieren optics in the literature [66,126,129,130,154,198,199,1013], this one is kept appropriately descriptive and visual rather than mathematically rigorous.

B.1 The Basic Fourier Processor with no Schlieren Present

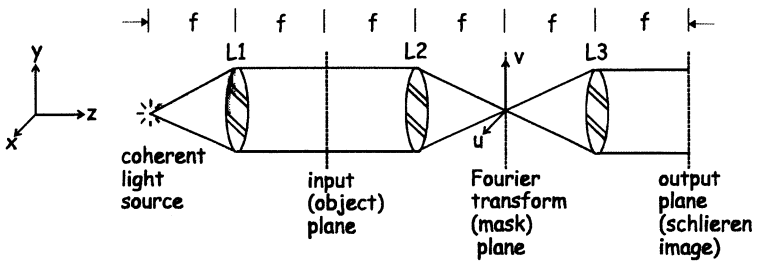

Fig. B.1. Diagram of the schlieren system as a Fourier optical processor.

Consider the schlieren system shown in Fig. B.1 as a Fourier optical processor. It is simplistic compared to a practical schlieren setup, but it serves for illustration. A coherent (monochromatic, "point") light source is used. Despite all that has been said on the advantages of incoherent light in schlieren imaging, a coherent light source is far simpler to deal with mathematically. Incoherent illumination is considered later, but for the moment a single monochromatic point source (helium-neon laser light at $\lambda = 0.6328$ μm) will suffice. As demonstrated in Chap. 7 and later here as well, the disadvantages of coherent illumination can be minimized by using a graded filter as a cutoff.

The spherical wavefront emanating from the light source along the optical z-axis is intercepted by lens L1, having focal length f. L1 thus collimates the light beam,

so that it now appears to emanate from a source at infinite distance. This light beam is, in fact, the spatial Fourier transform of the point light source [1014]. Physical optics represents such a beam by the complex amplitude of the optical wavefront. In codes like GLAD 4.6, the wavefront is modeled by a two-dimensional complex array in which, at each point along the z-axis, the real part A(x,y) represents beam amplitude and the imaginary part ϕ(x,y) represents phase:

$$f(x,y) = A(x,y)e^{j\phi(x,y)}$$

Lenses, mirrors, knife-edge cutoffs and the like are treated as matrix operators by which the beam matrix is multiplied. Special care is required on the issue of discrete sampling of the beam profile for computational purposes, lest aliasing confuse the results. The beam propagation between one optical element and the next along the z-axis is a diffraction process handled numerically by means of a Fast Fourier Transform (FFT) algorithm. This diffraction process is also modified by phase distortions due to the optical inhomogeneities that we call schlieren.

Coordinates x and y describe the 2-D profile of the light beam transverse to the optical axis. The beam after lens L1 is here chosen to be square and 2.56 ×2.56 cm in size. It is a planar electromagnetic wavefront with unit amplitude A(x,y) = 1 and zero phase ϕ(x,y) = 0, and it forms the initial condition of the problem at hand. The focal length f, which separates each optical element in Fig. B.1, is chosen to be 1 m. (These choices have more to do with the numerical resolution of the computer simulation than any practical embodiment.) The beam is numerically sampled every 0.01 cm, yielding a 256×256 array of schlieren pixels.

The input plane location in Fig. B.1 is reserved for the schlieren object. This might be a wind tunnel test section in parallel light, for example. But for the moment, let us assume no schlieren disturbance in the input plane.

The undistorted planar wavefront thus reaches, and is focused by, lens L2. Mathematically, this lens forms a Fourier transform of the light wavefront f(x,y) in its input plane. Replacing the x,y coordinates at the focus of L2 with u,v coordinates for clarity, this Fourier transform is given by:

$$F(u,v) = \int_{-\infty}^{\infty}\int_{-\infty}^{\infty} f(x,y)e^{-2\pi j(ux+vy)}dxdy$$

In this example the resulting Fourier spatial frequency spectrum at the lens focus is simply the Fraunhofer diffraction pattern of the square aperture in the input plane [938,1012], as shown in Fig. B.2.

Beyond the Fourier transform plane of Fig. B.2, lens L3 collects the diverging light beam and brings to focus in the output plane a conjugate image of the input plane. Mathematically, this image is obtained by the inverse Fourier transform of the cutoff-plane light distribution shown in Fig. B.2:

$$f(x,y) = \int_{-\infty}^{\infty}\int_{-\infty}^{\infty} F(u,v)e^{+2\pi j(ux+vy)}dudv$$

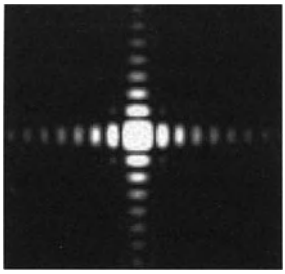

Fig. B.2. Enlarged view of schlieren focus with no disturbance in the input plane. On the scale of this example, the width of the diffraction pattern is about 1 mm.

This process exactly recovers the complex wavefront function f(x,y) in the output plane. In this preliminary discussion there is no schlieren object and no cutoff mask present, so one observes in the output only a brightly-illuminated square, the image of the square aperture in the input plane. We have described, in effect, the Fourier optics of a simple slide projector. However, the groundwork was laid not only for the schlieren technique, but also for the Foucault test, phase-contrast, and a key principle of optical processing: θ-modulation.

B.2 The Addition of a Schlieren Test Object

Now we place in the input plane of Fig. B.1 a phase distortion representing a schlieren object that we wish to render visible. Of many possible choices, a circular sinusoidal phase "ripple" is chosen. Centered on the optical axis, its radial x,y symmetry provides a simple test of different schlieren processing schemes.

Mathematically, this is accomplished by multiplying the beam array f(x,y) in the input plane by a matrix operator that replaces the (formerly zero) phase function of the input wavefront with the following:

$$\phi(x,y) = A \cdot \sin\left(2\pi n \cdot r / r_{\max}\right)$$

where A is the amplitude of the sinusoid in units of the light wavelength λ, n is the number of cycles across the beam width, $r \equiv \sqrt{x^2 + y^2}$ is the radial distance from the optical axis, and r_{max} is the radius of the beam itself. In this example r_{max} is 1.28 cm and convenient choices for a and n are 0.2λ and 2.0, respectively.

A contour plot of this input phase distribution is given in Fig. B.3a. Note that the amplitude A(x,y) of the beam has not been changed, and remains equal to unity as before. Neither the eye nor any traditional camera can see such a phase distribution at constant amplitude, but the schlieren technique will convert it to an amplitude distribution that should resemble Fig. B.3a.

For the moment, however, lens L2 now performs a Fourier transform upon the input wavefront as before. The input wavefront is still constrained by a square

aperture, but now also distorted by circular phase ripple as a result of having traversed a schlieren disturbance in the input plane. The diffraction pattern that results in the Fourier transform plane was computed using GLAD 4.6, and is displayed in Fig. B.3b. Remnants of the square-aperture Fraunhofer pattern can be seen, but the beam focus or point spread function is clearly dominated by the circular symmetry of the newly-imposed phase ripple.

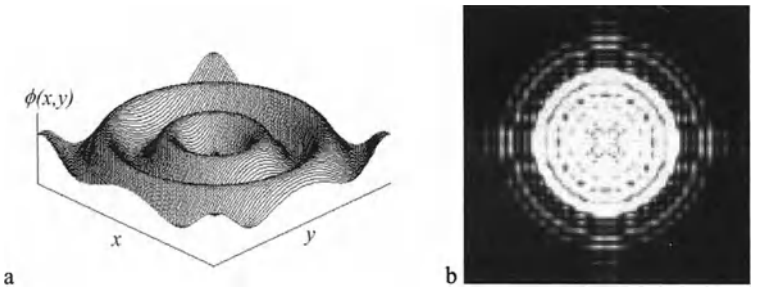

Fig. B.3. **a** Circular phase ripple function imposed upon the input plane, **b** Resulting diffraction pattern in the Fourier transform plane (pattern width ~ 1 mm)

The undisturbed Fourier spectrum of Fig. B.3b leads to the imaging of the input plane into the output plane of the optical processor by way of the inverse Fourier transform described earlier. However, this image cannot display phase, and since the amplitude is uniform, again only a bright square is seen (the projected image of the square input aperture).

B.3 The Schlieren Cutoff

In order to render the phase distribution visible, we now take advantage of the information in the input plane appearing at the focus of lens L2 as a diffraction pattern, the *Fourier spatial frequency spectrum*. The lowest spatial frequency, namely the "DC component" or background illumination, is centered on the optical axis in the middle of Fig. B.3b. Higher-frequency components, corresponding to finer features of the wavefront, appear further from the optical axis. An opaque spatial filter placed in the Fourier plane produces spatial frequency-band rejection [1014], and thus modifies the resulting image amplitude in the output plane.

Low-pass, high-pass, and bandpass spatial filters are described in the literature [129-132], and in Sect. 5.1.3. Some of these effects will be shown later, but for now the knife-edge of Foucault and Toepler is considered first.

A knife-edge that intersects the optical axis blocks exactly half of the spatial frequency plane. Mathematically, the wavefront is multiplied by an amplitude transmittance function that amounts to an opaque Fourier half-plane mask:

$$T(u,v) = \tfrac{1}{2}(1+\operatorname{sgn} v)$$

where sgn = 1 for $v \geq 0$ and -1 for $v < 0$ [130]. This has the effect of a horizontal knife-edge intercepting the beam focus from below with 50% cutoff. At this point, if not already, the complex integration goes far beyond hand calculations, and numerical integration by computer is absolutely required [1015].

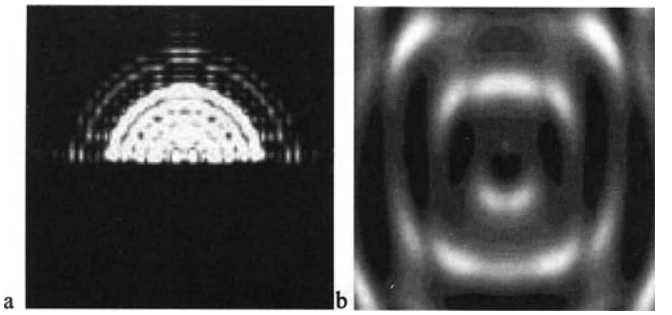

Fig. B.4. **a** Fourier spatial frequency spectrum of Fig. B.3, with bottom half truncated by knife-edge cutoff. **b** Resulting schlieren image in the output plane of the optical processor.

Carrying out this computation with the GLAD 4.6 program, the effect of the knife-edge cutoff is shown visually in Fig. B.4. With the bottom half of the Fourier spectrum truncated, the resulting image is not very useful compared to the input, Fig. B.3a. Indeed, phase has been transformed into amplitude, but there is vertical smearing and the radial symmetry is almost lost. This result echoes the earlier discussion of how a traditional knife-edge cutoff and coherent illumination are not compatible in schlieren optics (Sect. 7.1.1 and Fig. 7.2a).

We might expect to improve this situation, as some authors advocate [153], if we also allow the DC component (central maximum) and part of the lower sideband to pass the cutoff, Fig. B.5. However, though the image does brighten, a reasonable schlieren picture still fails to emerge. Interference among the unobscured parts of the diffraction pattern causes "ringing" or fringing, which misrepresents the number of sinusoidal peaks actually present in the input plane.

Following the logic of Chap. 7, we now apply a graded filter in the Fourier transform plane, Fig. B.6. Its transmission,

$$T(u,v) = T_0 + \text{const} \cdot v$$

is near 90% at the top of the spatial frequency spectrum, Fig. B.6a, but only about 60% at the bottom. Other choices of the width of the filter relative to the beam

waist could be made, but this one sufficiently makes the point: despite coherent illumination, the graded filter produces a realistic-looking schlieren image, Fig. B.6b. The familiar schlieren relief effect is evident. Although the vertical filter gradation causes schlieren sensitivity to fall to zero along a horizontal line through the image center, this is so familiar to a schlieren user that the eye ignores it. Similarly familiar is the radial antisymmetry of illumination about this line, which nonetheless indicates radial pattern symmetry to the trained eye. Compare Fig. B.6b to the input phase ripple function shown in Fig. B.3a, noting that only 10 gray levels are available in GLAD 4.6's bitmap output. The similar comparison shown in Fig. 7.2 should also be reviewed.

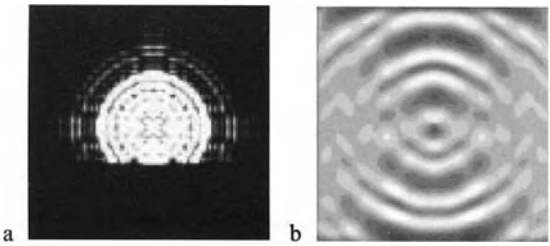

Fig. B.5. **a** The schlieren knife-edge now passes the DC component, upper sideband, and part of the lower sideband of the Fourier spectrum **b** The resulting schlieren image.

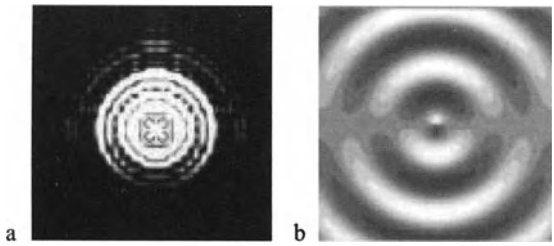

Fig. B.6. **a** A graded filter passes most of the Fourier spectrum, but with increasing attenuation from top to bottom. **b** The resulting schlieren image.

B.4 Other Spatial Filters

Beyond the knife-edge and graded filter, many other possibilities exist to filter or mask the Fourier spatial frequency spectrum in order to produce a schlieren image with desired characteristics. Let us first consider the classic microscopic techniques of bright- and dark-field illumination.

Microscopic brightfield illumination (Sect. 9.4.7) blocks the higher diffraction orders in the Fourier plane by way of an opaque mask with a central circular opening, but passes the central maximum and some of the lower orders. Objects thus appear dark against a bright field. Applied to the present example of schlieren imaging of a circular phase ripple disturbance, the result is shown in Fig. B.7.

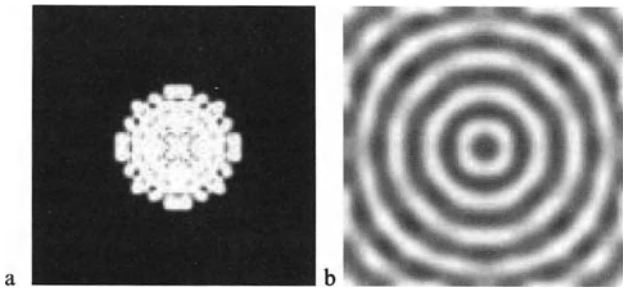

Fig. B.7. **a** The center of the Fourier spectrum – about ½ mm in diameter – is allowed to pass in bright-field schlieren imaging. **b** Resulting schlieren image.

Radial symmetry is approximately shown, as expected, but fringe formation in coherent light obscures the number of cycles that are actually present in the schlieren object. The result is analogous to that of the Erdmann interferometer (Sect. 5.4.2). As in the famous Abbe-Porter experiments [938,1011], information in the higher-order diffraction rings, required for faithful imaging, has been excluded by the low-pass brightfield spatial filter.

Darkfield imaging, on the other hand, blocks the central maximum with an opaque circular-spot mask, but allows all higher orders to pass: a high-pass filter. Results are shown in Fig. B.8.

Again the number of cycles actually present in the schlieren object is misrepresented by fringing. This result is analogous to that of the schlieren-interferometer with a focal filament (Sect. 5.4.2). Quantitative evaluations can be made, but at least in the case of coherent illumination, neither bright- nor dark-field spatial filtering is satisfactory for ordinary qualitative schlieren imaging.

Zernike's phase contrast method [295], discussed in Sect. 5.1.4, was invented as an improvement upon the spatial filtering schemes just described. By altering the phase and amplitude of the central diffraction maximum, phase contrast attempts to produce image contrast more subtly than by simply truncating segments of the Fourier spectrum.

To examine phase contrast properly, a weak schlieren object is required. Thus the same circular phase ripple as shown in Fig. B.3a is used, but now the peak amplitude is reduced by an order of magnitude to 0.02λ. This represents the weakest schlieren object likely to be observed, or the figure errors of even the best schlieren field elements.

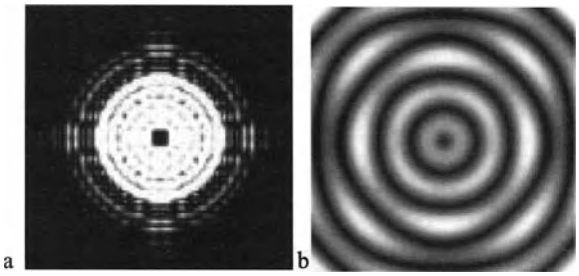

Fig. B.8. **a** The central maximum of the Fourier spectrum – about 0.12 mm across – is blocked in darkfield schlieren imaging. **b** Resulting schlieren image.

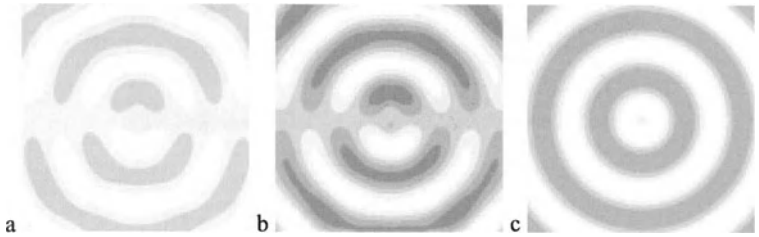

Fig. B.9. 0.02λ circular phase ripple imaged with **a** conventional schlieren knife-edge, **b** λ/2 half-plane phase plate, and **c** λ/4 phase "spot."

Results are shown in Fig. B.9 a-c. First, an ordinary schlieren knife-edge at nearly 50% cutoff is shown for comparison (Fig. B.9a), producing a very weak image. Next a λ/2 half-plane phase plate is used after Wolter [119], having unit transmittance but phase $\phi(u,v) = 0$ for $v \geq 0$ and $= \pi$ for $v < 0$. This has the effect of a horizontal "phase knife-edge,[1]" and does a better job of producing contrast for this weak disturbance (Fig. B.9b). Finally a λ/4 phase "spot" in the cutoff plane dephases the central diffraction maximum (Fig. B.9c). This third image is very close to being a true grayscale representation of the original schlieren object's phase distribution. It shows perfect radial symmetry and good contrast. However, some prefer the side-illuminated, antisymmetric relief effect of schlieren imaging to the results of phase contrast.

Finally, The Hoffman Modulation Contrast method [280-282], described earlier in terms of microscopic schlieren applications, is illustrated here by computational simulation. As illustrated in Fig. B.10a, a stepwise filter passes the upper sideband, blocks the lower sideband, and attenuates a central band through the Fourier

[1] Some authors see this approach and the Foucault knife edge as applications of a Hilbert transformation to the light beam [153,1017-1020].

spectrum. In this example the circular phase ripple of Fig. B.3 is the schlieren object once again, with $a = 0.2\lambda$ and n = 2.0. The central band of the Hoffman filter is about 0.2 mm wide, and transmits only 15% of the incident light. The resulting schlieren image, Fig. B.10b, is rather harshly illuminated, but is nevertheless a reasonable representation of the input phase distribution, second in quality only to the graded filter case (Fig. B.5b), and far superior to the dark- and bright-field images just shown.[2]

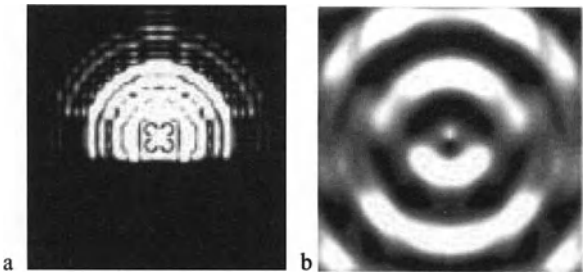

Fig. B.10. **a** Appearance of the Fourier spectrum after having been filtered by a Hoffman Modulation Contrast filter. **b** Resulting schlieren image.

B.5 Partially-Coherent and Polychromatic Illumination

Until now, fully-coherent illumination was assumed throughout this Appendix. That means both temporal coherence (monochromaticity) and spatial coherence (the ability to be focused to a point): laser light, in practical analogy. In this section we relax both constraints in turn. As already described in Chap. 7, most schlieren systems should and do use extended polychromatic light sources rather than lasers (though laser illumination with a graded-filter cutoff works well). The generality of coherent optical processing is lost in the incoherent case, but freedom from annoying coherent artifact noise is gained through multichannel redundancy. More to the present point, however, incoherent light is more troublesome to handle by Fourier optics, and has consequently been held for the last topic.

[2] In complete fairness to the Hoffman method, an extended (partially-coherent) light source is required in practice. Moreover, polarizer rotation allows variable transmission of the central band in order to optimize the contrast of the microscopic image.

To simulate incoherent illumination one must sum contributions from an array of many coherent points in the source plane of Fig. B.1 [129,588]. Each point source produces its own Fraunhofer diffraction pattern in the Fourier plane. The resulting array of point spread functions is added incoherently. The output schlieren image then becomes the sum of many mutually-incoherent narrow-band light beams. The 3-D Fourier optics calculation in (x,y,z) must be repeated for each of these many beams, sometimes taxing the available computer resources. To fully simulate incoherence, 50 or more separate point sources might be required. For partial coherence, however, 10 points will often suffice [588].

We thus take a first step in this direction by maintaining spatial coherence while relaxing temporal coherence: a white-light point source. As in sections B.2 and B.3, a circular phase ripple with $a = 0.2\lambda$ and n = 2.0 forms the schlieren object and an ordinary knife-edge is used. However, the light source now consists of 10 coincident illumination points at 10 different λ values more-or-less spanning the visible spectrum.

Because of polychromatic illumination, each point spread function in the Fourier plane is different, thus each is affected differently by the knife-edge. Repeating the case of Fig. B.5, the knife-edge is set to pass the DC component, top sideband, and part of the lower sideband of the Fourier spectrum. The resulting computed schlieren image, Fig. B.11a, shows improvement over its fully-coherent equivalent, Fig. B.5b: the "ringing" is reduced and the true number of sinusoidal peaks is better represented. Polychromatic fringe patterns overlap and smear, reducing fringe contrast somewhat in favor of a uniform gradation in image intensity [72]. Coherent artifact noise – not simulated here – is also reduced.

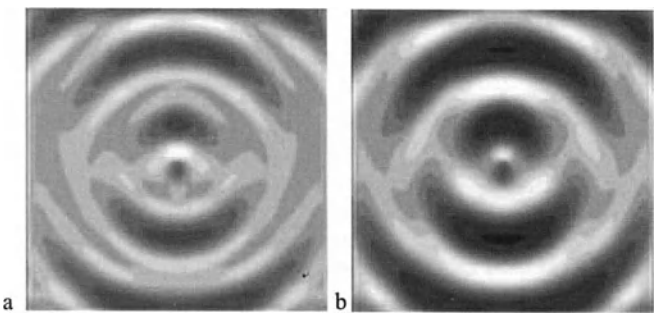

Fig. B.11. **a** Circular phase ripple schlieren image resulting from a polychromatic point source. **b** Schlieren image produced by an extended polychromatic light source.

Finally, we simulate reduced spatial as well as temporal coherence by distributing the 10 polychromatic point sources in an oblong spatial pattern centered about the optical axis. (In reality, a rectangular slit source contains an infinity of such points, but earlier simulations used only a line source of zero width [66,126].) The long axis of the present synthetic extended source is set parallel to the horizontal

knife-edge. The result is that some of the point spread functions, due to spatial location, are more severely obstructed than others by the knife-edge. In addition to the polychromatic effects described earlier, this further insures that all frequencies of the Fourier spectrum are redundantly represented in the final image, Fig. B.11b.

Fig. B.11b is a clear improvement over both fully-coherent schlieren, Fig. B.5b, and the case of the white-light point source, Fig. B.11a. It is similar in appearance to the graded-filter case discussed earlier (Fig. B.6b), and approaches being a realistic schlieren representation of the input phase function, Fig. B.3a. More point sources could be added to better simulate incoherence, yielding limited further improvement within the 10 gray levels available in GLAD 4.6 to display the result, but the point is already made.

Some advantages of relaxed coherence have thus been shown despite an increase in the computational complexity. Other advantages include the low cost of white-light sources compared to lasers, and the possibility that color schlieren and extended, matched source/cutoff masks can now be used. This assists directional filtering (θ-modulation) [71] in the x-y plane, as described in earlier chapters. The color schlieren technique, invented by Rheinberg [67] and covered in Sect. 5.2, is also analyzed in terms of Fourier optics by Bescos and Strand [69].

In conclusion, we see that Fourier optics provides the general theoretical background for the schlieren process. Practical examples require significant numerical computation, but software and hardware resources are available for the purpose (all present computations were done on a Pentium-class desktop computer). While geometric optics was used throughout this book for simplicity, it should now be clear that simple geometric theory is obeyed only as a first approximation to physical optics in schlieren and shadowgraph techniques.

Appendix C Parts List for a Simple Schlieren/ Shadowgraph System

Chap. 8 was devoted to a small, simple z-type schlieren system that can also be used for "focused" shadowgraphy. This Appendix lists the parts needed to build such a system. Typical vendors and prices are cited (ca. 2000), tho ugh none of these components is exclusive to a single manufacturer. Substitutions of comparable items are encouraged. The most expensive parts are the optical breadboard and mounts that can, however, be entirely homemade by the enterprising amateur to cut costs. Details on the suppliers of appropriate components are given in App. D. Cameras and video equipment for schlieren imaging are discussed in Sect. 7.3, but are not included in this parts list.

C.1 Optics

- Two 108 mm diameter by 864 mm focal length parabolic mirrors (f/8), first-surface aluminized and coated for protection, $\lambda/8$ surface accuracy, e.g. Edmund L32-122, $111US each. Other high-quality mirrors of different diameter can be used, but the f/number should be at least 6 to avoid astigmatism problems.
- One aspheric single-element condenser lens, typically 50 mm diameter f/1, though neither the diameter nor the f/number is critical, e.g. Edmund L43- 990, $33US each. Note that a camera lens, e.g. 50 mm diameter f/1.8, also serves as an acceptable condenser for the present purpose.
- One achromatic-doublet focusing lens of 50 mm diameter by 250 mm focal length, e.g. Edmund L32-919, $50US each, chosen to size the image for 35mm photography. For screen viewing and/or Polaroid photography a focal length of roughly ½ m is required: a single-element plano-convex or meniscus lens will suffice, e.g. Edmund L45-288, $30US each. Note that telephoto and zoom lenses intended for 35mm photography also accomplish this purpose well.

C.2 Illumination

- One tungsten-halogen headlamp or fog-lamp bulb, e.g. GE H3-55, $6US, available at automotive supply stores.
- One 0-30 VDC power supply, e.g. EZ Digital Model GP-4303A (90 W), $209US. Incandescent lamps can also be operated on AC power using, e.g., a Staco Variable Transformer Model 3PN221B. Battery operation is also feasible, though a rheostat voltage control is needed.

C.3 Miscellaneous Components

- One adjustable source-slit aperture, e.g. Ealing 61-1137, $195US. For economy, several fixed slit apertures can be made up from razor blades instead.
- One 100x100 mm ground glass screen, e.g. Edmund L45-656, $27US
- One 0.9 x 1.2 m or larger steel optical breadboard, e.g. Edmund L55-253, $1300US (optional, and replaceable by a steel plate on a standard workbench, for magnetic mounts, or just the workbench itself otherwise.)

C.4 Optical Mounts

- Two adjustable mirror mounts, e.g. Edmund L36-482, $141US each.
- Three 3-screw ring mounts, e.g. Edmund L36-605, $60US each.
- One screen holder for ground glass, e. g. Ealing 22-8700, $79US.
- One small filter holder for the knife-edge, e. g. Edmund L55-531, $95US.
- One 2-axis lead-screw drive for the schlieren cutoff, e.g. Edmund L55-020, $280US
- Eight magnetic base plates, e.g. Edmund L39-926, $84US each.
- Eight optical post holders, e.g. Edmund L03-646, $13US each.
- Eight optical posts, e.g. Edmund L36-495, $11US each.

Appendix D Suppliers of Schlieren Systems and Components

Such a listing as this will quickly become dated: the list given by Holder and North [98], for example, has long since ceased to be useful. Nevertheless an attempt is made to list current suppliers of systems and components circa 2000. There is no claim of comprehensiveness, but all suppliers known to the author are listed.

D.1 Complete Schlieren Systems

- Rudimentary 108 mm and 152 mm-aperture z-type schlieren systems are available from Edmund Industrial Optics, 101 E Gloucester Pike, Barrington, NJ 08007, phone 800-363-1992, fax 856-573-6295, www.edsci.com, Models L71-013 and -014, $355-$530US.
- The Optison Schlieren System, 50-120 mm aperture, intended for ultrasonic diagnostics research, is sold by Intec Research, 532 Weddell Drive, Suite no. 1, Sunnyvale, CA 94089, www.intec.com, phone 408-745-0383, fax 408-745-0956.
- Z-type schlieren equipment, intended for wind tunnel diagnostics, is available from Aerolab Inc., 9580 Washington Blvd., Laurel MD 20723, phone 301-776-6585, fax 301-776-2892, www.aerolab.com.
- NK Biotechnical Corp., 10850 Old County Road 15, Minneapolis, MN 55441, phone 800-462-3751, markets a small laser-illuminated lens-type schlieren system as part of their wind tunnel apparatus. www.nkb.com.
- A 100 mm-aperture z-type schlieren system, Model TE65, is available from TecQuipment Ltd., Bonsall Street, Nottingham NG10 2AN UK, phone +44 (0) 115 9722611, fax +44 (0) 115 9731520, www.tecquip.co.uk. The price is approximately $20,000US, including US delivery.

- Focusing schlieren systems, fixed and portable, with apertures up to 1 m or more are available by special order from Viewstar, Inc., 13 Burke Ave., Newport News, VA 23601, (757) 596-6113.
- Fixed and portable schlieren systems are available by special order from Industriefilm, D-65779 Kelkheim, Germany, phone +49 (0) 6195 – 63538, fax – 64158, www.schlierenoptics.de.
- The ATTO Schlierograph instrument for gel electrophoresis applications is available (only in Japan) from Atto Corp., Hongo 1-25-23, Bunkyo-ku, Tokyo 113-8425, Japan, www.atto.co.jp.
- Complete schlieren systems of 100-300 mm aperture, including color and video, are available (apparently only in Japan) from Mizojiri Optical Co. Ltd., 2-8-2 Nishi-shinagawa, Shinagawa-ku, Tokyo 141-0033, Japan, phone +81-03-3492-1900, fax +81-03-3492-1921.
- Complete schlieren systems in the 70-800 mm-diameter range are offered by the Tupolev Kazan State Technical University, International Cooperation Department, 10 Karl Marx Str., Kazan, Tatarstan 420111, Russia, phone +7 8432 385-044, fax +7 8432 366-032, email technopark@kai.ru. Contact with this supplier has been erratic, however, and as of Jan. 2001 it appears that the equipment is not currently available for export from Russia.

D.2 Schlieren Field Mirrors

- Parabolic $\lambda/8$ mirrors suitable for schlieren use are available in diameters up to 318 mm from Edmund Industrial Optics, 101 E Gloucester Pike, Barrington, NJ 08007, phone 800-363-1992, fax 856-573-6295, www.edsci.com. Prices range up to $1000US.
- Glass Mountain Optics, Inc., 9517 Old McNeil Rd., Austin, Texas 78758, phone 512-339-7442, fax -0589, has produced lightweight schlieren mirrors in the 700 mm range, $\lambda/8$ to $\lambda/4$, for a price of about $13,000US each. They have the capacity to grind mirrors up to 2.5 m diameter. Contact Larry Forest, www.glassmountain.com.
- Stefan Sydor Optics Inc., One Blossom Rd., Rochester, NY 14610-1009, phone 716-271-7300, fax -7309, can produce schlieren mirrors up to 1.3 m diameter.
- Space Optics Research Labs, 7 Stuart Road, Chelmsford, MA 01824, phone 978-250-8640, fax 978-256-5605, specializes in off-axis parabolic mirrors, which they can supply up to 400 mm in diameter. Mirror mounts are also available in sizes up to 600 mm. www.sorl.com.

- ARW Optical Corp., 6631-B Amsterdam Way, Wilmington, NC 28405, phone 910-452-7373, fax 910-452-6326, advertises the ability to produce schlieren mirrors.
- BSC Optics, 433 Live Oak Loop NE, Albuquerque, NM 87122, phone 505-856-6863, fax -6804 , www.bscoptics.com, sells used and surplus optics including schlieren mirrors.
- Cosmo Optics Inc., 238 Watkins Ave., Middletown, NY 10940, phone 914-343-2105, fax -9831, advertises the ability to produce schlieren mirrors.
- Galaxy Optics P.O. Box 2045, Buena Vista, CO 81211, phone 719-395-8242, manufactures precision telescopic parabolas up to 635 mm diameter. http://home.chaffee.net/~galaxy/.
- Pegasus Optics, P. O. Box 1389, Brackettville, Texas 78832-1389, phone 830-563-2578, fax –2965, manufactures precision telescopic parabolas up to 609 mm diameter. http://www.icstars.com/pegasus/.
- R.F. Royce Optics, 30 Holly Mar Hill Road, Northford, CT 06472, phone 203-484-7705, fax -9016, manufactures $\lambda/10$ telescopic parabolas up to 318 mm diameter and objective lenses up to 305 mm diameter. http:// www.rfroyce.com.
- Ealing Optical Works Ltd., Newquay, Cornwall, UK, Mr. E. O. Frisk, phone 01637 877 222, manufactures spherical mirrors up to 914 mm diameter with focal lengths up to 6 m.
- Surplus Shed, 407 Rt. 222, Blandon PA 19510, phone 877-7SURPLUS, sells used and surplus optics including schlieren mirrors at reasonable prices. www.surplusshed.com.
- Optical Surfaces Ltd., Godstone Rd., Kenley, Surrey CR8 5AA UK, phone 44-(0)-181-668-6126, fax: 44-(0)-181-660-7743, produces off-axis $\lambda/20$ parabolic mirrors up to 1 m diameter and spherical mirrors and flats up to 1.3 m diameter. www.optisurf.com.

D.3 Light Sources

- Quadtech, 5 Clock Tower Place, Suite 210 East, Maynard, MA 01754, phone 978-461-2100, www.quadtech.com, sells the Quadtech/Genrad 1531AB Strobotac (see Sect. 7.1) $4500US.
- High-Speed Photo-Systeme, Von-Linne-Str. 12, D-22880 Wedel, Germany, phone+ 49-4103-89379, fax + 49-4103-18254, www.HSPS.com/indexen.htm, offers for sale the Fischer Nanolite and the Früngel Combi-Spark light sources.

- Xenon Corporation , 20 Commerce Way, Woburn, MA 01801-9711, phone 800-XENON-XL, fax781-933-8804, also markets Nanolite-like spark sources, a high-intensity Nanopulse system, and linear, helical, and point-source flashlamps.
- Mercury- and xenon-arc lamps are available from Coherent-Ealing, Coherent Auburn Group, 2303 Lindbergh St., Auburn CA 95602, phone 800-343-4912; Oriel Instruments, 150 Long Beach Blvd., Stratford, CT 06615, phone 203-377-8282, fax 203-378-2457, www.oriel.com; and Melles-Griot, 16542 Millikan Avenue, Irvine, California 92606, phone 800-835-2626, fax 949-261-7589, www.mellesgriot.com.
- The Viewstar Model 955-5 3-Color Flashlamp with 5-10J microsecond flashes and adjustable delay times, is available from Viewstar, Inc., 13 Burke Ave., Newport News, VA 23601, (757) 596-6113, price about $10,000US.

D.4 Components

- Lenses and optical mounts suitable for schlieren use are available from a wide variety of sources including Edmund Industrial Optics, Oriel Instruments, Coherent-Ealing, Melles-Griot and many others.
- Wollaston prisms are available from:

  Karl Lambrecht Corp., 4204 N. Lincoln Ave., Chicago IL 60618, phone 773-472-5442, fax -2724.

  Lambda Research Optics, 17605 Fabrica Way, Suite A-D, Cerritos, CA 90703, phone 714-228-1192, fax -1193.

  OptoSigma, 2001 Deere Ave., Santa Ana, CA 92705, phone 714-851-5881, fax -5058.

  Optique de Précision J. Fichou, 30 rue de la Garenne, 94260 Fresnes, France, phone (33) 0146661518, fax (33) 0149840675.

  Coherent-Ealing, Coherent Auburn Group, 2303 Lindbergh St., Auburn CA 95602, phone 800-343-4912.

  Bernard Halle Nachfl. GmbH, Hubertusstrasse 10, D-12163 Berlin, Germany, phone (030) 791-6077, fax (030) 791-8527.

- Graded filters are available in the form of photographically-made Fuzzies soft-edged masks in five widths from DSC Labs, 3565 Nashua Drive, Mississauga, Ontario, Canada L4V 1R1, phone 905-673-3211, fax 905-673-0929, www.dsclabs.com.

- Optico Glass Fabrication, Inc., 3164 El Camino Real, Atascadero, CA 93422, Phone: 805/461-9402, Fax: 805/461-0420 produces flat mirrors up to 380 mm diameter and BK-7 glass windows up to 305 mm diameter.

D.5 Focusing Schlieren Lenses

- C&H Sales, 2176 E. Colorado Blvd., Pasadena, CA 91107, phone 800-325-9465 fax 626-796-4875, http://aaaim.com/CandH/index.htm, offers surplus optics including projection-TV lenses.
- Buhl Optical, 1009 Beech Avenue, Pittsburgh, PA 15233, phone 800-245-4574, fax 412-322-2640, www.buhloptical.com, sells projector lenses.
- Allen Gordon Enterprises, 1430 Cahuenga Blvd. Hollywood, CA 90029, phone 213-466-3561, fax 213-871-2193.
- Schneider Optics, Inc., 285 Oser Ave., Hauppauge, NY 11788, phone 631-761-5000, fax -5090, www.schneideroptics.com.
- Rodenstock Precision Optics, Inc., 4885 Colt Road, Rockford, IL 61109-2611, phone 800-467-8457, fax 815-874-6374, www.rodenstockoptics.com.

D.6 Miscellaneous

- Software for physical optics, ray tracing, and computed schlieren is available from:

  Applied Optics Research, 8127 Mesa Dr. no. B206, Austin, TX, phone 512-418-8569, fax 214-853-5516, http://www.aor.com, offers the GLAD physical optics and laser analysis software package.

  Lambda Research Corporation, 80 Taylor Street, P.O. Box 1400, Littleton, MA 01460-4400, phone 978-486-0766, fax -0755 markets the OSLO ray-tracing optical design software package.

  CIRA Scientific Visualization Group, 81043 Capua, Italy, phone +39 (0823) 623111, fax 623126, www.cira.it/research/vis, offers scientific visualization software Flowvis 4.1 with interactive schlieren post-processing capability.

- Lamp power supplies are available, among many sources, from TestMart, 851 Traeger Avenue, San Bruno, CA 94066, phone 650-624-0525, fax 650-624-0535, http://www.testmart.com. Staco variable AC transformers can be had

from ISE, Inc., 10100 Royalton Rd., Cleveland, OH 44133, USA, phone 440-237-3200, fax -1744, www.instserv.com.

- Glass cuvette cells suitable for schlieren studies in liquids are available from NSG Precision Cells, Inc. 195G Central Ave, Farmingdale, NY 11735.
- Retroreflective material in the form of 3M™ Scotchlite™ Reflective Sheetings can be obtained from 3M Traffic Control Materials Division, 3M Center, Building 225-5S-08, P.O. Box 33225, St. Paul, MN 55133-3225, phone 800-553-1380 Ext. 1&2, fax 800-591-9293, http://www.3m.com/safety.
- Light-shaping holographic diffusers are available from Edmund Industrial Optics; Physical Optics Corp., 20600 Gramercy Place, Building 100, Torrance, CA 90501, phone 310-320-3088, fax -8067, www.poc.com; and JML Optical Industries, Inc. 690 Portland Avenue Rochester, New York 14621, phone 716-342-8900, fax -6125, www.jmloptical.com.
- Fresnel lenses can be obtained from Edmund Industrial Optics and from Fresnel Optics, 1300 Mt. Read Blvd., Rochester, NY 14606, phone 716-647-1140, fax 716-254-4940, www.fresnel-optics.com.
- Hoffman Modulation Contrast imaging for microscopy is marketed by Modulation Optics, Inc., Subsidiary of Slant-Fin Corp., 100 Forest Dr., Greenvale, NY 11548-1205, phone 516-484-8882, fax 516-621-4768.
- Kodak Wratten gelatin color filters can be purchased from Edmund Industrial Optics.
- Refractive-index matching fluids are manufactured by Cargille Laboratories, Inc., 55 Commerce Road Cedar Grove, NJ 07009, phone 973-239-6633, fax – 6096, www.cargille.com.
- Stereo image viewers are available from 3D Concepts, P.O. Box 715, Carlisle, MA 01741, phone 978-371-5557, e-mail 3dman@ziplink.net, Internet address http://stereoscopy.com/3d-concepts/new.html.
- High-speed cameras compatible with schlieren and shadowgraphy are available from Redlake Imaging, 18450 Technology Dr., Suite A, Morgan Hill, CA 95037-5450, phone 408-779-6464, fax 408-778-6256, http://www.redlake.com, and from Cordin Scientific Imaging, 2230 South 3270 West, Salt Lake City, UT 84119, phone 801-972-5272, fax 801-972-8270, www.cordin.com.

Index

Color Plates

The following pages contain color plates numbered 1-48, as cited in numerical order in the text. In order to show as many examples as possible, these plates are identified by number with corresponding captions given below.

1. Microgram of sodium hydroxide (soda-lye) crystals under Rheinberg illumination at 100X. Photo by author.
2. Schardin's [2] prism-method color schlieren image of a burning match, reproduced courtesy of Springer-Verlag.
3. R. J. North's color schlieren image of a wedge airfoil in supersonic flow. Photo courtesy Nella North.
4. Supersonic flow past a flat-faced cylinder at Mach 3. 2-D dissection color schlieren photograph by the author.
5. Weak shock waves from the burst of a toy balloon. μsec 2-D dissection color schlieren photograph by the author.
6. Early Space Shuttle Orbiter model undergoing a transonic test in the former NASA-Ames 6x6 Supersonic Wind Tunnel, 2-D dissection color schlieren photograph by the author, ca. 1971.
7. As in Plate 6, but with supersonic airflow and a high model angle-of-attack.
8. A delta-winged version of the Space Shuttle Orbiter in supersonic flow.
9. Schardin's [2] schlieren method no. 3, the large-colored-grid-background method, reveals the flaws of a glass plate (courtesy of Springer-Verlag).
10. Full-scale schlieren image of displacement ventilation in a room, where chilled air from a register, below left, displaces warmer polluted air from a person and a computer (modeled by J. D. Miller).
11. Full-scale schlieren image of propane gas leaking from a valve [237] (modeled by J. D. Miller).
12. Schlieren image of an explosion beneath a full-sized aircraft seat occupied by a dummy, part of a study of aircraft hardening in response to incidents of international terrorism (research funded by the FAA, [793]).
13. Full-scale schlieren image of the convective plume from a gas-fired outdoor barbeque grill (modeled by J. D. Miller).

14. 2-D dissection color schlieren photograph of the convective plume from a burning wad of paper. Photo by the author.
15. High-speed wind tunnel test imaged by the Soviet-made IAB- 451 schlieren instrument using a prism attachment. Photo courtesy I. V. Ershov.
16. Band-lattice color schlieren photo of a mouth-blown glass plate, from Schardin [2] courtesy of Springer-Verlag.
17. Band-lattice color schlieren photo of a flawed glass plate, H. Herbrich photo reproduced by permission.
18. Band-lattice color schlieren image of a horizontal heating pipe (author photo).
19. Hypersonic test of a missile interceptor using Cords' 1-D dissection method (US Navy photo).
20. The tip vortex of a fan blade rolls up the convection column from an alcohol lamp. 2-D dissection color schlieren photo by J. K. Vandiver [386,387], reproduced by permission.
21. An overexpanded round supersonic jet discharging into free air, 2-D dissection color schlieren photo by the author.
22. As in Plate 22, but now underexpanded.
23. A supersonic bullet penetrates a telephone book sitting atop a stool. 2-D dissection color schlieren photo by the author.
24. A 0.22-caliber bullet is fired from a Thompson Contender marksman's pistol.
25. Supersonic bullet, blast wave, and propellant gases emerge from the muzzle of a 0.22-caliber rifle. 2-D dissection color schlieren photo by the author.
26. A High-Velocity Oxy-Fuel (HVOF) thermal spray gun ejects a supersonic plume of hot combustion gases in front of the 1 m parabolic mirror of the Penn State Gas Dynamics Lab (modeled by J. D. Miller).
27. The human thermal plume, modeled by Lara A. Settles ca. 1981. 2-D dissection color schlieren photo by the author.
28. A human cough expels warm air from the lungs. This schlieren image has been used to illustrate dozens of magazine articles on colds and influenza.
29. The thermal plume of a worker is suppressed by the ½ m/sec ventilation down-flow in a microelectronics clean room (modeled by A. J. Smits).
30. The turbulent convection plume from a candle flame after being disturbed by an ambient breeze. 2-D dissection color schlieren photo by the author.
31. A jet of propane gas from a 7 mm hose strikes a horizontal flat surface and rolls up in vortical structures. The propane flow rate is about 50 ml/sec.
32. A propane-filled soap bubble reveals soap-film striations and also acts as a weak lens to show the 4 colors of the 2-D dissection color schlieren method.
33. The diffraction of a planar shock wave around a sharp 90 ° corner in a shock tube is imaged by the round dissection color schlieren method. Image by Harald Kleine, reproduced by permission.

34. An AgN_3 pellet suspended on a fine wire explodes above a horizontal surface as seen by the round dissection color schlieren method. Image by Harald Kleine, reproduced by permission.
35. The interaction of a shock wave with a cylinder in a shock tube, as seen by the round dissection color schlieren method. Image courtesy Harald Kleine.
36. White-light, infinite-fringe Wollaston-prism schlieren interferogram of a flawed glass plate. Image by Heather Ferree and the author.
37. As in Plate 36, but the schlieren object is now the plume from a candle flame.
38. Gasoline fumes spill from an automotive tank while refueling, imaged by H. Herbrich using a portable 300 mm single-mirror coincident schlieren system. Photo reproduced by permission.
39. Faraday waves on the surface of a round pool of mercury, excited by a musical tone and imaged with the color band-lattice method. Photo by author.
40. As in Plate 39, but a square mercury pool and a higher-pitch tone were used.
41. The hydraulic analogy is invoked to visualize a supersonic double-wedge oblique compression using a color bullseye source filter. Photo by B. W. Skews, reproduced by permission.
42. A horizontal band-lattice schlieren photo of a Mach 3 shock wave/boundary-layer interaction under continuous illumination. Photo by author.
43. Color schlieren image of a supersonic missile model using the prism method [345]. US Govt. photograph.
44. 2-D flow over a planar wedge model in a supersonic wind tunnel. 2-D dissection color schlieren photo by the author.
45. Wolter's [119] quantitative color microgram of KSO_4 crystals, reproduced courtesy of Springer-Verlag.
46. Color-filter-adapted Hoffman Modulation Contrast microgram of rings formed by the dissolution of a saccharin crystal in alcohol. 100X photo by the author.
47. A Water Boatman of the family *Clorixidae* is supported by surface tension on a pool of water, locally depressing the surface and refracting light rays. The schlieren beam arrives from above and is reflected at an angle, giving a double image of the insect. Color band-lattice image by the author.
48. An explosion in the luggage container of a 1/6-scale Boeing 747 mockup ruptures the pressure hull of the aircraft in this aircraft-hardening simulation (research funded by the FAA, [793]; see also Color Plate 12).

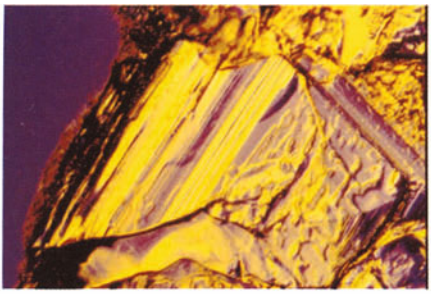
1

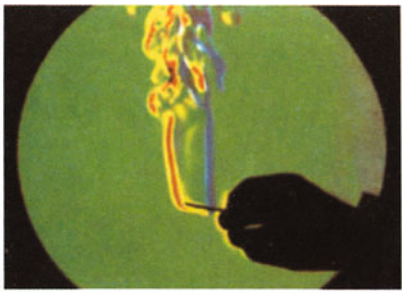
2

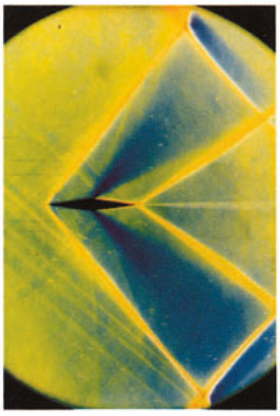
3

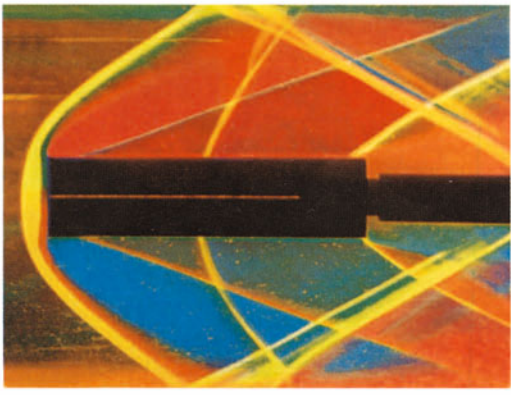
4

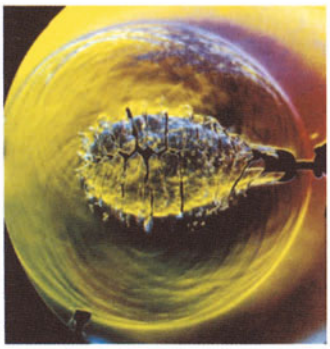
5


6


7

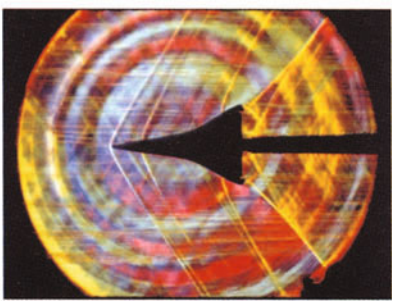
8

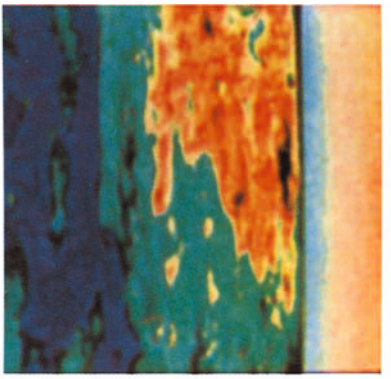
9

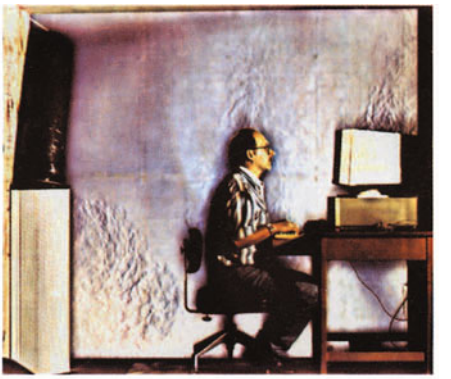
10


11


12


13

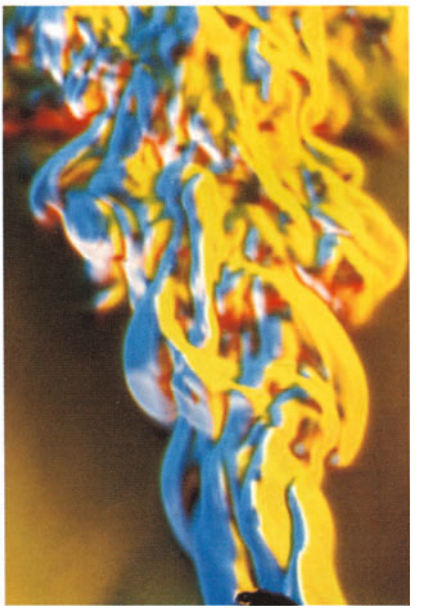
14

15

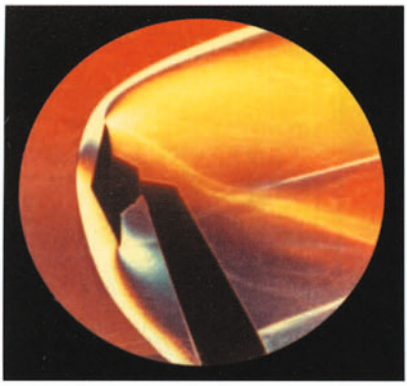

16

17

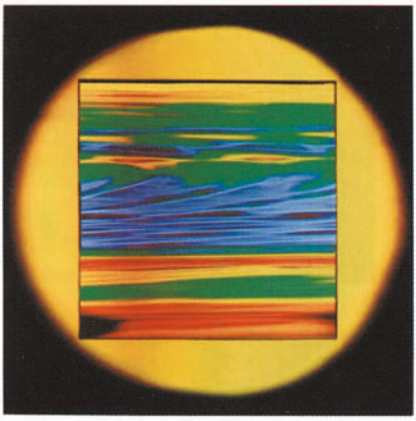

18

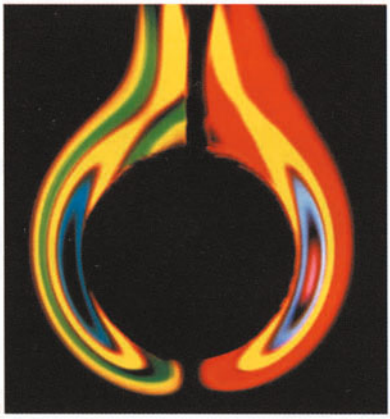

19

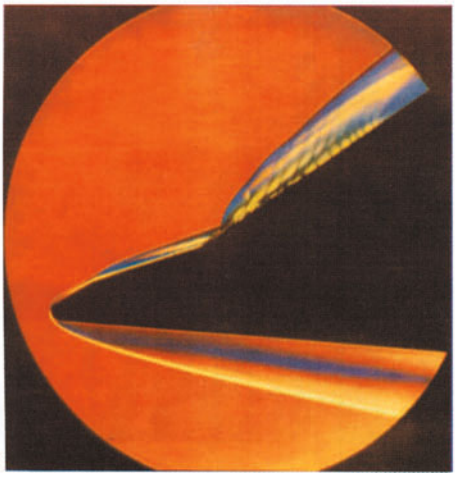

20

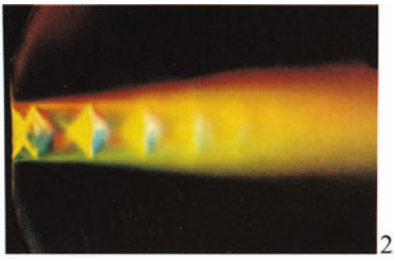
21

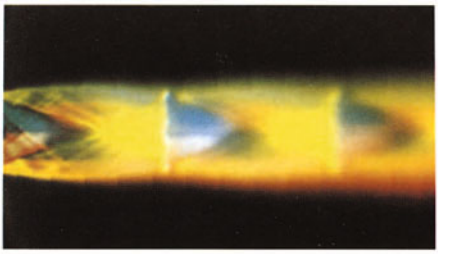
22

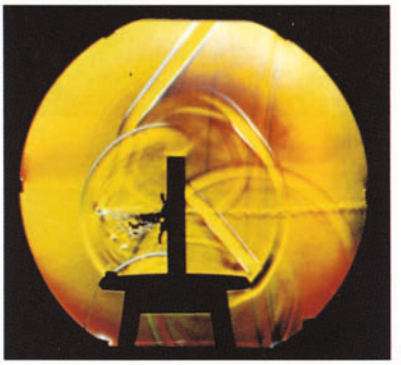
23

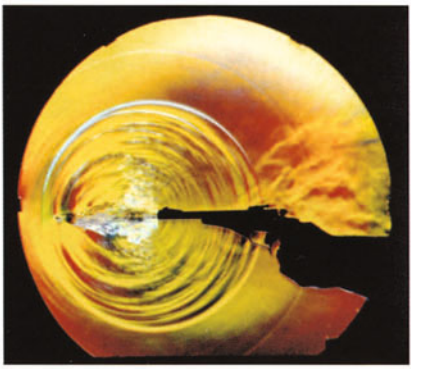
24

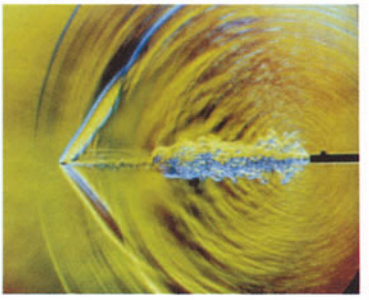
25


26

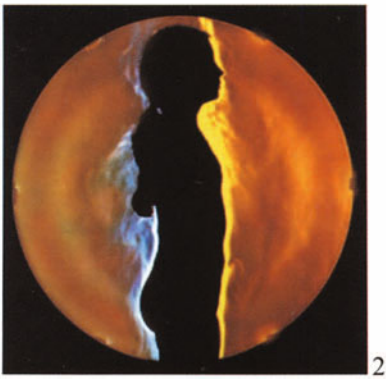
27

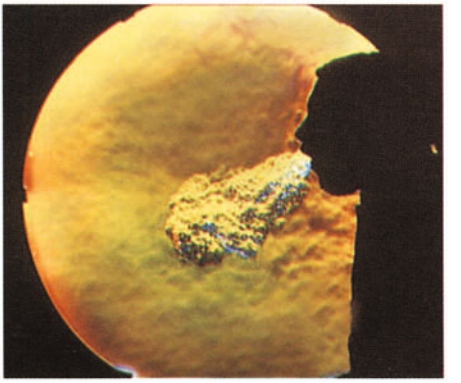
28


29

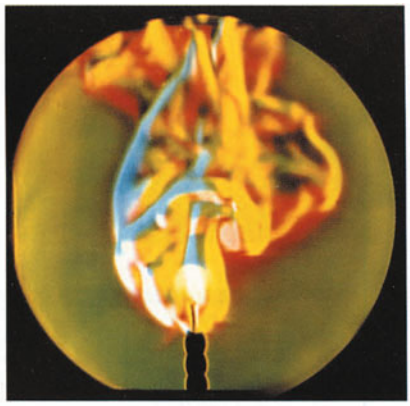
30

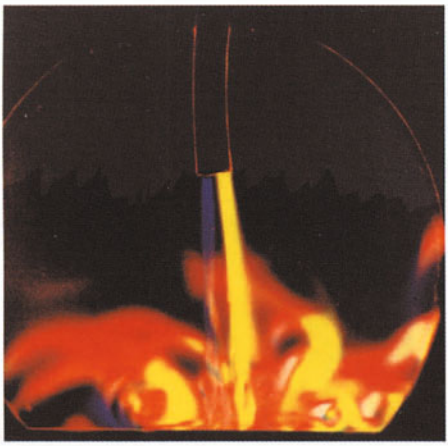
31

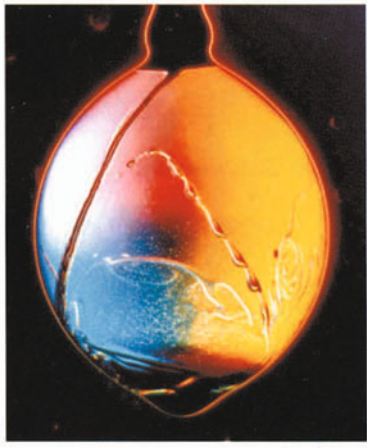
32

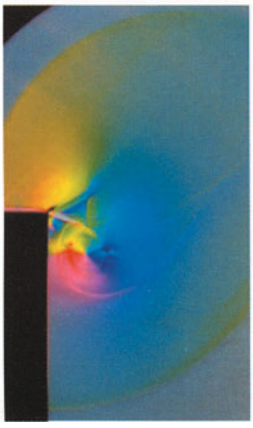
33

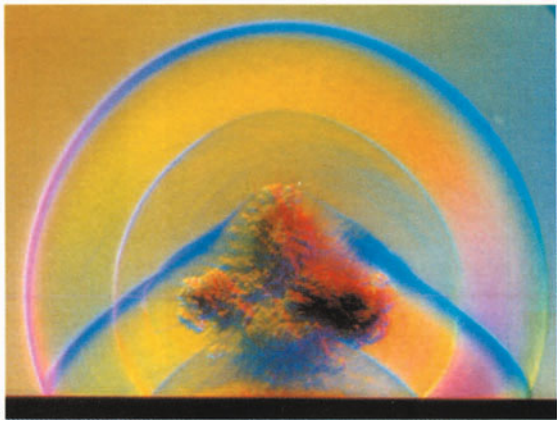
34


35

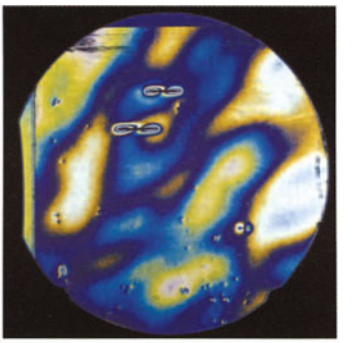
36

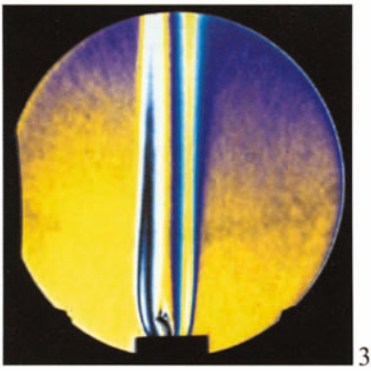
37


38

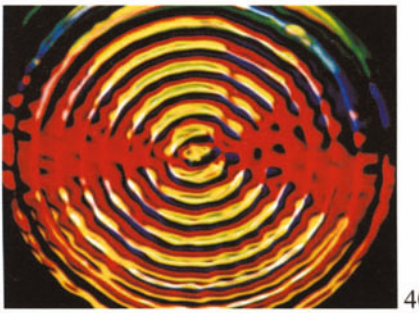
39

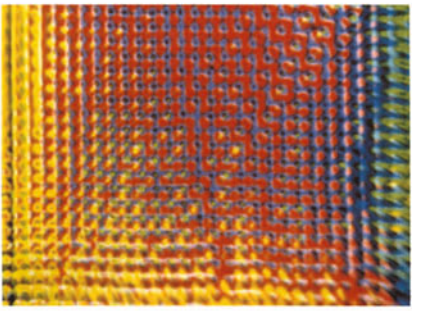
40

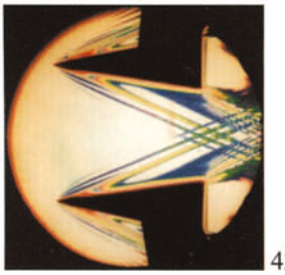
41


42

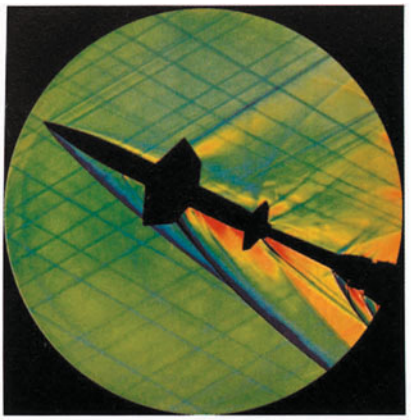

43

44

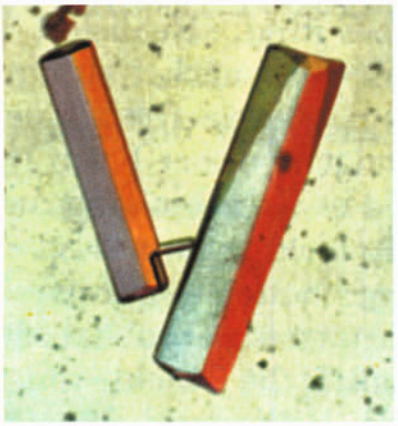

45

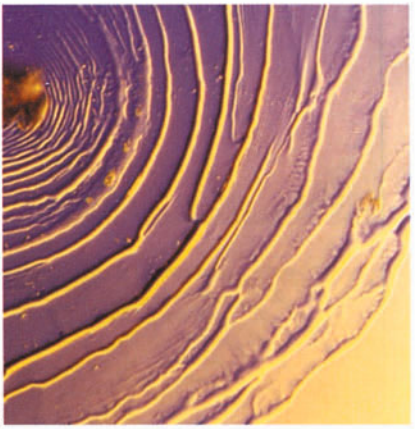

46

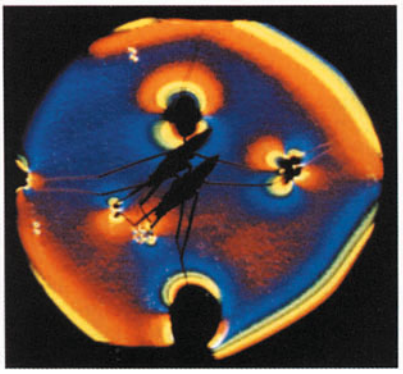

47

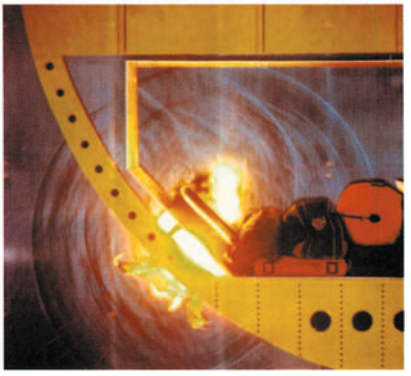

48